



MONASH University

Towards the prediction of properties in large clusters of ionic liquids with
quantum chemical methods

ZOE LUISA SEEGER

School of Chemistry

Faculty of Science

A thesis submitted for the degree of Doctor of Philosophy at

Monash University in 2020

Contents

Copyright notice	v
Abstract	vii
Declaration	xi
Acknowledgements	xiii
Abbreviations	xv
1 Introduction	1
1.1 What are ionic liquids?	1
1.2 Accurate quantum chemical methods	3
1.3 Quantum chemical methods for the prediction of energetic, physical, and spectroscopic properties of ionic liquids	7
1.4 Overview	66
1.5 References	69
2 Application of the fragment molecular orbital approach to large clusters	77
2.1 Introduction	77
2.2 Trends in Two- and Three-Body Effects in Multiscale Clusters of Ionic Liquids	79
2.3 References	91
3 In search of a DFT functional for geometry optimisations of large clusters	93
3.1 Introduction	93
3.2 A systematic study of DFT performance for geometry optimisations of ionic liquid clusters	95
3.3 References	159
4 Tuning DLPNO-CCSD(T): A high accuracy method at reduced cost	161
4.1 Introduction	161
4.2 A DLPNO-CCSD(T) benchmarking study of intermolecular interactions of ionic liquids	163
4.3 References	202
5 Sampling vast ionic liquid surfaces for the minima of bulk properties	203

5.1	Introduction	203
5.2	An intuitive approach to finding local minima in ionic materials: a balancing of starting geometry and dynamic evolution	205
5.3	References	246
6	Use of a cluster approach for the prediction of thermodynamic and transport properties	247
6.1	Introduction	247
6.2	Cluster approach to the prediction of thermodynamic and transport properties of ionic liquids	249
6.3	References	264
7	Conclusions	265
7.1	Future Work	268
	Appendices	269
A	A systematic study of DFT performance for geometry optimisations of ionic liquid clusters – Supporting Information	271
B	A DLPNO-CCSD(T) benchmarking study of intermolecular interactions of ionic liquids – Supporting Information	285
C	An intuitive approach to finding local minima in ionic materials: a balancing of starting geometry and dynamic evolution – Supporting Information	311
D	Cluster approach to the prediction of thermodynamic and transport properties of ionic liquids – Supporting Information	323

Copyright notice

© Zoe Luisa Seeger (2020).

I certify that I have made all reasonable efforts to secure copyright permissions for third-party content included in this thesis and have not knowingly added copyright content to my work without the owner's permission.

Abstract

Ionic liquids, a set of materials comprised entirely of ions, are considered designer liquids. This is due to the ease of substituting different ions, the ability to further functionalise these core constituents, and the myriad of ionic liquids possible from cation-anion combinations. Ionic liquids are tailored to exhibit properties such as electrochemical stability, thermal stability, high conductivity and low viscosity - and naturally have low flammability and volatility. For this reason, ionic liquids hold great promise in applications including catalysis, gas absorption, separation science, metal extraction, lubrication, drug design, organic synthesis and the booming field of energy storage. While the fields to which ionic liquids have been applied are widespread, the properties of these materials also vary considerably. In some sense this is advantageous as task-specific applications require a range of unique, finely-tuned properties. However, as yet a methodology to design task-specific ionic liquids does not exist.

A simplified explanation has not yet emerged that is able to ascertain physical properties of ionic liquids as a function of the constituent ions. Therefore, a complex model is needed to account for the nuanced interactions at play. The macroscopic properties of ionic liquids are a manifestation of the interaction energy of the system. The nature of the relationship between the macroscopic and microscopic remains elusive. It is the aim of this thesis to investigate, and facilitate the investigation, of this link with high level wavefunction-based methods in large scale clusters. Wavefunction-based methods and large clusters are two resource intensive endeavours, and as such have inhibited the study of ionic liquids at this level. The use of newly developed theories and new approaches to traditional theories can be exploited to facilitate these otherwise infeasible calculations.

The fragment molecular orbital (FMO) approach has been applied to second-order Møller Plesset perturbation theory (MP2) calculations of systems of up to 32 ion pairs (IPs). Two- and three-body effects were investigated to determine cutoffs that can be implemented such that two- and three-body calculations that contribute negligibly to the total energy can be avoided. It was found that 71% of two-body MP2 calculations are required in order to achieve an accuracy of 1 kJ mol⁻¹. In 32 IPs, up to 94% of the HF trimer calculations can be omitted without penalty. Two- and three-body cutoffs are suggested for each system size to reduce the cost of large scale calculations.

An extensive benchmarking of density functional theory (DFT) functionals and MP2-based methods has been performed on 2 and 4 IPs clusters of ionic liquids. The 2IP clusters were optimised with forty-three different approaches, where the wavefunction-based method/DFT functional, basis set, and the addition of dispersion correction was varied. Those with a promising performance in the 2IP structures were tested again with 4IP clusters. Some of the functionals with the best performance in the 2IP structures failed to accurately describe those of 4IPs. The functionals PBE-D3/cc-pVTZ, ω B97X-D/aug-cc-pVDZ and BLYP-D3/cc-pVTZ, and the MP2-based method FMO2-SRS-MP2/cc-pVTZ are recommended for the optimisation of larger clusters of ionic liquids.

Gold standard coupled cluster with single-, double-, and perturbative triple-excitations (CCSD(T)) scales formally as N^7 with chemical system size and thus the systems to which it can be applied are severely limited. The newly developed domain-based local pair natural orbital coupled-cluster method, DLPNO-CCSD(T), boasts CCSD(T) accuracy near the cost of a DFT calculation. The errors of DLPNO-CCSD(T) in the context of ionic liquids are presented for both protic and aprotic types. DLPNO-CCSD(T) with preset ‘TightPNO’ produces energies within chemical accuracy. Two further parameter sets have been devised to be used when spectroscopic accuracy is required.

A new methodology is presented in order to locate important minima contributing to bulk properties of condensed liquids. Four ion pair configurations are strategically created to span the potential energy surface of the materials before molecular dynamics is utilised to search the local region of each structure. Shorter molecular dynamics simulations are possible as no high energy barriers need to be traversed. Agglomerative clustering is then used to group similar

structures and thus find unique configurations. For the two ionic liquids tested geometries were located that had energies below those found by simulated annealing.

Macroscopic properties are a result of the subtle interplay of forces present at the atomic level. The nature of this relationship, however, remains elusive. Previous work in our group has shown that the ratio of total interaction energy to dispersion interaction energy correlates with melting point and dispersion interaction energy correlates with viscosity in single ion pairs. This research has been continued into 2IP structures to account for same-ion interactions. A full geometry screen was performed on twenty-four 2IP ionic liquids resulting in sixty-four unique, low energy geometries. Melting point trends were created with Boltzmann averages of the energies of the favourable structures. A generalised trend was established for the melting point that had not been present in the 1IP systems and its predictive power rivals that of molecular dynamics simulations.

Unravelling the structural motifs that influence the physicochemical properties of ionic liquids would truly unlock their potential.

Declaration

I hereby declare that this thesis contains no material which has been accepted for the award of any other degree or diploma at any university or equivalent institution and that, to the best of my knowledge and belief, this thesis contains no material previously published or written by another person, except where due reference is made in the text of the thesis.

This thesis includes two original papers published in peer reviewed journals, three submitted publications and one literature review publication. The core theme of the thesis is investigating methodologies to predict properties of ionic liquids using quantum calculations of large clusters. The ideas, development and writing up of all the papers in the thesis were the principal responsibility of myself, the student, working within the Faculty of Science graduate research programme under the supervision of Ekaterina I. Izgorodina.

The inclusion of co-authors reflects the fact that the work came from active collaboration between researchers and acknowledges input into team-based research.

I have not renumbered sections of submitted or published papers in order to generate a consistent presentation within the thesis.

Student name: Zoe Luisa Seeger

Student signature: 

Date: May, 2020

In the case of chapter 1, 2, 3, 4, 5, 6 my contribution to the work involved the following:

Thesis chapter	Publication title	Status	Student contribution	Co-author names and contribution	Monash student co-author
1	Quantum chemical methods for the prediction of energetic, physical, and spectroscopic properties of ionic liquids	Published	30% - Reviewed 150 papers, editing and images	1. Ekaterina I. Izgorodina - Manuscript, reviewing - 55%; 2. David L. A. Scarborough - reviewing - 10%; 3. Samuel Y. S. Tan - reviewing - 5%	1. N 2. N 3. N
2	Trends in Two- and Three-Body Effects in Multiscale Clusters of Ionic Liquids	Published	45% - Data collection, analysis, initial manuscript, images	1. Peter Halet - Analysis - 45%; 2. Santiago Barrera Acevedo - Data collection 2%; 3. Ekaterina I. Izgorodina - Manuscript, concept and supervision 8%	1. Y 2. N 3. N
3	A systematic study of DFT performance for geometry optimisations of large-scale clusters of ionic liquids	Submitted	85% - Data collection, analysis and manuscript	1. Ekaterina I. Izgorodina - Editing, concept and supervision 15%	1. N
4	A DLPNO-CCSD(T) benchmarking study for ionic liquids	Submitted	90% - Data collection, analysis and manuscript	1. Ekaterina I. Izgorodina - Editing and supervision - 10%	1. N
5	An intuitive approach to finding local minima in ionic liquids: a balancing of sampling and dynamic evolution	Submitted	90% - Data collection, analysis and manuscript	1. Ekaterina I. Izgorodina - Editing, concept and supervision - 10%	1. N
6	Cluster approach to the prediction of thermodynamic and transport properties of ionic liquids	Published	85% - Data collection, analysis and initial manuscript	1. Rika Kobayashi - Programme development - 2%; 2. Ekaterina I. Izgorodina - Manuscript, concept and supervision - 13%	1. N 2. N

Acknowledgements

It is with immense gratitude that I acknowledge the support and guidance of my supervisor, Katya Pas. It has been a pleasure to work with you and I have learnt so much because of you. I am indebted to my two life advisors, Nicole and Abhi. Also to those who I could always rely on and would drop everything to help me, Fi and Eunice. Those of the group who came before me and helped me learn the ropes and extended great kindness, Sam, Jason and Su. My office buddy whom I run ideas by everyday and can ask any question, Tom. The person I could go to who would unquestioningly put in time to give me scientific feedback, Peter. And those who have been integral in my constant learning and growing, putting up with my nonsense, and giving great feedback, Anh, Kaycee, Michael, Luke and Nathan.

Abbreviations

BF_4^-	tetrafluoroborate
C_1mim^+	1,3-dimethylimidazolium
C_1mpyr^+	N,N-dimethylpyrrolidinium
NTf_2^-	<i>bis</i> (trifluoromethylsulfonyl)amide
$\text{N}(\text{CN})_2^-$	dicyanamide
mes	mesylate
tos	tosylate
PF_6^-	hexafluorophosphate

AIMD	<i>ab initio</i> molecular dynamics
BSSE	basis set superposition error
CBS	complete basis set
CCSD(T)	coupled cluster with single, double and perturbative triple excitations
CP	counterpoise
DFT	density functional theory
DFT-D	dispersion corrected DFT functional
DFT-D3	DFT-D version 3
FMO	fragment molecular orbital
FMO2	two-body FMO
FMO3	three-body FMO
HBIL	hydrogen bonded ionic liquid dataset
HF	Hartree-Fock theory

IL	ionic liquid
IL174	aprotic ionic liquid single ion pair dataset
IP	ion pair
MAE	mean absolute error
MD	molecular dynamics
MP2	second-order Møller-Plesset perturbation theory
PES	potential energy surface
SRS-MP2	generalised spin ratio scaled MP2

Chapter 1

Introduction

The first chapter is intended to give the reader an overview of the target problems that this thesis explores and some of the proposed solutions that currently exist in the literature. Specifically, the chapter explains why ionic liquids have received attention from researchers for decades and why they are considered an environmentally friendly alternative in energy storage devices in 1.1. The chapter will then outline quantum chemical methods that have been used to progress the understanding of the fundamental causes of properties exhibited in ionic liquids. Section 1.3 is a literature review which thoroughly investigates quantum chemical methods and their part in unthreading the relationship between the fundamental forces of ionic liquids and their macroscopic representation as properties of materials. The chapter concludes with an overview of the thesis and details the remaining chapters and how they address predicting properties in large clusters of ionic liquids with quantum chemical methods – the aim of this research.

1.1 What are ionic liquids?

Ionic liquids have the capacity to revolutionise many fields of science provided that ionic liquids are fully understood. Ionic liquids (ILs) are organic salts composed of ions and are commonly defined to have a melting point below 100° C.¹ The lowering of melting temperatures in ionic liquids is achieved by 1) bulky anions and cations, 2) diffuse or shielded charges about the ions and 3) asymmetry in the geometries. These three characteristics have a compounding affect,

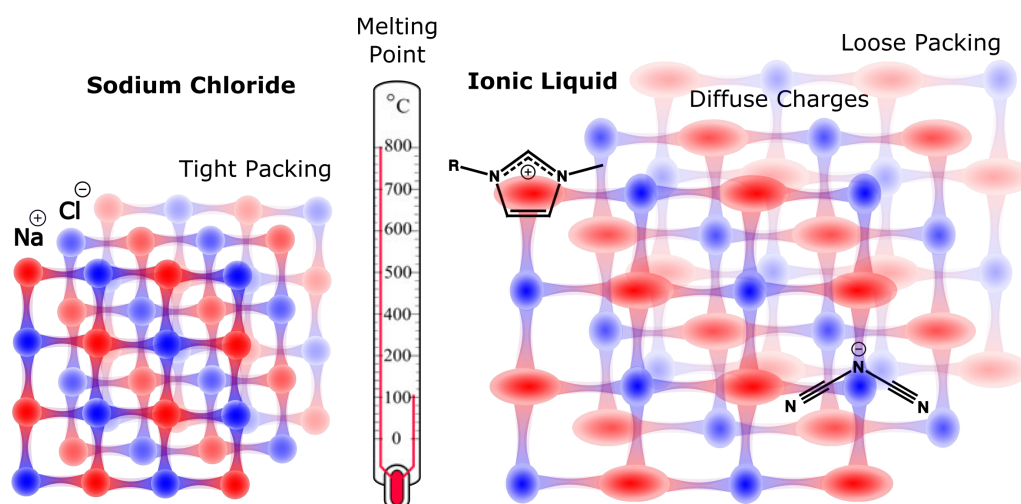


Figure 1.1: *Packing of an ionic liquid compared to a traditional salt.*

both decreasing the strength of interaction and increasing the distances in lattice packing, thus making crystallisation less favourable.^{2,3} This concept is demonstrated in Figure 1.1.

Ionic liquids have inherently appealing qualities: electrical conductivity, high thermal stability and negligible volatility. Furthermore, ion constituents can be readily interchanged and functionalised such that the material also exhibits a wide electrochemical window, lowered viscosity, the ability to solubilise a wide range of gases and solids, and low toxicity. Thus, ionic liquids have been studied in the context of electrolytes in batteries and solar cells,⁴⁻⁸ lubricants,^{9,10} gas absorption,^{11,12} drug design,¹³⁻¹⁵ and chemical synthesis.¹⁶ In the case of chemical synthesis, ionic liquids boast the ability to be highly recyclable, and as electrolytes, they would replace the current volatile organic electrolytes. As such, ionic liquids are considered ‘green’ as they enable the development of new technologies that are environmentally positive, especially in their application to energy storage issues.¹⁷

The mix and matching of ions is both promising and a hindrance in commercialising ionic liquids. There are estimated to be millions of trillions of candidate ionic liquids, and like in drug design, computational design is a promising avenue to refine structural motifs that give rise to optimum chemical properties.¹⁵ Intermolecular forces are manifested as macroscopic properties such as viscosity, melting point and conductivity, although it is not fully understood how the former governs the latter.¹⁸ This realisation means that in order to exploit ionic liquids a deeper understanding on the relationship between the intermolecular forces and physical properties is necessary. Both electrostatics and dispersion have been found to significantly

contribute to both the overall interaction energy and the unique properties of ionic liquids such as the cohesive energy and melting point.^{18–21} Additionally, charge-transfer,²² induction,²³ and exchange-repulsion play a lesser but significant role in shaping the resulting properties.²⁴ This intricate interplay of forces is difficult to grasp although progress has been made as outlined in the following review in section 1.3. Only a few studies have investigated the energy as a function of cluster size. The interaction energy per ion pair has been shown to increase in clusters from one to ten ion pairs due to many body effects.²⁵ Dispersion energy additionally increases rapidly per ion pair with increasing cluster sizes of at least up to eight ion pairs.²⁶ Thus, to accurately account for intermolecular forces larger clusters must be modelled.

1.2 Accurate quantum chemical methods

Traditionally, new materials have been designed and created by the laborious process of trial and error. In the age of technological advancements,^{27–29} the increasing availability of computational resources and subsequent development of efficient code^{30,31} has provided chemists with a secondary toolkit in probing ionic liquids – as a function of their electronic structure. Some notable quantum chemical methods are further detailed below.

First and foremost, couple cluster theory with singles, doubles and non-iterative triples, CCSD(T), is considered the gold standard in computational chemistry when it is extrapolated to the complete basis set (CBS).^{32,33} It scales as N^7 , compared to N^8 with iterative triples method CCSDT (where N is the number of basis functions) while still recovering the vast majority of correlation energy. Limiting computational cost is a common concern of theoretical chemists. Thus, CCSD(T) has been used extensively to benchmark cheaper methods in order to verify their use on ionic liquids and their interactions with materials, for example to understand interactions of ionic liquids with lignocellulose.^{34–37}

Perturbation theory is a decomposition scheme where the total energy is the sum of perturbation expansion of the energetic components and has CCSD(T) level accuracy.^{38–40} As the energy is built from the individual components – electrostatic, induction, exchange, charge-transfer, and dispersion terms – the theory can be used to correlate specific forces with certain behaviour. This powerful technique was used by London et al. to explain the attractive van der Waals forces in noble gases.⁴¹ The methodology has been improved to yield symmetry adapted

perturbation theory (SAPT).³⁸ SAPT has been used in the context of ionic liquids to identify the role of induction and dispersion in creating shallow minima in the potential energy surfaces of ionic liquids which goes some way in explaining their lowered melting points.⁴² A study by the Izgorodina group used SAPT on single ion pairs of ionic liquids and determined that all of the fundamental forces - electrostatic, exchange-repulsion, induction (also known as polarisability), and dispersion - contributed non-negligibly to the interaction energy and their interplay determined the interionic distances.⁴³

Calculations using a finite basis set are susceptible to basis set superposition error where electrons are artificially stabilised by the molecular orbitals of additional molecules of the system.⁴⁴ The extent of over-stabilisation can be determined *a posteriori* using the counterpoise approach by Boys and Bernardi,⁴⁵ where each molecule is recalculated in the presence of the basis functions of the system. To determine the counterpoise correction, $2N + 1$ calculations are required where N is the number of molecules. Determining the counterpoise correction is the bottleneck of large-scale wavefunction-based calculations. Counterpoise correction is required for obtaining accurate energies in calculations such as CCSD(T), density functional theory and Møller-Plesset perturbation theory.

Calculations using CCSD(T) and SAPT can be prohibitive due to their computational cost. New methods are often designed on the foundations of organic neutral systems which is partly due to the commonality of these systems and partly due to the straight-forward nature of their treatment.⁴⁶ Reliable methods for ionic species that correctly model weak dispersion forces, and are additionally affordable, are necessary in order to understand higher order properties and the structural moieties they are dependent on. Spin-ratio scaled second order Møller-Plesset perturbation theory (SRS-MP2) is a variant of the popular post-Hartree-Fock MP2 method for which the opposite spin and same spin correlation energies are scaled to reproduce CCSD(T)/CBS energies. The method has been recently designed to not only accurately model neutral species, but ionic liquid systems and radicals.^{46,47} Additionally, the method circumvents the need for counterpoise correction, making it more affordable than conventional MP2. It is basis set dependent and produces energies of $\pm 2 \text{ kJ mol}^{-1}$ when paired with the relatively small Dunning's cc-pVTZ basis set.

In order to extend the scope of quantum chemical methods into larger clusters – more than a few molecules – fragmentation methods are used to reduce the number of basis functions per calculation, and energies of these sub-calculations can be stitched back together reducing the cost dramatically. Additionally, the sub-calculations can be run in parallel. As well as reducing the cost, the calculations become accessible as common computers can be used to run the smaller sub-calculations in succession. One such fragmentation scheme is the fragment molecular orbital approach (FMO). FMO calculates each fragment in the Coulomb bath of the surrounding fragments which accounts for higher order induction effects. Two-body (for FMO2) and three-body effects are added (for FMO3) to the polarised monomers. In the case of ionic liquids FMO only considers the basis functions of three molecules at a time no matter the number of ion pairs considered. The monomer, dimer and trimer contributions for an FMO3 calculation are depicted in Figure 1.2 and the application to a two ion pair system is shown where each ion is a fragment and thus four monomer, six dimer and four trimer calculations are stitched together to recreate the total energy. The FMO approach has been tested in ionic liquid clusters of up to eight ion pairs, and with the inclusion of three-body effects obtains sub-kilojoule per mol accuracy.²⁶ The cost of calculating eight ion pairs decreased by 30% and the random access memory per central processing unit decreased by a factor of 14.5 when utilising FMO.

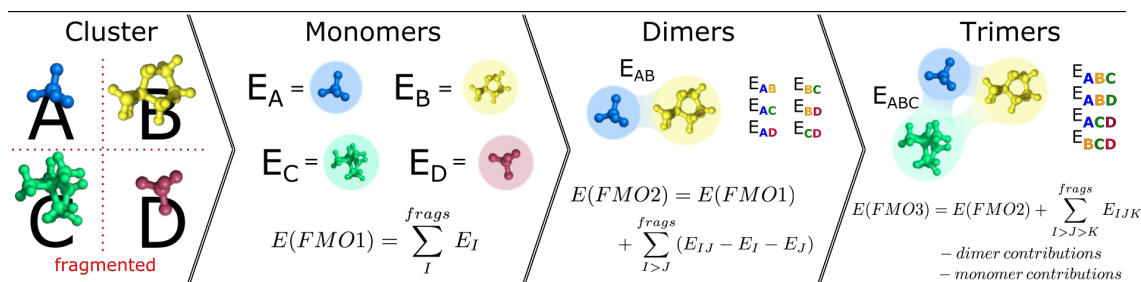


Figure 1.2: Illustration of the fragment molecular orbital approach (FMO): After fragmentation, monomer, dimer and trimer energies are calculated and stitched together.

Density functional theory is determined by the electron density distribution. It has garnered much use in chemical research as the simpler theory can be rendered much more quickly as the density is based on only the spatial coordinates of the atom centers. Density functional theory (DFT) truly is the best choice in terms of computational cost and can be extremely accurate. However functionals of this theory can act unpredictably in their ability to capture electron

correlation and exchange effects when arbitrary ionic liquids are considered.³⁷ Furthermore, functionals are known to produce large errors when determining intermolecular forces when dispersion is a large component.^{48,49} While it is not expected that DFT can be used to extract the energetics at a quality that allows for the understanding of the behaviour of ionic liquids, it is unknown how the inaccuracies of DFT functionals will affect optimisations of larger clusters of ionic liquids.^{50,51}

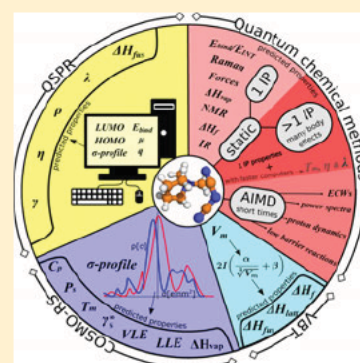
The following review provides an in-depth account of how wavefunction-based methods have contributed to predicting thermodynamic, physical and spectroscopic properties of ionic liquids. These techniques include quantum structure–property relationship (QSPR), a conductor-like screening model for realistic solvation (COSMO-RS), volume-based thermodynamics (VBT), small quantum chemical calculations and *ab initio* molecular dynamics (AIMD). AIMD while being very powerful, through which bond formation and breaking can be observed, remains very expensive and typical ionic liquid simulations run for 100's of picoseconds and contain less than 100 ion pairs. Ionic liquids are viscous materials and longer time scales are needed to allow for the movement of ions through the liquid, limiting the usefulness of the AIMD method.

Quantum Chemical Methods for the Prediction of Energetic, Physical, and Spectroscopic Properties of Ionic Liquids

Ekaterina I. Izgorodina,*[✉] Zoe L. Seeger, David L. A. Scarborough, and Samuel Y. S. Tan

Monash Computational Chemistry Group, School of Chemistry, Monash University, 17 Rainforest Walk, Clayton, Victoria 3800, Australia

ABSTRACT: The accurate prediction of physicochemical properties of condensed systems is a longstanding goal of theoretical (quantum) chemistry. Ionic liquids comprising entirely of ions provide a unique challenge in this respect due to the diverse chemical nature of available ions and the complex interplay of intermolecular interactions among them, thus resulting in the wide variability of physicochemical properties, such as thermodynamic, transport, and spectroscopic properties. It is well understood that intermolecular forces are directly linked to physicochemical properties of condensed systems, and therefore, an understanding of this relationship would greatly aid in the design and synthesis of functionalized materials with tailored properties for an application at hand. This review aims to give an overview of how electronic structure properties obtained from quantum chemical methods such as interaction/binding energy and its fundamental components, dipole moment, polarizability, and orbital energies, can help shed light on the energetic, physical, and spectroscopic properties of semi Coulomb systems such as ionic liquids. Particular emphasis is given to the prediction of their thermodynamic, transport, spectroscopic, and solubilizing properties.



CONTENTS

1. Introduction	6697	5.1. Melting points (T_m)	6714
1.1. Overview of terminology in quantum chemistry	6698	5.2. Heat of vaporization	6715
1.2. G3MP2	6698	5.3. Heat capacity	6715
1.3. CBS-QB3	6698	5.4. Transport properties	6715
1.4. MP2/CBS	6698	5.5. Activity coefficient at infinite dilution	6716
1.5. SCS-MP2	6699	5.6. Solubility	6717
1.6. SCS-IL-MP2	6699	5.7. Vapor-pressure equilibrium	6718
1.7. Counterpoise correction	6699	5.8. Noncontinuum models	6718
1.8. Fundamental forces	6699	6. Volume-Based Thermodynamics	6719
1.9. SAPT	6699	6.1. Comment on the prediction of volumes of ions	6720
1.10. EFP	6699	6.2. Lattice enthalpies	6720
1.11. Dispersion correction	6700	6.3. Melting points	6720
2. Intermolecular forces and their interplay in ionic liquids	6700	7. Quantum chemical calculations of single ion pairs	6721
2.1. Dispersion forces	6701	7.1. Melting points and transport properties	6721
2.2. Hydrogen bonding	6703	7.2. Heats of formation	6723
2.3. Many-body effects in ionic liquids	6704	7.3. Heats of vaporization	6724
3. Assessment and development of quantum chemical methods for ionic liquids	6706	7.4. Spectroscopic properties	6725
3.1. Comments on the accuracy of the GGA functionals for electronic structure properties	6707	8. Quantum chemical calculations of ionic clusters	6727
4. Quantitative structure–property relationship approach	6710	8.1. Thermodynamic data	6727
4.1. Density	6711	8.2. Spectroscopic properties	6729
4.2. Melting point and heat of fusion	6711	9. <i>Ab initio</i> molecular dynamics (AIMD)	6731
4.3. Transport properties	6712	9.1. Ion polarization	6732
5. COSMO-RS for thermodynamics of ionic liquids	6713	9.2. Dispersion correction	6734
		9.3. Proton dynamics	6734

Special Issue: Ionic Liquids

Received: August 9, 2016

Published: January 31, 2017

Chemical Reviews

Review

9.4. Thermodynamics data	6736
9.5. Power spectra	6736
9.6. NMR chemical shifts	6737
9.7. Electrochemical windows (ECWs)	6738
10. Summary and outlook	6738
Author Information	6739
Corresponding Author	6739
ORCID	6739
Notes	6739
Biographies	6739
Acknowledgments	6739
Abbreviations	6740
References	6740

1. INTRODUCTION

Ionic liquids are a fascinating class of low melting salts that consist entirely of ions¹ and form two large groups of aprotic and protic ionic liquids. The latter are defined as ionic liquids obtained by the proton transfer from a Brønsted acid to a Brønsted base.^{2,3} Figure 1 shows examples of aprotic and protic

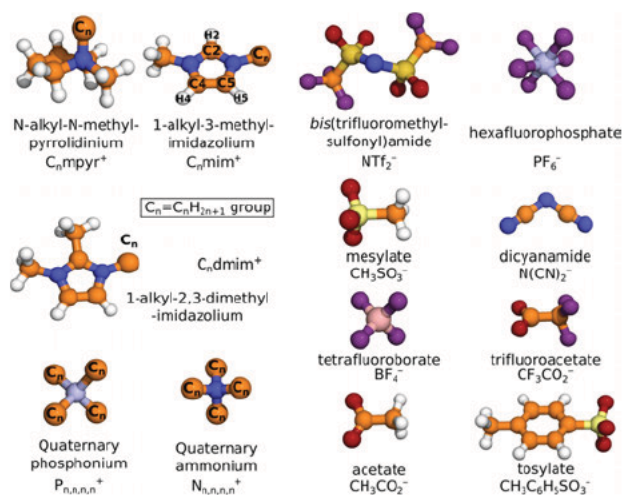


Figure 1. Chemical structures of typical cations and anions of aprotic and protic ionic liquids.

ionic liquids together with their abbreviations used in this review. Due to their unique nature (consisting entirely of ions), these materials have found their way into applications in almost every single branch of physical sciences,^{1,3} ranging from catalysis;^{4,5} separation science, such as liquid–liquid extraction^{6,7} and extraction of metals^{8,9} and hazardous waste;¹⁰ liquid mirror telescopes;¹¹ molecular gas capture, such as CO₂;^{12,13} active pharmaceutical ingredients;^{14,15} and alternative energy devices,^{16,17} such as metal ion batteries,¹⁸ fuel,¹⁹ and thermo electrochemical²⁰ and solar²¹ cells. ILs have become recognized by both the scientific community and the public as “green” solvents and electrolytes of the future, evidenced by the fact that ILs were selected as the most important British innovation of the 21st century by the Great British Innovation Vote.²² The number of ILs has been estimated in the trillions,²³ an impressive figure that allows for the unique tailoring of physical properties of ILs for their successful applications as both solvents and electrolytes. Not all ILs will find successful applications in electrochemical devices due to specific requirements that need to be satisfied, such as electrochemical and

thermal stability of electrolytes with high conductivity and preferably low viscosity.²⁴ To circumvent the latter, mixing ILs with traditional molecular solvents has proven far more beneficial in terms of their properties and, hence, their electrochemical applications.^{25,26}

An increase in the computational power and availability of computational resources has resulted in an increase of publications that use quantum chemical methods to offer theoretical underpinning to experimental data and prediction of physicochemical properties of ionic liquids. This review is designed to give an overview of how the electronic structure properties obtained from quantum chemical methods have contributed to the prediction of the energetic, physical, and spectroscopic properties of ionic liquids (see Figure 2). It has to

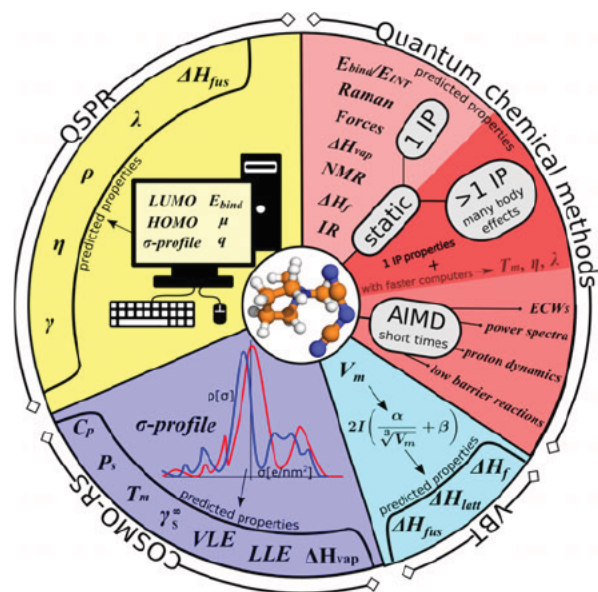


Figure 2. Overview of currently available computational approaches that apply electronic structure properties for the prediction of energetic, physical, and spectroscopic properties of ionic liquids.

be noted that classical molecular dynamics simulations of ionic liquids are not discussed here, as the topic fell outside the scope of this review. The Introduction contains a brief overview of quantum chemical terminology used in the field of ionic liquids. The first two sections of the review give a thorough insight into the energetic properties of ionic liquids, the current understanding of the complex interplay of intermolecular forces and many body effects that govern their properties, and a recent assessment and development of cost effective quantum chemical methods for studying multiscale clusters of ionic liquids. Four independent approaches—Quantum Structure–Property Relationship (QSPR), a Conductor like Screening Model for Realistic Solvation (COSMO RS), Volume Based Thermodynamics (VBT), and quantum chemical calculations of single ion pairs—have become rather popular due to their reduced cost. The review contains a section for each of these approaches with a description, the limitations, and the accuracy of each approach with the emphasis on the prediction of thermodynamic (melting point, lattice enthalpy, heat of vaporization, heat of formation, activity coefficients at infinite dilution, and liquid–liquid vapor–liquid equilibria) and transport (conductivity and viscosity) properties as well as spectroscopic

properties (nuclear magnetic resonance (NMR) chemical shifts, infrared (IR) and Raman spectra). It has to be noted that only studies that used electronic and molecular properties predicted from quantum chemical methods have been discussed in detail. The last two sections of the review present results from static multiscale calculations of ionic liquids and an exciting new direction in the field of ionic liquids, *ab initio* molecular dynamics (AIMD) simulations.

1.1. Overview of terminology in quantum chemistry

Schrödinger's equation is traditionally solved using either wave function based methods or density functional theory (DFT). The Hartree–Fock (HF) method represents the first building block for wave functions based correlated levels of *ab initio* theory. It accounts for the kinetic energy of nuclei and electrons and the potential energy of nuclei interacting with each other and electrons interacting with nuclei. The electron–electron interaction is approximated via the mean field, in which each electron interacts with the field of the other electrons in the system. Correlated levels of theory explicitly account for electron–electron interactions. The HF equation is solved iteratively using the self consistent field (SCF) method, in which the energy is minimized by changing molecular orbital coefficients.

In DFT, the energy of the system is written via the electron density, ρ , of the system:

$$E[\rho] = \hat{T}_s[\rho] + V_{ne}[\rho] + E_H[\rho] + E_{XC}[\rho] \quad (1)$$

where the first three terms refer to noninteracting electrons in the system. \hat{T}_s is the kinetic energy, V_{ne} is the potential energy of electrons interacting with nuclei, and E_H is the Hartree (or Coulomb) energy. The last term represents the exchange correlation potential, $v_{XC}[\rho] = \frac{\partial E_{XC}[\rho]}{\partial \rho}$, and it contains the rest of the unknown contributions. Due to the fact that the form of the exchange correlation potential is not formally known, the universal potential has not yet been designed. Kohn and Sham²⁷ revolutionized the DFT field by using the SCF method to obtain the solution of eq 1. This is the reason why DFT is often referred to as the Kohn–Sham (KS) formalism. DFT functionals are divided into groups based on their approximation of the exchange correlation potential. Perdew et al.²⁸ described the developments in DFT functionals as a ladder, with each rung representing a seminal development in the field. The first rung, based on the local spin density approximation, was not reliable for studying chemical systems.²⁷ The most notable rungs in terms of their accuracy for chemical systems are the second rung, based on the Generalized Gradient Approximation (GGA), the third rung, called meta GGA due to its inclusion of the kinetic energy gradient, and the fourth rung, called hybrid (also referred to as hyper GGA) due to its inclusion of exact HF exchange. The most widely used functionals in the field of ionic liquids include GGA based PBE,²⁹ BLYP^{30,31} and BP86,^{30,32} hybrid B3LYP³³ and PBE0,³⁴ and meta GGA M062X.³⁵

1.2. G3MP2

G3MP2 is a composite method based on the G3 theory designed by Curtiss et al.³⁶ to approximate the quality of CCSD(T) theory with a triple ζ quality basis set. The method uses MP2/6 31G(d)^{37–41} optimized geometry, and HF/6 31G(d) zero point vibrational energy followed by a series of single point energy calculations at the MP2⁴² and QCISD(T)⁴³ levels of theory in combination with Pople type basis sets. In

addition, spin–orbital correction for atoms and parametrized higher level corrections are added to the final energy.

1.3. CBS-QB3

CBS QB3 belongs to the family of methods based on a complete basis set (CBS) model chemistry approach introduced by Petersson et al.^{44–50} to introduce corrections for incomplete (i.e., truncated) basis sets that are usually used in quantum chemical methods to approximate the wave function. The approach is based on the asymptotic convergence of pair natural orbital expansions, thus allowing for extrapolation of a series of finite basis set calculations to an estimated CBS limit. The original CBS Q method utilized MP2 for geometry optimizations and frequency calculations, which was later replaced by a cheaper alternative, the B3LYP functional (see below).

Size consistent and size extensive methods of coupled cluster theory, proposed by Bartlett^{51,52} and Pople,⁴³ represent the state of the art methods in quantum chemistry. The “ultimate standard” of these methods is CCSDT(Q),⁵³ a coupled cluster (CC) method with iterative single (S), double (D), and triple (T) excitations and noniterative quadruple (Q) excitations. In order to produce high accuracy, CCSDT(Q) needs to be combined with a very large basis set,^{53,54} thus requiring a significant amount of computational resources and making its application for ionic liquid systems virtually impossible. The CCSD(T) method with noniterative triples coupled extrapolated to the complete basis set (CBS) limit, abbreviated as CCSD(T)/CBS, has been shown to achieve high accuracy and therefore has been considered the “gold standard” for studying the energetics of intermolecular complexes.^{53–55} The extrapolation^{56,57} is based on the asymptotic convergence of correlation consistent (cc) polarized (p) basis sets introduced by Dunning and co workers.^{58,59} The most widely used types are cc pVXZ and aug cc pVXZ, where X = D (double ζ basis set), T (triple ζ basis set), Q (quadruple ζ basis set), etc. and aug includes additional diffuse functions important for anionic species. The electronic energy of CCSD(T)/CBS is calculated as follows:

$$\begin{aligned} E(\text{CCSD(T)/CBS}) \\ = E(\text{MP2/CBS}) + [E(\text{CCSD(T)/DZ}) - E(\text{MP2/DZ})] \end{aligned} \quad (2)$$

where DZ is either cc pVDZ for the extrapolation of cc pVXZ basis sets or aug cc pVDZ for the extrapolation of aug cc pVXZ basis sets.

1.4. MP2/CBS

MP2/CBS uses the Dunning's basis set asymptotic convergence to extrapolate the MP2 correlation energy to a complete basis set limit. Due to limitations of current computational resources, extrapolation of (aug)cc pVTZ and (aug)cc pVQZ to a (aug)cc pVSZ limit is widely performed. It has been shown that for ionic liquids extrapolation of the original cc pVXZ works as accurately as the aug cc pVXZ basis set series.⁶⁰ MP2/CBS is calculated by means of Helgaker's approach:⁶¹

$$\text{MP2/CBS} = \frac{X^3 E_X^{\text{MP2}} - Y^3 E_Y^{\text{MP2}}}{X^3 - Y^3} \quad (3)$$

where X and Y are cardinal numbers of Dunning's basis sets, i.e. X = 3 for (aug)cc pVTZ and Y = 4 for (aug)cc pVQZ.

Chemical Reviews

Review

1.5. SCS-MP2

SCS MP2 is a modification of the second order Møller–Plesset perturbation theory,⁴² the lowest level of correlated methods of *ab initio* theory. The method was proposed by Grimme⁶² and was designed to scale the same spin (SS) and opposite spin (OS) components of the MP2 correlation energy as shown in eq 4 to reproduce reaction energies, reaction barriers, atomization energies, and heats of formation.^{63–65}

$$E_{\text{corr}}^{\text{MP2}} = c_{\text{OS}}E_{\text{OS}} + c_{\text{SS}}E_{\text{SS}} \quad (4)$$

1.6. SCS-IL-MP2

SCS IL MP2 is the recent modification of the SCS MP2 method proposed by the Izgorodina group to circumvent the inclusion of time consuming counterpoise correction.⁶⁰ The c_{OS} and c_{SS} coefficients in eq 4 were determined by scaling noncounterpoise corrected interaction energies of ionic liquid ion pairs calculated at the MP2 level of theory to reproduce the CCSD(T)/CBS correlation interaction energy. It has to be noted that due to a fundamentally different behavior of the HF method with respect to increasing basis set, only correlation interaction energies were considered in the fitting procedure. The best performing basis set was found to be cc pVTZ with $c_{\text{OS}} = 1.05$ and $c_{\text{SS}} = 0.68$.

1.7. Counterpoise correction

Counterpoise correction was introduced by Boys and Bernardi⁶⁶ to account for basis set superposition error (BSSE), a phenomenon inherent to *any* intermolecular complex calculation. BSSE represents a consequence of using a finite basis set in quantum chemical methods, and its effect vanishes in a complete basis set. BSSE manifests itself through artificial lowering of the energy of the system as a result of indistinguishable electrons occupying orbitals of interacting species to which they originally do not belong. Although the counterpoise correction behaves differently for HF, DFT functionals, and correlated levels of theory, such as MP2 and CCSD(T), it needs to be considered for any ionic liquid complex/cluster with any level of theory. By definition, the correction is small for the HF and DFT methods and increases with increasing complexity of recovering electron correlation in correlated levels of theory. The correction also increases drastically with increasing number of interacting species in the system.

1.8. Fundamental forces

Fundamental forces are represented by the following five types: electrostatics, exchange repulsion, induction, dispersion, and charge transfer.⁶⁷ Out of the five forces, exchange repulsion is the only interaction that cannot be explained in a classical way, as it is based purely on quantum chemical formulation and can be only loosely thought of as repulsion of electron densities of interacting molecules. The dispersion and charge transfer forces represent the most difficult terms to quantify. Dispersion describes interaction of instantaneous dipole moments on the electron density surface of interacting molecules generated by fluctuations in the density and, therefore, can be accurately accounted for at a correlated level of theory. Charge transfer is dependent on the way this force is defined, and therefore, direct comparison among energy decomposition schemes needs to be performed with caution.

1.9. SAPT

Symmetry Adapted Perturbation Theory (SAPT) and Effective Fragment Potential (EFP) belong to the family of energy decomposition schemes. SAPT^{68–70} is considered a state of the art method that decomposes interaction energy into five fundamental components—electrostatic, exchange repulsion, induction, dispersion, and charge transfer—based on the expansion of perturbation theory. In order to ensure that the wave function obeys the Pauli principle and is an eigenfunction of the unperturbed sum of the Hamiltonians of constituent monomers, $\hat{H}_A + \hat{H}_B$, the symmetry adapted perturbation procedure is applied. The SAPT approach partitions the Hamiltonian in the following way:

$$\hat{H} = \hat{F}_A + \hat{F}_B + \hat{W}_A + \hat{W}_B + V \quad (5)$$

where \hat{F}_A and \hat{F}_B are the Fock operators for monomers A and B, respectively. Similarly, \hat{W}_A and \hat{W}_B are the differences between the exact Coulomb operator and the Fock operator for each monomer, whereas V contains all the intermolecular terms. SAPT perturbs all of \hat{W}_A , \hat{W}_B , and V through varying orders to calculate the individual energy terms that are grouped together to produce five fundamental forces as follows:

$$E_{\text{electrostatic}} = E_{\text{Ind, Repl}}^{(0)} + E_{\text{Ind, Repl}}^{(1)} + E_{\text{Ind, Repl}}^{(2)} \quad (6)$$

$$E_{\text{exchange}} = E_{\text{Exch}}^{(1)} + E_{\text{Exch}}^{(2)} + E_{\text{Exch}}^{(3)} \quad (7)$$

$$E_{\text{induction}} = E_{\text{Ind, Repl}}^{(2)} + E_{\text{Ind, Repl}}^{(3)} + E_{\text{Ind, Repl}}^{(4)} + E_{\text{Exch-Ind, Repl}}^{(2)} + E_{\text{Exch-Ind, Repl}}^{(3)} + E_{\text{Exch-Ind, Repl}}^{(4)} + E_{\text{Exch-Ind, Repl}}^{(5)} + E_{\text{Exch-Ind, Repl}}^{(6)} \quad (8)$$

$$E_{\text{dispersion}} = E_{\text{Disp}}^{(2)} + E_{\text{Disp}}^{(3)} + E_{\text{Disp}}^{(4)} + E_{\text{Disp}}^{(5)} + E_{\text{Exch-Disp}}^{(2)} + E_{\text{Exch-Disp}}^{(3)} + E_{\text{Exch-Disp}}^{(4)} + E_{\text{Exch-Disp}}^{(5)} + E_{\text{Exch-Disp}}^{(6)} \quad (9)$$

$$E_{\text{charge-transfer}} = E_{\text{ind}}(\text{dimer basis}) - (\text{monomer basis}) \quad (10)$$

The powers in the form of (xy) denote the perturbations of the intermolecular potential, V (the power x), and the intramolecular contributions (the power y). Among all possible combinations, SAPT2 + 3 represents the highest level of truncation of SAPT theory implemented to date, as shown in eq 6–10.⁷¹ The “2” stands for the second order truncation for intermolecular contributions, whereas “3” represents third order intramolecular corrections within each ion, thus allowing for inclusion of electron correlation effects within each ion as well as between ions. Two other truncations, SAPT2 and SAPT2+, have been widely used in the literature. SAPT2 computes the terms in black and blue in eq 6–10, apart from intramolecular corrections for dispersion, $E_{\text{Disp}}^{(2)}$ and $E_{\text{Disp}}^{(2)}$, whereas SAPT2+ contains all terms in black and blue boxes. It has to be noted that in the SAPT formulation the charge transfer energy forms part of the induction term and vanishes in a complete basis set limit. It has been shown that, for ionic liquid ion pairs, SAPT2 + 3 in combination with aug cc pVDZ produces good agreement with CCSD(T)/CBS.⁷²

1.10. EFP

The EFP method is a fragmentation method developed by Gordon et al.^{73–75} originally to explicitly consider intermolecular interactions in solute–solvent systems, with solvent molecules used in calculations. It is a fragmentation approach, and the fragments are treated at the HF level of theory, with potentials being generated for each fragment. The method differentiates itself from other fragmentation methods based on how the intermolecular forces between fragments are derived when the fragments are allowed to interact via their potentials. The electrostatic contribution is treated using Stone's

distributed multipolar analysis truncated at the octopole term, and decays as R^{-1} , where R denotes distance.⁶⁷ To account for charge penetration, this contribution is damped with an exponentially decaying screening potential.⁷⁶ Exchange repulsion is calculated using a static localized molecular orbital basis.⁷⁷ Polarization is treated with dipole polarizability tensors centered on localized orbitals, and damped with a Gaussian type function.^{78,79} Dispersion is treated using a potential similar to the Lennard Jones potential:

$$E_{\text{Disp}} = \frac{C_6}{R^6} + \frac{C_8}{R^8} \quad (11)$$

The C_6 and C_8 coefficients were derived by fitting against SAPT dispersion, with C_8 being approximately a third of C_6 .⁸⁰ For charge transfer, a second order perturbation at the HF level of theory is used, with quasi atomic minimal basis set orbitals.^{78,81} It has to be noted that charge transfer is distinct from polarization in the EFP formulation, as opposed to it being a part of induction in SAPT.

1.11. Dispersion correction

A detailed overview on the history of the dispersion corrections can be found in the reviews of Klimeš and Michaelides,⁸² Doubson and Gould,⁸³ and Grimme et al.⁸⁴

GGA based DFT functionals are known to have short comings in the description of dispersion forces. To circumvent this problem, it has been suggested to add an empirical correction based on London dispersion forces⁸⁵ to the KS energy, thus referring to original functionals as dispersion corrected functionals (DFT D):

$$E_{\text{DFT-D}} = E_{\text{DFT}} + E_{\text{Disp}} \quad (12)$$

The dispersion correction has a general form as follows:

$$E_{\text{Disp}} = - \left(\frac{C_6(A, B)}{R_{AB}^6} + \frac{C_8(A, B)}{R_{AB}^8} + \frac{C_{10}(A, B)}{R_{AB}^{10}} \right) \quad (13)$$

where $C_n(A, B)$ are pairwise coefficients and R_{AB} is the interatomic distance between atoms A and B . The C_6 set of coefficients is the largest contributor to the dispersion energy. Among the suggested corrections, the second (D2)⁸⁶ and third (D3)⁸⁷ generation corrections by Grimme have become most widely used in the field of ionic liquids due to their simplicity and low computational cost. In accord with the London theory, the D2 correction accounts only for pairwise dispersion interactions as follows:

$$E_{\text{Disp}} = -s_6 \sum_{i=1}^{N-1} \sum_{j=i+1}^N \frac{C_6(i, j)}{R_{ij}^6} f_{\text{damp}}(R_{ij}) \quad (14)$$

where N is the number of atoms, s_6 is the global scaling coefficient for each DFT functional, C_6 coefficients are fitted for each atom–atom pair combinations as $\sqrt{C_6^i C_6^j}$, and f_{damp} is the damping function that corrects a steep behavior of the R^{-6} function at short interatomic distances to represent a chemical system.

Recently there has been development in incorporating many body dispersion interactions through the microscopic description of the frequency dependent polarizability of finite gap molecules and solids^{88,89} by means of the self consistent screening equation of classical electrodynamics.^{90,91} The third generation correction, D3, by Grimme includes three body effects of dispersion interactions, with the two body correction

also considering contributions from C_8 and C_{10} pairwise coefficients (for more detail see ref 87). Three body effects and higher order contributions in the two body effects have been shown to lead to significant improvements for the description of noncovalent bonding in neutral complexes.⁹²

It has to be noted that inclusion of the exact HF exchange, as demonstrated in hybrid meta GGA functionals such as M062X, already leads to good description of medium range electron correlation. Therefore, it is recommended not to combine hybrid meta GGA functionals with a large contribution from exact exchange with an explicit dispersion correction, as dispersion effects are more likely to be counted twice and therefore produce worse results for energetics. GGA functionals have been shown to work best with explicit dispersion corrections. For example, it has been established that M062X even slightly outperforms DFT D functionals for energetics of ionic liquid ion pairs, with DFT being a GGA functional, such as PBE or BLYP.^{93,94}

2. INTERMOLECULAR FORCES AND THEIR INTERPLAY IN IONIC LIQUIDS

Interaction energy, E_{INT} , is conceptually different from binding energy, E_{BIND} , as the former assesses the interaction strength based on geometries that ions adopt in an intermolecular complex, whereas the latter takes ions in their lowest energy geometry. Therefore, interaction energy does not include zero point vibrational energy (ZPVE) that accounts for the first vibrational level of the complex and individual ions, and deformation energy, E_{def} , that is usually positive and shows the amount of energy required for ions to undergo a structural change to adopt a new geometry in the intermolecular complex:

$$E_{\text{BIND}} = E_{\text{INT}} + \text{ZPVE} + E_{\text{def}} \quad (15)$$

ZPVE is not expected to contribute an appreciable amount to binding energy, as ions interact noncovalently, thus not affecting their first vibrational level. Some additional vibrations corresponding to interionic interactions appear in the far IR region and, hence, represent a negligible amount of energy. In many papers, binding energy is also referred to as dissociation energy when taken with a positive sign, as dissociation describes the reverse process of binding. In reality, ionic liquids are usually synthesized by a metathesis reaction in which an exchange of ions is observed. Therefore, interaction energy is a more realistic description of the interaction magnitude in ionic liquid systems, as ions do not exist on their own but instead are accompanied by counterions.

The magnitude of interaction between ions in ion pairs decreases with increasing charge delocalization on the anion and increasing shielding of the charge of the cation.^{95–100} The nature of interionic interactions in ionic liquids *from the energetic point of view* was slightly overlooked in the beginning due to the fact that ionic liquids comprised entirely of ions, and therefore, the main contribution to interaction was undoubtedly assigned to electrostatic (i.e., Coulomb) forces. In the past decade a great body of work has been performed by multiple groups, especially those of Hunt, Izgorodina, Kirchner, and Tsuzuki (for more detail, see below), to identify the extent of contribution from other fundamental forces to energetics of ionic liquids. A particular emphasis was given to quantifying London (i.e., dispersion) forces and hydrogen bonding.

2.1. Dispersion forces

In the early work of Tsuzuki et al.⁹⁶, ion pairs of varying ionic liquids were optimized at the HF/6 311G**^{101,102} level of theory, including [C₂mim][NTf₂], [C₂mim][BF₄], [C₂mim][PF₆], [C₂mim][CF₃CO₂], and [C₂mim][CF₃SO₃] as well as NTf₂⁻ based ILs coupled with C₂py⁺, N_{2,1,1,1}⁺, and C₂mpyr⁺ cations. A few configurations for each cation–anion combination were found, and their interaction energies were calculated using the HF and MP2 methods with a range of small to large basis sets and accounting for basis set superposition error through counterpoise correction by Boys and Bernardi.⁶⁶ For the optimized ion pairs of [C₂mim][BF₄], CCSD(T)/cc pVTZ showed similar interaction energies to those of MP2/6 311G*, and the latter was used to estimate the interaction energies of the rest of the ion pairs. The difference between the interaction energies of [C₂mim][BF₄] calculated at the MP2/cc pVQZ and HF/cc pVQZ levels was found to be 20 kJ mol⁻¹ on average, indicating the importance of electron correlation effects that are usually manifested as dispersion forces. The MP2/6 311G* interaction energies varied from -327.2 kJ mol⁻¹ for [C₂mim][BF₄] to -382.2 kJ mol⁻¹ for [C₂mim][CF₃CO₂]. For each cation–anion combination, at least four energetically favorable structures were identified, highlighting the importance of electrostatic forces and, hence, their nondirectional nature. The electrostatic energy was approximated as interaction of distributed multipoles of ions,⁶⁷ whereas the induction energy was calculated through interactions of polarizable sites on ions with the electronic field produced by multipoles of ions.¹⁰³ Although the electrostatic component was the leading contribution by far (>90%), the induction component was also shown to have a non negligible contribution, of up to 14%, to interaction energy (up to 45 kJ mol⁻¹). This work by Tsuzuki et al. was the very first indication that induction forces were important in ionic liquids. A similar conclusion of the main contribution of electrostatic forces to the stability of [C₂mim]Cl and [C₂mim]Br ion pairs was drawn in the study of Wang et al.¹⁰⁴ The B3LYP^{31,33}/6 31++G**^{37–41} level of theory was used to optimize multiple in plane configurations, in which the halide interacted with either the C2–H bond or hydrogens of the C=C backbone in the imidazolium ring. The magnitude of electrostatic interactions was estimated to fall >80% based on CHELPG derived atomic charges.¹⁰⁵ Later the Tsuzuki group work^{106,107} was extended to incorporate protic ionic liquids (PILs) based on the protonated ammonium cation, such as N_{2,2,1}H⁺ and N_{3,1,1}H⁺, and routinely used anions such as Cl⁻, BF₄⁻, CF₃SO₃⁻, and NTf₂⁻. For ion pairs of PILs, two different configurations were identified: (i) the anion interacts with alkyl groups, and (ii) the anion interaction directly with the N–H bond. Interaction energies for these ion pairs were compared to those with an aprotic ammonium cation, N_{2,1,1,1}⁺. The direct hydrogen bonding interaction was found to be stronger by 67 kJ mol⁻¹ on average, with the chloride showing the largest differences of up to 100 kJ mol⁻¹. The decomposition of interaction energy into electrostatic and induction components revealed a similar conclusion; that induction was even more important for protic ionic liquids contributing up to 21% of the interaction energy. It has to be noted that geometry optimizations performed at the HF level of theory in gas phase tend to produce shorter interionic distances due to gas phase not favoring charged species and the HF method not accounting for the dispersion component of interionic interactions. For example, in the [N_{2,2,1}H][NTf₂] and [N_{2,2,1}H][BF₄] ion pairs, the distances between the hydrogen

atom and the nitrogen on NTf₂⁻ and the fluorine on BF₄⁻ were as short as 1.670 and 1.709 Å. Shorter distances undoubtedly contribute to stronger interaction energies and are less likely to be observed in the bulk of PILs, as evidenced by the presented molecular dynamics simulations of [N_{2,2,1}H][NTf₂], placing the H...N distance >2 Å. It is expected that induction interaction decays faster than electrostatics, and therefore, the difference in ion pair interaction energies of protic and aprotic ionic liquids is predicted to reduce.

Tsuzuki et al.^{97,108} also investigated the effect of the alkyl chain conformation on the electrostatic and induction components in [C₄mim]X ionic liquids (X = Cl, Br, and I). Ion pairs with three different conformations of the butyl group, with respect to the central C–C bond, *trans–trans* (TT), *gauche–trans* (GT), and *gauche’ trans* (G’T), and varying positions of the halide anion around the cation, were optimized and analyzed using the methodology described above. The comparison of ion pair configurations with the same position of the anion showed a small difference in interaction energies, below 5.4 kJ mol⁻¹ across the anion series and conformational changes in the butyl group, thus supporting the evidence of crystal structures of [C₄mim]X^{109,110} of two conformers, TT and GT, coexisting in both chloride and bromide salts. The strength of the interionic interaction changed significantly depending on the position of the anion around the imidazolium ring, predominantly due to the change in the electrostatic component up to 57 kJ mol⁻¹, whereas the induction component changed only slightly. For example, in the case of the two lowest energy ion pair configurations (in which the anion is situated either in the C2–H plane or above it), induction reduces from 69 kJ mol⁻¹ for chloride to 63 kJ mol⁻¹ for bromide and to 55 kJ mol⁻¹ for iodide. The induction component was still larger compared to bulkier ionic liquid anions studied previously.⁹⁶ Potential energy surfaces were also constructed for the two lowest energy conformations of [C₁mim]X with respect to the distance between the halide ion (X = Cl and I) and the midpoint between two nitrogens atoms on the imidazolium ring of the C₁mim⁺ cation. The main differences are observed in the proximity of equilibrium structures, with energies becoming indistinguishable for both conformations, >3.6 Å for the chloride and >4.8 Å for the iodide, due to the electrostatic component decaying much more slowly compared to induction and hence becoming the domineering force at longer interionic distances.

Furthermore, undoubted evidence of the importance of induction and dispersion was then shown by the Kirchner group.^{111,112} Potential energy surfaces with respect to the cation...anion distance in the lowest energy ion pair configurations of [C₁mim]Cl, [C₁py]Cl, and [N_{2,1,1,1}]Cl were contrasted to that of NaCl as calculated by means of Symmetry Adapted Perturbation Theory (SAPT).⁶⁸ The inclusion of induction and dispersion forces in the description of interaction energy resulted in shallow energy profiles for ionic liquids, whereas almost no change was observed on the potential energy surface of NaCl, that exhibited a deeper and more distinct well. This work clearly identified that the equilibrium distance in ionic liquid ion pairs did not depend entirely on the electrostatic interactions. Hunt et al.¹¹³ used B3LYP/6 31++G(d,p)^{37–41} and the Natural Bond Order (NBO) analysis^{114–116} to study molecular orbitals of ion pair optimized geometries of [C₄mim]Cl, with the chloride occupying various positions around the ring. For the configurations of the chloride interaction with the C2–H bond, either in the plane of the

C2–H bond or above the ring, a significant orbital overlap between the p_π orbital on the chloride and the π orbital on the imidazolium ring was seen, which was also reflected in the net charge transfer of 0.16 e on average from the anion to the cation. This was the first publication that highlighted the contribution from the covalent type bonding into the interionic interactions, thus requiring higher correlated levels of theory to accurately predict their magnitude. Inclusion of more ion pairs into the ionic liquid cluster led to a further increase in contribution from dispersion forces (up to 30%), as was demonstrated by comparing the SCS MP2 and HF interaction energies of a two ion pair cluster of $[C_1\text{mim}]\text{Cl}$,¹¹¹ thus further highlighting the importance of correlated levels of theory for geometry optimizations of ionic liquids.

A thorough analysis of interaction energies and their fundamental components, calculated by means of SAPT2,⁶⁸ was conducted by the Izgorodina group.^{98,117} In their work, a large number of ionic liquid ion pairs (IPs) were optimized at the B3LYP/6-31+G(d) and MP2/6-31+G(d,p) levels of theory for pyrrolidinium and imidazolium based ionic liquids, respectively. $C_n\text{mpyr}^+$ and $C_n\text{mim}^+$ cations with varying alkyl chains ($n = 1-4$) were combined with 8 types of routinely used anions, such as Cl^- , Br^- , BF_4^- , PF_6^- , CH_3SO_3^- (mesylate), $\text{CH}_3\text{C}_6\text{H}_5\text{SO}_3^-$ (tosylate), $\text{N}(\text{CN})_2^-$ (dca), and NTf_2^- . For each cation–anion combination, 3 and 5 configurations were optimized for $C_n\text{mim}$ based and $C_n\text{mpyr}$ based IPs, respectively, making approximately 190 structures altogether. This work indicated that all four fundamental forces—electrostatic, exchange repulsion, induction, and dispersion—contributed to the interaction energy, and hence, the interplay of these forces governed the interionic distance in ion pairs. For example, dispersion forces were shown to contribute between 8 and 15% (which is equivalent to 28 to 59 kJ mol^{-1}) to the interaction energy, with imidazolium based ionic liquids generally producing stronger dispersion than pyrrolidinium based ones. Induction forces consistently contributed in the range of 6–12%, with chlorides and bromides generating the largest effect. For neutral intermolecular complexes, the concept of the direct linear correlation between intermolecular distances and corresponding interaction has been used to assess the strength of intermolecular interactions based solely on intermolecular distances, with shorter distances giving stronger interactions. In the case of ionic liquids, interplay among four intermolecular forces breaks this concept. For example, in the equilibrium geometry, the BF_4^- anion tends to be located further away (by 0.3 Å) from the cation—be it imidazolium or pyrrolidinium—compared to the NTf_2^- anion, yet the interaction energy for BF_4^- based IPs is >40 kJ mol^{-1} stronger compared to that of NTf_2^- . Spherical anions, such as chloride, bromide, and tetrafluoroborate, showed linear trends between the interaction energy and the distance between charge centers on ions in the homologous series of cations. This observation was attributed to strong contributions from electrostatic and induction forces in these anions. The interplay of all four fundamental forces indicates that the level of theory is important when optimizing ionic liquid IPs and larger clusters. State of the art results based on SAPT2 calculations clearly showcased that, in $[C_n\text{mim}]\text{Cl}$ and $[C_n\text{mim}]\text{Br}$ ion pairs (with $n = 1-4$), the halide preferred to interact above the imidazolium plane by 10 kJ mol^{-1} , on average, compared to in plane configurations.⁹⁸ A different observation¹¹⁸ was made based on B3LYP and MP2 results when combined with relatively small double ζ quality basis sets, such as 6-31++G(d,p) and cc-pVDZ, favoring the in plane

interaction of the chloride and the C2–H bond of the imidazolium ring by a few kJ mol^{-1} in $[C_4\text{mim}]\text{Cl}$ IPs. The varying alkyl chain on the imidazolium cation, while combined with the same anion, do not seem to change the order of IP stability. In the case of $[C_n\text{mim}][\text{NTf}_2]$ (with $n = 4, 6$, and 8), Logotheti et al.¹¹⁹ showed that 6 different configurations, whose binding energies were calculated with B3LYP/6-311+G*,^{101,102} followed the same trend in their stability with increasing alkyl chain.

Using far IR, Ludwig et al.¹²⁰ identified peaks at 70 and 130 cm^{-1} at 303 K that were assigned to the bending and the stretching vibrations of the hydrogen bonded ion pair in $[(\text{C}_6\text{H}_{13})_3\text{NH}][\text{CF}_3\text{SO}_3]$. While increasing temperature to 353 K, the two peaks disappeared, leaving behind one broad band centered at 100 cm^{-1} , which was attributed to the dispersion driven cation–anion interaction in which the anion interacted with hexyl groups. The Van't Hoff equation was used to establish the amount of energy required to undergo transition from the hydrogen bonded interaction to the dispersion driven one, which was found to be 34 kJ mol^{-1} . The difference in binding energies for ion pairs that corresponded to these types of interactions was calculated with and without the D3 explicit dispersion correction. Without the dispersion correction, this difference was large (almost 60 kJ mol^{-1}) but reduced close to the experimental value with the dispersion correction. The same trend persisted in larger clusters of 2 to 4 IPs, identifying the need to accurately account for dispersion forces for qualitative and quantitative results.

For larger ionic clusters consisting of 2 IPs, the chemical structure of the anion seemed to significantly affect the lowest energy configuration.¹²¹ The B3LYP D3/aug-cc-pVTZ level of theory was used to perform geometry optimizations of 2 IP clusters and calculate their binding energies. In the case of $[C_1\text{mim}]\text{Cl}$, the imidazolium rings preferred to stack and form the $\pi^+-\pi^+$ interactions,^{122,123} with the alternate charge configurations having slightly higher relative electronic energy (>3 kJ mol^{-1}). (Figure 1) For bulkier and more diffuse anions, such as nitrate, methylsulfate, trifluoromethylsulfonate, and tetrafluoroborate,¹²⁴ the alternate charge arrangement started to dominate the conformational space by at least 6 kJ mol^{-1} . This finding was attributed to the presence of a strong hydrogen bonding between the C2–H bond on the imidazolium ring and the anions studied, aided by the π delocalization of the anion (with the exception of the BF_4^- anion), thus providing the additional interplanar orbital overlap in high orbital energies. All cation–anion combinations studied generated a rather large number of accessible configurations within 10 kJ mol^{-1} , which fell within the systematic error of the B3LYP D3 functional,⁹⁴ further emphasizing the nondirectional nature of dominating interactions such as electrostatics and dispersion. For archetypical ionic liquids, such as $[\text{N}(\text{CH}_3)_4][\text{BF}_4]$ and $[C_n\text{mim}][\text{BF}_4]$ (with $n = 1, 3$, and 4), increase in cluster size, to include from 1 to 8 ion pairs, was shown to lead to a further increase in the dispersion component of up to 20%, that was estimated as the difference between the MP2 and HF interaction energies.¹²⁵ For ionic liquids, with the chloride, bromide, and dicyanamide anions and either the imidazolium or pyrrolidinium cation, dispersion forces were shown to contribute between 11 and 26% in clusters consisting of just 4 ion pairs.¹²⁶ The relative contributions correspond to the range of -68 to -81 kJ mol^{-1} per ion pair: an almost double increase compared to the range of -28 to -59 kJ mol^{-1} , as calculated for single pairs.⁹⁸ This further highlights the increase in

contribution from dispersion forces to an individual ion pair with increasing cluster size of ionic liquids. These *first principles* large scale calculations of ionic liquids showed for the first time the extent of significance of dispersion forces in the bulk of ionic liquids and require the development of quantum chemical methods that can accurately describe these dispersion forces.

Very little has been done in the area of the development of cost effective methods that allow for the decomposition of interaction energy in ionic liquids. SAPT is a state of the art approach that is very expensive and can only be applied to two molecule complexes at this stage. There is an implementation of three body effects for induction and dispersion forces within SAPT(DFT).¹²⁷ The latter utilizes the Kohn–Sham formula to calculate the energetic components⁶⁹ and therefore carries the same shortcomings as DFT functionals, especially for the prediction of dispersion forces. Recently Tan and Izgorodina⁷² have undertaken a study of the performance of the effective fragment potential method (EFP) against SAPT2+3 for intermolecular interactions in a large data set consisting of approximately 190 imidazolium and pyrrolidinium based ionic liquid ion pairs taken from their previous study.⁹⁸ While EFP is very promising for modeling intermolecular forces in large neutral systems,^{75–77,128–132} its shortcomings were amplified by the sheer magnitude of individual fundamental forces in ILs. It was suggested that EFP would not perform reliably for ionic liquids, as each of the five energetic components—electrostatics, exchange repulsion, induction, dispersion, and charge transfer—were derived for neutral molecules, in which the center of mass coincides with the center of charge. Significant errors were expected for charge transfer in particular. On the absolute scale, the five components predicted by EFP, as well as total interaction energy (i.e., the sum of the five components), differed significantly from those in SAPT2+3, falling in the range -63 to 70 kJ mol^{-1} for the best performing basis set, aug cc pVTZ. The two other basis sets, aug cc pVDZ and 6 311++G(d,p), produced larger errors. On the relative scale, the EFP method produced errors within 20%, on average, for all types of cation–anion combination, with the charge transfer component giving the largest deviations, as expected. It has to be noted that the EFP charge transfer component cannot be directly compared to that in the SAPT formulation because it disappears in a complete basis set in the latter. Overall, the relative errors were comparable to those obtained for the S22 and S66 databases in the earlier work of Flick et al.¹³² These databases were designed by Hobza et al.^{133,134} specifically to assess computational chemistry, and they consist of a well balanced series of intermolecular complexes, for example, complexes between small molecules, DNA base pairs, and amino acid pairs. These findings indicated that errors in the EFP method were not specific to ionic liquids as originally suggested. Due to the sheer magnitude of total interionic interactions, falling between -300 and -500 kJ mol^{-1} , it is not surprising that even an error of 10% would produce errors up to 50 kJ mol^{-1} . The most promising results came from scaling the EFP induction and dispersion terms with respect to SAPT2+3, with high values of correlation coefficient, R^2 , being obtained for all types of ionic liquids. The absolute errors reduced to <3 kJ mol^{-1} for typical ionic liquid anions such as BF_4^- and $\text{N}(\text{CN})_2^-$, and <11 kJ mol^{-1} for halides, thus paving the way toward cost effective methods for the calculation of induction and dispersion forces in ionic liquids based on first principles approaches. Recently, McDaniel et al.^{135,136} showed how SAPT(DFT) calculations performed on single ion pairs of

imidazolium based cations coupled with the BF_4^- and PF_6^- anions could be used to parametrize nonbonding terms in classical force fields to analyze dynamics of ions in the bulk and predict liquid density and heats of vaporization.

In summary, due to the importance of dispersion forces in ionic liquids, it is recommended that GGA functionals including the explicit dispersion correction, e.g. BLYP D3, and/or the newly modified MP2 method, SCS IL MP2, that accounts not only for dispersion but also counterpoise correction are to be used for future geometry optimizations of ionic liquid ion pairs and large clusters. For the accurate prediction of energetics of ionic liquids, especially larger clusters, the SCS IL MP2 method and the M062X functional are strongly recommended.

2.2. Hydrogen bonding

Hydrogen bonding in ionic liquids has been a topic of numerous scientific studies (for examples see two recent reviews from the Hunt¹³⁷ and Zhang¹³⁸ groups). In this review, the focus is given to the energetic decomposition of hydrogen bonding into four fundamental components, such as electrostatic, exchange repulsion, induction, and dispersion.⁶⁷ In the work of Tsuzuki et al.,⁹⁶ a difference of almost 15 kJ mol^{-1} in interaction energy (MP2/6 311G*) was observed between $[\text{C}_2\text{mim}][\text{BF}_4]$ and $[\text{C}_2\text{dmim}][\text{BF}_4]$, with the latter producing a more stable ion pair. This observation was translated into the fact that hydrogen bonding was not the main contributor to attractive interactions in C_nmim based ionic liquids. In the work of Dong et al.,¹³⁹ two configurations were calculated of the anions BF_4^- and PF_6^- interacting with the C2–H bond of the imidazolium cation, C_2mim^+ and C_4mim^+ , respectively, from above and below the plane. In both configurations the hydrogen bonds formed were of nondirectional nature and displayed varying bond lengths between the hydrogen atoms on the imidazolium ring and fluorine atoms on the anion. Three levels of theory, MP2 and two double hybrid functionals, B2PLYP⁸⁶ and B2PLYPD,¹⁴⁰ coupled with the 6 31++G(d,p) basis set, showed differences in the range of up to 10 kJ mol^{-1} for both configurations, indicating that both configurations are energetically stable.

In the study of Izgorodina et al.,¹⁴¹ the SAPT2/aug cc pVDZ calculations were performed on MP2/6 311+G(3df2p) optimized structures of neutral and charged complexes of model systems based on all possible combinations of CH_4 , CH_2F_2 , and CHF_3 with fluoride, chloride, or HF molecule. The presence of the halide anion immediately resulted in stronger interactions and distinct wells on the potential energy surface. The electrostatic contribution not only increased in magnitude 10 fold but also affected the corresponding induction and dispersion forces, thus resulting in an even larger increase in interaction energy overall. SAPT2 was also applied to ion pairs of $[\text{C}_2\text{mim}]\text{Cl}$ that were constructed to include nonlinear hydrogen bonding interactions (i.e., the chloride interacts with the C2–H bond and hydrogens of the C=C backbone in the plane of the ring) as well as typical interionic interactions (i.e., the chloride interacts above and below the imidazolium ring). No significant difference in the breakdown of energetic components was observed among these configurations, with the electrostatic component (calculated as the sum of electrostatic, exchange repulsion, and induction contributions) consistently contributing between 75 and 78% (see Figure 3). Both induction and dispersion forces were non negligible, falling in the range of 36 – 64 kJ mol^{-1} . From the fundamental

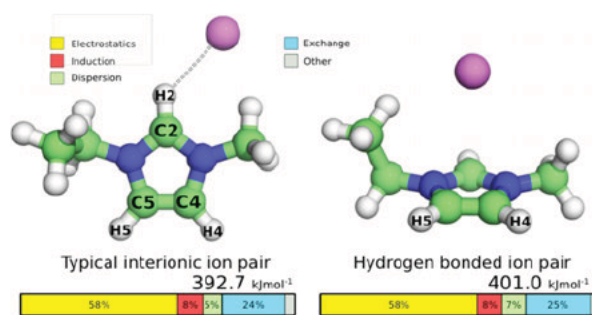


Figure 3. Comparison of fundamental forces calculated with SAPT2/aug-cc-pVDZ in imidazolium-based ion pairs with hydrogen bonding (structure on the left) and typical interionic interaction (structure on the right).

point of view, it should not come as a surprise that the presence of charges should impart much greater stability to intermolecular complexes. Charges are known to be highly polarizable, thus inducing dipole moments in interacting species. This effect does not only increase induction forces but also magnifies instantaneous dipole moments on the electron density surface, hence resulting in increased dispersion.

In the study of Rozas et al.,¹⁴² a similar observation was made for the ion pair of the guanidinium chloride. In addition, three other possible intermolecular complexes were studied by combining guanidine or guanidinium cations with either chloride or HCl. These complexes were optimized at the MP2/aug-cc-pVDZ level of theory, and interaction energies were improved with G3MP2 and corrected for BSSE. The inclusion of charge, on either the cation, anion, or both, led to a significant increase in interaction energies. The electrostatic component in the guanidinium chloride complex was estimated by subtracting the interaction energy of the complex between guanidine and HCl from that of guanidinium chloride and accounting for the acidity/basicity difference between guanidine and HCl. The resulting number of 75% was close to SAPT2 results reported previously for [C₂mim]Cl ion pairs.¹⁴¹ From the energetic point of view, hydrogen bonding in ionic liquids appears to be rather nonunique, which also suggests that no unique treatment of hydrogen bonding is required as long as quantum chemical methods can accurately describe two fundamental forces: induction and dispersion.

2.3. Many-body effects in ionic liquids

As in any condensed system, thermodynamic and transport properties of ionic liquids are governed by many body effects that are a consequence of ions interacting with each other in the bulk. Many body effects manifest themselves through an increase in interaction energy among ions when normalized to one ion pair due to the nonadditive nature of fundamental intermolecular forces. The phenomenon of many body effects is also referred to as cooperativity, the term widely used with respect to hydrogen bonded complexes.^{143–145} Induction forces are recognized as nonadditive in nature, and therefore, commonly used pairwise potentials are not adequate enough to treat bulk intermolecular interactions in condensed systems, for which induction forces dominate. Water is a classic example that requires the inclusion of not only three and four body interactions but also five body interactions to accurately treat the intermolecular interactions in the bulk.^{146,147} Recently, the nonadditive nature of dispersion forces has been highlighted in a number of condensed molecular systems starting from the

classical example of Ar₂–hydrogenhalide systems^{148,149} to π conjugated polynaphthalene derivatives interacting with a gold surface,¹⁵⁰ carbon nanostructured materials,¹⁵¹ and molecular crystals of pharmaceuticals, biologically relevant systems, and many other functional materials.^{152–154} As has been shown above, induction and dispersion forces are important in ionic liquids, and therefore, many body effects are expected to play an important role. The best way to extract many body effects is by performing quantum chemical calculations (be it electron density based or wave function based) on large clusters consisting of tens and hundreds of ions, thus mimicking the bulk of ionic liquids. Calculations need to be performed at a reliable level of theory that can accurately describe both induction and dispersion components of interaction energy to draw reliable conclusions on many body effects.

Early in 2006, Kößmann et al.¹⁵⁵ studied cooperativity (i.e., many body) effects of hydrogen bonding in “linear” chains of [C₁mim]Cl optimized at the BP86^{30,32}/TZVP^{156,157} level of theory. The chains were constructed by including the in plane interactions of the chloride anion through either the C2–H bond or the C–H bond off the C=C backbone. The DFT results indicated that the counterpoise corrected interaction energies per ion pair were lower for two and three ion paired clusters by at least 15 kJ mol^{−1} compared to that of the lowest energy single ion pair, which was found to be the in plane configuration of the chloride interacting with the C2–H bond. Only with inclusion of five ion pairs does the cluster become more energetically stable than the single ion pair, thus indicating that cooperative effects become important for larger clusters of ionic liquids. Although these results might indicate the anticooperative effect of hydrogen bonding for smaller clusters (i.e., the decrease in interaction energy per ion pair with increasing number of ions), these clusters were not designed to produce the lowest energy structures, whereas their interaction energies were compared to the lowest energy single ion pair. The other configurations used in the construction of the chains were up to almost 100 kJ mol^{−1} higher in energy. Therefore, it might not be surprising that no clear trend in many body effects was observed for smaller chained clusters. Later, Köddermann et al.¹⁵⁸ identified an increase in binding energy per ion pair of up to 30 kJ mol^{−1} (calculated at the B3LYP/6-31+G* level of theory and normalized to the lowest energy ion pair) in a number of two ion paired clusters of [C₂mim][NTf₂], which was the first indication that many body effects were present even in smaller clusters. In 2008, Ballone et al.¹⁵⁹ optimized a number of neutrally charged clusters of the [C₄mim][CF₃SO₃] ionic liquid varying in size from 1 to 30 ion pairs using the PBE functional. The structures were not claimed to be the global minimum for each cluster size; however, a combination of optimization algorithms were applied to ensure the reproducibility of the optimized clusters, thus ensuring that low energy clusters were indeed obtained for each size. Cohesive energies of these clusters were calculated in the same way as interaction energies, normalized to the cohesive energy of one ion pair and plotted against $N^{-1/3}$ (where N is the number of ions in the cluster). The trend was found to have two slopes: one with a steep slope from 1 to 4 ion pairs in the cluster, and the second, a more gradual slope from 4 to 30 ion pairs in the cluster. The cohesive energy consistently became 75 kJ mol^{−1} larger magnitude with increasing number of ions in the cluster, thus further providing the evidence of the nonadditive many body effects that contribute to interionic interactions in the bulk of ionic liquids. In 2010 Angenendt and

Chemical Reviews

Review

Johansson¹⁶⁰ showed that the B3LYP/6 311+G* binding energy per ion pair (not corrected for BSSE) consistently decreased by over 60 kJ mol⁻¹ from 1 to 5 ion paired clusters of [C₂mim]X ionic liquids (X = BF₄, PF₆, and NTf₂). The ionic clusters were constructed using a “mindless” approach with no particular pattern, and yet, the many body effects strongly manifested themselves.

The recent development of the Fragment Molecular Orbital (FMO) approach by Kitaura et al.¹⁶¹ offers a unique opportunity to incorporate two and three body effects for condensed systems such as ionic liquids. A few excellent reviews have been published on the history and fundamentals of the FMO approach (for example, see refs 162 and 163). In a nutshell, the approach fragments a large molecular system such as a polypeptide¹⁶⁴ or silicon based polymer,¹⁶⁵ into computationally feasible fragments by “breaking” single covalent bonds electrostatically and allocating the electron pair from the bond to one of the two resulting fragments. This results in a positively and a negatively charged species. Certain rules apply when deciding which bonds can be broken to avoid any sacrifice in the chemical integrity of the molecule. For example, conjugated groups such as the phenyl ring, or highly polar bonds such as the peptide C(=O)–NH bond, are recommended to be left intact.¹⁶² In the case of ionic liquids, this approach is ideal, as ionic liquid ions already represent positively and negatively charged species, thus requiring no fundamental change to the methodology or detachment of chemical bonds. Individual fragments are placed in the Coulomb bath that is represented by the combined electron densities of the fragments. Their energies are self consistently converged, thus generating the optimized electrostatic potential.¹⁶⁶ The electronic energy of the system is calculated by adding energies of intermolecular interactions in the form of two body, FMO2 (i.e., all possible two ion pair combinations),¹⁶⁷ and three body FMO3, (i.e., all possible three ion pair combinations),¹⁶⁸ fragments to the converged energies of individual fragments, FMO1, as shown in eq 16. Both two and three body energies are calculated in the presence of the converged electrostatic potential generated by individual fragments. The methodology can be extended to incorporate higher body effects, although it has been shown that three body contributions are already sufficient to accurately predict electronic energies of large molecules and water clusters at both the HF and MP2 levels of theory^{169–171} (see Figure 4)

$$\begin{aligned}
 E(\text{FMO1}) &= \sum_I^N E_I \\
 E(\text{FMO2}) &= E(\text{FMO1}) + \sum_{I>J}^N (E_{IJ} - E_I - E_J) \\
 E(\text{FMO3}) &= E(\text{FMO2}) + \sum_{I>J}^N [(E_{IJK} - E_I - E_J - E_K) \\
 &\quad - (E_{IJ} - E_I - E_J) - (E_{JK} - E_J - E_K) - (E_{IK} - E_I - E_K)]
 \end{aligned}
 \quad (16)$$

It has to be noted that quantum chemical codes contain default options that introduce cut offs for the inclusion of two and three body effects, as some fragments are separated by long distances and contribute an insignificant amount to the total electronic energy. The default parameters used in the quantum chemical package, GAMESS US,^{172,173} were established for isolated large molecules, and therefore, some of these might not

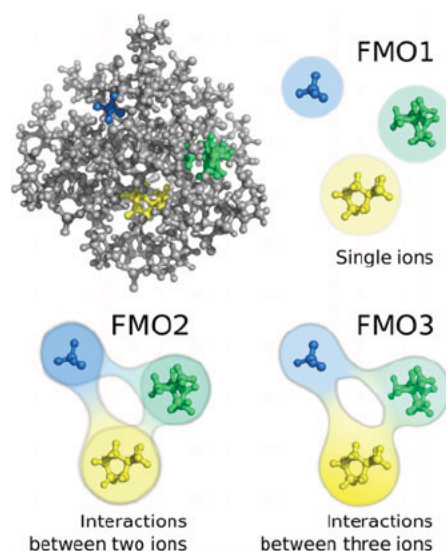


Figure 4. Application of the Fragment Molecular Orbital approach to studying multiscale clusters of ionic liquids.

be reliably transferred to large scale clusters of condensed systems, as the cut offs are dependent on the individual fragment size as well as the size of the cluster.

The first application of the FMO approach was shown by the Gordon group for energetic protic ionic liquids based on the triazolium cation.^{163,174} Errors within chemical accuracy for both FMO2 MP2 and FMO3 MP2 were found in the work of Carlson et al. with FMO3 MP2/6 31+G(d,p) for two ion paired clusters of 1 hydroxyethyl 4 amino 1,2,4 triazolium nitrate, thus suggesting that three body effects might be minor.¹⁷⁴ Clusters consisting of three ion pairs of 1,2,4 triazolium dinitramide and 1 amino 1,2,4 triazolium dinitramide also generated an insignificant difference between FMO2 MP2 and FMO3 MP2 in combination with a smaller 6 31+G(d) basis set.¹⁶³

Later the Izgorodina group¹²⁵ applied the FMO method in combination with the MP2 level of theory to study multiscale clusters of archetypical ionic liquids based on the BF₄⁻ anion coupled with a quaternary ammonium cation, N(CH₃)₄⁺, and C_nmim cations (n = 1, 3, and 4). Since the MP2 level of theory is a post HF method, the MP2 interaction energy can be separated into the HF component, that predominantly treats electrostatic, exchange repulsion, and induction forces, and the MP2 correlation component, that recovers dispersion forces. The full MP2 and both FMO2 MP2 and FMO3 MP2 were performed on M062X/cc pVDZ optimized geometries coupled with the Ahlrichs TZVPP¹⁷⁵ basis set. The ionic clusters were constructed to incorporate the most energetically stable configurations, in which the anion interacted either above/below the imidazolium ring or in the plane of the C2–H bond.¹⁴¹ The MP2 interaction energy calculated per one ion pair was found to increase with increasing cluster size above 60 kJ mol⁻¹, going from 1 to 2 ion pairs, slowly converging for eight ion pair clusters and thus confirming the presence of many body effects. The differences between the FMO2/3 MP2 and MP2 interaction energies showed that two body effects were essential for both the HF and MP2 levels of theory and all cluster sizes, indicating the need to properly account for dispersion forces in pairwise interactions. The importance of three body effects was evident for the HF method, contributing

up to 90% to the difference between the FMO3 HF and full MP2 interaction energies, whereas these were within chemical accuracy ($<4 \text{ kJ mol}^{-1}$) for the MP2 correlation energy. The former highlights the importance of induction forces that can only be accounted for by going beyond pairwise interactions. The extent of electron correlation on three body effects and, hence, dispersion forces could not be clearly determined, as more data for larger scale clusters of 16 and 32 ion pairs, as well as anions of varying basicity, are required to draw solid conclusions. Overall, the FMO3 MP2 method produced an accuracy of 0.2 kJ mol^{-1} averaged over all cluster sizes. This work clearly identified that many body effects were important in ionic liquids and that the FMO approach, with up to three body effects, can be applied to studying energetics of ionic liquids reliably and accurately. The FMO approach has been implemented in GAMESS US,^{172,173} and its performance is augmented with multilevel parallelization by means of the generalized distributed data interface (GDDI),¹⁷⁶ which translates into using multiple cores for performing calculations on individual fragments and higher order (i.e., two body and three body) fragments. Therefore, the FMO approach can be made to scale linearly with cluster size on massively parallel computers.¹⁷⁷

3. ASSESSMENT AND DEVELOPMENT OF QUANTUM CHEMICAL METHODS FOR IONIC LIQUIDS

The studies by Tsuzuki, Kirchner, and Izgorodina clearly highlighted the need for more accurate quantum chemical methods for studying ionic liquids. In the work of Tsuzuki et al.,¹⁷⁸ interaction energies calculated at the MP2/cc pVTZ and CCSD(T)/cc pVTZ levels were compared for multiple ion pair configurations of $[\text{C}_4\text{mim}][\text{Cl}]$ and $[\text{C}_4\text{mim}][\text{Br}]$ with alkyl chains adopting the GT, TT, and G'T conformations discussed above in section 1. Ion pair geometries were optimized at the MP2/6-311G** level of theory, and CCSD(T)/cc pVTZ was approximated using a composite approach on the following formula:

$$\begin{aligned} E(\text{CCSD(T)/cc-pVTZ}) \\ = E(\text{MP2/cc-pVTZ}) + [E(\text{CCSD(T)/6-31G*}) \\ - E(\text{MP2/6-31G*})] \end{aligned} \quad (17)$$

MP2/6-31G* underestimated interaction energies of $[\text{C}_4\text{mim}]\text{X}$ ion pairs by as much as 23.5 kJ mol^{-1} for $\text{X} = \text{Cl}^-$ and 8.4 kJ mol^{-1} for $\text{X} = \text{Br}^-$. The MP2/cc pVTZ level of theory produced accurate interaction energies within 2.4 kJ mol^{-1} for the chloride anion and 1.3 kJ mol^{-1} for the iodide, on average, which was the first indication that MP2 combined with Dunning's triple ζ quality basis set could be reliably used to predict interaction energies of ionic liquids.

In the work of Hunt et al.,¹¹⁸ relative electronic energies of the four most energetically stable ion pair configurations of $[\text{C}_4\text{mim}]\text{Cl}$, calculated with the B3LYP functional and two wave function based correlated levels of theory such as MP2 and CCSD, were compared to those of CCSD(T)/cc pVDZ. B3LYP combined with 6-31++G(d,p) predicted these configurations to fall within 5.6 kJ mol^{-1} of each other, whereas CCSD(T)/cc pVDZ produced a wider range of differences up to 16.7 kJ mol^{-1} , which is well beyond the systematic error of the CCSD(T) method. MP2 appeared to be dependent on the basis set, with a smaller basis set such as 6-31++G(d,p) producing a different trend in relative stabilities of these

configurations compared to cc pVDZ. In the work of Koßmann et al.,¹⁵⁵ BP86 and B3LYP functionals with the TZVP basis set^{156,157} showed opposite trends in relative stability of ion pairs coupled with a shorter chained cation, C_1mim^+ , compared to the MP2/TZVP binding energies. BP86 favored the in plane configuration over the above plane configuration by 23 kJ mol^{-1} , whereas B3LYP followed the MP2 trend by favoring the above the plane configuration by 5 kJ mol^{-1} . These findings also identified the importance of careful selection of the DFT functional as well as basis set for studying energetics of ionic liquids.

Zahn and Kirchner¹⁷⁹ studied the performance of DFT functionals with explicit dispersion for the prediction of binding energies of $[\text{C}_4\text{mim}][\text{N}(\text{CN})_2]$ ion pairs by varying the position of the dicyanamide anion around the imidazolium ring (either above the imidazolium ring plane or near the C2–H bond) and the conformation of the butyl chain. GGA functionals such as BP86, BLYP, TPSS, and PBE and hybrid functionals such as B3LYP and PBE0 were coupled with the second generation of explicit correction, D2, by Grimme⁸⁶ and the dispersion corrected atom centered potential (DCACP) by von Lilienfeld.¹⁸⁰ In the latter, an effective potential based on atom centered, nonlocal higher angular momentum terms was added to the exchange correlation potential. The potential was originally optimized with respect to higher correlated levels of *ab initio* theory such as MP2 with the view of improving the description of weak dispersion interactions in aromatic systems. Although all DFT methods applied produced rather large average errors, between 16 and 35 kJ mol^{-1} compared to the reference MP2/TZVPP values, the inclusion of the D2 correction significantly reduced the errors to below 5 kJ mol^{-1} , with the DCACP slightly underperforming. The latter might be a consequence of parameters taken from the DCACP optimized to MP2, which is known to produce larger errors for imidazolium based ionic liquids.⁶⁰ In the study by Grimme et al., potential energy surfaces of the ion pair dissociation, originally optimized at the B3LYP/TZVPP level of theory for three ionic liquids, $[\text{P}_{4,4,4,1}]\text{Cl}$, $[\text{C}_4\text{mim}][\text{N}(\text{CN})_2]$, and $[\text{C}_4\text{mim}][\text{CH}_3\text{COO}]$, were assessed by applying either the third generation of explicit dispersion correction, D3,⁸⁷ or the nonlocal van der Waals density potential proposed by Vydrov and van Voorhis, abbreviated as VV10,¹⁸¹ as both approaches were successful in the description of intermolecular interaction in between neutral molecules.^{92,182} Here these were applied to the GGA based PBE functional^{29,183} and hybrid functionals such as B3LYP³³ and revPBE38 (a revised version of the PBE functional where 38 stands for $3/8 = 37.5$ and represents the contribution of the HF exact exchange) in combination with the def2 QZVP^{184,185} basis set. It has to be noted that the VV10 potential is conceptually different from the D3 correction, as it is based on the nonlocal correlation energy that allows for the missing long range description of dispersion interactions. VV10 depends only on the electron density, thus avoiding any explicit orbital dependence, and vanishes in the uniform density limit by construction. Compared to the original functionals, the corrected functionals improved errors from 28 kJ mol^{-1} to below a chemical accuracy of 4 kJ mol^{-1} , on average, although they still overestimated the interaction energy by up to 8 kJ mol^{-1} around the equilibrium geometry. The D3 correction only slightly outperformed the VV10 potential. The main finding identified that the dispersion contribution remained significant at the interionic distance of up to 6 \AA .

An extensive body of work was conducted by the Izgorodina group, identifying the limitations of both the DFT and MP2 levels of theory for studying binding energies and interaction energies of pyrrolidinium and imidazolium based ionic liquids.^{93,94} The database of ionic liquid ion pairs described in section 1^{98,117} was used for these assessment studies. In addition, ion pairs of protic ionic liquids⁹⁴ based on primary, secondary, and tertiary ammonium cations, such as $[C_nNH_3]X$, $[C_nCH_2NH_2]X$, and $[C_n(CH_3)_2NH]X$, as well as 1-methylimidazolium and *N*-methylpyrrolidinium cations, were also considered in the study with $X = Cl^-$, ClO_4^- , NO_3^- , CF_3COO^- , CF_2HCOO^- , $CH_3SO_3^-$, and $CF_3SO_3^-$, thus making 236 ion pair structures altogether. The state of the art level of theory, CCSD(T)/CBS, considered the benchmark method for studying intermolecular interactions⁵⁵ was applied based on the MP2/CBS energies as shown in eq 2, where DZ represents a double quality basis set such as aug cc pVDZ (for systems with ≤ 20 atoms), cc pVDZ (for systems with ≤ 29 atoms), and def2 SVP¹⁸⁵ (for systems with >30 atoms). MP2/CBS was achieved by extrapolation of cc pVTZ and cc pVQZ by means of Helgaker's approach⁶¹ in eq 3. A number of DFT functionals (BLYP, BP86, PBE, PW91,^{29,186,187} OLYP,^{188,189} TPSS,¹⁹⁰ XLYP,¹⁹¹ B3LYP, O3LYP,¹⁹² PBE0, TPSSH,¹⁹⁰ TPSS0,¹⁹⁰ and X3LYP¹⁹¹) were used for comparison, including double hybrids such as B2PLYP⁸⁶ and mPW2PLYP¹⁹³ as well as meta GGA functionals of the Minnesota family such as M05, M05 2X, M06, M06 L, M06 2X, M08HX, and M08SO.^{35,194–196} A third generation of the explicit dispersion correction (D3) by Grimme⁸⁷ was also tested in combination with BLYP, BP86, PBE, TPSS, B3LYP, and B2PLYP. Surprisingly, all DFT functionals appeared to depend on the basis set and inclusion of the counterpoise correction. None of the GGA functionals performed well, generating mean absolute errors between 10 and 46 kJ mol⁻¹, with PBE producing the least error, on average. Hybrid functionals generally performed better, although maximum deviations were still rather large (>10 kJ mol⁻¹). Surprisingly, hybrid functionals such as B3LYP and TPSS0 performed better with double ζ basis sets without counterpoise correction, whereas meta GGA functionals of the Minnesota family needed at least a triple ζ basis set to produce good results. Addition of the D3 dispersion correction led to significant improvement, with PBE D3, B3LYP D3, and BLYP D3 in combination with 6-311+G(3df,2p) and counterpoise correction producing average errors of 4 kJ mol⁻¹ and a maximum error of 11.4 kJ mol⁻¹, and therefore, these methods are recommended for studying the energetics of ionic liquids. It has to be noted that functionals with double the amount of the exact HF exchange, such as M052X and M062X, already produced accurate and reliable results for interaction energies and, therefore, can also be recommended for studying ionic liquids. The HF exchange is known to improve the treatment of the medium range correlation, and therefore, addition of the D3 correction would "over describe" electron correlation. Poor performance was observed for double hybrid functionals with average errors >30 kJ mol⁻¹. Although the inclusion of the dispersion correction improved errors, these were still higher than those of PBE D3, B3LYP D3, and BLYP D3. The main outcome of this work was that, for GGA functionals, the dispersion correction is needed for the accurate prediction of energetics of ionic liquids. Overall, MP2 interaction energies with counterpoise correction were below 3 kJ mol⁻¹, on average, from those of CCSD(T)/CBS. Counterintuitively, the MP2 level of theory, when combined with cc pVTZ, showed

similar results to those with aug cc pVTZ, indicating that the presence of diffuse functions, in the already triple ζ basis set, was not necessary for accurate results. The SCS MP2 method produced larger errors compared to MP2, with interaction energies without the counterpoise correction and an aug cc pVTZ basis set which were surprisingly as low as those of the standard MP2 method.

Recently Dion et al.¹⁹⁷ developed a nonlocal density functional that treats long range dispersion interactions for general geometries. The functional, abbreviated as DRSL, introduces a nonlocal correction based on a parametrized kernel that was successfully applied to the noble gas dimers and benzene dimers. A limitation in the exchange energy of all GGA functionals lies in its gradient expansion that needs to vary depending on the type of density, with solids and surfaces requiring the violation of the expansion due to slow varying densities for the accurate treatment of atomization and total energies.¹⁹⁸ A compromise was to include the enhancement factor into the exchange energy to recover the gradient expansion over a wide range of densities.¹⁹⁸ Kohanoff et al.¹⁹⁹ studied the performance of the original DRSL functional as well as its modification with the enhancement factor, $F_X(s)$, for two ion paired clusters of $[C_n\text{mim}]Cl$, $[C_n\text{mim}][PF_6]$, and $[C_4\text{mim}][CF_3SO_3]$ (with $n = 1, 2, 4$, and 12):

$$F_X(s) = 1 + \kappa - \frac{\kappa}{1 + \mu s^2/\kappa} \quad (18)$$

where $s = \frac{|\nabla \rho|}{2k_F \rho}$, k_F is the Fermi momentum, and κ and μ are parameters fitted to reproduce the interaction energies of the S22 data set that consists of intermolecular complexes of hydrogen bonding, dispersion driven, and mixed nature. $\kappa = 1$ was found to give the best performance, and therefore, the new functional was termed the $\kappa = 1$ functional. Overall, the DRSL and $\kappa = 1$ functionals showed improved results for the prediction of intermolecular distances and molecular volumes with relative errors of 2%, on average, over the pure local density approximation (LDA)²⁷ functional and the GGA based PBE functional as compared to crystal structures, especially for PF_6 based ionic liquids. In the same series, LDA and PBE did not fare as well for interaction energies, with the latter consistently under binding as compared to MP2/6-31G* interaction energies. It has to be noted that although the LDA functional showed overbinding, it occurs only due to underestimation of the intermolecular distances by 5%. Although comparison to higher correlated levels of theory was not available, the new modification to the exchange energy, coupled with the nonlocal description of the correlation potential, shows promising results for further development of DFT functionals to accurately predict the energetics of ionic liquids.

3.1. Comments on the accuracy of the GGA functionals for electronic structure properties

The main disadvantage of the GGA functionals is the inaccurate prediction of the HOMO and LUMO orbital energies^{200–203} because of the continuum approximation used in local GGA based exchange correlation potentials.^{29,204,205} For a system with an integer number of electrons, the exact exchange correlation potential shows integer discontinuity between the region on the electron deficient side of the integer and those on the electron abundant side of the integer. This means that there is a system dependent difference between these two regions at all points in space. The exact HOMO and LUMO energies

represent ionization potential and electron affinity, respectively.²⁰⁴ Instead, local DFT functionals introduce an average of integer discontinuity,²⁰⁶ thus leading to erroneous predictions of band gaps and electronic excitations.^{200–202,205,206} As a result, the electronic properties of condensed systems relying on orbital energies cannot be accurately predicted, with band gaps being underestimated by up to 100% in the case of solids.^{207–209} It has to be noted that the inclusion of the D3 correction does not alter the behavior of GGA functionals with respect to integer discontinuity, especially at large separations.²¹⁰ In general, the HOMO energy is shown to be shifted up by 50% for molecular systems, with hybrid functionals improving the HOMO energy and producing larger errors for the HOMO–LUMO gap.²⁰⁰ For example, it is a rather common practice to shift energies of molecular orbitals, generated with DFT calculations in either isolated ions or ion pair configurations of ionic liquids, in order to align binding energies of atomic orbitals in experimentally measured photoelectron spectra.^{211–215} This shortcoming of GGA functionals may also lead to a flawed description of chemical reactivity and electrochemical processes in ionic liquid ions due to artificial charge transfer between the anion HOMO orbital and the cation LUMO orbital.^{210,216} It has been shown that the addition of a fraction of the exact HF exchange improves the prediction of the band gap in solids such as semiconductors,^{207,208,217–219} although the improvement depends on the inherent band gap of the material, with some requiring a larger fraction of the exchange than the others.²²⁰ For example, in the work of Ong et al.²¹⁶ the electrochemical windows of $[\text{C}_3\text{mpyr}]\text{X}$ and $[\text{C}_4\text{mim}]\text{X}$ (where $\text{X} = \text{NTf}_2^-$, BF_4^- , and PF_6^-) were predicted using the PBE functional with a fraction of the HF exchange on structures taken from equilibrated molecular dynamics (MD) simulations without further relaxation. In their work, molecular orbitals and the density of states were shifted using the exchange potential to reproduce a common reference: a vacuum slab attached to the ionic liquid cell. Good agreement was achieved between predicted and experimental results only when the alignment of molecular orbitals was introduced, further highlighting the deficiencies of GGA functionals for the prediction of electrochemical properties of condensed materials. Due to the reliable prediction of molecular orbital energies, the cathodic and anodic limits that are defined through the LUMO and HOMO energies, respectively, could be calculated. A finer detail in which species give rise to either the cathodic or the anodic limit may be identified based on the HOMO and LUMO energies. The study identified that, in $[\text{C}_4\text{mim}][\text{BF}_4]$ and $[\text{C}_4\text{mim}][\text{PF}_6]$, the cation was responsible for both the cathodic and anodic limits of the electrochemical window, whereas, in the case of $[\text{C}_3\text{mpyr}][\text{NTf}_2]$, the anion was the main contributor to the reduction and oxidation of the ionic liquid. For homologous series of ionic liquids, based on the same cation, the PBE functional, coupled with MD equilibrated structures, was shown by Dhungana et al.²²¹ to adequately predict the electrochemical windows of $[\text{C}_2\text{mim}]\text{X}$ and $\text{X} = \text{SCN}^-$, $\text{C}(\text{CN})_3^-$, $\text{N}(\text{CN})_2^-$, and $\text{B}(\text{CN})_4^-$, with the anion having the nitrile group incorporated in its structure. It has to be pointed out that extra care needs to be taken in the prediction of electrochemical windows of ionic liquids comprising varying cations and anions, with the Ong approach, described above,²¹⁶ being the most reliable. The HF method still gives the most accurate HOMO energies and reference orbitals for higher correlated levels of theory without the need for additional alignment of orbitals.

Therefore, the development of cost effective methods based on the HF method remains ideal for ionic liquids.

The Izgorodina group⁶⁰ improved on the CCSD(T)/CBS benchmark interaction energies for approximately 186 aprotic ionic liquid ion pairs⁹⁸ by using CCSD(T)/aug cc pVDZ and MP2/CBS based on the extrapolation of the aug cc pVTZ and aug cc pVQZ basis sets in eqs 2 and 3. Small differences, within 1 kJ mol^{-1} , were found between the CCSD(T)/CBS interaction energies calculated with either augmented (aug cc pVXZ) or nonaugmented (cc pVXZ) types of Dunning's basis sets (where $\text{X} = 3$ and 4). A series of 17 basis sets, including cc pVXZ and aug cc pVXZ ($\text{X} = 2, 3$, and 4), were used with the MP2 level of theory for the calculation of interaction energies. The latter were counterpoise corrected, with the BSSE effect exceeding 10 kJ mol^{-1} for 63% of the studied ion pairs. Even among triple ζ quality basis sets, the electron correlation recovery at the MP2 level strongly depended on the basis set and the anion type, ranging from 80 to 100%, highlighting the need for careful selection of the basis set to describe electron correlation in ILs. Since counterpoise correction requires a significant amount of computational time, this focused on modifying the SCS MP2 method by fitting the opposite, c_{OS} , and same spin, c_{SS} , coefficients (see eq 4) in the MP2 correlation energy to reproduce the CCSD(T)/CBS correlation interaction energy without the need for counterpoise correction. The bootstrapping technique,²²² a robust sampling approach, was used to establish confidence intervals for fitted coefficients with >10,000 replicates. Out of the 17 basis sets used, cc pVTZ produced the best statistical measures, with a mean average error of 0.03 kJ mol^{-1} , a standard deviation of 1.55 kJ mol^{-1} , and the narrowest confidence intervals for the fitted coefficients (see Figure 5). The significance of the new

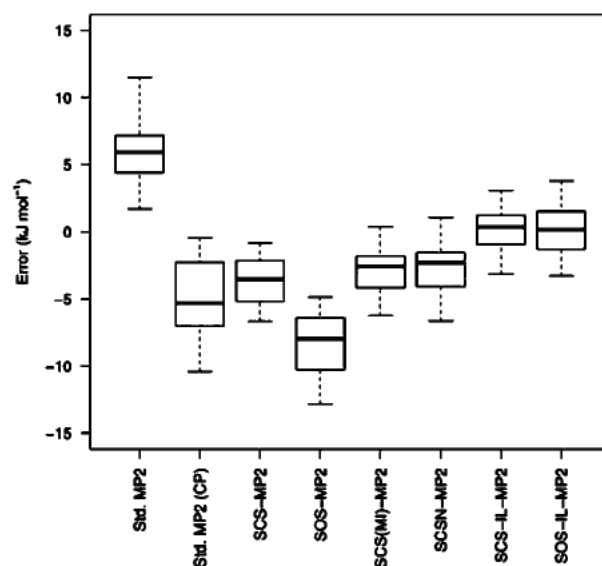


Figure 5. Comparison of errors (in kJ mol^{-1}) in the form of a box plot for interaction energies of IL ion pairs for the standard MP2 method (with and without the counterpoise correction), original SCS-MP2 and SOS-MP2 methods, and all available modifications of the SCS-MP2 method: SCSN, SCS(MI), SCS-IL-MP2, and SOS-IL-MP2. Errors are calculated with respect to CCSD(T)/CBS benchmark data. Reproduced with permission from Figure 12 of *J. Chem. Theory Comput.* 2014, 10, 3111–3122. Copyright 2014 American Chemical Society.

method, termed SCS IL MP2 (SCS MP2 for ionic liquids), was confirmed through its application to the prediction of interaction energies of larger ionic liquid clusters consisting of 2 and 4 ion pairs.¹²⁶ Overall, 15 types of ionic liquids based on 1,3-dimethylimidazolum, *N*-methyl *N'*-methyl(ethyl)pyrrolidinium, and *N*-ethylpyridinium cations (the latter was not originally included in the fitting procedure) coupled with a diverse range of anions, such as chloride, bromide, BF₄[−], and N(CN)₂[−]. Unprecedentedly, small maximum errors within chemical accuracy (4 kJ mol^{−1}) and average relative errors of <2.3% were observed for the clusters studied, with the error decreasing from 2 to 4 ion pairs due to lengthening of the intermolecular distance among ions. As expected, the largest errors were obtained for the bromide based ionic liquids, as the bromide anion with four fully occupied electron shells requires a larger than triple ζ basis set for the accurate description of electron correlation. Other methods, such as the original SCS MP2, with either cc-pVTZ or cc-pVQZ and MP2/CBS, failed to accurately predict interaction energies, with maximum errors exceeding 40 kJ mol^{−1}. In the same work, the SCS IL MP2 was also successfully combined with the FMO approach, with the three body effects accurately reproducing CCSD(T)/CBS interaction energies to within 1 kJ mol^{−1}. Flexible c_{OS} and c_{SS} coefficients (see eq 4) were implemented in the GAMESS US software, thus allowing for geometry optimizations of large ionic liquids at the FMO2/3 SCS IL MP2 level of theory with CCSD(T)/CBS quality. The availability of feasible benchmark methods for large scale clusters of ionic liquids will pave the way toward further development of cost effective wave function based methods and classical intermolecular potentials for molecular dynamics simulations.

Apart from the FMO approach, another method with great potential is that of density functional tight binding (DFTB),^{223–226} which has been shown to be up to 1000 times faster than traditional DFT. The DFTB method is based on the Foulkes and Haydock ansatz,²²⁷ which represents the electron density as the sum of a reference density, ρ_0 , and a small fluctuation, $\delta\rho$. The Kohn–Sham formalism can then be rewritten with respect to the $\rho_0 + \delta\rho$ sum, with the DFTB energy becoming:

$$E = \sum_i n_i \varepsilon_i + E_{\text{rep}}[\rho_0] + E^1[\rho_0, \delta\rho] + E^2[\rho_0, (\delta\rho)^2] + E^3[\rho_0, (\delta\rho)^3] \quad (19)$$

where ρ_0 stands for the sum of atomic electronic densities calculated by means of standard DFT, the first and second terms are attractive (i.e., binding) and repulsive terms that depend only on the reference density, and the last three terms account for the fluctuation in the electron density to the first, second, and third order expansion of the DFT energy. The first order approximation is DFTB1, which does not include a self-consistent procedure for the optimization of atomic electron densities.^{224,226} This approach can only be applied to systems that do not exhibit significant interactions between atomic electron densities, such as hydrocarbons²²⁸ and strongly ionic systems, such as NaCl,²²⁹ which is not the case for the majority of molecular systems. DFTB2 and DFTB3 methods^{223–225,230,231} account for charge fluctuations in atoms bound through covalent bonding that can only be achieved through the self-consistent procedure. The second order term in eq 19 depends on the chemical hardness of an atom as defined by Hubbard,²³² whereas the third order term accounts

for the change in the chemical hardness of an atom with its charged state. Since explicit DFT calculations are performed for individual atoms and molecules, the computation time of DFTB methods has been drastically reduced, allowing for fast calculations for chemical systems with several thousands atoms. For condensed systems with hydrogen bonding, the third order expansion in eq 19 has been shown to be significant.²²⁴ DFTB can also be augmented with an empirical correction to account for dispersion forces.²³³ The dispersion correction is calculated through C_6^{AB} coefficients of atomic polarizabilities *A* and *B* using the Slater–Kirkwood combination rule²³⁴ for both C_6^{AB} and R_{AB} quantities:

$$E_{\text{disp}} = - \sum_{AB} f(R_{AB}) \frac{C_6^{AB}}{R_{AB}^6} \quad (20)$$

The Irlé group²³⁵ pioneered the application of the DFTB3 method to studying large scale clusters of ionic liquids based on imidazolium cations. Clusters consisting of 1–4 ion pairs of nitrates coupled with the C₁mim⁺, C₂mim⁺, and C₄mim⁺ cations were optimized with DFTB3, and their energies were improved with M062X/6-311G(d,p). For each cluster size, a number of starting structures were generated using a stochastic “Kick” algorithm²³⁶ of “mindless chemistry”, allowing for the alkyl chain on the imidazolium cation to freely rotate. Both DFTB3 and M062X showed excellent agreement in the ranking of lower energy clusters for clusters of 2 to 4 ion pairs. In the case of single ion pairs, a proton transfer between the proton on the C2–H bond and the nitrate anion was observed, and this was attributed to poor correspondence between DFTB3 and M062X. This is an important outcome, as it further identifies the danger of drawing conclusions from structures of single ion pairs of ionic liquids. In the case of [C₂mim][NO₃] larger scale clusters, consisting of 6–15 ion pairs were studied with the view of determining the convergence behavior of binding energy per ion pair. Both DFTB3 and M062X showed rapid convergence of binding energy, for clusters with 10 ion pairs, to −528 and −559 kJ mol^{−1}, respectively, whereby producing a consistent difference between the two methods (see Figure 6). Overall, excellent agreement in trends and thermodynamically stable structures indicates a promising and exciting new method for studying large scale clusters of ionic liquids. The DFTB3 method has already been successfully applied by the Irlé group to understanding the mechanism of cellobiose hydrolysis to glucose²³⁷ and glucose transformation to 5-hydroxynethylfurfural²³⁸ in ionic liquids.

Recently Page et al.²³⁹ have demonstrated the reliability of the DFTB3 method in combination with the dispersion correction²³³ for studying energetics of protic ionic liquids such as ethylammonium nitrate, propylammonium nitrate, and butylammonium nitrate. The lower energy structures, and therefore thermodynamically more stable structures, were generated for clusters consisting of 2–10, 15, and 20 ion pairs. In order to achieve this, a number of initial structures were randomly generated using the “Kick” algorithm:²³⁶ e.g. between 1000 and 2000 initial structures for smaller sized clusters (≤ 10 ion pairs) and 5000 structures for larger sized clusters (≥ 15 ion pairs). Larger clusters were then subjected to single point calculations with M062X/6-311G(d,p), whereas smaller clusters were fully reoptimized with M062X/6-311G(d,p). Both DFTB3 D and M062X show the same trend in binding energies per ion pairs that decrease with increasing cluster size and already show convergence at 7 ion pairs. The

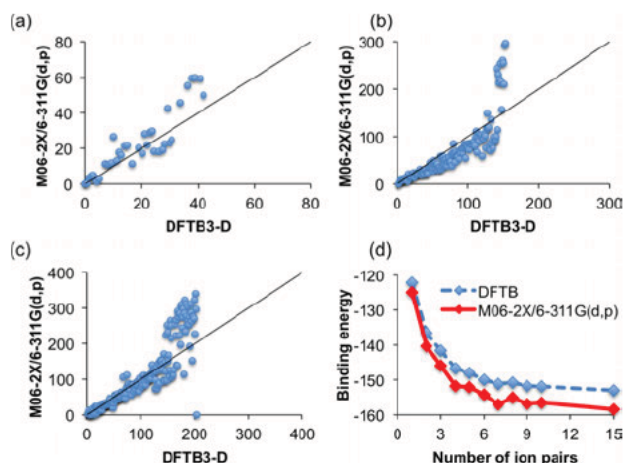


Figure 6. Comparison of relative energies (in kcal mol⁻¹) for (a) 2 (39 unique structures), (b) 6 (152 unique structures), and (c) 15 ethylammonium nitrate (EAN) ion-pair clusters (204 unique structures), computed using DFTB3 and M06-2X/6-311G(d,p). DFTB3 energies are fully optimized. M06-2X/6-311G(d,p) are single-point energies. (d) Binding energies (kcal mol⁻¹ per ion pair) for EAN clusters, as a function of cluster size, computed using DFTB3 and M06-2X/6-311G(d,p). Reproduced with permission from Figure 4 of *J. Chem. Theory Comput.* 2014, 10, 4633–4643. Copyright 2014 American Chemical Society.

absolute differences in binding energies are a little high and fall systematically within 40 kJ mol⁻¹. This is a good outcome, as the DFTB3 method may be further scaled to better reproduce M062X energies. For smaller clusters, the back proton transfer from the cation to the anion was again observed, further highlighting the deficiency of the gas phase to accurately predict geometries of ionic liquids with enhanced hydrogen bonding. The DFTB3 method was combined with the molecular dynamics formulation to predict the structural arrangement in the bulk of ionic liquids at 298 K. The DFTB3 D results were compared to neutron diffraction data²⁴⁰ and showed remarkable correspondence between the two sets of data. Overall, the performance of the DFTB3 D method is very promising for performing molecular dynamics simulations of ionic liquids with the view of predicting their bulk structure. For the accurate prediction of thermodynamic data, the DFTB3 method needs to be further parametrized to achieve better performance. A brief comparison of the technical aspects of the GGA+D3, SCS IL MP2, and DFTB3 D methods is given in Figure 7.

	GGA+D3	SCS-IL-MP2	DFTB3-D
Cheap	✓	✗	✓
Ions	10-100's	10-100's	1000's
Type of Calculation	Energy, Gradient	Energy, Gradient	Energy, Gradient
Accuracy	10 kJ/mol	< 4 kJ/mol	10 - 40 kJ/mol
Additional Advantages:	AIMD < 32 IPs 100 ps	+ FMO3 + Massively Parallel	Rapid global minimum search

Figure 7. Comparison of the GGA+D3, SCS-IL-MP2, and DFTB3-D methods.

4. QUANTITATIVE STRUCTURE–PROPERTY RELATIONSHIP APPROACH

The Quantitative Structure–Property Relationship (QSPR) approach is a widely used strategy to predict physicochemical properties of ionic liquids including melting point, transport properties, such as conductivity and viscosity, thermal decomposition temperature, and glass transition temperature, solubility, and dilution coefficients at infinite dilution. The reason behind the popularity of QSPR is in its simplicity, as it combines a number of well defined descriptors in either a linear or nonlinear fashion to achieve the least deviation for a particular property from experimental data (see Figure 8). The

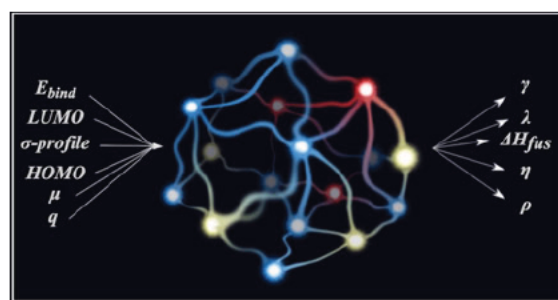


Figure 8. Schematic representation of nonlinear algorithms used in the QSPR approach for the prediction of physicochemical properties of ionic liquids.

fitting procedure usually comprises a *training set* that has an extensive series of experimental data on a wide range of ionic liquids and a *validation set* that includes ionic liquids that are excluded from the original fit. Descriptors vary in their type and include constitutional, topological, thermodynamic, geometrical, and quantum mechanical information. The latter are obtained from electronic structure (*i.e. ab initio*) calculations and can contain orbital energies, ionization potentials, atomic charges, ionic volumes, electrostatic energies, *etc.* There have been a number of excellent reviews detailing the use of molecular descriptors.^{241–243} In the current review the emphasis is given to the inclusion of data from electronic structure calculations into the QSPR approach, with the view of highlighting the accuracy and limitations of quantum mechanical descriptors on the quality of the proposed QSPR models.

Although quantum mechanical descriptors are more complex, these have advantages over the other types of descriptors due to the ability to recover the electronic structure information that is specific to a particular type of ion or a functional group.

Quantum mechanical descriptors are derived from the optimized structure of single ions. Some of these form a group of three dimensional (3D) descriptors that translate intricate details of geometrical parameters such as bond lengths and bond angles to the resulting QSPR model, whereas the others are taken from the analysis of molecular orbital energies, partial charges, charged surface areas, and molecular orbital populations. These quantum mechanical descriptors, based on the electronic structure, are expected to mimic the reactivity and strength of interactions among counterions in the bulk of ionic liquids.

4.1. Density

In the work of Rybinska et al.,²⁴⁴ ionic structures were optimized at three levels of theory—semi empirical PM7, HF/6 311+G*, and B3LYP/6 311+G*—to generate 3D quantum mechanical descriptors that were subsequently fitted to reproduce experimental density. The test set comprised 6 ionic liquids coupled with six types of routinely used cations (imidazolium, pyrrolidinium, ammonium, phosphonium, pyridinium, and piperidinium) and 27 different anions. Two weighted descriptors, one for each ion, were used in the resulting QSPR models. Overall, each level of theory used for geometry optimization affected both the geometric parameters of 3D structures and the quality of the QSPR models, with HF producing the best correlation, with a coefficient of determination (R^2) value of 0.95, and PM7 performing only marginally worse than HF. Surprisingly, B3LYP, which is usually considered superior to the HF method for geometry optimization, produced the R^2 value of 0.86. It is remarkable how just two descriptors could already predict the density of ionic liquids with up to 87% reliability. This is also partially due to the fact that density is less sensitive to the details of intermolecular interactions in the bulk of ionic liquids compared to thermodynamic and transport properties.

4.2. Melting point and heat of fusion

As reviewed by Valderrama,²⁴³ for the prediction of melting points, the QSPR models can give the maximum deviation in a wide range of 25 to 102 K. The maximum errors tend to become smaller when a QSPR model is limited to a particular type of ionic liquids, e.g. the same cation or the same anion. An increase, not only in the sheer number of ionic liquids included in the training set, but also their types seemed to further increase errors.

Separation of QSPR descriptors into cationic and anionic improved the prediction of melting points of imidazolium ionic liquids comprised of 22 different cations and 11 different anions.²⁴⁵ Inclusion of a quantum chemical descriptor such as the charge distribution on ions was shown to produce equally good correlations when combined with topological descriptors. The predicted melting points varied from as little as 0.4 to 53 K. This outcome was still rather impressive due to a wide range of melting points and the neglect of intermolecular interactions in ionic liquids.

Early models by Katrizky et al.²⁴⁶ showed that the inclusion of quantum chemical descriptors could produce reliable QSPR models for the prediction of melting points. Their first study focused on bromide salts of imidazolium and benzimidazolium ionic liquids. Ions were optimized at a semi empirical level of theory, AM1.²⁴⁷ The salts were further separated into four subsets with regard to the substituent on the imidazolium ring. The QSPR models for the four subsets used 5 descriptors out of the 16 best performing descriptors, with only two of them being topological and the rest quantum mechanical. Some notable descriptors include the HOMO–LUMO energy gap, orbital population, maximum partial charges on nitrogen and oxygen atoms, and charged surface areas. The models had R^2 values in the range between 0.69 and 0.94, with the corresponding standard deviations falling between 14 and 29 K. In addition, the R^2 values appeared to correlate well with the number of points included in the training set, with the R^2 numbers further deviating from 1.0 with an increase of data points in the set. The same methodology was applied to pyridinium bromides.²⁴⁸ Two proposed QSPR models with

either two or six descriptors produced R^2 values of <0.79 and standard deviations of <26 K, on average. Many descriptors, when considered individually, resulted in poor correlations. One quantum mechanical descriptor, total entropy of atoms, was among the best performing descriptors. In both studies, melting points could still be predicted with a maximum deviation of >90 K.

Trohalaki et al.²⁴⁹ studied 1 substituted 4 amino 1,2,4 triazolium bromide and nitrates using HF/6 31G** for geometry optimization of ions. A simple three parameter model was proposed that relied entirely on electrostatic and quantum mechanical descriptors, such as the Fukui nucleophilicity index, the area weighted surface charge of hydrogen bonded acceptor atoms, and the LUMO orbital energy of the ion. Atomic partial charges were taken from Natural Bond Analysis calculations. Bromide and nitrate salts were treated separately, and the resulting QSPR models had the R^2 value of >0.9 for each anion type, with significant differences being observed in the fitted coefficients. The study was later extended to incorporate nitrocyanimides with the same type of cation.²⁵⁰ The level of theory was also improved to MP2/6 31G** to account for electron correlation. Quantum chemical descriptors were augmented with topological and structural descriptors to ensure better correlations. 120 various descriptors were trialled in the study. A QSPR model was fitted for each type of anion. Nitrate salts appeared to produce the largest absolute errors. It has to be pointed out that these salts also have the widest melting point range, between –55 and 55 °C, which might contribute to the appearance of larger errors. These resulting models based on a higher level of theory performed worse than those previously reported by Trohalaki et al. that were based on a lower level of theory. For the nitrocyanimides, the use of the HOMO orbital energy on the substituent of the cation appeared to be enough to produce excellent correlations with $R^2 > 0.9$, with only seven ionic liquids being included in the test and with a relatively narrow range of melting points from –11 to 11 °C. These two studies highlighted that the level of theory was important. The range of melting points also affected the correlation.

Inclusion of electronic structure calculations of the single ion pair in QSPR led to excellent linear correlations for the prediction of the heat of fusion of 44 imidazolium based ionic liquids coupled with routinely used anions.²⁵¹ Based on the semi empirical calculations with the semi empirical PM3^{252,253} method, the QSPR model consisted of six quantum mechanical descriptors, such as dipole moment, LUMO energy, interionic interaction energies, and 3D geometric parameters. The R^2 value was as high as 0.9, with a standard deviation of 4.8 kJ mol^{–1}. The electronic structure properties taken from direct calculations of single ion pairs appear to provide a better estimate of interionic interactions in the bulk of ionic liquids, thus resulting in better correlations overall. The use of quantum chemical descriptors from PM3 was also demonstrated in the work of Eike et al.,²⁵⁴ who managed to predict melting points of 75 tetralakylammonium bromides and 34 *N* hydroxyalkyl trialkylammonium bromides with the R^2 coefficient of 0.77. Inclusion of electronic descriptors allowed for the largest error to be reduced from 110 to 82 K, thus further highlighting the importance of considering the electronic structure of ions in these predictive models.

4.3. Transport properties

Viscosity and ionic conductivity have been proven harder to predict, partially due to the lack of experimental data. Some ionic liquids either are solid or have high viscosities at room temperature. As a result, only medium sized sets of ionic liquids have been explored in the QSPR approach. Unless stated otherwise, quantum chemical descriptors are generated at the HF/6 31G** level of theory.

In the original study of Tochigi and Yamamoto,²⁵⁵ both multilinear and polynomial regression analyses were used to predict conductivity and viscosity. The experimental data comprise a diverse set of cations (ammonium, pyrrolidinium, piperidinium, pyridinium, and imidazolium) and anions (BF_4^- , PF_6^- , Cl^- , Br^- , NTf_2^- , CX_3COO^- , $\text{C}_n\text{F}_{2n+1}\text{BF}_3^-$, EtOSO_3^- , $\text{C}_4\text{F}_9\text{SO}_3^-$, $\text{CF}_3\text{SO}_2\text{NCOCF}_3^-$, and $\text{C}_3\text{F}_7\text{COO}^-$, where $X = \text{F}$ and H and $n = 1-4$). The nonlinear regression proved to be more reliable in the prediction of both properties, especially for the regions of low and high conductivity. The R^2 coefficient of 0.97 was achieved for 139 conductivity points, and the errors spanned a range of -1.98 to 1.44 mS cm^{-1} . For the viscosity prediction, 329 points were used, with the polynomial regression producing the correlation coefficient of 0.91, with errors spanning the range of -0.42 to 0.66 on the logarithmic scale. In both QSPR models, the temperature at which the properties were measured was explicitly included in the equation. Important quantum chemical descriptors included the ionization potential, the orbital energy of the LUMO, the dipole moment, and the charge on the nitrogen atom.

Bini et al.²⁵⁶ applied the heuristic method to predict the conductivity and viscosity of NTf_2^- based ionic liquids at two temperatures: 293 and 353 K. Four types of cations, such as imidazolium, pyridinium, piperidinium, and morpholinium, with linear alkyl and oxyalkyl chains, were included in the study. Quantum chemical descriptors came from geometry optimizations of ions and vibrational frequencies of cations performed at the B3LYP level of theory. Partial atomic charges were extracted from the Natural Bond Analysis as implemented in the Gaussian software. Out of an extensive pool of descriptors, two quantum chemical descriptors, the moment of inertia and the maximum net charge on the hydrogen atom, proved to be the most statistically significant. It is remarkable that the importance of these descriptors did not change on going from lower to higher temperature. It has to be noted that the correlation coefficient improved within 10% at 353 K, despite the fact that the actual dispersion of experimental data points increased compared to that at 293 K. Two different quantum chemical descriptors, the fractional negative surface area and the Fukui 1 electron reactivity index for the carbon atom, were found to be critical to finding the best fit for viscosity at the lower temperature. Both descriptors indirectly account for the strength of the cation–anion interaction. Although the overall R^2 value was found to be satisfactory, >0.87 , the correlation in the region of low viscosity was rather poor. The inhomogeneity within the experimental data was ruled out as a potential explanation. It is suggested that the non Newtonian behavior of some of the ionic liquids might be responsible for the poor correlation. As in the case of conductivity, a more reliable correlation was observed at the higher temperature. Two different descriptors accounting for the cation–anion interaction, including quantum chemical type, were established to be important at 353 K.

In the extensive study by Han et al.,²⁵⁷ ionic liquids were divided into groups by the anion, BF_4^- and NTf_2^- , and the

cation, 1 ethyl 3 methylimidazolium (C_2mim^+) and 1 butyl 3 methylimidazolium (C_4mim^+). Four groups contained a small number of ionic liquids, between 17 and 24. In the QSPR modeling of viscosity, all four quantum chemical descriptors were used for tetrafluoroborate ionic liquids to find the best correlation, whereas for the other groups, the number of quantum chemical descriptors fell between 2 and 3 out of 4. The most striking outcome in this study highlighted that, in order to produce correlations with $R^2 > 0.91$, different quantum chemical descriptors were needed for all four sets, even for two imidazolium cations that only differed by the length of their alkyl chains. Therefore, it may be concluded that there are appreciable differences in structural arrangement and intermolecular interactions of ionic liquids depending on their cation–anion combination, thus leading to a unique selection of descriptors that are critical for the prediction of viscosity.

In the work of Yu et al.,²⁵⁸ the QSPR modeling was developed to predict the viscosity of two sets of ionic liquids: (1) a set of 23 dicyanamide based ionic liquids coupled with imidazolium, pyridinium, pyrrolidinium, sulfonium, ammonium, guanidinium, and pyrazolium and (2) a set of 19 ionic liquids based on tributyl(3 amino propyl) phosphonium coupled with carboxylates of proteinogenic α amino acids. In the first set, four descriptors were used, with two of them being of quantum chemical type, which included: the sum of solvent accessible surface areas of hydrogen bonding acceptor atoms selected by threshold charge,²⁵⁹ and the average Fukui atomic 1 electron reactivity index²⁶⁰ for a carbon atom. The former quantifies the hydrogen bonding ability of the cation, whereas the latter is defined as the product of the HOMO and LUMO molecular orbital coefficients divided by the corresponding HOMO–LUMO gap and therefore identifies atoms that are more likely to lose or accept electrons. For the second set, three out of four descriptors were quantum chemical and included the Fukui reactivity index for the oxygen atom, the difference between partial positively and negatively charged surface areas, and the descriptor that characterizes the size and polarity of the molecule. Both correlations produced statistically sound fits with $R^2 > 0.9$. The descriptors used in the QSPR modeling were aimed at capturing the cation–anion electrostatic interaction as well as interionic hydrogen bonding and van der Waals interaction. The statistical importance of these descriptors indicated the effect of not only the interionic interactions but also the structural arrangement on viscosity in ionic liquids.

A larger number of 106 ionic liquids coupled with the NTf_2^- anion were subjected to the QSPR modeling to predict their viscosity at eight different temperatures from 283 to 343 K.²⁶¹ Ten different types of cations were included in the study, ranging from commonly used ones, such as imidazolium and pyrrolidinium, to guanidinium and sulfonium. Echoing previous studies, quantum chemical descriptors were found to be critical in producing reliable correlations ($R^2 > 0.82$). These descriptors ranged from solvent accessible partial charge distributions on atoms to orbital occupancy and orbital energies, including those of unoccupied molecular orbitals. Eight different equations were generated due to varying factors contributing to the change in viscosity with increasing temperature. Electrostatic interactions were found to be important in the full temperature range, whereas van der Waals interactions affected viscosity to a greater extent at low temperatures and steric structural and geometric effects outperformed other factors at higher temperatures. This

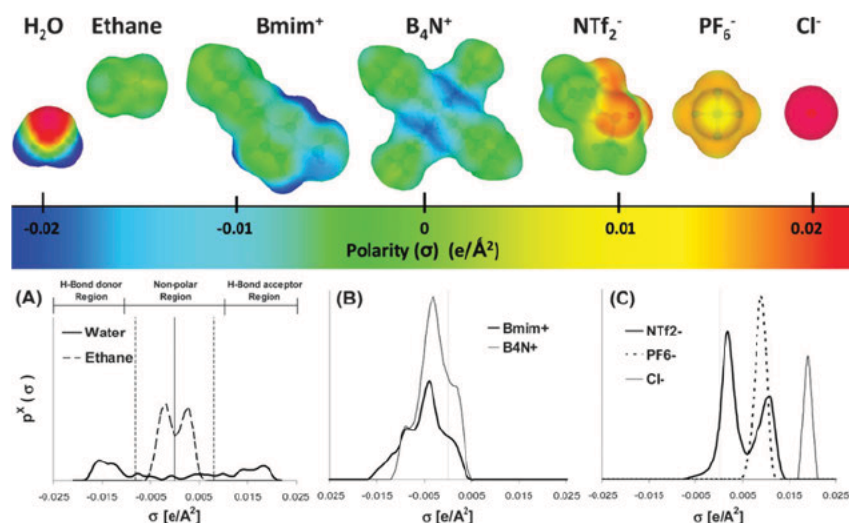


Figure 9. Examples of charge densities and σ -profiles for commonly used ionic liquid ions. Reproduced with permission from Figure 1 of *Phys. Chem. Chem. Phys.* 2010, 12, 1991–2000. Reproduced by permission of the PCCP Owner Societies.

study clearly identified the interplay of energetic and structural factors affecting viscosity changes with increasing temperature, thus further emphasizing the importance of treating all types of intermolecular interactions in ionic liquids equally well to predict their viscosity.

5. COSMO-RS FOR THERMODYNAMICS OF IONIC LIQUIDS

COSMO RS represents a conductor like screening model for realistic solvation.^{262,263} The methodology is based on the COSMO approach, which assumes that a solute molecule is placed in a cavity of a perfect conductor resembling the solute molecular shape. The role of the conductor is to fully screen the electric field of the solute generated by surface polarizability charge densities, σ , thus preventing solute molecules from interacting with each other and forming a well defined reference state for the solute. COSMO and other continuum polarizable models calculate the solvation energy by solving the Poisson equation self consistently, assuming that the polarization of the solvent is homogeneous and therefore can be simply described by a static dielectric constant. The resulting solvation energy captures only the electrostatic component of the solvation process. For polar solvents, the charge density is far from homogeneous due to the presence of functional groups that can engage in various types of interactions with the solute, especially hydrogen bonding. Therefore, the assumption of the linear and homogeneous response from the solvent represents an unrealistic scenario.

COSMO RS circumvents this issue by introducing explicit interactions between charge densities (also referred to σ profiles) of the solute and the solvent²⁶⁴ (see Figure 9). Quantum chemical calculations are performed to generate σ profiles separately for the solute and solvent molecules. All possible electrostatic contact interactions for the solvent σ profile are calculated, thus forming an ensemble of contact segment interactions, with each individual interaction being characterized by *local* charge densities. The inclusion of possible solute–solvent interactions in this simple manner avoids the need for a tedious task of screening corresponding intermolecular complexes though geometry optimization. In addition, COSMO RS also includes the dispersion energy that

depends on the atom surface and is added by summing contributions from all atoms. The ensemble of individual contact interactions serves as a partition function that is used to calculate the chemical potential, thus making it a solvent specific function. This function provides a link to thermodynamic quantities such as heat of vaporization and heat capacity as well as transport properties. In the presence of the solute, the solvent chemical potential is integrated over the σ profile of the solute to generate physical properties of the solute such as solubility and miscibility.

For a solvent, S , consisting of a few components, the σ profile of the entire solvent, $p_S(\sigma)$, can be expressed through the sum of σ profiles of its individual components, $p^X(\sigma)$, weighted by their mole fraction, x_i :

$$p_S(\sigma) = \sum_{i \in S} x_i p^{X_i}(\sigma) \quad (21)$$

Since it is assumed that the molecular interactions can be entirely described by $p_S(\sigma)$, the distribution function of the chemical potential, $\mu_S(\sigma)$, on the solvent surface, can be integrated over the surface of a solute, X , to produce the chemical potential of the solute X in solvent S :

$$\mu_S^{X_i} = \mu_{C,S}^{X_i} + \int p^{X_i}(\sigma) \mu_S(\sigma) d\sigma \quad (22)$$

where $\mu_{C,S}^{X_i}$ represents adjustable parameters. Knowing the chemical potential of the solute X in solvent, $\mu_S^{X_i}$, and the chemical potential of the pure solute X , $\mu_{X_i}^{X_i}$, allows for the prediction of the activity coefficient of the solute X in the solvent S .²⁶²

The $\gamma_S^{X_i}$ coefficient becomes the activity coefficient of X at infinite dilution in S , γ_S^∞ , when $\mu_S^{X_i} = \mu_S^{X_i^\infty}$.

$$\gamma_S^{X_i} = \exp\left(\frac{\mu_S^{X_i} - \mu_{X_i}^{X_i}}{RT}\right) \quad (23)$$

The chemical potentials can be used to predict the solubility of the solute X in solvent S and, hence, generate the liquid–liquid equilibrium (LLE) phase diagrams. For example, for a

binary system, the phase diagram is calculated using the following expression:

$$\mu_S^{X_1} + RT \ln x_{X_1}^1 = \mu_S^{X_2} + RT \ln x_{X_1}^2 \quad (24)$$

where 1 and 2 represent the two phases of the binary system.

The activity coefficient in eq 24 becomes the vapor pressure of the solute X above the mixture (p_X^X) when $\mu_S^{X_1} = \mu_{gas}^X$. The chemical potential of the pure compound X in the gas phase can be calculated as follows:²⁶⁵

$$\mu_{gas}^{X_i} = E_{gas}^{X_i} - E_{COSMO}^{X_i} - E_{vdW}^{X_i} - \omega_{Ring} \eta_{Ring}^{X_i} + \eta_{gas} \quad (25)$$

where $\mu_{gas}^{X_i}$ and $\mu_{COSMO}^{X_i}$ are the electronic energies of the solute in the gas phase and in the COSMO conductor, respectively, and $E_{vdW}^{X_i}$ is the van der Waals or dispersion energy. The other parameters refer to the number of ring atoms in the molecule ($\eta_{Ring}^{X_i}$) and the link between the reference state's energy in the gas phase and liquid.

In COSMO RS, ionic liquids can be treated in two ways. In the first approach, the ionic liquid ions are considered separately and the chemical potential of the solvent is constructed using the 50:50 ratio of cations to anions. The second approach takes a single ion pair into account. The effect of these two approaches was studied for 40 ionic liquids for the prediction of liquid entropy.²⁶⁶ Overall, good correlations within 2% were achieved between experimental and predicted liquid entropies over a wide range of temperatures. In general, only a marginal difference of 0.4% was observed between the two approaches mentioned above. Larger deviations of up to 5.2% were discovered when ionic liquids were analyzed individually. It was concluded that for weakly coordinating ions the predicted entropy did not depend on the approach being used, whereas for strongly coordinating ions it was advisable to use ion pairs to predict liquid entropy with higher accuracy. These findings stemmed from the fact that weakly coordinated ions changed their orientation in the ion pair when going from gas phase to solvent (COSMO calculations with infinite dielectric constant) geometry optimizations, with final geometries revealing almost noninteracting ions. Strongly coordinating ions did not experience any change when solvation effects were introduced, staying almost "locked" in their gas phase arrangement.

5.1. Melting points (T_m)

The Krossing group²⁶⁷ have done extensive research in this area by drawing back on the definition of the melting point from the second law of thermodynamics:

$$T_m = \frac{\Delta H_{fus}}{\Delta S_{fus}} \quad (26)$$

where ΔH_{fus} is the heat of fusion and ΔS_{fus} is the entropy of fusion. In the original work, the heat of fusion was treated using the volume based approach in which the lattice enthalpy was correlated to the effective radii, r , of ionic liquid ions, whereas the entropy of fusion was treated in a similar manner as previously developed for neutral organic molecules:

$$T_m = \frac{cr^3}{a \log \sigma + b\tau + 1} \quad (27)$$

where the radius, r , was found from the molecular volumes determined from COSMO calculations at the BP86/TZVP level of theory. A database of 67 ionic liquids with measured

melting points spanning a range of 337 K was used to fit the coefficients in eq 27 by least squares regression analysis. The R^2 values and average errors depended on the number of ionic liquids included in the regression analysis, with inclusion of more diverse cations and anions worsening the resulting fit. For the whole test, 0.67 was obtained for the R^2 value with an average error of 36.4 K. The maximum error was still very high at 116 K, which corresponds to a third of the melting point range used. In an attempt to improve the correlation, two types of directed interactions were included—ring interaction enthalpy for ring containing cations and van der Waals interaction enthalpy for nonring containing ions—in the heat of fusion calculated using COSMO RS, assuming that an ionic liquid consisted of a 50:50 ratio of the cation and anion at 25 °C. The correlation was improved only slightly, producing the R^2 value of 0.80, the average error of 24.5 K, and the maximum error of 89 K.

Further work by the Krossing group²⁶⁸ identified that the nonparameterized volume based approach did not adequately described the lattice enthalpy, underestimating this quantity to be between 20 and 140 kJ mol⁻¹ due to the lack of dispersive interactions. No direct correlations were found between the heat of vaporization and solvation energies calculated from COSMO RS calculations and experimentally measured thermodynamic properties, including the heat of fusion and lattice enthalpy.²⁶⁸ Lattice enthalpy could only be correlated to the COSMO RS solvation enthalpy calculated in an ideal conductor with infinite dielectric constant ($R^2 = 0.84$). For a better correlation, additional terms needed to be included, such as the solvent accessible surface (\hat{S}), enthalpic contributions from rotational, translational, and vibrational degrees of freedom (H_g^*), and ionic volume (r_m^3):

$$\Delta H_{latt} = a\Delta_{solv}H^\infty + bH^\infty + bH_g^* + cr_m^3 + d\hat{S} + e \quad (28)$$

The correlation was improved to the R^2 value of 0.92, and the average error dropped to 8.3 kJ mol⁻¹.

The Krossing group^{269,270} used this correlation from eq 28 for lattice enthalpy to predict melting points of a wide range of 520 organic salts, including protic ionic liquids. As expected for a large number of data points, the statistical measures were rather low. The correlation coefficient R^2 was only 0.45, with the average error of 36.1 K. COSMO calculations used gas phase optimized structures of individual ions at the BP86/TZVP level of theory. The improvement on this correlation was achieved by adding solvation enthalpies associated with hydrogen bonding and electrostatic interactions in COSMO RS. Instead of the gas phase enthalpic contribution to total energy, the gas phase entropic contribution was used. The relative error dropped only slightly to 33.5 K. The modified correlation still generated a number of outliers with deviations of up to 34.4% (which is equivalent to 175 K on the absolute scale). The appearance of outliers was attributed to difficulties in measuring the melting point, with decomposition of ionic liquids being suspected prior to melting. Overall, the average error of 33.5 K was achieved for a wide range of organic salts at the expense of nine optimized parameters. It was suggested that, despite large errors, high throughput screening of novel ionic liquids may be achieved with the developed correlation. To summarize, this is the best correlation that has been achieved to date that relates COSMO and COSMO RS calculations on individual ions with melting points of corresponding ionic liquids.

5.2. Heat of vaporization

In the past decade, the COSMO RS approach has also been applied to study heat of vaporization. Diedenhofen et al.²⁷¹ used the COSMO RS approach to predict vapor pressure and vaporization enthalpy for a series of [C_nmim][NTf₂] ionic liquids, where *n* = 2, 4, 6, and 8. Two strategies were used to predict the enthalpy. In the first strategy, the partial pressure is directly calculated in COSMO RS calculations and the reciprocal relationship between the partial pressure and temperature is used to extract the vaporization enthalpy as follows:

$$\ln(p(T)) = A - \frac{B}{T} \quad (29)$$

where the product of the slope, *B*, and the gas constant, *R*, represents the vaporization enthalpy. In the second strategy, the enthalpy of vaporization is calculated based on the following sum:

$$-(\Delta_{\text{vap}} G_{\text{cation}}^0(T) + \Delta_{\text{vap}} G_{\text{anion}}^0(T) + \Delta_{\text{vap}} G_{\text{ion pair}}(T)) \quad (30)$$

where $\Delta_{\text{vap}} G_{\text{cation}}^0$ and $\Delta_{\text{vap}} G_{\text{anion}}^0$ are the virtual Gibbs free energies of vaporization of the cation and the anion, respectively, whereas $\Delta_{\text{vap}} G_{\text{ion pair}}$ represents the heat of formation of the ion pair. The second strategy assumes that ionic liquids evaporate as ion pairs. COSMO calculations were performed at the BP86/TZVP for geometry optimizations. In COSMO RS calculations, ionic liquids were treated as a 50:50 combination of individual cations and anions. Both strategies produced very good correlations with experiment, with the largest deviation being 1.4 kJ mol⁻¹ for [C₃mim][NTf₂]. From this study it can be concluded that considering the vaporization as ion pairs correlates very well with experiment.

Preiss et al.²⁶⁸ determined COSMO RS vaporization enthalpies of a larger set of 14 imidazolium based ILs. The correlation coefficient between experimental and predicted enthalpies was found to be as low as 0.49, with the average error of 8.1 kJ mol⁻¹, with stronger coordinating anions, such as nitrates, producing errors >15 kJ mol⁻¹. It was suggested that, for a more rigorous correlation, single ion pairs needed to be considered in COSMO RS calculations, thus making the approach time consuming.

5.3. Heat capacity

Preiss et al.²⁷² established that ionic volumes could be most accurately estimated using a combination of COSMO calculations and the BP86/TZVP level of theory. When compared to X ray crystal structures of the ionic liquids studied, an average error of as low as 4.3% was found, indicating high accuracy of the DFT + COSMO combination. Ionic liquids included in the study represented a wide range of cations and anions. Heat capacity was correlated using the ionic volumes, taken as the sum of the cationic and anionic volumes:

$$C_p = iV_m + j \quad (31)$$

Two temperatures, 298 and 323 K, were used for correlations, with both temperatures producing excellent correlations with the *R*² value of 0.97 and the average relative error of 4.7%. Good correlations suggest that it is more likely that the ionic arrangement in the bulk does not affect the heat capacity measured.

5.4. Transport properties

The Krossing group²⁷³ explored the Arrhenius equation that relates activation energy with viscosity and conductivity:

$$\eta = Ae^{\Delta E/RT} \quad (32)$$

The first step was to predict the dielectric constant of ionic liquids. Using the data from Weingärtner's group, dielectric constants for 40 ionic liquids were correlated using the following expression:

$$\epsilon_r^* = a + b \frac{V_m}{V_0} + c \frac{\Delta G_{\text{solv}}^{*,\infty}}{G_0} \quad (33)$$

where *V*₀ = 1 m³ and *G*₀ = 1 kJ mol⁻¹. The estimation of dielectric constant for any ionic liquid allowed for calculations of solvation energies for a particular ionic liquid. Solvation energies were calculated using COSMO RS and BP86/TZVP optimized geometries of individual ions. Viscosity was fitted to the following expression:

$$\ln\left(\frac{\eta}{\eta_0}\right) = d + e \ln r_m^* + f \ln \sigma + g \frac{\Delta G_{\text{solv}}^*}{G_0} \quad (34)$$

A weak correlation was found with the *R*² value of 0.6, and this poor behavior was observed due to the presence of outliers, ionic liquids coupled with the BF₄⁻ and PF₆⁻ anions. In order to circumvent this issue, an additional term describing the symmetry of each ion (*σ*₊ for the cation and *σ*₋ for the anion) was introduced, with the symmetry of the ionic liquid defined as *σ* = $\sqrt{\sigma_+ \sigma_-}$. A much better correlation was obtained with the *R*² of 0.81 and the average error of 0.21 log units. Surprisingly, the correlation even improved slightly by replacing the solvation energy at a particular dielectric constant, ΔG_{solv}^* , with that of an ideal conductor with infinite dielectric constant, $\Delta G_{\text{solv}}^{*,\infty}$. This simplification resulted in a slightly lower average error of 0.17 log units.

The same correlation as in eq 34 using $\Delta G_{\text{solv}}^{*,\infty}$ was used for electrical conductivity and produced good statistics (*R*² of 0.71 and the root mean squared (RMS) error of 0.25 log units). A simpler correlation based on the Walden rule was achieved. The Walden rule states that the product of molar conductivity and viscosity is constant for a particular electrolyte, thus making the two properties interdependent. By using the predicted viscosity, the molar conductivity could be predicted by using the following expression:

$$\log \frac{\Lambda_m}{\Lambda_0} = s \log \frac{\eta_0}{\eta_{\text{calc}}} + \log C \quad (35)$$

Although the correlation was slightly worse (*R*² of 0.71 and the RMS error of 0.27 log units), it required only the already established correlation for viscosity. The correlation for viscosity requires at least five parameters and the knowledge of the solvation energy, ionic symmetry, and effective ionic radius. It would be insightful to see if the treatment of an ionic liquid as an ion pair would improve the correlations. In summary, these approximations may still produce some serious outliers, and therefore, the predicted results should be treated with caution.

The use of charge densities and *σ* profiles from COSMO RS calculations on individual ions has recently been pioneered in the QSPR approach to predict the viscosity²⁷⁴ and heat capacity²⁷⁵ of ionic liquids. In both studies, good correlations

were achieved by incorporating polar and nonpolar areas of charge densities of both cations and anions, with the anion playing a more important role. The work of Zhao et al.²⁷⁴ employed 1502 experimental points of 89 ionic liquids of 10 types of cations over a range of temperatures and, in the case of imidazolium ionic liquids, over a range of pressures. Their QSPR model used a multilinear regression (MLR) analysis and a nonlinear algorithm, support vector machine, to generate QSPR models only using the surface charge density area of σ profiles for individual cations and anions as descriptors that were taken from previous COSMO calculations at the BP/TZVP level of theory (for more detail, see the COSMOIL database^{276,277}). Significant descriptors included the surface charge density in nonpolar regions on both cations and anions, as well as polar regions on the anions. The latter are indicative of the hydrogen bonding ability of anions. The outcomes of this QSPR work are consistent with previously published data.²⁵⁵ First, the nonlinear algorithm produced better correlations, with the average absolute deviation of 6.6% and with the maximum deviation of 28%. In contrast, the MLR method produced the average error of >10% with a significant number of predicted viscosity values deviating above 20% up to 68%. Second, nonpolar regions on both cations and anions appeared to be more important than the polar regions. This suggests that interionic dispersion interactions might play a vital role in understanding the factors governing IL viscosity. The most convincing conclusion indicates that for more reliable and accurate prediction of viscosity, nonlinear correlations must be explored.

A similar strategy was employed for the prediction of the heat capacity of 46 ionic liquids.²⁷⁵ Both the MLR and a nonlinear artificial neural network algorithm performed well, producing R^2 coefficients of >0.98 and average errors of <2.7%. In the QSPR models, descriptors included the surface charge density of the nonpolar regions of ions and polar regions of only anions. Both studies clearly identify the importance of interionic (predominantly dispersion) interactions and strong hydrogen bonding in the prediction of heat capacity.

5.5. Activity coefficient at infinite dilution

For a number of 38 organic compounds,²⁷⁸ such as alkanes, alkenes, benzylalkenes, alcohols, polar organic solvents, and chloromethanes, the COSMO RS approach was applied to predict their activity coefficients at infinite dilution using eq 23 in three ionic liquids, [C₄mpyr][BF₄], [C₂mim][NTf₂], and [C₂dmim][NTf₂], at two elevated temperatures, 314 and 344 K. Overall, the prediction at 314 K was in good agreement with experimental data, with RMS deviations falling in the same range as in nonionic polar solvents, falling between 0.278 and 0.524 units on the natural logarithm scale in the [C₂dmim][NTf₂] < [C₂mim][NTf₂] < [C₄mpyr][BF₄] series. There are some notable exceptions, such as dichloromethane, whose activity coefficient was underestimated in all three ionic liquids. The deviation was originally attributed to the fact that the initial parametrization of the COSMO RS model was not performed from the acidic proton of the C2–H bond in the imidazolium ring. This hypothesis does not support the fact that the largest RMS deviation of 0.524 units on the natural logarithm scale for activity coefficients was produced in the [C₄mpyr][BF₄] ionic liquid that did not have acidic protons. Additionally, the predicted coefficients for 2,2,4 trimethylpentane, tetrachloromethane, and methanol showed the largest deviations from experiment in [C₄mpyr][BF₄]. For the second elevated

temperature of 344 K, similar RMS values were observed for [C₂mim][NTf₂] and [C₄mpyr][BF₄], whereas the RMS value was nearly halved for the [C₂dmim][NTf₂] ionic liquid at 344 K.

The COSMO RS approach was used to predict the activity coefficient at infinite dilution of organic compounds in the routinely used ionic liquids based on the trihexyltetradecyl phosphonium cation, P_{6,6,6,14}⁺, coupled with the Cl[−], BF₄[−], (C₂F₅)₃PF₃[−], and NTf₂[−] anions.²⁷⁹ The COSMO RS model was first benchmarked against experimental data for [P_{6,6,6,14}][Phosphate] and produced the average relative error of 11.5%. The application of the parametrization to the other phosphonium based ionic liquids was in good agreement with experimentally measured activity coefficients, deviating between 8 and 15%, on average. The theoretical prediction successfully identified that [P_{6,6,6,14}][BF₄] had a moderate selectivity for separation of benzene–alcohol mixtures.

In the study of Kurnia et al.,²⁸⁰ the COSMO RS model was applied to a broad range of 53 ionic liquids to predict the infinite dilution coefficients of water. Overall, 280 experimental data points at different temperatures for each ionic liquid were used for the prediction. Ionic liquids considered in the study consisted of commonly used cations and anions of varying nature and size. In the study, the relative error was calculated by taking the predicted values as the benchmark; the average error was found to be 27.2%, with the maximum error reaching up to 68%. It is conventional to calculate the relative error with respect to experimental data as the benchmark. When recalculated, the average error becomes 50.3%, with some individual errors exceeding 240%. Larger errors are observed from ionic liquids that deviate from ideality, i.e. those displaying either very hydrophobic or hydrophilic nature. The ionic liquids with the trifluoroacetate, tosylate, thiocyanate, halides, mesylate, and dimethylphosphate anions displayed the largest relative errors of >100%. The experimental values of γ_s^∞ significantly varied from 0.02 to 9.36, and it is suggested that larger errors might also be observed as a result of the wide range of experimental data. Therefore, for these ionic liquids, the prediction of infinite dilution coefficients of water is not recommended. It is not clear whether the COSMO RS model was additionally parametrized before the analysis.

In a similar study by Matheswaran et al.,²⁸¹ infinite dilution coefficients of thiophene in 53 ionic liquids at different temperatures were predicted. The average relative error calculated with respect to experimental data was found to be 24.1% with a standard deviation of only 16.5%, and the largest deviation being 99.7%. These results indicate that COSMO RS can reliably predict solubility at infinite dilution of weakly polar molecules, such as thiophene. It has to be noted that the experimental values of γ_s^∞ varied over a narrower range, between 0.38 and 2.68, compared to a much wider range observed for water in similar ionic liquids. It appears that the solubility of thiophene is not affected by the structural arrangement of ionic liquids, as opposed to polar molecules such as water. Thiophene shows the preference for interactions with alkyl chains, thus identifying structural factors that can be fine tuned in ionic liquid ions to enhance its solubility.

In the work of Kato and Gmehling,²⁸² a new modification of the COSMO RS model²⁸³ was used to predict infinite dilution coefficients of organic solvents (alkanes, alkenes, cycloalkanes, cycloalkenes, aromatics, alcohols, ketones, esters, ethers, and water) in the [C_nmim][NTf₂] (n = 2, 4, 6, and 8) and [C₄mpyr][NTf₂] ionic liquids. In the new model termed

COSMO RS(OI), the parameters used in the formation were fitted over an extensive range of thermodynamic data for neutral molecular solvents, including activity coefficients at infinite dilution, enthalpy of mixing, solid–liquid equilibria, and vapor–liquid equilibria. The predicted dilution coefficients were underestimated by >100% on the relative error scale. Qualitatively, the COSMO RS(OI) produced similar trends in γ_s^∞ to those observed experimentally. For quantitative results, the parametrization of the COSMO RS model for the same class of ionic liquids appears to be very important.

5.6. Solubility

COSMO RS can be used to calculate statistical dynamics of a mixture and can produce chemical potentials that are able to derive liquid–liquid equilibrium (LLE) and vapor–liquid equilibrium (VLE).^{265,284} For a binary system, the chemical potentials of the two components can be calculated as shown in eq 22 based on the σ profiles in eq 21. The temperature is allowed to vary until the chemical potentials of all components are equal in both phases, thus identifying at which temperature this particular composition of system components is completely miscible (see eq 24). The resulting temperatures are plotted against the corresponding chemical compositions, thus producing an LLE phase diagram.

Wu et al.²⁸⁵ experimentally measured the upper critical solution temperature (UCST) for mixtures of 1 alkyl 3-methylimidazolium hexafluorophosphate, $[C_n\text{mim}][\text{PF}_6]$, with butan-1-ol. The COSMO RS was used to plot the LLE phase diagram, which turned out to be incomplete due to the COSMO RS ability to find LLEs for the compositions close to critical points, such as UCST, due to COSMOtherm software issues. An extrapolation technique was utilized to predict the UCST values, which were found within 3 K for the alkyl chains varying from pentyl through to octyl and the composition sensitivity of 0.12. The presence of three different conformers for the $C_4\text{mim}^+$ cation increased the error only slightly to ± 5 K, which does not show dependence of the predicted LLE diagrams on the cation conformer.

Domańska et al.²⁸⁶ predicted liquid–liquid phase equilibria of mixtures containing 1 alkyl 3-methylimidazolium methyl sulfate (with alkyl = methyl and butyl) and a range of solvents such as alcohols, ethers, and ketones. The standard protocol was used in the COSMO RS calculations as described above. A thermodynamic Boltzmann average was applied to the solvation energies of multiple conformers where needed. The predicted LLE curves were used to estimate the UCST that fell below the boiling points of the solvents used. Compared to experimental results, solubility values in $[C_4\text{mim}][\text{CH}_3\text{SO}_4]$ produced better agreement, with the ketones showing the least deviations from experiment. The better agreement for the butyl chain was attributed to the increased polarity of the methyl group that could not be captured in COSMO RS. Due to large deviations for $[C_4\text{mim}][\text{CH}_3\text{SO}_4]$, the predicted data could only be analyzed qualitatively.

In the follow up paper, Domańska et al.²⁸⁷ probed the liquid–liquid equilibrium of 1,3-dimethylimidazolium and 1-butylmethylimidazolium based ILs with saturated hydrocarbons (e.g., hexane, octane, and cyclohexane) and unsaturated hydrocarbons (e.g., benzene, toluene, xylene). Compared to their previous work,²⁸⁶ better agreement with experimental data was achieved for all hydrocarbons, particularly around room temperature, which was attributed to their reduced polarity compared to that of alcohols and ethers. The errors tended to

worsen with increasing alkyl chain on the hydrocarbon, further highlighting the COSMO RS's inability to capture the difference in polarity. The second reason for better agreement might lie in the fact that hydrocarbons are less likely to interact with ionic liquids due to low polarity and poor hydrogen bonding ability of the former. Comparing between ionic liquids, the same trend was observed, with $[C_4\text{mim}][\text{CH}_3\text{SO}_4]$ producing better comparisons compared to $[C_1\text{mim}][\text{CH}_3\text{SO}_4]$. The UCST values could not be again predicted by the COSMO RS approach, whereas experimentally these could not be determined due to the overlap with boiling points of hydrocarbons. From the predicted data, one could identify the regions in which the UCST values could be observed. Although COSMO RS does not result in excellent agreement with experiment for LLE phase diagrams, the approach can be used qualitatively to identify the solubilities of various solvents in ionic liquids and, hence, potential systems for experimental confirmation.

Sahandzhieva et al. used COSMO RS to probe the liquid–liquid equilibrium of $[C_4\text{mim}][\text{PF}_6]$ with alcohols such as ethanol, 1-propanol, and 1-butanol. All three binary systems had experimental upper critical solution temperatures. The calculated LLE phase diagrams showed poor agreement with experimental data, with the predicted UCST values being shifted by almost 40 K toward lower temperatures as well as significantly lower concentrations of alcohols to which the theoretical UCSTs corresponded. Alcohols are known for their strong hydrogen bonding, and perhaps they form specific intermolecular interactions with ionic liquid ions other than strong electrostatic interactions, thus resulting in poor agreement with experiment.

In an extensive series of work by M. Freire and J. Coutinho et al.,^{288–291} the LLE phase diagrams were generated for binary systems of ionic liquids based on the imidazolium, pyrrolidinium, pyridinium, and piperidinium cations with alcohols of varying alkyl chains and water. The comparison with experimental data showed satisfactory agreement, albeit only qualitative. The deviation from experiment appeared to increase for longer alkyl chains on the alcohol and hydrophobic anions, such as NTf_2^- and PF_6^- . Some outstanding differences in the prediction of VLE diagrams were observed.²⁸⁸ The COSMO RS generated similar profiles for 1-hexyl-3-methylimidazolium and 1-hexyl-2,3-dimethylimidazolium ionic liquids coupled with the NTf_2^- anion. As a result, the predicted LLE data were nearly identical, which is in disagreement with experimental data that showed the decrease in solubility with replacing the C2–H proton with the methyl group in the imidazolium ring. A large difference in the predicted UCST values was observed between mixtures of *N*-hexylpyridinium NTf_2^- and *N*-hexyl *N'*-methylpyrrolidinium NTf_2^- and hexan-1-ol, whereas the experiment showed similar solubilities of alcohols. In the case of water, the anion seemed to affect the deviations from experiment over the cation.²⁸⁹ COSMO RS incorrectly predicted the complete miscibility of water with $[C_4\text{mim}][\text{C}(\text{CN})_3]$, failed to predict solubility in the IL-rich region of $[C_4\text{mim}][\text{NTf}_2]$ and $[C_4\text{mim}][\text{PF}_6]$, and overestimated solubility in $[C_4\text{mim}][\text{NTf}_2]$ compared to $[C_4\text{mim}][\text{PF}_6]$.

In follow up papers, Friere et al.^{290,291} measured water solubility in a series of ionic liquids: $[C_n\text{mim}][\text{NTf}_2]$ ($n = 1–8$), $[C_4\text{mim}][\text{BF}_4]$, $[C_n\text{mim}][\text{PF}_6]$ ($n = 4, 6, 8$), $[C_4\text{dmim}][\text{PF}_6]$, $[C_3\text{mpy}][\text{NTf}_2]$, $[C_3\text{mpyr}][\text{NTf}_2]$, and $[C_4\text{mpyr}][\text{NTf}_2]$. They showed that the solubility was correctly predicted

when the C2–H proton was methylated for the 1 butyl 3 methylimidazolium cation, with a shorter alkyl chain compared to the previously published data on 1 hexyl 3 methylimidazolium cation.²⁸⁸ COSMO RS also reliably predicted the trend in water solubility with increasing hydrophobicity of the anion in the $\text{BF}_4^- < \text{PF}_6^- < \text{NTf}_2^-$ series.

In the case of very hydrophobic ionic liquids based on the $\text{P}_{6,6,14}^+$ cation,²⁹² the agreement for the LLE prediction was qualitatively as well as quantitatively good, with the predicted results being more accurate in the IL rich region. It was observed that the solubility prediction was better for NTf_2^- based ILs than those with BF_4^- and PF_6^- . It has been again confirmed that larger differences in polarity among components would generally result in better predictions of solubility values.

5.7. Vapor-pressure equilibrium

Banerjee et al.²⁹³ used the COSMO RS approach to determine Vapor–Liquid Equilibria (VLE) of imidazolium based ILs in a range of solvent binary systems. The COSMO RS model was reparametrized independently for non hydrogen bonding and hydrogen bonding solvents. In the former, the effective contact area was considered a scalable parameter by fitting it to VLE data for binary mixtures incorporating 17 different compounds, whereas in the latter both the effective contact area and the hydrogen bonding coefficients were fitted to reproduce VLE data for the same 17 compounds and 4 polar solvents. The parametrization produced average deviations within 4% for the total pressure in 96 systems. The parametrized model was applied to a set of five ionic liquids, $[\text{C}_1\text{mim}][\text{NTf}_2]$, $[\text{C}_2\text{mim}][\text{NTf}_2]$, $[\text{C}_4\text{mim}][\text{NTf}_2]$, $[\text{C}_1\text{mim}][(\text{CH}_3)_2\text{PO}_4]$, and $[\text{C}_1\text{mim}][\text{C}_2\text{H}_5\text{SO}_4]$, with acetone, 2 propanol, water, cyclohexane, benzene, and tetrahydrofuran. The predicted total pressures deviated from 2.7% for binary mixtures of ILs with acetone, to 10.6% for mixtures with water. Mixtures with benzene and cyclohexane produced equally large errors of 6%. The latter is particularly surprising, as neither benzene nor cyclohexane are expected to interact strongly with ionic liquid ions. These data indicate that further parametrization for ionic liquids might be needed to improve the errors in prediction.

In Freire's work,²⁸⁸ a difference in the predictive power of COSMO RS for the VLE of IL mixtures with alcohols was observed between ionic liquids with strong negative deviations from Raoult's law, such as NTf_2^- based ionic liquids, and those with positive deviations from Raoult's law, such as PF_6^- . Raoult's law determines the total pressure in the system by multiplication of the partial pressure of a component and its mole fraction. An opposite trend to the LLE diagrams was observed in the predicted VLE diagrams with increasing alkyl chain on the alcohol, with the deviations from experiment decreasing. The worst result was observed for the most polar alcohol in the study, methanol. In the case of IL mixtures with water, good quantitative agreement was achieved for the predicted VLE diagrams.²⁹⁰

5.8. Noncontinuum models

One of the recent developments of noncontinuum models is the reference interaction solvation model (RISM).^{256,294–297}

The original RISM approach was one dimensional and applied to atomic fluids represented by atoms as hard spheres. The approach generated atomic radial distribution functions by solving the RISM integral equation:

$$h_{\alpha\beta}(r) = \omega_{\alpha\mu}(r) \otimes c_{\mu\nu}(r) \otimes \omega_{\nu\gamma}(r) + \omega_{\alpha\mu}(r) \otimes c_{\mu\nu}(r) \otimes \rho h_{\nu\gamma}(r) \quad (36)$$

where $h_{\alpha\gamma}(r)$ and $c_{\mu\nu}(r)$ are total and direct site to site correlation functions, respectively, between interaction sites $\alpha(\mu)$ and $\gamma(\nu)$ belonging to different molecules, $\omega_{\alpha\mu}(r)$ is the matrix of intramolecular correlations, ρ is the number density, and \otimes determines convolution in real space and summation of repeating indices. The total correlation functions are comprised of two main contributions based on hard sphere potentials—the site–site Lennard Jones (LJ) potential and the electrostatic potential accounted by Coulomb's law. The equation is dependent on the same LJ parameters and atomic charges used in molecular dynamics simulations and is solved in a closed form using either the hypernetted chain approximation²⁹⁸ or the partially linear hypernetted chain approximation introduced by Kovalenko and Kirato (also known as KH closure),²⁹⁹ thus also allowing expression of the free energy function and other thermodynamic quantities in a closed form.²⁹⁸ Kovalenko and Hirato^{299–301} extended the RISM model to a 3D representation by generalizing the solute–solvent equation to infinite dilution. The RISM model can also account to a certain extent for a flexibility of alkyl chains through the rotational isomeric state approximation originally applied to understanding polymeric melts.³⁰² In addition, intermolecular correlations can be taken from optimized structures of molecular components, e.g. ionic liquid ions. The 3D RISM model was successfully incorporated into the Kohn–Sham (KS) formulation (termed as KS DFT/3D RISM), thus allowing for the self consistent solution of the solvation effects incorporated in the Fock operator of the solute and providing a microscopic description of these effects depending on the electronic structure of the solute.³⁰³

The original RISM model was first applied to the $[\text{C}_1\text{mim}]\text{X}$ (where $\text{X} = \text{Cl}^-$, BF_4^- , and PF_6^-) ionic liquids by the Chiappe group.²⁹⁴ Two different sets of values for the LJ parameters and charges of the imidazolium cation were taken from the force fields used by either Lynden Bell et al.³⁰⁴ or Shah and Maginn.³⁰⁵ In the case of the BF_4^- and PF_6^- anions, the parameters of the Lopes and Padua force fields were employed,^{306,307} with the exception of atomic charges on PF_6^- , that came from Lynden Bell et al.³⁰⁸ The pair radial distribution functions, $g(r)$, were compared to those of classical MD simulations performed by Youngs et al.³⁰⁹ In the case of the Cl^- based ionic liquids, good agreement was achieved, with both sets of the parameters for the cation producing similar results. In the case of the anions with multiple interaction sites, such as BF_4^- and PF_6^- , significant deviations were observed that could only be corrected for by representing the anion as a single interaction site.³¹⁰ Additional shortcomings of the approach came from the prediction of the solvation thermodynamics of water in ionic liquids with anions of multiple interaction sites. The excess chemical potential, compared to that of the ideal gas, was calculated to assess water solubility, with the more negative excess potential reflecting higher affinity for ionic liquids. Although the predicted solubility trend followed the experimental observation, the excess chemical potential was found to be only slightly negative for $[\text{C}_1\text{mim}][\text{BF}_4]$ and even positive in the case of $[\text{C}_1\text{mim}][\text{PF}_6]$. The predicted excess molar entropy and enthalpy of water in $[\text{C}_1\text{mim}][\text{PF}_6]$ were of the same sign as the experimental values but deviated significantly (>50%)

compared to experimental data for $[\text{C}_4\text{mim}][\text{PF}_6]$.³⁰⁵ The Chiappe group also estimated the solvation of simple ions such as positively and negative charged lithium and chloride ions in $[\text{C}_1\text{mim}][\text{PF}_6]$ and $[\text{C}_1\text{mim}]\text{Cl}$ using the RISM model.²⁹⁵ The same LJ parameters and atomic charges on the cation were used as in their original publication.²⁹⁴ The PF_6^- anion was treated as a single atom center, and the absolute magnitude of charges on Li^+ , Cl^- , and PF_6^- was set to the magnitude of 1.0, thus not accounting for any charge transfer. The separation of the excess molar entropy of solvation into individual components, such as Lennard Jones and electrostatic (such as translational and orientational), provided insight into the mechanism of solvation in these ionic liquids, with the orientational contribution showing the extent to which the liquid structure needs to change to solvate an ion. For example, the lithium cation was calculated to have positive orientational entropy in both ionic liquids, due to the fact that a structure of higher density needed to be created around this small and positively charged ion. Different trends were observed in excess solvation energy (defined as the difference between the excess chemical potential and excess entropic contribution) between the two ionic liquids, with the Li^+ and Cl^- cations preferring to solvate in $[\text{C}_1\text{mim}]\text{Cl}$ and the Li^- and Cl^- anions in $[\text{C}_1\text{mim}][\text{PF}_6]$. The solubility of the neutral species, such as water, is already accounted for by solvation entropy,²⁹⁴ whereas for charged species the role of solute–solvent interactions becomes important. This work identified the dependence of ion solvation on the structure of ionic liquids, thus making the mechanism of solvation rather complex. Although the RISM model was not designed to produce very accurate absolute values for solvation thermodynamics of liquids, in general,³¹¹ relative trends for ionic liquids are usually in good agreement with experiment and allow for fast screening of various solutes in a number of ionic liquids.

A more robust way of applying the RISM model for ionic liquids was shown through the KS DFT/3D RISM methodology. In the work of Malvaldi et al.,²⁹⁷ the self-consistent field (SCF) procedure was applied to $[\text{C}_1\text{mim}]\text{Cl}$ in combination with the LDA functional and a double ζ quality basis set. Prior to the SCF procedure, the site–site correlation functions, $h_{\alpha\beta}(r)$ (see eq 36), and solvent susceptibility of the bulk solvent were obtained from dielectric consistent RISM theory developed by Perkins and Pettitt (DRISM),³¹² which was shown to provide a good description of the dielectric properties of ions in polar solvents. The rest of the parameters were taken from force fields of Lynden Bell et al.³⁰⁴ In the DRISM formulation, the atomic charges were obtained self-consistently for optimized geometries using the multipole charge derived analysis³¹³ as implemented in the ADF package,^{314,315} with self-consistency being achieved at either the dipole level or the quadrupole level. The cation and anion were geometry optimized in gas phase and the IL density was taken from Prado et al.³¹⁶ The radial distribution functions (RDFs) were again compared to previously published classical MD simulations of Youngs et al.³⁰⁹ Both types of self-consistency for atomic charges did not show significant differences in the bulk structure as analyzed through the RDFs. The main shortcoming of the KS DFT/3D RISM theory, as applied to $[\text{C}_1\text{mim}]\text{Cl}$, came from the inability to predict the importance of the hydrogen bonding between the chloride and the C2–H bond on the imidazolium cation as observed in Car–Parrinello MD simulations.³¹⁷ It was partially attributed to the use of the LDA functional that does not recover interactions in ionic liquids accurately. Although in the

current work a rigid model for the methyl groups was used, it was suggested that, with longer alkyl chain rotation, the change in atomic charges due to the flexibility of the alkyl chain on the cation, as well as LJ parameters, might have a more pronounced effect on the solvation structure near the melting point of ionic liquids.^{318,319} The predicted dipole moment of the bulk ionic liquids of 2.57 D was in very good agreement with that from MD simulations.³¹⁶ The same was observed for the Gibbs free energy of solvation, which was calculated to be approximately 298 kJ mol^{−1}. This number is in agreement with the previously determined COSMO RS range of 280 and 400 kJ mol^{−1} for ionic liquids.³²⁰

One of the exciting potential applications of the KS DFT/3D RISM methodology is the prediction of chemical reaction kinetics in ionic liquids and electronic and structural factors affecting reaction barriers in these complex media. It was applied to understanding the Diels–Alder reaction between cyclopentadiene and acrolein in $[\text{C}_6\text{mim}][\text{PF}_6]$.²⁹⁶ Apart from the same parameters as described above,²⁹⁷ geometry optimizations of reactants, adducts, and transition states were performed with the OLYP functional and a triple ζ quality basis set, with electronic energies being improved with the M062X functional. It was shown that ionic liquid ions did not change the structure of reactants and adducts but affected the geometry of all four possible transition states, causing the asynchronous addition to be preferred. In addition, the proton of the C2–H bond was shown not to affect the outcome of the calculated results, which was further confirmed through more sophisticated quantum mechanics/molecular mechanics calculations of Diels–Alder reactions in a series of imidazolium based ionic liquids by Acevedo et al.^{321,322}

Overall, the KS DFT/3D RISM theory shows promising results for the prediction of solvation thermodynamics of ionic liquids and can be especially recommended for fast screening of a number of ionic liquids to determine potential candidates for applications at hand. More sophisticated calculations (be it quantum chemical, large scale calculations or *ab initio* MD simulations) are still recommended, as the RISM methodology relies on classical force field parameters that might not be ideal for some ionic liquids. In addition, the lack of dependence of rotational flexibility of functional groups (e.g., long alkyl chains) on atomic charge represents a significant drawback when studying phase transitions in ionic liquids. The development of more reliable force field parameters, the inclusion of rotational flexibility of functional groups, and the use of more reliable DFT functionals will certainly lead to more accurate results by the KS DFT/3D RISM theory.

6. VOLUME-BASED THERMODYNAMICS

Volume Based Thermodynamics (VBT) is an empirical approach which relates many physical properties of a material to its molecular volume (V). The lattice potential energy (U_{POT}) of a solid is the enthalpy of formation of the crystal from infinitely separated ions. It can be determined by a VBT relationship determined by Glasser and Jenkins:^{323–325}

$$U_{\text{POT}} = 2I \left(\frac{\alpha}{\sqrt[3]{V_m}} + \beta \right) \quad (37)$$

here V_m is molecular volume and I is the ionic strength factor of the chemical formula calculated as $\frac{1}{2} \sum_i n_i z_i^2$, where n_i is a stoichiometric coefficient of ion i in the chemical formula and z_i

represents its charge. For inorganic salts of the MX type comprising monovalent ions M and X, I becomes equal to 1. For the MX inorganic salts, the α and β parameters were parametrized to be 117.3 kJ mol⁻¹ nm and 51.9 kJ mol⁻¹, respectively.³²⁴

The volume can be found computationally through the sum of volumes of individual ions. The lattice enthalpy (ΔH_{latt}) relates to the potential energy through the following expression:

$$\Delta H_{latt} = U_{POT} + \left[p \left(\frac{n_m}{2} - 2 \right) + q \left(\frac{n_x}{2} - 2 \right) \right] RT \quad (38)$$

where p and q are stoichiometric coefficients in the chemical formula of a salt and n_m and n_x are equal to 3 for monatomic ions, 5 for linear polyatomic ions, and 6 for polyatomic ions. Thus, for the inorganic salts and ionic liquids of the MX type, the formula becomes rather simple:

$$\Delta H_{latt} = U_{POT} + 2RT \quad (39)$$

Conversion to Gibbs free energy is simply a matter of substitution of the lattice enthalpy and approximated entropy into the second law of thermodynamics. Entropy can also be determined in a VBT fashion due to contributions from Jenkins and Glasser:^{326,327}

$$S = kV_m + c \quad (40)$$

where k and c are empirical constants that have been derived separately for ionic liquids³²⁶ to be 1246.5 J K⁻¹ mol⁻¹ nm⁻³ and 29.5 J K⁻¹ mol⁻¹, respectively. The VBT approach relies on the fact that both lattice enthalpy and entropy of organic materials increase with increasing alkyl chains, thus allowing for the use of estimates for these thermodynamic quantities for methylene linkers.³²⁸ For ionic liquids, a different behavior was observed with increasing alkyl chain length on the cation,³²⁶ with the melting point decreasing only up to a certain chain length. After this point, the dispersion forces begin to dominate the intermolecular interactions,^{329–331} leading to an increase in melting point and in some cases formation of liquid crystals.^{332,333}

6.1. Comment on the prediction of volumes of ions

Gutowski et al.^{299,300} showed that B3LYP could be reliably used to predict volumes of ions based on the electron density calculated with the 0.001 au contour.^{334,335} Compared with volumes taken from crystallographic data, predicted volumes are in very good agreement and are expected to produce errors within ± 20 kJ mol⁻¹ for lattice enthalpies. Both aug cc pVDZ and TZVP basis sets were successfully used for the prediction of ion volumes. In the VBT approach, the volume of the ionic liquid ion pair is used in eqs 37–40 and is determined as the sum of the cation and anion volumes.

6.2. Lattice enthalpies

Gutowski et al.³³⁴ used eqs 38 and 39 to predict the lattice enthalpies of a series of protonated and methylated imidazolium ionic liquids substituted with nitro, cyano, and methyl groups in the ring and coupled with halides, monohydrogen sulfate, methylhydrogen sulfate, triflate, and tosylate. Mono, di, and trisubstituted ionic liquids were used for the NO₂ and CN functional groups, with tetra and penta substitutions being used for the methyl group. Since the molecular volume of ions did not vary significantly, the predicted lattice enthalpies had a narrow spread of data, within

13 kJ mol⁻¹ on average, across cations coupled with the same anion. A slightly wider distribution was observed across anions: up to 84 kJ mol⁻¹. The predicted lattice enthalpies were subsequently used to predict the Gibbs free energy of the ionic liquid formation from a solid imidazole and a liquid RX by means of a Born–Haber cycle. The entropic contributions were calculated using the Glasser approach described in eq 40, with the k and c parameters being taken from the organic database for the RX species.³²⁶ For several of the cyano and nitro imidazolium ionic liquids, the Gibbs free energy was negative, indicating the potential for successful synthesis of these ionic liquids, which was confirmed experimentally (for more detail see ref 334). It has to be pointed out that none of these reactions had exothermic reaction enthalpy, further reinforcing the importance of inclusion of phase transition melting and evaporation into the thermodynamic calculation.

Knowledge of the lattice energy of an ionic liquid and heats of formation of individual ions, $\Delta H_f^0(\text{cation})$ and $\Delta H_f^0(\text{anion})$, that form the ionic liquid allows for the back calculation of the ionic liquid heat of formation, $\Delta H_f^0(\text{IL})$, as shown in another work of Gutowski et al.:³³⁵

$$\Delta H_f^0(\text{IL}) = -\Delta H_{latt} + \Delta H_f^0(\text{cation}) + \Delta H_f^0(\text{anion}) \quad (41)$$

The heats of formation of ionic liquids can also be reliably calculated using isodesmic reactions, as has been confirmed in a number of publications by Emel'yanenko, Verevkin, and Henitz.^{336–338} Gutowski et al.³³⁴ used the MP2/CBS level of theory to predict $\Delta H_f^0(\text{IL})$, with the temperature correction being calculated at the optimization level of theory, B3LYP/TZVP. The CBS convergence was achieved by extrapolating the aug cc pVTZ and aug cc pVQZ basis sets. The comparison between the quantum chemical heats of formation and those from eq 41 revealed that the VBT approach fell rather short of the accurate prediction of the lattice enthalpies, with errors averaging 400 kJ mol⁻¹ for picrate based ionic liquids. Nitrate based ionic liquids showed the lowest errors. It has to be pointed out that again the lattice enthalpies formed a very narrow distribution of 20 kJ mol⁻¹ on average among the 46 salts studied. This is in contrast with the quantum chemical heats of formation ranging from -56.6 to 172.0 kJ mol⁻¹. It was observed that the errors in U_{POT} fluctuated across the cation type, and in order to improve the performance of the VBT approach, 23 ionic liquids were subjected to a linear regression analysis, resulting in a new set of the α and β parameters. The errors were drastically reduced to <15 kJ mol⁻¹ on average, indicating that specific parameters were required for each class of ionic liquids. The major limitation of the VBT approach lies in the assumption that lattice energy can be predicted based on the molecular volumes of individual ions. Dispersion interactions have been shown to be very important,^{98,111} varying for each particular cation–anion combination, and therefore, coupled with the fact that volumes of ionic liquids do not vary significantly, omission of these forces in the VBT approach will undoubtedly result in poor correlation.

6.3. Melting points

The Gibbs solvation energies (ΔG_{solv}) and Gibbs lattice energy (ΔG_{latt}) can be used to determine the ΔG_{fus} according to the Born–Fajans–Haber cycle as follows:

$$\Delta G_{fus} = \Delta G_{latt} - \Delta G_{solv} \quad (42)$$

The melting point can be subsequently found by calculating ΔG_{fus} over a range of temperatures by extrapolating it to 0 kJ mol⁻¹. As ΔG_{sol} is temperature dependent, it is important to include a temperature correction, which can be determined by the difference in lattice energies at the new and reference temperatures. The extrapolation also allows us to determine factors affecting melting of ionic materials. Krossing et al.³²⁰ used a Born–Fajans–Haber cycle to indirectly calculate the Gibbs free energy of fusion, ΔG_{fus} , from which melting points were extracted by extrapolating ΔG_{fus} to zero. By the same token, a negative Gibbs free energy of fusion would indicate the presence of a particular ionic liquid in liquid state at room temperature. Ions were optimized with BP86/SV(P),^{339,340} and the COSMO solvation model and solvation energies were calculated for isolated ions. The ΔG_{sol} of the ion pair was found as the sum of solvation energies of the cation and the anion. The solvation free energy was taken to be the difference of the species between the COSMO solvation model and the gas phase. The predicted melting points were in good agreement with experimental results, although with a relatively low sensitivity of 4 kJ mol⁻¹ for each 1 K in temperature. This suggests that ΔG_{fus} should be predicted below chemical accuracy in order to reduce errors in predicted melting points. The distribution of melting points in the study was rather narrow: between -19 and 23 °C. The model in this form could not be successfully applied to studying a wide range of ionic liquids, with additional modifications needed to improve the sensitivity of prediction. For more details, see the section on COSMO RS applications.

7. QUANTUM CHEMICAL CALCULATIONS OF SINGLE ION PAIRS

Early works attempted to correlate thermodynamic, transport, and spectroscopic properties of ionic liquids with interaction energies of single ion pairs. These represented the first steps in identifying the importance of dispersion interactions even between cations and anions. No direct correlations were found between the ion pair interaction energy and experimentally measured physical properties, such as melting point, conductivity, and viscosity, thus providing further insight into how the inclusion of many body effects in ionic liquids is critical to predicting their properties.

7.1. Melting points and transport properties

Turner et al.³⁴¹ attempted the correlation of the interaction energy of single ion pairs of $[C_n\text{mim}][X]$ ionic liquids and their melting point, where $n = 1-4$ and $X = F^-$, Cl^- , Br^- , and I^- . Geometry optimizations of ion pairs were performed in the gas phase at the HF and MP2 levels of theory using Pople type basis sets: 3 21G, 6 31G*, and 6 31+G*. The interaction energies were calculated by taking the difference between the ion pair electronic energy and the sum of electronic energies of the cation and anion, with no counterpoise correction being taken into account. In the case of ion pair optimizations of $[C_2\text{mim}]F$, the resulting structures strongly depended on the level of theory, with the HF level favoring the hydrogen abstraction by the fluoride from the ring and MP2 predicting the addition of the fluoride to the ring. Only one out of five possible ion pair structures of the anion interacting with the imidazolium ring was located at the MP2 level of theory. This outcome may also be a result of the use of a gas phase setup with relatively small basis sets. HF is less affected by the counterpoise (CP) correction than MP2, and therefore, it is

rather difficult to judge the effect of various levels and basis sets on interaction energy. Therefore, a quantitative comparison between the HF and MP2 levels of theory cannot be achieved. It has to be pointed out that the relative stability of interionic complexes is best to be assessed through interaction energies and not total electronic energies, as was achieved in this work. The comparison of interaction energies was only made for the ion pair configuration, in which the anion interacted above the imidazolium ring. In contrast to total electronic energies, interaction energies vary *only slightly* (i.e., within the error of the calculation) from ethyl through butyl at the same level of theory. No general trend was found between interaction energies and melting points for all ionic liquids under study. Linear correlations were achieved in the series of $[C_n\text{mim}]Cl$, $[C_n\text{mim}]I$, $[C_2\text{mim}]X$, and $[C_4\text{mim}]X$ (with $n = 2$ and 4 and $X = Cl^-$, Br^- , and I^-). The $C_3\text{mim}^+$ cation produced the lowest melting points for chlorides and bromides. It was suggested that a better packing of cations with an even number of carbons in the alkyl chain must affect their melting points to a greater extent.

Early work attempted to correlate geometric factors of ions to their physical properties. For example, Li et al.³⁴² defined the charge lever moment (CLM) of an ionic liquid ion with the view of correlating the predicted moments with the shear viscosity of various ILs. The CLM contains information on the distribution of atomic charge and mass of the ion by considering its moment of inertia. The approximation assumes that an ion is a rigid body and thus is better suited to those that are less flexible and have fewer conformations. Since the ionic rotation proceeds via a diffusive mechanism, the strength of interionic interactions slows down the rotation and hence prevents fast “hopping” of ions among accessible conformations on the potential energy surface. From the classical transition state theory, this is reflected in larger barriers that need to be overcome for the “hopping” to occur. Therefore, it is expected that ions with larger CLM values will sample the conformational space more rapidly than those with smaller values. Structure calculations were performed using the B3LYP/6 31G(d,p) level of theory, and atomic charges were calculated with the CHELPG scheme. Since the lever value depends on the shortest vector between the center of charge and the center of mass, different conformations of longer alkyl chains may affect CLM values up to 50% in $C_4\text{mim}^+$ and 40% in $C_4\text{mpyr}^+$. In this work, in the case of long alkyl chains, the maximum CLM value was used for correlations. The CLM approach was applied to a series of $[C_n\text{mim}][NTf_2]$ ionic liquids, including those methylated in the C2 position of the ring and branched alkyl chains. Although a good linear correlation was obtained, some obvious deviations were also encountered for branched alkyl chains and were attributed to the loss of rotational flexibility for branched chains. Similar anomalies were observed for longer alkyl chained ammonium cations in a series of NTf_2^- based ionic liquids coupled with ammonium, pyrrolidinium, and piperidinium cations. The main limitations of the approach are the disregard for dispersion interactions between alkyl chains as well as flexibility of the alkyl chains in the lever moment. It appears that the CLM approach can be used to retrospectively shed light on the role of alkyl chains in viscosity trends for known ionic liquids.

Early attempts¹¹¹ to predict melting points of ionic liquids across anions based on ion pair interaction energies were not successful, as no clear trends could be achieved for imidazolium cations coupled with SCN^- , BF_4^- , $AlCl_4^-$, Cl^- , and $N(CN)_2^-$.

The information on the magnitude of ion pair interactions and types of possible interaction modes can be used to rationalize experimental data. For example, in the work of Hunt et al.,³⁴³ the decreasing binding energy in the series of $[\text{C}_4\text{mim}]\text{Cl}$, $[\text{C}_4\text{mim}][\text{BF}_4]$, and $[\text{C}_4\text{mim}][\text{NTf}_2]$ ionic liquids, from -376 kJ mol^{-1} to -315 kJ mol^{-1} , was related to decreasing viscosity and decreasing melting point. In this anionic series, the number of interaction sites increases from 1 to at least 5 from Cl^- to NTf_2^- and so does the number of energetically stable ion pair configurations as shown by Tsuzuki et al.,⁹⁶ thus potentially resulting in a flattening of the potential energy surface. As a consequence, a free energy profile would consist of local minima (i.e., ion pair configurations) connected through low energy barriers that can be accessible at room temperature, allowing ions to be more mobile in the ionic environment, thus resulting in lower viscosity and lower melting point. This phenomenon refers to the energy landscape paradigm introduced by Goldstein.³⁴⁴ This argument was successfully applied by the Kirchner and Izgorodina groups to shed light on the effect of methylation at the C2 position of the imidazolium ring on the thermodynamics and transport properties of ionic liquids.^{112,345} Prior to these studies, it had been observed that a small chemical structure modification, such as methylation at the C2 position in the imidazolium ring, could lead to a drastically increased viscosity^{345–352} and melting point^{346,351,353–357} in imidazolium based ionic liquids regardless of the counteranion. Earlier, Tsuzuki³⁵⁸ identified that the rotational barrier of the ethyl group in the 1 ethyl 2,3, dimethylimidazolium cation increased to 20 kJ mol^{-1} from as low as 4.6 kJ mol^{-1} in the nonmethylated analogue of the cation (as calculated with MP2/cc pVTZ on MP2/6 311G* optimized geometries). In 2007, Hunt³⁵⁹ observed no differences in binding energies of ion pairs of nonmethylated and C2 methylated chloride based ionic liquids, suggesting that entropy may have played an important role in the observed increase in both melting point and viscosity in methylated ILs. In 2008, Zahn et al.¹¹² performed calculations of the potential energy surface of ion pairs, $[\text{C}_1\text{mim}]\text{Cl}$ and $[\text{C}_1\text{dmim}]\text{Cl}$, by rotating the chloride ion from above the plane configuration to below the plane configuration. All geometries were optimized at the MP2/cc pVTZ level of theory, and electronic energies were improved with SCS MP2/aug cc pVTZ. Low barriers as small as 10 kJ mol^{-1} were obtained for the C_1mim^+ cation, whereas the barrier increased to 40 kJ mol^{-1} for the cation in the C2 methylated position. The increase in the barrier for methylated imidazolium ionic liquids explains their higher melting points due to significant energy requirements to sustain the anion mobility. In the work of Izgorodina et al.,³⁴⁵ the potential energy surfaces were calculated at the MP2/aug cc pVDZ level of theory for ion pairs of $[\text{C}_3\text{mim}]\text{I}$ and $[\text{C}_3\text{dmim}]\text{I}$ to explain the increased viscosity of the methylated imidazolium ionic liquids by 5 fold coupled with the iodide, NTf_2^- , BF_4^- , and PF_6^- anions (see Figure 10). In addition to the anion, moving from above the plane configuration to below the plane configuration, the anion was also allowed to move across the plane of the C2–H bond. In the former scenario, the barrier increased from 15 to 43 kJ mol^{-1} by replacing the C_1mim^+ cation with the methylated version, whereas when the anion moves in the plane of the C2–H bond, the barrier was found to be well within the kinetic energy range for the C_1mim^+ cation and increased to as much as 53 kJ mol^{-1} for the C_1dmim^+ cation. These numbers indicate that the anion mobility requires a significant amount of energy that is not accessible at room

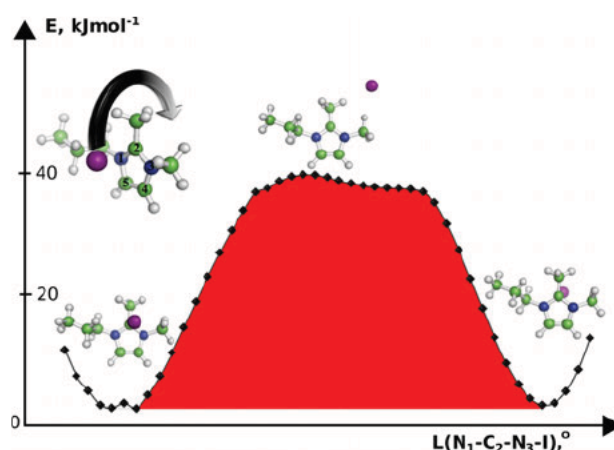


Figure 10. Relaxed scan of the potential energy surface of the iodide anion moving from above to below the C_2dmim^+ ring, optimized with respect to the N1 C2 N3 I dihedral angle, L , at the MP2/aug-cc-pVDZ level of theory. Adapted from the TOC graphic of *J. Phys. Chem. B* 2011, 115, 14688–14697. Copyright 2011 American Chemical Society.

temperature. This conclusion is in good agreement with the classical MD study by Zhang and Maginn³⁶⁰ that predicted lower mobility of ions in C2 methylated imidazolium ionic liquids (such as C_2dmim^+ and C_4dmim^+) compared to nonmethylated (C_2mim^+ and C_4mim^+) ones. In addition, larger activation barriers (by 7 kJ mol^{-1} on average) were observed for the dissociation of ion pairs in the methylated analogues. Both studies represented the first examples of how interaction energies and potential energy surfaces of ionic liquids can be used to explain trends in thermodynamics and transport properties.

No straightforward correlations were found between the cation–anion binding energy and transport properties such as self diffusion coefficient, conductivity, and heat of vaporization.^{361,362} The Izgorodina group^{98,117} proposed a different approach to correlation of binding/interaction energies of ionic liquid ion pairs and their thermodynamic (e.g., melting point) and transport (e.g., viscosity and conductivity) properties. Based on the second law of thermodynamics at equilibrium ($\Delta G = \Delta H - T\Delta S = 0$), it was postulated that, at the point of melting, the total interaction energy should correlate with the enthalpy of fusion, while the dispersion component of the interaction energy should correlate with the entropy of fusion. This hypothesis was based on the fact that during the melting process ions in the corners of the lattice obtain enough kinetic energy to break the high order symmetry, thus transforming the solid into a liquid. The melting is usually accompanied by increased volume and hence increased cation–anion distance. The latter was demonstrated in *ab initio* molecular dynamics simulations for an imidazolium ionic liquid³⁶³ (for more detail, see section 8). The entropy of fusion arises from increased randomization of the positions and motions of ions compared to their original crystalline state, thus resulting in an increase of disorder. Since dispersion interactions decay very fast with increasing distance between ions ($\sim R^{-6}$), it was thus hypothesized that the strength of these forces should be proportional to the increased degree of disorder and hence the entropy of fusion. Contrary to this behavior, electrostatic forces change linearly with cation–anion distance and are not expected to change significantly upon melting, thus represent

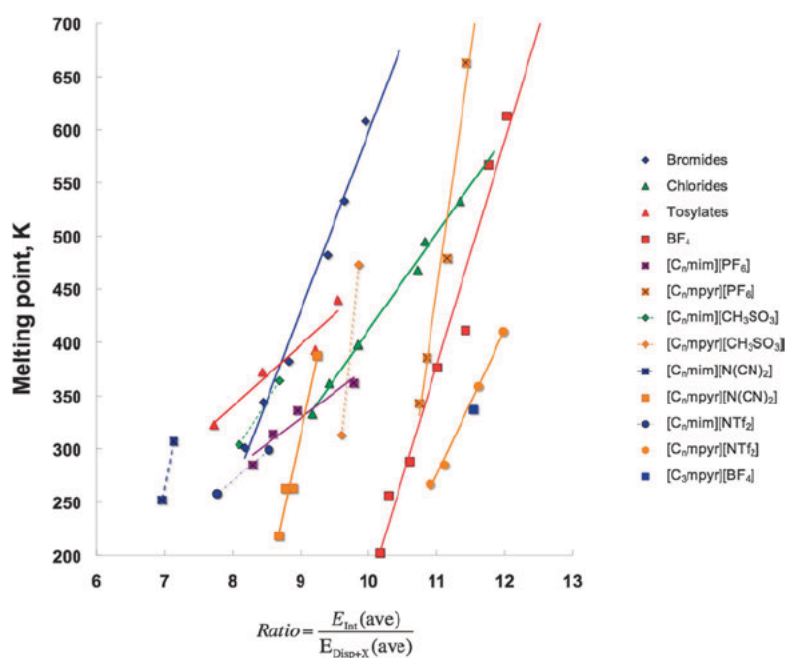


Figure 11. Correlation between experimental melting points (in K) and the ratio of the average interaction energy, $E_{\text{int}}(\text{ave})$, to the average dispersion component, $E_{\text{Disp}+\chi}(\text{ave})$. For chlorides, bromides, tosylates, and tetrafluoroborates, both imidazolium- and pyrrolidinium-type cations were considered in the same correlation. Reproduced from ref 98 by permission of the PCCP Owner Societies.

ing the enthalpy of fusion. The evidence of this behavior was observed in classical MD simulations of Fakhraee and Gholami³⁶⁴ performed for imidazolium ionic liquids with ester functionalized alkyl chains coupled with Br^- , NO_3^- , NTf_2^- , PF_6^- , and BF_4^- anions. It was shown that dispersion forces decreased in the range of 10 to almost 40 kJ mol^{-1} when going from room temperature to 550 K, which corresponds to a nearly 39% change on the relative scale. Contrary to this observation, electrostatic forces decreased consistently by 20 kJ mol^{-1} for all the ILs studied, which corresponded to <10% on average. Thus, the ratio of interaction energy to its dispersion component was suggested to correlate with melting point, T_m , of ionic liquids:

$$T_m = \frac{\Delta H_{\text{fus}}}{\Delta S_{\text{fus}}} \approx \frac{E_{\text{INT}}}{E_{\text{Disp}}} \quad (43)$$

It was also hypothesized that transport properties such as conductivity and viscosity should correlate with the dispersion component due to the fact that an ion's mobility is more likely to be affected by the strength of dispersion forces. The ratio in eq 43 was tested on a series of C_nmim and C_nmpyr based ionic liquid ion pairs ($n = 1-4$), with each cation–anion combination being represented by a few energetically favorable configurations as described above (see section 1). The Boltzmann distribution of these configurations was included to calculate average total interaction energy and average dispersion components for each cation–anion combination. It has to be noted that since single ion pairs were used as models for ILs in this approach, only ionic liquids whose melting points still decreased with increasing alkyl chain length were considered in eq 43. Overall, excellent correlations were established for spherical like anions such as chloride, bromide, and tetrafluoroborates, and these were attributed to the strongest electrostatic and induction contributions in their

ionic liquids (see Figure 11). For the rest of the cation–anion combinations, only individual correlations in the anionic series and a particular class of cation were observed, with slopes varying significantly depending on the anion/cation type. This finding strongly suggested that the structural arrangement of ionic liquids, the nature of both cation and anion, and the interplay of intermolecular forces governed thermodynamic properties in ionic liquids. Due to the lack of experimental data, only conductivity values were correlated with the dispersion component. The conductivity of C_nmpyr based ILs was surprisingly found to be insensitive to the dispersion component, where C_nmim based ILs produced excellent correlations for BF_4^- , $\text{N}(\text{CN})_2^-$, and NTf_2^- anions. It appears that entropic effects must play a more important role in pyrrolidinium ionic liquids than in imidazolium ILs. This study represented a seminal work identifying the importance of the interplay between both electrostatic and dispersion forces in ionic liquids in the prediction of their thermodynamic and transport properties. In the light of this work, it is highly recommended that generalized approaches to studying the energetics of ionic liquids be carefully tested on a series of ionic liquids for reliable predictions.

7.2. Heats of formation

Emel'yanenko, Verevkin, and Heintz³³⁸ showed how a series of isodesmic reactions could be used to predict the heats of formation of ionic liquids in the gas phase, $\Delta_f H_m^0(\text{g})$, using the methodology originally proposed by Raghavachari et al.³⁶⁵ In the case of $[\text{C}_4\text{mim}][\text{N}(\text{CN})_2]$, a series of three different isodesmic reactions were considered incorporating molecular species (such as HCN , CH_4 , NH_3 , etc.) whose heats of formation are well known.³⁶⁶ The reaction enthalpies of these isodesmic reactions were calculated using two quantum chemical methods, G3MP2, a composite method of the G3 theory, and B3LYP/6-31+G(d), and the $\Delta_f H_m^0(\text{g})$ values of $[\text{C}_4\text{mim}][\text{N}(\text{CN})_2]$ were extracted. The lowest energy

geometry of the ion pair was determined through geometry optimizations of 30 different structures at the B3LYP/6-31+G(d) level of theory accounting for the flexible rotation of the alkyl chain. This lowest geometry was used for the subsequent calculations of the heats of formation. The B3LYP functional produced heats of formation that varied by almost 30 kJ mol⁻¹ depending on the isodesmic reaction, revealing its inherent incapability of capturing finer differences in the chemical structure. On the other hand, G3MP2 produced very similar heats of formation that were within 5 kJ mol⁻¹ of each other as well as the experimental value. Compared to B3LYP, G3MP2 is a more reliable method for the prediction of thermodynamics properties of chemical reactions due to its composite nature that accounts for electron correlation effects at high correlated levels of theory such as QCISD. The Gibbs free energies of the [C₄mim][N(CN)₂] formation from individual cations and anions were also predicted using the G3MP2 method and were found to be 307.4 and 293.7 kJ mol⁻¹ at two different temperatures, 298 and 423 K, respectively. Although these numbers fall short of the experimental value of 363.4 kJ mol⁻¹ measured at 298 K, they were among the first indication that the ion pairing was energetically too strong to dissociate (dissociation constant, K_p , <10⁻³⁴), thus suggesting that ionic liquids are more likely to exist as ion pairs in the gas phase. The described methodology was confirmed to work for the prediction of the $\Delta_f H_m^0(g)$ of 1 ethyl 3-methylimidazolium thiocyanate.³⁶⁷ The most stable confirmation of the ion pair, in which the anion interacts above the C2–H bond of the imidazolium ring, was used in G3MP2 calculations. An excellent agreement of <2 kJ mol⁻¹ between the predicted and experimental gaseous heats of formation was observed, further highlighting the robustness of the G3MP2 method for the calculation of heats of formation. Low errors also indicate that ionic liquids are thermodynamically more likely to exist as single ion pairs.

The molar enthalpy of formation of any compound in the liquid state, $\Delta_f H_m^0(l)$, is related to the molar heat of formation in the gas phase, $\Delta_f H_m^0(g)$, through the enthalpy of vaporization, $\Delta_f^v H(298\text{ K})$:

$$\Delta_f H_m^0(g) = \Delta_f H_m^0(l) + \Delta_f^v H(298\text{ K}) \quad (44)$$

$\Delta_f H_m^0(l)$ can be measured using high precision combustion calorimetry. Using the G3MP2 based methodology for the prediction of $\Delta_f H_m^0(g)$ as established by Emel'yanenko, Verevkin, and Heintz,³³⁸ the enthalpy of vaporization of an ionic liquid can be easily estimated from eq 44. This approach has been used to predict the enthalpy of vaporization of a number of ionic liquids, [C_nmim][NO₃] (n = 2 and 4),³³⁶ 1-methylimidazolium nitrate,³³⁷ and 1-ethanol-3-methylimidazolium dicyanamide.³⁶⁸

The CBS-QB3 method was also used and showed slightly superior performance when compared to G3MP2 for the prediction of enthalpy of formation for [C₂mim][N(CN)₂] and [C₄mim][N(CN)₂], thus further highlighting that G3MP2 is a reliable method for the prediction of the gaseous heat of formation.³⁶⁹ Although isodesmic reactions are commonly used in the prediction of heats of formation, a certain degree of deviation is expected depending on which bonds are conserved in these reactions. For example, in the case of monosubstituted tetrazolium cations, the difference from 12 up to 52 kJ mol⁻¹ was observed in the predicted heats of formation using four types of isodesmic reactions in which the substituent in the

tetrazole ring was moved around four different nitrogen centers.³⁷⁰ Instead of isodesmic reactions, atomization reactions for the formation of the ion pair can be used to extract the enthalpy of formation. There is a significant advantage of using atomization energies, as no additional thermodynamic data are required as in the case of isodesmic reactions, thus resulting in more reliable data. Due to the bond cleavage accompanying atomization reactions, these are more likely to result in larger errors. In the case of nitrate based ionic liquids, the enthalpy of formation is underestimated within 7 kJ mol⁻¹ when atomization energies are used,^{336,337} whereas, for NTf₂⁻ based ionic liquids, the enthalpy is overestimated by the same amount.³⁶⁹ Verevkin et al.³⁷¹ recognized the potential in correcting atomization energies to improve the performance of the CBS-QB3 method. The predicted heats of formation of [C_nmim]Br (n = 1–8) in the gas phase were linearly fitted against the experimental values with the correlation coefficient of 0.998. Another solution is to use chemical reactions whose reaction energies can be predicted with high accuracy. For example, the reaction of pyridine interacted with chlorinated butane in the gas phase was used to successfully predict the gaseous enthalpy of formation of butyl pyridinium chloride, based on the CBS-QB3 method.³⁷²

In the study of Verevkin et al.,³⁶⁹ it was established that the enthalpy of vaporization changed linearly in the series of [C_nmim][NTf₂] with increasing alkyl chain from n = 2–8. A nearly linear relation was also observed for the G3MP2 predicted heats of formation in the series of ammonium based nitrates, [NR₄][NO₃], with R varying from methyl to butyl through ethyl.³⁷³ Similar differences were also observed in the predicted gaseous heats of formation for C₂mim and C₄mim based ionic liquids coupled with varying anions such as BF₄⁻, PF₆⁻, NO₃⁻, Cl⁻, NTf₂⁻, and N(CN)₂⁻. This renders the application of the group additivity method³⁷⁴ reliable for the prediction of enthalpies of vaporization and heats of formation for any length of alkyl chain as long as the values of the parental system with the shortest chain are known. The additivity parameters are slightly different for ionic liquids compared to those of organic compounds.³⁶⁹ The group additivity method was successfully applied to the prediction of enthalpy of formation of 1-ethanol-3-methylimidazolium dicyanamide,³⁶⁸ with an error of 13 kJ mol⁻¹. Later Verevkin et al.³⁷⁵ successfully applied the established methodology^{338,369} to predict enthalpies of formation and vaporization of the [C₄mim]Cl ionic liquid using additional data from DSC measurements.

7.3. Heats of vaporization

Vaporization is a physical process of a compound undergoing the phase transition in which the liquid–vapor equilibrium is achieved. In the case of neutral compounds, individual molecules amass enough kinetic energy to break free from the molecular interactions in the bulk. In the case of ionic liquids, the vaporization process is hindered by the fact that individual cations and anions are not stable on their own in the gas phase as opposed to neutral species such as ion pairs which are significantly favored thermodynamically. This is reflected in much stronger interaction energies in single ion pairs of ionic liquids in the range 300–450 kJ mol⁻¹ compared to organic molecules of similar size.⁹⁸ This suggests that larger amounts of kinetic energy are required to evaporate them, and it is not surprising that ionic liquids are known to possess low volatility at ambient temperatures and decompose at much higher

temperatures compared to traditional organic based electrolytes. It has been confirmed experimentally that ionic liquids evaporate predominantly as ion pairs,^{376–378} with heats of vaporization³⁶⁹ falling in the range 135–165 kJ mol^{−1}.

An early attempt to establish whether an archetypical ionic liquid such as [C₄mim][PF₆] evaporated as an ion pair was achieved by predicting its thermodynamic properties, such as entropy, S^0 , heat capacity, C_p , and $-(G^0(T) - H^0(0\text{ K}))/T$ assuming that either contact ion pairs or single cations and anions were present in the gas phase.³⁷⁹ Geometry optimizations and frequency calculations were performed at the HF/6 31G(d) level of theory, and electronic energies were improved with MP2/6 31+G(d). The entropy was evaluated using the vibrational and rotational partition functions based on the standard physical chemistry formulas,³⁸⁰ a commonly used approach. Experimentally, it was established that this ionic liquid decomposes at 473 K. The dissociation constant of the ion pair was estimated to be 7×10^{-31} at 500 K, which was suggested to be in agreement with the experientially estimated value of $<10^{-11}$ at 500 K. Therefore, it was concluded that the ion pair represented the ideal gas state of [C₄mim][PF₆]. Significant differences³⁸¹ of up to 90% were obtained between those predicted with B3LYP/6 311++G(d,p) and the measured molar heat capacities of [C_nmim][NTf₂] using the same methodology, with n ranging from 1 to 18. It was hypothesized that an approximation beyond hindered rotor should be applied to recover the rotational energy contribution. Recently it has also been shown that long alkyl chains could indeed easily change their configuration from linear to *gauche* and *trans* depending on the position of the halide anion without an applicable change to ion pair interaction energy,³⁸² thus further supporting the proposed hypothesis.

Hess's law allows us to use a series of isodesmic reactions containing species with known heats of formation to extract the heat of formation of a compound of interest. In addition, isodesmic reactions preserve the number of formally identical bonds on both sides of the equation, thus reducing the error in the estimated heat of formation. This strategy was applied to study derivatives of triazolium cations that contain three nitrogen centers compared to two in imidazolium based cations.³⁸³ MP2/6 311++G(d,p) was used to optimize the geometries of ions and ion pairs. For other molecules in the isodesmic reactions, the data were taken from the G2 data set. The theoretical heats of formation were rather large, ranging between 1121 and 1701.2 kJ mol^{−1} for monosubstituted cations, indicating that these cations may harbor a great amount of energy when synthesized. The advantage of quantum chemical methods is their ability to predict reaction barriers. In this work the 1,2 monosubstituted and 1,3 monosubstituted cations were subjected to a decomposition process by forming the corresponding azidinium cation and releasing the N₂ molecule. Due to the multireference character of the nitrogen molecule and hence transition states, the completely renormalized CCSD(T) method, CR CCSD(T), was used to predict both activation barriers and reaction energies. 1,2 monosubstituted cations were established to follow a two step process, whereas 1,3 monosubstituted cations needed only one step. The barriers of the first transition state for both types of cations were found to fall between 80 and 120 kJ mol^{−1}, whereas the reaction energies for the 1,2 monosubstituted cations were found to release a much larger amount of energy, by 91 kJ mol^{−1} on average, thus making them promising materials for hypergolic applications. On average, the MP2

method underperformed the CR CCSD(T) method by 19 kJ mol^{−1} for the reaction energies and 9 kJ mol^{−1} for activation energies, further highlighting the importance of the method selection for studying chemical reactions involving ionic liquid ions.

In a study of Li et al.,³⁸⁴ 32 ion pairs were considered consisting of a series of conjugated cations of the amino acids protonated at the nitrogen center, such as alanine and glycine, and routinely used anions, such as tetrafluoroborate, nitrate and chloride. Interaction energies of the clusters were calculated at the B3LYP/6 311++G(d,p) level of theory and CP corrected. The only qualitative relationship was found between the interaction energy and experimental melting point. Amino acids such as serine and threonine contain an additional OH group each that can engage in intramolecular hydrogen bonding with the protonated NH₃⁺ group, thus further strengthening the overall intermolecular interaction. A correction of 30 kJ mol^{−1} was applied to ionic liquids, whose carboxyl group did not participate in intramolecular hydrogen bonds. This seemed to improve the overall correlation between interaction energy and melting point, making it quantitative with the R^2 value of 0.79 and the average deviation of 30 K for predicted melting points. Ionic liquids coupled with chloride and nitrate anions still formed a number of outliers. It has to be pointed out that the majority of the optimized ion pairs incorporating the chloride, nitrate, and trifluoroacetate anions represented complexes between two neutral species. It is not surprising that in the absence of a stabilizing medium (e.g., a continuum polarizable model or explicit ionic liquid ions) the gas phase tends to favor neutral species, thus forcing the back transfer of the proton from the protonated base to the deprotonated acid. A similar situation was observed in energetic protic ionic liquids based on triazolium cations.³⁸³ The formation of neutral complexes between the acid and the base was favored over ionic ones between protonated base and deprotonated acid for up to 144 kJ mol^{−1}, even for strongly basic anions such as ClO₄[−] and NO₃[−]. Both studies highlighted the importance of the stabilizing polarizable medium in the form of the Conductor like Polarizable Continuum Model³⁸⁵ and the need for larger sized clusters to reliably account for proton transfer in protic ionic liquids.³⁸⁶

7.4. Spectroscopic properties

Wave function and electron density based methods have become invaluable in analyzing the spectral features of ionic liquids. Ion pair calculations of ionic liquids have been widely employed to assign their vibrational bands in IR and Raman spectra.³⁸⁷ DFT calculations tend to overestimate stretching vibrational frequencies, and it is common to apply scaling factors of <1.0 to improve the prediction of IR and Raman spectra. The fingerprint region is usually less affected by the type of DFT functional used, and predicted bands from this region compare well with experimentally measured spectra. It has to be pointed out that theoretical low to medium frequency vibrational modes ($<2000\text{ cm}^{-1}$) tend to be rather mixed, especially for an ion pair, due to the presence of intermolecular interactions affecting energy levels of specific vibrations for individual ions. This slightly complicates the assignment of experimental bands and leads to broad bands.³⁸⁷ Unless stated otherwise, the results on vibrational frequencies refer to the B3LYP functional. Scaling factors are not specifically discussed further in the text, as these are particularly sensitive to the system size with respect to the number of ion pairs, the level of

theory, and the basis set used³⁸⁸ and need to be determined specifically for each theory basis set combination, as has been demonstrated before for conformers of the isolated C_2mim^+ cation,³⁸⁹ single ion pairs of $[C_nmim][BF_4]$ (where $n = 2, 3$, and 4),³⁹⁰ and clusters of protic ionic liquids.³⁸⁶

One of the typical features in IR spectra of ionic liquids is the presence of a number of peaks in the low frequency (i.e., tetrahertz) region which is attributed to cation–anion interactions.^{387,391–395} A distinct peak observed between 20 and 200 cm^{-1} , depending on the anion type and methyl substitution of the imidazolium ring, correlated well with the B3LYP/6 31+G* binding energies of corresponding ion pairs, in which the anion interacted with the C2–H bond.³⁹² The prediction of cation–anion peaks can only be achieved by means of ion pair and/or multiscale calculations that properly describe interionic interactions in the bulk of ionic liquids.

Vibrational frequency calculations on individual ions allow for the analysis of ion conformers that are more likely to be present in the liquid phase in both IR and Raman spectra.^{110,359,396–406} For example, the studies of Berg et al.^{407,408} tested various conformers of the NTf_2^- anion and the C_4mim^+ and C_6mim^+ cations as calculated with either B3LYP or MP2. Speciation mechanisms of small metal ions such as Li^+ and Al^{3+} have been investigated by studying complexes between these metal cations and ionic liquid anions and comparing their predicted spectra with experimental ones to identify thermodynamically stable species in mixtures with ionic liquids.^{409–412} B3LYP calculations have been helpful in identifying the dissolution mechanism of water,^{413–415} polyols,⁴¹⁶ and *o*-chloronitrobenzene⁴¹⁷ in imidazolium ionic liquids by studying how the predicted spectra change upon inclusion of solvated molecules in the subsequent ion pair calculations.

Many studies have revealed that individual ions were not considered a reliable model for studying particular vibrations, such as those associated with cation–anion interactions^{392,418} and stretching vibrations such as the C2–H stretch in imidazolium based ionic liquids.^{419,420} In the work of Cha et al.,⁴¹⁹ the position of this vibration in the $[C_4mim]X$ ionic liquids ($X = Cl^-, Br^-,$ and BF_4^-) was affected by a few factors, including the type of anion and the use of the CPCM solvation approach, with water as solvent in the calculation. A more diffuse anion such as BF_4^- showed the least shift in the stretch when compared with the predicted spectrum of the isolated cation. Surprisingly, the CPCM solvation approach produced almost identical stretches for the C2–H and C4,5–H bonds in all three ionic liquids studied. This observation suggests that the full dissociation of ion pairs is expected in water, which was in agreement with experimental data. Very similar findings were also observed in the works of Katsyuba et al.⁴²¹ for an extensive series of imidazolium ionic liquids and Holomb et al.⁴⁰⁰ for $[C_4mim][BF_4]$. A detailed analysis of B3LYP/6 31G* generated vibrational frequencies of ion pairs of imidazolium ionic liquids was published by Katsyuba et al.⁴²¹ Multiple ion pair configurations and varying alkyl chains (including ethyl, propyl, butyl, and allyl) were considered in the study coupled with the Cl^-, Br^-, BF_4^- , and PF_6^- anions. The spectral features of individual ion pairs were linked to the position of the anion around the imidazolium ring. Broadening of the bands, associated with stretching of the B–F, P–F, and C–H bonds, was attributed to the presence of strong cation–anion interactions arising from a mix of energetically stable ion pairs, further confirming the importance of considering single

ion pairs as models for the assignment of IR and Raman spectra of ionic liquids. Later Lassègues et al.⁴²² highlighted that the C2–H stretching vibration did not change when the BF_4^- anion was replaced with a bulkier and more diffuse anion such as NTf_2^- . Frequency calculations on the isolated C_nmim^+ cations ($n = 2, 3$, and 4) were already accurate enough to assign the C2–H stretching mode in experimental spectra. In the work of Shukla et al.,⁴²³ the predicted vibrational frequencies of $[C_4mim]X$ ion pairs ($X = Cl^-, Br^-,$ and I^-) formed a nearly perfect linear correlation with experimentally observed bands. Only one type of ion pair configuration, in which the halide interacted in the C2–H bond, was considered, and the scaling factor of 0.9835 was fitted to reproduce stretching vibrations above 2900 cm^{-1} . Perfectly linear correlations were also established for vibrational frequencies of ion pairs of $[C_nmim][BF_4]$ ($n = 2, 3$, and 4), with the scaling factors of 0.963 and 0.916 being fitted for B3LYP/6 311+G(2d,p) and HF/6 311+G(2d,p) methods, respectively.³⁹⁰

A distinct difference in the low frequency spectra was observed between nonmethylated and C2 methylated imidazolium ionic liquids coupled with the NTf_2^- anion.³⁹⁵ The B3LYP/6 31+G* calculations on ion pairs of $[C_2mim][NTf_2]$ predicted two bands at 98.9 and 121.0 cm^{-1} , corresponding to the C4,5–H and C2–H bonds, respectively. Both bands reproduced a broad experimentally recorded peak at 83.5 cm^{-1} , which was assigned to hydrogen bonding driven cation–anion interaction. The theoretical band at 121.0 cm^{-1} disappeared from the predicted spectrum of the $[C_2dmim][NTf_2]$ ion pair, in which the anion interacted above the imidazolium ring. This was in agreement with the experimental spectrum that exhibited a series of peaks between 100 and 200 cm^{-1} , which were attributed to Coulomb driven cation–anion interactions.

DFT calculations have been proven invaluable in supporting the hypothesis that ionic liquids evaporate as single ion pairs. The study of Akai et al.³⁷⁶ confirmed that the vaporization process of $[C_2mim][CF_3SO_3]$ resulted in the appearance of single ion pairs in the vapor phase that was isolated and mixed with neon to record matrix isolation IR spectra. The B3LYP/6 311++G(3df,3pd) predicted vibrational frequencies of the thermodynamically preferred ion pair configuration, in which the anion interacted above the C2–H bond with all three oxygens forming equal hydrogen bonds and the resulting IR spectrum correlated well with experiment. A slightly different conclusion was drawn³⁷⁷ from the same type of experiment performed on $[C_2mim][NTf_2]$. The second thermodynamically stable ion pair configuration was tentatively assigned to be present in the vapor phase. Based on the B3LYP/6 311+G(d,p) predicted spectra, it was concluded that 1-methylimidazolium acetate evaporated as neutral molecules such as 1-methylimidazole and acetic acid,⁴²⁴ a fact that was also confirmed experimentally using mass spectrometry.^{378,425}

DFT calculations have been shown to be successful in the prediction of NMR chemical shifts. Chemical shifts are calculated as well as measured as nuclear magnetic shielding constants with respect to a reference constant, usually tetramethylsilane (TMS). From the quantum chemical point of view, these constants are dependent on the gauge of the vector potential of the external magnetic field,³⁷ thus preventing the comparison among calculated magnetic constants. The gauge invariance of molecular orbitals on magnetic field can be achieved through either a complete basis set (which is time consuming) or inclusion of local gauge

origins to define the vector potential. The latter was first adapted by Ditchfield in the form of gauge invariant atomic orbitals (GIAO),⁴²⁶ with local gauge being placed at the center of each atomic orbital. The GIAO approach was successfully implemented with the self consistent field procedure of HF and DFT calculations by Pulay et al.,⁴²⁷ thus making NMR chemical shift calculations straightforward and routine.

In the study of Palomar et al.,⁴²⁸ the gas phase was used in ion pair geometry optimizations and NMR chemical shift calculations of the ring protons in the imidazolium ring in $[C_n\text{mim}][PF_6]$ ($n = 1, 4$, and 8), $[C_4\text{mim}]\text{Br}$, and $[C_4\text{mim}][BF_4]$ using the B3LYP/6-31++G** level of theory. Additionally, the effect of a polarizable continuum model (PCM)^{429,430} and explicit solvent (three water molecules on the proton chemical shifts of $[C_1\text{mim}][PF_6]$) was systematically studied. Three solvents, benzene, dichloromethane, and water, were used in combination with the PCM model, whereas three water molecules were included in the calculation to account for explicit solvent. Out of the ring protons, the largest differences were observed for the H2 proton, followed by the H4 and H5 protons. The position of the peaks corresponding to these protons depended on the anion type for the gas phase geometries as well as the solvent type used in the PCM model, in the case of $[C_1\text{mim}][PF_6]$. The chemical shifts of the H2 proton shifted downfield going from a nonpolar solvent such as benzene to a polar solvent such as water by >1.5 ppm. This observation was in accordance with the lengthening of the interionic $H_2\cdots F$ bond with increasing solvent polarity. Explicit water molecules shifted the H2 proton in the opposite direction by almost 0.8 ppm with inclusion of three water molecules. Isolated imidazolium cations produced a peak shifted downfield by almost 2.5 ppm with respect to that in ion pairs. The use of water as solvent on an isolated cation produced the H2 peak that was very close to the one in the $[C_1\text{mim}][PF_6]$ ion pair. This study highlighted the sensitivity of the H2, H4, and H5 protons to their local environment. Due to the lack of experimental results, no conclusions could be drawn with respect to the accuracy of the predicted proton NMR shifts. Very similar conclusions were also presented in the work of Katsyuba et al.⁴³¹ for ion pair configurations of $[C_2\text{mim}][BF_4]$ calculated at the B3LYP/6-31G* level of theory. The ion pair configuration, in which the anion interacted above the imidazolium plane, optimized with the PCM model and dichloromethane as solvent, gave the best comparison with proton NMR chemical shifts measured in CD_2Cl_2 . Excellent linear correlations between experimental and predicted chemical shifts of the ring protons were also established.

Chen et al.⁴³² studied the effect of ion pair configuration and the level of theory on predicted proton NMR chemical shifts in imidazolium ionic liquids coupled with chloride, BF_4^- , PF_6^- , CH_3COO^- , CF_3COO^- , $C_2H_5OSO_3^-$, $CH_3C_6H_5SO_3^-$, and $N(CN)_2^-$. The HF and MP2 methods together with a series of DFT functionals, such as B3LYP,^{30,31,33} PBE0,^{29,34,205} X3LYP,¹⁹¹ mPW91PW91,^{29,186,187,205,433} M062X,³⁵ and TPSSH,¹⁹⁰ were combined with Pople and Dunning's type basis sets for two preferable ion pair configurations in which the anion interacted either above the imidazolium plane (configuration 1) or in the plane of the C2–H bond (configuration 2). In all the ILs studied, the anion preferred to interact above the imidazolium plane, closer to the C2–H bond. All the levels of theory and basis sets produced very similar deviations from experimental data, indicating that the proton NMR chemical shifts were insensitive to the level of theory, particularly

electron correlation effects. The largest deviations came for the H2 proton, with configuration 1 producing the least error with respect to experiment. It was also established that the predicted proton NMR chemical shift of the H2 atom strongly depended on the cation–anion distance, with elongation of the distance resulting in a decrease of the H2 chemical shift, thus bringing it closer to experimental values. Among the other ring protons, the backbone H4 and H5 protons gave the second largest deviations for the chloride and acetate anions due to their strong hydrogen bonding ability, that could only be considered in multiscale calculations. No obvious correlation was found between the ion pair binding energy and the predicted H2 proton shift, suggesting that the basicity of the anion was not responsible for the changes in the H2 chemical shift. Overall, the proton NMR chemical shifts were found to be sensitive to the position of the anion and, hence, the structural arrangement of the bulk of the ionic liquid, thus suggesting that, in combination with quantum chemical methods, 1H NMR can quickly probe the liquid structure of ionic liquids.

Recently in the work of Strauch et al.,⁴³⁴ a linear relationship was observed between the calculated 1H NMR chemical shift of the N–H bond and the calculated deuteron quadrupole coupling constant in single ion pairs of triethylammonium ionic liquids coupled with the NTf_2^- , triflate, and mesylate anions. Both B3LYP/6-31+G* and B3LYP D3/6-31+G* were used in the study, although no comment with regard to how clusters were constructed was made. This trend reflected the increased strength of the cation–anion interaction in the $NTf_2^- < \text{Triflate} < \text{Mesylate}$ series and was maintained in ionic clusters of up to four ion pairs. Typically, changes within 1 ppm were observed in the proton chemical shift going from a single ion pair to clusters of four ion pairs. Only slight differences were observed between dispersion corrected and nondispersion corrected functionals, with the explicit dispersion correction favoring stronger interionic interaction and, hence, a slightly stronger downfield shift of the proton in the NH group. This further supports the conclusion drawn in the work of Chen et al.⁴³¹ about the relative insensitivity of the proton chemical shift with respect to the level of theory.

8. QUANTUM CHEMICAL CALCULATIONS OF IONIC CLUSTERS

Only a handful of studies have been performed on multiscale clusters of ionic liquids due to the computational expense associated with quantum chemical calculations, especially for the prediction of secondary molecular properties such as vibrational frequencies, IR and Raman intensities, and NMR chemical shifts. It has to be noted that calculations of molecular properties (such as dipole moments, charge distribution, polarizability, etc.) of individual ions within ionic clusters become dependent on the use of additional approaches that allow for the localization of molecular orbitals on atoms. These localized orbitals can be subsequently used to predict individual dipole moments and charge distribution.

8.1. Thermodynamic data

Due to the significance of many body effects, Ludwig⁴³⁵ proposed to use a cluster approach with the view of predicting thermodynamic data such as enthalpy and entropy of vaporization and boiling point. The cluster approach searches for minimum energy structures of clusters consisting of multiple ion pairs and calculates vibrational frequencies corresponding to these minima. The electronic energy is

corrected for zero point vibrational energy and augmented with translational, rotational, vibrational, and electronic contributions that are temperature dependent and calculated based on the partition functions for each contribution:

$$q_{\text{tot}} = q_{\text{trans}} \cdot q_{\text{rot}} \cdot q_{\text{vib}} \cdot q_{\text{elec}} \quad (45)$$

Individual partition functions are extracted from frequency calculations as implemented in GAUSSIAN09⁴³⁶ and follow the standard physical chemistry formulas (e.g., as described by McQuarrie³⁸⁰). The enthalpy of vaporization is defined as the difference between the enthalpies of the system in gas and liquid phases. In the Ludwig approach, it is assumed that an ionic liquid evaporates as an ion pair and the liquid phase can be approximated by a cluster consisting of multiple ion pairs. Thus, the enthalpy of vaporization can be expressed as

$$\Delta H_{\text{vap}}(T, p) = H_1(T, p) - \left(\frac{H_n(T, p)}{n} \right) \quad (46)$$

where 1 and n represent the number of ion pairs in the system and H_1 and H_n are enthalpies of one and n ion pair clusters, respectively. Standard conditions of room temperature at 298.15 K and pressure of 1 atm are assumed. Since the boiling point, T_b , occurs when $G_{\text{gas}}(T_b, p) = G_{\text{liq}}(T_b, p)$, comparison of the Gibbs free energy of 1 ion pair with that of the n pair cluster with varying temperature allows for extraction of the boiling point. Trouton's rule can then be used to calculate the entropy of vaporization:

$$\Delta S_{\text{vap}}(T_b, p) = \frac{\Delta H_{\text{vap}}(T_b, p)}{T_b} \quad (47)$$

The Kirchner group showed the successful application of this rule for the accurate prediction of vaporization enthalpies of water.⁴³⁷ Ludwig applied the cluster approach to calculate the thermodynamic data of $[\text{C}_n\text{mim}][\text{SCN}]$. Ionic clusters consisting of 2 to 14 ion pairs as well as single ion pairs were optimized at the RHF/3 21G* level of theory. Two configurations of ion pairs, in which the anion interacts with the C2–H bond and the C=C backbone, were both considered as the reference point for one ion pair. The relative energy difference between two configurations was rather large, at 50 kJ mol^{−1}. The binding energy normalized to one ion pair was shown to steadily increase by >40 kJ mol^{−1} with increasing numbers of ion pairs and convergence when the cluster consisted of at least 10 ion pairs. Larger clusters were shown to better predict the enthalpy of vaporization. Using two ion pair configurations as reference points, the enthalpy of vaporization was predicted to be 90 and 140 kJ mol^{−1}, with the latter number being obtained from the higher energy ion pair. The experimental enthalpy of vaporization was measured to be 145 kJ mol^{−1}, which is in good agreement with one of the predicted values. The boiling points were estimated to be between 880 and 940 K, which is in good agreement with experimental estimates for $[\text{C}_n\text{mim}][\text{NTf}_2]$.⁴³⁸ The entropy of vaporization was estimated to be between 112 and 160 kJ mol^{−1} for ionic clusters consisting of 6 and 10 ion pairs, respectively. This range is also in good agreement with experimental entropies for $[\text{C}_n\text{mim}][\text{NTf}_2]$.⁴³⁸ The main limitations of the cluster approach are the use of the HF method, as it does not account for dispersion interactions, and not for screening for lower energy structures of clusters used. It has to be noted that the approach requires vibrational frequency calculations for large scale clusters, which becomes computationally less feasible with

larger basis sets, and the screening for all lowest energy cluster structures becomes very time consuming.

Good prediction of enthalpy of vaporization might come as a surprise provided how important dispersion forces are in ionic liquids. Although the HF method does not recover any of those significant forces, the agreement is perhaps “too good to be true”. In 2013 Verevkin et al.³⁸¹ found a linear relationship between the enthalpy of vaporization and the alkyl chain on the imidazolium cation. Moreover, the slope was very gradual, thus leading to small changes in enthalpy from ethyl to octadecyl. In the latter, dispersion forces undoubtedly play a critical role in the bulk structure as well physicochemical properties of these ionic liquids. It has been proven that ionic liquids evaporate as ion pairs, and therefore, the linear dependence might not be as surprising, as the interaction energy between the cation and anion is expected to also change only slightly. The fortunate result of the HF method is associated with the use of larger clusters to obtain “the right result for the wrong reason”. It has to be pointed out that the binding energy per ion pair of *any* multiple ion cluster *increases due to the increasing number of interionic interactions*, and therefore, it is not surprising that even the HF method might arrive at an experimentally comparable result when a significant number of ions is present in the cluster.

Recently Ludwig et al.⁴³⁹ applied their cluster approach to the prediction of vaporization enthalpies of protic ionic liquids based on the triethylammonium, $\text{NH}(\text{C}_2\text{H}_5)_3^+$, cation and the NTf_2^- , mesylate, CH_3SO_3^- , and triflate, CF_3SO_3^- , anions. Experimentally it was established that compared to aprotic ionic liquids previously studied, the vaporization enthalpy of these protic ionic liquids was consistently lower, between 16 and 59 kJ mol^{−1}. This observation was supported by the calculated binding energies per ion pair of large clusters consisting of 10 ion pairs that predicted a 30 kJ mol^{−1} weaker interaction in the cluster of $[\text{NH}(\text{C}_2\text{H}_5)_3][\text{NTf}_2]$ compared to the same sized cluster of $[\text{C}_2\text{mim}][\text{CH}_3\text{SO}_3]$ as calculated using B3LYP D3/6 31+G*. The presence of strong hydrogen bonding as well as dispersion interaction between the ammonium cation and an ionic liquid anion in single ion pairs calculated in the gas phase was attributed to the observed difference in vaporization enthalpies.

In the study of Dong et al.,⁴⁴⁰ the Ludwig approach was applied to predict enthalpies of vaporization of the $[\text{C}_2\text{mim}][\text{NTf}_2]$, $[\text{C}_2\text{dmim}][\text{NTf}_2]$, $[\text{C}_2\text{mim}]\text{Cl}$, and $[\text{C}_2\text{H}_5\text{NH}_3][\text{NO}_3]$ ionic liquids. Clusters consisting of 2, 4, 8, 10, and 12 ion pairs were geometry optimized at the M062X/3 21G* level of theory and the thermodynamic data was extracted as described above. Different configurations of ion pairs, including those consisting of neutral species such as imidazole and the protonated anion, were used as a reference point to represent the gas phase. The predicted enthalpies of vaporization showed different trends for each of the ionic liquids studied. In the case of the NTf_2^- based ILs, the enthalpy of vaporization was found to peak at the medium sized clusters with four and eight ion paired clusters producing results that were close to experimental data. In the case of $[\text{C}_2\text{mim}]\text{Cl}$, the enthalpy showed convergence at four ion pairs, whereas, in the case of the protic ionic liquids, the enthalpy almost linearly increased from 2 to 10 ion pairs. Different configurations of reference ion pairs did not affect the predicted enthalpy of the NTf_2^- based ionic liquids, whereas larger differences were found for the other ionic liquids. The latter could be attributed to inclusion of higher energy ion pairs as reference points. The presence of neutral species in ion pairs

in the gas phase was ruled out, as the latter produced much larger deviations from experiment. Although some of the cluster sizes produced good agreement with experiment, varying trends of the enthalpy of vaporization with increasing cluster size revealed the strong dependence of the approach on the geometry of clusters. Further studies are required to study two effects, such as the location of the global minimum for each cluster and more accurate levels of theory on the prediction of thermodynamic data using this approach. The latter was demonstrated by Emel'yanenko et al.⁴⁴¹ when B3LYP and dispersion corrected B3LYP functionals were applied within the Ludwig approach to predict the enthalpy of vaporization of ethylammonium nitrate. Clusters consisting of 2 to 12 ion pairs were optimized at the B3LYP/6-31+G* level of theory, and the binding energies were corrected with counterpoise correction and Grimme's D3 correction. Two different trends were obtained with the B3LYP and B3LYP D3 functionals, with the latter producing much better agreement with the experimental enthalpy of vaporization of 105.3 kJ mol⁻¹ as well as a clear convergence of the enthalpy with increasing size of the cluster. It was established that the cluster consisting of six ion pairs was already reliable for the prediction, and the calculated enthalpy of vaporization changed within 15 kJ mol⁻¹. In their work, the formation of a neutral complex between ethylamine and the nitric acid was used as the reference point for the gas phase and the predicted enthalpies of large clusters were almost 100 kJ mol⁻¹ higher. B3LYP, on its own, failed to show convergence of many body effects, even for the largest clusters, and fell almost 50 kJ mol⁻¹ short of the experimental enthalpy.

The cluster approach was used by the Ludwig group to find correlations between electronic energies and experimental melting points of a range of imidazolium ionic liquids coupled with the NTf₂⁻ anion.^{393,442} The cation varied from imidazolium to monomethyl, dimethyl, trimethyl, tetramethyl, and pentamethyl substituted imidazolium cation, thus consistently changing the hydrogen bonding ability of the cation. The clusters were optimized at a low level of theory, HF/3-21G*, and electronic energies were counterpoise corrected, and normalized electronic energies, called binding energies per ion pair, were calculated as $(E_4 - 4E_1)/4$, where E_1 and E_4 are counterpoise corrected electronic energies for a single ion pair and four ion pair clusters, respectively. Only a loose linear correlation was observed between binding energies per ion pair and corresponding melting points, with hydrogen bonding contributing to a wide spread of data points. Higher levels of theory need to be applied to also include dispersion forces in order to identify whether linear correlations exist between binding energies of larger clusters and experimental melting points.

The Ludwig cluster approach can be formulated in a general manner based on the quantum cluster equilibrium (QCE) methodology, which has one significant difference. Instead of one particular cluster size, a series of clusters of consistently increasing size are considered for the same system. The QCE approach was originally proposed by Weinhold,^{443,444} and successfully applied by Weinhold and Ludwig, to studying the structure and thermodynamics properties of condensed systems such as ammonia, amides, water, methanol, and ethanol.^{445–452} The QCE approach assumes that a liquid phase can be described by clusters, consisting of i molecules or monomers that are in equilibrium with each other such that their chemical potentials, μ_i , can be defined as

$$\mu_1 = \frac{\mu_2}{2} = \dots = \frac{\mu_i}{i} = \dots = \frac{\mu_c}{c} \quad (48)$$

where c is the largest cluster size. Each cluster can be optimized using a quantum chemical method, and therefore, an individual partition function, q_i , can be assigned and their components easily evaluated using standard physical chemistry formulas as described in detail by Kirchner.^{453,454} Using the definition of

the mole number, $n_i = q_i \left[\frac{n_1}{q_1} \right]^i N_A^{i-1}$, for each cluster size and the particle conservation rule, the total number of moles, n_A , can be expressed as

$$n_A = n_1 + \left[\frac{2q_2 N_A}{q_1^2} \right] n_1^2 + \left[\frac{3q_3 N_A}{q_1^3} \right] n_1^3 + \dots + \left[\frac{cq_c N_A}{q_1^c} \right] n_1^c \quad (49)$$

Equation 49 has multiple solutions with respect to the population number, N_i , for each individual cluster. From the fundamental point of view, there exists a solution with physically meaningful population values and the lowest Gibbs free energy calculated based on the set of partition functions, q_i , at a particular temperature and pressure. The solution of eq 49 can be achieved iteratively until the lowest Gibbs free energy is identified.

The standard formula of the pressure dependence on volume and the total partition function, $P = kT \left(\frac{\partial \ln Q}{\partial V} \right)_T$, can be applied to arrive at a third degree polynomial relating the volume of the system with N_i , the number of i th order clusters. The solution of this polynomial needs to be found iteratively. By plotting the isobars of the volume dependence on temperature, one can determine the phase transition temperature of melting. Originally, the HF method was used in the QCE approach. Later, the Kirchner group⁴⁵³ compared the performance of various DFT functionals and the MP2 method for studying the thermodynamic properties of water. Due to the importance of the cooperativity effects in water, clusters consisting of up to seven water molecules were considered in the QCE model. The B3LYP and MP2 levels of theory performed the best only when combined with a large triple ζ quality basis set, such as TZVPP. The effect of the level of theory and basis set was even more evident in the case of hydrogen fluoride clusters with strong hydrogen bonding.^{455,456} Even the CCSD(T)/CBS and MP2/QZVP methods failed to accurately predict the volume change at the boiling point of hydrogen fluoride, whereas MP2/TZVP produced very good results. It appears that the level of theory strongly affects intermolecular distances in large clusters during the geometry optimization, and therefore, benchmark levels of theory are needed to generate more balanced optimized clusters. More studies into the effect of higher levels of theory and varying size of clusters on the structural arrangement are needed. Overall, the QCE approach combined with higher correlated levels of theory may prove invaluable for the prediction of thermodynamic data of ionic liquids (especially in light of the locality of electronic effects in the bulk of ionic liquids⁴⁵⁷), as it allows for much faster screening of novel materials than even classical molecular dynamics simulations.

8.2. Spectroscopic properties

The Ludwig group pioneered the identification of cation–anion vibrations in both protic and aprotic ionic liquids based on multiscale calculations.^{392,418,458–460} They showed that the

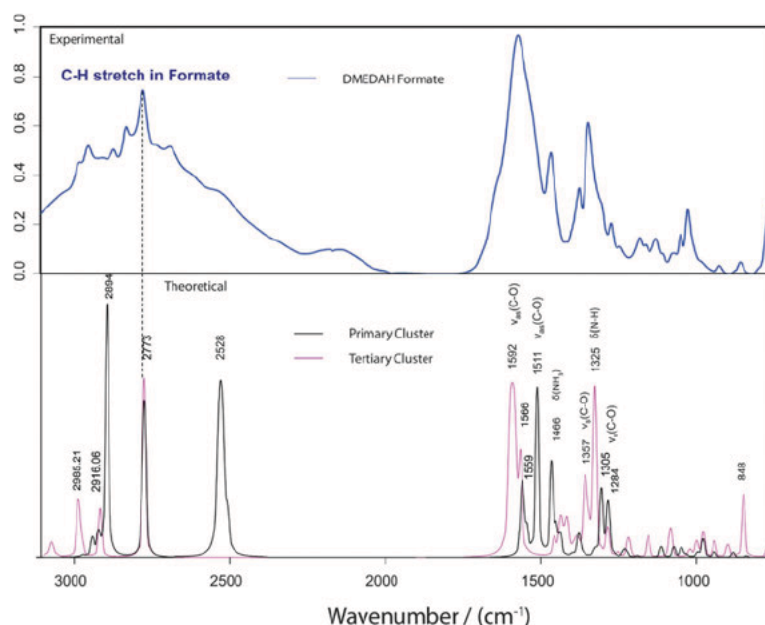


Figure 12. Calculated (bottom graph) and experimental (top graph) FTIR spectra of *N,N*-dimethylethylenediammonium formate. In the bottom graph, the primary amine protonated cluster is shown in black and the tertiary amine protonated cluster is shown in magenta. Predicted spectra are normalized to the C–H stretch of formate at 2773 cm^{-1} . Scaling factors of 0.933 and 0.961 were used for the primary and tertiary protonated clusters, respectively. Reproduced from ref 386 by permission of the PCCP Owner Societies.

inclusion of more ion pairs in the B3LYP/6-31+G(d) calculations produces more peaks in the low frequency region (below 500 cm^{-1}) for both aprotic, $[\text{C}_4\text{mim}][\text{NO}_3]$, and protic, $[\text{C}_3\text{H}_7\text{NH}_3][\text{NO}_3]$ and $[(\text{CH}_3)_2\text{NH}][\text{NO}_3]$, ionic liquids, allowing for assignment of low intensity peaks arising from intermolecular interactions.^{392,418} In protic ionic liquids, distinct peaks in the regions of 199 to 224 cm^{-1} and 134 to 159 cm^{-1} were observed and attributed to symmetric and asymmetric stretches of the N–H \cdots O hydrogen bonds, respectively. These peaks could not be accurately assigned based on single ion pair calculations due to the lack of predicted vibrational modes in the tetrahertz region. Similar calculations consisting of up to 8 ion pairs were performed for a series of C_2mim based ionic liquids coupled with the SCN^- , $\text{N}(\text{CN})_2^-$, $\text{C}_2\text{H}_5\text{OSO}_3^-$, and NTf_2^- anions.⁴⁵⁸ Binding energy per ion pair of 6 ion paired clusters correlated linearly with the strongest peak that corresponds to the cation–anion interaction in the region between 80 and 120 cm^{-1} .

The size of ionic clusters was shown to affect the length of the C–H bonds in $[\text{C}_n\text{mim}][\text{SCN}]$ ($n = 1, 2$) depending on the local environment of the ions.⁴⁶¹ 1, 2, 3, 4, and 6 ion paired clusters were optimized at the B3LYP/6-31+G* level of theory. Theoretical chemical shifts were referenced to the TMS signal at 32.06 ppm. The predicted NMR chemical shifts of the ring protons, from all of the clusters, were plotted against the corresponding C–H bond length, the frequency of the C–H stretching vibration scaled with the factor of 0.96 and deuterium quadrupole coupling constants. The latter was calculated using the methodology described by Huber et al.^{462,463} A linear correlation was found between the proton chemical shift and the C–H bond length, whereas a cubic relationship was established for the stretching vibration and quadrupole coupling constants. With these relationships, the knowledge of experimentally measured proton chemical shifts can lead to the prediction of other quantities, such as relaxation times and

relaxation rates, that are usually not readily available from experiments requiring particular setups. These relaxation quantities, in turn, allow for the prediction of dynamics in ionic liquids based on simple measurements of proton NMR chemical shifts.

Vibrational frequency calculations performed on ionic clusters can also help identify the impact that solvated molecules have on the liquid structure. For example, the predicted spectrum of a cluster of CO_2 interacting with two ion pairs of $[\text{C}_4\text{mim}][\text{CF}_3\text{COO}]$ showed no difference to the spectrum calculated for the isolated cluster,⁴⁶⁴ which was in agreement with experimental observation that the CO_2 molecules did not disrupt the liquid structure, and thus, these are more likely to occupy the already existing voids.

Simons et al.³⁸⁶ established that clusters consisting of two ion pairs were needed to predict IR spectra of protic ionic liquids that are obtained by a proton transfer between diamines and a weak acid. In their work, *N,N*-dimethylethylenediamine was used as the diamine and contained one primary ($-\text{NH}_2$) and one tertiary ($\text{N}(\text{CH}_3)_2$) amine center. When combined with a weak acid, such as formic or acetic acid, it appeared that both centers were protonated, whereas in the case of a strong acid, such as HNTf_2 , the primary center was almost exclusively protonated. Clusters consisting of two ammonium cations and two anions (either acetate or formate) were sufficient in reproducing the experimental IR spectra (see Figure 12). In the case of formic and acetic acids, two types of clusters had to be considered, in which either the primary or tertiary centers were protonated. In order to maintain the proton transfer from the acid to the base, these clusters were optimized at the M062X/cc-pVDZ level of theory using the CPCM approach with ethanol as the solvent. The predicted spectra were scaled with respect to a distinct and strong band in the experimental spectra. In the case of the formate, the C–H stretching vibration represented the reference band, whereas, in the case

of the acetate, the C–C stretch was selected. The scaling factors were slightly different for both cases—0.933 for the formate and 0.961 for the acetate—further highlighting the importance of individual scaling for each ionic liquid. The combination of two types of clusters was in excellent agreement with experiment, further confirming that both primary and tertiary centers were protonated when a weak acid was used for the proton transfer.

In the recent publication by Ludwig,⁴⁶⁵ the comparison of the far IR spectra of tetramethylammonium nitrate and trimethylammonium nitrate showed a strong influence of dispersion interaction between ion pairs observed in larger ionic clusters on the position of vibrational bands corresponding to intermolecular interactions. This clearly highlights the importance of the accurate treatment of dispersion forces even in protic ionic liquids in order to predict their far IR vibrational spectra. This conclusion was further supported by Knorr et al.,^{466–468} who identified that for any cation capable of forming hydrogen bonding, such as 1 (2 hydroxyethyl) 3 methylimidazolium, the intermolecular interactions with other cations strongly influenced the prediction of their IR spectra. For example, the O–H stretching region could only be explained when a cluster of four ion pairs was considered, with the cations forming cyclic hydrogen bonding through the hydroxyl groups.

Bagno et al.⁴⁶⁹ studied the prediction of NMR chemical shifts of $[\text{C}_4\text{mim}][\text{BF}_4]$ and $[\text{C}_4\text{mim}][\text{CH}_3\text{OSO}_3]$ based on ionic clusters taken from classical MD simulations⁴⁷⁰ using the Lopes and Padua force fields on periodic simulation boxes consisting of 27 ion pairs. 125 and 70 clusters were extracted from MD simulation of the $[\text{C}_4\text{mim}][\text{BF}_4]$ and $[\text{C}_4\text{mim}][\text{CH}_3\text{OSO}_3]$ ionic liquids, respectively, and were subjected to ONIOM type calculations⁴⁷¹ for the prediction of ^1H and ^{13}C NMR chemical shifts referenced to the TMS signal, in which the systems were divided into two layers. The first layer, the quantum mechanical (QM) part, consisting of a few ions, was carried out using the B3LYP/cc pVTZ level of theory, whereas the second layer, the molecular mechanics (MM) part, comprising the rest of the cluster, came from the performed MD simulations. The QM part of the extracted clusters was selected based on the distance between the reference cation and neighboring ions, with the cutoff distance varying between 6 and 10 Å. The QM layer in a fraction of clusters was selected by taking single ion pairs, whereas in others two anions closest to the C2–H bond together with neighboring ions within 7.8 Å were considered. The predicted NMR shifts were averaged over all atoms of the same type within each cluster. Isolated ion pairs predicted the largest shift for the H2 proton of 13.31 and 11.37 ppm for $[\text{C}_4\text{mim}][\text{BF}_4]$ and $[\text{C}_4\text{mim}][\text{CH}_3\text{OSO}_3]$, respectively. Depending on the cluster type, the shift decreased drastically, to between 6.57 and 7.45 ppm for $[\text{C}_4\text{mim}][\text{BF}_4]$ and between 7.17 and 7.48 ppm for $[\text{C}_4\text{mim}][\text{CH}_3\text{OSO}_3]$. The isolated cation was predicted to have a shift of 6.62 ppm. The ^{13}C chemical shifts varied only slightly within clusters for both ionic liquids. This finding suggested insensitivity of the carbon magnetic shielding to the structural arrangement of the ionic liquid, with the isolated cation already producing good agreement with experiment. Inclusion of more ions around the reference cation resulted in an increase of the H2 NMR chemical shift and a decrease of the mean absolute errors for proton chemical shifts from 1.22 to 0.12 ppm for $[\text{C}_4\text{mim}][\text{BF}_4]$ and from 0.73 to 0.20 ppm for $[\text{C}_4\text{mim}][\text{CH}_3\text{OSO}_3]$. This study clearly identified the importance of long range interactions in ionic liquids for the accurate prediction of their

molecular properties, such as proton NMR chemical shift. It was recommended to include at least the first solvation shell around the reference ion to ensure reliable results.

9. AB INITIO MOLECULAR DYNAMICS (AIMD)

One of the main disadvantages of classical molecular dynamics simulations is their inability to directly observe bond breaking and bond forming, thus limiting their application to studying chemical reactions and transport and solvation mechanisms associated with significant changes to electronic structure (e.g., formation of strong donor–acceptor bonds). In a quantum chemical method (also referred to as *ab initio*), be it wave function based or electron density based, all electrons are treated quantum mechanically, thus allowing for observation and quantification of chemical processes. Historically, quantum chemical methods are also known as *ab initio* methods, translating from Latin as “from the beginning”, to highlight the fundamental nature of Schrödinger’s equation, which does not contain any empirical parameters. A marriage of an *ab initio* method and the molecular dynamics formalism results in *ab initio* molecular dynamics, which combines the Newtonian equations of motion in molecules with the quantum mechanical description of electrons within these molecules, thus representing the “holy grail” of theoretical and computational chemistry—the ability to study the behavior of a molecular system in real time from a quantum mechanical point of view. This unified approach was originally proposed by Car and Parrinello⁴⁷² 30 years ago, giving rise to what now is known as Car–Parrinello Molecular Dynamics (CPMD). The KS equations are easily solved using the self consistent field approximation, originally applied for the HF method by diagonalization of the Fock matrix with the set of orthogonal molecular orbitals. In order to circumvent the computational cost involving the minimization of the energy functional with respect to molecular orbitals, a concept of *dynamic simulated annealing* was applied. In this approach, the energy functional was introduced into the MD formulation and the velocities of nuclei and electrons were slowed down until the temperature of the system approached absolute zero, thus reaching the equilibrium state of the energy. It has to be pointed out that in this formulation the velocities of nuclei are real, whereas those of electrons are fictitious. Car and Parrinello proved⁴⁷² that the energy solved using the MD formulation was identical to the conventional solution of the KS equations, thus drastically reducing the computational cost of CPMD simulations. Unlike classical MD simulations,^{473–476} fluctuations in atomic partial charge distribution on ions and hence charge transfer among ions,^{477–481} polarization effects³¹⁶ due to intermediate changes in the structural arrangement such as ion pairing and cage formation,^{482–484} and many body effects are explicitly accounted for by a quantum chemical method throughout the simulation. Although polarizable force fields can account for polarization effects either directly or indirectly,^{473,485} these rely on additional implementation of time consuming terms that describe polarization effects⁴⁸⁶ and many body effects⁴⁸⁷ in ionic condensed systems. The major limitation of any AIMD simulation lies in the lack of computational resources that would allow for longer simulations, as current AIMD simulations reported for ionic liquids run between 50 and 100 ps for simulation boxes of 30 to 40 ion pairs.⁴⁷⁹ For condensed systems that are bound through strong intermolecular forces such as ionic liquids, simulation time is the main obstacle. Ionic liquids are usually referred to as

“sluggish” due to the decreased mobility of ions as a result of these strong forces, thus requiring longer equilibration times, and are on the scale of 5 to 10 ns before trajectories can be recorded to produce a statistically sound analysis of transport and thermodynamic properties.⁴⁷⁵ The size of a simulation box is determined by the size of individual ions, with long and bulky functional groups further restricting ion mobility to some extent.⁴⁸⁸ For more accurate and reliable results for ionic liquids, large simulation boxes consisting of hundreds of molecules and long computational times are required,⁴⁸⁹ further reducing the simulation time. Due to the importance of many body effects¹²⁵ and dispersion forces^{98,490,491} in ionic liquids, the AIMD approach represents a direct way of accounting for these effects without the need for further methodology development.

The only consideration that needs to be taken into account in the AIMD approach is the fact that, due to the sluggish nature of ionic liquid ions equilibrium, AIMD simulations might not properly describe high barrier chemical reactions, as they would prevent ions from sampling nearby maxima and minima separated by barriers that are larger than the kinetic energy of ions. The solution to this obstacle is the use of powerful techniques that accelerate rare events by enhancing the sampling of the free energy landscape and later reconstructing it as the probability function of collective variables that are carefully predefined on the potential energy surface. There are a number of methods that follow the same philosophy, such as metadynamics^{492–495} and umbrella sampling.^{496–499} For low barrier reactions such as proton transfer, short runs of equilibrium AIMD simulations are already enough to understand the proton dynamics in ionic liquids.^{500,501}

Currently, AIMD simulations have been performed to analyze the liquid structure and spectroscopic properties of protic⁴⁸³ and aprotic ionic liquids^{317,502–504} and their mixtures with each other,⁵⁰⁵ water,^{500,506} and other molecules.^{501,507–509} AIMD has helped elucidate the mechanism of solvation of electrons⁵¹⁰ as well as the extent of ion pairing and the hydrogen bonding dynamics in typical ionic liquids.^{500,506,511,512} Some exciting new applications also include the analysis of kinetics of low barrier reactions such as proton transfer of tryptophan in ionic liquids,⁵¹³ reversible decomposition of formic acid into CO₂ and H₂ in [C₁mim][CH₃COO],⁵¹⁴ and carbene formation induced by CO₂ addition in imidazolium ionic liquids.⁵¹⁵

The first AIMD simulations of ionic liquids were performed by Del Pópolo et al. to predict the liquid structure of the [C₁mim]Cl ionic liquid⁵⁰² and analyze the proton transfer of a single HCl molecule in this ionic liquid.⁵⁰¹ In their work, the GGA PBE functional²⁹ was used together with norm conserving pseudopotentials for core electrons⁵¹⁶ and a nonorthogonal basis set of atom centered orbitals, as implemented in the SIESTA program.⁵¹⁷ Two simulation boxes consisting of 8 and 24 ion pairs were considered in the periodic boundary conditions with temperature set at 425 K. For the smaller systems, the simulation ran for 39 ps, whereas for the larger box only one trajectory of 3.5 ps was feasible. Both simulation boxes produced very similar RDFs for the cation–anion distances calculated with respect to the center of the imidazolium cation, producing the same first solvation shell and indicating that the cation–anion interactions were strong, thus governing the liquid structure of the ionic liquid. When compared to classical MD simulations, a striking difference was

observed for the H–Cl site–site distribution functions, with the AIMD simulations also showing the existence of *directional* hydrogen bonding between the chloride anion and the C2–H bond of the ring with a distinct peak at 2.2 Å and producing a red shift in the stretching vibration of this bond. This was the first observation that both cation–anion interactions, in which the anion was located either above or in the plane of the imidazolium ring, were favorable in the bulk. The size of the simulation box became important for the cation–cation and anion–anion radical distributions, i.e. the second solvation shell. Some significant differences in geometric parameters were observed in AIMD simulations of a single ion pair, especially for angles and dihedral angles corresponding to the most occupied positions of the anion around the ring, thus highlighting the importance of large scale calculations for the accurate elucidation of the structure and energetics of ionic liquids. Similar observations of the strong in plane hydrogen bonding between the C2–H bond and the chloride anion were obtained by Bühl et al.⁵⁰³ with the BP86 functional and plane wave basis sets in CPMD calculations. In their simulations, 25 and 41 ion pairs were placed in a periodic box followed by short simulations of 5.3 and 2.3 ps, respectively. The lone pair of the chloride anion was shown to donate to the antibonding of the $\sigma^*(\text{C–H})$ orbital of the cation: a pattern revealing itself as a distinct peak in the cation–anion radical distribution functions in both small and large boxes. In the AIMD simulations for the same ionic liquid, [C₁mim]Cl, by Bhargava and Balasubramanian,³¹⁷ differences in the cation–cation radical distribution functions were observed. In their work, the Car–Parrinello Molecular Dynamics (CPMD)⁴⁷² combined with the BLYP functional was used to predict the liquid structure of the ionic liquid. The radical distribution functions did not show appreciable differences compared to those of previous AIMD simulations with the PBE functional.⁵⁰² The main difference came for the cation–cation RDF that displayed a distinct peak at 4.1 Å, otherwise absent in classical MD simulations repeated in the same work. It was suggested that a longer simulation time of 9.5 ps for a simulation periodic box of 32 ion pairs resulted in the cations exploring a larger space of available configurations, leading to the cations preferring to stack through long range π – π stacking interactions, also observed in the crystal structure.⁵¹⁸ The size of the simulation box and the simulation time appeared to be important for the prediction of long range cation–cation and anion–anion interactions.

9.1. Ion polarization

Lynden Bell and co workers were the first ones to show that ionic liquid ions displayed increased dipole moments in the bulk of ionic liquids.³¹⁶ AIMD simulations similar to their original work⁵⁰² were performed on 8 ion pairs of [C₁mim]Cl using periodic boundary conditions at 450 K. Dipole moments of ions in the structure were analyzed using a scheme of Marzari and Vanderbilt⁵¹⁹ to localize KS orbitals (originally extending through the whole space of the simulation box) and apply the Wannier representation to extract dipole moments for individual atoms. The latter were recalculated to a dipole moment of an individual ion with *N* atoms and *M* orbitals as follows:

$$\mu = \sum_{I=1}^N Z_I \mathbf{R}_I - 2 \sum_{A=1}^M \mathbf{r}_A \quad (50)$$

where *R* is the atom center and *r* is the Wannier orbital center. Five hundred configurations for both cations and anions were

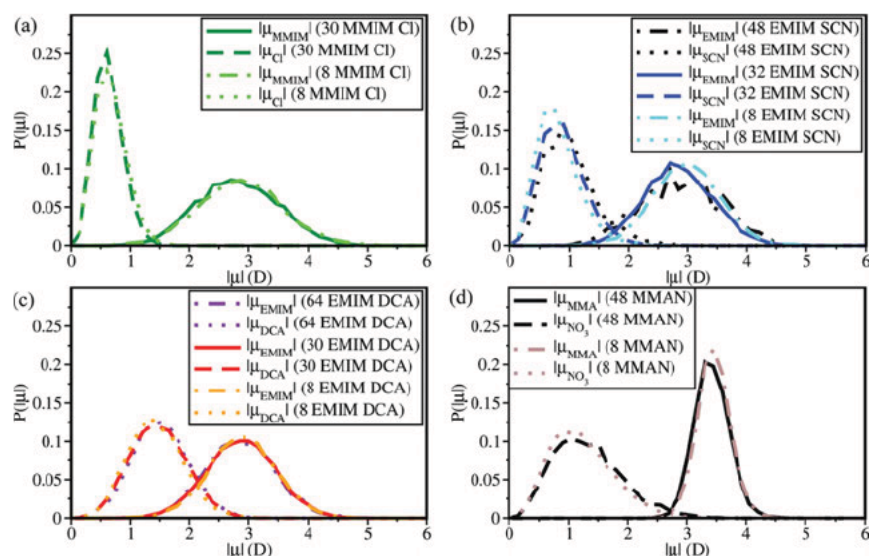


Figure 13. Dipole moment distribution in periodic simulation boxes of varying size (between 8 and 64 ion pairs) of ionic liquids: (a) $[\text{C}_1\text{mim}]\text{Cl}$, (b) $[\text{C}_2\text{mim}][\text{SCN}]$, (c) $[\text{C}_2\text{mim}][\text{N}(\text{CN})_2]$, and (d) $[\text{CH}_3\text{NH}_3][\text{NO}_3]$. Reproduced from Figure 2 of *J. Chem. Theory Comput.* 2011, 7, 3040 3044. Copyright 2011 American Chemical Society.

selected from AIMD trajectories⁵⁰² to generate a distribution of dipole moments. A significant polarization of both cations and anions by an average of 0.7 D was observed. The dipole moment distribution of the cation was predicted to be very broad, with an average of 2.67 D, compared to 2.2 D for an isolated cation in similar simulations. The most impressive result was obtained for the chloride anion, whose dipole moment peaked at 0.56 D compared to zero dipole moment in the absence of other ions. This was a seminal work, establishing the importance of ion polarization in ionic liquids. Further confirmation came from the work of Bhargava and Balasubramanian,⁵⁰⁷ who performed AIMD simulations of $[\text{C}_4\text{mpm}][\text{PF}_6]$ on a periodic box of 12 ion pairs using the BLYP potential. A similar broadening of the dipole moment distribution for both the cation and anion was observed, with the PF_6^- anion, which possessed a zero dipole moment in the isolated state, becoming strongly polarized and extending its dipole moment beyond 2 D. Similar results of the increase in dipole moments of ions were also obtained from MP2 and PBE calculations for ionic clusters consisting of 2 to 8 ion pairs of $[\text{C}_1\text{mim}]\text{Cl}$ ^{477,520} as well as other typical ionic liquids, such as $[\text{N}(\text{CH}_3)_4][\text{BF}_4]$ and $[\text{C}_n\text{mim}][\text{BF}_4]$ (where $n = 1, 3$, and 4).⁵²¹ Krekeler et al.⁵²² performed a systematic study comparing the dipole moments calculated for structures of $[\text{C}_1\text{mim}]\text{Cl}$, based on classical MD simulations and DFT calculations. The former were performed on 239 ion pairs with the Lopes and Padua force fields^{306,307} at 425 K and the Wang force fields⁵²³ at 0 K. Ionic clusters consisting of 2, 4, and 8 ion pairs were extracted from classical MD simulations and reoptimized with the PBE functional. Dipole moments of ions in these clusters were calculated using Wannier orbitals. The PBE optimized clusters were subsequently reoptimized in classical MD simulations to allow for comparison of dipole moments from classical MD simulations with those from DFT. As a rule, the MD simulations produced lower and narrower dipole moments by at least 1.0 D, further identifying the need for AIMD simulations to properly account for the electrostatic properties of ions in the bulk of ionic liquids.

In the work of Wendler et al.,⁴⁷⁷ AIMD simulations were performed on the 30 ion pair box of $[\text{C}_2\text{mim}][\text{N}(\text{CN})_2]$ with the BLYP functional and the D2 dispersion correction (further in the text abbreviated as BLYP D2) at two temperatures, 333 and 400 K. Structures from equilibrated classical MD simulations were used as the starting point, and the box was allowed to equilibrate for 5 ps. An interval of 3 ps was used to record trajectories up to 39 ps and calculate dipole moments of ions using Wannier orbitals. A wide fluctuation in the dipole moment distribution was almost identical for each interval, thus highlighting that polarization was a rather localized effect independent of the bulk liquid structure. As expected, temperature affected the dipole moment distribution, with ions becoming less polarized with increasing temperature due to the increase in interionic distances. The locality of dipole moments was originally suggested and confirmed by Wendler et al.⁴⁵⁷ in a series of AIMD simulations of ionic clusters of varying sizes: from 8 to 64 ion pairs. These calculations were performed for four ionic liquids, $[\text{C}_1\text{mim}]\text{Cl}$, $[\text{C}_2\text{mim}][\text{SCN}]$, $[\text{C}_2\text{mim}][\text{N}(\text{CN})_2]$, and $[\text{CH}_3\text{NH}_3][\text{NO}_3]$, using the same BLYP D2 functional, apart from the protic ionic liquid, for which the BLYP functional was augmented with dispersion corrected atom centered potentials (DCACPs) as described in section 1.^{179,180} Snapshots of equilibrated classical MD simulations were used as starting structures for consequent AIMD simulations, allowing for 5 ps of equilibration before trajectories were analyzed. The most impressive observation was that all ionic liquid ions exhibited a very large fluctuation in the dipole moment distribution that did not change going from small clusters of 8 ion pairs to larger clusters of 48 and 64 ion pairs (see Figure 13). Despite ionic liquids being governed by long range electrostatic interactions, the electronic effects associated with ion polarization exhibited a very local nature. This represents a very powerful conclusion that ensures that as long as good starting structures (e.g., as those from classical MD simulations) are selected, short time AIMD simulations should provide reliable information about the liquid structure and dynamics of ions in ionic liquids as well as their electronic properties, such as dipole moments and vibrational spectra.⁴⁷⁹

9.2. Dispersion correction

The description of dispersion forces is critical in the prediction of the liquid structure of ionic liquid ions that can form specific intermolecular interactions such as π - π stacking of imidazolium rings⁵¹⁸ or functionalized methanide anions.³⁸⁵ The ultimate role of dispersion forces, even in ionic liquids driven by hydrogen bonding such as imidazolium based ionic liquids, has been shown through a series of AIMD simulations by the Kirchner group⁴⁹¹ for the $[\text{C}_2\text{mim}][\text{C}_2\text{H}_5\text{OSO}_3]$ ionic liquids. The original PBE functional, as well as the PBE functional augmented with the D2 dispersion correction, was used in a periodic box of 32 ion pairs, with the simulations being performed for 19 ps. The cation-anion radical distribution functions did not reveal any significant difference between the two functionals. This translated into almost identical power spectra that are discussed further in the text. The main deviation came from long range cation-cation and anion-anion interactions, showing the increased population of the π - π stacking interaction sites for cations and the sulfur-sulfur interaction sites for the anions. The cation also appeared to preserve its environment for twice as long when dispersion forces were properly accounted for. The inclusion of dispersion led to decreased and, hence, more realistic diffusion rates of ions as well as slow hydrogen bonding dynamics. Although the GGA functionals are already reliable in predicting the liquid structure qualitatively, for quantitative results on dynamics, it is crucial to include the dispersion correction.

Contrary to the $[\text{C}_1\text{mim}]\text{Cl}$ results described above, AIMD simulations⁵²⁴ revealed the importance of the anion interacting with the imidazolium ring from above or below the plane in C_2mim based ionic liquids coupled with cyano based anions such as SCN^- , $\text{N}(\text{CN})_2^-$, and $\text{B}(\text{CN})_4^-$. The simulations employed the BLYP functional with the D3 dispersion correction, a double ζ basis set, and the core-electron pseudopotentials of Hutter et al.⁵²⁵⁻⁵²⁸ and were carried out at 398 K to enhance the sampling of the available configuration space. Between 22 and 32 ion pairs were placed in a periodic box, with the simulation times ranging between 42 and 60 ps depending on the anion size. Starting structures were generated by classical MD simulations based on the Lopes and Padua OPLS AA force fields.^{306,307} In the AIMD bulk structure, the π - π stacking of the imidazolium ring was predominantly observed in the case of $[\text{C}_2\text{mim}][\text{SCN}]$, with its occurrence drastically dropping for other bulkier anions. Diffusion coefficients were estimated based on the mean square displacements of ions and showed very fast dynamics of ions in $[\text{C}_2\text{mim}][\text{SCN}]$ and $[\text{C}_2\text{mim}][\text{B}(\text{CN})_4]$, whereas the diffusion process in $[\text{C}_2\text{mim}][\text{N}(\text{CN})_2]$ was very slow: four times slower compared to that of $[\text{C}_2\text{mim}][\text{SCN}]$. These values did not correlate well with viscosity measured at 363.15 K, with $[\text{C}_2\text{mim}][\text{SCN}]$ being the most viscous despite showing the slowest dynamics. The difference in simulation and experimental temperatures as well as short simulation times were attributed to these deviations, further confirming that longer simulation runs are required for a quantitative description of the diffusion process in ionic liquids. A difference between experimental and simulation temperatures of 35 K might represent a more important factor, as the experimental viscosity values fell in a very narrow range of 3.8 to 5.4 mPa s. The viscosity in ionic liquids was found to follow the traditional Vogel-Fulcher-Tammann behavior,^{529,530} that assumes the exponential behavior of this property with respect to the temperature difference, $T - T_0$, where T_0 is the glass transition

temperature. Ionic liquids were shown to have different pre exponential factors as well as strength parameters⁵³¹ under the exponent for a homologous series of ionic liquids coupled with the same anion, e.g. NTf_2^- .⁵³² This finding suggests that a higher temperature might produce a different trend in viscosity in these cyano based ionic liquids. Regardless of this outcome, this work clearly identified that the liquid structure depended on both the cation and anion, with smaller, linear anions such as Cl^- and SCN^- favoring the imidazolium ring π - π stacking, whereas bulkier anions such as dicyanamide and tetracyanoborate disrupt the stacking in the bulk. The liquid structure *per se* would not be indicative of how mobile ionic liquids are, with a structurally different ionic arrangement leading to similar diffusion coefficients.

9.3. Proton dynamics

AIMD simulations are the best technique today to understand hydrogen bonding dynamics in ionic liquids, as these reveal the structural arrangement in the first and second solvation shells, thus allowing for the prediction of the effect of molecular solvents on the hydrogen bonding network in ionic liquids. This has been demonstrated for a number of ionic liquids by the Kirchner group.^{500,506,511,512}

The first AIMD study of a protic ionic liquid, methyl ammonium nitrate, was performed by Zahn et al. using the BP86 functional in a periodic box of 48 ion pairs using the CPMD method.⁴⁷² The Amber⁵³³ force field was used in classical MD simulations to generate the starting structures for AIMD. Equilibration was carried out for 5 ps, with an additional time of 1.92 ps for relaxation with the thermostat settings at 400 K. The actual simulation was performed for 19.35 ps at the same temperature. The autocorrelation function of Rapaport was applied to study the ion pairing dynamics in this ionic liquid. The liquid structure, represented by an extended hydrogen bonding network, exhibits a large degree of directionality. Only 1.8 out of three available oxygen atoms are involved in the hydrogen bonding at a time, with a negligible amount of 2 fold hydrogen bonds. The dynamics revealed long lived ion pairs, with 85% of them being kept in tact even after 14.5 ps of the simulation, which was beyond the duration of the simulation. The presence of long lived ion pairs was independent of the initial ion arrangement. Individual ions were found to almost freely rotate on the scale of 2 ps within these ion pairs. This suggests that the liquid structure of the protic ionic liquid consisted of long lived cages, with ions "rattling" around tiny areas similar to ions of NaCl oscillating in the corners of the crystal lattice. It has to be noted that no proton transfer between the cation and the anion was observed throughout the simulation, which is in good agreement with strong basicity of the nitrate anion that would prevent the back proton transfer from the methylammonium cation.

In the study of Zahn et al.,⁵⁰⁶ 48 ion pairs of methylammonium nitrate and 4 water molecules (which corresponds to 1.6 wt % of water in the mixture) were included in AIMD simulations at 400 K, thus allowing for the water molecules to essentially be solvated by the ionic liquid ions. The BP86 functional^{30,32} was used in these simulations. The equilibration procedure was applied for the first 4.39 ps, with the simulation running for 25.25 ps. The cation was found to form stronger hydrogen bonding and longer living hydrogen bonded complexes with the water molecules. In the mixture, water was established to have its dipole moment distribution shifted to lower values compared to that of pure water, thus

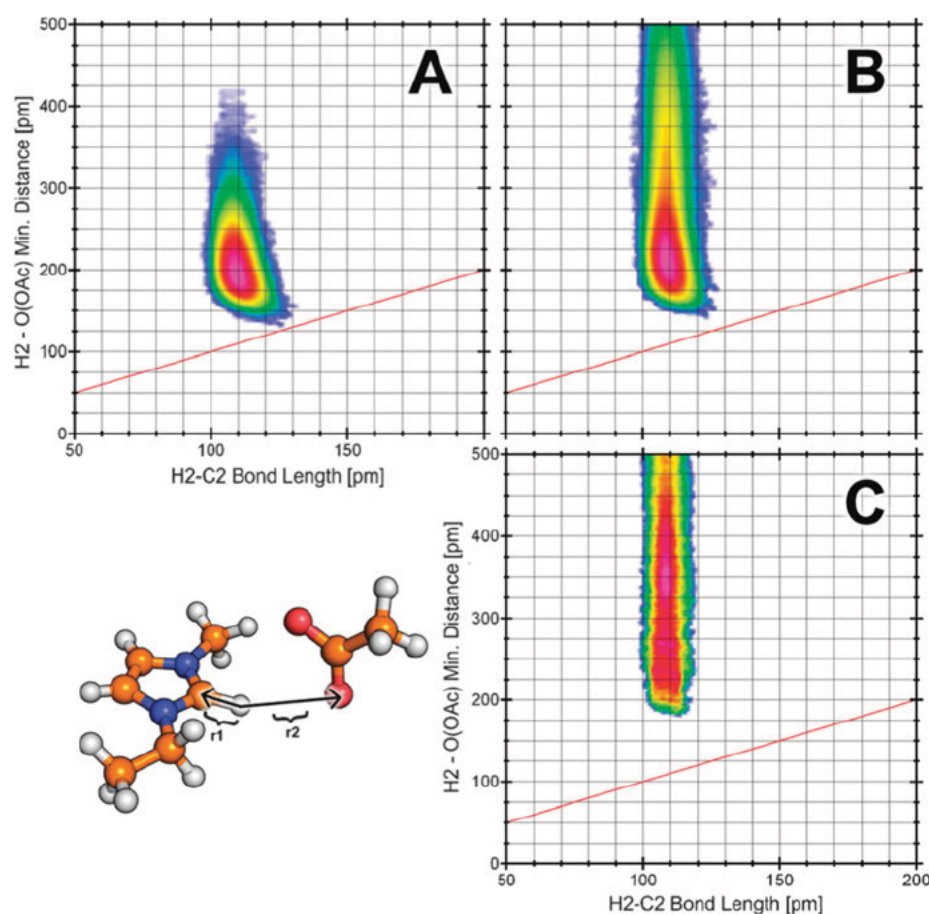


Figure 14. Combined distribution function showing the proton transfer from the C_2mim^+ cation to the acetate anion. The red line indicates the configurations at which $r_1 = r_2$. Reproduced from ref 500 with permission of the PCCP Owner Societies.

decreased the polarization of water in ILs compared to the bulk of water. The dipole moment was calculated from the maximally localized Wannier centers,^{519,534–536} which was successfully validated for water mixtures. Comparing the power spectrum of pure water to that of the IL–water mixture indicates a significant red shift of the O–H stretches, thus further supporting the idea of reduced polarization of water molecules in ionic liquids. It has to be noted that the dipole moment distribution of either the cation or the anion did not change when going from the neat IL to the IL–water mixture, which is also reflected in almost identical cation–anion, cation–cation, and anion–anion radical distribution functions calculated with respect to the center of mass for the cation and the anion for both cases.

Different conclusions were observed in the study of Brehm et al. on mixtures of water with an imidazolium based ionic liquid, $[C_2mim][CH_3COO]$.^{500,511} AIMD simulations were performed on periodic boxes of varying composition: (a) 31 ion pairs for the neat IL, (b) 27 ion pairs and 81 water molecules (75.9 wt % of IL), (c) 3 ion pairs and 300 water molecules (86 wt % of IL), and (d) 128 water molecules for the neat water. The BLYP D2 functional as well as double ζ quality basis sets and pseudopotentials of Hutter et al.^{525–527} were used. The starting configurations were taken from classical MD simulations using the OLPS AA force fields⁵³⁷ with the modifications of Liu et al.⁵³⁸ for imidazolium based ionic liquids. Each configuration was allowed to run for 10 ps, with the final box size being

averaged over these configurations in the last 5 ps. All simulations ran for at least 47 ps for each composition. Water molecules were found to form strong hydrogen bonds with the acetate anion. Addition of water changed the liquid structure of ionic liquids, with the cations no longer forming π – π stacking interactions regardless of the water content. The ordered structure of the acetate ionic liquid appears to drastically change upon water addition. In the neat IL, the acetate anion exclusively interacted in the plane of the C2–H bond, thus blocking interference of any other neutral species from interacting with the bond. An effect of this strong cation–anion interaction was also shown in AIMD simulations of 1 ethyl 3 methylimidazole 2 ylidene solvated in 1 methyl 3 ethyl imidazolium acetate, forcing the carbene molecule to interact with alkyl chains on the imidazolium cation.⁵³⁹ It is not surprising that as a result of this insufficient stability arising from the alkyl chains, the carbene is usually very reactive in acetate based ionic liquids.⁵⁴⁰ Binary mixtures of ionic liquids with water showed a different trend. Due to the disruption of the π – π stacking interaction of imidazolium rings, the anion started to additionally show a preference for interacting with the cation from above/below the imidazolium ring, thus blocking the water molecules from accessing the ring directly. Water was found to be more strongly polarized when interacting with the anion compared to neat water. In instances in which water interacted with the cation, a decrease in the dipole moment of water was again observed, as in the case of

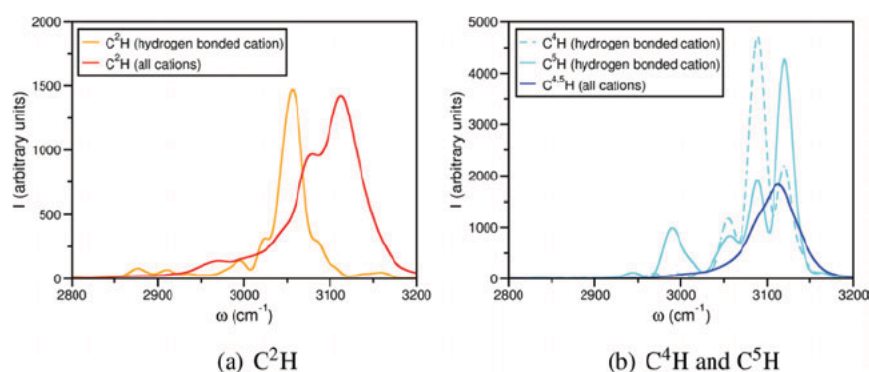


Figure 15. Power spectra of (a) C2–H vibrations and (b) C4–H and C5–H vibrations of all cations and of strongly hydrogen bonded cations in the region 2800–3200 cm^{−1}. Reproduced from Figure 7 of *J. Chem. Theory Comput.* 2012, 8, 1570–1579. Copyright 2012 American Chemical Society.

methylammonium nitrate.⁵⁰⁶ The simulation of the neat IL identified a few instances for which the C2–H bond was almost broken, with the proton being almost transferred to the anion (see Figure 14). This finding suggests that the presence of carbene impurities may be inevitable in this nominally aprotic ionic liquid that appears to exhibit the behavior of a protic ionic liquid. The back proton transfer between the imidazolium cation and the anion was much less likely to be observed with increasing water content, due to changes in the liquid structure. This study further highlighted the value of AIMD simulations to study the proton dynamics, especially in ionic liquids that were previously considered typically aprotic.

9.4. Thermodynamics data

The vaporization process of 1 ethyl 3 methylimidazolium ethylsulfate^{363,490} was investigated by comparing the change in the liquid structure at three temperatures, 300 K, 400 K, and 600 K, with 400 K being closest to the experimental temperature of vaporization. The same computational protocol as the one described in the previous publication by Wendler et al.⁴⁷⁷ was used in the study. The bulk simulations were also compared to those for a single ion pair, recorded between 295 and 340 ps. The AIMD simulation at 300 K revealed a typical cation–anion arrangement, with the anion occupying both energetically favorable positions: above/below the imidazolium ring and in the plane of the C2–H bond. As the temperature increased to 400 K, the cation–anion distance lengthened, leading to the anion predominantly residing above/below the plane. The emphasis of the hydrogen bonding shifted toward a typical interionic interaction, which produced similar radial distribution functions when compared to the gas phase simulation of an ion pair at 400 K. The free energy surface of the C2(cation)–S(anion) distance was plotted for the bulk ionic liquid at 300 K and the gas phase ion pair at 600 K. A striking difference between the shapes and positions of the two curves was observed, with the former displaying the minimum at a shorter distance on a much flatter surface. This work confirmed that ionic liquids did, in fact, undergo a significant structural change close to the vaporization temperature, favoring the formation of typical ion pairs and approaching the preferred energetic state observed in the gas phase.⁴⁹⁰ This was a confirmation that imidazolium based ionic liquids did indeed evaporate as liquid ion pairs.

Currently, solubility properties of ionic liquids can only be analyzed qualitatively based on their liquid structure. For example, studies performed by the Kirchner group to understand the solvation mechanism of CO₂^{509,515} and

SO₂⁵⁰⁸ in ionic liquids carried important insight into the type of interactions that these gases imposed in the bulk of ionic liquids. In the case of the CO₂ molecule, the anion played the defining role in the solvation process, whereas SO₂ tended to equally interact with both the cation and anion. The quantitative thermodynamic characterization of the solvation process is not yet available due to short running times of current AIMD simulations.

9.5. Power spectra

IR spectra carry invaluable information not only about the chemical structure of ions but also about intermolecular interactions, especially hydrogen bonding, in ionic liquids, as has been demonstrated by the Ludwig group.^{393,458} The low frequency regime, below 200 cm^{−1}, is particularly indicative of strong cation–anion interactions evidenced in a series of ionic liquids.^{391,541} Fundamentally, IR spectra are calculated from changes in dipole moments of individual atoms that are affected not only by chemical bonds but also by intra and intermolecular interactions. The development of the procedure to maximally localized Wannier orbitals in condensed periodic systems^{542–544} allows for the calculation of time dependent dipole moments for individual atoms in AIMD simulations based on the Fourier transformation of autocorrelation functions of atom's velocities, thus generating power spectra.^{545,546} These spectra have been demonstrated to reliably predict experimental IR spectra of traditional condensed systems such as water and ice from short time trajectories of AIMD simulations.^{546,547} The Kirchner group identified that, for ionic liquids, the autocorrelation functions summed over all time steps provided an excellent prediction of their IR spectra, as was first demonstrated for a number of imidazolium based ionic liquids.⁵⁴⁸ AIMD simulations usually produce red shifted IR spectra for condensed systems such as water due to the exclusion of electron mass following each nucleus and the use of an incomplete basis set.^{546,549,550} These two effects were shown to be successfully corrected through the inclusion of a fictitious electron mass of 450 au,^{546,548} and thus, the vibrational frequency could be effectively recalculated using the reduced mass of the nuclei involved in the vibration as $\omega \sqrt{1 + \frac{\delta M}{M}}$ (where M is the sum of masses of the nuclei and δM is the sum of masses of fictitious electrons associated with the nuclei). The inclusion of fictitious masses of electrons is known to slow down AIMD simulations, thus affecting the energy convergence, which needs to be carefully monitored.^{546,548}

The procedure to generate power spectra from AIMD trajectories was implemented in the TRAVIS software,^{551,552} a powerful code that also enables the extraction of other valuable information such as radial distribution functions, molecule/ion displacements, and diffusion coefficients. The use of the harmonic oscillator approximation to calculate vibrational frequencies results in predicted intensities to be of the same magnitude.⁵⁵² Due to the influence of anharmonic effects on vibrations in condensed systems, it is common to observe additional broadening and overlap of experimental bands, thus changing their intensities. As a result, predicted intensities of harmonic vibrations can only be considered in a qualitative manner. Atom velocities can be easily recalculated to predict IR spectral lines of individual cations and anions (see Figure 15), thus allowing for a thorough analysis of the influence of intermolecular interactions on the distribution of bands in IR spectra.

The first studies reporting power spectra of ionic liquids were performed by the Balasubramanian^{517,553,554} and Kirchner⁵⁴⁸ groups. In the study of Wendler,⁵⁴⁸ the size of the periodic box and simulation time were assessed with respect to the quality of generated IR spectra for $[\text{C}_1\text{mim}]\text{Cl}$, $[\text{C}_2\text{mim}][\text{SCN}]$, $[\text{C}_2\text{mim}][\text{N}(\text{CN})_2]$, and $[\text{C}_4\text{mim}]\text{Y}$, where $\text{Y} = \text{Cl}^-$, SCN^- , and $\text{N}(\text{CN})_2^-$. Due to the locality of the electronic effects in ionic liquids,^{457,555} both 8 and 32 ion pair periodic boxes produced similar IR spectra. Slow dynamics of ions that are usually present in long lived cages⁴⁸³ reflects the finding that AIMD simulations of already 10 ps were sufficient to produce convergence and, hence, generate high quality power spectra. Single ion pairs could reproduce the experimental spectra in the fingerprint and higher frequency regions, $>1000\text{ cm}^{-1}$, but failed to adequately describe the low frequency region due to the neglect of interionic interactions in the bulk of ionic liquids⁴⁷⁷ (see Figure 16). Static DFT calculations on larger clusters of aprotic¹³⁹ and protic³⁸⁶ ionic liquids, consisting of a few ion pairs, were shown to adequately predict experimental IR spectra. A number of low frequency vibrations were also predicted from AIMD simulations of $[\text{C}_4\text{mim}][\text{PF}_6]$ in the study of Sarangi et al.⁵⁵³ These are positive outcomes highlighting the ability of short time AIMD spectra in assigning IR spectra of ionic liquids and their mixtures with molecular solvents and gases to specific vibrations observed in experiment. Examples of the prediction of power spectra include systems of SO_2 solvated in $[\text{C}_2\text{mim}][\text{SCN}]$,⁵⁰⁸ binary mixtures of $[\text{C}_2\text{mim}]\text{Cl}$ and $[\text{C}_2\text{mim}][\text{SCN}]$,⁵⁵⁵ and mixtures of $[\text{C}_2\text{mim}][\text{CH}_3\text{COO}]$ and water.⁵⁵⁶

Although Wannier orbitals are a powerful tool to predict dipole moments of condensed systems based on localized molecular orbitals, the approach is computationally demanding and can lead to spurious oscillations of dipole moments. The most cost effective way to counteract this issue is to use the radical Voronoi tessellation by Gellatly and Finney⁵⁵⁷ that partitions the system into well defined geometric domains occupied by individual molecules. The domains are determined based on van der Waals radii of atoms and distances between them.^{558,559} The original Voronoi approach did not distinguish between heterogeneous atoms, whereas the inclusion of the radical plane division allowed for inclusion of the overlap between atomic radii of different sizes, thus resulting in a reliable description of hydrogen bonded interactions between molecules.⁵⁵⁷ Integration over the electron density associated with each molecular domain can be subsequently used to obtain individual molecular dipole moments and, hence, generate

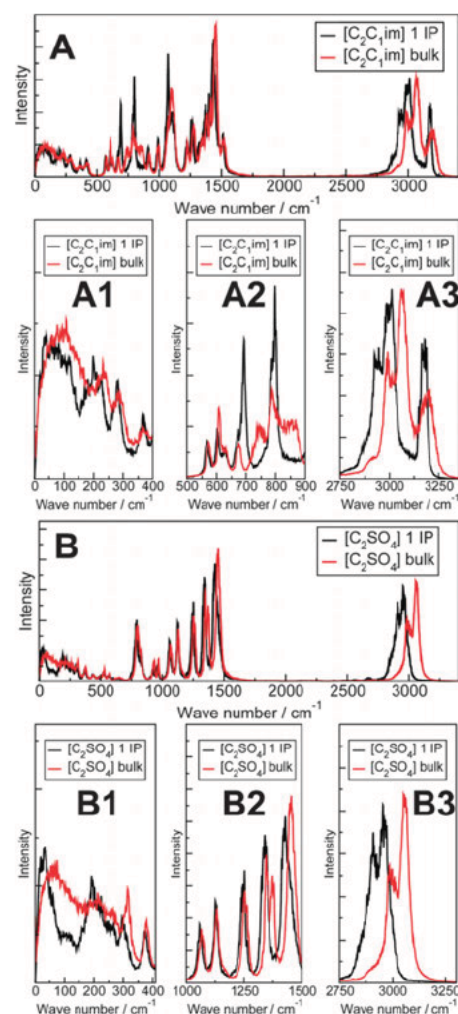


Figure 16. Comparison of the predicted power spectra of $[\text{C}_2\text{mim}]\text{-}[\text{Ethylsulfate}]$ obtained from the calculations of a single ion pair (1 IP, black line) and the bulk (red line). Reproduced from ref 490 with permission of the PCCP Owner Societies.

power spectra. This approach with some modifications was implemented in the TRAVIS code by the Kirchner group.⁵⁶⁰ Excellent agreement between power spectra with the Wannier orbitals and the radical Voronoi tessellation was observed for condensed systems including traditional solvents such as methanol, benzene, and phenol and mixtures of $[\text{C}_2\text{mim}][\text{CH}_3\text{COO}]$ and water.⁵⁶⁰

9.6. NMR chemical shifts

Bagno et al.⁵⁶¹ used snapshots from AIMD simulations to predict proton NMR chemical shifts of $[\text{C}_2\text{mim}]\text{Cl}$. The AIMD simulations were performed using the originally proposed CPMD formulation⁴⁷² on periodic simulation boxes consisting of either 7 or 20 ion pairs. Short time simulations, within 3.5 ps, were performed for each simulation box, with geometries at sequential time steps being extracted for further calculation of proton NMR chemical shifts. These clusters consisted of the reference cation, three anions closest to the H2, H4, and H5 atoms, and neighboring ions within 7.8 Å, thus including the first solvation shell as identified earlier.⁴⁶⁹ A two layer approach based on the Morokuma's ONIOM approach⁴⁷¹ was again applied to study clusters. The first layer, consisting of the

reference cation and the three closest anions, was treated at the B3LYP/cc pVTZ and/or B3LYP/6 31G(d) levels of theory, whereas the rest of the cluster was calculated with HF/3 21G. The predicted proton NMR chemical shifts were averaged over time steps for each cluster time in the statistical analysis. It has to be pointed out that the NMR shifts of the ring protons showed a very broad distribution of up to 10 ppm. The averaged proton NMR chemical shifts differed up to 0.5 ppm depending on the size of the simulation box of the original CPMD simulation as well as the cluster size chosen for subsequent NMR calculations. The smallest simulation box with 9 ion pairs produced the best results for the ring protons, with the H2 shift deviating from experiment by <0.5 ppm. Overall, all types of clusters taken from CPMD simulations produced errors of <0.55 ppm on average, perhaps due to the locality of the electronic properties in ionic liquids, thus making it an effective tool for the prediction of proton NMR of ILs and providing a solid link between the structural arrangement and experimentally observed proton chemical shifts.

9.7. Electrochemical windows (ECWs)

Recently Zhang and Maginn⁵⁶² have successfully applied AIMD simulations to predict the electrochemical window of ionic liquids. As was shown by Ong et al.²¹⁶ the electrochemical window could be reliably calculated as the orbital energy difference of the HOMO and LUMO. AIMD simulations with the PBE functional used snapshots from 2 ns classical MD simulations^{360,478} of eight ion pairs in a periodic simulation box. Statistically similar results were produced from 12 and 16 ion pairs. The previously established approach was extended by relaxing snapshots from classical MD simulations with CPMD simulations for 300 steps at 300 K, with the final configuration being quenched to the minimum in 3000 steps using simulated annealing. The relaxation procedure was established to be particularly important, as it produced better agreement with experimental values. The new methodology was applied to 14 ionic liquids based on two anions, such as 1,2,4 triazolidine and 2 (cyano) pyrrolide, and 7 types of imidazolium and phosphonium based cations. The predicted electrochemical windows were in excellent agreement with experimental data with an average error of 0.34 eV and a maximum error of 0.7 eV. When the relaxation and quenching steps were not followed through in the AIMD simulations, the average error increased 2 fold up to 0.67 eV (see Table 1). This finding might be indicative of an inadequate description of the liquid structure of ionic liquids using classical MD simulations. Overall, the new methodology is very robust for the prediction of ECWs of novel ionic liquids.

In the work of Dhungana et al.,²²¹ a similar methodology to that of Zhang and Maginn was used to predict the ECWs of cyano based ionic liquids, $[C_2mim]X$ and $X = SCN^-$, $C(CN)_3^-$, $N(CN)_2^-$, and $B(CN)_4^-$. AIMD simulations with the PBE functional and double ζ basis set were performed on snapshots from classical MD simulations^{306,307} equilibrated for 6 ns, allowing for relaxation for 300 steps without the subsequent quenching. The quenching was not performed, as the liquid structure was intended to adjust its bond lengths and angle without a significant change to the liquid structure. Excellent agreement was achieved with experimental data. Analysis of the HOMOs and LUMOs revealed that, in the case of the $B(CN)_4^-$ anion, both the cathodic and anodic limits of the electrochemical window came from the cation, thus making this anion a rather poor electron donor and widening its ECW.

Table 1. Comparison of Calculated and Experimental^b Electrochemical Windows (in V) for a Group of Ionic Liquids Containing 2 (Cyano)pyrrolide (CNPyrr) and 1,2,4 Triazolidine (124triz) Anions^a

IL	AIMD-sp	AIMD-min	exp.
$[P_{2224}][CNPyrr]$	3.10 ± 0.02	3.32 ± 0.05	3.7
$[P_{2224}][124triz]$	3.26 ± 0.01	3.90 ± 0.04	4.6
$[P_{222mom}][CNPyrr]$	2.95 ± 0.02	3.45 ± 0.03	3.3
$[P_{222mom}][124triz]$	3.19 ± 0.01	4.01 ± 0.04	
$[P_{222mom}][CNPyrr]$	3.03 ± 0.01	3.36 ± 0.05	3.5
$[P_{222mom}][H4triz]$	3.29 ± 0.02	4.15 ± 0.04	4.2
$[P_{66614}][CNPyrr]$	3.28 ± 0.01	3.50 ± 0.04	3.7
$[P_{66614}][124triz]$	3.25 ± 0.02	3.79 ± 0.06	4.2
$[EMIM][CNPyrr]$	2.17 ± 0.01	2.66 ± 0.03	2.4
$[EMIM][124triz]$	2.49 ± 0.02	3.41 ± 0.05	2.9
$[BMIM][CNPyrr]$	2.23 ± 0.02	2.82 ± 0.02	2.9
$[BMIM][124triz]$	2.34 ± 0.02	3.27 ± 0.06	3.3
$[PY_{14}][CNPyrr]$	3.48 ± 0.02	3.63 ± 0.05	3.3
$[PY_{14}][124triz]$	3.67 ± 0.02	4.10 ± 0.05	3.7
rmsd	0.67	0.34	

^aCalculated results for two types of simulations are presented: (a) no additional relaxation and quenching to ensure the global minimum, labeled AIMD-sp, and (b) additional relaxation and quenching to ensure the global minimum, labeled AIMD-min. Reproduced from Table 6 of *J. Phys. Chem. B* 2014, 118, 6250–6255. Copyright 2014 American Chemical Society. ^bExperimental data are taken from ref 549 and *J. Electrochem. Soc.* 2013, 160, A1604–A1610.

More studies are needed to understand the effect of quenching on the prediction of ECWs in ionic liquids.

10. SUMMARY AND OUTLOOK

Quantum chemical calculations have been invaluable in understanding the complex interplay of intermolecular forces in ionic liquids and the relationship to their thermodynamic and transport properties. The importance of three fundamental forces—Coulomb, induction, and dispersion—in governing the physicochemical properties of ionic liquids has been established, thus identifying the need for correlated levels of theory to accurately predict the energetics of ionic liquid clusters. It has been convincingly evidenced in multiple publications that inclusion of dispersion interactions has led to much better agreement with experimental data. From the energetic point of view, hydrogen bonding appeared to be equivalent to typical interionic interactions, suggesting that no unique treatment was needed to accurately account for bulk interactions in ILs. Many body effects up to third order have been confirmed to be crucial for induction forces and, potentially, dispersion forces, suggesting that pairwise potentials are not adequate to capture interactions in ionic liquids. More studies are needed to identify the extent of three body effects on dispersion forces. These findings clearly indicate that individual ions and single ion pairs do not serve as reliable models for studying the physicochemical properties of semi Coulomb systems such as ionic liquids, and therefore, they need to be used with caution. Although the QSPR, VBT, COSMO RS, and noncontinuum solvation models have been successful in the prediction of the physicochemical properties of ionic liquids, these often rely on additional parametrization for a new class of ionic liquids. Their main limitation comes from the exclusion of many body effects in their formulation, thus stymieing their predictive power to design novel ionic materials. Attempts to find direct

correlations between electronic structure properties, such as orbital energies, dipole moments, and binding/interaction energy in ion pairs and experimental data, have been unsuccessful, further highlighting the need to consider larger clusters of ionic liquids to ensure the predictive power of quantum chemical methods. On the positive side, electronic structure properties appear to be of local nature, thus allowing for the prediction of spectroscopic properties such as NMR chemical shifts, power IR, and Raman spectra and electrochemical windows using relatively medium sized clusters of 8 ion pairs. Further development and application of the quantum cluster equilibrium approach coupled with newly developed cost effective methods may provide a powerful tool for fast screening of ionic liquids to select those with desirable properties for an application at hand.

Ab initio molecular dynamics simulations have been powerful in providing insight into the liquid structure, proton dynamics, and low barrier chemical reactions. Due to limitations in computational resources, these simulations are only feasible on the scale of up to 100 ps, which is not sufficient to generate reliable statistical data and to compute ion mobility and, hence, transport properties. Ionic liquids have also proven to be rather complex in their behavior, undergoing drastic structural change depending on the environment, such as the presence of a solvent. Therefore, it is recommended to conduct studies on varying types of ionic liquids for definitive and general conclusions.

There has been significant development in cost effective quantum chemical methods such as modifications of the SCS MP2 method and the DFTB3 D approach for studying energetics of ionic liquids, making calculations of tens of ion pairs feasible. These advancements will provide necessary benchmark data needed for further development and refinement of classical force fields, as has been already demonstrated for some ionic systems.^{309,520,563,564} Due to their robust methodology, AIMD simulations will prove invaluable for studying solvation mechanisms in ionic liquids for solutes ranging from molecular gases such as CO₂ to large biologically relevant molecules. Another advantage of AIMD simulations will come from the analysis of kinetics of chemical reactions as well as ubiquitous proton and transfer processes. As computational power continues to grow in the next 10 years, longer runs of AIMD simulations will become feasible, thus leading to the reliable prediction of physicochemical properties of novel ionic liquids and their mixtures with traditional solvents. These developments are expected to result in a robust and reliable methodology for fast screening of technologically and industrially advanced materials based on ionic liquids for a myriad of applications ranging from energy and storage devices to medical research.

AUTHOR INFORMATION

Corresponding Author

*E mail: katya.pas@monash.edu.

ORCID

Ekaterina I. Izgorodina: 0000-0002-2506-4890

Notes

The authors declare no competing financial interest.

Biographies

Ekaterina I. Izgorodina was educated at the Higher Chemistry College affiliated with the Russian Academy of Sciences and graduated with both a Bachelor's degree in Chemistry and a Master's of Science degree in Theoretical Chemistry. She obtained her Dr. Rer. Nat. degree in 2004 from the University of Münster under the supervision of Prof. Stefan Grimme. After a postdoctoral position with Prof. Michelle L. Coote at the Australian National University, she joined the School of Chemistry at Monash University in 2006 as a Research Fellow in Prof. Douglas R. MacFarlane's group. From 2008 until 2016 she has held two prestigious fellowships from the Australian Research Council, an Australian Post-Doctoral Fellowship, and later a Future Fellowship, that allowed her to establish the Monash Computational Chemistry Group. Her group specializes in the assessment and development of cost-effective quantum chemical methods for studying the energetics of multiscale clusters of condensed systems based on ionic liquids. Her research marries these cost-effective methods with molecular dynamics formulation to pave the way toward robust and accurate *ab initio* molecular dynamics simulations of condensed materials with a view of predicting not only their properties but also kinetic mechanisms of chemical reactions, including proton and electron transfer processes. Her passion lies in the understanding of the role of intermolecular forces and structural arrangement on the physicochemical properties of condensed systems and the development of new materials for applications in energy devices, such as metal-ion batteries and solar and fuel cells; gas capture, such as CO₂; and the pharmaceutical industry. She is an Associate Professor in the School Chemistry at Monash University who strongly contributes to the teaching program through the curriculum development in computational and physical chemistry.

Zoe L. Seeger is a current Ph.D. student in the Monash Computational Chemistry Group. She completed her Bachelor's degree with Honours at Monash University in 2015. She works on using *ab initio* molecular dynamics to develop robust approaches for the prediction of physical properties of condensed systems based on ionic liquids, and her passion lies at the junction of chemistry and computing.

David L. A. Scarborough was awarded a Ph.D. in chemistry from Monash University in 2015 under the supervision of Dr. Christopher Thompson and Assoc. Prof. Ekaterina Izgorodina. His research includes *ab initio* and DFT modelling of ionic liquids, the stability and behavior of radicals in ionic liquids, and the spectroscopic properties of organic-based conjugated materials. He also has an interest in multireference methods and chemical education.

Samuel Y. S. Tan is a senior Ph.D. student in the Monash Computational Chemistry Group. He completed a Bachelor's of Science degree with Honours with majors in Mathematics and Chemistry. His current research revolves around the development of cost-effective quantum chemical methods for the accurate prediction of noncovalent interactions of ionic liquids and intermolecular complexes in general. He is very much interested in applications of these methods to biochemistry, and his passion lies in predictive modelling.

ACKNOWLEDGMENTS

The authors acknowledge generous support from the Australian Research Council through a Discovery Project Grant and a Future Fellowship for E.I. Z.L.S. and S.Y.S.T. are grateful to the Department of Education and Training for Australian Postgraduate Awards.

ABBREVIATIONS

	where X = D (double ζ basis set), T (triple ζ basis set), Q (quadruple ζ basis set), etc. and aug includes additional diffuse functions
(aug)cc pVXZ	important for anionic species
6 311++G(d,p)	triple ζ Pople type basis set with double diffuse functions “++” and polarization functions for non hydrogen atoms “d” and hydrogen atoms “p”; other commonly used basis sets of this type include 6 311G**, 6 31++G**, and 6 31+G(d,p)
6 311G*	triple ζ Pople type basis set (* defines polarization functions as in 6 31G(d))
6 31G(d)	double ζ Pople type basis set (d stands for polarization functions for non hydrogen atoms)
AIMD	<i>ab initio</i> molecular dynamics
B(3)LYP	Becke–Lee–Yang–Parr DFT functional
BSSE	basis set superposition error
C2 H	carbon in the imidazolium cation between two nitrogen atoms
CBS	complete basis set
CC	coupled cluster with single (S), double (D), and triple (T) excitations and noniterative quadruple (Q) excitations
COSMO RS	conductor like screening model for realistic solvation
CP	counterpoise correction
CPCM	solvation approach
CPMD	Car–Parrinello molecular dynamics
D(2)(3)	dispersion correction functionals
DFT	density functional theory
DFTB(N)	density functional tight binding (N = 1,2,3)
FMO	fragment molecular orbital approach
GAMESS US	the general atomic and molecular electronic structure system
GGA	generalized gradient approximation
HF	Hartree–Fock theory
HOMO	highest occupied molecular orbital
IL	ionic liquid
IP	ion pair
KS	Kohn–Sham formalism
LDA	local density approximations
LJ	Lennard Jones potential
LLE	liquid–liquid equilibrium
LUMO	lowest unoccupied molecular orbital
MD	molecular dynamics
MOY2X	Minnesota family of DFT functionals with Y = 5 and 6 being commonly used
MP2	Møller–Plesset perturbation theory
PBE(0)	Perdew–Burke–Ernzerhof exchange correlation
QSPR	quantitative structure–property relationship
R ²	coefficient of determination
RDF	radial distribution function
RISM	reference interaction solvation model
RMS	root mean squared
SAPT	symmetry adapted perturbation theory
SCF	self consistent field
SCS IL MP2	spin component scaled for ionic liquids MP2
SCS MP2	spin component scaled MP2
TMS	tetramethylsilane

TT	trans trans
TZVP, TZVPP	triple ζ Ahlrichs’ type basis sets where P stands for polarization functions
VBT	volume based thermodynamics
VLE	vapor–liquid equilibrium

REFERENCES

- (1) Hallett, J. P.; Welton, T. Room-Temperature Ionic Liquids: Solvents for Synthesis and Catalysis. 2. *Chem. Rev.* **2011**, *111*, 3508–3576.
- (2) Greaves, T. L.; Drummond, C. J. Protic Ionic Liquids: Properties and Applications. *Chem. Rev.* **2008**, *108*, 206–237.
- (3) Greaves, T. L.; Drummond, C. J. Protic Ionic Liquids: Evolving Structure–Property Relationships and Expanding Applications. *Chem. Rev.* **2015**, *115*, 11379–11448.
- (4) Sheldon, R. Catalytic Reactions in Ionic Liquids. *Chem. Commun.* **2001**, 2399–2407.
- (5) Plechkova, N. V.; Seddon, K. R. Applications of Ionic Liquids in the Chemical Industry. *Chem. Soc. Rev.* **2008**, *37*, 123–150.
- (6) Zhao, H.; Xia, S. Q.; Ma, P. S. Use of Ionic Liquids as ‘Green’ Solvents for Extractions. *J. Chem. Technol. Biotechnol.* **2005**, *80*, 1089–1096.
- (7) Poole, C. F.; Poole, S. K. Extraction of Organic Compounds with Room Temperature Ionic Liquids. *J. Chromatogr. A* **2010**, *1217*, 2268–2286.
- (8) Abbott, A. P.; Frisch, G.; Hartley, J.; Ryder, K. S. Processing of Metals and Metal Oxides Using Ionic Liquids. *Green Chem.* **2011**, *13*, 471–481.
- (9) Billard, I.; Ouadi, A.; Gaillard, C. Liquid-Liquid Extraction of Actinides, Lanthanides, and Fission Products by Use of Ionic Liquids: From Discovery to Understanding. *Anal. Bioanal. Chem.* **2011**, *400*, 1555–1566.
- (10) Visser, A. E.; Swatoski, R. P.; Reichert, W. M.; Mayton, R.; Sheff, S.; Wierzbicki, A.; Davis, J. H.; Rogers, R. D. Task-Specific Ionic Liquids Incorporating Novel Cations for the Coordination and Extraction of Hg²⁺ and Cd²⁺: Synthesis, Characterization, and Extraction Studies. *Environ. Sci. Technol.* **2002**, *36*, 2523–2529.
- (11) Borra, E. F.; Seddiki, O.; Angel, R.; Eisenstein, D.; Hickson, P.; Seddon, K. R.; Worden, S. P. Deposition of Metal Films on an Ionic Liquid as a Basis for a Lunar Telescope. *Nature* **2007**, *447*, 979–981.
- (12) Vijayraghavan, R.; Pas, S. J.; Izgorodina, E. I.; MacFarlane, D. R. Diamino Protic Ionic Liquids for CO₂ Capture. *Phys. Chem. Chem. Phys.* **2013**, *15*, 19994–19999.
- (13) MacDowell, N.; Florin, N.; Buchard, A.; Hallett, J.; Galindo, A.; Jackson, G.; Adjiman, C. S.; Williams, C. K.; Shah, N.; Fennell, P. An Overview of CO₂ Capture Technologies. *Energy Environ. Sci.* **2010**, *3*, 1645–1669.
- (14) Hough, W. L.; Smiglak, M.; Rodriguez, H.; Swatoski, R. P.; Spear, S. K.; Daly, D. T.; Pernak, J.; Grisel, J. E.; Carliss, R. D.; Soutullo, M. D.; et al. The Third Evolution of Ionic Liquids: Active Pharmaceutical Ingredients. *New J. Chem.* **2007**, *31*, 1429–1436.
- (15) Petkovic, M.; Seddon, K. R.; Rebelo, L. P. N.; Pereira, C. S. Ionic Liquids: A Pathway to Environmental Acceptability. *Chem. Soc. Rev.* **2011**, *40*, 1383–1403.
- (16) Armand, M.; Endres, F.; MacFarlane, D. R.; Ohno, H.; Scrosati, B. Ionic-Liquid Materials for the Electrochemical Challenges of the Future. *Nat. Mater.* **2009**, *8*, 621–629.
- (17) MacFarlane, D. R.; Forsyth, M.; Howlett, P. C.; Kar, M.; Passerini, S.; Pringle, J. M.; Ohno, H.; Watanabe, M.; Yan, F.; Zheng, W. Ionic Liquids and Their Solid-State Analogues as Materials for Energy Generation and Storage. *Nat. Rev. Mat.* **2016**, *1*, 15005 (pp 15).
- (18) Scrosati, B.; Garche, J. Lithium Batteries: Status, Prospects and Future. *J. Power Sources* **2010**, *195*, 2419–2430.
- (19) Noda, A.; Susan, A. B.; Kudo, K.; Mitsushima, S.; Hayamizu, K.; Watanabe, M. Brønsted Acid-Base Ionic Liquids as Proton-Conducting Nonaqueous Electrolytes. *J. Phys. Chem. B* **2003**, *107*, 4024–4033.

- (20) Abraham, T. J.; MacFarlane, D. R.; Pringle, J. M. Seebeck Coefficients in Ionic Liquids -Prospects for Thermo-Electrochemical Cells. *Chem. Commun.* **2011**, 47, 6260–6262.
- (21) Gratzel, M. Conversion of Sunlight to Electric Power by Nanocrystalline Dye-Sensitized Solar Cells. *J. Photochem. Photobiol., A* **2004**, 164, 3–14.
- (22) Great British Innovation Vote, <http://www.topbritishinnovations.org/> (accessed August 1, 2016).
- (23) Rogers, R. D.; Seddon, K. R. Ionic Liquids - Solvents of the Future? *Science* **2003**, 302, 792–793.
- (24) MacFarlane, D. R.; Forsyth, M.; Howlett, P. C.; Pringle, J. M.; Sun, J.; Annat, G.; Neil, W.; Izgorodina, E. I. Ionic Liquids in Electrochemical Devices and Processes: Managing Interfacial Electrochemistry. *Acc. Chem. Res.* **2007**, 40, 1165–1173.
- (25) Crosthwaite, J. M.; Aki, S.; Maginn, E. J.; Brennecke, J. F. Liquid Phase Behavior of Imidazolium-Based Ionic Liquids with Alcohols. *J. Phys. Chem. B* **2004**, 108, 5113–5119.
- (26) Heintz, A. Recent Developments in Thermodynamics and Thermophysics of Non-Aqueous Mixtures Containing Ionic Liquids. A Review. *J. Chem. Thermodyn.* **2005**, 37, 525–535.
- (27) Kohn, W.; Sham, L. J. Self-Consistent Equations Including Exchange and Correlation Effects. *Phys. Rev.* **1965**, 140, A1133–A1138.
- (28) Perdew, J. P.; Ruzsinszky, A.; Tao, J.; Staroverov, V. N.; Scuseria, G. E.; Csonka, G. I. Prescription for the Design and Selection of Density Functional Approximations: More Constraint Satisfaction with Fewer Fits. *J. Chem. Phys.* **2005**, 123, 062201.
- (29) Perdew, J. P.; Burke, K.; Ernzerhof, M. Generalized Gradient Approximation Made Simple. *Phys. Rev. Lett.* **1996**, 77, 3865–3868.
- (30) Becke, A. D. Density-Functional Exchange-Energy Approximation with Correct Asymptotic Behavior. *Phys. Rev. A: At., Mol., Opt. Phys.* **1988**, 38, 3098–3100.
- (31) Lee, C.; Yang, W.; Parr, R. G. Development of the Colle-Salvetti Correlation-Energy Formula into a Functional of the Electron Density. *Phys. Rev. B: Condens. Matter Mater. Phys.* **1988**, 37, 785–789.
- (32) Perdew, J. P. Density-Functional Approximation for the Correlation Energy of the Inhomogeneous Electron Gas. *Phys. Rev. B: Condens. Matter Mater. Phys.* **1986**, 33, 8822–8824.
- (33) Becke, A. D. Density-Functional Thermochemistry. III. The Role of Exact Exchange. *J. Chem. Phys.* **1993**, 98, 5648–5652.
- (34) Adamo, C.; Barone, V. Toward Reliable Density Functional Methods without Adjustable Parameters: The PBE0 Model. *J. Chem. Phys.* **1999**, 110, 6158–6170.
- (35) Zhao, Y.; Truhlar, D. G. The M06 Suite of Density Functionals for Main Group Thermochemistry, Thermochemical Kinetics, Non-covalent Interactions, Excited States, and Transition Elements: Two New Functionals and Systematic Testing of Four M06-Class Functionals and 12 Other Functionals. *Theor. Chem. Acc.* **2008**, 120, 215–241.
- (36) Curtiss, L. A.; Redfern, P. C.; Raghavachari, K.; Rassolov, V.; Pople, J. A. Gaussian-3 Theory Using Reduced Møller-Plesset Order. *J. Chem. Phys.* **1999**, 110, 4703–4709.
- (37) Ditchfield, R.; Miller, D. P.; Pople, J. A. Self-Consistent Molecular Orbital Methods. XI. Molecular Orbital Theory of NMR Chemical Shifts. *J. Chem. Phys.* **1971**, 54, 4186–4193.
- (38) Franci, M. M.; Pietro, W. J.; Hehre, W. J.; Binkley, J. S.; Gordon, M. S.; DeFrees, D. J.; Pople, J. A. Self-Consistent Molecular Orbital Methods. XXIII. A Polarization-Type Basis Set for Second-Row Elements. *J. Chem. Phys.* **1982**, 77, 3654–3665.
- (39) Hehre, W. J.; Ditchfield, R.; Pople, J. A. Self-Consistent Molecular Orbital Methods. XII. Further Extensions of Gaussian Type Basis Sets for Use in Molecular Orbital Studies of Organic Molecules. *J. Chem. Phys.* **1972**, 56, 2257–2261.
- (40) Binning, R. C.; Curtiss, L. A. Compact Contracted Basis Sets for Third-Row Atoms: Ga–Kr. *J. Comput. Chem.* **1990**, 11, 1206–1216.
- (41) Hariharan, P. C.; Pople, J. A. The Influence of Polarization Functions on Molecular Orbital Hydrogenation Energies. *Theor. Chim. Acta* **1973**, 28, 213–222.
- (42) Møller, C.; Plesset, M. S. Note on an Approximation Treatment for Many-Electron Systems. *Phys. Rev.* **1934**, 46, 618–622.
- (43) Pople, J. A.; Head-Gordon, M.; Raghavachari, K. Quadratic Configuration Interaction. A General Technique for Determining Electron Correlation Energies. *J. Chem. Phys.* **1987**, 87, 5968–5975.
- (44) Montgomery, J. A.; Frisch, M. J.; Ochterski, J. W.; Petersson, G. A. A Complete Basis Set Model Chemistry. VI. Use of Density Functional Geometries and Frequencies. *J. Chem. Phys.* **1999**, 110, 2822–2827.
- (45) Montgomery, J. A.; Frisch, M. J.; Ochterski, J. W.; Petersson, G. A. A Complete Basis Set Model Chemistry. VII. Use of the Minimum Population Localization Method. *J. Chem. Phys.* **2000**, 112, 6532–6542.
- (46) Montgomery, J. A.; Ochterski, J. W.; Petersson, G. A. A Complete Basis Set Model Chemistry. IV. An Improved Atomic Pair Natural Orbital Method. *J. Chem. Phys.* **1994**, 101, 5900–5909.
- (47) Ochterski, J. W.; Petersson, G. A.; Montgomery, J. A. A Complete Basis Set Model Chemistry. V. Extensions to Six or More Heavy Atoms. *J. Chem. Phys.* **1996**, 104, 2598–2619.
- (48) Petersson, G. A.; Al-Laham, M. A. A Complete Basis Set Model Chemistry. II. Open-Shell Systems and the Total Energies of the First-Row Atoms. *J. Chem. Phys.* **1991**, 94, 6081–6090.
- (49) Petersson, G. A.; Bennett, A.; Tensfeldt, T. G.; Al-Laham, M. A.; Shirley, W. A.; Mantzaris, J. A. Complete Basis Set Model Chemistry. I. The Total Energies of Closed-Shell Atoms and Hydrides of the First-Row Elements. *J. Chem. Phys.* **1988**, 89, 2193–2218.
- (50) Petersson, G. A.; Tensfeldt, T. G.; Montgomery, J. A. A Complete Basis Set Model Chemistry. III. The Complete Basis Set-Quadratic Configuration Interaction Family of Methods. *J. Chem. Phys.* **1991**, 94, 6091–6101.
- (51) Bartlett, R. J.; Purvis, G. D. Many-Body Perturbation Theory, Coupled-Pair Many-Electron Theory, and the Importance of Quadruple Excitations for the Correlation Problem. *Int. J. Quantum Chem.* **1978**, 14, 561–581.
- (52) Purvis, G. D.; Bartlett, R. J. A Full Coupled-Cluster Singles and Doubles Model: The Inclusion of Disconnected Triples. *J. Chem. Phys.* **1982**, 76, 1910–1918.
- (53) Řezáč, J.; Hobza, P. Describing Noncovalent Interactions Beyond the Common Approximations: How Accurate Is the “Gold Standard,” CCSD(T) at the Complete Basis Set Limit? *J. Chem. Theory Comput.* **2013**, 9, 2151–2155.
- (54) Demovicova, L.; Hobza, P.; Řezáč, J. Evaluation of Composite Schemes for CCSDT(Q) Calculations of Interaction Energies of Noncovalent Complexes. *Phys. Chem. Chem. Phys.* **2014**, 16, 19115–19121.
- (55) Řezáč, J.; Hobza, P. Benchmark Calculations of Interaction Energies in Noncovalent Complexes and Their Applications. *Chem. Rev.* **2016**, 116, 5038–5071.
- (56) DeYonker, N. J.; Cundari, T. R.; Wilson, A. K. The Correlation Consistent Composite Approach (Ccca): An Alternative to the Gaussian-N Methods. *J. Chem. Phys.* **2006**, 124, 114104.
- (57) Helgaker, T.; Jørgensen, P.; Olsen, J. *Molecular Electronic-Structure Theory*; Wiley: 2000; pp 908.
- (58) Dunning, T. H. Gaussian Basis Sets for Use in Correlated Molecular Calculations. I. The Atoms Boron through Neon and Hydrogen. *J. Chem. Phys.* **1989**, 90, 1007–1023.
- (59) Woon, D. E.; Dunning, T. H. Gaussian Basis Sets for Use in Correlated Molecular Calculations. IV. Calculation of Static Electrical Response Properties. *J. Chem. Phys.* **1994**, 100, 2975–2988.
- (60) Rigby, J.; Izgorodina, E. I. New SCS- and SOS-MP2 Coefficients Fitted to Semi-Coulombic Systems. *J. Chem. Theory Comput.* **2014**, 10, 3111–3122.
- (61) Halkier, A.; Helgaker, T.; Jørgensen, P.; Klopper, W.; Koch, H.; Olsen, J.; Wilson, A. K. Basis-Set Convergence in Correlated Calculations on Ne, N₂, and H₂O. *Chem. Phys. Lett.* **1998**, 286, 243–252.
- (62) Grimme, S. Improved Second-Order Møller Plesset Perturbation Theory by Separate Scaling of Parallel- and Antiparallel-Spin Pair Correlation Energies. *J. Chem. Phys.* **2003**, 118, 9095–9102.

- (63) Goumans, T. P. M.; Ehlers, A. W.; Lammertsma, K.; Würthwein, E.-U.; Grimme, S. Improved Reaction and Activation Energies of [4 + 2] Cycloadditions, [3,3] Sigmatropic Rearrangements and Electrocyclizations with the Spin-Component-Scaled MP2Method. *Chem. - Eur. J.* **2004**, *10*, 6468–6475.
- (64) Hyla-Kryspin, L.; Grimme, S. Comprehensive Study of the Thermochemistry of First-Row Transition Metal Compounds by Spin Component Scaled MP2 and MP3Methods. *Organometallics* **2004**, *23*, 5581–5592.
- (65) Grimme, S. Accurate Calculation of the Heats of Formation for Large Main Group Compounds with Spin-Component Scaled MP2Methods. *J. Phys. Chem. A* **2005**, *109*, 3067–3077.
- (66) Boys, S. F.; Bernardi, F. The Calculation of Small Molecular Interactions by the Differences of Separate Total Energies. Some Procedures with Reduced Errors. *Mol. Phys.* **1970**, *19*, 553–566.
- (67) Stone, A. J. *The Theory of Intermolecular Forces*, 2nd ed.; OUP: Oxford, 2013; pp 323.
- (68) Jeziorski, B.; Moszynski, R.; Szalewicz, K. Perturbation Theory Approach to Intermolecular Potential Energy Surfaces of Van Der Waals Complexes. *Chem. Rev.* **1994**, *94*, 1887–1930.
- (69) Misquitta, A. J.; Podeszwa, R.; Jeziorski, B.; Szalewicz, K. Intermolecular Potentials Based on Symmetry-Adapted Perturbation Theory with Dispersion Energies from Time-Dependent Density-Functional Calculations. *J. Chem. Phys.* **2005**, *123*, 214103.
- (70) Lao, K. U.; Schäffer, R.; Jansen, G.; Herbert, J. M. Accurate Description of Intermolecular Interactions Involving Ions Using Symmetry-Adapted Perturbation Theory. *J. Chem. Theory Comput.* **2015**, *11*, 2473–2486.
- (71) Turney, J. M.; Simmonett, A. C.; Parrish, R. M.; Hohenstein, E. G.; Evangelista, F. A.; Fermann, J. T.; Mintz, B. J.; Burns, L. A.; Wilke, J. J.; Abrams, M. L.; et al. Psi4: An Open-Source Ab Initio Electronic Structure Program. *WIREs: Comput. Mol. Sci.* **2012**, *2*, 556–565.
- (72) Tan, S. Y. S.; Izgorodina, E. I. Comparison of the Effective Fragment Potential Method with Symmetry-Adapted Perturbation Theory in the Calculation of Intermolecular Energies for Ionic Liquids. *J. Chem. Theory Comput.* **2016**, *12*, 2553–2568.
- (73) Day, P. N.; Jensen, J. H.; Gordon, M. S.; Webb, S. P.; Stevens, W. J.; Krauss, M.; Garmer, D.; Basch, H.; Cohen, D. An Effective Fragment Method for Modeling Solvent Effects in Quantum Mechanical Calculations. *J. Chem. Phys.* **1996**, *105*, 1968–1986.
- (74) Gordon, M. S.; Freitag, M. A.; Bandyopadhyay, P.; Jensen, J. H.; Kairys, V.; Stevens, W. J. The Effective Fragment Potential Method: A Qm-Based Mm Approach to Modeling Environmental Effects in Chemistry. *J. Phys. Chem. A* **2001**, *105*, 293–307.
- (75) Gordon, M. S.; Slipchenko, L.; Li, H.; Jensen, J. H. Chapter 10 the Effective Fragment Potential: A General Method for Predicting Intermolecular Interactions. *Annu. Rep. Comput. Chem.* **2007**, *3*, 177–193.
- (76) Slipchenko, L. V.; Gordon, M. S. Electrostatic Energy in the Effective Fragment Potential Method: Theory and Application to Benzene Dimer. *J. Comput. Chem.* **2007**, *28*, 276–291.
- (77) Ghosh, D.; Kosenkov, D.; Vanovschi, V.; Williams, C. F.; Herbert, J. M.; Gordon, M. S.; Schmidt, M. W.; Slipchenko, L. V.; Krylov, A. I. Noncovalent Interactions in Extended Systems Described by the Effective Fragment Potential Method: Theory and Application to Nucleobase Oligomers. *J. Phys. Chem. A* **2010**, *114*, 12739–12754.
- (78) Li, H.; Gordon, M. S.; Jensen, J. H. Charge Transfer Interaction in the Effective Fragment Potential Method. *J. Chem. Phys.* **2006**, *124*, 214108.
- (79) Slipchenko, L. V.; Gordon, M. S. Damping Functions in the Effective Fragment Potential Method. *Mol. Phys.* **2009**, *107*, 999–1016.
- (80) Adamovic, I.; Gordon, M. S. Dynamic Polarizability, Dispersion Coefficient C_6 and Dispersion Energy in the Effective Fragment Potential Method. *Mol. Phys.* **2005**, *103*, 379–387.
- (81) Lu, W. C.; Wang, C. Z.; Schmidt, M. W.; Bytautas, L.; Ho, K. M.; Ruedenberg, K. Molecule Intrinsic Minimal Basis Sets. I. Exact Resolution of Ab Initio Optimized Molecular Orbitals in Terms of Deformed Atomic Minimal-Basis Orbitals. *J. Chem. Phys.* **2004**, *120*, 2629–2637.
- (82) Klimeš, J.; Michaelides, A. Perspective: Advances and Challenges in Treating Van Der Waals Dispersion Forces in Density Functional Theory. *J. Chem. Phys.* **2012**, *137*, 120901.
- (83) Dobson, J. F.; Gould, T. Calculation of Dispersion Energies. *J. Phys.: Condens. Matter* **2012**, *24*, 073201.
- (84) Grimme, S.; Hansen, A.; Brandenburg, J. G.; Bannwarth, C. Dispersion-Corrected Mean-Field Electronic Structure Methods. *Chem. Rev.* **2016**, *116*, 5105–5154.
- (85) London, F. The General Theory of Molecular Forces. *Trans. Faraday Soc.* **1937**, *33*, 8b–26.
- (86) Grimme, S. Semiempirical GGA-Type Density Functional Constructed with a Long-Range Dispersion Correction. *J. Comput. Chem.* **2006**, *27*, 1787–1799.
- (87) Grimme, S.; Antony, J.; Ehrlich, S.; Krieg, H. A Consistent and Accurate Ab Initio Parametrization of Density Functional Dispersion Correction (DFT-D) for the 94 Elements H–Pu. *J. Chem. Phys.* **2010**, *132*, 154104.
- (88) Tkatchenko, A.; DiStasio, R. A.; Car, R.; Scheffler, M. Accurate and Efficient Method for Many-Body Van Der Waals Interactions. *Phys. Rev. Lett.* **2012**, *108*, 236402.
- (89) Tkatchenko, A.; Scheffler, M. Accurate Molecular Van Der Waals Interactions from Ground-State Electron Density and Free-Atom Reference Data. *Phys. Rev. Lett.* **2009**, *102*, 073005.
- (90) Oxtoby, D. W.; Gelbart, W. M. Collisional Polarizability Anisotropies of the Noble Gases. *Mol. Phys.* **1975**, *29*, 1569–1576.
- (91) Thole, B. T. Molecular Polarizabilities Calculated with a Modified Dipole Interaction. *Chem. Phys.* **1981**, *59*, 341–350.
- (92) Goerigk, L.; Grimme, S. A Thorough Benchmark of Density Functional Methods for General Main Group Thermochemistry, Kinetics, and Noncovalent Interactions. *Phys. Chem. Chem. Phys.* **2011**, *13*, 6670–6688.
- (93) Izgorodina, E. I.; Bernard, U. L.; MacFarlane, D. R. Ion-Pair Binding Energies of Ionic Liquids: Can DFT Compete with Ab Initio-Based Methods? *J. Phys. Chem. A* **2009**, *113*, 7064–7072.
- (94) Zahn, S.; MacFarlane, D. R.; Izgorodina, E. I. Assessment of Kohn-Sham Density Functional Theory and Møller-Plesset Perturbation Theory for Ionic Liquids. *Phys. Chem. Chem. Phys.* **2013**, *15*, 13664–13675.
- (95) Izgorodina, E. I.; Forsyth, M.; MacFarlane, D. R. Towards a Better Understanding of ‘Delocalized Charge’ in Ionic Liquid Anions. *Aust. J. Chem.* **2007**, *60*, 15–20.
- (96) Tsuzuki, S.; Tokuda, H.; Hayamizu, K.; Watanabe, M. Magnitude and Directionality of Interaction in Ion Pairs of Ionic Liquids: Relationship with Ionic Conductivity. *J. Phys. Chem. B* **2005**, *109*, 16474–16481.
- (97) Tsuzuki, S.; Katoh, R.; Mikami, M. Analysis of Interactions between 1-Butyl-3-Methylimidazolium Cation and Halide Anions (Cl[−], Br[−] and I[−]) by Ab Initio Calculations: Anion Size Effects on Preferential Locations of Anions. *Mol. Phys.* **2008**, *106*, 1621–1629.
- (98) Izgorodina, E. I.; Golze, D.; Maganti, R.; Armel, V.; Taige, M.; Schubert, T. J. S.; MacFarlane, D. R. Importance of Dispersion Forces for Prediction of Thermodynamic and Transport Properties of Some Common Ionic Liquids. *Phys. Chem. Chem. Phys.* **2014**, *16*, 7209–7221.
- (99) Lehmann, S. B. C.; Roatsch, M.; Schoppke, M.; Kirchner, B. On the Physical Origin of the Cation-Anion Intermediate Bond in Ionic Liquids Part I. Placing a (Weak) Hydrogen Bond between Two Charges. *Phys. Chem. Chem. Phys.* **2010**, *12*, 7473–7486.
- (100) Dong, K.; Zhang, S.; Wang, D.; Yao, X. Hydrogen Bonds in Imidazolium Ionic Liquids. *J. Phys. Chem. A* **2006**, *110*, 9775–9782.
- (101) Krishnan, R.; Binkley, J. S.; Seeger, R.; Pople, J. A. Self-Consistent Molecular Orbital Methods. XX. A Basis Set for Correlated Wave Functions. *J. Chem. Phys.* **1980**, *72*, 650–654.
- (102) McLean, A. D.; Chandler, G. S. Contracted Gaussian Basis Sets for Molecular Calculations. I. Second Row Atoms, Z = 11–18. *J. Chem. Phys.* **1980**, *72*, 5639–5648.

- (103) Stone, A. J. Distributed Polarizabilities. *Mol. Phys.* **1985**, *56*, 1065–1082.
- (104) Wang, Y.; Li, H.; Han, S. The Chemical Nature of the $C-H^+ \cdots X^-$ ($X = Cl$ or Br) Interaction in Imidazolium Halide Ionic Liquids. *J. Chem. Phys.* **2006**, *124*, 044504.
- (105) Chirlian, L. E.; Francl, M. M. Atomic Charges Derived from Electrostatic Potentials: A Detailed Study. *J. Comput. Chem.* **1987**, *8*, 894–905.
- (106) Tsuzuki, S.; Shinoda, W.; Miran, M. S.; Kinoshita, H.; Yasuda, T.; Watanabe, M. Interactions in Ion Pairs of Protic Ionic Liquids: Comparison with Aprotic Ionic Liquids. *J. Chem. Phys.* **2013**, *139*, 174504.
- (107) Yasuda, T.; Kinoshita, H.; Miran, M. S.; Tsuzuki, S.; Watanabe, M. Comparative Study on Physicochemical Properties of Protic Ionic Liquids Based on Allylammonium and Propylammonium Cations. *J. Chem. Eng. Data* **2013**, *58*, 2724–2732.
- (108) Tsuzuki, S.; Tokuda, H.; Mikami, M. Theoretical Analysis of the Hydrogen Bond of Imidazolium C2-H with Anions. *Phys. Chem. Chem. Phys.* **2007**, *9*, 4780–4784.
- (109) Nakakoshi, M.; Shiro, M.; Fujimoto, T.; Machinami, T.; Seki, H.; Tashiro, M.; Nishikawa, K. Crystal Structure of 1-Butyl-3-Methylimidazolium Iodide. *Chem. Lett.* **2006**, *35*, 1400–1401.
- (110) Ozawa, R.; Hayashi, S.; Saha, S.; Kobayashi, A.; Hamaguchi, H.-o. Rotational Isomerism and Structure of the 1-Butyl-3-Methylimidazolium Cation in the Ionic Liquid State. *Chem. Lett.* **2003**, *32*, 948–949.
- (111) Zahn, S.; Uhlig, F.; Thar, J.; Spickermann, C.; Kirchner, B. Intermolecular Forces in an Ionic Liquid ([Mmim][Cl]) Versus Those in a Typical Salt (NaCl). *Angew. Chem., Int. Ed.* **2008**, *47*, 3639–3641.
- (112) Zahn, S.; Bruns, G.; Thar, J.; Kirchner, B. What Keeps Ionic Liquids in Flow? *Phys. Chem. Chem. Phys.* **2008**, *10*, 6921–6924.
- (113) Hunt, P. A.; Kirchner, B.; Welton, T. Characterising the Electronic Structure of Ionic Liquids: An Examination of the 1-Butyl-3-Methylimidazolium Chloride Ion Pair. *Chem. - Eur. J.* **2006**, *12*, 6762–6775.
- (114) Foster, J. P.; Weinhold, F. Natural Hybrid Orbitals. *J. Am. Chem. Soc.* **1980**, *102*, 7211–7218.
- (115) Reed, A. E.; Curtiss, L. A.; Weinhold, F. Intermolecular Interactions from a Natural Bond Orbital, Donor-Acceptor Viewpoint. *Chem. Rev.* **1988**, *88*, 899–926.
- (116) Reed, A. E.; Weinstock, R. B.; Weinhold, F. Natural Population Analysis. *J. Chem. Phys.* **1985**, *83*, 735–746.
- (117) Bernard, U. L.; Izgorodina, E. I.; MacFarlane, D. R. New Insights into the Relationship between Ion-Pair Binding Energy and Thermodynamic and Transport Properties of Ionic Liquids. *J. Phys. Chem. C* **2010**, *114*, 20472–20478.
- (118) Hunt, P. A.; Gould, I. R. Structural Characterization of the 1-Butyl-3-Methylimidazolium Chloride Ion Pair Using *Ab Initio* Methods. *J. Phys. Chem. A* **2006**, *110*, 2269–2282.
- (119) Logotheti, G. E.; Ramos, J.; Economou, I. G. Molecular Modeling of Imidazolium-Based $[Tf_2n^-]$ Ionic Liquids: Microscopic Structure, Thermodynamic and Dynamic Properties, and Segmental Dynamics. *J. Phys. Chem. B* **2009**, *113*, 7211–7224.
- (120) Fumino, K.; Fossog, V.; Stange, P.; Paschek, D.; Hempelmann, R.; Ludwig, R. Controlling the Subtle Energy Balance in Protic Ionic Liquids: Dispersion Forces Compete with Hydrogen Bonds. *Angew. Chem., Int. Ed.* **2015**, *54*, 2792–2795.
- (121) Matthews, R. P.; Welton, T.; Hunt, P. A. Hydrogen Bonding and π - π Interactions in Imidazolium-Chloride Ionic Liquid Clusters. *Phys. Chem. Chem. Phys.* **2015**, *17*, 14437–14453.
- (122) Geronimo, L.; Jiten Singh, N.; Kim, K. S. Nature of Anion-Templated $\pi^+ \cdots \pi^+$ Interactions. *Phys. Chem. Chem. Phys.* **2011**, *13*, 11841–11845.
- (123) Seth, S. K.; Manna, P.; Singh, N. J.; Mitra, M.; Jana, A. D.; Das, A.; Choudhury, S. R.; Kar, T.; Mukhopadhyay, S.; Kim, K. S. Molecular Architecture Using Novel Types of Non-Covalent π -Interactions Involving Aromatic Neutrals, Aromatic Cations and π -Anions. *CrystEngComm* **2013**, *15*, 1285–1288.
- (124) Matthews, R. P.; Ashworth, C.; Welton, T.; Hunt, P. A. The Impact of Anion Electronic Structure: Similarities and Differences in Imidazolium Based Ionic Liquids. *J. Phys.: Condens. Matter* **2014**, *26*, 284112.
- (125) Izgorodina, E. I.; Rigby, J.; MacFarlane, D. R. Large-Scale *Ab Initio* Calculations of Archetypical Ionic Liquids. *Chem. Commun.* **2012**, *48*, 1493–1495.
- (126) Rigby, J.; Barrera Acevedo, S.; Izgorodina, E. I. Novel SCS-IL-MP2 and SOS-IL-MP2 Methods for Accurate Energetics of Large-Scale Ionic Liquid Clusters. *J. Chem. Theory Comput.* **2015**, *11*, 3610–3616.
- (127) Podeszwa, R.; Szalewicz, K. Three-Body Symmetry-Adapted Perturbation Theory Based on Kohn-Sham Description of the Monomers. *J. Chem. Phys.* **2007**, *126*, 194101.
- (128) Gordon, M. S.; Smith, Q. A.; Xu, P.; Slipchenko, L. V. Accurate First Principles Model Potentials for Intermolecular Interactions. *Annu. Rev. Phys. Chem.* **2013**, *64*, 553–578.
- (129) Adamovic, I.; Li, H.; Lamm, M. H.; Gordon, M. S. Modeling Styrene-Styrene Interactions. *J. Phys. Chem. A* **2006**, *110*, 519–525.
- (130) Smith, Q. A.; Gordon, M. S.; Slipchenko, L. V. Effective Fragment Potential Study of the Interaction of DNA Bases. *J. Phys. Chem. A* **2011**, *115*, 11269–11276.
- (131) Slipchenko, L. V.; Gordon, M. S. Water-Benzene Interactions: An Effective Fragment Potential and Correlated Quantum Chemistry Study. *J. Phys. Chem. A* **2009**, *113*, 2092–2102.
- (132) Flick, J. C.; Kosenkov, D.; Hohenstein, E. G.; Sherrill, C. D.; Slipchenko, L. V. Accurate Prediction of Noncovalent Interaction Energies with the Effective Fragment Potential Method: Comparison of Energy Components to Symmetry-Adapted Perturbation Theory for the S22 Test Set. *J. Chem. Theory Comput.* **2012**, *8*, 2835–2843.
- (133) Jurečka, P.; Šponer, J.; Černý, J.; Hobza, P. Benchmark Database of Accurate (MP2 and CCSD(T) Complete Basis Set Limit) Interaction Energies of Small Model Complexes, DNA Base Pairs, and Amino Acid Pairs. *Phys. Chem. Chem. Phys.* **2006**, *8*, 1985–1993.
- (134) Řezáč, J.; Riley, K. E.; Hobza, P. S66: A Well-Balanced Database of Benchmark Interaction Energies Relevant to Biomolecular Structures. *J. Chem. Theory Comput.* **2011**, *7*, 2427–2438.
- (135) McDaniel, J. G.; Choi, E.; Son, C. Y.; Schmidt, J. R.; Yethiraj, A. *Ab Initio* Force Fields for Imidazolium-Based Ionic Liquids. *J. Phys. Chem. B* **2016**, *120*, 7024–7036.
- (136) McDaniel, J. G.; Schmidt, J. R. Physically-Motivated Force Fields from Symmetry-Adapted Perturbation Theory. *J. Phys. Chem. A* **2013**, *117*, 2053–2066.
- (137) Hunt, P. A.; Ashworth, C. R.; Matthews, R. P. Hydrogen Bonding in Ionic Liquids. *Chem. Soc. Rev.* **2015**, *44*, 1257–1288.
- (138) Dong, K.; Zhang, S.; Wang, J. Understanding the Hydrogen Bonds in Ionic Liquids and Their Roles in Properties and Reactions. *Chem. Commun.* **2016**, *52*, 6744–6764.
- (139) Dong, K.; Song, Y.; Liu, X.; Cheng, W.; Yao, X.; Zhang, S. Understanding Structures and Hydrogen Bonds of Ionic Liquids at the Electronic Level. *J. Phys. Chem. B* **2012**, *116*, 1007–1017.
- (140) Schwabe, T.; Grimme, S. Double-Hybrid Density Functionals with Long-Range Dispersion Corrections: Higher Accuracy and Extended Applicability. *Phys. Chem. Chem. Phys.* **2007**, *9*, 3397–3406.
- (141) Izgorodina, E. I.; MacFarlane, D. R. Nature of Hydrogen Bonding in Charged Hydrogen-Bonded Complexes and Imidazolium-Based Ionic Liquids. *J. Phys. Chem. B* **2011**, *115*, 14659–14667.
- (142) Rozas, I.; Alkorta, I.; Elguero, J. Hydrogen Bonds and Ionic Interactions in Guanidine/Guanidinium Complexes: A Computational Case Study. *Struct. Chem.* **2008**, *19*, 923–933.
- (143) Frank, H. S.; Wen, W.-Y. Ion-Solvent Interaction. Structural Aspects of Ion-Solvent Interaction in Aqueous Solutions: A Suggested Picture of Water Structure. *Discuss. Faraday Soc.* **1957**, *24*, 133–140.
- (144) Del Bene, J.; Pople, J. A. Intermolecular Energies of Small Water Polymers. *Chem. Phys. Lett.* **1969**, *4*, 426–428.
- (145) Kollman, P. A.; Allen, L. C. Hydrogen Bonded Dimers and Polymers Involving Hydrogen Fluoride, Water, and Ammonia. *J. Am. Chem. Soc.* **1970**, *92*, 753–759.
- (146) Barnes, P.; Finney, J. L.; Nicholas, J. D.; Quinn, J. E. Cooperative Effects in Simulated Water. *Nature* **1979**, *282*, 459–464.

- (147) Stone, A. J. Water from First Principles. *Science* **2007**, *315*, 1228–1229.
- (148) Moszynski, R.; Wormer, P. E. S.; Heijmen, T. G. A.; van der Avoird, A. Symmetry-Adapted Perturbation Theory of Nonadditive Three-Body Interactions in Van Der Waals Molecules. II. Application to the Ar₂ Hf Interaction. *J. Chem. Phys.* **1998**, *108*, 579–589.
- (149) Cooper, A. R.; Hutson, J. M. Nonadditive Intermolecular Forces from the Spectroscopy of Van Der Waals Trimers: Calculations on Ar₂. *J. Chem. Phys.* **1993**, *98*, 5337–5351.
- (150) Wagner, C.; Fournier, N.; Ruiz, V. G.; Li, C.; Müllen, K.; Rohlfing, M.; Tkatchenko, A.; Temirov, R.; Tautz, F. S. Non-Additivity of Molecule-Surface Van Der Waals Potentials from Force Measurements. *Nat. Commun.* **2014**, *5*, 5568.
- (151) Gobre, V. V.; Tkatchenko, A. Scaling Laws for Van Der Waals Interactions in Nanostructured Materials. *Nat. Commun.* **2013**, *4*, 2341.
- (152) DiStasio, R. A.; von Lilienfeld, O. A.; Tkatchenko, A. Collective Many-Body Van Der Waals Interactions in Molecular Systems. *Proc. Natl. Acad. Sci. U. S. A.* **2012**, *109*, 14791–14795.
- (153) Reilly, A. M.; Tkatchenko, A. Van Der Waals Dispersion Interactions in Molecular Materials: Beyond Pairwise Additivity. *Chem. Sci.* **2015**, *6*, 3289–3301.
- (154) DiStasio, R. A., Jr.; Gobre, V. V.; Tkatchenko, A. Many-Body Van Der Waals Interactions in Molecules and Condensed Matter. *J. Phys.: Condens. Matter* **2014**, *26*, 213202.
- (155) Köfmann, S.; Thar, J.; Kirchner, B.; Hunt, P. A.; Welton, T. Cooperativity in Ionic Liquids. *J. Chem. Phys.* **2006**, *124*, 174506.
- (156) Schäfer, A.; Horn, H.; Ahlrichs, R. Fully Optimized Contracted Gaussian Basis Sets for Atoms Li to Kr. *J. Chem. Phys.* **1992**, *97*, 2571–2577.
- (157) Schäfer, A.; Huber, C.; Ahlrichs, R. Fully Optimized Contracted Gaussian Basis Sets of Triple Zeta Valence Quality for Atoms Li to Kr. *J. Chem. Phys.* **1994**, *100*, 5829–5835.
- (158) Köddermann, T.; Wertz, C.; Heintz, A.; Ludwig, R. Ion-Pair Formation in the Ionic Liquid 1-Ethyl-3-Methylimidazolium Bis-(Triflyl)Imide as a Function of Temperature and Concentration. *ChemPhysChem* **2006**, *7*, 1944–1949.
- (159) Ballone, P.; Pinilla, C.; Kohanoff, J.; Del Pópolo, M. G. Neutral and Charged 1-Butyl-3-Methylimidazolium Triflate Clusters: Equilibrium Concentration in the Vapor Phase and Thermal Properties of Nanometric Droplets. *J. Phys. Chem. B* **2007**, *111*, 4938–4950.
- (160) Angenendt, K.; Johansson, P. Ionic Liquid Structures from Large Density Functional Theory Calculations Using Mindless Configurations. *J. Phys. Chem. C* **2010**, *114*, 20577–20582.
- (161) Kitaura, K.; Ikeo, E.; Asada, T.; Nakano, T.; Uebayasi, M. Fragment Molecular Orbital Method: An Approximate Computational Method for Large Molecules. *Chem. Phys. Lett.* **1999**, *313*, 701–706.
- (162) Gordon, M. S.; Fedorov, D. G.; Pruitt, S. R.; Slipchenko, L. V. Fragmentation Methods: A Route to Accurate Calculations on Large Systems. *Chem. Rev.* **2012**, *112*, 632–672.
- (163) Gordon, M. S.; Mullin, J. M.; Pruitt, S. R.; Roskop, L. B.; Slipchenko, L. V.; Boatz, J. A. Accurate Methods for Large Molecular Systems. *J. Phys. Chem. B* **2009**, *113*, 9646–9663.
- (164) Nakano, T.; Kaminuma, T.; Sato, T.; Akiyama, Y.; Uebayasi, M.; Kitaura, K. Fragment Molecular Orbital Method: Application to Polypeptides. *Chem. Phys. Lett.* **2000**, *318*, 614–618.
- (165) Ishikawa, T.; Mochizuki, Y.; Imamura, K.; Nakano, T.; Mori, H.; Tokiwa, H.; Tanaka, K.; Miyoshi, E.; Tanaka, S. Application of Fragment Molecular Orbital Scheme to Silicon-Containing Systems. *Chem. Phys. Lett.* **2006**, *430*, 361–366.
- (166) Nakano, T.; Kaminuma, T.; Sato, T.; Fukuzawa, K.; Akiyama, Y.; Uebayasi, M.; Kitaura, K. Fragment Molecular Orbital Method: Use of Approximate Electrostatic Potential. *Chem. Phys. Lett.* **2002**, *351*, 475–480.
- (167) Fedorov, D. G.; Kitaura, K. Pair Interaction Energy Decomposition Analysis. *J. Comput. Chem.* **2007**, *28*, 222–237.
- (168) Fedorov, D. G.; Kitaura, K. The Three-Body Fragment Molecular Orbital Method for Accurate Calculations of Large Systems. *Chem. Phys. Lett.* **2006**, *433*, 182–187.
- (169) Fedorov, D. G.; Kitaura, K. Second Order Møller-Plesset Perturbation Theory Based Upon the Fragment Molecular Orbital Method. *J. Chem. Phys.* **2004**, *121*, 2483–2490.
- (170) Fedorov, D. G.; Kitaura, K. The Importance of Three-Body Terms in the Fragment Molecular Orbital Method. *J. Chem. Phys.* **2004**, *120*, 6832–6840.
- (171) Fedorov, D. G.; Ishimura, K.; Ishida, T.; Kitaura, K.; Pulay, P.; Nagase, S. Accuracy of the Three-Body Fragment Molecular Orbital Method Applied to Møller Plesset Perturbation Theory. *J. Comput. Chem.* **2007**, *28*, 1476–1484.
- (172) Gordon, M. S.; Schmidt, M. W. In Theory and Applications of Computational Chemistry: The First Forty Years. Dykstra, C. E., Frenking, G., Kim, K. S., Scuseria, G. E., Eds.; *Advances in Electronic Structure Theory: Gamess a Decade Later*; Elsevier: 2005; pp 1167–1189.
- (173) Schmidt, M. W.; Baldridge, K. K.; Boatz, J. A.; Elbert, S. T.; Gordon, M. S.; Jensen, J. H.; Koseki, S.; Matsunaga, N.; Nguyen, K. A.; Su, S. General Atomic and Molecular Electronic Structure System. *J. Comput. Chem.* **1993**, *14*, 1347–1363.
- (174) Carlson, P. J.; Bose, S.; Armstrong, D. W.; Hawkins, T.; Gordon, M. S.; Petrich, J. W. Structure and Dynamics of the 1-Hydroxyethyl-4-Amino-1,2,4-Triazolium Nitrate High-Energy Ionic Liquid System. *J. Phys. Chem. B* **2012**, *116*, 503–512.
- (175) Weigend, F.; Häser, M.; Patzelt, H.; Ahlrichs, R. Ri-MP2: Optimized Auxiliary Basis Sets and Demonstration of Efficiency. *Chem. Phys. Lett.* **1998**, *294*, 143–152.
- (176) Fedorov, D. G.; Olson, R. M.; Kitaura, K.; Gordon, M. S.; Koseki, S. A New Hierarchical Parallelization Scheme: Generalized Distributed Data Interface (Gddi), and an Application to the Fragment Molecular Orbital Method (Fmo). *J. Comput. Chem.* **2004**, *25*, 872–880.
- (177) Izgorodina, E. I. Towards Large-Scale, Fully *Ab Initio* Calculations of Ionic Liquids. *Phys. Chem. Chem. Phys.* **2011**, *13*, 4189–4207.
- (178) Tsuzuki, S.; Arai, A. A.; Nishikawa, K. Conformational Analysis of 1-Butyl-3-Methylimidazolium by CCSD(T) Level *Ab Initio* Calculations: Effects of Neighboring Anions. *J. Phys. Chem. B* **2008**, *112*, 7739–7747.
- (179) Zahn, S.; Kirchner, B. Validation of Dispersion-Corrected Density Functional Theory Approaches for Ionic Liquid Systems. *J. Phys. Chem. A* **2008**, *112*, 8430–8435.
- (180) von Lilienfeld, O. A.; Tavernelli, I.; Rothlisberger, U.; Sebastiani, D. Optimization of Effective Atom Centered Potentials for London Dispersion Forces in Density Functional Theory. *Phys. Rev. Lett.* **2004**, *93*, 153004.
- (181) Vydrov, O. A.; Van Voorhis, T. Nonlocal Van Der Waals Density Functional: The Simpler the Better. *J. Chem. Phys.* **2010**, *133*, 244103.
- (182) Hujo, W.; Grimme, S. Performance of the Van Der Waals Density Functional vv10 and (Hybrid)GGA Variants for Thermochemistry and Noncovalent Interactions. *J. Chem. Theory Comput.* **2011**, *7*, 3866–3871.
- (183) Zhang, Y.; Yang, W. Comment on "Generalized Gradient Approximation Made Simple". *Phys. Rev. Lett.* **1998**, *80*, 890–890.
- (184) Weigend, F.; Furche, F.; Ahlrichs, R. Gaussian Basis Sets of Quadruple Zeta Valence Quality for Atoms H–Kr. *J. Chem. Phys.* **2003**, *119*, 12753–12762.
- (185) Weigend, F.; Ahlrichs, R. Balanced Basis Sets of Split Valence, Triple Zeta Valence and Quadruple Zeta Valence Quality for H to Rn: Design and Assessment of Accuracy. *Phys. Chem. Chem. Phys.* **2005**, *7*, 3297–3305.
- (186) Perdew, J. P.; Chevary, J. A.; Vosko, S. H.; Jackson, K. A.; Pederson, M. R.; Singh, D. J.; Fiolhais, C. Atoms, Molecules, Solids, and Surfaces: Applications of the Generalized Gradient Approximation for Exchange and Correlation. *Phys. Rev. B: Condens. Matter Mater. Phys.* **1992**, *46*, 6671–6687.
- (187) Perdew, J. P.; Chevary, J. A.; Vosko, S. H.; Jackson, K. A.; Pederson, M. R.; Singh, D. J.; Fiolhais, C. Erratum: Atoms, Molecules, Solids, and Surfaces: Applications of the Generalized Gradient

Approximation for Exchange and Correlation. *Phys. Rev. B: Condens. Matter Mater. Phys.* **1993**, *48*, 4978–4978.

(188) Hoe, W.-M.; Cohen, A. J.; Handy, N. C. Assessment of a New Local Exchange Functional Optx. *Chem. Phys. Lett.* **2001**, *341*, 319–328.

(189) Handy, N. C.; Cohen, A. J. Left-Right Correlation Energy. *Mol. Phys.* **2001**, *99*, 403–412.

(190) Tao, J.; Perdew, J. P.; Staroverov, V. N.; Scuseria, G. E. Climbing the Density Functional Ladder: Nonempirical Meta-Generalized Gradient Approximation Designed for Molecules and Solids. *Phys. Rev. Lett.* **2003**, *91*, 146401.

(191) Xu, X.; Goddard, W. A. The X3lyp Extended Density Functional for Accurate Descriptions of Nonbond Interactions, Spin States, and Thermochemical Properties. *Proc. Natl. Acad. Sci. U. S. A.* **2004**, *101*, 2673–2677.

(192) Cohen, A. J.; Handy, N. C. Dynamic Correlation. *Mol. Phys.* **2001**, *99*, 607–615.

(193) Schwabe, T.; Grimme, S. Towards Chemical Accuracy for the Thermodynamics of Large Molecules: New Hybrid Density Functionals Including Non-Local Correlation Effects. *Phys. Chem. Chem. Phys.* **2006**, *8*, 4398–4401.

(194) Zhao, Y.; Truhlar, D. G. Density Functional for Spectroscopy: No Long-Range Self-Interaction Error, Good Performance for Rydberg and Charge-Transfer States, and Better Performance on Average Than B3LYP for Ground States. *J. Phys. Chem. A* **2006**, *110*, 13126–13130.

(195) Zhao, Y.; Truhlar, D. G. Exploring the Limit of Accuracy of the Global Hybrid Meta Density Functional for Main-Group Thermochemistry, Kinetics, and Noncovalent Interactions. *J. Chem. Theory Comput.* **2008**, *4*, 1849–1868.

(196) Zhao, Y.; Truhlar, D. G. A New Local Density Functional for Main-Group Thermochemistry, Transition Metal Bonding, Thermochemical Kinetics, and Noncovalent Interactions. *J. Chem. Phys.* **2006**, *125*, 194101.

(197) Dion, M.; Rydberg, H.; Schröder, E.; Langreth, D. C.; Lundqvist, B. I. Erratum: Van Der Waals Density Functional for General Geometries. *Phys. Rev. Lett.* **2005**, *95*, 109902.

(198) Perdew, J. P.; Ruzsinszky, A.; Csonka, G. I.; Vydrov, O. A.; Scuseria, G. E.; Constantin, L. A.; Zhou, X.; Burke, K. Restoring the Density-Gradient Expansion for Exchange in Solids and Surfaces. *Phys. Rev. Lett.* **2008**, *100*, 136406.

(199) Kohanoff, J.; Pinilla, C.; Youngs, T. G. A.; Artacho, E.; Soler, J. M. Dispersion Interactions in Room-Temperature Ionic Liquids: Results from a Non-Empirical Density Functional. *J. Chem. Phys.* **2011**, *135*, 154505.

(200) Zhang, G.; Musgrave, C. B. Comparison of DFT Methods for Molecular Orbital Eigenvalue Calculations. *J. Phys. Chem. A* **2007**, *111*, 1554–1561.

(201) Allen, M. J.; Tozer, D. J. Eigenvalues, Integer Discontinuities and NMR Shielding Constants in Kohn–Sham Theory. *Mol. Phys.* **2002**, *100*, 433–439.

(202) Borgoo, A.; Tozer, D. J. Negative Electron Affinities from DFT: Influence of Asymptotic Exchange–Correlation Potential and Effective Homogeneity under Density Scaling. *J. Phys. Chem. A* **2012**, *116*, 5497–5500.

(203) Tozer, D. J. Relationship between Long-Range Charge-Transfer Excitation Energy Error and Integer Discontinuity in Kohn–Sham Theory. *J. Chem. Phys.* **2003**, *119*, 12697–12699.

(204) Perdew, J. P.; Parr, R. G.; Levy, M.; Balduz, J. L. Density-Functional Theory for Fractional Particle Number: Derivative Discontinuities of the Energy. *Phys. Rev. Lett.* **1982**, *49*, 1691–1694.

(205) Perdew, J. P.; Levy, M. Comment on “Significance of the Highest Occupied Kohn–Sham Eigenvalue”. *Phys. Rev. B: Condens. Matter Mater. Phys.* **1997**, *56*, 16021–16028.

(206) Perdew, J. P.; Levy, M. Physical Content of the Exact Kohn–Sham Orbital Energies: Band Gaps and Derivative Discontinuities. *Phys. Rev. Lett.* **1983**, *51*, 1884–1887.

(207) Wang, C. S.; Pickett, W. E. Density-Functional Theory of Excitation Spectra of Semiconductors: Application to Si. *Phys. Rev. Lett.* **1983**, *51*, 597–600.

(208) Sham, L. J.; Schlüter, M. Density-Functional Theory of the Energy Gap. *Phys. Rev. Lett.* **1983**, *51*, 1888–1891.

(209) Chan, M. K. Y.; Ceder, G. Efficient Band Gap Prediction for Solids. *Phys. Rev. Lett.* **2010**, *105*, 196403.

(210) Grimme, S.; Hujo, W.; Kirchner, B. Performance of Dispersion-Corrected Density Functional Theory for the Interactions in Ionic Liquids. *Phys. Chem. Chem. Phys.* **2012**, *14*, 4875–4883.

(211) Krischok, S.; Ötting, R.; Beenken, W. J. D.; Himmerlich, M.; Lorenz, P.; Höfft, O.; Bahr, S.; Kemper, V.; Schaefer, J. A. A Comparative Study on the Electronic Structure of the 1-Ethyl-3-Methylimidazolium Bis(Trifluoromethylsulfonyl)Amide Room-Temperature Ionic Liquid by Electron Spectroscopy and First Principles Calculations. *Z. Phys. Chem.* **2006**, *220*, 1407–1416.

(212) Strasser, D.; Goulay, F.; Kelkar, M. S.; Maginn, E. J.; Leone, S. R. Photoelectron Spectrum of Isolated Ion-Pairs in Ionic Liquid Vapor. *J. Phys. Chem. A* **2007**, *111*, 3191–3195.

(213) Krischok, S.; Eremitchenko, M.; Himmerlich, M.; Lorenz, P.; Uhlir, J.; Neumann, A.; Ötting, R.; Beenken, W. J. D.; Höfft, O.; Bahr, S. Temperature-Dependent Electronic and Vibrational Structure of the 1-Ethyl-3-Methylimidazolium Bis(Trifluoromethylsulfonyl)-Amide Room-Temperature Ionic Liquid Surface: A Study with XPS, UPS, MIES, and HREELS. *J. Phys. Chem. B* **2007**, *111*, 4801–4806.

(214) Ulbrich, A.; Reinmöller, M.; Beenken, W. J. D.; Krischok, S. Surface Electronic Structure of [Xmim]Cl Probed by Surface-Sensitive Spectroscopy. *ChemPhysChem* **2012**, *13*, 1718–1724.

(215) Weingarh, D.; Czekaj, I.; Fei, Z.; Foelske-Schmitz, A.; Dyson, P. J.; Wokaun, A.; Kötz, R. Electrochemical Stability of Imidazolium Based Ionic Liquids Containing Cyano Groups in the Anion: A Cyclic Voltammetry, XPS and DFT Study. *J. Electrochem. Soc.* **2012**, *159*, H611–H615.

(216) Ong, S. P.; Andreussi, O.; Wu, Y.; Marzari, N.; Ceder, G. Electrochemical Windows of Room-Temperature Ionic Liquids from Molecular Dynamics and Density Functional Theory Calculations. *Chem. Mater.* **2011**, *23*, 2979–2986.

(217) Alkauskas, A.; Broqvist, P.; Devynck, F.; Pasquarello, A. Band Offsets at Semiconductor–Oxide Interfaces from Hybrid Density-Functional Calculations. *Phys. Rev. Lett.* **2008**, *101*, 106802.

(218) Chan, K. T.; Neaton, J. B.; Cohen, M. L. First-Principles Study of Metal Adatom Adsorption on Graphene. *Phys. Rev. B: Condens. Matter Mater. Phys.* **2008**, *77*, 235430.

(219) Muscat, J.; Wander, A.; Harrison, N. M. On the Prediction of Band Gaps from Hybrid Functional Theory. *Chem. Phys. Lett.* **2001**, *342*, 397–401.

(220) Paier, J.; Marsman, M.; Hummer, K.; Kresse, G.; Gerber, I. C.; Ángyán, J. G. Screened Hybrid Density Functionals Applied to Solids. *J. Chem. Phys.* **2006**, *124*, 154709.

(221) Dhungana, K. B.; Faria, L. F. O.; Wu, B.; Liang, M.; Ribeiro, M. C. C.; Margulis, C. J.; Castner, E. W. Structure of Cyano-Anion Ionic Liquids: X-Ray Scattering and Simulations. *J. Chem. Phys.* **2016**, *145*, 024503.

(222) Efron, B. Better Bootstrap Confidence Intervals. *J. Am. Stat. Assoc.* **1987**, *82*, 171–185.

(223) Elstner, M. The SCC-DFTB Method and Its Application to Biological Systems. *Theor. Chem. Acc.* **2006**, *116*, 316–325.

(224) Elstner, M.; Seifert, G. Density Functional Tight Binding. *Philos. Trans. R. Soc. A* **2014**, *372*, 20120483.

(225) Yang, York, D.; Cui, Q.; Elstner, M.; Yu, H. Extension of the Self-Consistent-Charge Density-Functional Tight-Binding Method: Third-Order Expansion of the Density Functional Theory Total Energy and Introduction of a Modified Effective Coulomb Interaction. *J. Phys. Chem. A* **2007**, *111*, 10861–10873.

(226) Oliveira, A. F.; Seifert, G.; Heine, T.; Duarte, H. A. Density-Functional Based Tight-Binding: An Approximate DFT Method. *J. Braz. Chem. Soc.* **2009**, *20*, 1193–1205.

- (227) Foulkes, W. M. C.; Haydock, R. Tight-Binding Models and Density-Functional Theory. *Phys. Rev. B: Condens. Matter Mater. Phys.* **1989**, *39*, 12520–12536.
- (228) Porezag, D.; Frauenheim, T.; Köhler, T.; Seifert, G.; Kaschner, R. Construction of Tight-Binding-Like Potentials on the Basis of Density-Functional Theory: Application to Carbon. *Phys. Rev. B: Condens. Matter Mater. Phys.* **1995**, *51*, 12947–12957.
- (229) Elstner, M. SCC-DFTB: What Is the Proper Degree of Self-Consistency? *J. Phys. Chem. A* **2007**, *111*, 5614–5621.
- (230) Gaus, M.; Cui, Q.; Elstner, M. DFTB3: Extension of the Self-Consistent-Charge Density-Functional Tight-Binding Method (SCC-DFTB). *J. Chem. Theory Comput.* **2011**, *7*, 931–948.
- (231) Seifert, G.; Porezag, D.; Frauenheim, T. Calculations of Molecules, Clusters, and Solids with a Simplified Lcao-DFT-Lda Scheme. *Int. J. Quantum Chem.* **1996**, *58*, 185–192.
- (232) Elstner, M.; Porezag, D.; Jungnickel, G.; Elsner, J.; Haugk, M.; Frauenheim, T.; Suhai, S.; Seifert, G. Self-Consistent-Charge Density-Functional Tight-Binding Method for Simulations of Complex Materials Properties. *Phys. Rev. B: Condens. Matter Mater. Phys.* **1998**, *58*, 7260–7268.
- (233) Elstner, M.; Hobza, P.; Frauenheim, T.; Suhai, S.; Kaxiras, E. Hydrogen Bonding and Stacking Interactions of Nucleic Acid Base Pairs: A Density-Functional-Theory Based Treatment. *J. Chem. Phys.* **2001**, *114*, 5149–5155.
- (234) Halgren, T. A. The Representation of Van Der Waals (vdW) Interactions in Molecular Mechanics Force Fields: Potential Form, Combination Rules, and vdW Parameters. *J. Am. Chem. Soc.* **1992**, *114*, 7827–7843.
- (235) Addicoat, M. A.; Fukuoka, S.; Page, A. J.; Irle, S. Stochastic Structure Determination for Conformationally Flexible Heterogenous Molecular Clusters: Application to Ionic Liquids. *J. Comput. Chem.* **2013**, *34*, 2591–2600.
- (236) Addicoat, M. A.; Page, A. J.; Brain, Z. E.; Flack, L.; Morokuma, K.; Irle, S. Optimization of a Genetic Algorithm for the Functionalization of Fullerenes. *J. Chem. Theory Comput.* **2012**, *8*, 1841–1851.
- (237) Nishimura, Y.; Yokogawa, D.; Irle, S. Theoretical Study of Cellobiose Hydrolysis to Glucose in Ionic Liquids. *Chem. Phys. Lett.* **2014**, *603*, 7–12.
- (238) Arifin; Puripat, M.; Yokogawa, D.; Parasuk, V.; Irle, S. Glucose Transformation to 5-Hydroxymethylfurfural in Acidic Ionic Liquid: A Quantum Mechanical Study. *J. Comput. Chem.* **2016**, *37*, 327–335.
- (239) Addicoat, M. A.; Stefanovic, R.; Webber, G. B.; Atkin, R.; Page, A. J. Assessment of the Density Functional Tight Binding Method for Protic Ionic Liquids. *J. Chem. Theory Comput.* **2014**, *10*, 4633–4643.
- (240) Hayes, R.; Imberti, S.; Warr, G. G.; Atkin, R. Pronounced Sponge-Like Nanostructure in Propylammonium Nitrate. *Phys. Chem. Chem. Phys.* **2011**, *13*, 13544–13551.
- (241) Weis, D. C.; MacFarlane, D. R. Computer-Aided Molecular Design of Ionic Liquids: An Overview. *Aust. J. Chem.* **2012**, *65*, 1478–1486.
- (242) Das, R. N.; Roy, K. Advances in Qspr/Qstr Models of Ionic Liquids for the Design of Greener Solvents of the Future. *Mol. Diversity* **2013**, *17*, 151–196.
- (243) Valderrama, J. O. Myths and Realities About Existing Methods for Calculating the Melting Temperatures of Ionic Liquids. *Ind. Eng. Chem. Res.* **2014**, *53*, 1004–1014.
- (244) Rybinska, A.; Sosnowska, A.; Barycki, M.; Puzyn, T. Geometry Optimization Method Versus Predictive Ability in Qspr Modeling for Ionic Liquids. *J. Comput.-Aided Mol. Des.* **2016**, *30*, 165–176.
- (245) López-Martin, I.; Burello, E.; Davey, P. N.; Seddon, K. R.; Rothenberg, G. Anion and Cation Effects on Imidazolium Salt Melting Points: A Descriptor Modelling Study. *ChemPhysChem* **2007**, *8*, 690–695.
- (246) Katritzky, A. R.; Jain, R.; Lomaka, A.; Petrukhin, R.; Karelson, M.; Visser, A. E.; Rogers, R. D. Correlation of the Melting Points of Potential Ionic Liquids (Imidazolium Bromides and Benzimidazolium Bromides) Using the Codessa Program. *J. Chem. Inf. Comput. Sci.* **2002**, *42*, 225–231.
- (247) Dewar, M. J. S.; Zoebisch, E. G.; Healy, E. F.; Stewart, J. J. P. Development and Use of Quantum Mechanical Molecular Models. 76. Aml: A New General Purpose Quantum Mechanical Molecular Model. *J. Am. Chem. Soc.* **1985**, *107*, 3902–3909.
- (248) Katritzky, A. R.; Lomaka, A.; Petrukhin, R.; Jain, R.; Karelson, M.; Visser, A. E.; Rogers, R. D. Qspr Correlation of the Melting Point for Pyridinium Bromides, Potential Ionic Liquids. *J. Chem. Inf. Comput. Sci.* **2002**, *42*, 71–74.
- (249) Trohalaki, S.; Pachter, R. Prediction of Melting Points for Ionic Liquids. *QSAR Comb. Sci.* **2005**, *24*, 485–490.
- (250) Trohalaki, S.; Pachter, R.; Drake, G. W.; Hawkins, T. Quantitative Structure Property Relationships for Melting Points and Densities of Ionic Liquids. *Energy Fuels* **2005**, *19*, 279–284.
- (251) Zhu, J.; Bai, L.; Chen, B.; Fei, W. Thermodynamical Properties of Phase Change Materials Based on Ionic Liquids. *Chem. Eng. J.* **2009**, *147*, 58–62.
- (252) Stewart, J. J. P. Optimization of Parameters for Semiempirical Methods I. Method. *J. Comput. Chem.* **1989**, *10*, 209–220.
- (253) Stewart, J. J. P. Optimization of Parameters for Semiempirical Methods II. Applications. *J. Comput. Chem.* **1989**, *10*, 221–264.
- (254) Eike, D. M.; Brennecke, J. F.; Maginn, E. J. Predicting Melting Points of Quaternary Ammonium Ionic Liquids. *Green Chem.* **2003**, *5*, 323–328.
- (255) Tochigi, K.; Yamamoto, H. Estimation of Ionic Conductivity and Viscosity of Ionic Liquids Using a Qspr Model. *J. Phys. Chem. C* **2007**, *111*, 15989–15994.
- (256) Bini, R.; Malvaldi, M.; Pitner, W. R.; Chiappe, C. Qspr Correlation for Conductivities and Viscosities of Low-Temperature Melting Ionic Liquids. *J. Phys. Org. Chem.* **2008**, *21*, 622–629.
- (257) Han, C.; Yu, G.; Wen, L.; Zhao, D.; Asumana, C.; Chen, X. Data and Qspr Study for Viscosity of Imidazolium-Based Ionic Liquids. *Fluid Phase Equilib.* **2011**, *300*, 95–104.
- (258) Yu, G.; Zhao, D.; Wen, L.; Yang, S.; Chen, X. Viscosity of Ionic Liquids: Database, Observation, and Quantitative Structure-Property Relationship Analysis. *AIChE J.* **2012**, *58*, 2885–2899.
- (259) Stanton, D. T.; Jurs, P. C. Development and Use of Charged Partial Surface Area Structural Descriptors in Computer-Assisted Quantitative Structure-Property Relationship Studies. *Anal. Chem.* **1990**, *62*, 2323–2329.
- (260) Franke, A. *Theoretical Drug Design Methods*; Elsevier Science Publishers: 1984; Vol. 7, pp 412.
- (261) Yu, G.; Wen, L.; Zhao, D.; Asumana, C.; Chen, X. Qspr Study on the Viscosity of Bis(Trifluoromethylsulfonyl)Imide-Based Ionic Liquids. *J. Mol. Liq.* **2013**, *184*, 51–59.
- (262) Klamt, A.; Eckert, F.; Arlt, W. COSMO-RS: An Alternative to Simulation for Calculating Thermodynamic Properties of Liquid Mixtures. *Amu. Rev. Chem. Biomol. Eng.* **2010**, *1*, 101–122.
- (263) Klamt, A. The COSMO and COSMO-RS Solvation Models. *WIREs: Comput. Mol. Sci.* **2011**, *1*, 699–709.
- (264) Palomar, J.; Torrecilla, J. S.; Lemus, J.; Ferro, V. R.; Rodriguez, F. A COSMO-RS Based Guide to Analyze/Quantify the Polarity of Ionic Liquids and Their Mixtures with Organic Cosolvents. *Phys. Chem. Chem. Phys.* **2010**, *12*, 1991–2000.
- (265) Eckert, F.; Klamt, A. Fast Solvent Screening Via Quantum Chemistry: COSMO-RS Approach. *AIChE J.* **2002**, *48*, 369–385.
- (266) Preiss, U.; Emel'yanenko, V. N.; Verevkin, S. P.; Himmel, D.; Paulechka, Y. U.; Krossing, I. Temperature-Dependent Prediction of the Liquid Entropy of Ionic Liquids. *ChemPhysChem* **2010**, *11*, 3425–3431.
- (267) Preiss, U.; Bulut, S.; Krossing, I. In Silico Prediction of the Melting Points of Ionic Liquids from Thermodynamic Considerations: A Case Study on 67 Salts with a Melting Point Range of 337 °C. *J. Phys. Chem. B* **2010**, *114*, 11133–11140.
- (268) Preiss, U.; Verevkin, S. P.; Koslowski, T.; Krossing, I. Going Full Circle: Phase-Transition Thermodynamics of Ionic Liquids. *Chem. - Eur. J.* **2011**, *17*, 6508–6517.
- (269) Preiss, U. P.; Beichel, W.; Erle, A. M. T.; Paulechka, Y. U.; Krossing, I. Is Universal, Simple Melting Point Prediction Possible? *ChemPhysChem* **2011**, *12*, 2959–2972.

- (270) Beichel, W.; Preiss, U. P.; Verevkin, S. P.; Koslowski, T.; Krossing, I. Empirical Description and Prediction of Ionic Liquids Properties with Augmented Volume-Based Thermodynamics. *J. Mol. Liq.* **2014**, *192*, 3–8.
- (271) Diedenhofen, M.; Klamt, A.; Marsh, K.; Schäfer, A. Prediction of the Vapor Pressure and Vaporization Enthalpy of 1-N-Alkyl-3-Methylimidazolium-Bis-(Trifluoromethanesulfonyl) Amide Ionic Liquids. *Phys. Chem. Chem. Phys.* **2007**, *9*, 4653–4656.
- (272) Preiss, U. P. R. M.; Slattery, J. M.; Krossing, I. *In Silico* Prediction of Molecular Volumes, Heat Capacities, and Temperature-Dependent Densities of Ionic Liquids. *Ind. Eng. Chem. Res.* **2009**, *48*, 2290–2296.
- (273) Eiden, P.; Bulut, S.; Köchner, T.; Friedrich, C.; Schubert, T.; Krossing, I. *In Silico* Predictions of the Temperature-Dependent Viscosities and Electrical Conductivities of Functionalized and Nonfunctionalized Ionic Liquids. *J. Phys. Chem. B* **2011**, *115*, 300–309.
- (274) Zhao, Y.; Huang, Y.; Zhang, X.; Zhang, S. A Quantitative Prediction of the Viscosity of Ionic Liquids Using S[Σ]-Profile Molecular Descriptors. *Phys. Chem. Chem. Phys.* **2015**, *17*, 3761–3767.
- (275) Zhao, Y.; Zeng, S.; Huang, Y.; Afzal, R. M.; Zhang, X. Estimation of Heat Capacity of Ionic Liquids Using S σ -Profile Molecular Descriptors. *Ind. Eng. Chem. Res.* **2015**, *54*, 12987–12992.
- (276) Diedenhofen, M.; Klamt, A. COSMO-RS as a Tool for Property Prediction of IL Mixtures – a Review. *Fluid Phase Equilib.* **2010**, *294*, 31–38.
- (277) Eckert, F.; Klamt, A. COSMOlogic Predicting Solutions. <http://www.cosmologic.de/>; **2013**.
- (278) Diedenhofen, M.; Eckert, F.; Klamt, A. Prediction of Infinite Dilution Activity Coefficients of Organic Compounds in Ionic Liquids Using COSMO-RS. *J. Chem. Eng. Data* **2003**, *48*, 475–479.
- (279) Banerjee, T.; Khanna, A. Infinite Dilution Activity Coefficients for Trihexyltetradecyl Phosphonium Ionic Liquids: Measurements and COSMO-RS Prediction. *J. Chem. Eng. Data* **2006**, *51*, 2170–2177.
- (280) Kurnia, K. A.; Pinho, S. P.; Coutinho, J. A. P. Evaluation of the Conductor-Like Screening Model for Real Solvents for the Prediction of the Water Activity Coefficient at Infinite Dilution in Ionic Liquids. *Ind. Eng. Chem. Res.* **2014**, *53*, 12466–12475.
- (281) Matheswaran, P.; Wilfred, C. D.; Kurnia, K. A.; Ramli, A. Overview of Activity Coefficient of Thiophene at Infinite Dilution in Ionic Liquids and Their Modeling Using COSMO-RS. *Ind. Eng. Chem. Res.* **2016**, *55*, 788–797.
- (282) Kato, R.; Gmehling, J. Systems with Ionic Liquids: Measurement of Vle and ρ Data and Prediction of Their Thermodynamic Behavior Using Original Unifac, Mod. Unifac(DO) and COSMO-RS(OI). *J. Chem. Thermodyn.* **2005**, *37*, 603–619.
- (283) Grensemann, H.; Gmehling, J. Performance of a Conductor-Like Screening Model for Real Solvents Model in Comparison to Classical Group Contribution Methods. *Ind. Eng. Chem. Res.* **2005**, *44*, 1610–1624.
- (284) Klamt, A.; Eckert, F. OSMO-RS: A Novel and Efficient Method for the a Priori Prediction of Thermophysical Data of Liquids. *Fluid Phase Equilib.* **2000**, *172*, 43–72.
- (285) Wu, C. T.; Marsh, K. N.; Deev, A. V.; Boxall, J. A. Liquid-Liquid Equilibria of Room-Temperature Ionic Liquids and Butan-1-OL. *J. Chem. Eng. Data* **2003**, *48*, 486–491.
- (286) Domańska, U.; Pobudkowska, A.; Eckert, F. Liquid + Liquid Phase Equilibria of 1-Alkyl-3-Methylimidazolium Methylsulfate with Alcohols, or Ethers, or Ketones. *J. Chem. Thermodyn.* **2006**, *38*, 685–695.
- (287) Domańska, U.; Pobudkowska, A.; Eckert, F. Liquid-Liquid Equilibria in the Binary Systems (1,3-Dimethylimidazolium, or 1-Butyl-3-Methylimidazolium Methylsulfate + Hydrocarbons). *Green Chem.* **2006**, *8*, 268–276.
- (288) Freire, M. G.; Santos, L. M. N. B. F.; Marrucho, I. M.; Coutinho, J. A. P. Evaluation of COSMO-RS for the Prediction of LLE and VLE of Alcohols + Ionic Liquids. *Fluid Phase Equilib.* **2007**, *255*, 167–178.
- (289) Freire, M. G.; Neves, C. M. S. S.; Carvalho, P. J.; Gardas, R. L.; Fernandes, A. M.; Marrucho, I. M.; Santos, L. M. N. B. F.; Coutinho, J. A. P. Mutual Solubilities of Water and Hydrophobic Ionic Liquids. *J. Phys. Chem. B* **2007**, *111*, 13082–13089.
- (290) Freire, M. G.; Ventura, S. P. M.; Santos, L. M. N. B. F.; Marrucho, I. M.; Coutinho, J. A. P. Evaluation of COSMO-RS for the Prediction of LLE and VLE of Water and Ionic Liquids Binary Systems. *Fluid Phase Equilib.* **2008**, *268*, 74–84.
- (291) Freire, M. G.; Carvalho, P. J.; Gardas, R. L.; Marrucho, I. M.; Santos, L. M. N. B. F.; Coutinho, J. A. P. Mutual Solubilities of Water and the [C_nmim][Tf₂n] Hydrophobic Ionic Liquids. *J. Phys. Chem. B* **2008**, *112*, 1604–1610.
- (292) Freire, M. G.; Carvalho, P. J.; Gardas, R. L.; Santos, L. M. N. B. F.; Marrucho, I. M.; Coutinho, J. A. P. Solubility of Water in Tetradecyltriethylphosphonium-Based Ionic Liquids. *J. Chem. Eng. Data* **2008**, *53*, 2378–2382.
- (293) Banerjee, T.; Singh, M. K.; Khanna, A. Prediction of Binary VLE for Imidazolium Based Ionic Liquid Systems Using COSMO-RS. *Ind. Eng. Chem. Res.* **2006**, *45*, 3207–3219.
- (294) Bruzzzone, S.; Malvaldi, M.; Chiappe, C. A Rism Approach to the Liquid Structure and Solvation Properties of Ionic Liquids. *Phys. Chem. Chem. Phys.* **2007**, *9*, 5576–5581.
- (295) Bruzzzone, S.; Malvaldi, M.; Chiappe, C. Solvation Thermodynamics of Alkali and Halide Ions in Ionic Liquids through Integral Equations. *J. Chem. Phys.* **2008**, *129*, 074509.
- (296) Chiappe, C.; Malvaldi, M.; Pomelli, C. S. *Ab Initio* Study of the Diels Alder Reaction of Cyclopentadiene with Acrolein in a Ionic Liquid by KS-DFT/3D-RISM-KH Theory. *J. Chem. Theory Comput.* **2010**, *6*, 179–183.
- (297) Malvaldi, M.; Bruzzzone, S.; Chiappe, C.; Gusarov, S.; Kovalenko, A. *Ab Initio* Study of Ionic Liquids by KS-DFT/3D-RISM-KH Theory. *J. Phys. Chem. B* **2009**, *113*, 3536–3542.
- (298) Singer, S. J.; Chandler, D. Free Energy Functions in the Extended Rism Approximation. *Mol. Phys.* **1985**, *55*, 621–625.
- (299) Kovalenko, A.; Hirata, F. First-Principles Realization of a Van Der Waals Maxwell Theory for Water. *Chem. Phys. Lett.* **2001**, *349*, 496–502.
- (300) Kovalenko, A.; Hirata, F. Three-Dimensional Density Profiles of Water in Contact with a Solute of Arbitrary Shape: A Rism Approach. *Chem. Phys. Lett.* **1998**, *290*, 237–244.
- (301) Kovalenko, A.; Hirata, F. Self-Consistent Description of a Metal Water Interface by the Kohn Sham Density Functional Theory and the Three-Dimensional Reference Interaction Site Model. *J. Chem. Phys.* **1999**, *110*, 10095–10112.
- (302) Schweizer, K. S.; Curro, J. G. Integral Equation Theory of Polymer Melts: Intramolecular Structure, Local Order, and the Correlation Hole. *Macromolecules* **1988**, *21*, 3070–3081.
- (303) Sato, H.; Kovalenko, A.; Hirata, F. Self-Consistent Field, *Ab Initio* Molecular Orbital and Three-Dimensional Reference Interaction Site Model Study for Solvation Effect on Carbon Monoxide in Aqueous Solution. *J. Chem. Phys.* **2000**, *112*, 9463–9468.
- (304) Lynden-Bell, R. M.; Atamas, N. A.; Vasilyuk, A.; Hanke, C. G. Chemical Potentials of Water and Organic Solutes in Imidazolium Ionic Liquids: A Simulation Study. *Mol. Phys.* **2002**, *100*, 3225–3229.
- (305) Shah, J. K.; Maginn, E. J. Monte Carlo Simulations of Gas Solubility in the Ionic Liquid 1-N-Butyl-3-Methylimidazolium Hexafluorophosphate. *J. Phys. Chem. B* **2005**, *109*, 10395–10405.
- (306) Canongia Lopes, J. N.; Deschamps, J.; Pádua, A. A. H. Modeling Ionic Liquids Using a Systematic All-Atom Force Field. *J. Phys. Chem. B* **2004**, *108*, 2038–2047.
- (307) Canongia Lopes, J. N.; Deschamps, J.; Pádua, A. A. H. Modeling Ionic Liquids Using a Systematic All-Atom Force Field. *J. Phys. Chem. B* **2004**, *108*, 11250–11250.
- (308) Hanke, C. G.; Price, S. L.; Lynden-Bell, R. M. Intermolecular Potentials for Simulations of Liquid Imidazolium Salts. *Mol. Phys.* **2001**, *99*, 801–809.
- (309) Youngs, T. G. A.; Del Pópolo, M. G.; Kohanoff, J. Development of Complex Classical Force Fields through Force Matching to *Ab Initio* Data: Application to a Room-Temperature Ionic Liquid. *J. Phys. Chem. B* **2006**, *110*, 5697–5707.

- (310) Shim, Y.; Choi, M. Y.; Kim, H. J. A Molecular Dynamics Computer Simulation Study of Room-Temperature Ionic Liquids. I. Equilibrium Solvation Structure and Free Energetics. *J. Chem. Phys.* **2005**, *122*, 044510.
- (311) Hirata, F. *Molecular Theory of Solvation*; Kluwer Academic Publishers: New York, Boston, Dordrecht, London, Moscow, 2004; Vol. 24, pp 358.
- (312) Perkyns, J.; Pettitt, B. M. A Site Site Theory for Finite Concentration Saline Solutions. *J. Chem. Phys.* **1992**, *97*, 7656–7666.
- (313) Swart, M.; van Duijnen, P. T.; Snijders, J. G. A Charge Analysis Derived from an Atomic Multipole Expansion. *J. Comput. Chem.* **2001**, *22*, 79–88.
- (314) te Velde, G.; Bickelhaupt, F. M.; Baerends, E. J.; Fonseca Guerra, C.; van Gisbergen, S. J. A.; Snijders, J. G.; Ziegler, T. Chemistry with ADF. *J. Comput. Chem.* **2001**, *22*, 931–967.
- (315) Fonseca Guerra, C.; Snijders, G. J.; te Velde, G.; Baerends, J. E. Towards an Order-N DFT Method. *Theor. Chem. Acc.* **1998**, *99*, 391–403.
- (316) Prado, C. E. R.; Pópolo, M. G. D.; Youngs, T. G. A.; Kohanoff, J.; Lynden-Bell, R. M. Molecular Electrostatic Properties of Ions in an Ionic Liquid. *Mol. Phys.* **2006**, *104*, 2477–2483.
- (317) Bhargava, B. L.; Balasubramanian, S. Intermolecular Structure and Dynamics in an Ionic Liquid: A Car Parrinello Molecular Dynamics Simulation Study of 1,3-Dimethylimidazolium Chloride. *Chem. Phys. Lett.* **2006**, *417*, 486–491.
- (318) Yan, T.; Burnham, C. J.; Del Pópolo, M. G.; Voth, G. A. Molecular Dynamics Simulation of Ionic Liquids: The Effect of Electronic Polarizability. *J. Phys. Chem. B* **2004**, *108*, 11877–11881.
- (319) Köddermann, T.; Paschek, D.; Ludwig, R. Molecular Dynamic Simulations of Ionic Liquids: A Reliable Description of Structure, Thermodynamics and Dynamics. *ChemPhysChem* **2007**, *8*, 2464–2470.
- (320) Krossing, I.; Slatery, J. M.; Daguenet, C.; Dyson, P. J.; Oleinikova, A.; Weingärtner, H. Why Are Ionic Liquids Liquid? A Simple Explanation Based on Lattice and Solvation Energies. *J. Am. Chem. Soc.* **2006**, *128*, 13427–13434.
- (321) Acevedo, O.; Jorgensen, W. L.; Evanseck, J. D. Elucidation of Rate Variations for a Diels Alder Reaction in Ionic Liquids from Qm/Mm Simulations. *J. Chem. Theory Comput.* **2007**, *3*, 132–138.
- (322) Acevedo, O.; Jorgensen, W. L. Quantum and Molecular Mechanical Monte Carlo Techniques for Modeling Condensed-Phase Reactions. *WIRES: Comput. Mol. Sci.* **2014**, *4*, 422–435.
- (323) Jenkins, H. D. B.; Roobottom, H. K.; Passmore, J.; Glasser, L. Relationships among Ionic Lattice Energies, Molecular (Formula Unit) Volumes, and Thermochemical Radii. *Inorg. Chem.* **1999**, *38*, 3609–3620.
- (324) Jenkins, H. D. B.; Tudela, D.; Glasser, L. Lattice Potential Energy Estimation for Complex Ionic Salts from Density Measurements. *Inorg. Chem.* **2002**, *41*, 2364–2367.
- (325) Glasser, L.; Jenkins, H. D. B. Volume-Based Thermodynamics: A Prescription for Its Application and Usage in Approximation and Prediction of Thermodynamic Data. *J. Chem. Eng. Data* **2011**, *56*, 874–880.
- (326) Glasser, L. Lattice and Phase Transition Thermodynamics of Ionic Liquids. *Thermochim. Acta* **2004**, *421*, 87–93.
- (327) Jenkins, H. D. B.; Glasser, L. Standard Absolute Entropy, S°_{298} Values from Volume or Density. I. Inorganic Materials. *Inorg. Chem.* **2003**, *42*, 8702–8708.
- (328) Glasser, L. Thermodynamic Estimation: Ionic Materials. *J. Solid State Chem.* **2013**, *206*, 139–144.
- (329) Canongia Lopes, J. N. A.; Pádua, A. A. H. Nanostructural Organization in Ionic Liquids. *J. Phys. Chem. B* **2006**, *110*, 3330–3335.
- (330) Shimizu, K.; Tariq, M.; Gomes, M. F. C.; Rebelo, L. P. N.; Canongia Lopes, J. N. Assessing the Dispersive and Electrostatic Components of the Cohesive Energy of Ionic Liquids Using Molecular Dynamics Simulations and Molar Refraction Data. *J. Phys. Chem. B* **2010**, *114*, 5831–5834.
- (331) Almeida, H. F. D.; Freire, M. G.; Fernandes, A. M.; Lopes-da-Silva, J. A.; Morgado, P.; Shimizu, K.; Filipe, E. J. M.; Canongia Lopes, J. N.; Santos, L. M. N. B. F.; Coutinho, J. A. P. Cation Alkyl Side Chain Length and Symmetry Effects on the Surface Tension of Ionic Liquids. *Langmuir* **2014**, *30*, 6408–6418.
- (332) Holbrey, J. D.; Seddon, K. R. The Phase Behaviour of 1-Alkyl-3-Methylimidazolium Tetrafluoroborates; Ionic Liquids and Ionic Liquid Crystals. *J. Chem. Soc., Dalton Trans.* **1999**, 2133–2140.
- (333) Gordon, C. M.; Holbrey, J. D.; Kennedy, A. R.; Seddon, K. R. Ionic Liquid Crystals: Hexafluorophosphate Salts. *J. Mater. Chem.* **1998**, *8*, 2627–2636.
- (334) Gutowski, K. E.; Holbrey, J. D.; Rogers, R. D.; Dixon, D. A. Prediction of the Formation and Stabilities of Energetic Salts and Ionic Liquids Based on *Ab Initio* Electronic Structure Calculations. *J. Phys. Chem. B* **2005**, *109*, 23196–23208.
- (335) Gutowski, K. E.; Rogers, R. D.; Dixon, D. A. Accurate Thermochemical Properties for Energetic Materials Applications. II. Heats of Formation of Imidazolium-, 1,2,4-Triazolium-, and Tetrazolium-Based Energetic Salts from Isodesmic and Lattice Energy Calculations. *J. Phys. Chem. B* **2007**, *111*, 4788–4800.
- (336) Emel'yanenko, V. N.; Verevkin, S. P.; Heintz, A.; Schick, C. Ionic Liquids. Combination of Combustion Calorimetry with High-Level Quantum Chemical Calculations for Deriving Vaporization Enthalpies. *J. Phys. Chem. B* **2008**, *112*, 8095–8098.
- (337) Emel'yanenko, V. N.; Verevkin, S. P.; Heintz, A.; Voss, K.; Schulz, A. Imidazolium-Based Ionic Liquids. 1-Methyl Imidazolium Nitrate: Thermochemical Measurements and *Ab Initio* Calculations. *J. Phys. Chem. B* **2009**, *113*, 9871–9876.
- (338) Emel'yanenko, V. N.; Verevkin, S. P.; Heintz, A. The Gaseous Enthalpy of Formation of the Ionic Liquid 1-Butyl-3-Methylimidazolium Dicyanamide from Combustion Calorimetry, Vapor Pressure Measurements, and *Ab Initio* Calculations. *J. Am. Chem. Soc.* **2007**, *129*, 3930–3937.
- (339) Eichkorn, K.; Treutler, O.; Öhm, H.; Häser, M.; Ahlrichs, R. Auxiliary Basis Sets to Approximate Coulomb Potentials. *Chem. Phys. Lett.* **1995**, *240*, 283–290.
- (340) Eichkorn, K.; Weigend, F.; Treutler, O.; Ahlrichs, R. Auxiliary Basis Sets for Main Row Atoms and Transition Metals and Their Use to Approximate Coulomb Potentials. *Theor. Chem. Acc.* **1997**, *97*, 119–124.
- (341) Turner, E. A.; Pye, C. C.; Singer, R. D. Use of *Ab Initio* Calculations toward the Rational Design of Room Temperature Ionic Liquids. *J. Phys. Chem. A* **2003**, *107*, 2277–2288.
- (342) Li, H.; Ibrahim, M.; Agberemi, I.; Kobrak, M. N. The Relationship between Ionic Structure and Viscosity in Room-Temperature Ionic Liquids. *J. Chem. Phys.* **2008**, *129*, 124507.
- (343) Hunt, P. A.; Gould, I. R.; Kirchner, B. The Structure of Imidazolium-Based Ionic Liquids: Insights from Ion-Pair Interactions. *Aust. J. Chem.* **2007**, *60*, 9–14.
- (344) Goldstein, M. Viscous Liquids and the Glass Transitions. *J. Chem. Phys.* **1969**, *51*, 3728–3739.
- (345) Izgorodina, E. I.; Maganti, R.; Armel, V.; Dean, P. M.; Pringle, J. M.; Seddon, K. R.; MacFarlane, D. R. Understanding the Effect of the C2 Proton in Promoting Low Viscosities and High Conductivities in Imidazolium-Based Ionic Liquids: Part I. Weakly Coordinating Anions. *J. Phys. Chem. B* **2011**, *115*, 14688–14697.
- (346) Bonhôte, P.; Dias, A.-P.; Papageorgiou, N.; Kalyanasundaram, K.; Grätzel, M. Hydrophobic, Highly Conductive Ambient-Temperature Molten Salts. *Inorg. Chem.* **1996**, *35*, 1168–1178.
- (347) Nishida, T.; Tashiro, Y.; Yamamoto, M. Physical and Electrochemical Properties of 1-Alkyl-3-Methylimidazolium Tetrafluoroborate for Electrolyte. *J. Fluorine Chem.* **2003**, *120*, 135–141.
- (348) Min, G.-H.; Yim, T.; Lee, H. Y.; Kim, H.-J.; Mun, J.; Kim, S.; Oh, S. M.; Kim, Y. G. Synthesis and Physicochemical Properties of Ionic Liquids: 1-Alkenyl-2,3-Dimethylimidazolium Tetrafluoroborates. *Bull. Korean Chem. Soc.* **2007**, *28*, 1562–1566.
- (349) Carda-Broch, S.; Berthod, A.; Armstrong, D. W. Solvent Properties of the 1-Butyl-3-Methylimidazolium Hexafluorophosphate Ionic Liquid. *Anal. Bioanal. Chem.* **2003**, *375*, 191–199.

- (350) Strehmel, V.; Laschewsky, A.; Wetzel, H.; Gornitz, E. Free Radical Polymerization of N-Butyl Methacrylate in Ionic Liquids. *Macromolecules* **2006**, *39*, 923–930.
- (351) Fredlake, C. P.; Crosthwaite, J. M.; Hert, D. G.; Aki, S. N. V. K.; Brennecke, J. F. Thermophysical Properties of Imidazolium-Based Ionic Liquids. *J. Chem. Eng. Data* **2004**, *49*, 954–964.
- (352) Kölle, P.; Dronskowski, R. Synthesis, Crystal Structures and Electrical Conductivities of the Ionic Liquid Compounds Butyldimethylimidazolium Tetrafluoroborate, Hexafluorophosphate and Hexafluoroantimonate. *Eur. J. Inorg. Chem.* **2004**, *2004*, 2989–2989.
- (353) Huddleston, J. G.; Visser, A. E.; Reichert, W. M.; Willauer, H. D.; Broker, G. A.; Rogers, R. D. Characterization and Comparison of Hydrophilic and Hydrophobic Room Temperature Ionic Liquids Incorporating the Imidazolium Cation. *Green Chem.* **2001**, *3*, 156–164.
- (354) Wilkes, J. S.; Levisky, J. A.; Wilson, R. A.; Hussey, C. L. Dialkylimidazolium Chloroaluminate Melts: A New Class of Room-Temperature Ionic Liquids for Electrochemistry, Spectroscopy and Synthesis. *Inorg. Chem.* **1982**, *21*, 1263–1264.
- (355) Ngo, H. L.; LeCompte, K.; Hargens, L.; McEwen, A. B. Thermal Properties of Imidazolium Ionic Liquids. *Thermochim. Acta* **2000**, *357–358*, 97–102.
- (356) Kölle, P.; Dronskowski, R. Hydrogen Bonding in the Crystal Structures of the Ionic Liquid Compounds Butyldimethylimidazolium Hydrogen Sulfate, Chloride, and Chloroferrate(II,III). *Inorg. Chem.* **2004**, *43*, 2803–2809.
- (357) Domańska, U.; Marciniak, A. Liquid Phase Behaviour of 1-Hexyloxymethyl-3-Methyl-Imidazolium-Based Ionic Liquids with Hydrocarbons: The Influence of Anion. *J. Chem. Thermodyn.* **2005**, *37*, 577–585.
- (358) Tsuzuki, S. Factors Controlling the Diffusion of Ions in Ionic Liquids. *ChemPhysChem* **2012**, *13*, 1664–1670.
- (359) Hunt, P. A. Why Does a Reduction in Hydrogen Bonding Lead to an Increase in Viscosity for the 1-Butyl-2,3-Dimethyl-Imidazolium-Based Ionic Liquids? *J. Phys. Chem. B* **2007**, *111*, 4844–4853.
- (360) Zhang, Y.; Maginn, E. J. The Effect of C2 Substitution on Melting Point and Liquid Phase Dynamics of Imidazolium Based-Ionic Liquids: Insights from Molecular Dynamics Simulations. *Phys. Chem. Chem. Phys.* **2012**, *14*, 12157–12164.
- (361) Borodin, O. Relation between Heat of Vaporization, Ion Transport, Molar Volume, and Cation-Anion Binding Energy for Ionic Liquids. *J. Phys. Chem. B* **2009**, *113*, 12353–12357.
- (362) Borodin, O.; Vatamanu, J.; Smith, G. Bulk and Interfacial Behavior of Ionic Liquids from Molecular Dynamics Simulations. *ECS Trans.* **2010**, *33*, 583–599.
- (363) Malberg, F.; Brehm, M.; Holloczki, O.; Pensado, A. S.; Kirchner, B. Understanding the Evaporation of Ionic Liquids Using the Example of 1-Ethyl-3-Methylimidazolium Ethylsulfate. *Phys. Chem. Chem. Phys.* **2013**, *15*, 18424–18436.
- (364) Fakhraee, M.; Gholami, M. R. Biodegradable Ionic Liquids: Effects of Temperature, Alkyl Side-Chain Length, and Anion on the Thermodynamic Properties and Interaction Energies as Determined by Molecular Dynamics Simulations Coupled with *Ab Initio* Calculations. *Ind. Eng. Chem. Res.* **2015**, *54*, 11678–11700.
- (365) Raghavachari, K.; Stefanov, B. B.; Curtiss, L. A. Accurate Thermochemistry for Larger Molecules: Gaussian-2 Theory with Bond Separation Energies. *J. Chem. Phys.* **1997**, *106*, 6764–6767.
- (366) Pedley, J. B.; Naylor, R. D.; Kirby, S. P.; Pedley, J. B. *Thermochemical Data of Organic Compounds*; Chapman and Hall: London, 1986; pp 792.
- (367) Zaitsau, D. H.; Emel'yanenko, V. N.; Verevkin, S. P.; Heintz, A. Sulfur-Containing Ionic Liquids. Rotating-Bomb Combustion Calorimetry and First-Principles Calculations for 1-Ethyl-3-Methylimidazolium Thiocyanate. *J. Chem. Eng. Data* **2010**, *55*, 5896–5899.
- (368) Emel'yanenko, V. N.; Zaitsau, D. H.; Verevkin, S. P.; Heintz, A. Imidazolium Based Ionic Liquids. 1-Ethanol-3-Methyl-Imidazolium Dicyanamide: Thermochemical Measurement and First-Principles Calculations. *Thermochim. Acta* **2011**, *518*, 107–110.
- (369) Verevkin, S. P.; Emel'yanenko, V. N.; Zaitsau, D. H.; Heintz, A.; Muzny, C. D.; Frenkel, M. Thermochemistry of Imidazolium-Based Ionic Liquids: Experiment and First-Principles Calculations. *Phys. Chem. Chem. Phys.* **2010**, *12*, 14994–15000.
- (370) Zorn, D. D.; Boatz, J. A.; Gordon, M. S. Electronic Structure Studies of Tetrazolium-Based Ionic Liquids. *J. Phys. Chem. B* **2006**, *110*, 11110–11119.
- (371) Verevkin, S. P.; Emel'yanenko, V. N.; Zaitsau, D. H.; Ralys, R. V.; Schick, C. Ionic Liquids: Differential Scanning Calorimetry as a New Indirect Method for Determination of Vaporization Enthalpies. *J. Phys. Chem. B* **2012**, *116*, 4276–4285.
- (372) Verevkin, S. P.; Zaitsau, D. H.; Emel'yanenko, V. N.; Ralys, R. V.; Schick, C.; Geppert-Rybczyńska, M.; Jayaraman, S.; Maginn, E. J. Benchmark Values: Thermochemistry of the Ionic Liquid [C₄py][Cl]. *Aust. J. Chem.* **2012**, *65*, 1487–1490.
- (373) Verevkin, S. P.; Emel'yanenko, V. N.; Krossing, I.; Kalb, R. Thermochemistry of Ammonium Based Ionic Liquids: Tetra-Alkyl Ammonium Nitrates - Experiments and Computations. *J. Chem. Thermodyn.* **2012**, *51*, 107–113.
- (374) Cohen, N.; Benson, S. W. Estimation of Heats of Formation of Organic Compounds by Additivity Methods. *Chem. Rev.* **1993**, *93*, 2419–2438.
- (375) Verevkin, S. P.; Zaitsau, D. H.; Emel'yanenko, V. N.; Schick, C.; Jayaraman, S.; Maginn, E. J. An Elegant Access to Formation and Vaporization Enthalpies of Ionic Liquids by Indirect DSC Experiment and *in Silico* Calculations. *Chem. Commun.* **2012**, *48*, 6915–6917.
- (376) Akai, N.; Kawai, A.; Shibuya, K. Ion-Pair Structure of Vaporized Ionic Liquid Studied by Matrix-Isolation F₂IR Spectroscopy with DFT Calculations: A Case of 1-Ethyl-3-Methylimidazolium Trifluoromethanesulfonate. *J. Phys. Chem. A* **2010**, *114*, 12662–12666.
- (377) Akai, N.; Parasz, D.; Kawai, A.; Shibuya, K. Cryogenic Neon Matrix-Isolation F₂IR Spectroscopy of Evaporated Ionic Liquids: Geometrical Structure of Cation Anion 1:1 Pair in the Gas Phase. *J. Phys. Chem. B* **2009**, *113*, 4756–4762.
- (378) Earle, M. J.; Esperanca, J. M. S. S.; Gilea, M. A.; Canongia Lopes, J. N.; Rebelo, L. P. N.; Magee, J. W.; Seddon, K. R.; Widegren, J. A. The Distillation and Volatility of Ionic Liquids. *Nature* **2006**, *439*, 831–834.
- (379) Paulechka, Y. U.; Kabo, G. J.; Blokhin, A. V.; Vydrov, O. A.; Magee, J. W.; Frenkel, M. Thermodynamic Properties of 1-Butyl-3-Methylimidazolium Hexafluorophosphate in the Ideal Gas State. *J. Chem. Eng. Data* **2003**, *48*, 457–462.
- (380) McQuarrie, D. A. *Statistical Mechanics*; Harper and Row: New York, 1976.
- (381) Verevkin, S. P.; Zaitsau, D. H.; Emel'yanenko, V. N.; Yermalayev, A. V.; Schick, C.; Liu, H.; Maginn, E. J.; Bulut, S.; Krossing, I.; Kalb, R. Making Sense of Enthalpy of Vaporization Trends for Ionic Liquids: New Experimental and Simulation Data Show a Simple Linear Relationship and Help Reconcile Previous Data. *J. Phys. Chem. B* **2013**, *117*, 6473–6486.
- (382) Umebayashi, Y.; Hamano, H.; Tsuzuki, S.; Canongia Lopes, J. N.; Pádua, A. A. H.; Kameda, Y.; Kohara, S.; Yamaguchi, T.; Fujii, K.; Ishiguro, S. -i. Dependence of the Conformational Isomerism in 1-Butyl-3-Methylimidazolium Ionic Liquids on the Nature of the Halide Anion. *J. Phys. Chem. B* **2010**, *114*, 11715–11724.
- (383) Pimenta, I. S. O.; Elzey, S.; Boatz, J. A.; Gordon, M. S. Pentazole-Based Energetic Ionic Liquids: A Computational Study. *J. Phys. Chem. A* **2007**, *111*, 691–703.
- (384) Li, W.; Wu, X.; Qi, C.; Rong, H.; Gong, L. Study on the Relationship between the Interaction Energy and the Melting Point of Amino Acid Cation Based Ionic Liquids. *J. Mol. Struct.: THEOCHEM* **2010**, *942*, 19–25.
- (385) Chesman, A. S. R.; Hodgson, J. L.; Izgorodina, E. I.; Urbatsch, A.; Turner, D. R.; Deacon, G. B. Batten, S. R. Anion Anion Interactions in the Crystal Packing of Functionalized Methanide Anions: An Experimental and Computational Study. *Cryst. Growth Des.* **2014**, *14*, 1922–1932.
- (386) Simons, T. J.; Verheyen, T.; Izgorodina, E. I.; Vijayaraghavan, R.; Young, S.; Pearson, A. K.; Pas, S. J.; MacFarlane, D. R. Mechanisms

- of Low Temperature Capture and Regeneration of CO₂ Using Diamino Protic Ionic Liquids. *Phys. Chem. Chem. Phys.* **2016**, *18*, 1140–1149.
- (387) Talaty, E. R.; Raja, S.; Storhaug, V. J.; Dölle, A.; Carper, W. R. Raman and Infrared Spectra and *Ab Initio* Calculations of C₂-4mim Imidazolium Hexafluorophosphate Ionic Liquids. *J. Phys. Chem. B* **2004**, *108*, 13177–13184.
- (388) Scott, A. P.; Radom, L. Harmonic Vibrational Frequencies: An Evaluation of Hartree Fock, Møller Plesset, Quadratic Configuration Interaction, Density Functional Theory, and Semiempirical Scale Factors. *J. Phys. Chem.* **1996**, *100*, 16502–16513.
- (389) Umabayashi, Y.; Fujimori, T.; Sukizaki, T.; Asada, M.; Fujii, K.; Kanzaki, R.; Ishiguro, S.-i. Evidence of Conformational Equilibrium of 1-Ethyl-3-Methylimidazolium in Its Ionic Liquid Salts: Raman Spectroscopic Study and Quantum Chemical Calculations. *J. Phys. Chem. A* **2005**, *109*, 8976–8982.
- (390) Heimer, N. E.; Del Sesto, R. E.; Meng, Z.; Wilkes, J. S.; Carper, W. R. Vibrational Spectra of Imidazolium Tetrafluoroborate Ionic Liquids. *J. Mol. Liq.* **2006**, *124*, 84–95.
- (391) Wulf, A.; Fumino, K.; Ludwig, R. Spectroscopic Evidence for an Enhanced Anion Cation Interaction from Hydrogen Bonding in Pure Imidazolium Ionic Liquids. *Angew. Chem., Int. Ed.* **2010**, *49*, 449–453.
- (392) Fumino, K.; Wulf, A.; Ludwig, R. The Potential Role of Hydrogen Bonding in Aprotic and Protic Ionic Liquids. *Phys. Chem. Chem. Phys.* **2009**, *11*, 8790–8794.
- (393) Fumino, K.; Peppel, T.; Geppert-Rybczynska, M.; Zaitsau, D. H.; Lehmann, J. K.; Verevkin, S. P.; Kockerling, M.; Ludwig, R. The Influence of Hydrogen Bonding on the Physical Properties of Ionic Liquids. *Phys. Chem. Chem. Phys.* **2011**, *13*, 14064–14075.
- (394) Roth, C.; Peppel, T.; Fumino, K.; Kockerling, M.; Ludwig, R. The Importance of Hydrogen Bonds for the Structure of Ionic Liquids: Single-Crystal X-Ray Diffraction and Transmission and Attenuated Total Reflection Spectroscopy in the Terahertz Region. *Angew. Chem., Int. Ed.* **2010**, *49*, 10221–10224.
- (395) Fumino, K.; Wulf, A.; Ludwig, R. Strong, Localized, and Directional Hydrogen Bonds Fluidize Ionic Liquids. *Angew. Chem., Int. Ed.* **2008**, *47*, 8731–8734.
- (396) Blokhin, A. V.; Paulechka, Y. U.; Strechan, A. A.; Kabo, G. J. Physicochemical Properties, Structure, and Conformations of 1-Butyl-3-Methylimidazolium Bis(Trifluoromethanesulfonyl)Imide [C₄mim]⁺Ntf₂[−] Ionic Liquid. *J. Phys. Chem. B* **2008**, *112*, 4357–4364.
- (397) Fujimori, T.; Fujii, K.; Kanzaki, R.; Chiba, K.; Yamamoto, H.; Umabayashi, Y.; Ishiguro, S.-i. Conformational Structure of Room Temperature Ionic Liquid N-Butyl-N-Methyl-Pyrrolidinium Bis-(Trifluoromethanesulfonyl) Imide - Raman Spectroscopic Study and DFT Calculations. *J. Mol. Liq.* **2007**, *131*, 132–132, 216–224.
- (398) Fujii, K.; Fujimori, T.; Takamuku, T.; Kanzaki, R.; Umabayashi, Y.; Ishiguro, S.-i. Conformational Equilibrium of Bis(Trifluoromethanesulfonyl) Imide Anion of a Room-Temperature Ionic Liquid: Raman Spectroscopic Study and DFT Calculations. *J. Phys. Chem. B* **2006**, *110*, 8179–8183.
- (399) Fujii, K.; Seki, S.; Fukuda, S.; Kanzaki, R.; Takamuku, T.; Umabayashi, Y.; Ishiguro, S.-i. Anion Conformation of Low-Viscosity Room-Temperature Ionic Liquid 1-Ethyl-3-Methylimidazolium Bis-(Fluorosulfonyl) Imide. *J. Phys. Chem. B* **2007**, *111*, 12829–12833.
- (400) Holomb, R.; Martinelli, A.; Albinsson, L.; Lassègues, J. C.; Johansson, P.; Jacobsson, P. Ionic Liquid Structure: The Conformational Isomerism in 1-Butyl-3-Methyl-Imidazolium Tetrafluoroborate ([Bmim][BF₄]). *J. Raman Spectrosc.* **2008**, *39*, 793–805.
- (401) Endo, T.; Kato, T.; Tozaki, K.-i.; Nishikawa, K. Phase Behaviors of Room Temperature Ionic Liquid Linked with Cation Conformational Changes: 1-Butyl-3-Methylimidazolium Hexafluorophosphate. *J. Phys. Chem. B* **2010**, *114*, 407–411.
- (402) Sobota, M.; Nikiforidis, I.; Hieringer, W.; Paape, N.; Happel, M.; Steinrück, H.-P.; Görling, A.; Wasserscheid, P.; Laurin, M.; Libuda, J. Toward Ionic-Liquid-Based Model Catalysis: Growth, Orientation, Conformation, and Interaction Mechanism of the [Tf₂n][−] Anion in [Bmim][Tf₂n] Thin Films on a Well-Ordered Alumina Surface. *Langmuir* **2010**, *26*, 7199–7207.
- (403) Xiao, D.; Hines, L. G., Jr.; Holtz, M. W.; Song, K.; Bartsch, R. A.; Quitevis, E. L. Effect of Cation Symmetry on the Low-Frequency Spectra of Imidazolium Ionic Liquids: Oke and Raman Spectroscopic Measurements and DFT Calculations. *Chem. Phys. Lett.* **2010**, *497*, 37–42.
- (404) Umabayashi, Y.; Mitsugi, T.; Fujii, K.; Seki, S.; Chiba, K.; Yamamoto, H.; Canongia Lopes, J. N.; Pádua, A. A. H.; Takeuchi, M.; Kanzaki, R. Raman Spectroscopic Study, DFT Calculations and Md Simulations on the Conformational Isomerism of N-Alkyl-N-Methylpyrrolidinium Bis-(Trifluoromethanesulfonyl) Amide Ionic Liquids. *J. Phys. Chem. B* **2009**, *113*, 4338–4346.
- (405) Lassègues, J. C.; Grondin, J.; Holomb, R.; Johansson, P. Raman and *Ab Initio* Study of the Conformational Isomerism in the 1-Ethyl-3-Methyl-Imidazolium Bis(Trifluoromethanesulfonyl)Imide Ionic Liquid. *J. Raman Spectrosc.* **2007**, *38*, 551–558.
- (406) Kiefer, J.; Pye, C. C. Structure of the Room-Temperature Ionic Liquid 1-Hexyl-3-Methylimidazolium Hydrogen Sulfate: Conformational Isomerism. *J. Phys. Chem. A* **2010**, *114*, 6713–6720.
- (407) Berg, R. W.; Rüisager, A.; Van Buu, O. N.; Fehrmann, R.; Harris, P.; Tomaszowska, A. A.; Seddon, K. R. Crystal Structure, Vibrational Spectroscopy and *Ab Initio* Density Functional Theory Calculations on the Ionic Liquid Forming 1,1,3,3-Tetramethylguanidinium Bis((Trifluoromethyl)Sulfonyl)Amide. *J. Phys. Chem. B* **2009**, *113*, 8878–8886.
- (408) Berg, R. W.; Deetlefs, M.; Seddon, K. R.; Shim, I.; Thompson, J. M. Raman and *Ab Initio* Studies of Simple and Binary 1-Alkyl-3-Methylimidazolium Ionic Liquids. *J. Phys. Chem. B* **2005**, *109*, 19018–19025.
- (409) Umabayashi, Y.; Mitsugi, T.; Fukuda, S.; Fujimori, T.; Fujii, K.; Kanzaki, R.; Takeuchi, M.; Ishiguro, S.-i. Lithium Ion Solvation in Room-Temperature Ionic Liquids Involving Bis-(Trifluoromethanesulfonyl) Imide Anion Studied by Raman Spectroscopy and DFT Calculations. *J. Phys. Chem. B* **2007**, *111*, 13028–13032.
- (410) Rocher, N. M.; Izgorodina, E. I.; Rüther, T.; Forsyth, M.; MacFarlane, D. R.; Rodopoulos, T.; Horne, M. D.; Bond, A. M. Aluminium Speciation in 1-Butyl-1-Methylpyrrolidinium Bis-(Trifluoromethylsulfonyl)Amide/AlCl₃ Mixtures. *Chem. - Eur. J.* **2009**, *15*, 3435–3447.
- (411) Lassègues, J.-C.; Grondin, J.; Aupetit, C.; Johansson, P. Spectroscopic Identification of the Lithium Ion Transporting Species in LiTf₂-Doped Ionic Liquids. *J. Phys. Chem. A* **2009**, *113*, 305–314.
- (412) Umabayashi, Y.; Mori, S.; Fujii, K.; Tsuzuki, S.; Seki, S.; Hayamizu, K.; Ishiguro, S.-i. Raman Spectroscopic Studies and *Ab Initio* Calculations on Conformational Isomerism of 1-Butyl-3-Methylimidazolium Bis-(Trifluoromethanesulfonyl)Amide Solvated to a Lithium Ion in Ionic Liquids: Effects of the Second Solvation Sphere of the Lithium Ion. *J. Phys. Chem. B* **2010**, *114*, 6513–6521.
- (413) Köddermann, T.; Wertz, C.; Heintz, A.; Ludwig, R. The Association of Water in Ionic Liquids: A Reliable Measure of Polarity. *Angew. Chem., Int. Ed.* **2006**, *45*, 3697–3702.
- (414) Zhang, L.; Xu, Z.; Wang, Y.; Li, H. Prediction of the Solvation and Structural Properties of Ionic Liquids in Water by Two-Dimensional Correlation Spectroscopy. *J. Phys. Chem. B* **2008**, *112*, 6411–6419.
- (415) Stange, P.; Fumino, K.; Ludwig, R. Ion Speciation of Protic Ionic Liquids in Water: Transition from Contact to Solvent-Separated Ion Pairs. *Angew. Chem., Int. Ed.* **2013**, *52*, 2990–2994.
- (416) Papanyan, Z.; Roth, C.; Paschek, D.; Ludwig, R. Understanding the Dissolution of Polyols by Ionic Liquids Using the Example of a Well-Defined Model Compound. *ChemPhysChem* **2011**, *12*, 2400–2404.
- (417) Xiao, C.-x.; Wang, H.-z.; Mu, X.-d.; Kou, Y. Ionic-Liquid-Like Copolymer Stabilized Nanocatalysts in Ionic Liquids I. Platinum Catalyzed Selective Hydrogenation of O-Chloronitrobenzene. *J. Catal.* **2007**, *250*, 25–32.

- (418) Fumino, K.; Wulf, A.; Ludwig, R. Hydrogen Bonding in Protic Ionic Liquids: Reminiscent of Water. *Angew. Chem., Int. Ed.* **2009**, *48*, 3184–3186.
- (419) Cha, S.; Ao, M.; Sung, W.; Moon, B.; Ahlstrom, B.; Johansson, P.; Ouchi, Y.; Kim, D. Structures of Ionic Liquid-Water Mixtures Investigated by IR and NMR Spectroscopy. *Phys. Chem. Chem. Phys.* **2014**, *16*, 9591–9601.
- (420) Chang, H.-C.; Jiang, J.-C.; Tsai, W.-C.; Chen, G.-C.; Lin, S. H. Hydrogen Bond Stabilization in 1,3-Dimethylimidazolium Methyl Sulfate and 1-Butyl-3-Methylimidazolium Hexafluorophosphate Probed by High Pressure: The Role of Charge-Enhanced C–H···O Interactions in the Room-Temperature Ionic Liquid. *J. Phys. Chem. B* **2006**, *110*, 3302–3307.
- (421) Katsyuba, S. A.; Zvereva, E. E.; Vidiš, A.; Dyson, P. J. Application of Density Functional Theory and Vibrational Spectroscopy toward the Rational Design of Ionic Liquids. *J. Phys. Chem. A* **2007**, *111*, 352–370.
- (422) Lassègues, J.-C.; Grondin, J.; Cavagnat, D.; Johansson, P. New Interpretation of the C–H Stretching Vibrations in Imidazolium-Based Ionic Liquids. *J. Phys. Chem. A* **2009**, *113*, 6419–6421.
- (423) Shukla, M.; Srivastava, N.; Saha, S. Theoretical and Spectroscopic Studies of 1-Butyl-3-Methylimidazolium Iodide Room Temperature Ionic Liquid: Its Differences with Chloride and Bromide Derivatives. *J. Mol. Struct.* **2010**, *975*, 349–356.
- (424) Berg, R. W.; Canongia Lopes, J. N.; Ferreira, R.; Rebelo, L. P. N.; Seddon, K. R.; Tomaszowska, A. A Raman Spectroscopic Study of the Vapor Phase of 1-Methylimidazolium Ethanoate, a Protic Ionic Liquid. *J. Phys. Chem. A* **2010**, *114*, 10834–10841.
- (425) Leal, J. P.; Esperança, J. M. S. S.; Minas da Piedade, M. E.; Canongia Lopes, J. N.; Rebelo, L. P. N.; Seddon, K. R. The Nature of Ionic Liquids in the Gas Phase. *J. Phys. Chem. A* **2007**, *111*, 6176–6182.
- (426) Ditchfield, R. Self-Consistent Perturbation Theory of Diamagnetism. *Mol. Phys.* **1974**, *27*, 789–807.
- (427) Wolinski, K.; Hinton, J. F.; Pulay, P. Efficient Implementation of the Gauge-Independent Atomic Orbital Method for NMR Chemical Shift Calculations. *J. Am. Chem. Soc.* **1990**, *112*, 8251–8260.
- (428) Palomar, J.; Ferro, V. R.; Gilarranz, M. A.; Rodriguez, J. J. Computational Approach to Nuclear Magnetic Resonance in 1-Alkyl-3-Methylimidazolium Ionic Liquids. *J. Phys. Chem. B* **2007**, *111*, 168–180.
- (429) Miertuš, S.; Scrocco, E.; Tomasi, J. Electrostatic Interaction of a Solute with a Continuum. A Direct Utilization of *Ab Initio* Molecular Potentials for the Prediction of Solvent Effects. *Chem. Phys.* **1981**, *55*, 117–129.
- (430) Cossi, M.; Scalmani, G.; Rega, N.; Barone, V. New Developments in the Polarizable Continuum Model for Quantum Mechanical and Classical Calculations on Molecules in Solution. *J. Chem. Phys.* **2002**, *117*, 43–54.
- (431) Katsyuba, S. A.; Griaiznova, T. P.; Vidiš, A.; Dyson, P. J. Structural Studies of the Ionic Liquid 1-Ethyl-3-Methylimidazolium Tetrafluoroborate in Dichloromethane Using a Combined DFT-NMR Spectroscopic Approach. *J. Phys. Chem. B* **2009**, *113*, 5046–5051.
- (432) Chen, S.; Vijayaraghavan, R.; MacFarlane, D. R.; Izgorodina, E. I. *Ab Initio* Prediction of Proton NMR Chemical Shifts in Imidazolium Ionic Liquids. *J. Phys. Chem. B* **2013**, *117*, 3186–3197.
- (433) Adamo, C.; Barone, V. Exchange Functionals with Improved Long-Range Behavior and Adiabatic Connection Methods without Adjustable Parameters: The Mpw and Mpw1pw Models. *J. Chem. Phys.* **1998**, *108*, 664–675.
- (434) Strauch, M.; Bonsa, A.-M.; Golub, B.; Overbeck, V.; Michalik, D.; Paschek, D.; Ludwig, R. Deuteron Quadrupole Coupling Constants and Reorientational Correlation Times in Protic Ionic Liquids. *Phys. Chem. Chem. Phys.* **2016**, *18*, 17788–17794.
- (435) Ludwig, R. Thermodynamic Properties of Ionic Liquids – a Cluster Approach. *Phys. Chem. Chem. Phys.* **2008**, *10*, 4333–4339.
- (436) Frisch, M. J.; Trucks, G. W.; Schlegel, H. B.; Scuseria, G. E.; Robb, M. A.; Cheeseman, J. R.; Scalmani, G.; Barone, V.; Mennucci, B.; Petersson, G. A. et al. *Gaussian 09*; Gaussian Inc.: Wallingford, CT, USA, 2009.
- (437) Spickermann, C.; Lehmann, S. B. C.; Kirchner, B. Introducing Phase Transitions to Quantum Chemistry: From Trouton's Rule to First Principles Vaporization Entropies. *J. Chem. Phys.* **2008**, *128*, 244506.
- (438) Zaitsau, D. H.; Kabo, G. J.; Strechan, A. A.; Paulechka, Y. U.; Tschersich, A.; Verevkin, S. P.; Heintz, A. Experimental Vapor Pressures of 1-Alkyl-3-Methylimidazolium Bis-(Trifluoromethylsulfonyl)Imides and a Correlation Scheme for Estimation of Vaporization Enthalpies of Ionic Liquids. *J. Phys. Chem. A* **2006**, *110*, 7303–7306.
- (439) Zaitsau, D. H.; Emel'yanenko, V. N.; Stange, P.; Schick, C.; Verevkin, S. P.; Ludwig, R. Dispersion and Hydrogen Bonding Rule: Why the Vaporization Enthalpies of Aprotic Ionic Liquids Are Significantly Larger Than Those of Protic Ionic Liquids. *Angew. Chem., Int. Ed.* **2016**, *55*, 11682–11686.
- (440) Dong, K.; Zhao, L.; Wang, Q.; Song, Y.; Zhang, S. Are Ionic Liquids Pairwise in Gas Phase? A Cluster Approach and *in Situ* IR Study. *Phys. Chem. Chem. Phys.* **2013**, *15*, 6034–6040.
- (441) Emel'yanenko, V. N.; Boeck, G.; Verevkin, S. P.; Ludwig, R. Volatile Times for the Very First Ionic Liquid: Understanding the Vapor Pressures and Enthalpies of Vaporization of Ethylammonium Nitrate. *Chem. - Eur. J.* **2014**, *20*, 11640–11645.
- (442) Peppel, T.; Roth, C.; Fumino, K.; Paschek, D.; Köckerling, M.; Ludwig, R. The Influence of Hydrogen-Bond Defects on the Properties of Ionic Liquids. *Angew. Chem., Int. Ed.* **2011**, *50*, 6661–6665.
- (443) Weinhold, F. Quantum Cluster Equilibrium Theory of Liquids: Illustrative Application to Water. *J. Chem. Phys.* **1998**, *109*, 373–384.
- (444) Weinhold, F. Quantum Cluster Equilibrium Theory of Liquids: General Theory and Computer Implementation. *J. Chem. Phys.* **1998**, *109*, 367–372.
- (445) Ludwig, R.; Weinhold, F. Quantum Cluster Equilibrium Theory of Liquids: Freezing of Qc/3-21g Water to Tetraikaidecahedral "Bucky-Ice". *J. Chem. Phys.* **1999**, *110*, 508–515.
- (446) Ludwig, R.; Weinhold, F.; Farrar, T. C. Quantum Cluster Equilibrium Theory of Liquids: Temperature Dependent Chemical Shifts, Quadrupole Coupling Constants and Vibrational Frequencies in Liquid Ethanol. *Mol. Phys.* **1999**, *97*, 479–486.
- (447) Ludwig, R.; Weinhold, F.; Farrar, T. C. Quantum Cluster Equilibrium Theory of Liquids: Molecular Clusters and Thermodynamics of Liquid Ethanol. *Mol. Phys.* **1999**, *97*, 465–477.
- (448) Ludwig, R. Isotopic Quantum Effects in Liquid Methanol. *ChemPhysChem* **2005**, *6*, 1376–1380.
- (449) Ludwig, R. The Structure of Liquid Methanol. *ChemPhysChem* **2005**, *6*, 1369–1375.
- (450) Ludwig, R.; Weinhold, F.; Farrar, T. C. Experimental and Theoretical Studies of Hydrogen Bonding in Neat, Liquid Formamide. *J. Chem. Phys.* **1995**, *102*, 5118–5125.
- (451) Ludwig, R.; Weinhold, F.; Farrar, T. C. Theoretical Study of Hydrogen Bonding in Liquid and Gaseous N-Methylformamide. *J. Chem. Phys.* **1997**, *107*, 499–507.
- (452) Ludwig, R.; Weinhold, F.; Farrar, T. C. Quantum Cluster Equilibrium Theory of Liquids Part II: Temperature Dependent Chemical Shifts, Quadrupole Coupling Constants and Vibrational Frequencies in Liquid Ammonia. *Ber. Bunsenges. Phys. Chem.* **1998**, *102*, 205–212.
- (453) Kirchner, B. Cooperative Versus Dispersion Effects: What Is More Important in an Associated Liquid Such as Water? *J. Chem. Phys.* **2005**, *123*, 204116.
- (454) Kirchner, B. Theory of Complicated Liquids: Investigation of Liquids, Solvents and Solvent Effects with Modern Theoretical Methods. *Phys. Rep.* **2007**, *440*, 1–111.
- (455) Friedrich, J.; Perl, E.; Roatsch, M.; Spickermann, C.; Kirchner, B. Coupled Cluster in Condensed Phase. Part I: Static Quantum Chemical Calculations of Hydrogen Fluoride Clusters. *J. Chem. Theory Comput.* **2011**, *7*, 843–851.

- (456) Spickermann, C.; Perl, E.; von Domaros, M.; Roatsch, M.; Friedrich, J.; Kirchner, B. Coupled Cluster in Condensed Phase. Part II: Liquid Hydrogen Fluoride from Quantum Cluster Equilibrium Theory. *J. Chem. Theory Comput.* **2011**, *7*, 868–875.
- (457) Wendler, K.; Zahn, S.; Dommert, F.; Berger, R.; Holm, C.; Kirchner, B.; Delle Site, L. Locality and Fluctuations: Trends in Imidazolium-Based Ionic Liquids and Beyond. *J. Chem. Theory Comput.* **2011**, *7*, 3040–3044.
- (458) Fumino, K.; Wulf, A.; Ludwig, R. The Cation Anion Interaction in Ionic Liquids Probed by Far-Infrared Spectroscopy. *Angew. Chem., Int. Ed.* **2008**, *47*, 3830–3834.
- (459) Wulf, A.; Fumino, K.; Ludwig, R.; Taday, P. F. Combined Thz, Fir and Raman Spectroscopy Studies of Imidazolium-Based Ionic Liquids Covering the Frequency Range 2–300 cm^{-1} . *ChemPhysChem* **2010**, *11*, 349–353.
- (460) Fumino, K.; Fossog, V.; Stange, P.; Wittler, K.; Polet, W.; Hempelmann, R.; Ludwig, R. Ion Pairing in Protic Ionic Liquids Probed by Far-Infrared Spectroscopy: Effects of Solvent Polarity and Temperature. *ChemPhysChem* **2014**, *15*, 2604–2609.
- (461) Wulf, A.; Fumino, K.; Michalik, D.; Ludwig, R.; IR, N. M. R. Properties of Ionic Liquids: Do They Tell Us the Same Thing? *ChemPhysChem* **2007**, *8*, 2265–2269.
- (462) Huber, H. Deuterium Quadrupole Coupling Constants. A Theoretical Investigation. *J. Chem. Phys.* **1985**, *83*, 4591–4598.
- (463) Ludwig, R.; Weinhold, F.; Farrar, T. C. Effective O-17 Quadrupole Moments for the Calibrated Computation of Quadrupole Coupling Parameters at Different Levels of Theory. *J. Chem. Phys.* **1996**, *105*, 8223–8230.
- (464) Cabaco, M. I.; Besnard, M.; Danten, Y.; Coutinho, J. A. P. Solubility of CO_2 in 1-Butyl-3-Methylimidazolium-Trifluoroacetate Ionic Liquid Studied by Raman Spectroscopy and DFT Investigations. *J. Phys. Chem. B* **2011**, *115*, 3538–3550.
- (465) Ludwig, R. The Effect of Dispersion Forces on the Interaction Energies and Far Infrared Spectra of Protic Ionic Liquids. *Phys. Chem. Chem. Phys.* **2015**, *17*, 13790–13793.
- (466) Knorr, A.; Stange, P.; Fumino, K.; Weinhold, F.; Ludwig, R. Spectroscopic Evidence for Clusters of Like-Charged Ions in Ionic Liquids Stabilized by Cooperative Hydrogen Bonding. *ChemPhysChem* **2016**, *17*, 447–447.
- (467) Knorr, A.; Ludwig, R. Cation-Cation Clusters in Ionic Liquids: Cooperative Hydrogen Bonding Overcomes Like-Charge Repulsion. *Sci. Rep.* **2015**, *5*, 17505.
- (468) Knorr, A.; Fumino, K.; Bonsa, A.-M.; Ludwig, R. Spectroscopic Evidence of 'Jumping and Pecking' of Cholinium and H-Bond Enhanced Cation-Cation Interaction in Ionic Liquids. *Phys. Chem. Chem. Phys.* **2015**, *17*, 30978–30982.
- (469) Bagno, A.; D'Amico, F.; Saielli, G. Computing the NMR Spectrum of a Bulk Ionic Liquid Phase by Qm/Mm Methods. *J. Phys. Chem. B* **2006**, *110*, 23004–23006.
- (470) Bagno, A.; D'Amico, F.; Saielli, G. Computer Simulation of Diffusion Coefficients of the Room-Temperature Ionic Liquid [Bmim][BF₄]: Problems with Classical Simulation Techniques. *J. Mol. Liq.* **2007**, *131*, 132–132.
- (471) Karadakov, P. B.; Morokuma, K. Oniom as an Efficient Tool for Calculating NMR Chemical Shielding Constants in Large Molecules. *Chem. Phys. Lett.* **2000**, *317*, 589–596.
- (472) Car, R.; Parrinello, M. Unified Approach for Molecular Dynamics and Density-Functional Theory. *Phys. Rev. Lett.* **1985**, *55*, 2471–2474.
- (473) Salanne, M. Simulations of Room Temperature Ionic Liquids: From Polarizable to Coarse-Grained Force Fields. *Phys. Chem. Chem. Phys.* **2015**, *17*, 14270–14279.
- (474) Lynden-Bell, R. M.; Del Pópolo, M. G.; Youngs, T. G. A.; Kohanoff, J.; Hanke, C. G.; Harper, J. B.; Pinilla, C. C. Simulations of Ionic Liquids, Solutions, and Surfaces. *Acc. Chem. Res.* **2007**, *40*, 1138–1145.
- (475) Maginn, E. J. Molecular Simulation of Ionic Liquids: Current Status and Future Opportunities. *J. Phys.: Condens. Matter* **2009**, *21*, 373101.
- (476) Maginn, E. J.; Elliott, J. R. Historical Perspective and Current Outlook for Molecular Dynamics as a Chemical Engineering Tool. *Ind. Eng. Chem. Res.* **2010**, *49*, 3059–3078.
- (477) Wendler, K.; Dommert, F.; Zhao, Y. Y.; Berger, R.; Holm, C.; Delle Site, L. Ionic Liquids Studied across Different Scales: A Computational Perspective. *Faraday Discuss.* **2012**, *154*, 111–132.
- (478) Zhang, Y.; Maginn, E. J. A Simple Aimd Approach to Derive Atomic Charges for Condensed Phase Simulation of Ionic Liquids. *J. Phys. Chem. B* **2012**, *116*, 10036–10048.
- (479) Kirchner, B.; Hollóczy, O.; Canongia Lopes, J. N.; Pádua, A. A. H. Multiresolution Calculation of Ionic Liquids. *WIREs: Comput. Mol. Sci.* **2015**, *5*, 202–214.
- (480) Schmidt, J.; Krekeler, C.; Dommert, F.; Zhao, Y.; Berger, R.; Site, L. D.; Holm, C. Ionic Charge Reduction and Atomic Partial Charges from First-Principles Calculations of 1,3-Dimethylimidazolium Chloride. *J. Phys. Chem. B* **2010**, *114*, 6150–6155.
- (481) Lynden-Bell, R. M.; Youngs, T. G. A. Simulations of Imidazolium Ionic Liquids: When Does the Cation Charge Distribution Matter? *J. Phys.: Condens. Matter* **2009**, *21*, 424120.
- (482) Zhang, Y.; Maginn, E. J. Direct Correlation between Ionic Liquid Transport Properties and Ion Pair Lifetimes: A Molecular Dynamics Study. *J. Phys. Chem. Lett.* **2015**, *6*, 700–705.
- (483) Zahn, S.; Thar, J.; Kirchner, B. Structure and Dynamics of the Protic Ionic Liquid Monomethylammonium Nitrate ([CH₃NH₃][NO₃]) from Ab Initio Molecular Dynamics Simulations. *J. Chem. Phys.* **2010**, *132*, 124506.
- (484) Holloczki, O.; Malberg, F.; Welton, T.; Kirchner, B. On the Origin of Ionicity in Ionic Liquids. Ion Pairing Versus Charge Transfer. *Phys. Chem. Chem. Phys.* **2014**, *16*, 16880–16890.
- (485) Borodin, O. Polarizable Force Field Development and Molecular Dynamics Simulations of Ionic Liquids. *J. Phys. Chem. B* **2009**, *113*, 11463–11478.
- (486) Schmoltingruber, M.; Lesch, V.; Schröder, C.; Heuer, A.; Steinhauser, O. Comparing Induced Point-Dipoles and Drude Oscillators. *Phys. Chem. Chem. Phys.* **2015**, *17*, 14297–14306.
- (487) Salanne, M.; Rotenberg, B.; Jahn, S.; Vuilleumier, R.; Simon, C.; Madden, P. A. Including Many-Body Effects in Models for Ionic Liquids. *Theor. Chem. Acc.* **2012**, *131*, 1–16.
- (488) Zhang, Y.; Xue, L.; Khabaz, F.; Doerfler, R.; Quitevis, E. L.; Khare, R.; Maginn, E. J. Molecular Topology and Local Dynamics Govern the Viscosity of Imidazolium-Based Ionic Liquids. *J. Phys. Chem. B* **2015**, *119*, 14934–14944.
- (489) Zhang, Y.; Maginn, E. J. Molecular Dynamics Study of the Effect of Alkyl Chain Length on Melting Points of [C_nmim][PF₆] Ionic Liquids. *Phys. Chem. Chem. Phys.* **2014**, *16*, 13489–13499.
- (490) Malberg, F.; Pensado, A. S.; Kirchner, B. The Bulk and the Gas Phase of 1-Ethyl-3-Methylimidazolium Ethylsulfate: Dispersion Interaction Makes the Difference. *Phys. Chem. Chem. Phys.* **2012**, *14*, 12079–12082.
- (491) Pensado, A. S.; Brehm, M.; Thar, J.; Seitsonen, A. P.; Kirchner, B. Effect of Dispersion on the Structure and Dynamics of the Ionic Liquid 1-Ethyl-3-Methylimidazolium Thiocyanate. *ChemPhysChem* **2012**, *13*, 1845–1853.
- (492) Sutto, L.; Marsili, S.; Gervasio, F. L. New Advances in Metadynamics. *WIREs: Comput. Mol. Sci.* **2012**, *2*, 771–779.
- (493) Barducci, A.; Bonomi, M.; Parrinello, M. Metadynamics. *WIREs: Comput. Mol. Sci.* **2011**, *1*, 826–843.
- (494) Spiwok, V.; Scur, Z.; Hosek, P. Enhanced Sampling Techniques in Biomolecular Simulations. *Biotechnol. Adv.* **2015**, *33*, 1130–1140.
- (495) Valsson, O.; Tiwary, P.; Parrinello, M. Enhancing Important Fluctuations: Rare Events and Metadynamics from a Conceptual Viewpoint. *Annu. Rev. Phys. Chem.* **2016**, *67*, 159–184.
- (496) Kästner, J. Umbrella Sampling. *WIREs: Comput. Mol. Sci.* **2011**, *1*, 932–942.
- (497) Torrie, G. M.; Valleau, J. P. Nonphysical Sampling Distributions in Monte Carlo Free-Energy Estimation: Umbrella Sampling. *J. Comput. Phys.* **1977**, *23*, 187–199.

- (498) Singh, S.; Chopra, M.; de Pablo, J. J. Density of States Based Molecular Simulations. *Annu. Rev. Chem. Biomol. Eng.* **2012**, *3*, 369 394.
- (499) Virmau, P.; Müller, M. Calculation of Free Energy through Successive Umbrella Sampling. *J. Chem. Phys.* **2004**, *120*, 10925 10930.
- (500) Brehm, M.; Weber, H.; Pensado, A. S.; Stark, A.; Kirchner, B. Proton Transfer and Polarity Changes in Ionic Liquid-Water Mixtures: A Perspective on Hydrogen Bonds from *Ab Initio* Molecular Dynamics at the Example of 1-Ethyl-3-Methylimidazolium Acetate-Water Mixtures - Part 1. *Phys. Chem. Chem. Phys.* **2012**, *14*, 5030 5044.
- (501) Del Pópolo, M. G.; Kohanoff, J.; Lynden-Bell, R. M. Solvation Structure and Transport of Acidic Protons in Ionic Liquids: A First-Principles Simulation Study. *J. Phys. Chem. B* **2006**, *110*, 8798 8803.
- (502) Del Pópolo, M. G.; Lynden-Bell, R. M.; Kohanoff, J. *Ab Initio* Molecular Dynamics Simulation of a Room Temperature Ionic Liquid. *J. Phys. Chem. B* **2005**, *109*, 5895 5902.
- (503) Bühl, M.; Chaumont, A.; Schurhammer, R.; Wipff, G. *Ab Initio* Molecular Dynamics of Liquid 1,3-Dimethylimidazolium Chloride. *J. Phys. Chem. B* **2005**, *109*, 18591 18599.
- (504) Ghatee, M. H.; Ansari, Y. *Ab Initio* Molecular Dynamics Simulation of Ionic Liquids. *J. Chem. Phys.* **2007**, *126*, 154502.
- (505) Brussel, M.; Brehm, M.; Voigt, T.; Kirchner, B. *Ab Initio* Molecular Dynamics Simulations of a Binary System of Ionic Liquids. *Phys. Chem. Chem. Phys.* **2011**, *13*, 13617 13620.
- (506) Zahn, S.; Wendler, K.; Delle Site, L.; Kirchner, B. Depolarization of Water in Protic Ionic Liquids. *Phys. Chem. Chem. Phys.* **2011**, *13*, 15083 15093.
- (507) Bhargava, B. L.; Balasubramanian, S. Insights into the Structure and Dynamics of a Room-Temperature Ionic Liquid: *Ab Initio* Molecular Dynamics Simulation Studies of 1-N-Butyl-3-Methylimidazolium Hexafluorophosphate ([Bmim][PF₆]) and the [Bmim][PF₆] CO₂Mixture. *J. Phys. Chem. B* **2007**, *111*, 4477 4487.
- (508) Firaha, D. S.; Kavalchuk, M.; Kirchner, B. SO₂ Solvation in the 1-Ethyl-3-Methylimidazolium Thiocyanate Ionic Liquid by Incorporation into the Extended Cation Anion Network. *J. Solution Chem.* **2015**, *44*, 838 849.
- (509) Hollóczki, O.; Kelemen, Z.; Könczöl, L.; Szieberth, D.; Nyulászi, L.; Stark, A.; Kirchner, B. Significant Cation Effects in Carbon Dioxide Ionic Liquid Systems. *ChemPhysChem* **2013**, *14*, 315 320.
- (510) Wang, Z.; Zhang, L.; Chen, X.; Cukier, R. I.; Bu, Y. Excess Electron Solvation in an Imidazolium-Based Room-Temperature Ionic Liquid Revealed by *Ab Initio* Molecular Dynamics Simulations. *J. Phys. Chem. B* **2009**, *113*, 8222 8226.
- (511) Brehm, M.; Weber, H.; Pensado Alfonso, S.; Stark, A.; Kirchner, B. Liquid Structure and Cluster Formation in Ionic Liquid/Water Mixtures - an Extensive *Ab Initio* Molecular Dynamics Study on 1-Ethyl-3-Methylimidazolium Acetate/Water Mixtures - Part 2. *Phys. Chem.* **2013**, *227*, 177 204.
- (512) Thar, J.; Brehm, M.; Seitsonen, A. P.; Kirchner, B. Unexpected Hydrogen Bond Dynamics in Imidazolium-Based Ionic Liquids. *J. Phys. Chem. B* **2009**, *113*, 15129 15132.
- (513) Klähn, M.; Seduraman, A.; Wu, P. Proton Transfer between Tryptophan and Ionic Liquid Solvents Studied with Molecular Dynamics Simulations. *J. Phys. Chem. B* **2011**, *115*, 8231 8241.
- (514) Bhargava, B. L.; Yasaka, Y.; Klein, M. L. Hydrogen Evolution from Formic Acid in an Ionic Liquid Solvent: A Mechanistic Study by *Ab Initio* Molecular Dynamics. *J. Phys. Chem. B* **2011**, *115*, 14136 14140.
- (515) Hollóczki, O.; Firaha, D. S.; Friedrich, J.; Brehm, M.; Cybik, R.; Wild, M.; Stark, A.; Kirchner, B. Carbene Formation in Ionic Liquids: Spontaneous, Induced, or Prohibited? *J. Phys. Chem. B* **2013**, *117*, 5898 5907.
- (516) Troullier, N.; Martins, J. L. Efficient Pseudopotentials for Plane-Wave Calculations. *Phys. Rev. B: Condens. Matter Mater. Phys.* **1991**, *43*, 1993 2006.
- (517) Soler, J. M.; Artacho, E.; Gale, J. D.; García, A.; Junquera, J.; Ordejón, P.; Sánchez-Portal, D. The Siesta Method for *Ab Initio* Order-N Materials Simulation. *J. Phys.: Condens. Matter* **2002**, *14*, 2745 2779.
- (518) Arduengo, A. J.; Dias, H. V. R.; Harlow, R. L.; Kline, M. Electronic Stabilization of Nucleophilic Carbenes. *J. Am. Chem. Soc.* **1992**, *114*, 5530 5534.
- (519) Marzari, N.; Vanderbilt, D. Maximally Localized Generalized Wannier Functions for Composite Energy Bands. *Phys. Rev. B: Condens. Matter Mater. Phys.* **1997**, *56*, 12847 12865.
- (520) Dommert, F.; Schmidt, J.; Krekeler, C.; Zhao, Y. Y.; Berger, R.; Delle Site, L.; Holm, C. Towards Multiscale Modeling of Ionic Liquids: From Electronic Structure to Bulk Properties. *J. Mol. Liq.* **2010**, *152*, 2 8.
- (521) Rigby, J.; Izgorodina, E. I. Assessment of Atomic Partial Charge Schemes for Polarisation and Charge Transfer Effects in Ionic Liquids. *Phys. Chem. Chem. Phys.* **2013**, *15*, 1632 1646.
- (522) Krekeler, C.; Schmidt, J.; Zhao, Y. Y.; Qiao, B.; Berger, R.; Holm, C.; Delle Site, L. Study of 1,3-Dimethylimidazolium Chloride with Electronic Structure Methods and Force Field Approaches. *J. Chem. Phys.* **2008**, *129*, 174503.
- (523) Wang, Y.; Izvekov, S.; Yan, T.; Voth, G. A. Multiscale Coarse-Graining of Ionic Liquids. *J. Phys. Chem. B* **2006**, *110*, 3564 3575.
- (524) Weber, H.; Kirchner, B. Complex Structural and Dynamical Interplay of Cyano-Based Ionic Liquids. *J. Phys. Chem. B* **2016**, *120*, 2471 2483.
- (525) VandeVondele, J.; Hutter, J. Gaussian Basis Sets for Accurate Calculations on Molecular Systems in Gas and Condensed Phases. *J. Chem. Phys.* **2007**, *127*, 114105.
- (526) Goedecker, S.; Teter, M.; Hutter, J. Separable Dual-Space Gaussian Pseudopotentials. *Phys. Rev. B: Condens. Matter Mater. Phys.* **1996**, *54*, 1703 1710.
- (527) Hartwigsen, C.; Goedecker, S.; Hutter, J. Relativistic Separable Dual-Space Gaussian Pseudopotentials from H to Rn. *Phys. Rev. B: Condens. Matter Mater. Phys.* **1998**, *58*, 3641 3662.
- (528) Krack, M. Pseudopotentials for H to Kr Optimized for Gradient-Corrected Exchange-Correlation Functionals. *Theor. Chem. Acc.* **2005**, *114*, 145 152.
- (529) Tammann, G.; Hesse, W. The Dependence of the Viscosity on the Temperature in Supercooled Liquids. *Z. Anorg. Allg. Chem.* **1926**, *156*, 245 257.
- (530) Fulcher, G. S. Analysis of Recent Measurements of the Viscosity of Glasses. *J. Am. Ceram. Soc.* **1925**, *8*, 339 355.
- (531) Angell, C. A. Formation of Glasses from Liquids and Biopolymers. *Science* **1995**, *267*, 1924 1935.
- (532) Bulut, S.; Eiden, P.; Beichel, W.; Slattery, J. M.; Beyersdorff, T. F.; Schubert, T. J. S.; Krossing, I. Temperature Dependence of the Viscosity and Conductivity of Mildly Functionalized and Non-Functionalized [Tf₂n]⁺ Ionic Liquids. *ChemPhysChem* **2011**, *12*, 2296 2310.
- (533) Wang, J.; Wolf, R. M.; Caldwell, J. W.; Kollman, P. A.; Case, D. A. Development and Testing of a General Amber Force Field. *J. Comput. Chem.* **2004**, *25*, 1157 1174.
- (534) Rapaport, D. C. Hydrogen Bonds in Water. *Mol. Phys.* **1983**, *50*, 1151 1162.
- (535) Wannier, G. H. The Structure of Electronic Excitation Levels in Insulating Crystals. *Phys. Rev.* **1937**, *52*, 191 197.
- (536) Kirchner, B.; Hutter, J. Solvent Effects on Electronic Properties from Wannier Functions in a Dimethyl Sulfoxide/Water Mixture. *J. Chem. Phys.* **2004**, *121*, 5133 5142.
- (537) Kaminski, G. A.; Friesner, R. A.; Tirado-Rives, J.; Jorgensen, W. L. Evaluation and Reparametrization of the Opls-Aa Force Field for Proteins Via Comparison with Accurate Quantum Chemical Calculations on Peptides. *J. Phys. Chem. B* **2001**, *105*, 6474 6487.
- (538) Liu, Z.; Huang, S.; Wang, W. A Refined Force Field for Molecular Simulation of Imidazolium-Based Ionic Liquids. *J. Phys. Chem. B* **2004**, *108*, 12978 12989.
- (539) Thomas, M.; Brehm, M.; Hollóczki, O.; Kirchner, B. How Can a Carbene Be Active in an Ionic Liquid? *Chem. - Eur. J.* **2014**, *20*, 1622 1629.

- (540) Kelemen, Z.; Holloczki, O.; Nagy, J.; Nyulaszi, L. An Organocatalytic Ionic Liquid. *Org. Biomol. Chem.* **2011**, *9*, 5362–5364.
- (541) Fumino, K.; Wulf, A.; Verevkin, S. P.; Heintz, A.; Ludwig, R. Estimating Enthalpies of Vaporization of Imidazolium-Based Ionic Liquids from Far-Infrared Measurements. *ChemPhysChem* **2010**, *11*, 1623–1626.
- (542) Berghold, G.; Mundy, C. J.; Romero, A. H.; Hutter, J.; Parrinello, M. General and Efficient Algorithms for Obtaining Maximally Localized Wannier Functions. *Phys. Rev. B: Condens. Matter Mater. Phys.* **2000**, *61*, 10040–10048.
- (543) Thomas, J. W.; Ifitimie, R.; Tuckerman, M. E. Field Theoretic Approach to Dynamical Orbital Localization in *Ab Initio* Molecular Dynamics. *Phys. Rev. B: Condens. Matter Mater. Phys.* **2004**, *69*, 125105.
- (544) Resta, R.; Sorella, S. Electron Localization in the Insulating State. *Phys. Rev. Lett.* **1999**, *82*, 370–373.
- (545) Ifitimie, R.; Thomas, J. W.; Tuckerman, M. E. On-the-Fly Localization of Electronic Orbitals in Car Parrinello Molecular Dynamics. *J. Chem. Phys.* **2004**, *120*, 2169–2181.
- (546) Ifitimie, R.; Tuckerman, M. E. Decomposing Total IR Spectra of Aqueous Systems into Solute and Solvent Contributions: A Computational Approach Using Maximally Localized Wannier Orbitals. *J. Chem. Phys.* **2005**, *122*, 214508.
- (547) Sprik, M.; Hutter, J.; Parrinello, M. *Ab Initio* Molecular Dynamics Simulation of Liquid Water: Comparison of Three Gradient-Corrected Density Functionals. *J. Chem. Phys.* **1996**, *105*, 1142–1152.
- (548) Wendler, K.; Brehm, M.; Malberg, F.; Kirchner, B.; Delle Site, L. Short Time Dynamics of Ionic Liquids in Amd-Based Power Spectra. *J. Chem. Theory Comput.* **2012**, *8*, 1570–1579.
- (549) Gaigeot, M. P.; Vuilleumier, R.; Sprik, M.; Borgis, D. Infrared Spectroscopy of N-Methylacetamide Revisited by *Ab Initio* Molecular Dynamics Simulations. *J. Chem. Theory Comput.* **2005**, *1*, 772–789.
- (550) Tangney, P.; Scandolo, S. How Well Do Car Parrinello Simulations Reproduce the Born–Oppenheimer Surface? Theory and Examples. *J. Chem. Phys.* **2002**, *116*, 14–24.
- (551) Brehm, M.; Kirchner, B. Travis – a Free Analyzer and Visualizer for Monte Carlo and Molecular Dynamics Trajectories. *J. Chem. Inf. Model.* **2011**, *51*, 2007–2023.
- (552) Thomas, M.; Brehm, M.; Fligg, R.; Vohringer, P.; Kirchner, B. Computing Vibrational Spectra from *Ab Initio* Molecular Dynamics. *Phys. Chem. Chem. Phys.* **2013**, *15*, 6608–6622.
- (553) Sarangi, S. S.; Reddy, S. K.; Balasubramanian, S. Low Frequency Vibrational Modes of Room Temperature Ionic Liquids. *J. Phys. Chem. B* **2011**, *115*, 1874–1880.
- (554) Bhargava, B. L.; Balasubramanian, S. *Ab Initio* Molecular Dynamics Simulation of a 1-Ethyl-3-Methylimidazolium Fluoride Hydrogen Fluoride Mixture. *J. Phys. Chem. B* **2008**, *112*, 7566–7573.
- (555) Brussel, M.; Brehm, M.; Pensado, A. S.; Malberg, F.; Ramzan, M.; Stark, A.; Kirchner, B. On the Ideality of Binary Mixtures of Ionic Liquids. *Phys. Chem. Chem. Phys.* **2012**, *14*, 13204–13215.
- (556) Thomas, M.; Brehm, M.; Hollóczki, O.; Kelemen, Z.; Nyulaszi, L.; Pasinszki, T.; Kirchner, B. Simulating the Vibrational Spectra of Ionic Liquid Systems: 1-Ethyl-3-Methylimidazolium Acetate and Its Mixtures. *J. Chem. Phys.* **2014**, *141*, 024510.
- (557) Gellatly, B. J.; Finney, J. L. Calculation of Protein Volumes: An Alternative to the Voronoi Procedure. *J. Mol. Biol.* **1982**, *161*, 305–322.
- (558) Batista, E. R.; Xantheas, S. S.; Jónsson, H. Multipole Moments of Water Molecules in Clusters and Ice Ih from First Principles Calculations. *J. Chem. Phys.* **1999**, *111*, 6011–6015.
- (559) Rousseau, B.; Peeters, A.; Van Alsenoy, C. Atomic Charges from Modified Voronoi Polyhedra. *J. Mol. Struct.: THEOCHEM* **2001**, *538*, 235–238.
- (560) Thomas, M.; Brehm, M.; Kirchner, B. Voronoi Dipole Moments for the Simulation of Bulk Phase Vibrational Spectra. *Phys. Chem. Chem. Phys.* **2015**, *17*, 3207–3213.
- (561) Bagno, A.; D'Amico, F.; Saielli, G. Computing the ¹H NMR Spectrum of a Bulk Ionic Liquid from Snapshots of Car Parrinello Molecular Dynamics Simulations. *ChemPhysChem* **2007**, *8*, 873–881.
- (562) Zhang, Y.; Shi, C.; Brennecke, J. F.; Maginn, E. J. Refined Method for Predicting Electrochemical Windows of Ionic Liquids and Experimental Validation Studies. *J. Phys. Chem. B* **2014**, *118*, 6250–6255.
- (563) Mondal, A.; Balasubramanian, S. Quantitative Prediction of Physical Properties of Imidazolium Based Room Temperature Ionic Liquids through Determination of Condensed Phase Site Charges: A Refined Force Field. *J. Phys. Chem. B* **2014**, *118*, 3409–3422.
- (564) Dommert, F.; Wendler, K.; Qiao, B.; Delle Site, L.; Holm, C. Generic Force Fields for Ionic Liquids. *J. Mol. Liq.* **2014**, *192*, 32–37.

1.4 Overview

It is concluded in section 1.3 that three-body effects are crucial in accurately capturing induction and dispersion forces in ionic liquids. As such, single ion pairs do not serve as reliable models for studying the more complex physicochemical properties that are a product of the dynamic interplay of forces. However, few studies have modelled multiscale clusters of ionic liquids with wavefunction-based methods due to the associated computational cost.

The aim herein is to facilitate the prediction of properties of ionic liquids from large scale wavefunction-based methods. This is done in a number of ways:

- I. Examining the energetics of larger clusters of ionic liquids that can be linked to structural motifs
- II. Exploring quantum chemical methods that have the potential to be used as cheaper alternatives with high accuracy
- III. Identifying key low energy geometries in larger clusters that contribute to physicochemical properties of ionic liquids
- IV. Investigating the link between fundamental forces and desired properties in larger clusters of ionic liquids

The aims above are achieved in the chapters 2-6 as follows:

Chapter 2 focuses on the fragment molecule orbital approach and its application in ionic liquid clusters of 4, 8 and 16 ion pairs. The approach reduces the cost of larger scale calculations and thus allows for studying systems with energetics similar to a bulk liquid. An analysis is undertaken where cutoff criteria for both two- and three-body effects (Figure 1.2) are presented to further reduce the computer resources needed and therefore expand what can be explored by quantum chemical methods. The research also explores how structural arrangements adopted by ionic liquids impacts the Hartree-Fock and dispersion forces and thus the properties they exhibit. By enabling the study of larger clusters it is expected that the nuances of the governing forces in ionic liquids will be revealed such that physicochemical properties can be directly linked with energies.

Chapter 3 determines suitable density functional theory (DFT) functionals and Møller-Plesset perturbation theory (MP2) variants for the optimisation of larger cluster of ionic liquids. While optimisations of single ions and ion pairs are commonplace in the literature, few articles exist that optimise larger clusters with *ab initio* methods. Whether functionals can reproduce geometries of high level wavefunction-based methods is unknown. This chapter use forty-three approaches with varying basis sets and dispersion corrections to determine a cost effective method that can be applied to the optimisation of large scale clusters.

Chapter 4 introduces domain-based local pair natural orbital coupled-cluster method (DLPNO-CCSD(T)) as an alternative for expensive but accurate gold standard coupled cluster single-, double-, and perturbative triple-excitations (CCSD(T)). By limiting the doubles and triples calculated at a coupled cluster level, DLPNO-CCSD(T) has the ability to drastically increase the number of atoms considered at such a high accuracy. This work is the first benchmarking study of DLPNO methods for ionic liquid systems and identifies if the long-range electrostatic forces or strong intermolecular dispersion can be recovered by the method with a high degree of accuracy. Secondly, the study identifies the method parameters required to produce sub-kilojoule per mol accuracy in order for the method to be used in a predictive context.

Chapter 5 presents a methodology for locating important minima of condensed systems which contribute to macroscopic properties. Configurations are created that span the potential energy surface of the material. The local area of each configuration is then explored using molecular dynamics. Agglomerative clustering has been used to groups geometries of nearby minima and the lowest energy structure is used as the representative geometry. The study produced excess geometries of the ionic liquids investigated such that key low energy structural features could be examined. The methodology provides the geometries from which physical properties can be predicted using ensemble averages.

Chapter 6 investigates relationships between interaction energy components – that define the amount of energy needed for molecules to dissociate – and physical and thermodynamic properties: conductivity and melting point. The study attempts to form a foundation in understanding how forces such as dispersion govern these physicochemical properties as well as develop a predictive tool. In order to fulfil this aim, extensive geometry screens are

performed for a set of two ion pair systems through which favourable structural arrangements can be linked to the ions present. The interaction energies are then correlated with conductivity and melting point.

Lastly, the conclusions of the work herein is given in Chapter 7 which states the main findings and the significance of the research. Further work is suggested that would shine further light on the topics discussed.

1.5 References

- [1] John S. Wilkes. A Short History of Ionic Liquids—from Molten Salts to Neoteric Solvents. *Green Chemistry* **4**(2) (2002), 73–80. DOI: [10.1039/B110838G](https://doi.org/10.1039/B110838G).
- [2] Ekaterina I. Izgorodina, Uditha L. Bernard, Pamela M. Dean, Jennifer M. Pringle, and Douglas R. MacFarlane. The Madelung Constant of Organic Salts. *Crystal Growth & Design* **9**(11) (2009), 4834–4839. DOI: [10.1021/cg900656z](https://doi.org/10.1021/cg900656z).
- [3] Pamela M. Dean, Jennifer M. Pringle, and Douglas R. MacFarlane. Structural Analysis of Low Melting Organic Salts : Perspectives on Ionic Liquids. *Physical Chemistry Chemical Physics* **12**(32) (2010), 9144–9153. DOI: [10.1039/C003519J](https://doi.org/10.1039/C003519J).
- [4] A. Guerfi, M. Dontigny, P. Charest, M. Petitclerc, M. Lagacé, A. Vijh, and K. Zaghib. Improved Electrolytes for Li-Ion Batteries: Mixtures of Ionic Liquid and Organic Electrolyte with Enhanced Safety and Electrochemical Performance. *Journal of Power Sources* **195**(3) (2010), 845–852. DOI: [10.1016/j.jpowsour.2009.08.056](https://doi.org/10.1016/j.jpowsour.2009.08.056).
- [5] Debbie S. Silvester and Richard G. Compton. Electrochemistry in Room Temperature Ionic Liquids: A Review and Some Possible Applications. *Zeitschrift für Physikalische Chemie* **220**(10) (2006), 1247–1274. DOI: [10.1524/zpch.2006.220.10.1247](https://doi.org/10.1524/zpch.2006.220.10.1247).
- [6] Makoto Ue, Masayuki Takeda, Akiko Toriumi, Asao Kominato, Rika Hagiwara, and Yasuhiko Ito. Application of Low-Viscosity Ionic Liquid to the Electrolyte of Double-Layer Capacitors. *Journal of The Electrochemical Society* **150**(4) (2003), A499–A502. DOI: [10.1149/1.1559069](https://doi.org/10.1149/1.1559069).
- [7] Peng Wang, Shaik M. Zakeeruddin, Pascal Comte, Ivan Exnar, and Michael Grätzel. Gelation of Ionic Liquid-Based Electrolytes with Silica Nanoparticles for Quasi-Solid-State Dye-Sensitized Solar Cells. *Journal of the American Chemical Society* **125**(5) (2003), 1166–1167. DOI: [10.1021/ja029294+](https://doi.org/10.1021/ja029294+).
- [8] Di Wei and Ari Ivaska. Applications of Ionic Liquids in Electrochemical Sensors. *Analytica Chimica Acta* **607**(2) (2008), 126–135. DOI: [10.1016/j.aca.2007.12.011](https://doi.org/10.1016/j.aca.2007.12.011).
- [9] Chengfeng Ye, Weimin Liu, Yunxia Chen, and Laigui Yu. Room-Temperature Ionic Liquids: A Novel Versatile Lubricant. *Chemical Communications* (21) (2001), 2244–2245. DOI: [10.1039/B106935G](https://doi.org/10.1039/B106935G).

- [10] Zhuo Zeng, Benjamin S. Phillips, Ji-Chang Xiao, and Jean'ne M. Shreeve. Polyfluoroalkyl, Polyethylene Glycol, 1,4-Bismethylenebenzene, or 1,4-Bismethylene-2,3,5,6-Tetrafluorobenzene Bridged Functionalized Dicationic Ionic Liquids: Synthesis and Properties as High Temperature Lubricants. *Chemistry of Materials* **20**(8) (2008), 2719–2726. DOI: [10.1021/cm703693r](https://doi.org/10.1021/cm703693r).
- [11] Alexia Finotello, Jason E. Bara, Dean Camper, and Richard D. Noble. Room-Temperature Ionic Liquids: Temperature Dependence of Gas Solubility Selectivity. *Industrial & Engineering Chemistry Research* **47**(10) (2008), 3453–3459. DOI: [10.1021/ie0704142](https://doi.org/10.1021/ie0704142).
- [12] Mahinder Ramdin, Theo W. de Loos, and Thijs J.H. Vlugt. State-of-the-Art of CO₂ Capture with Ionic Liquids. *Industrial & Engineering Chemistry Research* **51**(24) (2012), 8149–8177. DOI: [10.1021/ie3003705](https://doi.org/10.1021/ie3003705).
- [13] Marsha R. Cole, Min Li, Bilal El-Zahab, Marlene E. Janes, Daniel Hayes, and Isiah M. Warner. Design, Synthesis, and Biological Evaluation of β -Lactam Antibiotic-Based Imidazolium- and Pyridinium-Type Ionic Liquids. *Chemical Biology & Drug Design* **78**(1) (2011), 33–41. DOI: [10.1111/j.1747-0285.2011.01114.x](https://doi.org/10.1111/j.1747-0285.2011.01114.x).
- [14] Julia L. Shamshina, Patrick S. Barber, and Robin D. Rogers. Ionic Liquids in Drug Delivery. *Expert Opinion on Drug Delivery* **10**(10) (2013), 1367–1381. DOI: [10.1517/17425247.2013.808185](https://doi.org/10.1517/17425247.2013.808185).
- [15] Julia L. Shamshina, Steven P. Kelley, Gabriela Gurau, and Robin D. Rogers. Chemistry: Develop Ionic Liquid Drugs. *Nature News* **528**(7581) (2015), 188. DOI: [10.1038/528188a](https://doi.org/10.1038/528188a).
- [16] Robin D. Rogers and Kenneth R. Seddon. Ionic Liquids - Solvents of the Future? *Science* **302**(5646) (2003), 792–793. DOI: [10.1126/science.1090313](https://doi.org/10.1126/science.1090313).
- [17] Douglas R. MacFarlane, Naoki Tachikawa, Maria Forsyth, Jennifer M. Pringle, Patrick C. Howlett, Gloria D. Elliott, James H. Davis, Masayoshi Watanabe, Patrice Simon, and C. Austen Angell. Energy Applications of Ionic Liquids. *Energy & Environmental Science* **7**(1) (2014), 232–250. DOI: [10.1039/C3EE42099J](https://doi.org/10.1039/C3EE42099J).
- [18] Uditha L. Bernard, Ekaterina I. Izgorodina, and Douglas R. MacFarlane. New Insights into the Relationship between Ion-Pair Binding Energy and Thermodynamic and Transport

- Properties of Ionic Liquids. *The Journal of Physical Chemistry C* **114**(48) (2010), 20472–20478. DOI: [10.1021/jp1048875](https://doi.org/10.1021/jp1048875).
- [19] Karina Shimizu, Mohammad Tariq, Margarida F. Costa Gomes, Luís P. N. Rebelo, and José N. Canongia Lopes. Assessing the Dispersive and Electrostatic Components of the Cohesive Energy of Ionic Liquids Using Molecular Dynamics Simulations and Molar Refraction Data. *The Journal of Physical Chemistry B* **114**(17) (2010), 5831–5834. DOI: [10.1021/jp101910c](https://doi.org/10.1021/jp101910c).
- [20] Patricia A. Hunt, Barbara Kirchner, and Tom Welton. Characterising the Electronic Structure of Ionic Liquids: An Examination of the 1-Butyl-3-Methylimidazolium Chloride Ion Pair. *Chemistry – A European Journal* **12**(26) (2006), 6762–6775. DOI: [10.1002/chem.200600103](https://doi.org/10.1002/chem.200600103).
- [21] Chihiro Wakai, Alla Oleinikova, Magnus Ott, and Hermann Weingärtner. How Polar Are Ionic Liquids? Determination of the Static Dielectric Constant of an Imidazolium-Based Ionic Liquid by Microwave Dielectric Spectroscopy. *The Journal of Physical Chemistry B* **109**(36) (2005), 17028–17030. DOI: [10.1021/jp053946+](https://doi.org/10.1021/jp053946+).
- [22] Oldamur Hollóczki, Friedrich Malberg, Tom Welton, and Barbara Kirchner. On the Origin of Ionicity in Ionic Liquids. Ion Pairing versus Charge Transfer. *Physical Chemistry Chemical Physics* **16**(32) (2014), 16880–16890. DOI: [10.1039/C4CP01177E](https://doi.org/10.1039/C4CP01177E).
- [23] Dmitry Bedrov, Oleg Borodin, Zhe Li, and Grant D. Smith. Influence of Polarization on Structural, Thermodynamic, and Dynamic Properties of Ionic Liquids Obtained from Molecular Dynamics Simulations. *The Journal of Physical Chemistry B* **114**(15) (2010), 4984–4997. DOI: [10.1021/jp911670f](https://doi.org/10.1021/jp911670f).
- [24] Ekaterina I. Izgorodina and Douglas R. MacFarlane. Nature of Hydrogen Bonding in Charged Hydrogen-Bonded Complexes and Imidazolium-Based Ionic Liquids. *The Journal of Physical Chemistry B* **115**(49) (2011), 14659–14667. DOI: [10.1021/jp208150b](https://doi.org/10.1021/jp208150b).
- [25] Ralf Ludwig. Thermodynamic Properties of Ionic Liquids—a Cluster Approach. *Physical Chemistry Chemical Physics* **10**(29) (2008), 4333–4339. DOI: [10.1039/B803572E](https://doi.org/10.1039/B803572E).

- [26] Ekaterina I. Izgorodina, Jason Rigby, and Douglas R. MacFarlane. Large-Scale *Ab Initio* Calculations of Archetypical Ionic Liquids. *Chemical Communications* **48**(10) (2012), 1493–1495. DOI: [10.1039/C1CC15056A](https://doi.org/10.1039/C1CC15056A).
- [27] Eric J. Bylaska, Mathias Jacquelin, Wibe A. de Jong, Jeff R. Hammond, and Michael Klemm. Performance Evaluation of NWChem *Ab Initio* Molecular Dynamics (AIMD) Simulations on the Intel® Xeon Phi™ Processor. In: *High Performance Computing*. Ed. by Julian M. Kunkel, Rio Yokota, Michela Taufer, and John Shalf. Lecture Notes in Computer Science. Cham, 2017, pp.404–418. DOI: [10.1007/978-3-319-67630-2_30](https://doi.org/10.1007/978-3-319-67630-2_30).
- [28] Carsten Kutzner, Szilárd Páll, Martin Fechner, Ansgar Esztermann, Bert L. de Groot, and Helmut Grubmüller. More Bang for Your Buck: Improved Use of GPU Nodes for GROMACS 2018. *Journal of Computational Chemistry* **40**(27) (2019), 2418–2431. DOI: [10.1002/jcc.26011](https://doi.org/10.1002/jcc.26011).
- [29] Yudong Cao, Jonathan Romero, Jonathan P. Olson, Matthias Degroote, Peter D. Johnson, Mária Kieferová, Ian D. Kivlichan, Tim Menke, Borja Peropadre, Nicolas P. D. Sawaya, Sukin Sim, Libor Veis, and Alán Aspuru-Guzik. Quantum Chemistry in the Age of Quantum Computing. *Chemical Reviews* **119**(19) (2019), 10856–10915. DOI: [10.1021/acs.chemrev.8b00803](https://doi.org/10.1021/acs.chemrev.8b00803).
- [30] Frank Neese. Software Update: The ORCA Program System, Version 4.0. *WIREs Computational Molecular Science* **8**(1) (2018), e1327. DOI: [10.1002/wcms.1327](https://doi.org/10.1002/wcms.1327).
- [31] Robert M. Parrish, Lori A. Burns, Daniel G. A. Smith, Andrew C. Simmonett, A. Eugene DePrince, Edward G. Hohenstein, Uğur Bozkaya, Alexander Yu. Sokolov, Roberto Di Remigio, Ryan M. Richard, Jérôme F. Gonthier, Andrew M. James, Harley R. McAlexander, Ashutosh Kumar, Masaaki Saitow, Xiao Wang, Benjamin P. Pritchard, Prakash Verma, Henry F. Schaefer, Konrad Patkowski, Rollin A. King, Edward F. Valeev, Francesco A. Evangelista, Justin M. Turney, T. Daniel Crawford, and C. David Sherrill. Psi4 1.1: An Open-Source Electronic Structure Program Emphasizing Automation, Advanced Libraries, and Interoperability. *Journal of Chemical Theory and Computation* **13**(7) (2017), 3185–3197. DOI: [10.1021/acs.jctc.7b00174](https://doi.org/10.1021/acs.jctc.7b00174).

- [32] George D. Purvis and Rodney J. Bartlett. A Full Coupled-cluster Singles and Doubles Model: The Inclusion of Disconnected Triples. *The Journal of Chemical Physics* **76**(4) (1982), 1910–1918. DOI: [10.1063/1.443164](https://doi.org/10.1063/1.443164).
- [33] Trygve Helgaker, Poul Jorgensen, and Jeppe Olsen. *Molecular Electronic-Structure Theory*. 2014.
- [34] Ceila Fong-Padrón, Enrique M. Cabaleiro-Lago, and Jesús Rodríguez-Otero. Water Interaction with Ion Pairs from Ionic Liquids. Computational Study and Performance Assessment of Several Common Functionals. *Chemical Physics Letters* **593** (2014), 181–188. DOI: [10.1016/j.cplett.2014.01.013](https://doi.org/10.1016/j.cplett.2014.01.013).
- [35] Benjamin G. Janesko. Modeling Interactions between Lignocellulose and Ionic Liquids Using DFT-D. *Physical Chemistry Chemical Physics* **13**(23) (2011), 11393–11401. DOI: [10.1039/C1CP20072K](https://doi.org/10.1039/C1CP20072K).
- [36] Stefan Grimme, Waldemar Hujo, and Barbara Kirchner. Performance of Dispersion-Corrected Density Functional Theory for the Interactions in Ionic Liquids. *Physical Chemistry Chemical Physics* **14**(14) (2012), 4875–4883. DOI: [10.1039/C2CP24096C](https://doi.org/10.1039/C2CP24096C).
- [37] Stefan Zahn, Douglas R. MacFarlane, and Ekaterina I. Izgorodina. Assessment of Kohn–Sham Density Functional Theory and Møller–Plesset Perturbation Theory for Ionic Liquids. *Physical Chemistry Chemical Physics* **15**(32) (2013), 13664–13675. DOI: [10.1039/C3CP51682B](https://doi.org/10.1039/C3CP51682B).
- [38] Kazuo Kitaura and Keiji Morokuma. A New Energy Decomposition Scheme for Molecular Interactions within the Hartree-Fock Approximation. *International Journal of Quantum Chemistry* **10**(2) (1976), 325–340. DOI: [10.1002/qua.560100211](https://doi.org/10.1002/qua.560100211).
- [39] Dmitri G. Fedorov and Kazuo Kitaura. Pair Interaction Energy Decomposition Analysis. *Journal of Computational Chemistry* **28**(1) (2007), 222–237. DOI: [10.1002/jcc.20496](https://doi.org/10.1002/jcc.20496).
- [40] Peifeng Su and Hui Li. Energy Decomposition Analysis of Covalent Bonds and Intermolecular Interactions. *The Journal of Chemical Physics* **131**(1) (2009), 014102. DOI: [10.1063/1.3159673](https://doi.org/10.1063/1.3159673).
- [41] Hinne Hettema. *Quantum Chemistry: Classic Scientific Papers*. 2000.

- [42] Stefan Zahn, Frank Uhlig, Jens Thar, Christian Spickermann, and Barbara Kirchner. Intermolecular Forces in an Ionic Liquid ([Mmim][Cl]) versus Those in a Typical Salt (NaCl). *Angewandte Chemie International Edition* **47**(19) (2008), 3639–3641. DOI: [10.1002/anie.200705526](https://doi.org/10.1002/anie.200705526).
- [43] Ekaterina I. Izgorodina, Dorothea Golze, Radha Maganti, Vanessa Armel, Maria Taige, Thomas J. S. Schubert, and Douglas R. MacFarlane. Importance of Dispersion Forces for Prediction of Thermodynamic and Transport Properties of Some Common Ionic Liquids. *Physical Chemistry Chemical Physics* **16**(16) (2014), 7209–7221. DOI: [10.1039/C3CP53035C](https://doi.org/10.1039/C3CP53035C).
- [44] Pavel Hobza author. *Non-Covalent Interactions: Theory and Experiment*. In collab. with Klaus Müller-Dethlefs author and Royal Society of Chemistry. RSC Theoretical and Computational Chemistry Series 2. Cambridge, 2010.
- [45] S. F. Boys and F. Bernardi. The Calculation of Small Molecular Interactions by the Differences of Separate Total Energies. Some Procedures with Reduced Errors. *Molecular Physics* **19**(4) (1970), 553–566. DOI: [10.1080/00268977000101561](https://doi.org/10.1080/00268977000101561).
- [46] Samuel Tan, Santiago Barrera Acevedo, and Ekaterina I. Izgorodina. Generalized Spin-Ratio Scaled MP2 Method for Accurate Prediction of Intermolecular Interactions for Neutral and Ionic Species. *The Journal of Chemical Physics* **146**(6) (2017), 064108. DOI: [10.1063/1.4975326](https://doi.org/10.1063/1.4975326).
- [47] Samuel Y. S. Tan, Luke Wylie, Ivan Begic, Dennis Tran, and Ekaterina I. Izgorodina. Application of Spin-Ratio Scaled MP2 for the Prediction of Intermolecular Interactions in Chemical Systems. *Physical Chemistry Chemical Physics* **19**(42) (2017), 28936–28942. DOI: [10.1039/C7CP04391K](https://doi.org/10.1039/C7CP04391K).
- [48] Alston J. Misquitta, Bogumil Jeziorski, and Krzysztof Szalewicz. Dispersion Energy from Density-Functional Theory Description of Monomers. *Physical Review Letters* **91**(3) (2003), 033201. DOI: [10.1103/PhysRevLett.91.033201](https://doi.org/10.1103/PhysRevLett.91.033201).
- [49] O. Anatole von Lilienfeld, Ivano Tavernelli, Ursula Rothlisberger, and Daniel Sebastiani. Optimization of Effective Atom Centered Potentials for London Dispersion Forces in Density Functional Theory. *Physical Review Letters* **93**(15) (2004), 153004. DOI: [10.1103/PhysRevLett.93.153004](https://doi.org/10.1103/PhysRevLett.93.153004).

- [50] Stefan Grimme, Waldemar Hujo, and Barbara Kirchner. Performance of Dispersion-Corrected Density Functional Theory for the Interactions in Ionic Liquids. *Physical Chemistry Chemical Physics* **14**(14) (2012), 4875–4883. DOI: [10.1039/C2CP24096C](https://doi.org/10.1039/C2CP24096C).
- [51] Eva Perlt, Promit Ray, Andreas Hansen, Friedrich Malberg, Stefan Grimme, and Barbara Kirchner. Finding the Best Density Functional Approximation to Describe Interaction Energies and Structures of Ionic Liquids in Molecular Dynamics Studies. *The Journal of Chemical Physics* **148**(19) (2018), 193835. DOI: [10.1063/1.5013122](https://doi.org/10.1063/1.5013122).

Chapter 2

Application of the fragment molecular orbital approach to large clusters

2.1 Introduction

To understand transport and thermodynamic properties of ionic liquids it is critical that the materials are modelled via methods that can obtain accurate energies.¹ The fragment molecular orbital approach (FMO) is a fragmentation scheme that reduces the cost of a quantum chemical calculation by only considering up to N fragments in tandem.² In practice, FMO2 or FMO3 are generally enough to accurately reproduce energies whereby two-body contributions (FMO2), or two- and three-body contributions (FMO3) are added to monomer energies, although corrections up to the number of fragments is possible.³⁻⁶ The approach greatly reduces cost such that quantum chemical calculations of larger numbers of ion pairs are possible. As such, classical force fields which include only two-body interactions and do not consider quantum electronic effects, and density functional theory which captures these effects inconsistently among ionic liquids, can be replaced with quantum chemical methods and provide qualitative *and* quantitative insight.⁷

In the next section (2.2), a publication of *The Journal of Physical Chemistry B* is presented that focuses on the use of the fragment molecular orbital approach in conjunction with second-order Møller Plesset perturbation theory (MP2) in systems of ionic liquids. The premise of

the study is that dimers and trimers that do not contribute to the energy of the system can be eliminated to reduce the cost of the calculation permitting calculations of larger systems that more accurately represent a bulk liquid. An FMO2 calculation, for example, consists of one-body and two-body contributions. At large distances, a two-body correction may equal the sum of the one-body contributions such that there is no interaction between the pair and the two-body calculation can be omitted. By studying the distance of these many-body interactions and their associated energy, cutoffs can be put in place that reduce computational cost and have little to no consequence on the calculated energy.

In clusters of 4, 8, 16 and 32 ion pairs the Hartree-Fock (HF) and correlation components of the MP2 calculations were investigated as electrostatics and dispersion, respectively. Although HF dimer energy contributions are non-negligible for all distances, a relationship has been proposed for the size of the cluster and the distance cutoff for two-body correlation energies. This relationship revealed that dispersion forces penetrate an ion's third solvation shell, much further than was previously thought. Three-body cutoffs have been suggested and in some cases 94% of the trimer calculations can be avoided. Contributions of three-body dispersion can be greater than 80 kJ mol^{-1} and as such three body dispersion effects are essential in creating realistic models of ionic liquids.

Trends in Two- and Three-Body Effects in Multiscale Clusters of Ionic Liquids

Published as part of *The Journal of Physical Chemistry virtual special issue "Mark S. Gordon Festschrift"*.

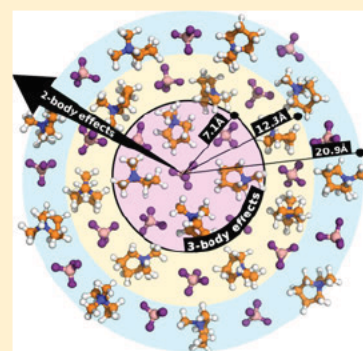
Peter Halat,[†] Zoe L. Seeger,[†] Santiago Barrera Acevedo,[‡] and Ekaterina I. Izgorodina^{*,†}

[†]Monash Computational Chemistry Group, School of Chemistry, Monash University, 17 Rainforest Walk, Clayton, Victoria 3800, Australia

[‡]School of Mathematical Sciences, Monash University, 9 Rainforest Walk, Clayton, Victoria 3800., Australia

Supporting Information

ABSTRACT: Applications of higher correlated levels of *ab initio* theory to condensed systems require a significant amount of computational resources. The recent development of the fragment molecular orbital (FMO) approach alleviates this issue by splitting the system into individual fragments and achieves the accuracy of the method by accounting for all possible two body and three body interactions. In this work a comprehensive application of the FMO approach in combination with a second order of Møller–Plesset perturbation theory method, MP2, is presented for multiscale clusters of ionic liquids such as $[C_1mim]X$, $[C_1mpyr]X$, $[C_2py]X$, and $[NMe_4]X$, where $X =$ chloride and tetrafluoroborates, BF_4^- , with the clusters varying in size from 4, 8, 16, to 32 ion pairs. Reliable cutoff criteria for the inclusion of two body and three body interactions are identified for both HF energy and MP2 correlation energy to achieve the desired accuracy of 1 kJ mol^{-1} . The importance of two body and three body interactions in ionic liquids is also discussed.



INTRODUCTION

Multiscale calculations are important for the prediction of bulk structure and physicochemical properties of condensed systems such as liquids and solids. Of particular interest are electrolyte materials based on traditional solvents and ionic liquids.¹ The latter represent a fascinating class of materials consisting entirely of ions.² These have been shown to be excellent replacements for traditional organic electrolytes such as ethylene carbonate due to their unique properties including low flammability, negligible vapor pressure, and high ionic conductivity.^{3–5} Strong Coulombic interactions prevent ionic liquids from becoming as fluid as organic electrolytes at room temperature. Mixtures of ionic liquids with conventional organic solvents have been found to possess reduced viscosity that can potentially lead to enhanced performance of electrochemical devices such as metal ion batteries, solar, and fuel cells.^{6,7} Physicochemical properties of ionic liquids can be tailored by manipulating cation–anion combinations. It has been estimated that trillions of potential ionic liquids may be synthesized.⁸ Coupled with the fact that organic solvents help reduce viscosity, a myriad of mixtures would need to be screened to determine suitable candidates for electrochemical devices. This represents a huge task requiring significant time and effort in the laboratory.

Computational chemistry methods can screen properties of novel ionic liquids and their mixtures in a more robust way. From the theoretical point of view, ionic liquids are challenging as all five fundamental forces, electrostatics, exchange–

repulsion, induction, dispersion, and charge transfer, play an important role in governing their energetics.^{9–11} In particular, dispersion forces have been identified as significant, contributing up to 20% of the total interaction energy for single ion pairs as well as for multiscale clusters of ionic liquids. The dispersion component appeared to depend on the cation type, with imidazolium based cations giving rise to stronger dispersion forces compared to pyrrolidinium ones coupled with the same anion. This finding requires the inclusion of counterpoise correction to account for basis set superposition error as well as the use of correlated levels of theory for accurate calculations of interaction energy. Recently, our group have published modifications of the second order Møller–Plesset perturbation theory method, MP2, that allow for calculations of interaction energies of multiscale clusters of ionic liquids within unprecedented CCSD(T)/CBS accuracy.^{12,13} Wavefunction based methods even as low as MP2 are still computationally infeasible for multiscale calculations of ionic liquids beyond eight ion pairs with medium sized ions due to the increasing demand on computational resources.¹⁴ Although density functional theory can be applied to relatively large clusters (up to 48 ion pairs depending on ion size),^{15–22} it is not known how these fare for the prediction of energetics of these clusters due to the lack of benchmark data.

Received: October 6, 2016

Revised: December 13, 2016

Published: December 19, 2016

The current trend in the field of ionic liquids is to find cost effective and reliable *ab initio* methods that can be combined with molecular dynamics (MD) simulations to allow for the prediction of physicochemical properties of these complex materials *from first principles*. At the moment, *ab initio* MD simulations employing DFT functionals can only be carried out for short times of 100 ps, thus preventing them from studying a wide range of chemical reactions in ionic liquids and predicting their thermodynamics and transport properties.¹⁸

A development of the fragment molecular orbital (FMO) approach by Kitaura^{23–25} and later Federov^{26–31} and Gordon^{32–35} allows for the division of larger molecular systems into computationally feasible fragments. For ionic liquids, ions represent the smallest building blocks within the system and, therefore, serve as individual fragments without the need to break bonds. In the approach, individual fragments are placed in a Coulombic bath and their energies are self consistently iterated with respect to the electric field, generated by the bath. The total electronic energy of the system is calculated as the sum of electronic energies of individual fragments (i.e., one body FMO1) as well as all possible combinations of two fragment (i.e., two body, FMO2) and three fragment (i.e., three body, FMO3) interactions. Originally, the FMO approach was used in combination with the Hartree–Fock level of theory, thus disregarding dispersion interactions arising from electron correlation effects. Recently the FMO approach has been extended to correlated methods of perturbation theory such as MP2^{26,28} and coupled cluster theory such as CCSD.^{36,37} Our group have validated the use of ions as individual fragments for clusters of archetypical ionic liquids consisting of 2 to 8 ion pairs for both HF and MP2 levels of theory.¹⁴ These ionic liquids were based on the tetrafluoroborate anion coupled with tetramethylammonium, NMe_4^+ , and a series of 1 alkyl 3 ethylimidazolium cations, C_nmim^+ . The performance of FMO2 and FMO3 showed different trends for HF energy and dispersion components of electronic energies. Two body interactions were found to be critical for the energetics of these clusters for both HF and MP2 methods, whereas three body effects were established to be equally important only for induction forces as calculated at the HF level of theory. The contribution from three body effects from dispersion forces, calculated as the difference between MP2 and HF electronic energies, fell below chemical accuracy and was suggested to be negligible in the studied clusters of ionic liquids.

Induction is a nonadditive force whereas dispersion is considered more of an additive force. It has been assumed that for multiscale systems only two body effects are important for dispersion. In this work we have extended the FMO2 and FMO3 applications to eight ionic liquids based on quaternary ammonium, pyrrolidinium, imidazolium, and pyridinium cations coupled with tetrafluoroborates, BF_4^- , and chloride anions. Both anions represent good models for ionic liquids. BF_4^- based ionic liquids are routinely used ionic liquids in the field and are especially used as electrolytes for metal ion batteries and solar cells,¹⁰ whereas chlorides have been found to form strong interionic bonds, bordering on covalency.³⁸ The size of ionic clusters systematically varied as 4, 8, 16, and 32 ion pairs to analyze the dependence of two and three body effects with respect to cluster size as well as ionic liquid type. Previously the cutoff criteria for two body and three body contributions to the total energy were identified for single molecules and are currently used by default in the FMO code as

implemented in GAMESS US.³⁹ To the best of our knowledge these cutoff distances have not been tested for multiscale clusters representing condensed systems such as ionic liquids. Therefore, the main goal of this study was to identify cutoff criteria for both two and three body effects at both HF and MP2 levels of theory of semi Coulombic condensed systems.

THEORETICAL PROCEDURES

All quantum chemical calculations were carried out using the GAMESS US package. All ionic liquid clusters studied were geometry optimized at the FMO2 MP2/cc pVDZ level of theory using individual ions as independent fragments and accounting for all possible two body effects. The optimization was confirmed as complete when traditional geometry convergence criteria used for determining a minimum on the potential energy of a single molecule were met. No frequency calculations were performed on the optimized structures due to a significant demand on computer resources in the case of these large clusters. Electronic energies were improved at both the FMO2 and FMO3 MP2 levels of theory in combination with cc pVTZ basis set. The latter was shown to perform best for energetics of ionic liquid clusters.^{12,13}

In the initial step of any FMO calculation the HF energies of individual ions are calculated self consistently using the modified Fock operator that contains the environmental electrostatic potential explicitly.^{29,30} The latter consists of one electron nuclear attraction and two electron repulsion components and represents the combined polarization effect of surrounding ions. Each two body and three body interaction is calculated using the same environmental potential, thus leading to inclusion of polarization (i.e., induction) effects at both the individual ion level and the combination of two and three ions.

Previously Fedorov and Kitaura³⁰ showed that the interaction energy from two body interactions could be divided into four terms: electrostatic (ES), exchange–repulsion (EX), charge transfer with higher order mixed terms (CT+mix), and dispersion (D):

$$\Delta E_{\text{INT}}^{\text{IJ}} = \Delta E_{\text{INT}}^{\text{ES}} + \Delta E_{\text{INT}}^{\text{EX}} + \Delta E_{\text{INT}}^{\text{CT+mix}} + \Delta E_{\text{INT}}^{\text{D}} \quad (1)$$

It has to be noted that in the FMO3 calculations performed here no bond was detached and therefore there was no need for a bond detachment atom correction.

The first three terms in eq 1 comprised the HF energy, whereas the last term in eq 1, dispersion, was calculated at the MP2 level of theory in this study and is simply referred to as the dispersion component. It has to be pointed out that in this case the dispersion component corresponded to the MP2 correlation energy, which is considered a good approximation for the dispersion energy in condensed systems. Our groups successfully used this definition of dispersion before to analyze the importance of dispersion in single ion pairs of ionic liquids.¹⁰ The same energy decomposition shown in eq 1 was used to analyze the contribution from three body interactions. Although the electrostatic component cancels out due to the additive nature of electrostatic forces, the induction effect arising from the environmental electrostatic potential remains together with contributions from exchange–repulsion, charge transfer, and dispersion.

In our previous work the decomposition of interaction energy was performed for an extensive series of ionic liquid ion pairs.^{10,11} It was found that the electrostatic component of the HF energy dominated the two body contributions, whereas

charge transfer contributed the least in the order of a few kJ mol^{-1} . Therefore, it is expected that in ionic liquid clusters two body interactions at the HF level of theory are expected to be predominantly driven by electrostatics, whereas the induction forces are expected to play a significant role in three body contributions of the HF energy due to their nonadditive nature.

Radial distribution functions (RDFs) were used to analyze the structural arrangement of ions in the clusters studied and were constructed in the following manner. The distance between two ions was defined through their center of mass. For each cluster, the calculated interionic distances were split into areas with an increment of 0.2 Å. The corresponding RDF was plotted as a histogram that counted the number of distances within each area, and a smooth curve was placed over the histogram counts for a clearer visual representation. To allow for an unbiased comparison, the number of distances on RDF graphs will be given in percentage and is referred to as density of ions.

In the FMO approach, as implemented in GAMESS US, a unitless R_{AB} factor is used to define the interfragment distance:

$$R_{AB} = \min \left\{ \frac{R_{AB}^I}{R_I^{\text{vdW}} + R_J^{\text{vdW}}} \right\} \quad (2)$$

where R_{AB}^I is the distance between the atom I on fragment A and the atom J on fragment B, R_I^{vdW} and R_J^{vdW} are van der Waals radii of the atoms I and J , respectively. Atoms I and J are the atoms from the respective fragments with the shortest distance between them. This unitless measure results in an unbiased criterion for the interionic distance regardless of the nature of the atoms, be it two hydrogen atoms or two non hydrogen atoms. It can be easily converted to a corresponding distance in Ångströms by multiplication with the sum of van der Waals radii of atom I and atom J . Further in the text the interionic distance is defined as the shortest distance between atoms in two separate ions as defined in eq 2.

The R_{AB} distance, from eq 2, serves as the basis for cutoff criteria for discarding two and three body interactions in the energy calculations. There are two sets of cutoff criteria that are used in GAMESS US, with one pertaining to two body interactions and the other to three body interactions. In this study, the Mulliken approximation²⁵ was not used to approximate both one electron and two electron components of the environment electrostatic potential (i.e., RESPAP was set to 0 and RESPPC was set to -1, the latter switches off the approximation completely) due to large errors.¹⁴ No cutoff distances for the inclusion of two and three body effects were used in the benchmark FMO calculations, thus accounting for all possible two body and three body contributions (i.e., RESDIM = 100, RCORSD = 50 and RITRIM(1) = 50, 50, 50, 50). These calculations are referred to as full FMO calculations further in the text. For more details on how cutoffs can be introduced in FMO calculations; see ref 40. Cutoff distances for both FMO2 and FMO3 were analyzed on the basis of the results of these full FMO calculations. The selection of the cutoff distances, referred to as R_{cutoff} with respect to cluster size and ionic liquid type will be discussed further in the text.

RESULTS AND DISCUSSION

Construction of Ionic Clusters. Eight different ionic liquids, consisting of four types of cations and two types of anions, were considered. The cations chosen for this study were

modeled on routinely used cations in the field of ionic liquids and include the N,N' dimethylpyrrolidinium cation ($C_1\text{mpyr}^+$), 1,3 dimethylimidazolium ($C_1\text{mim}^+$), N ethylpyridinium ($C_2\text{py}^+$), and tetramethylammonium ($N\text{Me}_4^+$). Chloride and tetrafluoroborates (BF_4^-) were selected as anions on the basis of not only their frequent use in the field but also the strength of interionic interactions that they tend to form. Chlorides are known to form very strong hydrogen bonds with cations, with the character of this bond bordering on covalency. The latter is strongly supported by strong interionic interactions exhibited by chloride based ion pairs.^{10,38} On the contrary, the BF_4^- anion represents a good model for a typical ionic liquid anion with the negative charge dissociated over the whole structure.

A few starting geometries of two ion pair clusters in the alternating charge arrangement were optimized for each ionic liquid, with the cation being rotated to allow for various interaction modes with the anion. The lowest energy configurations established for each ionic liquid were subsequently used to construct larger ionic clusters. The optimized two ion pair clusters were placed side by side and reoptimized to generate a few 4 ion pair clusters for each ionic liquid. From this pool of clusters the lowest energy structures of 4 ion pair clusters were selected and are given in Figure 1. Clusters of larger sizes, consisting of 8, 16, and 32 ion pairs, were constructed in the same manner, while ensuring that the volume was minimized. The latter requirement implied that linear structures were dismissed and more box like arrange

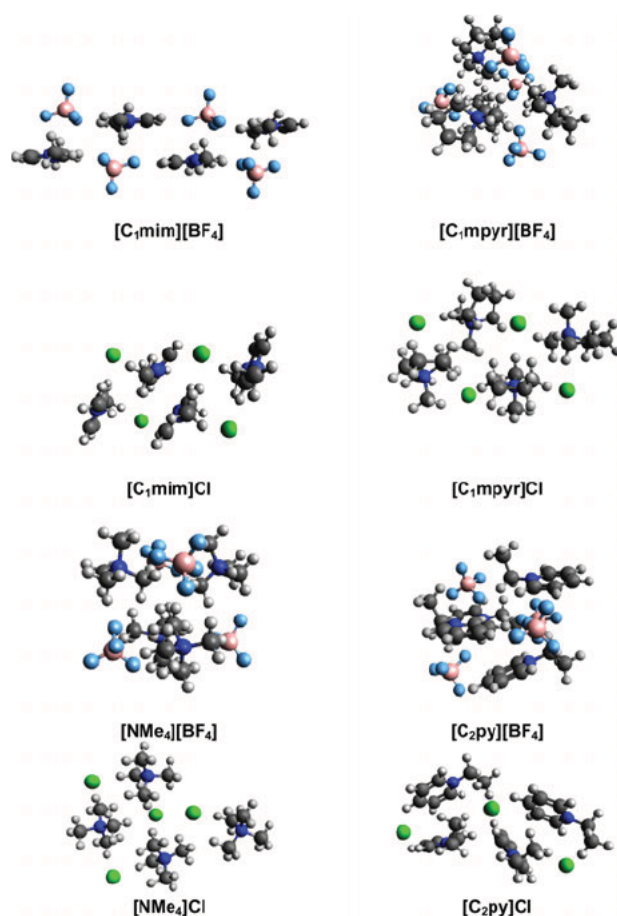


Figure 1. Optimized structures of 4-ion-pair clusters.

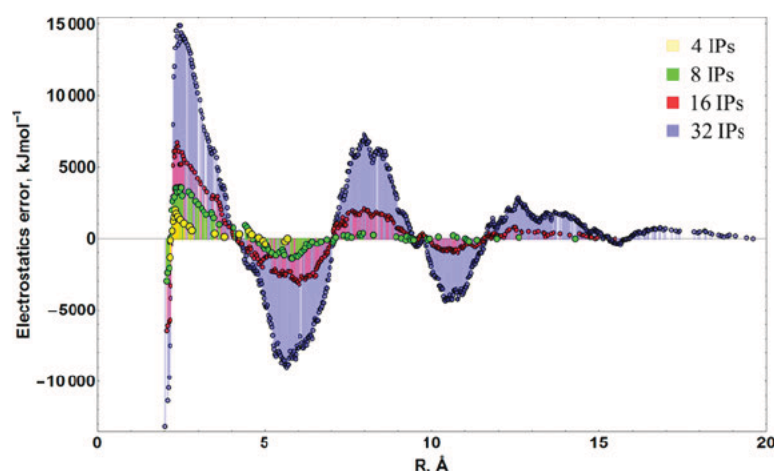


Figure 2. Deviations of HF energy (in kJ mol^{-1}) with respect to the interionic distance, R , for 4-, 8-, 16-, and 32-ion-pair clusters of $[\text{C}_1\text{mpyr}][\text{BF}_4]$.

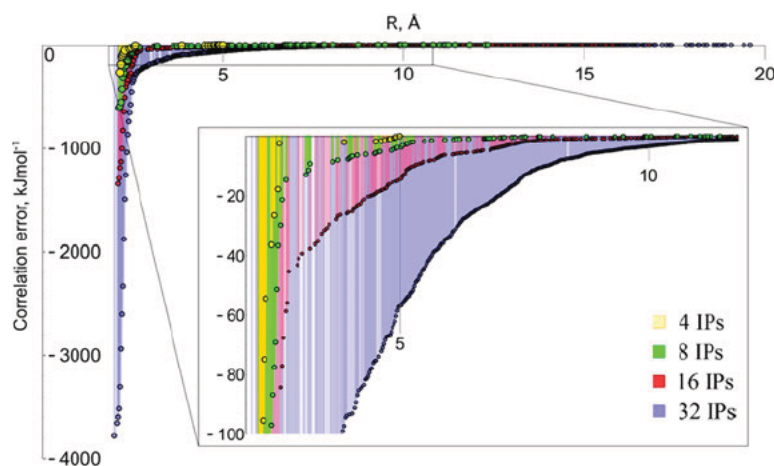


Figure 3. Deviations of correlation energy (in kJ mol^{-1}) with respect to the interionic distance, R , for 4-, 8-, 16-, and 32-ion-pair clusters of $[\text{C}_1\text{mpyr}][\text{BF}_4]$.

ments were subjected to geometry optimizations. Geometry optimizations of 32 ion pair clusters were feasible for only three ionic liquids due to increased demands on computer resources. It has to be pointed out that it was outside the scope of this study to generate the lowest energy configuration for each cluster size. As only electronic energies are discussed further in the text, the availability of not fully screened geometries of large clusters will not change the conclusions drawn with respect to the extent of two and three body contributions to the total energy of the cluster. For more detail on the cluster geometries, see the [Supporting Information](#).

Two-Body Effects. The behavior of the electronic energy with respect to the interionic distance is discussed separately for the HF energy and dispersion (i.e., the MP2 correlation energy). In the FMO calculation the HF energy of each individual ion is obtained self consistently in the Coulomb bath generated by the electron density of the rest of the ions, thus accounting for polarization effects by the whole cluster. The converged environmental electrostatic potential for each ion is also applied to calculate two body effects noniteratively. The FMO2 energy incorporates the sum of energies of all individual fragments as well as the contribution from two body interactions and the electrostatic potential as shown here:

$$E(\text{FMO2}) = \sum_{I=1}^N E_I + \sum_{I>J}^N (E_{IJ} - E_I - E_J) + \sum_{I>J}^N \text{Tr}(\Delta \mathbf{D}^{IJ} \mathbf{V}^{IJ}) \quad (3)$$

where I and J represent individual fragments, N is the total number of fragments, \mathbf{V}^{IJ} is the environmental electrostatic potential, and \mathbf{D}^{IJ} is the difference in the density of the IJ ion pair and the two corresponding ions, I and J . Each IJ ion pair is calculated within the environment electrostatic potential generated by the remainder of the ions. In this part of the study the combined behavior of the second and third sums is thoroughly analyzed. The induction effects arising from the environment potential were included in the HF energy.

The total energy from all possible two body contributions formed the benchmark for each cluster studied. Within each cluster, the distances between all possible pairs of ions were tabulated and the corresponding two body contribution identified. For each unique value of the interionic distance, energy contributions from all two body combinations whose shortest interionic distance fell within this range were summed, with a deviation to the benchmark value being determined.

Cutoff interionic distances, R_{cutoff} were determined for each cluster when the deviation fell and remained below 1 kJ mol^{-1} .

HF Energy. A typical trend found for the HF energy of two body effects with increasing interionic distance is shown in Figure 2 for 4, 8, 16, and 32 ion pair clusters of $[\text{C}_1\text{mim}][\text{BF}_4]$. The interionic distances converted from the unitless measure, R , to Ångströms was used in the x axis. As one can see, a periodic behavior is observed in this case, with huge oscillations in energies (up to $15\,000 \text{ kJ mol}^{-1}$) from extreme positives to extreme negatives, with the magnitude of these oscillation becoming larger with increasing cluster size. Although these oscillations (Figure 2) cross the x axis multiple times, resulting in negligible deviations, the periodicity with which this occurs is unique to each ionic liquid. Therefore, the convergence over the whole range of distances needs to be considered. Even for the 32 ion pair clusters, the deviation did not remain below 1 kJ mol^{-1} until an interionic distance of 20 Å. Other types of ionic liquids exhibited the same behavior (for more detail, see the Supporting Information). This periodic behavior is not unusual for the HF energy as repulsive anion–anion and cation–cation interactions strongly contribute to the final energy. It has to be pointed out that a typical classical MD simulation of ionic liquids contains a simulation box from 16 to 32 ion pairs. It is suggested that *the same cutoff for pairwise HF interactions cannot be universally used for all cluster sizes of ionic liquids*. With respect to FMO calculations, this finding clearly highlights that *all* two body interactions need to be included at the HF level for accurate results.

Dispersion. Different behavior is observed for the MP2 correlation energy. The deviation from the benchmark values follows a typical decay of $1/R^6$ function, thus converging rather fast with increasing interionic distance. An example of such a behavior is shown in Figure 3 for the clusters of $[\text{NMe}_4][\text{BF}_4]$. As the cluster size doubles, the number of all possible two interionic distances nearly quadruples and so does the deviation. As a result, the cutoff distance for which the deviation falls below 1 kJ mol^{-1} needs to be scaled for each cluster size. For medium sized clusters consisting of 4 and 8 ion pairs, the two body dispersion contribution becomes negligible beyond 5 Å, whereas for medium to large sized clusters of up to 32 ion pairs, the contribution does not become negligible below 8 Å regardless of ionic liquid type and structural arrangement. The latter was assessed through RDFs calculated as described in Theoretical Procedures. Examples of RDFs for two ionic liquids, $[\text{C}_1\text{mim}]\text{Cl}$ and $[\text{NMe}_4][\text{BF}_4]$, are shown Figure 4. As expected, the tetramethylammonium based ionic liquid clusters clearly exhibit a symmetric arrangement of ions with well defined peaks in a narrow range of distances, whereas the imidazolium based IL clusters demonstrate a wider range of interionic distances. Even the 4 ion pair cluster of $[\text{C}_1\text{mim}]\text{Cl}$ contains distances of up to 10 Å, in stark contrast to that of $[\text{NMe}_4][\text{BF}_4]$ with the maximum distance within 5 Å.

Independence of the cutoff distance for two body dispersion effects on structural arrangement is further evidenced in Table 1 that presents ranges of the unitless cutoff distances (eq 2) and corresponding averages across each cluster size and ionic liquid studied here. Analysis of the average unitless cutoffs reveals that these gradually increase with cluster size. This trend can be best described as $\log_2(N) - 0.5$ (where N is the number of ion pairs) and can be subsequently used to evaluate the cutoff distance for each cluster. Within each cluster size the cutoff distances fall into a consistently narrow range of 0.4, which is

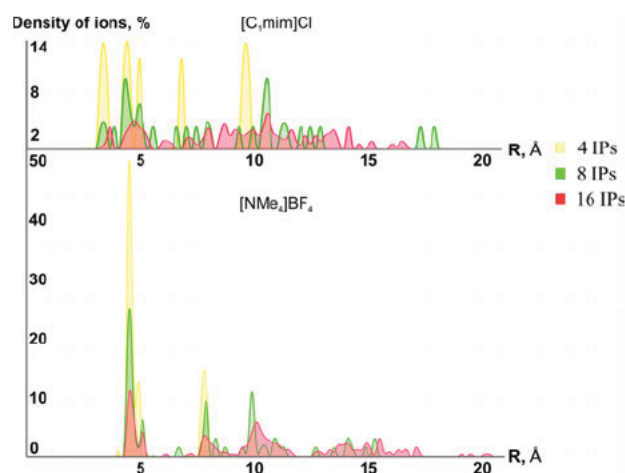


Figure 4. RDFs for 4, 8, and ion-pair clusters of $[\text{C}_1\text{mim}]\text{Cl}$ (top) and $[\text{NMe}_4][\text{BF}_4]$ (bottom).

also reflected in the small values (between 0.13 and 0.22) of the standard deviation.

Table 2 shows relative numbers of two body dispersion interactions in percentage that need to be included in the FMO2 calculation to satisfy the deviation of $<1 \text{ kJ mol}^{-1}$. On average 71% of two body correlation calculations need to be performed *regardless of cluster size and ionic liquid type* (Figure 5), with a maximum of 78% for medium to large sized clusters. The trend in Figure 5 is almost linear and can be easily extrapolated to larger clusters, highlighting the need to include at least 70% of two body interactions regardless of cluster size. For 32 ion pair clusters two body interactions within 12 Å need to be included, indicating that for each ion even the third solvation shell strongly contributes to both HF interactions and dispersion forces. As a result, FMO2 calculations can only be sped up by less than a third. To this end, the extent of two body correlation effects depends on the cluster size for ionic liquids with no clear relationship with the bulk structure, with the cutoff distance consistently increasing with increasing cluster size. This finding clearly indicates that dispersion is less of a local effect as has been previously assumed and needs to be scaled up depending on the cluster size using $\log_2(N) - 0.5$ (where N is the number of ion pairs). In general, the maximum cutoffs (Table 1) are recommended as accurate cutoff distances for MP2 correlation energy in FMO2 calculations of multiscale clusters of ionic liquids. These cutoff distances can be directly used as the RESDIM parameter in the current implementation of the FMO code in GAMESS US.

Three-Body Effects. Three body effects arise from induction forces as well as exchange–repulsion and charge transfer. The importance of induction is the main reason polarizable force fields improve the prediction of thermodynamic and transport properties of ionic liquids. Recently, three body effects were also found to be important to treat interatomic dispersion in neutral molecular systems.^{41–49} In this section, the extent of three body effects in both the HF energy (including induction through the environment electrostatic potential; see the third sum in eq 4) and dispersion are discussed. In the FMO approach, these effects are expressed as the last sum below:

Table 1. Average Cutoff Distances That Give Errors $<1 \text{ kJ mol}^{-1}$ for MP2 Correlation Energy, $R_{\text{cutoff}}^{\text{av}}$ (Unitless as in Eq 2), Standard Deviations (st dev), Unitless Maximum (max) Cutoff Distances (with Values in Å Given in Parentheses), and Distribution of Cutoff Distances with Respect to Increasing Cluster Size

cluster size, no. of IPs	av R_{cutoff}	st dev	max R_{cutoff}	range R_{cutoff}	IL system with max R_{cutoff}
4	1.71	0.22	1.88 (4.79)	1.28 1.88	[NMe ₄][BF ₄]
8	2.46	0.16	2.65 (6.65)	2.23 2.65	[C ₂ py]Cl
16	3.36	0.22	3.61 (9.24)	2.96 3.61	[C ₂ py][BF ₄]
32	4.47	0.13	4.62 (11.78)	4.39 4.62	[C ₁ mpyr][BF ₄]

Table 2. Relative average, Standard Deviation (st dev), and Maximum (max) Number of Two Body Interactions with Errors $<1 \text{ kJ mol}^{-1}$ for MP2 Correlation Energy with Respect to Increasing Cluster Size

no. of IPs	average (%)	st dev (%)	max (%)	IL with max %
4	71	10	86	[NMe ₄][BF ₄]
8	70	6	78	[C ₁ mpyr][BF ₄]
16	71	5	77	[C ₂ py]Cl
32	74	3	75	[C ₁ mpyr][BF ₄], [NMe ₄][BF ₄]

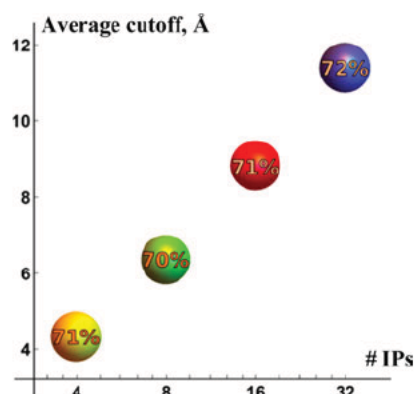


Figure 5. Relationship between cluster size (number of ion pairs on x -axis) and cutoff distance for dispersion (in Å on y -axis). The size of the spheres is scaled with respect to the relative number of two-body interactions whose contribution is shown in % inside of the spheres.

$$\begin{aligned}
 E(\text{FMO3}) = E(\text{FMO2}) + \sum_{I>J>K}^N \{ & (E_{IJK} - E_I - E_J - E_K) \\
 & - (E_{IJ} - E_I - E_J) - (E_{JK} - E_J - E_K) \\
 & - (E_{KI} - E_K - E_I) \} + \sum_{I>J>K}^N \text{Tr}(\Delta\Delta D^{IJK} V^{IJK})
 \end{aligned} \quad (4)$$

where E_{IJK} represents the energy of a three body system, D^{IJK} is the three body difference matrix, and V^{IJK} is the environment electrostatic potential.

Trend in Three-Body Effects with Increasing Cluster Size. Previously, our group showed that three body effects were critical at the HF level due to nonadditive induction forces, whereas the contribution from dispersion appeared below chemical accuracy.¹⁴ In this study a larger number of ionic liquids has been included, with clusters of 32 ion pairs available.

Figure 6 shows the total energy from three body contributions from the HF energy and the MP2 correlation energy taken from full FMO3 calculations. All energy contributions are negative and are given in Figure 6 on the absolute scale. It is expected that as the cluster doubles, the number of all possible three body interactions increase approximately by a factor of 2^3 . Therefore, it is not surprising that the HF energy starts to non negligibly contribute to the total energy already for 8 ion pair clusters, in some cases approaching as much as 283 kJ mol^{-1} for 32 ion pairs. In the case of some ionic liquids, dispersion forces also show a significant contribution to total energy, especially for chloride based ionic liquids. For example, 16 ion pair clusters of [C₁mim]Cl and [C₂py]Cl have a contribution in the range of $66\text{--}83 \text{ kJ mol}^{-1}$, which suggests that three body effects in dispersion cannot be neglected for some ionic liquids. It has to be noted that with increasing size of the ionic cluster, the contribution from dispersion forces will become significant regardless of the ionic liquid type due to the sheer number of three body interaction possible, defined as $\frac{N(N-1)(N-2)}{6}$, where N is the number of ions. Even if each individual contribution is seemingly negligible, their combined effect cannot be overlooked. This phenomenon is clearly observed in the case of 32 ion pair clusters of [C₁mpyr][BF₄] and [NMe₄][BF₄].

Further analysis of Figure 6 reveals that the behaviors of three body contributions depend on the structural arrangement and the type of ionic liquid. For the HF energy the contribution is non negligible for all ionic liquids studied, although the extent of this contribution varies rather significantly. Ionic liquids based on the C₁mpyr⁺ and NMe₄⁺ cations tend to have a

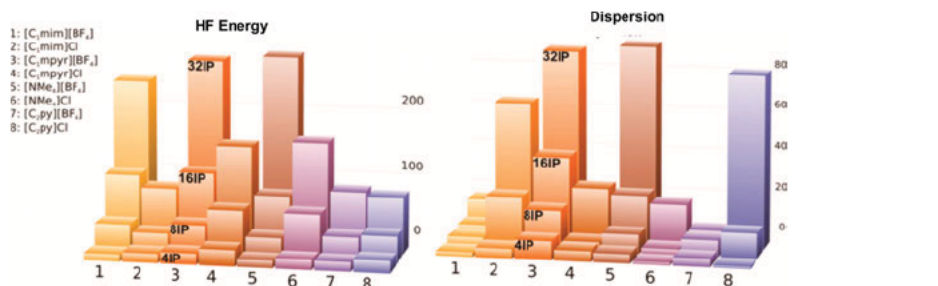


Figure 6. Three-body contributions (in kJ mol^{-1}) for HF energy (left) and correlation energy (right). Energy values are given on the absolute scale.

steep increase in the attractive contribution to the HF energy with increasing cluster size. This observation can be attributed to the fact that these ionic liquids form structures with alternate charge arrangement, similar to that of NaCl (Figure 7). In

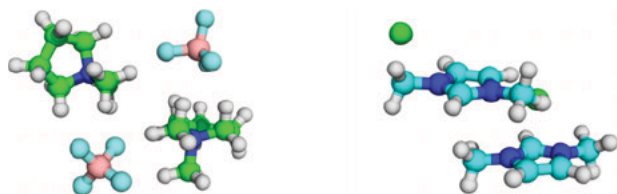


Figure 7. Structures depicting a typical alternate-charge arrangement found in the 16-ion-pair cluster of $[C_1\text{mpyr}][\text{BF}_4]$ (left) and a $\pi^+ \pi^-$ stacking interaction found in the 16-ion-pair cluster of $[C_1\text{mim}]\text{Cl}$ (right).

contrast to this trend, the $C_1\text{mim}^+$ and $C_2\text{py}^+$ cations can form $\pi^+ - \pi^-$ stacking interaction with each other⁵⁰ and, as a result, three body contribution from the HF energy is not as strong. On the contrary, their three body dispersion is significant and can no longer be neglected. The presence of imidazolium and pyridinium based cations does not automatically guarantee the significance of three body dispersion. All clusters of $[C_1\text{mim}][\text{BF}_4]$ show a very small (within chemical accuracy) contribution from dispersion and in this particular case three body interactions can be neglected. This finding further supports the fact that the bulk structure of the ionic liquid is a result of the importance of three body dispersion. To this end, it appears that the inclusion of both three body HF energy and dispersion is necessary to study the structural arrangement and energetics of multiscale clusters of ionic liquids.

Selection of Cutoff Criteria for Three-Body Interactions. A three body interaction can be described by three interionic distances, as shown in Figure 8. Therefore, three types of range

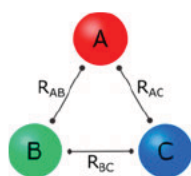


Figure 8. Graphical representation of three-body interactions.

restrictions based on the R_{AB} , R_{BC} , and R_{AC} distances can be potentially used to analyze the behavior of the three body contribution to the total energy with increasing cluster size. There are three models that can be used to estimate the significance of three body effects based on the interionic distances. The first model is based on using one interionic

distance restriction, in which at least one of the three interionic distances needs to fall within the set cutoff distance for a three body system to be included in the calculation. This model, further referred to in the text as the 1R model, is the most inclusive restriction model as it is not sensitive to the position of the third fragment in the system, allowing for possible combinations to be included. The latter makes this model very general. 2R and 3R models can be defined in the similar manner that requires two and three interionic distances, respectively, to fall within the set cutoff distance. The 3R model is the best model out of the three due to the fact that it considers all three distances, R_{AB} , R_{BC} , and R_{AC} , in the system before discarding it. Further in the text the behavior of all three models is discussed on the basis of the benchmark FMO3 calculations.

HF Energy. Analysis of three body contributions was performed in the same manner as for two body effects, with cutoff distances being identified when the electronic energy deviates below 1 kJ mol^{-1} with respect to the benchmark data (for more detail see Theoretical Procedures). The three body correction as shown in eq 3 contains contributions from corresponding two body interactions. The criteria below were established assuming all two body HF and dispersion interactions were included in the calculation.

Table 3 compares the performance of 1R, 2R, and 3R models in terms of the average unitless cutoff distances and corresponding average number of three body interactions. As one can see, the cutoff distances for the 1R model are shorter compared to those of the 2R and 3R model. Because the 1R model is insensitive to the position of the third ion, a significantly larger relative number of three body systems needs to be included in the calculation to achieve the desired accuracy. As a rule, the 1R model needs more than double the number of three body interactions compared to the 3R model. In contrast to this behavior, the 2R model tends to have the lowest number of three body interactions needed to achieve the deviation of 1 kJ mol^{-1} . The latter appears to be more robust in identifying the most important three body combinations and therefore is highly recommended.

Figure 9 shows typical trends in three body HF and dispersion contributions for all three models, 1R, 2R, and 3R, in 16 ion pair clusters of $[\text{NMe}_4][\text{BF}_4]$ and $[C_1\text{mim}]\text{Cl}$. The $[\text{NMe}_4][\text{BF}_4]$ ionic liquid represents an excellent example of the structural arrangement, in which the alternate charge pattern dominate, whereas the $[C_1\text{mim}]\text{Cl}$ ionic liquid contains distinct motifs of cation–cation interactions. As one can see, these ionic liquids show a strikingly different behavior in three body effects for two types of structural arrangement, clearly indicating that these effects are sensitive to the immediate environment of each ion. The 1R and 2R models exhibit a more distinct trend for both the HF energy and dispersion, with the

Table 3. Comparison of 1R, 2R, and 3R Models for Three Body HF Energy for Average Relative Number of Three Body Interactions (no. of three body) and Cutoff Distances, R_{cutoff} (Unitless as in Eq 2), with Standard Deviation in Parentheses with Respect to Increasing Cluster Size

no. of IPs	1R model		2R model		3R model	
	no. of three-body %	R_{cutoff}	no. of three-body %	R_{cutoff}	no. of three-body %	R_{cutoff}
4	67 (16)	0.88 (0.04)	41 (8)	0.97 (0.04)	33 (14)	1.58 (0.36)
8	54 (6)	0.93 (0.03)	20 (5)	1.10 (0.24)	26 (14)	2.13 (0.37)
16	41 (3)	0.97 (0.03)	11 (8)	1.25 (0.42)	16 (8)	2.45 (0.27)
32	25 (1)	0.99 (0.03)	6 (1)	1.70 (0.13)	6 (1)	2.57 (0.09)

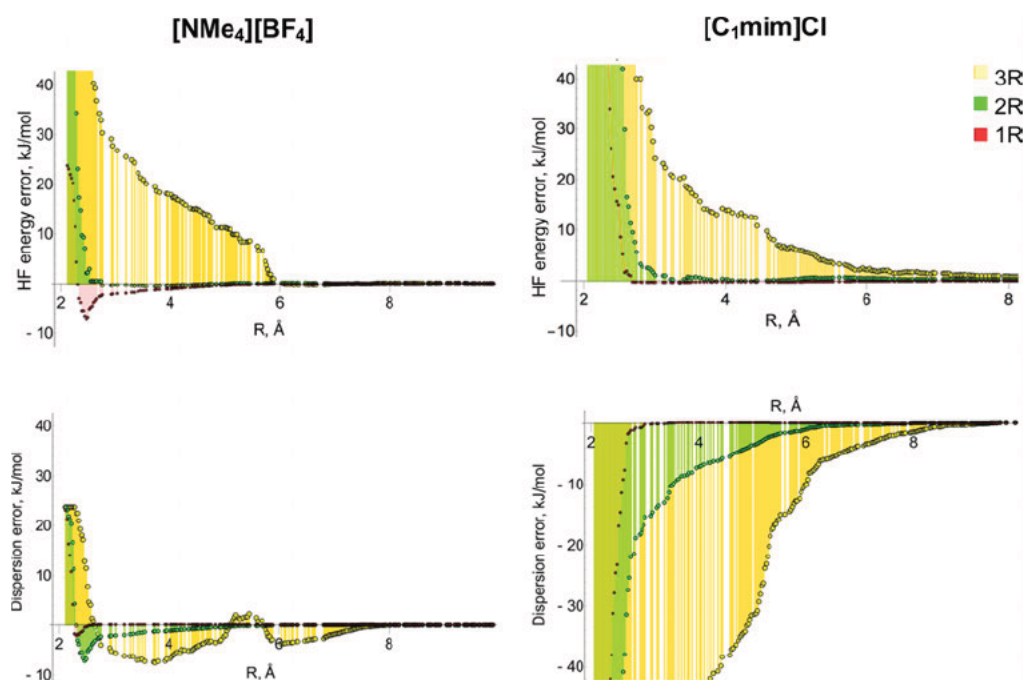


Figure 9. Deviations of HF and correlation energies (kJ mol^{-1}) with respect to the interionic distance, R , for 16-ion-pair clusters of $[\text{NMe}_4][\text{BF}_4]$ (left) and $[\text{C}_1\text{mim}]\text{Cl}$ (right).

former being consistently underestimated and the latter being overestimated. The 3R model shows a large degree of periodicity due to its sensitivity of the position of the third ion with respect to the other two. Rather unexpectedly, the effect of dispersion appears to extend much further by at least a couple of Å than that of the HF energy. On the basis of the relative number of three body interactions (Table 3) that need to be included to achieve 1 kJ mol^{-1} of accuracy and coupled with a smooth behavior of three body HF energy and dispersion, the 2R model can be concluded to be the most robust out of the three.

As shown in Table 3 the unitless cutoff distance steadily increases for the 2R model with increasing cluster size with no particular trend. It has to be pointed out that the standard deviation decreases in the same direction, indicating that the cutoff distance becomes more independent of the structural arrangement of ions in the bulk and, therefore, the importance of three body interactions consistently decreases with distance. The latter trend clearly indicates that three body effects appear to be more localized compared to two body effects. In the case of 16 and 32 ion pair clusters, the maximum number of required three body interactions was found to be 34% and 8%, respectively. It has to be pointed out that in 32 ion pair clusters 8% corresponds to nearly 400 three body interactions. A similar calculation for 16 ion pair clusters identifies that 190 of three body interactions corresponds to 34%. As a result, the inclusion of three body interactions in 32 ion pair clusters still requires double the computer time needed for 16 ion pair clusters. Because calculations of three body interactions are the most time consuming, this finding will allow for a reduction in cost of FMO3 calculations by more than two thirds, which constitutes a significant savings of computer resources. Due to relatively large fluctuations in standard deviations for multiscale clusters up to 16 ion pairs, maximum cutoff distances established for each cluster size are recommended for future

FMO3 calculations, as shown in Table 4. For more detail on the maximum cutoffs and corresponding ionic liquid systems see the Supporting Information.

Table 4. Recommended Unitless Cutoffs for HF Energy and Dispersion (MP2 Correlation Energy) in FMO3 Calculations of Ionic Liquids

no. of IPs	2R Model			
	HF		MP2 correlation	
	unitless	Å	unitless	Å
4	1.01	2.14	1.07	1.82
8	1.65	4.79	1.77	4.45
16	2.25	6.08	2.40	6.50
32	1.83	4.69	2.15	5.49

Dispersion. Similar data obtained for three body interactions of MP2 correlation energy and presented in Table 5, reveal that dispersion forces are as important as contributions from HF energy. Comparison of Tables 3 and 5 indicates that the average cutoff distances for correlation energy are slightly longer for all three models. More three body interactions need to be included to achieve the accuracy of 1 kJ mol^{-1} in the 3R model compared to the 2R model. The latter was again found to be the most robust, allowing for most of three body interactions to be discarded for larger clusters without any sacrifice in accuracy. This is reflected in the smooth behavior of three body contribution deviations in the 2R model (Figure 9). Their relative number consistently decreases with increasing cluster size, reaching 25% and 11% on average for 16 and 32 ion pair clusters, respectively, thus allowing for a significant reduction in computation time. In terms of average values, the cutoff distance has almost converged for 32 ion pair clusters, thus demonstrating the local nature of dispersion forces in three body interactions.

Table 5. Comparison of 1R, 2R, and 3R Models for Three Body Dispersion for Average Relative Number of Three Body Interactions with Standard Deviation in Parentheses and Cutoff Distances, R_{cutoff} (Unitless as in Eq 2), with Respect to Increasing Cluster Size

no. of IPs	1R Model		2R Model		3R Model	
	no. of three-body %	R_{cutoff}	no. of three-body %	R_{cutoff}	no. of three-body %	R_{cutoff}
4	61 (19)	0.88 (0.03)	37 (9)	0.96 (0.06)	48 (19)	1.76 (0.32)
8	53 (9)	0.93 (0.04)	27 (6)	1.38 (0.33)	37 (8)	2.36 (0.22)
16	44 (3)	1.01 (0.04)	25 (10)	2.03 (0.26)	31 (7)	2.95 (0.10)
32	28 (1)	1.03 (0.05)	11 (1)	2.14 (0.02)	15 (1)	3.21 (0.04)

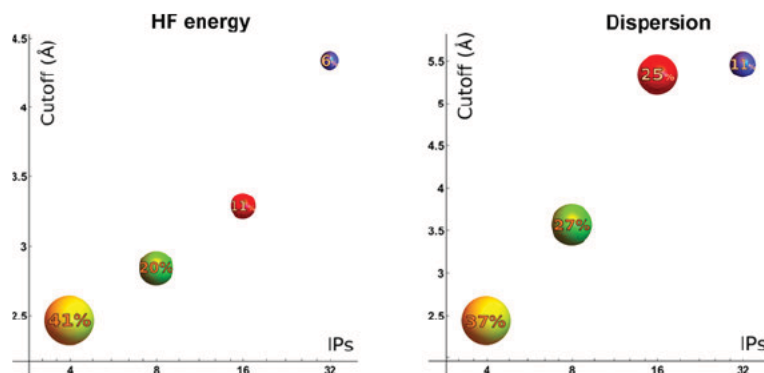


Figure 10. Relationship between cluster size (number of ion pairs on x -axis) and cutoff distance for HF energy (left) and dispersion (right) (in Å on y -axis) in the 2R model. The size of the spheres is scaled with respect to relative number of three-body interactions whose contribution is shown in % inside of the spheres.

Table 6. Performance of FMO3 Calculations for Three Body HF and MP2 Correlation Energy Using the Cutoffs Recommended in Table 4

IL	no. of IPs/cutoff	% three-body		error, kJ mol ⁻¹		
		HF	MP2 correlation	HF	MP2 correlation	total
[C ₇ mim][BF ₄]	8/1.77	46	45	0.01	0.28	0.29
[C ₇ mim]Cl		33	33	0.57	0.57	0.01
[C ₇ mpyr][BF ₄]		32	32	0.23	0.38	0.61
[C ₇ mpyr]Cl		30	30	0.57	1.16	0.59
[NMe ₄][BF ₄]		36	36	0.09	0.18	0.26
[NMe ₄]Cl	16/2.40	33	33	0.6	0.89	0.29
[C ₂ py][BF ₄]		38	38	0.07	0.14	0.08
[C ₂ py]Cl		33	33	0.12	0.78	0.66
[C ₇ mim][BF ₄]		42	42	0.02	0.21	0.19
[C ₇ mim]Cl		45	45	0.26	0.41	0.15
[C ₇ mpyr][BF ₄]		32	31	0.05	0.12	0.07
[C ₇ mpyr]Cl		35	35	0.83	0.65	0.18
[NMe ₄][BF ₄]		29	29	0.15	0.06	0.09
[NMe ₄]Cl		36	36	0.72	0.62	0.10
[C ₂ py][BF ₄]		32	31	0.10	0.38	0.49
[C ₂ py]Cl		40	40	0.23	0.95	0.72

Due to large standard deviations, the recommended cutoff distances for MP2 correlation energy shown in Table 5 are based on the maximum ones found for each cluster size. It has to be pointed out that dispersion forces extend further than HF energy by at least 0.5 Å. The converted recommended cutoffs reflect the necessity to include at least the first solvation shell for each ion to account for three body interactions regardless of cluster size. This finding is not surprising, as molecular properties such as dipole moment and vibrational spectra related to electronic structure are confirmed by *ab initio* MD simulations to be local in nature for common ionic liquids.^{15,16,51} In our work they appear to be truly converged

for dispersion forces at the first solvation shell (Figure 10). Although the trend in the HF energy appears not to converge considering average cutoffs, it is converged when one analyzes the recommended (i.e., maximum) cutoff distances (Table 4).

Overall, three body dispersion forces appear to be localized compared to two body dispersion forces and the cutoff distance is expected to converge with larger cluster sizes. The 2R model appears to be the most robust, achieving spectroscopic accuracy for electronic energy and discards almost 70% of the three body interactions for clusters consisting of at least 16 ion pairs.

Applications of Established Cutoff Distances in FMO3 Calculations of Ionic Liquids with GAMESS-US. The current

implementation of the FMO code in GAMESS US supports two types of models for the HF method: 1R model and 2R model. As has been established earlier, the 2R model provides an excellent tradeoff between the number of two and three body interactions and the resulting accuracy of electronic energy. The unitless cutoffs recommended in Table 4 were independently tested for the 8 and 16 ion pair ionic liquid clusters discussed above; i.e., the FMO3 calculations were performed using the RITRIM(1) parameters set to 1.77 each for 8 ion pair clusters and 2.40 each for 16 ion pair clusters. For increased accuracy of the MP2 correlation energy the same cutoff was used for both HF and MP2 correlation energy for each cluster size. The performance of the FMO3 MP2 method for three body effects is presented in Table 6. It has to be noted that all possible two body interactions were included in the calculations.

Analysis of Table 6 reveals that 36% of three body interactions on average were included for both sizes of ionic liquid clusters, thus allowing for almost two thirds of savings with regard to computer time. It is interesting to note that three body effects are indeed insensitive to the structural arrangement of the ionic liquid, resulting in very small variations in the % values. As was already established in Figure 9, the HF energy tends to have positive deviations, whereas MP2 correlation energy gives negative ones. As a result, the overall deviation is below 1 kJ mol⁻¹ due to the opposing effects of the HF energy and dispersion.

CONCLUSIONS

A comprehensive analysis of two and three body effects of the FMO approach coupled with the MP2 method has been performed on a wide range of ionic liquid clusters consisting of imidazolium, purrolidinium, quaternary ammonium, and pyridinium cations and typical anions such as chloride and tetrafluoroborate. The clusters varies in size from 4, 8, 16, to 32 ion pairs, thus accounting for up to 64 ions in the system. Overall, two body and three body effects for both HF and MP2 correlation energy were established to be important. Surprisingly, three body effects for dispersion forces, defined here as MP2 correlation energy, can contribute for up to 80 kJ mol⁻¹, making then far from non negligible in these semi Coulombic systems. The behavior of three body contributions was found to depend on the structural arrangement of ions in the cluster. Counterintuitively, ionic liquids with a typical alternate charge arrangement exhibited a much stronger contribution from three body dispersion compared to those with $\pi^+ - \pi^+$ stacking interactions.

Analysis of the extent of importance of two body effects revealed that these cannot be discarded at all at the HF level of theory due to a periodic behavior of two body contributions with increasing interionic distance between ions. The HF energy continues to oscillate for the whole range of interionic distances, even up to 20 Å in 32 ion pair clusters. However, MP2 correlation energy follows an expected convergent trend, with cutoff distances linearly increasing with cluster size regardless of the structural arrangement of ions in the clusters. The linear increase was found to follow the trend $\log_2(N) - 0.5$ (where N is the number of ion pairs), extending up to 12 Å in 32 ion pair clusters. On average, 71% of two body MP2 correlation calculations need to be performed to achieve accuracy of 1 kJ mol⁻¹, thus suggesting that an identical cutoff for dispersion cannot be used for varying cluster sizes.

Generally, three body effects were established to be much more localized than two body effects. Three possible models, 1R, 2R, and 3R, analyzed in this work were based on the number of interionic distances considered in a three ion system to discard three body interactions. The 2R model based on considering two lowest interionic distances was found to be the most robust. The model allows to achieve accuracy of 1 kJ mol⁻¹ in electronic energy by including the lowest number of three body interactions. Three body effects were found not to extend beyond the first solvation shell (in the range of 5–6.5 Å), with the MP2 correlation energy converging by almost 2 Å slower than the HF one. Due to the local nature of three body effects, between 11 and 30% of three body effects are needed in FMO3 calculations of large sized clusters of ionic liquids. The established cutoffs for two and three body effects will allow for a systematic study of dispersion forces on the structural arrangement of ions in the bulk of ionic liquids and the correlation with their thermodynamic and transport properties. This work is currently underway.

ASSOCIATED CONTENT

Supporting Information

The Supporting Information is available free of charge on the ACS Publications website at DOI: 10.1021/acs.jpcb.6b10101.

Optimized structures of the ionic liquid clusters analyzed, radial distribution functions of all clusters, FMO1, FMO2, and FMO3 electronic energies (both HF and MP2) of clusters taken from full FMO3/cc pVTZ calculations, graphs with deviations of two body contributions for the HF energy and MP2 correlation energy with interionic distance, unitless cutoff distances identified each ionic liquid cluster for two body and three body contributions for the HF energy and dispersion, individual relative number of two body and three body fragments (in %) corresponding to selected cutoff distances for both HF and MP2 correlation energy (PDF)

AUTHOR INFORMATION

Corresponding Author

*E. I. Izgorodina. E mail: katya.pas@monash.edu.

ORCID

Ekaterina I. Izgorodina: 0000-0002-2506-4890

Notes

The authors declare no competing financial interest.

ACKNOWLEDGMENTS

The authors gratefully acknowledge a generous allocation of computer resources through the Monash eResearch Centre, the National Computational Infrastructure, and the Pawsey Super computing Centre. This work is generously supported by the Australian Research Council through a Discovery Project Grant and a Future Fellowship for E.I. Zoe Seeger acknowledges support by the Australian Government through her Australian Postgraduate Award.

REFERENCES

- (1) Izgorodina, E. I. Towards Large-Scale, Fully *Ab Initio* Calculations of Ionic Liquids. *Phys. Chem. Chem. Phys.* **2011**, *13*, 4189–4207.
- (2) Hallett, J. P.; Welton, T. Room-Temperature Ionic Liquids: Solvents for Synthesis and Catalysis. *Chem. Rev.* **2011**, *111*, 3508–3576.

- (3) MacFarlane, D. R.; Forsyth, M.; Howlett, P. C.; Kar, M.; Passerini, S.; Pringle, J. M.; Ohno, H.; Watanabe, M.; Yan, F.; Zheng, W.; et al. Ionic Liquids and Their Solid-State Analogues as Materials for Energy Generation and Storage. *Nat. Rev. Mater.* **2016**, *1*, 15005.
- (4) MacFarlane, D. R.; Forsyth, M.; Howlett, P. C.; Pringle, J. M.; Sun, J.; Annat, G.; Neil, W.; Izgorodina, E. I. Ionic Liquids in Electrochemical Devices and Processes: Managing Interfacial Electrochemistry. *Acc. Chem. Res.* **2007**, *40*, 1165–1173.
- (5) Plechkova, N. V.; Seddon, K. R. Applications of Ionic Liquids in the Chemical Industry. *Chem. Soc. Rev.* **2008**, *37*, 123–150.
- (6) Crosthwaite, J. M.; Aki, S.; Maginn, E. J.; Brennecke, J. F. Liquid Phase Behavior of Imidazolium-Based Ionic Liquids with Alcohols. *J. Phys. Chem. B* **2004**, *108*, 5113–5119.
- (7) Heintz, A. Recent Developments in Thermodynamics and Thermophysics of Non-Aqueous Mixtures Containing Ionic Liquids. A Review. *J. Chem. Thermodyn.* **2005**, *37*, 525–535.
- (8) Rogers, R. D.; Seddon, K. R. Ionic Liquids - Solvents of the Future? *Science* **2003**, *302*, 792–793.
- (9) Bernard, U. L.; Izgorodina, E. I.; MacFarlane, D. R. New Insights into the Relationship between Ion-Pair Binding Energy and Thermodynamic and Transport Properties of Ionic Liquids. *J. Phys. Chem. C* **2010**, *114*, 20472–20478.
- (10) Izgorodina, E. I.; Golze, D.; Maganti, R.; Armel, V.; Taige, M.; Schubert, T. J. S.; MacFarlane, D. R. Importance of Dispersion Forces for Prediction of Thermodynamic and Transport Properties of Some Common Ionic Liquids. *Phys. Chem. Chem. Phys.* **2014**, *16*, 7209–7221.
- (11) Tan, S. Y. S.; Izgorodina, E. I. Comparison of the Effective Fragment Potential Method with Symmetry-Adapted Perturbation Theory in the Calculation of Intermolecular Energies for Ionic Liquids. *J. Chem. Theory Comput.* **2016**, *12*, 2553–2568.
- (12) Rigby, J.; Izgorodina, E. I. New SCS- and SOS-MP2 Coefficients Fitted to Semi-Coulombic Systems. *J. Chem. Theory Comput.* **2014**, *10*, 3111–3122.
- (13) Rigby, J.; Barrera Acevedo, S.; Izgorodina, E. I. Novel SCS-IL-MP2 and SOS-IL-MP2 Methods for Accurate Energetics of Large-Scale Ionic Liquid Clusters. *J. Chem. Theory Comput.* **2015**, *11*, 3610–3616.
- (14) Izgorodina, E. I.; Rigby, J.; MacFarlane, D. R. Large-Scale *Ab Initio* Calculations of Archetypical Ionic Liquids. *Chem. Commun.* **2012**, *48*, 1493–1495.
- (15) Wendler, K.; Brehm, M.; Malberg, F.; Kirchner, B.; Delle Site, L. Short Time Dynamics of Ionic Liquids in Aimd-Based Power Spectra. *J. Chem. Theory Comput.* **2012**, *8*, 1570–1579.
- (16) Wendler, K.; Zahn, S.; Dommert, F.; Berger, R.; Holm, C.; Kirchner, B.; Delle Site, L. Locality and Fluctuations: Trends in Imidazolium-Based Ionic Liquids and Beyond. *J. Chem. Theory Comput.* **2011**, *7*, 3040–3044.
- (17) Zahn, S.; Thar, J.; Kirchner, B. Structure and Dynamics of the Protic Ionic Liquid Monomethylammonium Nitrate ($[\text{CH}_3\text{NH}_3]^+[\text{NO}_3]^-$) from *Ab Initio* Molecular Dynamics Simulations. *J. Chem. Phys.* **2010**, *132*, 124506.
- (18) Kirchner, B.; Hollóczy, O.; Canongia Lopes, J. N.; Pádua, A. A. H. Multiresolution Calculation of Ionic Liquids. *WIREs: Comput. Mol. Sci.* **2015**, *5*, 202–214.
- (19) Lehmann, S. B. C.; Roatsch, M.; Schoppke, M.; Kirchner, B. On the Physical Origin of the Cation-Anion Intermediate Bond in Ionic Liquids Part I. Placing a (Weak) Hydrogen Bond between Two Charges. *Phys. Chem. Chem. Phys.* **2010**, *12*, 7473–7486.
- (20) Malberg, F.; Brehm, M.; Holloczki, O.; Pensado, A. S.; Kirchner, B. Understanding the Evaporation of Ionic Liquids Using the Example of 1-Ethyl-3-Methylimidazolium Ethylsulfate. *Phys. Chem. Chem. Phys.* **2013**, *15*, 18424–18436.
- (21) Malberg, F.; Pensado, A. S.; Kirchner, B. The Bulk and the Gas Phase of 1-Ethyl-3-Methylimidazolium Ethylsulfate: Dispersion Interaction Makes the Difference. *Phys. Chem. Chem. Phys.* **2012**, *14*, 12079–12082.
- (22) Pensado, A. S.; Brehm, M.; Thar, J.; Seitsonen, A. P.; Kirchner, B. Effect of Dispersion on the Structure and Dynamics of the Ionic Liquid 1-Ethyl-3-Methylimidazolium Thiocyanate. *ChemPhysChem* **2012**, *13*, 1845–1853.
- (23) Kitaura, K.; Ikeo, E.; Asada, T.; Nakano, T.; Uebayasi, M. Fragment Molecular Orbital Method: An Approximate Computational Method for Large Molecules. *Chem. Phys. Lett.* **1999**, *313*, 701–706.
- (24) Nakano, T.; Kaminuma, T.; Sato, T.; Akiyama, Y.; Uebayasi, M.; Kitaura, K. Fragment Molecular Orbital Method: Application to Polypeptides. *Chem. Phys. Lett.* **2000**, *318*, 614–618.
- (25) Nakano, T.; Kaminuma, T.; Sato, T.; Fukuzawa, K.; Akiyama, Y.; Uebayasi, M.; Kitaura, K. Fragment Molecular Orbital Method: Use of Approximate Electrostatic Potential. *Chem. Phys. Lett.* **2002**, *351*, 475–480.
- (26) Fedorov, D. G.; Ishimura, K.; Ishida, T.; Kitaura, K.; Pulay, P.; Nagase, S. Accuracy of the Three-Body Fragment Molecular Orbital Method Applied to Møller Plesset Perturbation Theory. *J. Comput. Chem.* **2007**, *28*, 1476–1484.
- (27) Fedorov, D. G.; Kitaura, K. The Importance of Three-Body Terms in the Fragment Molecular Orbital Method. *J. Chem. Phys.* **2004**, *120*, 6832–6840.
- (28) Fedorov, D. G.; Kitaura, K. Second Order Møller-Plesset Perturbation Theory Based Upon the Fragment Molecular Orbital Method. *J. Chem. Phys.* **2004**, *121*, 2483–2490.
- (29) Fedorov, D. G.; Kitaura, K. The Three-Body Fragment Molecular Orbital Method for Accurate Calculations of Large Systems. *Chem. Phys. Lett.* **2006**, *433*, 182–187.
- (30) Fedorov, D. G.; Kitaura, K. Pair Interaction Energy Decomposition Analysis. *J. Comput. Chem.* **2007**, *28*, 222–237.
- (31) Fedorov, D. G.; Olson, R. M.; Kitaura, K.; Gordon, M. S.; Koseki, S. A New Hierarchical Parallelization Scheme: Generalized Distributed Data Interface (GDDI), and an Application to the Fragment Molecular Orbital Method (FMO). *J. Comput. Chem.* **2004**, *25*, 872–880.
- (32) Gordon, M. S.; Mullin, J. M.; Pruitt, S. R.; Roskop, L. B.; Slipchenko, L. V.; Boatz, J. A. Accurate Methods for Large Molecular Systems. *J. Phys. Chem. B* **2009**, *113*, 9646–9663.
- (33) Gordon, M. S.; Fedorov, D. G.; Pruitt, S. R.; Slipchenko, L. V. Fragmentation Methods: A Route to Accurate Calculations on Large Systems. *Chem. Rev.* **2012**, *112*, 632–672.
- (34) Pruitt, S. R.; Bertoni, C.; Brorsen, K. R.; Gordon, M. S. Efficient and Accurate Fragmentation Methods. *Acc. Chem. Res.* **2014**, *47*, 2786–2794.
- (35) Pruitt, S. R.; Steinmann, C.; Jensen, J. H.; Gordon, M. S. Fully Integrated Effective Fragment Molecular Orbital Method. *J. Chem. Theory Comput.* **2013**, *9*, 2235–2249.
- (36) Fedorov, D. G.; Kitaura, K. Coupled-Cluster Theory Based Upon the Fragment Molecular-Orbital Method. *J. Chem. Phys.* **2005**, *123*, 134103.
- (37) Findlater, A. D.; Zahariev, F.; Gordon, M. S. Combined Fragment Molecular Orbital Cluster in Molecule Approach to Massively Parallel Electron Correlation Calculations for Large Systems. *J. Phys. Chem. A* **2015**, *119*, 3587–3593.
- (38) Rigby, J.; Izgorodina, E. I. Assessment of Atomic Partial Charge Schemes for Polarisation and Charge Transfer Effects in Ionic Liquids. *Phys. Chem. Chem. Phys.* **2013**, *15*, 1632–1646.
- (39) Schmidt, M. W.; Baldridge, K. K.; Boatz, J. A.; Elbert, S. T.; Gordon, M. S.; Jensen, J. H.; Koseki, S.; Matsunaga, N.; Nguyen, K. A.; Su, S. General Atomic and Molecular Electronic Structure System. *J. Comput. Chem.* **1993**, *14*, 1347–1363.
- (40) Fedorov, D. G.; Kitaura, K. *The Fragment Molecular Orbital Method*; CRC Press, Taylor and Francis Group: Boca Raton, London, NY, 2009.
- (41) Stone, A. J. Water from First Principles. *Science* **2007**, *315*, 1228–1229.
- (42) Moszynski, R.; Wormer, P. E. S.; Heijmen, T. G. A.; van der Avoird, A. Symmetry-Adapted Perturbation Theory of Nonadditive Three-Body Interactions in van der Waals Molecules. II. Application to the Ar_2Hf Interaction. *J. Chem. Phys.* **1998**, *108*, 579–589.

- (43) DiStasio, R. A.; von Lilienfeld, O. A.; Tkatchenko, A. Collective Many-Body van der Waals Interactions in Molecular Systems. *Proc. Natl. Acad. Sci. U. S. A.* **2012**, *109*, 14791–14795.
- (44) Gobre, V. V.; Tkatchenko, A. Scaling Laws for van der Waals Interactions in Nanostructured Materials. *Nat. Commun.* **2013**, *4* (2341), 1–6.
- (45) Reilly, A. M.; Tkatchenko, A. van der Waals Dispersion Interactions in Molecular Materials: Beyond Pairwise Additivity. *Chem. Sci.* **2015**, *6*, 3289–3301.
- (46) Robert, A. D., Jr.; Vivekanand, V. G.; Alexandre, T. Many-Body van der Waals Interactions in Molecules and Condensed Matter. *J. Phys.: Condens. Matter* **2014**, *26*, 213202.
- (47) Tkatchenko, A.; DiStasio, R. A.; Car, R.; Scheffler, M. Accurate and Efficient Method for Many-Body van der Waals Interactions. *Phys. Rev. Lett.* **2012**, *108*, 236402.
- (48) Tkatchenko, A.; Scheffler, M. Accurate Molecular van der Waals Interactions from Ground-State Electron Density and Free-Atom Reference Data. *Phys. Rev. Lett.* **2009**, *102*, 073005.
- (49) Wagner, C.; Fournier, N.; Ruiz, V. G.; Li, C.; Müllen, K.; Rohlfing, M.; Tkatchenko, A.; Temirov, R.; Tautz, F. S. Non-Additivity of Molecule-Surface van der Waals Potentials from Force Measurements. *Nat. Commun.* **2014**, *5*, 5568.
- (50) Matthews, R. P.; Welton, T.; Hunt, P. A. Hydrogen Bonding and π - π Interactions in Imidazolium-Chloride Ionic Liquid Clusters. *Phys. Chem. Chem. Phys.* **2015**, *17*, 14437–14453.
- (51) Zahn, S.; Wendler, K.; Delle Site, L.; Kirchner, B. Depolarization of Water in Protic Ionic Liquids. *Phys. Chem. Chem. Phys.* **2011**, *13*, 15083–15093.

2.3 References

- [1] Ekaterina I. Izgorodina. Towards Large-Scale, Fully *Ab Initio* Calculations of Ionic Liquids. *Physical Chemistry Chemical Physics* **13**(10) (2011), 4189–4207. DOI: [10.1039/C0CP02315A](https://doi.org/10.1039/C0CP02315A).
- [2] Kazuo Kitaura, Eiji Ikeo, Toshio Asada, Tatsuya Nakano, and Masami Uebayasi. Fragment Molecular Orbital Method: An Approximate Computational Method for Large Molecules. *Chemical Physics Letters* **313**(3) (1999), 701–706. DOI: [10.1016/S0009-2614\(99\)00874-X](https://doi.org/10.1016/S0009-2614(99)00874-X).
- [3] Ekaterina I. Izgorodina, Jason Rigby, and Douglas R. MacFarlane. Large-Scale *Ab Initio* Calculations of Archetypical Ionic Liquids. *Chemical Communications* **48**(10) (2012), 1493–1495. DOI: [10.1039/C1CC15056A](https://doi.org/10.1039/C1CC15056A).
- [4] Dmitri G. Fedorov, Kazuya Ishimura, Toyokazu Ishida, Kazuo Kitaura, Peter Pulay, and Shigeru Nagase. Accuracy of the Three-Body Fragment Molecular Orbital Method Applied to Møller–Plesset Perturbation Theory. *Journal of Computational Chemistry* **28**(9) (2007), 1476–1484. DOI: [10.1002/jcc.20645](https://doi.org/10.1002/jcc.20645).
- [5] Dmitri G. Fedorov and Kazuo Kitaura. The Importance of Three-Body Terms in the Fragment Molecular Orbital Method. *The Journal of Chemical Physics* **120**(15) (2004), 6832–6840. DOI: [10.1063/1.1687334](https://doi.org/10.1063/1.1687334).
- [6] Dmitri G. Fedorov and Kazuo Kitaura. Second Order Møller–Plesset Perturbation Theory Based upon the Fragment Molecular Orbital Method. *The Journal of Chemical Physics* **121**(6) (2004), 2483–2490. DOI: [10.1063/1.1769362](https://doi.org/10.1063/1.1769362).
- [7] Stefan Zahn, Douglas R. MacFarlane, and Ekaterina I. Izgorodina. Assessment of Kohn–Sham Density Functional Theory and Møller–Plesset Perturbation Theory for Ionic Liquids. *Physical Chemistry Chemical Physics* **15**(32) (2013), 13664–13675. DOI: [10.1039/C3CP51682B](https://doi.org/10.1039/C3CP51682B).

Chapter 3

In search of a DFT functional for geometry optimisations of large clusters

3.1 Introduction

Quantum chemists have consistently sought to obtain predictive power in the pursuit of determining task-specific ionic liquids. Wavefunction-based methods provide a highly accurate account of the geometry they are supplied with. However, the global minimum and other interesting minima must first be located. It has been determined that ion arrangements of ionic liquid clusters of one and two ion pairs are dependent on the size and electron distribution of both the anion and cation.¹⁻³ Thus, it is not obvious *a priori* which minima are important. Vast potential energy surfaces require geometry screening processes where numerous configurations are optimised, and inhibits accurate modelling of large scale clusters. It is common procedure to optimise at a lower level of theory, although as of yet the effect of density functional theory (DFT) functional on the resulting optimised geometry of large scale clusters has not been tested.

Section 3.2 contains a manuscript submitted to *The Journal of Chemical Theory and Computation*. DFT functionals and second order Møller-Plesset perturbation theory- (MP2) based methods have been applied to a set of two ion pair (2IP) structures of 1-methyl-3-methylimidazolium tetrafluoroborate ([C₁mim][BF₄]) and chloride ([C₁mim]Cl). The benchmark geometries were

optimised with FMO3-SRS-MP2/cc-pVTZ. SRS-MP2 is an MP2 variant that scales the correlation energy to reproduce CCSD(T) accuracy,^{4,5} while FMO3 fragments the calculation such that the cost becomes scalable with system size while accounting for up to three-body effects.⁶⁻⁹ Further explanations for SRS-MP2 and the FMO approach can be found in section 1.2. Forty-three different approaches were tested where the functionals/wavefunction-based methods, basis sets and dispersion corrections vary. Promising theories were further tested in eight 4IP ionic liquid clusters.

The functionals ω B97X-D/cc-pVDZ, M06-2X/aug-cc-pVDZ, B3LYP-D3/cc-pVTZ and TPSS-D3/cc-pVTZ were some of the best performing functionals for the 2IP systems. However, implementation with 4IP systems found them to be inaccurate. All of the methods that performed the best for 4IP systems also performed well for the 2IP systems. These were PBE-D3/cc-pVTZ followed by ω B97X-D/aug-cc-pVDZ, then BLYP-D3/cc-pVTZ and lastly FMO2-SRS-MP2/cc-pVTZ. These four methods/basis sets had maximum RMSD values below 1.0 Å. This study provides chemists with a hierarchy of accuracy for optimisation techniques when investigating larger clusters of ionic liquids.

A systematic study of DFT performance for geometry optimisations of ionic liquid clusters

*Zoe L. Seeger and Ekaterina I. Izgorodina**

School of Chemistry, Monash University, 17 Rainforest Walk, Clayton, Victoria 3800, Australia

Keywords: DFT, functionals, density functional theory, MP2, benchmarking, optimization, clusters, ionic liquids

Abstract

Clusters of two ion pairs of imidazolium-based ionic liquids were optimised with 43 different levels of theory, including DFT functionals and MP2-based methods combined with varying Dunning's basis sets, and added dispersion corrections. Better performing DFT functionals were then applied to clusters consisting of four ion pairs. Excellent performance of some DFT functionals for the two ion pair clusters did not always match that of the four ion paired clusters, despite interionic distances remaining constant between the optimised two and four ion-paired clusters of the same ionic liquid. Combinations of DFT functional and basis set such as ω B97X-D/cc-pVDZ, M06-2X/aug-cc-pVDZ, B3LYP-D3/cc-pVTZ and TPSS-D3/cc-pVTZ gave excellent results for geometry optimisation of two ion-paired clusters of imidazolium ionic liquids, but gave larger deviations when applied to the four ion paired clusters of varying ionic liquids. Empirical dispersion corrections were seen to be crucial in correctly capturing correlation effects in the studied ionic liquid clusters, becoming more important in larger clusters. Dunning's double- ζ basis

set, cc-pVDZ, is associated with the smallest root mean squared deviations for geometries; however, it also produces the largest deviations in total electronic energies. ω B97X-D and M06-2X produced the best performance with the augmented version of this basis set. The triple- ζ basis set, cc-pVTZ, leads to the best performance of most of the DFT functionals (especially the dispersion-corrected ones) used, whereas its augmented version, aug-cc-pVTZ, was not seen to improve results. The combinations of functional and basis set that gave the best geometry and energetics in both 2 and 4 ion-paired clusters were PBE-D3/cc-pVTZ, ω B97X-D/aug-cc-pVDZ and BLYP-D3/cc-pVTZ. All three combinations are recommended for geometry optimisations of larger clusters of ionic liquids. PBE-D3/cc-pVTZ performed the best with an average deviation of 2.3 kJ mol⁻¹ and a standard deviation of 3.4 kJ mol⁻¹ for total electronic energy when applied to 4 ion-paired clusters. Geometries optimised with FMO2-SRS-MP2/cc-pVTZ produced total energy within 2.0 kJ mol⁻¹ off the benchmark in two ion-paired clusters, with the cc-pVDZ basis set performing unsurprisingly poorly with the same method. The error increased to 4.8 kJ mol⁻¹ on average in four ion-paired clusters, with the smallest RMSD deviations in geometries when compared to the benchmark ones. This study is the first report that investigated the performance of DFT functionals for 2- and 4 ion-paired clusters of a wide range of ionic liquids consisting of commonly used cations such as pyrrolidinium, imidazolium, pyridinium and ammonium. It also identified the importance of assessing the performance of quantum chemical methods for ionic liquids on a variety of cation-anion combinations.

Introduction

Ionic liquids, discovered over a century ago, remain prevalent in the current literature and research into their application continues to grow in areas spanning catalysis,¹⁻³ electrochemical sensing,⁴⁻⁶

separation,⁷⁻⁹ gas absorption,^{10,11} and biomass processing.^{12,13} Interest in ionic liquids remains strong due to a sheer number of potential cation-anion combinations of varying chemical structure, thus offering endless amounts of possibilities to produce materials of varying physicochemical properties. Among these properties of interest are low melting point, thermal and electrochemical stability, negligible volatility, high conductivity and low viscosity.

The prediction of thermodynamic and transport properties of ionic liquids has been a holy grail of molecular dynamics simulations and quantum chemical calculations since the first applications of ionic liquids.¹⁴⁻¹⁶ Quantum chemical methods have been of particular interest as they provide accurate energetic insight into the interplay of fundamental forces – electrostatics, induction, exchange and dispersion – in ionic liquids. The work previously conducted in our group has identified a strong relationship between electrostatics and dispersion forces calculated for two ion-paired clusters of imidazolium- and pyrrolidinium-based ionic liquids and their melting point and conductivity.^{17,18} Two features of ionic liquids represent the main difficulty of turning the proposed methodology into a high-throughput approach – many-body effects and shallow potential energy surfaces.

The importance of many-body effects in ionic liquids has been demonstrated in a number of ionic liquids, with the ratio of electrostatic, induction and dispersion forces varying on a series of factors ranging from the length of alkyl chain on the cation, to the functionality of interaction sites on the anion. Ludwig *et al.* showed that many-body effects led to a continuing increase of interaction energy per ion pair in clusters of imidazolium-based ionic liquids consisting of up to ten ion pairs.¹⁹ Dispersion interactions increase rapidly with increasing cluster size in up to at least eight ion pairs of imidazolium-based ionic liquids coupled with the tetrafluoroborate anion.²⁰ In general, increases in both induction and dispersion interactions was observed going from 8 to 32-

ion paired clusters of commonly used ionic liquids based on imidazolium and pyrrolidinium cations.²¹ The magnitude of the increase was identified to strongly depend on the cation-anion combination. Strength and interplay of interionic interactions in turn affect the optimised geometry. Koßmann *et al.* found that the hydrogen bond distances in dimethylimidazolium chloride increased asymptotically while increasing in up to nine ion pairs in a linear chain.²² Matthews *et al.* have shown that low energy two ion-paired structures of dimethylimidazolium chloride could not be located by combining lower energy structures of single ion pairs highlighting that the potential energy surfaces of larger systems require re-examination.²³ Our group identified that interionic distances in imidazolium chlorides and acetates had already converged at two ion-paired clusters when an implicit solvation model was used during geometry optimisation.²⁴

Significant contributions of dispersion forces among ionic liquid ions lead to shallow potential energy surfaces.²⁵ The main consequence of this phenomenon is the existence of many energetically favourable configurations of large-scale clusters of ionic liquids.^{18,26} The location of the global minimum – as well as other energetically accessible local minima of multiple ion clusters – are essential in ensuring that the fundamental forces from these clusters can be translated to bulk properties of ILs. The accurate description of dispersion forces was shown to be critical at identifying the correct bulk structure of ionic liquids, which in turn affects the prediction of their physicochemical properties.^{27,28}

In the case of imidazolium ionic liquids there is a competition between Coulombic cation-anion interactions and the $\pi^+-\pi^+$ stacking of imidazolium cations as originally demonstrated for triazolium cations.²⁹ The former leads to an alternating charge structure in the ionic liquid bulk. Matthews *et al.* have found that conversions between alternating-charge structures and $\pi^+-\pi^+$ stacked structures in dimers of 1,3-dimethylimidazolium chloride have a low energy barrier of less

than 6 kJ mol⁻¹.²³ The small energy differences in structural arrangements likely explain the prevalence of $\pi^+-\pi^+$ stacking in molecular dynamics simulations of 1-ethyl-3-methylimidazolium with anions chloride or thiocyanate.³⁰ The $\pi^+-\pi^+$ stacking was observed in crystal structures of 1-ethyl-3-methylimidazolium nitrate³¹ and 1,3-dimethylimidazolium with either triflate³² or *bis*(trifluoromethanesulfonyl)imide.³³ The aggregation of alkyl chains has also been documented in the literature.^{34–36} A systematic and elegant study by Kirchner *et al.* demonstrated how an increase of alkyl chain length on the imidazolium cation going from ethyl to octyl gradually increases nanosegregation of the bulk structure into polar and non-polar domains driven by van der Waals interactions among the alkyl chains.¹⁴ The effect of hydrogen bonding in imidazolium ionic liquids on their macroscopic properties has been extensively demonstrated in experiment. Mid- and far-FTIR spectra showed that highly directional hydrogen bonds were responsible for the reduction of melting points and viscosities. A similar observation was also made for 1-ethyl-3-methylimidazolium *bis*(trifluoromethylsulfonyl)imide and 1-ethyl-2,3-dimethylimidazolium *bis*(trifluoromethylsulfonyl)imide in a study by Fumino *et al.*³⁷ Furthermore, a series of theoretical studies confirmed that substituting the hydrogen atom in the C2 position of the imidazolium ring with a methyl group created a larger barrier between energetically preferable configurations, thus explaining their higher melting points and increased viscosity values with respect to commonly used imidazolium ionic liquids.^{38–40}

Two ion-paired clusters of imidazolium- and pyrrolidinium-based ionic liquids exhibiting same-ion interactions have been fully configurationally screened to determine lower-energy configurations when coupled with the tetrafluoroborate, and dicyanamide anions.¹⁸ Global minimum structures exhibiting the stacking of cations were only found for imidazolium chlorides with shorter alkyl chains on the cation. $\pi^+-\pi^+$ interactions were competitive in the imidazolium

dicyanamide structures for imidazolium cations with longer alkyl chains and were not favourable for any of the imidazolium tetrafluoroborates. Hence, it was found that the preferred arrangements of smaller-sized clusters of ionic liquids are dependent on the nature and size of the anion as well as the cation. Therefore, it is important to identify reliable and cost-effective quantum chemical methods that can be applied to studying the geometry and energetics of large-scale clusters of ionic liquids.

Locating all possible minima becomes an arduous task when the cost of quantum chemical methods used is considered. Density functional theory (DFT) has become popular for studying clusters of ionic liquids due to its low cost.^{41,42} Early DFT functionals based on the generalised gradient approximation (GGA) such as PBE,⁴³ BLYP^{44,45} and PW91⁴⁶ fell short of the accurate prediction of interaction energies in pyrrolidinium-based ion pairs, producing errors above 14 kJ mol⁻¹.⁴⁷ Inclusion of 54% of Hartree-Fock (HF) exchange in a meta-GGA functional, such as M05-2X,⁴⁸ reduced the error to within chemical accuracy. Grimme's development of the empirical dispersion correction, especially its third generation, D3,⁴⁹⁻⁵¹ greatly improved the description of non-covalent interactions in the S22 dataset at equilibrium and extended intermolecular distances. In the context of ionic liquids, DFT functionals augmented with the D3 correction have been tested to study the potential energy curve of imidazolium single ion pairs as a function of the cation to anion distance.⁵² Interaction energy errors with respect to CCSD(T)/CBS were within chemical accuracy for all D3 corrected functionals (B3LYP-D3, revPBE-D3 and revPBE38-D3) at the equilibrium interaction energy, however larger deviations occurred at shorter distances. Dispersion effects were also shown to be important in ionic liquids driven by hydrogen bonding as in the case of imidazolium-based ionic liquids.⁵³

Hunt demonstrated that for 1-butyl-3-methyl-imidazolium chloride and 1-butyl-2,3-dimethyl-imidazolium chloride B3LYP/6-31++G(d,p) could only provide to a qualitative description of the located configurations of single ion pairs as the dispersion effects could not be fully recovered.⁴⁰ Hunt and Gould compared the performance of B3LYP, MP2 and CCSD(T) for studying energetics of single ion-paired configurations of 1-butyl-3-methylimidazolium chloride.⁵⁴ B3LYP/ 6-31++G(d,p) was unable to correctly determine their relative stability. MP2/6-31++G(d,p) was found to be a superior choice by correctly predicting the relative stability when compared to CCSD(T)/aug-cc-pVDZ. B3LYP/ 6-31++G(d,p) performed poorer in configurations, in which the chloride interacted with the cation above the imidazolium ring. Matthews *et al.* optimised clusters of two ion pairs of 1,3-dimethylimidazolium (C_{1mim}^+) chloride, nitrate, methyl sulfate, trifluoromethanesulfonate and tetrafluoroborate with B3LYP-D3/6-311+G(d,p) to study structural and energetic differences.⁵⁵ The dominant structure of the cation with the chloride anion had the imidazolium rings stacked in an antiparallel orientation, with an alternating charge structure being only 3.3 kJ mol⁻¹ higher in energy. On the other hand, for $[C_{1mim}][NO_3]$ and $[C_{1mim}][CH_3SO_4]$ the $\pi^+-\pi^+$ stacked configuration was > 6.4 kJ mol⁻¹ higher in energy than that with an alternating charge. The ionic liquids of the larger anions (with the exception of chloride) favoured an alternating charge structure. A further study used B3LYP-D3/aug-cc-pVTZ to optimise clusters of single and double ion pairs of 1,3-dimethylimidazolium chloride.⁵⁶ Both alternating charge and $\pi^+-\pi^+$ stacked ion pair configurations were found to have similar energetics.

Dispersion also appears to be well accounted for when using meta-GGA functionals with 54% of the HF exchange, such as M05-2X and M06-2X, when applied to a database consisting of single ion pairs of commonly used aprotic ionic liquids, IL174.^{47,57} In this study B3LYP was used for geometry optimisation of pyrrolidinium-based ion pairs, whereas MP2 was applied for

imidazolium-based ones. 16 different DFT functionals applied to the IL174 database found that the addition of diffuse functions to double- ζ basis sets improved interaction energies when paired with GGA, meta-GGA and GGA DFT-D functionals compared to triple- ζ basis sets without any diffuse functions.⁵⁸ GGA and meta-GGA functionals with the D3 empirical correction and triple zeta basis set performed well when compared to the benchmark interaction energies calculated with the gold standard method, a coupled cluster method with singles and doubles and non-iterative triples, CCSD(T) within the complete basis set (CBS). Out of the DFT functionals used, M06-2X and TPSS-D3 coupled with the 6-311++G(3df,2p) basis set performed the best with a mean absolute error (MAE) of 4.1 and 4.7 kJ mol⁻¹, respectively. PBE-D3 and BLYP-D3 with the same basis set obtained mean absolute errors of 5.1 and 5.2 kJ mol⁻¹, respectively. BP86-D3 had a higher mean absolute error of 8.3 kJ mol⁻¹. PBE, without the dispersion correction, outperformed other GGA functionals - BP86 and BLYP - with a mean absolute error of 11.4 kJ mol⁻¹, BP86 and BLYP had MAEs > 20 kJ mol⁻¹. An MAE of 5.3 kJ mol⁻¹ was produced by a hybrid functional, B3LYP-D3, which is an improvement by 17.1 kJ mol⁻¹ over the B3LYP functional itself.

Garcia *et al.* published a benchmarking study of DFT functionals and their performance in the prediction of binding energy of single ion pairs of 54 ionic liquids.⁵⁹ Geometries that were initially optimized with B3LYP/6-31G*, were re-optimised with a range of functionals including PBE, BLYP, PBE-D2, B3LYP-D2, ω B97X-D and M06-2X and basis sets 6-31G*, 6-31+G**, 6-311+G** and aug-cc-pVDZ. Geometries and energies were compared to those of MP2/aug-cc-pVDZ. B3LYP-D2/6-31+G* obtained an RMSD of interaction energy in single ion pairs of 3.5 kJ mol⁻¹, whereas the geometries had slightly shortened intermolecular distances resulting in larger dispersion energies compared to the benchmark. The PBE and B3LYP functionals with and without dispersion corrections with 6-31+G** led to very small RMSDs in geometry. ω B97X and

ω B97X-D had equally small RMSDs for geometry and deviated below 2 kJ mol⁻¹ on average for binding energies regardless of the basis set used. Their excellent performance was attributed to a better description of charge-transfer. Overall, all studied functionals produced geometries within chemical accuracy when compared to MP2/aug-cc-pVDZ.

Firaha *et al.* investigated the effect of dispersion corrected functionals in *ab initio* molecular dynamics.⁶⁰ 32 ion pairs of 1-butyl-3-methylimidazolium triflate with BLYP and BLYP-D3 were simulated with periodic boundaries. The inclusion of D3 corrections resulted in shorter interionic distances between the cations and anions. RDF peaks corresponding to interionic hydrogen bonds occurred at longer distances and had larger intensities suggesting that either the frequency of hydrogen bonds increases or they become stronger. This observation was also accompanied with a decrease in alkyl-alkyl interactions and hence, microheterogeneity in the system.

Single ion pairs of 8 imidazolium-based ionic liquids were optimised with a series of DFT functionals ranging from GGA to hybrid and meta-GGA functionals and the 6-311+G(d,p) basis set by Lage-Estebanez and compared with MP2 geometries.⁶¹ MP2/311+G(d,p) was used as a benchmark method. Dispersion played a larger role in determining the position of asymmetric anions. For example, in ion pairs of 1,3-dimethylimidazolium thiocyanate and 1-ethyl-3-methylimidazolium dicyanamide, the functionals without the empirical dispersion correction favoured configurations, in which the anion interacted in the plane of the ring. Inclusion of the empirical dispersion correction the anion optimised to above/below the imidazolium ring. The M06 family of functionals optimized to similar structures. The interionic distance in the ion pair of 1,3-dimethylimidazolium thiocyanate decreased by 1 Å when dispersion-corrected functionals were used, which closely resembled the MP2 optimized geometry. On the other hand, the

dispersion correction had no effect on the interionic distance in the ion pair of 1-ethyl-3-methylimidazolium thiocyanate. Overall, M06-2X and M06-L had the lowest mean absolute errors below 4.7 kJ mol^{-1} , followed by wB97X-D with an MAE of 7.2 kJ mol^{-1} .

Perlt *et al.* calculated the dissociation energy curves of a 3 ion-paired cluster of ethylammonium nitrate and a 2 ion-paired cluster of 1-ethyl-3-methylimidazolium acetate using the domain-based local pair natural orbital (DLPNO) implementation of the CCSD(T) method as the benchmark. The performance of a series of DFT functionals were tested for the prediction of these dissociation curves.⁶² Goedecker-Teter-Hutter pseudopotentials for the core electrons and the TZVP basis set for the valence electrons were used in combination with these functionals. Although London dispersion forces were again highlighted as being crucial in studying ionic liquids, the performance of the chose functionals varied depending on the nature of ionic liquid. B3LYP-D3 and PBE0-D3 produced the lowest mean absolute deviations below 2.5 kJ mol^{-1} for both ionic liquids, with the composite method, B97-3c, producing an equally good performance. On the other hand, dispersion-corrected GGA functionals such as PBE-D3 and BP86-D3 had mean absolute deviations $> 7.5 \text{ kJ mol}^{-1}$. A study by Karu *et al.*⁶³ also identified that the inclusion of the empirical dispersion correction, D3, reduced mean average errors of PBE, SCAN and a double hybrid functional, B2LYP, when applied to studying interaction energies of single ion pairs of ionic liquids consisting of 4 different cations including pyridinium and ammonium ones and 12 different anions ranging from halides to dicyanamides. All three functionals gave MAEs below 4.7 kJ mol^{-1} , although maximum deviations of 15 kJ mol^{-1} and 17.7 kJ mol^{-1} were observed for PBE-D3 and SCAN-D3.

Geometry optimisations are the cornerstone of any investigation into energetics and properties of ionic liquids. Many studies described above detail the performance of DFT

functionals for the prediction of energetics of ionic liquids. This was achieved by applying these functionals to “static” geometries that were optimized at a constant level of theory – usually a DFT functional such as B3LYP. It is not clear how these functionals fair in geometry optimisation of large-scale clusters of ionic liquids and how their systematic errors influence the resulting arrangement of ions. In order to make a fair comparison large-scale clusters must be optimized with a benchmark method. The fragment molecular orbital approach (FMO)^{64–68} including three-body corrections (FMO3)^{69,70} has been validated in ionic liquid clusters and reproduces the conventional MP2 energies to within 0.2 kJ mol⁻¹ per ion pair at a significantly reduced cost.^{20,21} By dividing a large system into smaller fragments which can be treated at a high level of ab initio theory, the calculation scales linearly with molecular size. In this work, the FMO3 approach is paired with the spin-ratio scaled MP2 (SRS-MP2), that reproduces the gold standard method, CCSD(T)/CBS, to within 2 kJ mol⁻¹ per ion pair without the need for counterpoise correction.^{71,72}

This study investigates the performance of DFT functionals and MP2-based methods for geometry optimisation by applying them to a series of ionic liquid clusters consisting of two and four ion pairs. Four Dunning’s basis sets, cc-pVDZ, aug-cc-pVDZ, cc-pVTZ and aug-cc-pVTZ, were used with each selected level of theory. Two imidazolium-based ionic liquids coupled with the chloride and tetrafluoroborate anions were considered in constructing 2 ion-paired clusters. The former is a strongly coordinating anion, whereas the latter belongs to the weakly coordinating type, and thus represent excellent models for ionic liquid anions commonly used. For both ionic liquids, the lowest energy configurations located in our previous study were used as starting geometries. The best performing combinations of functionals/basis sets identified for the 2 ion-paired clusters were further considered in geometry optimisations of four ion paired structures of a series of ionic liquids based on the 1,3-dimethylimidazolium, N,N’-dimethylpyrrolidinium,

tetramethylammonium and N-methylpyridinium cations coupled with the Cl^- and BF_4^- anions. The performance of each DFT functional was compared to the geometries optimized with the benchmark method, FMO3-SRS-MP2/cc-pVTZ. Geometry and energetic criteria used to assess the performance included root mean squared deviations in geometry, total electronic energies calculated at the benchmark level of theory, and interaction energies and their Hartree-Fock and correlation components also calculated with FMO3-SRS-MP2/cc-pVTZ. Finally, recommendations for the best combinations of DFT functionals/basis sets were given for geometry optimisation of large-scale ionic liquid clusters.

Theoretical Calculations

Two ion-paired (2IP) low energy structures of ionic liquids 1-methyl-3-methylimidazolium tetrafluoroborate ($[\text{C}_1\text{mim}][\text{BF}_4]$) and chloride ($[\text{C}_1\text{mim}]\text{Cl}$), were first optimised with FMO2-SRS-MP2/cc-pVDZ and then DFT functionals and wavefunction-based methods were used for subsequent geometry optimisation.⁷³ The 2 ion-paired lower energy structures were taken from the previous study, in which a full configurational screen was performed for imidazolium-based ionic liquids.¹⁸ The two lower-energy configurations of $[\text{C}_1\text{mim}][\text{BF}_4]$ shown in Figure 1 have an alternating charge arrangement in conf1 and a T-shape arrangement of the imidazolium cations in conf2. One of the structures of $[\text{C}_1\text{mim}]\text{Cl}$ include the $\pi^+-\pi^+$ stacking of the imidazolium cations with the anions interacting with the C2-H bond in the plane of the ring in conf1. The second structure, conf2, had the anions exhibiting two modes of interaction - above the imidazolium ring and with the C2-H bond.

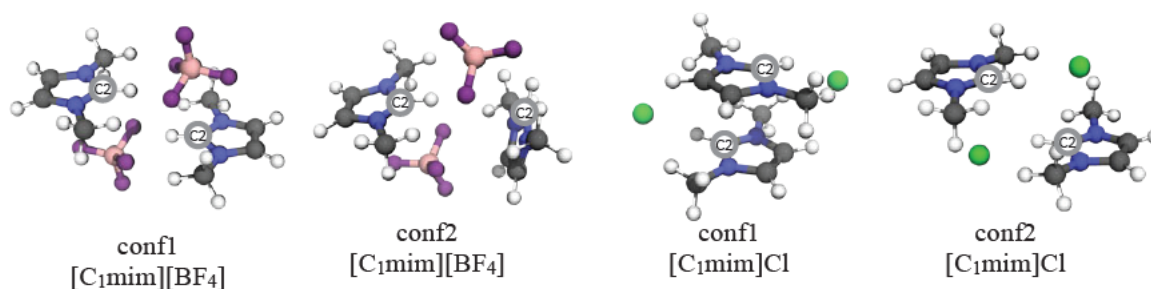


Figure 1. Two starting two ion-paired structures denoted as conf1 and conf2) of [C1mim][BF4] and [C1mim]Cl.

Seven density functionals and variations of wavefunction-based second-order Møller-Plesset perturbation method (MP2) were used for geometry optimisation. The following functionals were used:

- 1) General Gradient Approximation (GGA) functionals BLYP (B88 exchange⁴⁴ + LYP correlation⁴⁵), BP86 (B88 + P86⁷⁴) and PBE,⁴³
- 2) meta-GGA functional M06-2X,⁷⁵
- 3) hybrid functional B3LYP,⁷⁶
- 4) long-range corrected hybrid density functional ω B97X-D,⁷⁷
- 5) GGA-D3 BLYP-D3, BP86-D3 and PBE-D3,
- 6) meta-GGA + D3 functional– TPSS-D3⁷⁸ and
- 7) hybrid DFT + D3 functional – B3LYP-D3.

GGA functionals, PBE and BLYP, are used in research of condensed systems due to their compromise between cost and accuracy. Notably, they are used in *ab initio* molecular dynamics

simulations of ionic liquids to account for electron correlation and charge transfer between ions.^{79,80} These functionals as well as BP86 have been shown to improve greatly with the addition of empirical dispersion corrections and their reduced cost gives them priority over higher level functionals if they produce accurate geometries especially moving towards larger number of ion pairs.⁴⁹ A meta-GGA functional, M06-2X, a hybrid functional, B3LYP, and a long-range corrected functional, ω B97X-D, are extremely popular functionals and have been used extensively for optimisations of ionic liquids in the literature.^{81–91} Meta-GGA functional with D3 correction TPSS-D3 has previously been shown to perform well for single ion paired systems.⁵⁸

Wavefunction-based methods MP2⁹² and aforementioned SRS-MP2 were additionally used. SRS-MP2 calculations were performed according to the fragment molecular orbital approach (FMO) and include two- and three-body effects without any approximations and cutoffs.^{64,69} These methods were used with Dunning's correlation consistent basis sets: cc-pVDZ, cc-pVTZ, aug-cc-pVDZ and aug-cc-pVTZ, and are abbreviated in this text as VDZ, VTZ, aVDZ and aVTZ, respectively.^{93–95}

Accurate, "gold standard", CCSD(T) is limited to small and medium-sized clusters due to a scaling of N^7 , where N is the system size. MP2 provides a reasonable accuracy at a reduced scaling of N^5 , although it tends to overestimate correlation energy.⁹⁶ The accuracy of MP2 decreases however when treating van der Waals complexes.⁹⁷ The original modification of MP2, spin-component scaled MP2^{98,99} (SCS-MP2) by Grimme, provides higher quality reaction energies⁹⁷ by scaling the opposite- (E_{OS}) and same-spin (E_{SS}) components of the correlation energy (E_{corr}) where:

$$E_{corr} = c_{OS}E_{OS} + c_{SS}E_{SS} \quad (1)$$

The original SCS-MP2 method obtained the scaling coefficients through modelled on 51 chemical reactions of neutral molecules.⁹⁹ Parametrisation of the SRS-MP2 coefficients included the intermolecular datasets S22 and S66, commonly used for benchmarking quantum chemical methods, as well as 174 ion pairs from the IL174 dataset. The c_{OS} and c_{SS} coefficients were fitted to reproduce CCSD(T)/CBS by determining the optimum scaling coefficients.⁷¹ These coefficients depended on the extent of London dispersion forces, with dispersion-driven systems consistently producing the ratio > 1.0 . The parametrisation was also achieved without the need to introduce counterpoise correction in the MP2 correlation energy. An average error of 1.4 kJ mol^{-1} was obtained for the cc-pVTZ basis set. Due to the cost and excellent performance of the SRS-MP2 method for ionic liquids, it was considered the benchmark method in this study. Energies of all optimised geometries were improved with FMO3-SRS-MP2/cc-pVTZ and compared with those of the optimised FMO3-SRS-MP2/cc-pVTZ geometry.

A subset of these DFT- and MP2-modified methods were also used on a more diverse range of four ion-paired clusters of ionic liquids: $[\text{C}_1\text{mim}][\text{BF}_4]$; $[\text{C}_1\text{mim}]\text{Cl}$; N,N'-methyl-methylpyrrolidinium tetrafluoroborate ($[\text{C}_1\text{mpyr}][\text{BF}_4]$) and chloride ($[\text{C}_1\text{mpyr}]\text{Cl}$); tetramethylammonium tetrafluoroborate ($[\text{NMe}_4][\text{BF}_4]$) and chloride ($[\text{NMe}_4]\text{Cl}$); and 1-ethylpyrrolidinium tetrafluoroborate ($[\text{C}_2\text{py}][\text{BF}_4]$) and chloride ($[\text{C}_2\text{py}]\text{Cl}$). Four ion-paired clusters were previously optimised with FMO2-MP2/cc-pVDZ.²¹

Interaction energies (E_{INT}) were calculated via the following expression:

$$E_{INT} = E_{cluster} - \sum_i^{ions} E_i(ion) \quad (2)$$

where the ions were taken in the geometry adopted in the corresponding cluster. The SRS-MP2 method already accounts for the basis set superposition error due to the parameterised coefficients in the MP2 correlation energy. Counterpoise corrections for the HF level of theory were not considered as they were expected to be similar across the clusters studied and therefore, none of the conclusions drawn in the study should be affected. Interaction energies were divided into their HF component, which is predominantly electrostatics with some induction, and the correlation component that reliably captures London dispersion forces.

Differences in geometries were also analysed with root mean square deviations (RMSDs):

$$RMSD = \sum_i^{atom} \|a_i - b_i\|^2 \quad (3)$$

where a and b are vectors consisting of the Cartesian coordinates of the same atom, i , present in the two structures compared. The RMSD of each DFT functional/method was determined with respect to the benchmark geometry. Positions of all atoms were included in eq. 3.

Mean absolute errors (MAEs), and standard deviations (SDs) were used in the analysis of total and interaction energies. For each DFT functional/method the standard deviation was calculated using the following expression:

$$SD = \sqrt{\sum_i^N (x_i - \bar{x})^2 / (N - 1)} \quad (4)$$

where N is the number of geometries compared, x_i is the energy deviation of each geometry, and \bar{x} is the mean deviation of the given functional/method for all N geometries.

DFT calculations were carried out with Gaussian 09,¹⁰⁰ conventional MP2 calculations were performed with PSI4¹⁰¹ and fragment molecular orbital calculations were performed with GAMESS-US.⁶⁷

Interionic distances were calculated as distances between chemically accepted centres of ions labelled in Figure 2. All cation-anion distances in 2 and 4 ion-paired clusters were averaged. In addition, all cation-anion and anion-anion distances were averaged in 4 ion-paired clusters.

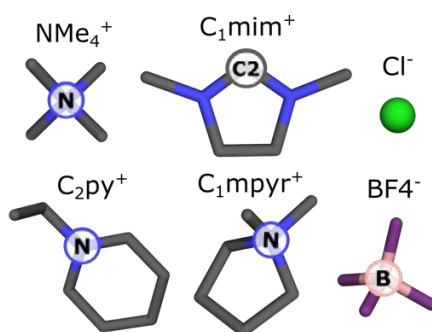


Figure 2. Positions used to calculate interionic distances.

Results and Discussion

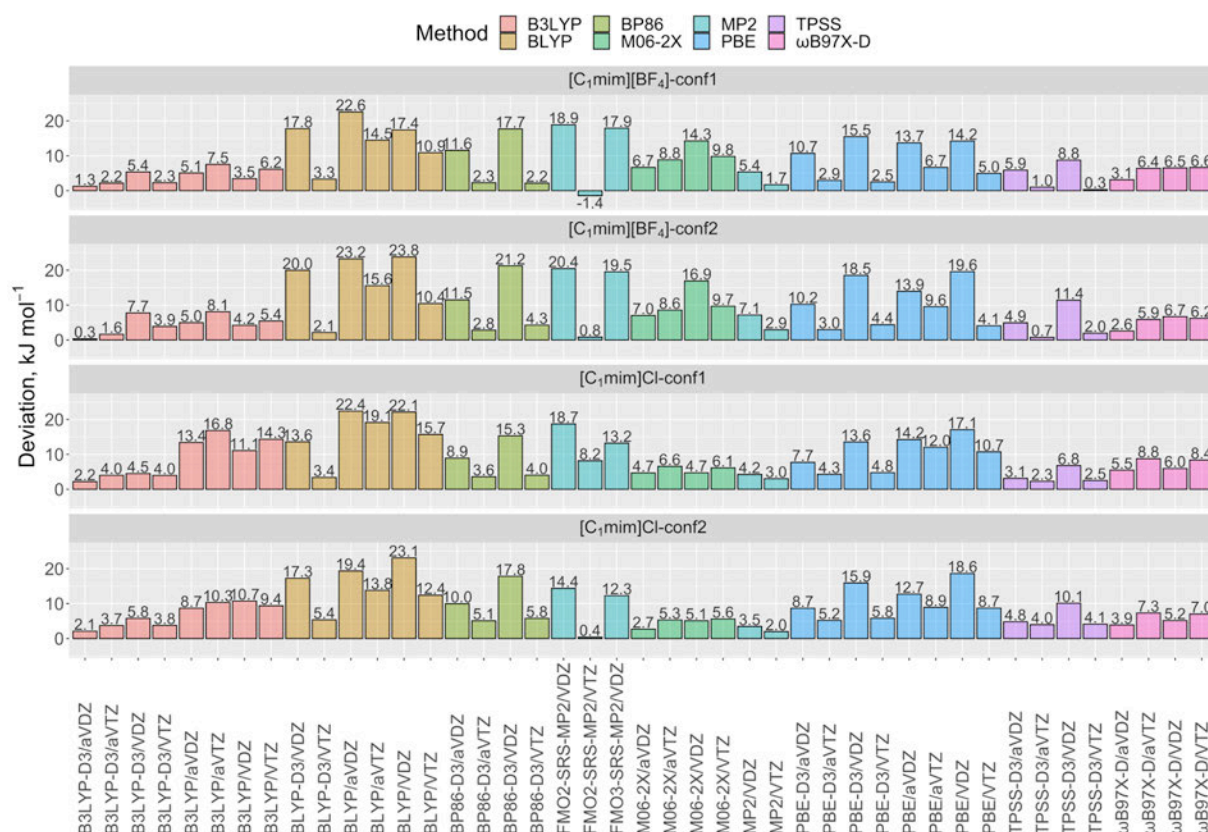


Figure 3. Deviations in total electronic energies of 2 ion-paired clusters with respect to FMO3-SRS-MP2/cc-pVTZ optimized geometry. Single point calculations performed with FMO3-SRS-MP2/cc-pVTZ for each geometry from the functional/method of optimisation (x axis).

Two ion pairs: influence of basis set on DFT functional performance

In order to understand the effect that each level of theory imposes on geometry, single point calculations were performed with the benchmark method – FMO3-SRS-MP2 in combination with Dunning’s cc-pVTZ basis set. Deviations of the resulting total electronic energies were calculated with respect to the total electronic energy of the structure optimized with FMO3-SRS-MP2/VTZ and are presented in Figure 3. Therefore, these deviations are indicative of the overall performance of each DFT functional/MP2-based method. Fig. 3 shows a comparison of these deviations for the

2 ion-paired geometries obtained from geometry optimisation of 2 different configurations of [C₁mim][BF₄] and [C₁mim]Cl, *i.e.* 4 clusters in total (for more detail see Figure 1). We screened all possible configurations of 2 ion-paired clusters of these ionic liquids in our previous work.¹⁸ In this study, the two lower energy configurations for each ionic liquid were chosen to perform geometry optimizations with varying levels of theory. The mean average values across these four clusters are given in Table 1. A lower bar in Fig. 3 indicates that on the potential energy surface the optimized geometry with a given method is closer to the benchmark method. All deviations were found to be positive, thus reinforcing the confidence in the benchmark method used. Only one exception was found in the case of the FMO2-SRS-MP2/cc-pVTZ optimisation of conf1 of [C₁mim][BF₄], where a geometry of a slightly lower energy by 1.4 kJ mol⁻¹ with respect to the benchmark was located.

For Dunning's cc-pVDZ basis set, three functionals, B3LYP-D3, ω B97X-D and B3LYP, were found to be the best performing functionals, with average mean errors of 5.8, 6.1 and 7.4 kJ mol⁻¹, respectively. A good performance of ω B97X-D is expected as it accounts for long-range correlation, whereas an excellent performance of B3LYP is rather unusual, considering the empirical dispersion correction does not compensate for the insufficient description of London dispersion forces. Notably, B3LYP outperforms functionals such as BP86-D3 (18.0 kJ mol⁻¹), M062-X (10.2 kJ mol⁻¹), PBE-D3 (15.9 kJ mol⁻¹) and TPSS-D3 (9.3 kJ mol⁻¹), with average mean errors given in brackets. As expected, FMO2-SRS-MP2 (18.1 kJ mol⁻¹) and FMO3-SRS-MP2 (15.7 kJ mol⁻¹), do not fare well in combination with cc-pVDZ. The best performing method overall is conventional MP2, with an average deviation of slightly above chemical accuracy of 5.1 kJ mol⁻¹.

Upon using the cc-pVTZ basis set, FMO2-SRS-MP2 unsurprisingly attains the geometry closest to the benchmark method with an average difference of only 2.0 kJ mol⁻¹. Functionals without the explicit dispersion correction, D3, namely B3LYP (8.8 kJ mol⁻¹), BLYP (12.4 kJ mol⁻¹) fair worse than B3LYP-D3 (3.5 kJ mol⁻¹), BP86-D3 (4.1 kJ mol⁻¹), PBE-D3 (4.4 kJ mol⁻¹) and TPSS-D3 (2.2 kJ mol⁻¹) where the latter is the best performing DFT functional (their average mean errors are given in brackets). The two functionals designed to accurately account for dispersion forces in non-covalently bound systems, M06-2X and ω B97X-D, produce errors of 7.8 and 7.1 kJ mol⁻¹, respectively, outside of chemical accuracy. Conventional MP2 performs only marginally worse than FMO2-SRS-MP2, with the average energy difference of 0.4 kJ mol⁻¹.

Going from the cc-pVDZ basis set to the cc-pVTZ basis set, the geometries of B3LYP and ω B97X-D become only marginally higher in energy by 1.2 kJ mol⁻¹ and 1.0 kJ mol⁻¹, respectively, which indicates small dependence of the functional on the basis set. While BLYP almost halves the associated error, the average difference of 12.4 kJ mol⁻¹ is still large. The most dramatic changes are seen in BP86-D3 and FMO2-SRS-MP2, whose difference to the benchmark decrease by 13.9 and 16.1 kJ mol⁻¹, respectively. In accordance with these results, the incorporation of the D3 correction has a large positive impact when paired with cc-pVTZ.

The switch to aug-cc-pVDZ led to geometries closer to the benchmark and lower average relative energies in the case of B3LYP-D3 (1.5 kJ mol⁻¹), M06-2X (5.3 kJ mol⁻¹) and ω B97X-D (3.8 kJ mol⁻¹) (their average mean errors are given in brackets). The best performing functional for geometry optimisation was found to be B3LYP-D3, whose average error is as little as 1.5 kJ mol⁻¹, which is 0.5 kJ mol⁻¹ lower in energy than any of the MP2 variants. In the case of B3LYP, BLYP, BP86-D3, PBE, PBE-D3 and TPSS-D3, the aug-cc-pVDZ basis set produced geometries similar

to the cc-pVTZ basis set. It has to be noted that SRS-MP2 does not perform well with Dunning's augmented basis sets and therefore, these basis sets were not used in combination with the conventional and modified MP2 methods.^{71,72}

Table 1. Average deviations in total electronic energy of varying levels of theory (kJ mol^{-1}) with respect to the benchmark geometry with FMO3-SRS-MP2/cc-pVTZ. Single point calculations performed with FMO3-SRS-MP2/cc-pVTZ for each geometry from the functional/method of optimisation. The last column provides the best performing basis set for each level of theory.

	VDZ	VTZ	aVDZ	aVTZ	Best performance
B3LYP	7.4	8.8	8.0	10.7	VDZ
B3LYP-D3	5.8	3.5	1.5	2.9	aVDZ
BLYP	21.6	12.4	21.9	15.7	VTZ
BLYP-D3	17.2	3.6	-	-	VTZ
BP86-D3	18.0	4.1	10.5	3.4	aVTZ
M06-2X	10.2	7.8	5.3	7.3	aVDZ
PBE	17.4	7.1	13.7	9.3	VTZ
PBE-D3	15.9	4.4	9.3	3.9	aVTZ
TPSS-D3	9.3	2.2	4.7	2.0	aVTZ
ω B97X-D	6.1	7.1	3.8	7.1	aVDZ
MP2	5.1	2.4	-	-	VTZ
FMO2-SRS-MP2	18.1	2.0	-	-	VTZ
FMO3-SRS-MP2	15.7	0.0	-	-	VTZ

The use of Dunning's aug-cc-pVTZ basis set does not bring significant changes to the performance of the majority of the DFT functionals employed, with average deviations within chemical accuracy when compared with the cc-pVTZ and aug-cc-pVDZ basis sets. Majority of these differences do not justify the use of this significantly larger basis set. For example, TPSS-D3 produced geometries similar to those with cc-pVTZ with a negligible energy difference of 0.2 kJ mol^{-1} . It was found to be the best performing functional with the average error of 2.0 kJ mol^{-1} .

BP86-D3 and PBE-D3 also had errors within chemical accuracy of 3.4 and 3.9 kJ mol⁻¹, respectively. Contrary to this, best performing functionals with the cc-pVDZ basis set - B3LYP and B3LYP-D3 - optimized to geometries higher in energy by further 2.7 and 1.4 kJ mol⁻¹, respectively. BP86-D3, TPSS-D3 and PBE-D3 show the best performance when combined with aug-cc-VTZ. The reduction in error within 1 kJ mol⁻¹ compared to that for cc-pVTZ does not balance a significant increase in computational resources required for the introduction of additional diffuse functions in the basis set.

To this end, the following combinations of DFT functionals and basis sets are recommended for geometry optimisations of larger clusters of imidazolium-based ionic liquids within chemical accuracy (average errors are given in brackets): B3LYP-D3/aVDZ (1.5 kJ mol⁻¹), FMO2-SRS-MP2/VTZ (2.0 kJ mol⁻¹), TPSS-D3/aVTZ (2.0 kJ mol⁻¹), TPSS-D3/VTZ (2.2 kJ mol⁻¹), MP2/VTZ (2.4 kJ mol⁻¹), B3LYP-D3/aVTZ (2.9 kJ mol⁻¹), BP86-D3/aVTZ (3.4 kJ mol⁻¹), B3LYP-D3/VTZ (3.5 kJ mol⁻¹), BLYP-D3/VTZ (3.6 kJ mol⁻¹), ω B97X-D/aVDZ (3.8 kJ mol⁻¹) and PBE-D3/aVTZ (3.9 kJ mol⁻¹). In terms of the cost vs accuracy compromise B3LYP-D3/aVDZ, TPSS-D3/VTZ and FMO2-SRS-MP2/VTZ are highly recommended for future studies.

Two ion pairs: influence of DFT functional on geometry and interaction energy

The differences in geometry can be assessed by separating the interaction energy into HF (predominantly electrostatics) and electron correlation (predominantly dispersion) components. Figure 4 shows deviations of interaction energy and its components – HF and correlation - calculated for the two-ion paired clusters optimized at the selected levels of theory. For comparison, interaction energy calculations were performed for all optimized geometries with the benchmark method, FMO3-SRS-MP2/cc-pVTZ. This comparison does not identify the

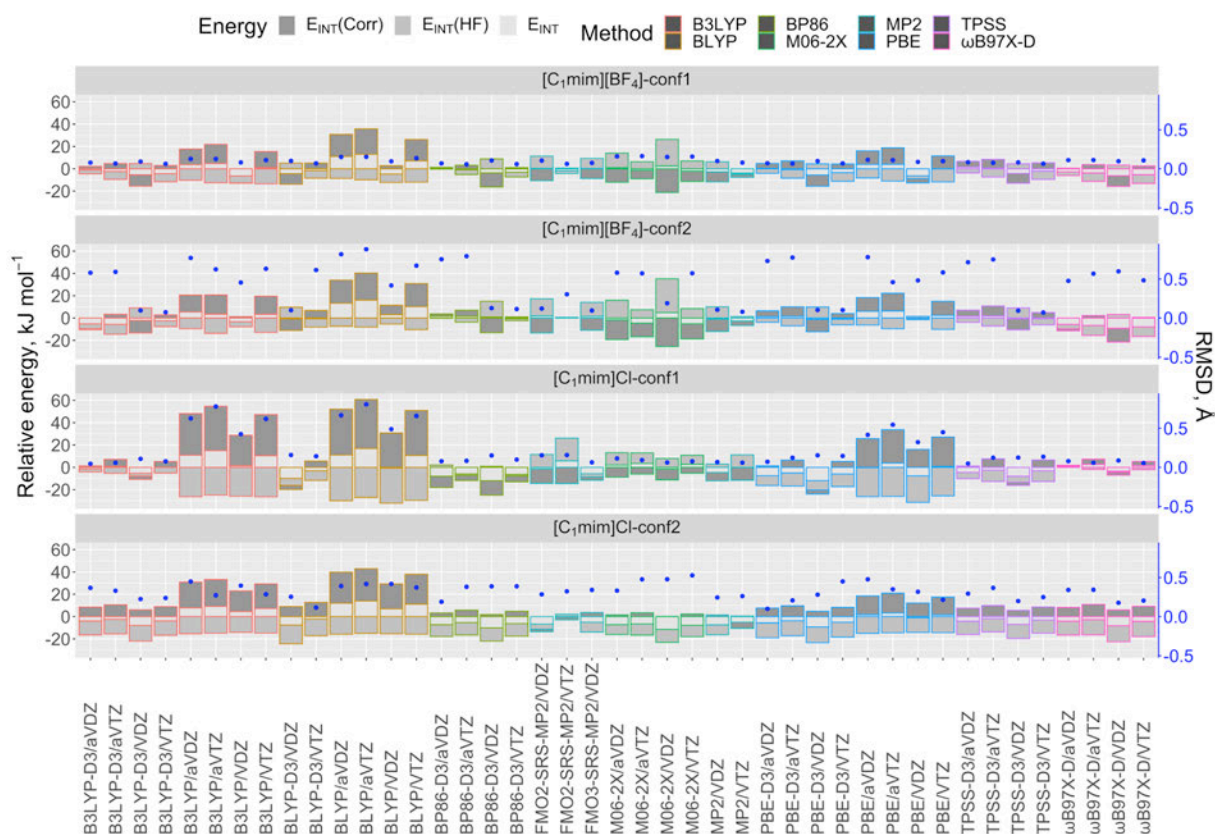


Figure 4. Deviations of total electronic energy from the FMO3-SRS-MP2/cc-pVTZ optimized geometry together with relative correlation (Corr) and Hatree-Fock (HF) interaction energy components (left y axis) and RMSDs in Å (right y axis) of 2 ion-paired clusters. Single point calculations performed with FMO3-SRS-MP2/cc-pVTZ for each geometry from the method of optimisation (x-axis). All energies are given in in kJ mol^{-1} .

accuracy of each DFT functional. Instead, it allows us to analyse the proximity of these optimized structures to the benchmark ones. Additionally, average RMSD values with respect to geometry are given to further ascertain this proximity. These energetic and geometric quantities are broken down by basis set and functional/method further in the text.

The 2 ion-paired clusters of [C₁mim][BF₄] optimized with FMO3-SRS-MP2/cc-pVTZ have very similar HF and correlation components of interaction energy. Both are within chemical accuracy, which is not surprising since their total energies differ within 1 kJ mol⁻¹. Despite the similarity in interaction energies, these configurations have a rather different arrangement of ionic liquid ions. The parallel arrangement of the imidazolium rings in conf1 leads to the C2...C2 interionic distance of 4.3 Å, while this distance elongates to 4.7 Å in the T-shaped conf2, in which the imidazolium rings are perpendicular to each other. Similarly, the B...B interionic distance is slightly longer by 0.2 Å in conf2. On average, the C2...B distances in these configurations are similar and are measured at 3.4 and 3.6 Å for conf1 and conf2, respectively, thus resulting in similar interaction energies.

The 2 ion-paired clusters of [C₁mim]Cl optimised with FMO3-SRS-MP2/VTZ also have a tiny difference of interaction energy of 1.9 kJ mol⁻¹. In this case, the difference is accompanied with larger deviations in the HF and correlation components of interaction energy between conf1 and conf2. The alternating charge structure in conf2 has a larger interaction HF energy by 16.5 kJ mol⁻¹. The $\pi^+-\pi^+$ stacking of the imidazolium rings in conf1 leads to a geometry that is stabilised through dispersion energy by 18.4 kJ mol⁻¹ compared to that of conf2. Stark differences in interaction energy components are reflected in interionic distances. The C2...C2 distances in conf1 and conf2 are 3.5 and 4.1 Å, respectively. A similar trend is observed in the cation-anion distances. The average C2...Cl distance is 3.9 Å for conf1 and a much shorter 3.2 Å for conf2.

Overall, total interaction energies differ from the benchmark in a range spanning nearly 29 kJ mol⁻¹ from -12.0 to 16.9 kJ mol⁻¹. There are no distinct trends when interaction energy becomes above or below that of the benchmark method. In our previous systematic work on the analysis

of total and interaction energies in lower-energy two-ion paired clusters of imidazolium- and pyrrolidinium-based ionic liquids, we established that structures with the strongest interaction energy do not necessarily have the lowest total energy due to the subtraction of deformation energies of ionic liquid ions in the former.¹⁸ Therefore, negative deviations of interaction energies from the benchmark should be considered with caution as these are not indicative of the level of theory locating a lower energy minimum. These deviations reveal subtle differences in the optimized structures with respect to the benchmark method. As discussed above, all DFT functionals/MP2-based methods produced positive deviations in their total energies of optimized structures of the 2 ion-paired clusters.

Across all the chosen levels of theory, the optimized geometries of conf1 of [C₁mim][BF₄], representing an alternating charge arrangement, have RMSDs < 0.2 Å highlighting that the geometries do not change significantly after optimization regardless of the functional/method and basis set combination. In contrast, the T-shaped conf2 configuration optimizes to geometries with the highest median RMSD of 0.6 Å, with 17 combinations of methods/basis sets out of the possible 43 returning geometries with an RMSD deviation > 0.5 Å with respect to the benchmark. The deviations of geometry reflect the difficulty to correctly identify the minimum for some DFT functionals. Although conf2 of [C₁mim][BF₄] has a slightly larger correlation component by 1.3 kJ mol⁻¹ compared to that of conf1, when dispersion forces are not completely accounted for, this minimum does not seem to be properly captured on the potential energy surface by some DFT functionals. For example, the BLYP/aVTZ geometry of conf2 of [C₁mim][BF₄] has an RMSD of 0.9 Å. The HF component of interaction energy is more negative than the benchmark by 8.2 kJ mol⁻¹, whereas the correlation component is calculated to be weaker by as much as 24 kJ mol⁻¹.

In general, geometry optimisations of conf2 of [C₁mim]Cl generate structures with a larger average deviation in geometry from the benchmark with the median RMSD of 0.3 Å compared to that of 0.1 Å in conf1. The conf2 interionic distances between the anions decrease by 0.3 Å and the cations increase by 0.1 Å on median. The cation-anion distances have a median distance of 0.1 Å longer than that in the benchmark geometry. The $\pi^+-\pi^+$ stacked conf1 of [C₁mim]Cl has the lowest median RMSD of 0.1 Å for BLYP and B3LYP in combination with the VTZ, aVDZ and aVTZ basis sets, whereas PBE/aVTZ has the largest RMSDs of 0.5 to 0.8 Å. The remaining B3LYP, BLYP and PBE functional/basis set combinations exclusively have RMSD values above 0.3 Å. These functionals clearly fail to describe the $\pi^+-\pi^+$ stacking accurately. In the cases with RMSDs > 0.5 Å, the average distances between the chloride and the C2 position on the cation is consistent with the benchmark geometry, however the distance between the C2 positions on different cations increases between 0.9 and 1.1 Å. The latter observation makes the cations forgo the $\pi^+-\pi^+$ stacking in favour of the alternating charge arrangement.

The median RMSDs of the DFT-D3 functionals (0.1 – 0.2 Å) are consistently lower than the median values of B3LYP, BLYP and PBE (0.3 – 0.6 Å) (the range of median values are given in brackets). The maximum RMSDs of the B3LYP method with the four basis sets span a range of 0.5 to 0.8 Å, while B3LYP-D3 with the four basis sets fall in a range of 0.2 to 0.6 Å. The M06-2X median RMSDs are slightly larger than those of DFT-D3 functionals (0.2 to 0.3 Å) and their maximum RMSDs are consistently larger (0.5 to 0.6 Å). The median RMSDs of ω B97X-D vary between 0.1 to 0.2 Å, whereas the maximum RMSDs fall between 0.5 and 0.6 Å.

Performance of cc-pVDZ basis set

In this section geometry optimisations performed with the cc-pVDZ basis set are discussed. The mean and standard deviations of total electronic and interaction energies of the optimised structures together with mean and maximum RMSD values with respect to the FMO3-SRS-MP2/VTZ geometry are given in Table 2 for each DFT functional/MP2-based method.

Table 2. Two ion-paired clusters: Mean errors (Mean) and standard deviations (SD) for total electronic energy (Total Energy), interaction energy (E_{INT}), HF interaction Energy ($E_{\text{INT}}(\text{HF})$) and correlation interaction energy ($E_{\text{INT}}(\text{Corr})$) energies, mean and maximum RMSD values for each functional and MP2-based method with the cc-pVDZ basis set with respect to the FMO3-SRS-MP2/cc-pVTZ geometry. All energies are given in kJ mol^{-1} and RMSD is given in Å.

Theory	Total Energy		E_{INT}		$E_{\text{INT}}(\text{HF})$		$E_{\text{INT}}(\text{Corr})$		RMSD	
	Mean	SD	Mean	SD	Mean	SD	Mean	SD	Mean	Max
B3LYP	7.4	4.1	-1.0	4.9	-12.7	9.7	11.8	13.4	0.3	0.5
B3LYP-D3	5.8	1.4	-5.2	2.4	-0.7	10.1	-4.5	8.0	0.1	0.2
BLYP	21.6	2.9	1.1	5.1	-14.9	11.9	16.0	12.8	0.4	0.5
BLYP-D3	17.2	2.6	-5.7	4.0	-2.1	11.9	-3.6	9.0	0.2	0.3
BP86-D3	18.0	2.4	-6.2	6.0	3.0	11.3	-9.2	7.3	0.2	0.4
M06-2X	10.2	6.3	-1.4	7.2	12.6	18.7	-14.1	11.6	0.2	0.5
PBE	17.4	2.3	-3.7	3.8	-9.5	11.3	5.8	9.8	0.3	0.5
PBE-D3	15.9	2.0	-7.0	4.7	-2.0	11.1	-5.0	7.3	0.2	0.3
TPSS-D3	9.3	2.0	-5.0	3.3	-1.1	9.8	-3.9	7.1	0.1	0.2
ω B97X-D	6.1	0.7	-6.8	2.5	-2.2	8.3	-4.6	8.2	0.2	0.6
MP2	5.1	1.6	-3.9	2.7	2.6	8.2	-6.5	5.5	0.1	0.2
FMO2-SRS-MP2	18.1	2.6	-1.5	3.8	8.3	8.8	-9.8	5.2	0.2	0.3
FMO3-SRS-MP2	15.7	3.5	-2.3	3.7	2.5	10.0	-4.8	6.5	0.1	0.3

Compared to total energy, interaction energy does not deviate significantly from that of the benchmark method regardless of the DFT functional/MP2-based method used. The deviation falls in a narrow range of -6.8 kJ mol^{-1} to 1.1 kJ mol^{-1} , with an average standard deviation of 4.4

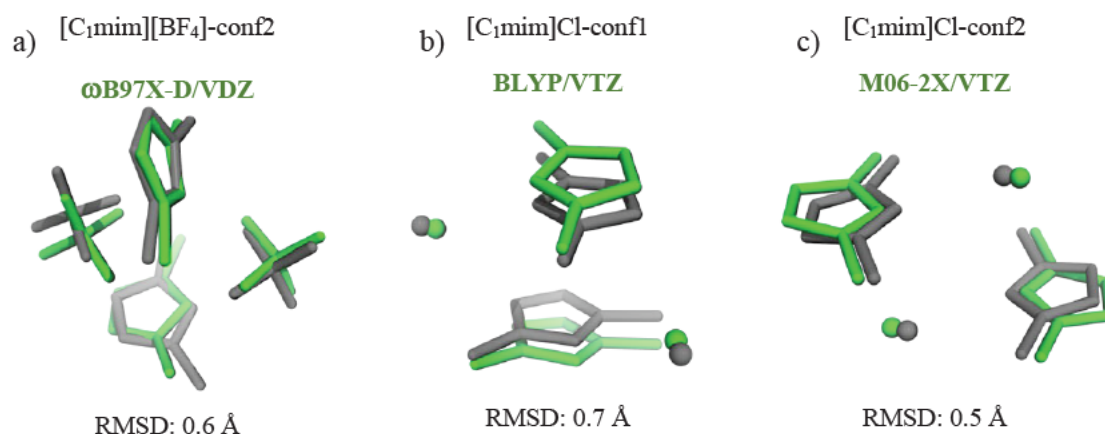


Figure 5. Alignment between the optimized geometry of DFT functional (green) and the optimized geometry of FMO3-SRS-MP2/cc-pVTZ (grey) and their RMSDs in two ion-paired clusters.

kJ mol^{-1} . This trend is accompanied with larger deviations in the HF and correlation components. In general, when the HF component becomes more negative, the correlation component appears to overcompensate by becoming less negative. Large standard deviations in these components $> 9 \text{ kJ mol}^{-1}$ indicate the presence of a systematic error in DFT functionals when carrying out geometry optimisations of ionic liquid clusters. Although the DFT functionals perform rather well on average with respect to the benchmark interaction energy, it is achieved through the error cancelation in the description of the HF and correlation components. Large discrepancies in energetic components result in RMSDs falling between 0.1 and 0.3 Å on average.

All four clusters of [C₁mim][BF₄] and [C₁mim]Cl with the smallest deviations of energy components (mean deviations in HF and correlation components are given in kJ mol^{-1} in brackets) come from dispersion-corrected functionals - B3LYP-D3 (-0.7, -4.5), BLYP-D3 (-2.1, -3.6), PBE-D3 (-2.0, -5.0), TPSS-D3 (-1.1, -3.9) and a range-separated functional, ω B97X-D (-2.2, -4.6). Average RMSDs for these functionals are among the smallest. For example, B3LYP-D3 and

ω B97X-D have average RMSDs of only 0.1 and 0.2 Å, respectively. There are some exceptions. The ω B97X-D largest RMSD of 0.60 Å is observed in conf2 of [C₁mim][BF₄] and its alignment with FMO3-SRS-MP2/VTZ is shown in Figure 5a. The largest deviation in geometries between these levels of theory lies in a displacement of one anion by 0.7 Å when optimized with ω B97X-D, whereby reducing the average cation-anion distance (C2...B) by 0.2 Å and the anion-anion distance (B...B) by 0.3 Å. Small deviations of the cation positions result in a comparatively shorter cation-cation distance of 4.4 compared to 4.7 Å in the benchmark geometry.

MP2/cc-pVDZ with an average deviation in total energy of 5.1 kJ mol⁻¹ has small deviations in HF and correlation components and the largest RMSD of only 0.2 Å. This method performs equally well for both imidazolium-based ionic liquids.

Based on the total energy and interaction energy, the preferred DFT functionals to use with the VDZ basis set are ω B97X-D and B3LYP-D3. In terms of similarity in geometries, B3LYP-D3 performs the best with a maximum RMSD of 0.2 Å. Both functionals produce HF and correlation components of interaction energy within or close to chemical accuracy (4 kJ mol⁻¹) off the benchmark results.

Performance of aug-cc-pVDZ basis set

In this section geometry optimisations performed with the aug-cc-pVDZ basis set are discussed. The mean and standard deviations of total electronic and interaction energies of the optimised structures together with mean and maximum RMSD values with respect to the FMO3-SRS-MP2/VTZ geometry are given in Table 3 for each DFT functional/MP2-based method.

Table 3. Two ion-paired clusters: Mean errors (Mean) and standard deviations (SD) for total electronic energy (Total Energy), interaction energy (E_{INT}), HF interaction Energy ($E_{\text{INT}}(\text{HF})$) and correlation interaction energy ($E_{\text{INT}}(\text{Corr})$) energies, mean and maximum RMSD values for each functional and MP2-based method with the aug-cc-pVDZ basis set with respect to the FMO3-SRS-MP2/cc-pVTZ geometry. All energies are given in kJ mol^{-1} and RMSD is given in Å.

Theory	Total Energy		E_{INT}		$E_{\text{INT}}(\text{HF})$		$E_{\text{INT}}(\text{Corr})$		RMSD	
	Mean	SD	Mean	SD	Mean	SD	Mean	SD	Mean	Max
B3LYP	8.0	4.0	7.0	3.1	-15.4	7.7	22.3	10.7	0.5	0.8
B3LYP-D3	1.5	0.9	-2.9	1.9	-5.8	4.6	2.8	4.0	0.3	0.6
BLYP	21.9	1.7	11.9	1.1	-15.4	10.3	27.3	9.8	0.5	0.8
BP86-D3	10.5	1.3	-3.3	5.1	-2.2	5.6	-1.0	6.1	0.3	0.8
M06-2X	5.3	2.0	-1.5	4.2	7.8	11.2	-9.3	8.0	0.3	0.6
PBE	13.7	0.7	2.9	2.7	-13.9	8.9	16.7	6.4	0.4	0.8
PBE-D3	9.3	1.4	-2.9	4.4	-7.5	4.5	4.6	2.6	0.2	0.7
TPSS-D3	4.7	1.1	-1.4	3.4	-6.2	3.8	4.8	2.7	0.3	0.7
ω B97X-D	3.8	1.3	-2.9	2.8	-4.8	5.4	1.9	4.3	0.3	0.5

In general, dispersion-corrected DFT functionals perform better with aug-cc-pVDZ compared to cc-pVDZ, producing smaller deviations in interaction energies. In terms of RMSD values, all DFT functionals show an increase in the mean values, with their maximum RMSD exceeding 0.5 Å. Conf2 of $[\text{C}_{1\text{mim}}][\text{BF}_4]$ has a mean and maximum RMSD of 0.5 and 0.9 Å, respectively, whereas conf1 of $[\text{C}_{1\text{mim}}]\text{Cl}$ has RMSDs above 0.6 Å when optimised with B3LYP and BLYP. PBE-D3 obtains the smallest average RMSD of 0.2 Å when compared to those with cc-pVDZ; however, the maximum RMSD is increased to 0.7 Å (up from 0.3 Å for cc-pVDZ). The maximum RMSD was determined for conf2 of $[\text{C}_{1\text{mim}}][\text{BF}_4]$, for which it is attributed to an increase in the cation-cation distance by 0.2 Å. In general, no obvious trends were observed in changes in interionic distances. In the case of B3LYP-D3/aVDZ, all the interionic distances are contracted by at least 0.2 Å. In the geometry of TPSS-D3/aVDZ the cation-cation and cation-anion distances

also become shorter by 0.1 to 0.2 Å. On the other hand, for conf1 of [C1mim]Cl, BLYP (RMSD of 0.7 Å) and B3LYP (RMSD of 0.6 Å) optimized to geometries with a significantly increased cation-cation distance by as much as 0.9 to 1.0 Å, whereas the anion-anion distance is reduced by 0.4 to 0.5 Å. The $\pi^+-\pi^+$ stacking remains intact, with the distance between the two cations increasing.

In terms of the combined performance for total and interaction energies, B3LYP-D3 (-5.8, 2.8), ω B97X-D (-4.8, 1.9) and TPSS-D3 (-6.2, 4.8) can be recommended, with mean deviations in HF and correlation components being given in kJ mol⁻¹ in brackets. Their standard deviations for the energy components within chemical accuracy clearly indicate the robustness of these functionals for geometry optimisation of ionic liquids when combined with aug-cc-pVDZ. One has to exercise caution when optimising ionic liquids exhibiting the $\pi^+-\pi^+$ stacking of imidazolium rings. All of the DFT functionals used in this study did not fare well in this scenario due to a significant change in arrangement that imidazolium cations undergo and therefore, for these ionic liquids the use of aug-cc-pVDZ is not recommended.

Performance of cc-pVTZ basis set

In this section geometry optimisations performed with the cc-pVTZ basis set are discussed. The mean and standard deviations of total electronic and interaction energies of the optimised structures together with mean and maximum RMSD values with respect to the FMO3-SRS-MP2/VTZ geometry are given in Table 4 for each DFT functional/MP2-based method.

Table 4. Two ion-paired clusters: Mean errors (Mean) and standard deviations (SD) for total electronic energy (Total Energy), interaction energy (E_{INT}), HF interaction Energy ($E_{\text{INT}}(\text{HF})$) and correlation interaction energy ($E_{\text{INT}}(\text{Corr})$) energies, mean and maximum RMSD values for each functional and MP2-based method with the cc-pVTZ basis set with respect to the FMO3-SRS-MP2/cc-pVTZ geometry. All energies are given in kJ mol^{-1} and RMSD is given in Å.

Theory	Total Energy		E_{INT}		$E_{\text{INT}}(\text{HF})$		$E_{\text{INT}}(\text{Corr})$		RMSD	
	Mean	SD	Mean	SD	Mean	SD	Mean	SD	Mean	Max
B3LYP	8.8	4.0	5.5	4.2	-16.9	6.4	22.4	10.1	0.4	0.6
B3LYP-D3	3.5	0.8	-2.7	2.0	-7.6	3.6	5.0	2.9	0.1	0.2
BLYP	12.4	2.4	9.8	1.8	-16.9	8.7	26.7	9.6	0.5	0.7
BLYP-D3	3.6	1.3	-1.9	1.0	-9.5	3.7	7.5	3.5	0.2	0.6
BP86-D3	4.1	1.5	-4.2	2.8	-4.5	4.6	0.4	4.2	0.2	0.4
M06-2X	7.8	2.3	-3.1	4.5	3.4	9.0	-6.5	6.7	0.3	0.6
PBE	7.1	3.1	1.2	1.1	-15.4	7.0	16.6	6.8	0.3	0.6
PBE-D3	4.4	1.4	-3.9	2.2	-9.4	3.7	5.5	1.9	0.2	0.5
TPSS-D3	2.2	1.6	-2.2	1.2	-8.6	2.7	6.3	1.7	0.1	0.2
ω B97X-D	7.1	0.9	-4.0	4.0	-8.0	4.7	4.0	3.7	0.2	0.5
MP2	2.4	0.7	-2.9	2.1	3.0	5.6	-5.9	3.9	0.1	0.3
FMO2-SRS-MP2	2.0	4.2	0.9	3.3	5.0	10.4	-4.1	7.1	0.2	0.3

With respect to cc-pVDZ, all DFT functionals achieve a better performance for geometry optimisation of 2 ion-paired clusters. Mean RMSD values fall consistently between 0.1 and 0.2, with the exception of BLYP and B3LYP. GGA functionals fall short in reducing their error to reach chemical accuracy. The dispersion-corrected functionals – B3LYP-D3, BLYP-D3, BP86-D3, PBE-D3 and TPSS-D3 – achieve mean deviations and standard deviations of interaction energy well within chemical accuracy. Recently developed functionals, ω B97X-D and M06-2X, also show an outstanding performance with mean deviations of -4.0 and -3.1 kJ mol^{-1} , respectively, highlighting the importance of a larger basis set for the description of London dispersion forces in semi-Coulombic systems such as ionic liquids. The use of this larger basis set becomes critical to

achieve the needed performance for geometry optimisation of either dispersion-corrected or meta-GGA/range-separated functionals. The excellent performance of these functionals achieved through overestimation of the HF component in the range of 4.5 to 9.5 kJ mol⁻¹ and underestimation of the correlation component in a similar range of 4.0 to 7.5 kJ mol⁻¹. M06-2X represents an exception in this series through underestimation of the HF component and overestimation of the correlation component. The only functional, BP86-D3, has the mean absolute deviations of individual components and standard deviations associated with these below 4.6 kJ mol⁻¹. Standard deviations in both energy components tend to be within chemical accuracy for the dispersion-corrected functionals used, with the exception for M06-2X and the GGA functionals. This suggests that a triple- ζ quality basis set improves the systematic error for dispersion-corrected functionals and ω B97X-D.

Trends in the HF and correlation components of interaction energy are also reflected in large maximum RMSD values above 0.4 Å observed for the majority of functionals with the exception of B3LYP-D3 and TPSS-D3. Coupled with small median RMSD values, this suggests that optimisation of only some configurations resulted in a different geometry compared to the benchmark method. For example, in the B3LYP-D3 optimized geometry of conf2 of [C₁mim]Cl, the anion-anion and cation-anion distances were optimized to be shorter by 0.4 and 0.1 Å, respectively, whereas the cation-cation distance is longer by 0.1 Å. Nor surprising that this geometry gave absolute deviations in the energy components > 9 kJ mol⁻¹. For comparison, the B3LYP-D3 optimisation of conf2 of [C₁mim][BF₄] produced negligible deviations in the average cation-cation, anion-anion and cation-anion distances, which are in turn reflected in small deviations of the HF and correlation components of - 5.2 kJ mol⁻¹ and 2.8 kJ mol⁻¹, respectively.

Overall, ionic liquid clusters exhibiting the $\pi^+-\pi^+$ stacking represented a challenge for geometry optimisation with GGA functionals as well as M062X. The conf1 cluster of [C₁mim]Cl optimised with BLYP/VTZ is displayed in Figure 5b. The geometry of BLYP/VTZ (shown in green) produces an RMSD of 0.7 Å and is contrasted with that of FMO3-SRS-MP2/VTZ. The distance between the C2 positions of the cation rings drastically increases from 3.6 Å for the benchmark method to 4.7 Å for BLYP, whereas the distance between the chloride anions becomes shorter by 0.5 Å. Not surprisingly that energetically this results in an underestimation of the correlation energy component by 26.8 kJ mol⁻¹ and an overestimation of the HF energy component by 15.7 kJ mol⁻¹. A similar trend is observed in the BLYP/VTZ optimized geometry of conf2 of [C₁mim], in which the cations are further apart by 0.4 Å and the anions draw nearer to one another by 0.3 Å, giving the overall RMSD of 0.4 Å.

The M06-2X optimisation of the conf2 cluster of [C₁mim]Cl is contrasted to the FMO3-SRS-MP2/VTZ optimized geometry in Figure 5c. The cation-cation distance is 0.1 Å longer than that of the benchmark and as the imidazolium rings move away from each other, which is accompanied by the chloride anions moving in between the stacked cations, producing an RMSD of 0.5 Å. This geometry has an overestimated HF component by over 10 kJ mol⁻¹, whereas the correlation component is close to that of the benchmark geometry due to the predominantly unchanged cation-anion distance. On the other hand, the M06-2X optimized geometry of conf1 of [C₁mim]Cl has a small RMSD of 0.1 Å and relatively small absolute deviations in the HF and correlation components < 8 kJ mol⁻¹ due to a shortening of the cation-anion distances by 0.1 Å.

FMO2-SRS-MP2 and MP2 perform equally well compared to dispersion-corrected DFT functionals, with the former producing the lowest mean deviations in total and interaction energies among the functionals/MP2-based methods studied with cc-pVTZ. FMO2-SRS-MP2 has larger

standard deviations between 7 and 10 kJ mol⁻¹ for individual components of interaction energy, suggesting the importance of induction effects in these clusters as two-body effects do not allow for explicit inclusion of induction forces. The maximum RMSD value does not exceed 0.3 Å.

Based on the combined performance statistics for total energy, interaction energy and RMSD, DFT functionals such as BP86-D3, B3LYP-D3, BP86-D3 and TPSS-D3 can be recommended for geometry optimisation of ionic liquids when coupled with cc-pVTZ. Other functionals, especially GGA ones, should be used with caution as these do not capture nuances of London dispersion forces in ionic liquids. Although FMO2-SRS-MP2 produces the best statistics for total and interaction energy, the exclusion of induction effects through the omission of three-body effects might not produce a reliable geometry for some ionic liquids, for which these effects are crucial.

Performance of aug-cc-pVTZ basis set

In this section geometry optimisations performed with the aug-cc-pVTZ basis set are discussed. The mean and standard deviations of total electronic and interaction energies of the optimised structures together with mean and maximum RMSD values with respect to the FMO3-SRS-MP2/VTZ geometry are given in Table 5 for each DFT functional/MP2-based method.

Table 5. Two ion-paired clusters: Mean errors (Mean) and standard deviations (SD) for total electronic energy (Total Energy), interaction energy (E_{INT}), HF interaction Energy ($E_{\text{INT}}(\text{HF})$) and correlation interaction energy ($E_{\text{INT}}(\text{Corr})$) energies, mean and maximum RMSD values for each functional and MP2-based method with the aug-cc-pVTZ basis set with respect to the FMO3-SRS-MP2/cc-pVTZ geometry. All energies are given in kJ mol^{-1} and RMSD is given in Å.

Theory	Total Energy		E_{INT}		$E_{\text{INT}}(\text{HF})$		$E_{\text{INT}}(\text{Corr})$		RMSD	
	Mean	SD	Mean	SD	Mean	SD	Mean	SD	Mean	Max
B3LYP	10.7	4.3	8.1	5.2	-16.5	5.7	24.5	10.6	0.5	0.8
B3LYP-D3	2.9	1.2	-2.4	2.6	-8.6	3.3	6.2	3.1	0.3	0.6
BLYP	15.7	2.4	15.0	1.8	-15.0	8.5	30.0	9.6	0.6	0.9
BP86-D3	3.4	1.2	-2.6	3.6	-5.1	4.2	2.4	4.8	0.3	0.8
M06-2X	7.3	1.7	-2.3	4.4	3.3	8.9	-5.6	6.5	0.3	0.6
PBE	9.3	2.2	4.3	1.3	-15.3	7.5	19.6	6.9	0.4	0.5
PBE-D3	3.9	1.1	-2.0	3.0	-9.9	3.1	7.9	1.5	0.3	0.8
TPSS-D3	2.0	1.5	-0.5	2.1	-9.1	2.2	8.6	1.1	0.3	0.8
ω B97X-D	7.1	1.3	-2.6	3.9	-8.0	4.8	5.3	3.8	0.3	0.6

In general, augmentation of the cc-pVTZ basis set does not lead to improvement in performance of the DFT functionals used. BP86-D3 is the only functional that shows a marginal improvement. The mean RMSD values increase by 0.1 Å from VTZ to aVTZ, with the maximum RMSD values exceeding 0.5 Å. Optimisations of the T-shaped conf2 cluster of $[\text{C}_{1\text{mim}}][\text{BF}_4]$ and the $\pi^+-\pi^+$ stacked conf1 cluster of $[\text{C}_{1\text{mim}}]\text{Cl}$ produce largest RMSD values, which is not surprising considering the same situation was observed for aug-cc-pVDZ. Due to a significant increase in computational cost, this basis set is not recommended to be used for geometry optimisation of ionic liquids.

Comments on the best functional/basis set combination

Table 6. Two ion paired clusters: mean deviations of total electronic energy (Total Energy) and interaction energy (EINT) in kJ mol⁻¹ for the best performing functionals/MP2-based methods for each basis set used together with mean and maximum RMSD values in Å.

Functional/Method	Basis set	Total Energy	E _{INT}	Mean RMSD	Max RMSD
MP2		5.1	-3.9	0.1	0.2
B3LYP-D3	VDZ	5.8	-5.2	0.1	0.2
ωB97X-D		6.1	-2.2	0.2	0.6
B3LYP-D3	aVDZ	1.5	-2.9	0.3	0.6
ωB97X-D		3.8	-2.9	0.3	0.5
TPSS-D3	VTZ	2.2	-2.2	0.1	0.2
B3LYP-D3		3.5	-2.7	0.1	0.2
BP86-D3		4.1	-4.2	0.2	0.4

Table 6 summarises the best performing DFT functionals/MP2-based methods for each basis set. Out of these combinations, the best geometries of imidazolium-based ionic liquids are obtained with B3LYP-D3/VTZ and TPSS-D3/VTZ due to the lowest RMSD values and lowest deviations in total and interaction energies. Among other combinations that can be recommended are ωB97X-D/aVDZ, B3LYP-D3/aVDZ and BP86-D3/VTZ. In general, the use of cc-pVTZ led to the best performance of dispersion-driven functionals, whereas aug-cc-pVDZ was found to be necessary to achieve a good performance for M06-2X and ωB97X-D.

Four ion paired clusters: influence of DFT functional on geometry, total electronic energy and interaction energy

The initial structures shown in Figure 6 were optimised with FMO2-MP2/cc-pVDZ and can be found in our previous work.²¹ Deviations of total energy and interaction energy and RMSDs are shown in Figure 7 for eight ionic liquids – [C₁mim][BF₄], [C₁mim]Cl, [C₁mpyr][BF₄], [C₁mpyr]Cl, [NMe₄][BF₄], [NMe₄]Cl, [C₂py][BF₄] and [C₂py]Cl. Based on the recommendations for the 2 ion-paired clusters of imidazolium-based ionic liquids, the following combinations of

functionals/basis sets were used B3LYP/VTZ, B3LYP-D3/aVDZ, B3LYP-D3/VTZ, BLYP/VTZ, BLYP-D3/VTZ, M06-2X/aVDZ, M06-2X/VTZ, PBE/VTZ, PBE-D3/VTZ, TPSS-D3/VTZ, ω B97X-D/VDZ, ω B97X-D/aVDZ and ω B97X-D/VTZ. In addition, the performance of wavefunction-based methods such as HF/VTZ, FMO2-SRS-MP2/VDZ, FMO2-SRS-MP2/VTZ and FMO3-SRS-MP2/VDZ was also contrasted.

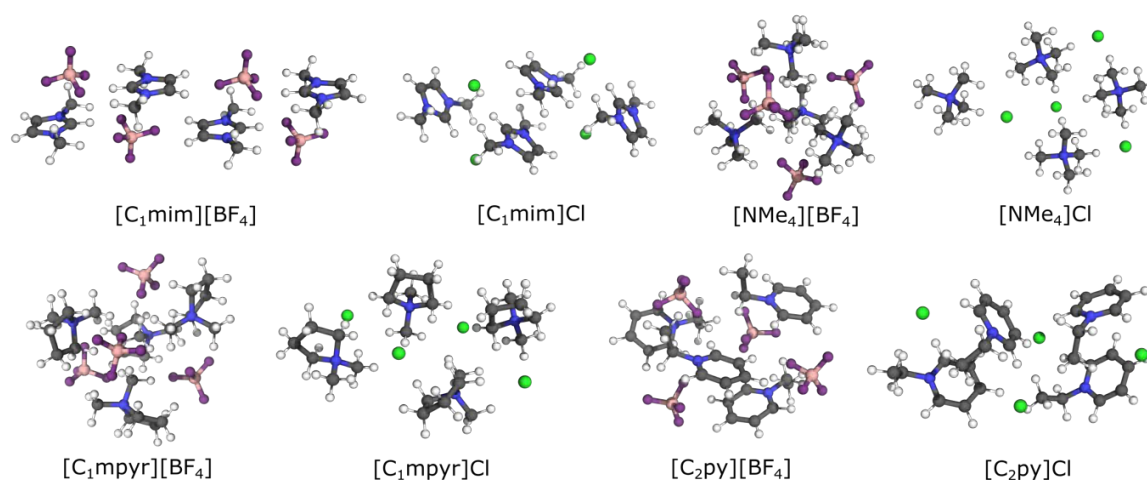


Figure 6. Starting structures of four ion-paired clusters of [C₁mim][BF₄], [C₁mim]Cl, [C₁mpyr][BF₄], [C₁mpyr]Cl, [NMe₄][BF₄], [NMe₄]Cl, [C₂py][BF₄] and [C₂py]Cl.

In our previous work, we extensively analysed interaction energies and corresponding HF and correlation components of the 4 ion paired clusters and these were used as starting geometries.²¹ Here we give a brief overview of the energetic landscape of these clusters studied.

Table 7. Interaction energy (E_{INT}), HF interaction energy ($E_{\text{INT}}(\text{HF})$), correlation interaction energy ($E_{\text{INT}}(\text{Corr})$) energy and the percentage of interaction energy of the correlation component ($\% E_{\text{INT}}(\text{Corr})$) of the four ion pair clusters per ion pair optimised and calculated with FMO3-SRS-MP2/cc-pVTZ.

Cluster	E_{INT}	$E_{\text{INT}}(\text{HF})$	$E_{\text{INT}}(\text{Corr})$	$\% E_{\text{INT}}(\text{Corr})$
[C ₁ mim][BF ₄]	-460.1	-408.5	-51.6	11.2
[C ₁ mim]Cl	-506.4	-439.8	-66.5	13.1
[C ₁ mpyr][BF ₄]	-468.8	-400.6	-68.3	14.6
[C ₁ mpyr]Cl	-508.1	-438.5	-69.6	13.7
[NMe ₄][BF ₄]	-478.2	-424.1	-54.1	11.3
[NMe ₄]Cl	-508.1	-448.7	-59.4	11.7
[C ₂ py][BF ₄]	-473.4	-400.5	-72.9	15.4
[C ₂ py]Cl	-488.9	-411.3	-77.7	15.9

Table 7 contains the interaction energy components of each cluster per ion pair as determined by FMO3-SRS-MP2/cc-pVTZ. The interaction energy of the tetrafluoroborate-based clusters span a range of -478.2 to -460.1 kJ mol⁻¹, whereas the chloride-based ones have stronger interaction energy falling in a range of -508.1 to -488.9 kJ mol⁻¹. The interaction energies increase in magnitude in the following order: [C₁mim][BF₄] < [C₁mpyr][BF₄] < [C₂py][BF₄] < [NMe₄][BF₄] < [C₂py]Cl < [C₁mim]Cl < [C₁mpyr]Cl < [NMe₄]Cl. The pyridinium-based ionic liquids have the largest correlation components of -72.9 and -77.7 kJ mol⁻¹ when coupled with BF₄⁻ and Cl⁻, respectively, while [C₁mim][BF₄] has the lowest contribution of -51.6 kJ mol⁻¹.

Deviations of the total electronic and interaction energies in the optimized 4 ion-paired clusters with respect to the benchmark method are given in Fig. 7 and Table 8.

The HF/VTZ combination was used to highlight the critical importance of dispersion forces for studying larger-scale clusters of ionic liquids. Not surprisingly, HF/VTZ consistently optimised to

configurations of much higher energy – up to 75 kJ mol^{-1} in the case of $[\text{C}_{1}\text{mim}]\text{Cl}$. These large deviations are accompanied with an increase in the cation-cation, cation-anion and anion-anion distances by 0.8 to 1.6 Å. The exclusion of London dispersion forces results in unrealistic geometries of ionic liquids.

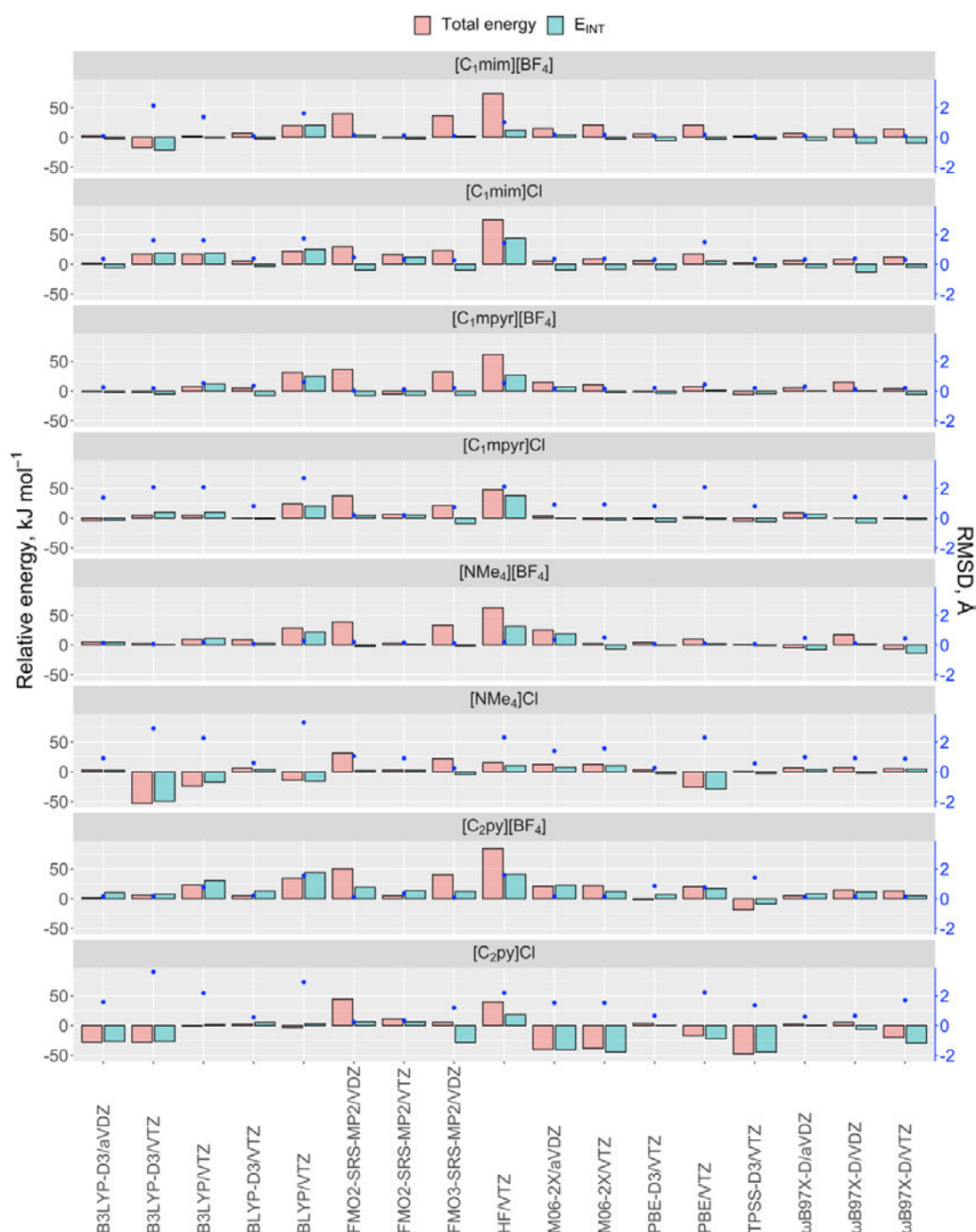


Figure 7. Four ion-paired clusters: Deviations of total electronic energies and interaction energies (left y axis) and mean RMSDs (right y axis) with respect to FMO3-SRS-MP2/cc-pVTZ optimised geometries. Single point calculations performed with FMO3-SRS-MP2/cc-pVTZ for each geometry from the method of optimisation (x axis).

Table 8. Four ion-paired clusters: Mean errors (Mean) and standard deviations (SD) for total electronic energy (Total), interaction energy (E_{INT}), HF interaction inergy ($E_{\text{INT}}(\text{HF})$) and correlation interaction energy ($E_{\text{INT}}(\text{Corr})$) energies, mean and maximum RMSD values for each functional and MP2-based method with the cc-pVTZ basis set with respect to the FMO3-SRS-MP2/cc-pVTZ geometry. All energies are given in kJ mol^{-1} and RMSDs are given in Å.

Theory	Total Energy		E_{INT}		$E_{\text{INT}}(\text{HF})$		$E_{\text{INT}}(\text{Corr})$		RMSD	
	Mean	SD	Mean	SD	Mean	SD	Mean	SD	Mean	Max
B3LYP/VTZ	4.8	14.1	8.4	14.2	-53.1	23.7	61.5	28.0	1.4	2.3
B3LYP-D3/aVDZ	-2.5	10.6	-3.0	10.9	1.0	16.7	-4.0	14.6	0.6	1.6
B3LYP-D3/VTZ	-8.7	22.6	-8.2	22.7	-24.3	25.1	16.2	41.0	1.6	3.6
BLYP/VTZ	17.8	17.2	18.1	17.4	-55.0	28.6	73.0	32.0	1.8	3.3
BLYP-D3/VTZ	4.9	2.8	1.2	6.3	-9.6	16.6	10.9	14.5	0.4	0.8
HF/VTZ	57.4	22.5	27.7	13.0	-65.6	28.4	93.3	30.8	1.4	2.3
M06-2X/aVDZ	7.1	20.4	1.2	19.6	29.7	30.9	-28.6	15.2	0.6	1.5
M06-2X/VTZ	4.7	19.1	-5.8	17.5	12.8	25.9	-18.6	16.8	0.7	1.6
PBE/VTZ	4.2	17.3	-3.7	15.1	-48.6	26.9	44.9	26.9	1.2	2.3
PBE-D3/VTZ	2.3	3.4	-2.5	4.9	-12.4	17.2	9.9	17.3	0.4	0.9
TPSS-D3/VTZ	-8.9	17.0	-9.4	14.5	-16.8	22.0	7.4	19.9	0.6	1.4
ω B97X-D/aVDZ	4.6	4.2	0.1	6.0	6.2	17.3	-6.1	17.4	0.4	1.0
ω B97X-D/VDZ	10.3	6.0	-3.1	7.9	11.6	20.9	-14.7	15.7	0.5	1.4
ω B97X-D/VTZ	2.6	11.7	-7.1	11.0	-9.9	22.5	2.8	17.6	0.6	1.7
FMO2-SRS-MP2/VDZ	38.5	6.6	2.0	9.1	23.3	24.2	-21.3	16.6	0.3	1.1
FMO2-SRS-MP2/VTZ	4.8	6.8	4.0	6.9	12.2	21.7	-8.3	17.7	0.3	0.9
FMO3-SRS-MP2/VDZ	26.8	11.2	-5.8	11.5	-2.5	20.9	-3.3	16.5	0.4	1.2

Increase in the number of ionic liquid ions in the cluster leads to a larger contribution of dispersion forces to interaction energy. As calculated with FMO3-SRS-MP2/VTZ, this contribution ranges from 11.2 to 15.9 %. This, in turn, results in increased deviations in total and interaction energy of the DFT functionals that do not fully describe dispersion forces. As expected, GGA functionals such as BLYP and PBE do not fare well, producing larger RMSD values of up to 3.3 Å and significant deviations (above 49 kJ mol^{-1} on the absolute scale) in the HF and

correlation components of interaction energy. 3 DFT functional/basis set combinations stand out due to their consistently excellent performance – BLYP-D3/VTZ, PBE-D3/VTZ and ω B97X-D/aVDZ. These combinations produce mean deviations in total energy below 4.9 kJ mol^{-1} , whereas mean deviations in interaction energies are well within chemical accuracy. Standard deviations for both quantities fall in a narrow range of 2.8 to 6.9 kJ mol^{-1} , indicating their consistently excellent performance for geometry optimisation of ionic liquid clusters. It is not surprising that these combinations also produced the lowest RMSD values, with the maximum not exceeding 1.0 \AA .

In general, the use of a diverse range of ionic liquids for geometry optimisation has revealed systematic errors for some functionals. Three of the 13 DFT functional/basis set combinations – B3LYP-D3/aVDZ, B3LYP-D3/VTZ and TPSS-D3/VTZ – produced mean total energies lower than the benchmark ones by between 2.5 and 8.9 kJ mol^{-1} on average. In contrast, the B3LYP-D3 and TPSS-D3 functionals performed well for the two ion-paired clusters of imidazolium-based ionic liquids, typically within chemical accuracy. In the case of the four ion-paired clusters, B3LYP-D3/aVDZ had largest negative deviations in total energy for $[\text{C}_2\text{py}]\text{Cl}$ ($-27.6 \text{ kJ mol}^{-1}$) and $[\text{C}_1\text{mpyr}]\text{Cl}$ (-4.7 kJ mol^{-1}), B3LYP-D3/VTZ for $[\text{NMe}_4]\text{Cl}$ ($-52.7 \text{ kJ mol}^{-1}$), $[\text{C}_2\text{py}]\text{Cl}$ ($-27.6 \text{ kJ mol}^{-1}$) and $[\text{C}_1\text{mim}][\text{BF}_4]$ ($-17.1 \text{ kJ mol}^{-1}$), and TPSS-D3/VTZ for $[\text{C}_2\text{py}]\text{Cl}$ ($-47.3 \text{ kJ mol}^{-1}$), and $[\text{C}_2\text{py}][\text{BF}_4]$ ($-18.6 \text{ kJ mol}^{-1}$). Pyridinium-based clusters consistently produced lower total energy structures with B3LYP-D3 and TPSS-D3. These ionic liquids have the largest contribution from London dispersion forces $> 15\%$ (see Table 7), indicating systematic errors that these functionals have when applied for geometry optimisation of ionic liquid clusters.

B3LYP-D3/VTZ also gave the largest RMSD values for $[\text{C}_2\text{py}]\text{Cl}$ and $[\text{C}_1\text{mim}][\text{BF}_4]$ with values of 3.6 and 2.1 \AA , respectively. For example, the B3LYP-D3/VTZ optimisation of $[\text{NMe}_4]\text{Cl}$ generates a geometry with an RMSD of 2.9 \AA when compared to the benchmark geometry and

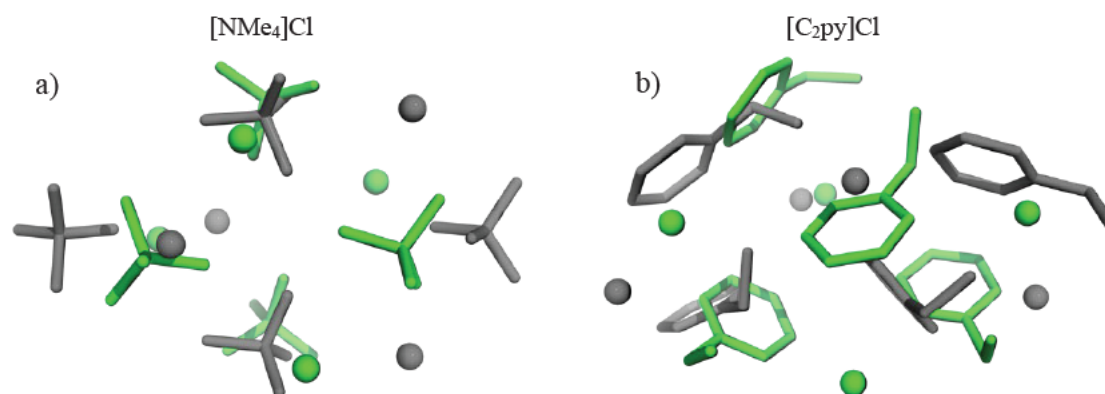


Figure 8. Four ion pair alignment between geometry of B3LYP-D3/cc-pVTZ (green) and the geometry of FMO3-SRS-MP2/cc-pVTZ (dark grey) for a) [NMe₄]Cl and b) [C₂py]Cl .

overestimates total energy by as much as 52.7 kJ mol⁻¹. Analysis of the B3LYP-D3/VTZ optimized geometries for the [NMe₄]Cl and [C₂py]Cl (see Fig. 8) reveals that this DFT functional/basis set combination converges to completely different structures compared to the benchmark ones, suggesting that the functional missed the local minima close to the starting geometries.

The B3LYP-D3/VTZ optimised structure of [NMe₄]Cl has shorter cation-cation, anion-anion and cation-anion distances by 1.1 Å, 0.4 Å and 0.6 Å on average, respectively. The benchmark method is in a more linear ionic arrangement that is expected to be less stable. Contrary to this observation, B3LYP-D3/VTZ pushed the ions into a more spherical arrangement to maximise the cation-anion interaction, thus also displaying stronger HF and correlation components. Cation-cation, anion-anion and cation-anion distances are also shortened in the [C₂py]Cl geometry by 0.5, 0.7 and 0.5 Å on average, respectively. The ethyl chains reorient to point outwards such that the rings are in closer proximity.

FMO2-SRS-MP2/VTZ and FMO3-SRS-MP2/VDZ have relatively low RMSD values of 0.3 and 0.4 Å on average, respectively. The former also produces low mean deviations in total energy of

4.8 kJ mol⁻¹ and interaction energy of 4.0 kJ mol⁻¹, accompanied by standard deviations of 6.8 kJ mol⁻¹. This indicates a consistent performance of the method across the ionic liquid clusters studied. It appears that the reliable description of dispersion forces outweighs the inclusion of induction forces. This is clearly demonstrated through a poor performance of FMO3-SRS-MP2/VDZ, whose mean deviation is well above the chemical accuracy at 26.8 kJ mol⁻¹.

To this end, the best geometries were obtained with PBE-D3/VTZ, BLYP-D3/VTZ, ω B97X-D/aVDZ and FMO2-SRS-MP2/VTZ. PBE-D3/VTZ performed the best, producing mean deviations in total and interaction energy well within chemical accuracy.

Conclusions

Two ion-paired clusters of [C₁mim][BF₄] and [C₁mim]Cl were optimised with various combinations of DFT functional/MP2-based method and Dunning's basis set and subsequently compared with the benchmark method, FMO3-SRS-MP2/cc-pVTZ. Single point calculations of the optimised geometries were performed with FMO3-SRS-MP2/cc-pVTZ to assess their proximity to the benchmark values. Out of the four basis sets used, cc-pVTZ led to an excellent performance of the dispersion-corrected DFT functionals such as BP86-D3, B3LYP-D3, BP86-D3 and TPSS-D3. M06-2X and ω B97X-D were found to produce the best results with the aug-cc-pVDZ. In general, aug-cc-pVDZ produced poorer geometries for the clusters involving $\pi^+ \cdots \pi^+$ stacking of their imidazolium rings, whereas aug-cc-pVTZ gave only marginal improvement over cc-pVTZ, thus not justifying the trade-off between cost and accuracy. GGA functionals such as BLYP, BP86 and PBE are not recommended for geometry optimisation of imidazolium-based ionic liquids as they do not completely account for dispersion forces that are critical in producing reliable geometries.

Four ion-paired clusters of [C₁mim][BF₄], [C₁mim]Cl, [C₁mpyr][BF₄], [C₁mpyr]Cl, [NMe₄][BF₄], [NMe₄]Cl, [C₂py][BF₄] and [C₂Py]Cl were optimized with better performing DFT functionals/methods as identified for the 2 ion-paired clusters. PBE-D3/VTZ, BLYP-D3/VTZ and ω B97X-D/aVDZ were found to perform consistently well for the selected ionic liquids, with average deviations of total and interaction energy falling within chemical accuracy. In the selected ionic liquids, dispersion forces contributed up to 15.9 % of the interaction energy. GGA functionals such as BLYP, BP86 and PBE as well as hybrid functional B3LYP, are not recommended for geometry optimisation of ionic liquids due to their poor performance in capturing subtle balances of dispersion forces. The study also identified the need to perform rigorous systematic studies of ionic liquid clusters consisting of varying cations and anions before a reliable conclusion on the performance of a DFT functional can be made. This was clearly demonstrated in a starkly different performance of B3LYP-D3 and TPSS-D3 for 2 and 4 ion-paired clusters of ionic liquids.

The importance of the accurate treatment of London dispersion forces in ionic liquids was demonstrated through a superior performance of FMO2-SRS-MP2/VTZ over FMO3-SRS-MP2/VDZ. The former produced mean deviations in total and interaction energies below 4.8 kJ mol⁻¹. PBE-D3/VTZ had the smallest mean deviations in total energy of 2.3 kJ mol⁻¹ and interaction energy of -2.5 kJ mol⁻¹. The four method/basis set combinations - PBE-D3/VTZ, BLYP-D3/VTZ, ω B97X-D/aVDZ and FMO2-SRS-MP2/VTZ - optimized to geometries with maximum RMSD values < 1.0 Å and therefore, these are confidently recommended for future studies of large-scale clusters of ionic liquids. It is important to notice that PBE-D3 and BLYP-D3 produce excellent results only in combination with a triple- ζ basis set. Both functionals can be reliably applied in *ab initio* MD simulations of ionic liquids of varying chemical nature.

References

- (1) Olivier-Bourbigou, H.; Magna, L.; Morvan, D. Ionic Liquids and Catalysis: Recent Progress from Knowledge to Applications. *Appl. Catal. A: Gen.* **2010**, *373* (1), 1–56. <https://doi.org/10.1016/j.apcata.2009.10.008>.
- (2) Hallett, J. P.; Welton, T. Room-Temperature Ionic Liquids: Solvents for Synthesis and Catalysis. 2. *Chem. Rev.* **2011**, *111* (5), 3508–3576. <https://doi.org/10.1021/cr1003248>.
- (3) Vekariya, R. L. A Review of Ionic Liquids: Applications towards Catalytic Organic Transformations. *J. Mol. Liq.* **2017**, *227*, 44–60. <https://doi.org/10.1016/j.molliq.2016.11.123>.
- (4) Shiddiky, M. J. A.; Torriero, A. A. J. Application of Ionic Liquids in Electrochemical Sensing Systems. *Biosens. Bioelectron.* **2011**, *26* (5), 1775–1787. <https://doi.org/10.1016/j.bios.2010.08.064>.
- (5) Abo-Hamad, A.; AlSaadi, M. A.; Hayyan, M.; Juneidi, I.; Hashim, M. A. Ionic Liquid-Carbon Nanomaterial Hybrids for Electrochemical Sensor Applications: A Review. *Electrochim. Acta* **2016**, *193*, 321–343. <https://doi.org/10.1016/j.electacta.2016.02.044>.
- (6) Bagheri, H.; Afkhami, A.; Khoshshafar, H.; Rezaei, M.; Sabounchei, S. J.; Sarlakifar, M. Simultaneous Electrochemical Sensing of Thallium, Lead and Mercury Using a Novel Ionic Liquid/Graphene Modified Electrode. *Anal. Chim. Acta* **2015**, *870*, 56–66. <https://doi.org/10.1016/j.aca.2015.03.004>.
- (7) Han, D.; Row, K. H. Recent Applications of Ionic Liquids in Separation Technology. *Molecules* **2010**, *15* (4), 2405–2426. <https://doi.org/10.3390/molecules15042405>.

- (8) Berthod, A.; Ruiz-Ángel, M. J.; Carda-Broch, S. Recent Advances on Ionic Liquid Uses in Separation Techniques. *J. Chromatogr. A* **2018**, *1559*, 2–16. <https://doi.org/10.1016/j.chroma.2017.09.044>.

- (9) Riaño, S.; Binnemans, K. Extraction and Separation of Neodymium and Dysprosium from Used NdFeB Magnets: An Application of Ionic Liquids in Solvent Extraction towards the Recycling of Magnets. *Green Chem.* **2015**, *17* (5), 2931–2942. <https://doi.org/10.1039/C5GC00230C>.

- (10) Cui, G.; Zhang, F.; Zhou, X.; Huang, Y.; Xuan, X.; Wang, J. Acylamido-Based Anion-Functionalized Ionic Liquids for Efficient SO₂ Capture through Multiple-Site Interactions. *ACS Sustainable Chem. Eng.* **2015**, *3* (9), 2264–2270. <https://doi.org/10.1021/acssuschemeng.5b00526>.

- (11) Baghban, A.; Mohammadi, A. H.; Taleghani, M. S. Rigorous Modeling of CO₂ Equilibrium Absorption in Ionic Liquids. *Int. J. Greenh. Gas Control* **2017**, *58*, 19–41. <https://doi.org/10.1016/j.ijggc.2016.12.009>.

- (12) George, A.; Brandt, A.; Tran, K.; S. Zahari, S. M. S. N.; Klein-Marcuschamer, D.; Sun, N.; Sathitsuksanoh, N.; Shi, J.; Stavila, V.; Parthasarathi, R.; Singh, S.; M. Holmes, B.; Welton, T.; A. Simmons, B.; P. Hallett, J. Design of Low-Cost Ionic Liquids for Lignocellulosic Biomass Pretreatment. *Green Chem.* **2015**, *17* (3), 1728–1734. <https://doi.org/10.1039/C4GC01208A>.

- (13) da Costa Lopes, A. M.; Bogel-Lukasik, R. Acidic Ionic Liquids as Sustainable Approach of Cellulose and Lignocellulosic Biomass Conversion without Additional Catalysts. *ChemSusChem* **2015**, *8* (6), 947–965. <https://doi.org/10.1002/cssc.201402950>.

- (14) Elfgén, R.; Hollóczki, O.; Kirchner, B. A Molecular Level Understanding of Template Effects in Ionic Liquids. *Acc. Chem. Res.* **2017**, *50* (12), 2949–2957. <https://doi.org/10.1021/acs.accounts.7b00436>.
- (15) Kirchner, B.; Hollóczki, O.; Canongia Lopes, J. N.; Pádua, A. A. H. Multiresolution Calculation of Ionic Liquids. *Wiley Interdiscip. Rev. Comput. Mol. Sci.* **2015**, *5* (2), 202–214. <https://doi.org/10.1002/wcms.1212>.
- (16) Izgorodina, E. I.; Seeger, Z. L.; Scarborough, D. L. A.; Tan, S. Y. S. Quantum Chemical Methods for the Prediction of Energetic, Physical, and Spectroscopic Properties of Ionic Liquids. *Chem. Rev.* **2017**, *117* (10), 6696–6754. <https://doi.org/10.1021/acs.chemrev.6b00528>.
- (17) Izgorodina, E. I.; Golze, D.; Maganti, R.; Armel, V.; Taïge, M.; Schubert, T. J.; MacFarlane, D. R. Importance of Dispersion Forces for Prediction of Thermodynamic and Transport Properties of Some Common Ionic Liquids. *Phys. Chem. Chem. Phys.* **2014**, *16* (16), 7209–7221. <https://doi.org/10.1039/C3CP53035C>.
- (18) Seeger, Z. L.; Kobayashi, R.; Izgorodina, E. I. Cluster Approach to the Prediction of Thermodynamic and Transport Properties of Ionic Liquids. *J. Chem. Phys.* **2018**, *148* (19), 193832. <https://doi.org/10.1063/1.5009791>.
- (19) Ludwig, R. Thermodynamic Properties of Ionic Liquids—a Cluster Approach. *Phys. Chem. Chem. Phys.* **2008**, *10* (29), 4333–4339. <https://doi.org/10.1039/B803572E>.
- (20) Izgorodina, E.; Rigby, J.; MacFarlane, D. Large-Scale Ab Initio Calculations of Archetypical Ionic Liquids. *Chem. Commun.* **2012**, 48 (10), 1493–1495. <https://doi.org/10.1039/C1CC15056A>.

- (21) Halat, P.; Seeger, Z. L.; Barrera Acevedo, S.; Izgorodina, E. I. Trends in Two- and Three-Body Effects in Multiscale Clusters of Ionic Liquids. *J. Phys. Chem. B* **2017**, *121* (3), 577–588. <https://doi.org/10.1021/acs.jpcc.6b10101>.
- (22) Koßmann, S.; Thar, J.; Kirchner, B.; Hunt, P. A.; Welton, T. Cooperativity in Ionic Liquids. *J. Chem. Phys.* **2006**, *124* (17), 174506. <https://doi.org/10.1063/1.2191493>.
- (23) P. Matthews, R.; Welton, T.; A. Hunt, P. Competitive Pi Interactions and Hydrogen Bonding within Imidazolium Ionic Liquids. *Phys. Chem. Chem. Phys.* **2014**, *16* (7), 3238–3253. <https://doi.org/10.1039/C3CP54672A>.
- (24) Chen, S.; I. Izgorodina, E. Prediction of ¹H NMR Chemical Shifts for Clusters of Imidazolium-Based Ionic Liquids. *Phys. Chem. Chem. Phys.* **2017**, *19* (26), 17411–17425. <https://doi.org/10.1039/C7CP02951A>.
- (25) Zahn, S.; Uhlig, F.; Thar, J.; Spickermann, C.; Kirchner, B. Intermolecular Forces in an Ionic Liquid ([Mmim][Cl]) versus Those in a Typical Salt (NaCl). *Angew. Chem. Int. Ed.* **2008**, *47* (19), 3639–3641. <https://doi.org/10.1002/anie.200705526>.
- (26) Saielli, G. Computational Spectroscopy of Ionic Liquids for Bulk Structure Elucidation. *Adv. Theory Simul.* **2018**, *1* (10), 1800084. <https://doi.org/10.1002/adts.201800084>.
- (27) Firaha, D. S.; Kavalchuk, M.; Kirchner, B. SO₂ Solvation in the 1-Ethyl-3-Methylimidazolium Thiocyanate Ionic Liquid by Incorporation into the Extended Cation–Anion Network. *J. Solution Chem.* **2015**, *44* (3), 838–849. <https://doi.org/10.1007/s10953-015-0321-5>.

- (28) Weber, H.; Kirchner, B. Complex Structural and Dynamical Interplay of Cyano-Based Ionic Liquids. *J. Phys. Chem. B* **2016**, *120* (9), 2471–2483. <https://doi.org/10.1021/acs.jpcc.6b00098>.
- (29) Li, H.; Boatz, J. A.; Gordon, M. S. Cation–Cation Π – π Stacking in Small Ionic Clusters of 1,2,4-Triazolium. *J. Am. Chem. Soc.* **2008**, *130* (2), 392–393. <https://doi.org/10.1021/ja076406u>.
- (30) Brüssel, M.; Brehm, M.; S. Pensado, A.; Malberg, F.; Ramzan, M.; Stark, A.; Kirchner, B. On the Ideality of Binary Mixtures of Ionic Liquids. *Phys. Chem. Chem. Phys.* **2012**, *14* (38), 13204–13215. <https://doi.org/10.1039/C2CP41926B>.
- (31) S. Wilkes, J.; J. Zaworotko, M. Air and Water Stable 1-Ethyl-3-Methylimidazolium Based Ionic Liquids. *J. Chem. Soc. Chem. Comm.* **1992**, 0 (13), 965–967. <https://doi.org/10.1039/C39920000965>.
- (32) Wilkes, J. S.; Zaworotko, M. J. Manifestations of Noncovalent Interactions in the Solid State. Dimeric and Polymeric Self-Assembly in Imidazolium Salts via Face-to-Face Cation–Cation π -Stacking. *Supramol. Chem.* **1993**, *1* (3–4), 191–193. <https://doi.org/10.1080/10610279308035160>.
- (32) Deetlefs, M.; Hardacre, C.; Nieuwenhuyzen, M.; Padua, A. A. H.; Sheppard, O.; Soper, A. K. Liquid Structure of the Ionic Liquid 1,3-Dimethylimidazolium Bis(Trifluoromethyl)Sulfonylamide. *J. Phys. Chem. B* **2006**, *110* (24), 12055–12061. <https://doi.org/10.1021/jp060924u>.
- (34) Canongia Lopes, J. N. A.; Pádua, A. A. H. Nanostructural Organization in Ionic Liquids. *J. Phys. Chem. B* **2006**, *110* (7), 3330–3335. <https://doi.org/10.1021/jp056006y>.

(34) Chen, S.; Zhang, S.; Liu, X.; Wang, J.; Wang, J.; Dong, K.; Sun, J.; Xu, B. Ionic Liquid Clusters: Structure, Formation Mechanism, and Effect on the Behavior of Ionic Liquids. *Phys. Chem. Chem. Phys.* **2014**, *16* (13), 5893–5906. <https://doi.org/10.1039/C3CP53116C>.

(36) Liu, X.; Zhou, G.; Zhang, S.; Wu, G. Molecular Simulation of Imidazolium Amino Acid-Based Ionic Liquids. *Mol. Simul.* **2010**, *36* (14), 1123–1130. <https://doi.org/10.1080/08927022.2010.497923>.

(37) Fumino, K.; Wulf, A.; Ludwig, R. Strong, Localized, and Directional Hydrogen Bonds Fluidize Ionic Liquids. *Angew. Chem. Int. Ed.* **2008**, *47* (45), 8731–8734. <https://doi.org/10.1002/anie.200803446>.

(38) Zahn, S.; Bruns, G.; Thar, J.; Kirchner, B. What Keeps Ionic Liquids in Flow? *Phys. Chem. Chem. Phys.* **2008**, *10* (46), 6921–6924. <https://doi.org/10.1039/B814962N>.

(39) Izgorodina, E. I.; Maganti, R.; Armel, V.; Dean, P. M.; Pringle, J. M.; Seddon, K. R.; MacFarlane, D. R. Understanding the Effect of the C2 Proton in Promoting Low Viscosities and High Conductivities in Imidazolium-Based Ionic Liquids: Part I. Weakly Coordinating Anions. *J. Phys. Chem. B* **2011**, *115* (49), 14688–14697. <https://doi.org/10.1021/jp208573y>.

(40) Hunt, P. A. Why Does a Reduction in Hydrogen Bonding Lead to an Increase in Viscosity for the 1-Butyl-2,3-Dimethyl-Imidazolium-Based Ionic Liquids? *J. Phys. Chem. B* **2007**, *111* (18), 4844–4853. <https://doi.org/10.1021/jp067182p>.

(41) Červinka, C.; Klajmon, M.; Štejfa, V. Cohesive Properties of Ionic Liquids Calculated from First Principles. *J. Chem. Theory Comput.* **2019**, *15* (10), 5563–5578. <https://doi.org/10.1021/acs.jctc.9b00625>.

- (42) Chen, L.; Bryantsev, V. S. A Density Functional Theory Based Approach for Predicting Melting Points of Ionic Liquids. *Phys. Chem. Chem. Phys.* **2017**, *19* (5), 4114–4124. <https://doi.org/10.1039/C6CP08403F>.
- (43) Perdew, J. P.; Burke, K.; Ernzerhof, M. Generalized Gradient Approximation Made Simple. *Phys. Rev. Lett.* **1996**, *77* (18), 3865–3868. <https://doi.org/10.1103/PhysRevLett.77.3865>.
- (41) Becke, A. D. Density-Functional Exchange-Energy Approximation with Correct Asymptotic Behavior. *Phys. Rev. A* **1988**, *38*, 3098–3100. <https://doi.org/10.1103/PhysRevA.38.3098>.
- (45) Lee, C.; Yang, W.; Parr, R. G. Development of the Colle-Salvetti Correlation-Energy Formula into a Functional of the Electron Density. *Phys. Rev. B* **1988**, *37* (2), 785–789. <https://doi.org/10.1103/PhysRevB.37.785>.
- (46) Perdew, J. P.; Wang, Y. Pair-Distribution Function and Its Coupling-Constant Average for the Spin-Polarized Electron Gas. *Phys. Rev. B* **1992**, *46* (20), 12947–12954. <https://doi.org/10.1103/PhysRevB.46.12947>.
- (47) Izgorodina, E. I.; Bernard, U. L.; MacFarlane, D. R. Ion-Pair Binding Energies of Ionic Liquids: Can DFT Compete with Ab Initio-Based Methods? *J. Phys. Chem. A* **2009**, *113* (25), 7064–7072. <https://doi.org/10.1021/jp8107649>.
- (48) Zhao, Y.; Schultz, N. E.; Truhlar, D. G. Design of Density Functionals by Combining the Method of Constraint Satisfaction with Parametrization for Thermochemistry, Thermochemical Kinetics, and Noncovalent Interactions. *J. Chem. Theory Comput.* **2006**, *2* (2), 364–382. <https://doi.org/10.1021/ct0502763>.

(49) Grimme, S.; Antony, J.; Ehrlich, S.; Krieg, H. A Consistent and Accurate *Ab Initio* Parametrization of Density Functional Dispersion Correction (DFT-D) for the 94 Elements H-Pu. *J. Chem. Phys.* **2010**, *132* (15), 154104. <https://doi.org/10.1063/1.3382344>.

(50) Grimme, S. Semiempirical GGA-type density functional constructed with a long-range dispersion correction. *J. Comput. Chem.* **2006**, *27* (15), 1787–1799. <https://doi.org/10.1002/jcc.20495>.

(51) Grimme, S. Accurate description of van der Waals complexes by density functional theory including empirical corrections. *J. Comput. Chem.* **2004**, *25* (12), 1463–1473. <https://doi.org/10.1002/jcc.20078>.

(49) Grimme, S.; Hujo, W.; Kirchner, B. Performance of Dispersion-Corrected Density Functional Theory for the Interactions in Ionic Liquids. *Phys. Chem. Chem. Phys.* **2012**, *14* (14), 4875–4883. <https://doi.org/10.1039/C2CP24096C>.

(53) Izgorodina, E. I.; MacFarlane, D. R. Nature of Hydrogen Bonding in Charged Hydrogen-Bonded Complexes and Imidazolium-Based Ionic Liquids. *J. Phys. Chem. B* **2011**, *115* (49), 14659–14667. <https://doi.org/10.1021/jp208150b>.

(54) Hunt, P. A.; Gould, I. R. Structural Characterization of the 1-Butyl-3-Methylimidazolium Chloride Ion Pair Using *Ab Initio* Methods. *J. Phys. Chem. A* **2006**, *110* (6), 2269–2282. <https://doi.org/10.1021/jp0547865>.

(55) Matthews, R. P.; Ashworth, C.; Welton, T.; Hunt, P. A. The Impact of Anion Electronic Structure: Similarities and Differences in Imidazolium Based Ionic Liquids. *J. Phys.: Condens. Matter* **2014**, *26* (28), 284112. <https://doi.org/10.1088/0953-8984/26/28/284112>.

(56) Matthews, R. P.; Welton, T.; Hunt, P. A. Hydrogen Bonding and π - π Interactions in Imidazolium-Chloride Ionic Liquid Clusters. *Phys. Chem. Chem. Phys.* **2015**, *17* (22), 14437–14453. <https://doi.org/10.1039/C5CP00459D>.

(56) A. Marekha, B.; N. Kalugin, O.; Idrissi, A. Non-Covalent Interactions in Ionic Liquid Ion Pairs and Ion Pair Dimers: A Quantum Chemical Calculation Analysis. *Phys. Chem. Chem. Phys.* **2015**, *17* (26), 16846–16857. <https://doi.org/10.1039/C5CP02197A>.

(57) Zahn, S.; R. MacFarlane, D.; I. Izgorodina, E. Assessment of Kohn–Sham Density Functional Theory and Møller–Plesset Perturbation Theory for Ionic Liquids. *Phys. Chem. Chem. Phys.* **2013**, *15* (32), 13664–13675. <https://doi.org/10.1039/C3CP51682B>.

(59) García, G.; Atilhan, M.; Aparicio, S. Assessment of DFT Methods for Studying Acid Gas Capture by Ionic Liquids. *Phys. Chem. Chem. Phys.* **2015**, *17* (40), 26875–26891. <https://doi.org/10.1039/C5CP04283F>.

(59) Firaha, D. S.; Thomas, M.; Hollóczki, O.; Korth, M.; Kirchner, B. Can Dispersion Corrections Annihilate the Dispersion-Driven Nano-Aggregation of Non-Polar Groups? An *Ab Initio* Molecular Dynamics Study of Ionic Liquid Systems. *J. Chem. Phys.* **2016**, *145* (20), 204502. <https://doi.org/10.1063/1.4967861>.

(61) Lage-Estebanez, I.; del Olmo, L.; López, R.; García de la Vega, J. M. The Role of Errors Related to DFT Methods in Calculations Involving Ion Pairs of Ionic Liquids. *J. Comput. Chem.* **2017**, *38* (8), 530–540. <https://doi.org/10.1002/jcc.24707>.

(62) Perlth, E.; Ray, P.; Hansen, A.; Malberg, F.; Grimme, S.; Kirchner, B. Finding the Best Density Functional Approximation to Describe Interaction Energies and Structures of Ionic

Liquids in Molecular Dynamics Studies. *J. Chem. Phys.* **2018**, *148* (19), 193835. <https://doi.org/10.1063/1.5013122>.

(63) Karu, K.; Mišin, M.; Ers, H.; Sun, J.; Ivaništšev, V. Performance of SCAN Density Functional for a Set of Ionic Liquid Ion Pairs. *International Journal of Quantum Chemistry* **2018**, *118* (13), e25582. <https://doi.org/10.1002/qua.25582>.

(64) Kitaura, K.; Ikeo, E.; Asada, T.; Nakano, T.; Uebayasi, M. Fragment Molecular Orbital Method: An Approximate Computational Method for Large Molecules. *Chem. Phys. Lett.* **1999**, *313* (3), 701–706. [https://doi.org/10.1016/S0009-2614\(99\)00874-X](https://doi.org/10.1016/S0009-2614(99)00874-X).

(65) Nakano, T.; Kaminuma, T.; Sato, T.; Akiyama, Y.; Uebayasi, M.; Kitaura, K. Fragment Molecular Orbital Method: Application to Polypeptides. *Chem. Phys. Lett.* **2000**, *318* (6), 614–618. [https://doi.org/10.1016/S0009-2614\(00\)00070-1](https://doi.org/10.1016/S0009-2614(00)00070-1).

(66) Nakano, T.; Kaminuma, T.; Sato, T.; Fukuzawa, K.; Akiyama, Y.; Uebayasi, M.; Kitaura, K. Fragment Molecular Orbital Method: Use of Approximate Electrostatic Potential. *Chem. Phys. Lett.* **2002**, *351* (5), 475–480. [https://doi.org/10.1016/S0009-2614\(01\)01416-6](https://doi.org/10.1016/S0009-2614(01)01416-6).

(67) Fedorov, D. G.; Olson, R. M.; Kitaura, K.; Gordon, M. S.; Koseki, S. A New Hierarchical Parallelization Scheme: Generalized Distributed Data Interface (GDDI), and an Application to the Fragment Molecular Orbital Method (FMO). *J. Comput. Chem.* **2004**, *25* (6), 872–880. <https://doi.org/10.1002/jcc.20018>.

(68) Fedorov, D. G.; Kitaura, K. Second Order Møller-Plesset Perturbation Theory Based upon the Fragment Molecular Orbital Method. *J. Chem. Phys.* **2004**, *121* (6), 2483–2490. <https://doi.org/10.1063/1.1769362>.

- (69) Fedorov, D. G.; Kitaura, K. The Importance of Three-Body Terms in the Fragment Molecular Orbital Method. *J. Chem. Phys.* **2004**, *120* (15), 6832–6840. <https://doi.org/10.1063/1.1687334>.
- (70) Fedorov, D. G.; Ishimura, K.; Ishida, T.; Kitaura, K.; Pulay, P.; Nagase, S. Accuracy of the Three-Body Fragment Molecular Orbital Method Applied to Møller–Plesset Perturbation Theory. *J. Comput. Chem.* **2007**, *28* (9), 1476–1484. <https://doi.org/10.1002/jcc.20645>.
- (71) Tan, S.; Barrera Acevedo, S.; Izgorodina, E. I. Generalized Spin-Ratio Scaled MP2 Method for Accurate Prediction of Intermolecular Interactions for Neutral and Ionic Species. *J. Chem. Phys.* **2017**, *146* (6), 064108. <https://doi.org/10.1063/1.4975326>.
- (72) S. Tan, S. Y.; Wylie, L.; Begic, I.; Tran, D.; I. Izgorodina, E. Application of Spin-Ratio Scaled MP2 for the Prediction of Intermolecular Interactions in Chemical Systems. *Phys. Chem. Chem. Phys.* **2017**, *19* (42), 28936–28942. <https://doi.org/10.1039/C7CP04391K>.
- (73) Rigby, J.; Barrera Acevedo, S.; Izgorodina, E. I. Novel SCS-IL-MP2 and SOS-IL-MP2 Methods for Accurate Energetics of Large-Scale Ionic Liquid Clusters. *J. Chem. Theory Comput.* **2015**, *11* (8), 3610–3616. <https://doi.org/10.1021/acs.jctc.5b00551>.
- (74) Perdew, J. P. Density-Functional Approximation for the Correlation Energy of the Inhomogeneous Electron Gas. *Phys. Rev. B* **1986**, *33* (12), 8822–8824. <https://doi.org/10.1103/PhysRevB.33.8822>.
- (75) Zhao, Y.; Truhlar, D. G. The M06 Suite of Density Functionals for Main Group Thermochemistry, Thermochemical Kinetics, Noncovalent Interactions, Excited States, and Transition Elements: Two New Functionals and Systematic Testing of Four M06-Class

Functionals and 12 Other Functionals. *Theor. Chem. Account* **2008**, *120* (1), 215–241. <https://doi.org/10.1007/s00214-007-0310-x>.

(76) Becke, A. D. Density-functional Thermochemistry. III. The Role of Exact Exchange. *J. Chem. Phys.* **1993**, *98* (7), 5648–5652. <https://doi.org/10.1063/1.464913>.

(77) Chai, J.-D.; Head-Gordon, M. Long-Range Corrected Hybrid Density Functionals with Damped Atom–Atom Dispersion Corrections. *Phys. Chem. Chem. Phys.* **2008**, *10* (44), 6615–6620. <https://doi.org/10.1039/B810189B>.

(78) Tao, J.; Perdew, J. P.; Staroverov, V. N.; Scuseria, G. E. Climbing the Density Functional Ladder: Nonempirical Meta--Generalized Gradient Approximation Designed for Molecules and Solids. *Phys. Rev. Lett.* **2003**, *91* (14), 146401. <https://doi.org/10.1103/PhysRevLett.91.146401>.

(79) Thomas, M.; Kirchner, B. Classical Magnetic Dipole Moments for the Simulation of Vibrational Circular Dichroism by Ab Initio Molecular Dynamics. *J. Phys. Chem. Lett.* **2016**, *7* (3), 509–513. <https://doi.org/10.1021/acs.jpcclett.5b02752>.

(80) Tang, F.; Ohto, T.; Hasegawa, T.; Bonn, M.; Nagata, Y. $\pi + -\pi +$ Stacking of Imidazolium Cations Enhances Molecular Layering of Room Temperature Ionic Liquids at Their Interfaces. *Phys. Chem. Chem. Phys.* **2017**, *19* (4), 2850–2856. <https://doi.org/10.1039/C6CP07034E>.

(81) Sedghamiz, T.; Ghalami, F.; Sedghamiz, E.; Bahrami, M. Chiral Recognition of Propranolol Enantiomers by Chiral Ionic Liquid: A Quantum Chemical Calculation Analysis. *Comp. Theor. Chem.* **2018**, *1140*, 38–48. <https://doi.org/10.1016/j.comptc.2018.07.017>.

- (82) Xu, J.; Yi, L.; Mou, Y.; Cao, J.; Wang, C. Effect of a Molecule of Imidazolium Bromide Ionic Liquid on the Structure and Properties of Cytosine by Density Functional Theory. *Chem. Phys. Lett.* **2018**, *708*, 109–116. <https://doi.org/10.1016/j.cplett.2018.08.009>.
- (83) Shakourian-Fard, M.; Bayat, A.; Kamath, G. Effect of Mono-Vacant Defects on the Opto-Electronic Properties of Ionic Liquid Functionalized Hexagonal Boron-Nitride Nanosheets. *J. Mol. Liq.* **2018**, *249*, 1172–1182. <https://doi.org/10.1016/j.molliq.2017.11.140>.
- (84) Jolodar, O. G.; Ghauri, K.; Seddighi, M.; Shirini, F.; Bayat, Y. Preparation and Characterization of Ethane-1,2-Diaminium Trinitromethanide as a Novel Energetic Ionic Liquid. *J. Mol. Struct.* **2019**, *1186*, 448–457. <https://doi.org/10.1016/j.molstruc.2019.03.062>.
- (85) Patil, A. B.; Bhanage, B. M. Assessing Ionicity of Protic Ionic Liquids by Far IR Spectroscopy. *J. Mol. Liq.* **2018**, *252*, 180–183. <https://doi.org/10.1016/j.molliq.2017.12.131>.
- (86) Tankov, I.; Yankova, R.; Genieva, S.; Mitkova, M.; Stratiev, D. Density Functional Theory Study on the Ionic Liquid Pyridinium Hydrogen Sulfate. *J. Mol. Struct.* **2017**, *1139*, 400–406. <https://doi.org/10.1016/j.molstruc.2017.03.040>.
- (87) Parveen, F.; Patra, T.; Upadhyayula, S. Hydrolysis of Microcrystalline Cellulose Using Functionalized Bronsted Acidic Ionic Liquids – A Comparative Study. *Carbohydr. Polym.* **2016**, *135*, 280–284. <https://doi.org/10.1016/j.carbpol.2015.08.039>.
- (88) Bai, L.; Zhu, J.; Chen, B. Quantitative Structure–Property Relationship Study on Heat of Fusion for Ionic Liquids. *Fluid Phase Equilib.* **2011**, *312*, 7–13. <https://doi.org/10.1016/j.fluid.2011.09.005>.

- (89) Singh, D. K.; Rathke, B.; Kiefer, J.; Materny, A. Molecular Structure and Interactions in the Ionic Liquid 1-Ethyl-3-Methylimidazolium Trifluoromethanesulfonate. *J. Phys. Chem. A* **2016**, *120* (31), 6274–6286. <https://doi.org/10.1021/acs.jpca.6b03849>.
- (90) Bodo, E.; Mangialardo, S.; Ramondo, F.; Ceccacci, F.; Postorino, P. Unravelling the Structure of Protic Ionic Liquids with Theoretical and Experimental Methods: Ethyl-, Propyl- and Butylammonium Nitrate Explored by Raman Spectroscopy and DFT Calculations. *J. Phys. Chem. B* **2012**, *116* (47), 13878–13888. <https://doi.org/10.1021/jp3052714>.
- (91) Ara, G.; Rahman, A.; Halim, M. A.; Islam, Md. M.; Mollah, M. Y. A.; Rahman, M. M.; Susan, Md. A. B. H. One-Pot Synthesis of Aprotic Ionic Liquid through Solvent-Free Alkylation of an Organic Superbase. *Mater. Today* **2020**. <https://doi.org/10.1016/j.matpr.2020.04.704>.
- (92) Møller, Chr.; Plesset, M. S. Note on an Approximation Treatment for Many-Electron Systems. *Phys. Rev.* **1934**, *46* (7), 618–622. <https://doi.org/10.1103/PhysRev.46.618>.
- (93) Dunning, T. H. Gaussian Basis Sets for Use in Correlated Molecular Calculations. I. The Atoms Boron through Neon and Hydrogen. *J. Chem. Phys.* **1989**, *90* (2), 1007–1023. <https://doi.org/10.1063/1.456153>.
- (94) Kendall, R. A.; Dunning, T. H.; Harrison, R. J. Electron Affinities of the First-row Atoms Revisited. Systematic Basis Sets and Wave Functions. *J. Chem. Phys.* **1992**, *96* (9), 6796–6806. <https://doi.org/10.1063/1.462569>.
- (95) Woon, D. E.; Dunning, T. H. Gaussian Basis Sets for Use in Correlated Molecular Calculations. III. The Atoms Aluminum through Argon. *J. Chem. Phys.* **1993**, *98* (2), 1358–1371. <https://doi.org/10.1063/1.464303>.

- (96) Řezáč, J.; Hobza, P. Benchmark Calculations of Interaction Energies in Noncovalent Complexes and Their Applications. *Chem. Rev.* **2016**, *116* (9), 5038–5071. <https://doi.org/10.1021/acs.chemrev.5b00526>.
- (97) Hill, J. G.; Platts, J. A. Spin-Component Scaling Methods for Weak and Stacking Interactions. *J. Chem. Theory Comput.* **2007**, *3* (1), 80–85. <https://doi.org/10.1021/ct6002737>.
- (98) Gerenkamp, M.; Grimme, S. Spin-Component Scaled Second-Order Møller–Plesset Perturbation Theory for the Calculation of Molecular Geometries and Harmonic Vibrational Frequencies. *Chem. Phys. Lett.* **2004**, *392* (1), 229–235. <https://doi.org/10.1016/j.cplett.2004.05.063>.
- (99) Grimme, S. Improved Second-Order Møller–Plesset Perturbation Theory by Separate Scaling of Parallel- and Antiparallel-Spin Pair Correlation Energies. *J. Chem. Phys.* **2003**, *118* (20), 9095–9102. <https://doi.org/10.1063/1.1569242>.
- (100) Frisch, M. J.; Trucks, G. W.; Schlegel, H. B.; Scuseria, G. E.; Robb, M. A.; Cheeseman, J. R.; Scalmani, G.; Barone, V.; Petersson, G. A.; Nakatsuji, H.; Li, X.; Caricato, M.; Marenich, A. V.; Bloino, J.; Janesko, B. G.; Gomperts, R.; Mennucci, B.; Hratchian, H. P.; Ortiz, J. V.; Izmaylov, A. F.; Sonnenberg, J. L.; Williams-Young, D.; Ding, F.; Lipparini, F.; Egidi, F.; Goings, J.; Peng, B.; Petrone, A.; Henderson, T.; Ranasinghe, D.; Zakrzewski, V. G.; Gao, J.; Rega, N.; Zheng, G.; Liang, W.; Hada, M.; Ehara, M.; Toyota, K.; Fukuda, R.; Hasegawa, J.; Ishida, M.; Nakajima, T.; Honda, Y.; Kitao, O.; Nakai, H.; Vreven, T.; Throssell, K.; Montgomery, Jr., J. A.; Peralta, J. E.; Ogliaro, F.; Bearpark, M. J.; Heyd, J. J.; Brothers, E. N.; Kudin, K. N.; Staroverov, V. N.; Keith, T. A.; Kobayashi, R.; Normand, J.; Raghavachari, K.; Rendell, A. P.; Burant, J. C.; Iyengar, S. S.; Tomasi, J.; Cossi, M.; Millam, J. M.; Klene, M.; Adamo, C.; Cammi,

R.; Ochterski, J. W.; Martin, R. L.; Morokuma, K.; Farkas, O.; Foresman, J. B.; Fox, D. J. Gaussian 09, Revision E.01. **2016**.

(101) Parrish, R. M.; Burns, L. A.; Smith, D. G. A.; Simmonett, A. C.; DePrince, A. E.; Hohenstein, E. G.; Bozkaya, U.; Sokolov, A. Yu.; Di Remigio, R.; Richard, R. M.; Gonthier, J. F.; James, A. M.; McAlexander, H. R.; Kumar, A.; Saitow, M.; Wang, X.; Pritchard, B. P.; Verma, P.; Schaefer, H. F.; Patkowski, K.; King, R. A.; Valeev, E. F.; Evangelista, F. A.; Turney, J. M.; Crawford, T. D.; Sherrill, C. D. Psi4 1.1: An Open-Source Electronic Structure Program Emphasizing Automation, Advanced Libraries, and Interoperability. *J. Chem. Theory Comput.* **2017**, *13* (7), 3185–3197. <https://doi.org/10.1021/acs.jctc.7b00174>.

Supporting Information

Total and interaction energies of 2 and 4 ion-paired clusters; Cartesian coordinates of the optimized 2 and 4 ion-paired clusters.

Corresponding Author

*katya.pas@monash.edu

Author Contributions

The manuscript was written through contributions of all authors. All authors have given approval to the final version of the manuscript.

Funding Sources

This work was supported through the Australian Government Research Training Program.

Notes

None.

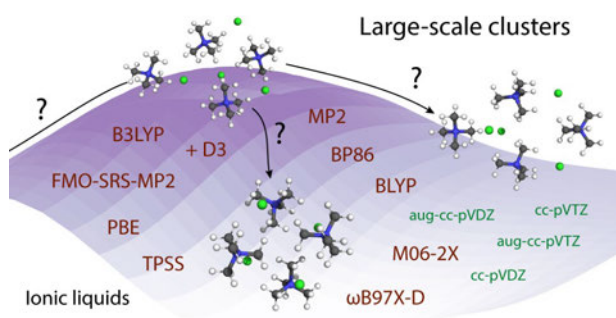
Acknowledgments

The authors gratefully acknowledge a generous allocation of computer resources through the Monash *e*Research Centre and the National Computational Infrastructure. This research was supported by an Australian Government Research Training Program (RTP) Scholarship.

Abbreviations

DFT, density functional theory; coupled cluster with singles, doubles and non-iterative triples, CCSD(T); FMO, fragment molecular orbital approach; HF, Hartree-Fock; [C₁mim][BF₄], 1-methyl-3-methylimidazolium tetrafluoroborate; [C₁mim]Cl, 1-methyl-3-methylimidazolium chloride; SRS-MP2, spin-component ratio scaling MP2; [C₁mpyr][BF₄], N,N'-methyl-methylpyrrolidinium tetrafluoroborate; [C₁mpyr]Cl, N,N'-methyl-methylpyrrolidinium chloride; [NMe₄][BF₄], tetramethylammonium tetrafluoroborate; [NMe₄]Cl, tetramethylammonium chloride; [C₂py][BF₄], 1-ethylpyrrolidinium tetrafluoroborate; [C₂py]Cl, 1-ethylpyrrolidinium chloride; VDZ, cc-pVDZ; VTZ, cc-pVTZ; aVDZ, aug-cc-pVDZ; aVTZ, aug-cc-pVTZ; SD, standard deviation; RMSD, root mean square deviation; MAE, mean absolute error;

For Table of Contents Only



This the first systematic study that assesses the performance of varying DFT functionals for geometry optimizations of 2 and 4 ion-paired clusters of ionic liquids consisting of imidazolium, pyrrolidinium, pyridinium and ammonium cations.

3.3 References

- [1] Patricia A. Hunt, Ian R. Gould, and Barbara Kirchner. The Structure of Imidazolium-Based Ionic Liquids: Insights From Ion-Pair Interactions. *Australian Journal of Chemistry* **60**(1) (2007), 9–14. DOI: [10.1071/CH06301](https://doi.org/10.1071/CH06301).
- [2] Ekaterina I. Izgorodina, Dorothea Golze, Radha Maganti, Vanessa Armel, Maria Taige, Thomas J. S. Schubert, and Douglas R. MacFarlane. Importance of Dispersion Forces for Prediction of Thermodynamic and Transport Properties of Some Common Ionic Liquids. *Physical Chemistry Chemical Physics* **16**(16) (2014), 7209–7221. DOI: [10.1039/C3CP53035C](https://doi.org/10.1039/C3CP53035C).
- [3] Zoe L. Seeger, Rika Kobayashi, and Ekaterina I. Izgorodina. Cluster Approach to the Prediction of Thermodynamic and Transport Properties of Ionic Liquids. *The Journal of Chemical Physics* **148**(19) (2018), 193832. DOI: [10.1063/1.5009791](https://doi.org/10.1063/1.5009791).
- [4] Samuel Y. S. Tan, Luke Wylie, Ivan Begic, Dennis Tran, and Ekaterina I. Izgorodina. Application of Spin-Ratio Scaled MP2 for the Prediction of Intermolecular Interactions in Chemical Systems. *Physical Chemistry Chemical Physics* **19**(42) (2017), 28936–28942. DOI: [10.1039/C7CP04391K](https://doi.org/10.1039/C7CP04391K).
- [5] Samuel Tan, Santiago Barrera Acevedo, and Ekaterina I. Izgorodina. Generalized Spin-Ratio Scaled MP2 Method for Accurate Prediction of Intermolecular Interactions for Neutral and Ionic Species. *The Journal of Chemical Physics* **146**(6) (2017), 064108. DOI: [10.1063/1.4975326](https://doi.org/10.1063/1.4975326).
- [6] Dmitri G. Fedorov, Ryan M. Olson, Kazuo Kitaura, Mark S. Gordon, and Shiro Koseki. A New Hierarchical Parallelization Scheme: Generalized Distributed Data Interface (GDDI), and an Application to the Fragment Molecular Orbital Method (FMO). *Journal of Computational Chemistry* **25**(6) (2004), 872–880. DOI: [10.1002/jcc.20018](https://doi.org/10.1002/jcc.20018).
- [7] Dmitri G. Fedorov and Kazuo Kitaura. On the Accuracy of the 3-Body Fragment Molecular Orbital Method (FMO) Applied to Density Functional Theory. *Chemical Physics Letters* **389**(1) (2004), 129–134. DOI: [10.1016/j.cplett.2004.03.072](https://doi.org/10.1016/j.cplett.2004.03.072).

- [8] Ekaterina I. Izgorodina, Jason Rigby, and Douglas R. MacFarlane. Large-Scale *Ab Initio* Calculations of Archetypical Ionic Liquids. *Chemical Communications* **48**(10) (2012), 1493–1495. doi: [10.1039/C1CC15056A](https://doi.org/10.1039/C1CC15056A).
- [9] Kazuo Kitaura, Eiji Ikeo, Toshio Asada, Tatsuya Nakano, and Masami Uebayasi. Fragment Molecular Orbital Method: An Approximate Computational Method for Large Molecules. *Chemical Physics Letters* **313**(3) (1999), 701–706. doi: [10.1016/S0009-2614\(99\)00874-X](https://doi.org/10.1016/S0009-2614(99)00874-X).

Chapter 4

Tuning DLPNO-CCSD(T): A high accuracy method at reduced cost

4.1 Introduction

When high accuracy is desired, the method of choice is gold standard coupled cluster with single-, double-, and perturbative triple-excitations (CCSD(T), see section 1.2). However, the systems that can be studied with this method are limited to tens of atoms due to the tremendous resources required. Recently developed domain-based local pair natural orbital coupled-cluster method, DLPNO-CCSD(T),¹⁻⁵ uses localised orbitals to reduce the virtual space and limits coupled cluster treatment of doubles and triples to those with sufficient electron occupation.⁶ The implementation of DLPNO-CCSD(T) has been designed to use a comparable amount of resources as density functional theory while obtaining coupled cluster level results. In practice, the method reproduces canonical CCSD(T) energies to within 1 kJ mol⁻¹ in neutral dimers when the parameters controlling the external space are chosen to be the most accurate of the predefined settings: ‘TightPNO’.^{7,8}

Section 4.2 contains a manuscript submitted to *The Journal of Chemical Theory and Computation*. The text is a benchmarking study – applying DLPNO-CCSD(T) to both protic and aprotic ionic liquids and assessing the errors against CCSD(T) values. The errors of DLPNO-CCSD(T)

in ionic liquids have not yet been assessed and DLPNO-CCSD(T) would be an asset in unlocking energies of larger systems that are currently inaccessible by traditional high accuracy methods. In addition to providing a detailed analysis of the performance in ionic liquids, the study also aims to fine-tune the parameters of the method in order to obtain spectroscopic accuracy (within 1 kJ mol^{-1}) such that the energies are truly of coupled cluster accuracy.

DLPNO-CCSD(T) with TightPNO settings is shown to produce energies within chemical accuracy and is recommended for use in ionic liquid calculations to reduce resource consumption when errors of up to 3 kJ mol^{-1} are acceptable. The accuracy of the DLPNO-CCSD(T) was found to be dependent on both the anion and cation involved. Halides, especially bromide systems were associated with the largest systematic errors and settings have been developed to obtain spectroscopic accuracy for these systems. Additionally, these setting also reduced the errors of hydrogen bonded ionic liquids to below 1 kJ mol^{-1} . Aprotic systems of tetrafluoroborate, dicyanamide, mesylate, hexafluorophosphate and tosylate required more doubles and triples to be treated at a couple cluster level, although settings for spectroscopic accuracy have also been recommended for these systems.

A DLPNO-CCSD(T) benchmarking study of intermolecular interactions of ionic liquids

*Zoe L. Seeger and Ekaterina I. Izgorodina**

School of Chemistry, Monash University, 17 Rainforest Walk, Clayton, Victoria 3800, Australia

Keywords: DLPNO, DLPNO-CCSD(T), CCSD(T), ionic liquids, benchmarking, benchmark, protic, aprotic, coupled cluster, domain-based local pair natural orbital

Abstract

The accuracy of correlation energy recovered by coupled cluster single-, double-, and perturbative triple-excitations, CCSD(T), has led to the method being considered the gold standard of computational chemistry. Due to its scalability of N^7 (where N is the number of basis functions), the application of CCSD(T) has been limited to medium-sized molecular systems. The recent development of alternative domain-based local pair natural orbital coupled-cluster method, DLPNO-CCSD(T), has significantly broadened the range of chemical systems to which CCSD(T) level calculations can be applied. Studying condensed systems, such as liquids and solids, requires inclusion of tens to hundreds of molecules in one simulation. Some of these, such as ionic liquids consisting entirely of organic-type ions, have a large contribution from dispersion forces that grow with increasing cluster size. In this work, the performance of DLPNO-CCSD(T) is validated for the prediction of correlation interaction energies of two data sets consisting of protic and aprotic

ionic liquids. Parameters controlling the external space, $T_{CutPairs}$, T_{CutPNO} and T_{CutMKN} , as well as the treatment of triple excitations, were probed to achieve spectroscopic accuracy for these semi-Coulombic systems. DLPNO-CCSD(T) readily gave chemical accuracy, with respect to conventional CCSD(T), for all of the systems tested when tight parameter settings were used, with systems containing the NTf₂⁻ anion achieving energies within 1 kJ mol⁻¹. Three additional settings, $T_{CutPairs}$ and T_{CutPNO} , and the iterative treatment of triple excitations were found important to attain spectroscopic accuracy depending on the anion type. Two new sets of parameters, labeled IL1PNO and IL2PNO, are put forward to ensure the reliable performance of DLPNO-CCSD(T) for halide-based and hydrogen bonded ionic liquids as well as to attain spectroscopic accuracy for all types of ionic liquids for future benchmarking.

Introduction

Despite their predominantly electrostatic nature, ionic liquids have been shown to possess a large contribution from dispersion forces that grow with an increasing number of ions in the system.¹ It has been demonstrated that dispersion forces have an enormous effect on the bulk structure of ionic liquids.² The accurate recovery of energetics has improved reliability of the prediction of physicochemical properties of ionic liquids.³ Furthermore, interaction energies have shown to provide insight into how macroscopic properties of ionic liquids are manifested. Interaction energies are strongly linked with melting point^{4,5} as well as conductivity,⁶ although the complex nature of the relationship demands further investigation.

Innovative new theory, Domain-based Local Pair Natural Orbital (DLPNO)⁷⁻¹⁰, is a milestone formulation in the endeavour of building a toolbox of reliable methods that provides extremely accurate results at a fraction of the computational cost. DLPNO takes advantage of the local nature of correlation by localising internal orbitals. These local molecular orbitals (LMOs) are created

through a Foster-Boys orbital rotation procedure to form non-orthogonal orbitals.¹¹ Furthermore, as devised by Saebø and Pulay, a set of spatially close projected atomic orbitals (PAOs) can be constructed for each LMO by projecting out only the occupied orbitals, thus manifesting the locality of the generated LMOs.¹² A reduction of the external space (which is much larger than the internal) is achieved through using an incomplete set of pair natural orbitals (PNOs) to represent the correlating orbitals specific for electron pair that are also localised.¹³ The PNOs are thus created as linear combinations of the PAOs.

Coupled cluster (CC) theory employing the DLPNO theory has been developed by Neese's group and have produced, among others, a series of methods such as DLPNO-CCSD in 2009⁸ followed by DLPNO-CCSD(T) in 2013⁹ and improved iterative triples in 2018¹⁰. Among these methods, DLPNO-CCSD(T) has demonstrated superb performance. For example, DLPNO-CCSD(T) was shown to recover > 95 % of the canonical triples energy and 99.8 % of the total correlation energy with various basis sets in medium-sized molecules including penicillin.¹⁰ Overall, inclusion of iterative triples was shown to improve the accuracy of absolute energies of the GMTKN30 database. The method boasts similar computational cost to density functional theory and linear scaling with system size.

The DLPNO theory introduces three main cutoffs to control the size of the molecular orbital external space. Estimated multipole Møller-Plesset second order perturbation theory (MP2) pair energies are compared with $T_{CutPairs}$ to determine electron pairs included in a subsequent coupled cluster calculation; these are called strong pairs. Pairs with energies less than the cutoff and larger than $T_{CutPairs} \times 10^{-2}$ are recalculated at the MP2 level with the semi-canonical orbitals (weak pairs) while the rest are accounted for with the MP2 estimate (skipped pairs). PNOs with occupation numbers less than T_{CutPNO} are dropped and this controls the size of the external space per electron

pair. T_{CutPNO} was identified to have the largest effect on error and the added pair energies calculated with MP2 helps to cancel some of the error introduced by this truncation.¹⁴ A third cutoff, T_{CutMKN} is used during the resolution-of-identity (RI) transformation to help with large-scale integral transformations and controls the fit to the PNOs. It has been shown to be insensitive to the cutoff value to a certain extent.⁷ T_{CutMKN} has been additionally used to construct the PAO domains from which the PNOs are expanded. In DLPNO-CCSD(T), triple natural orbitals (TNOs) are constructed with T_{CutTNO} with the threshold of $T_{\text{CutPNO}} \times 10^{-2}$ and T_{CutPNO} is converged at $T_{\text{CutTNO}} = 10^{-7}$.⁹

Liakos, Neese and co-workers have performed a benchmarking study on datasets including 51 reaction energies by Friedrich and Hänchen¹⁵ including isomerisations, hydrogenations, allylic shifts and oxidations; S66 dimers bound by hydrogen bonds and dispersion; 52 melatonin conformers differentiated in energy by intramolecular weak hydrogen bonds and aromatic-amide interactions; and 65 gas phase conformers of butane-1,4-diol that span almost 30 kJ mol⁻¹.¹⁶ The convergence of electronic energy with tightened T_{CutPairs} , T_{CutPNO} and T_{CutMKN} was explored. The research establishes three presets of the theory: LoosePNO ($T_{\text{CutPNO}} = 10^{-6}$, $T_{\text{CutPairs}} = 10^{-3}$, $T_{\text{CutMKN}} = 10^{-3}$), NormalPNO ($T_{\text{CutPNO}} = 3.33 \times 10^{-7}$, $T_{\text{CutPairs}} = 10^{-4}$, $T_{\text{CutMKN}} = 10^{-3}$), and TightPNO ($T_{\text{CutPNO}} = 10^{-7}$, $T_{\text{CutPairs}} = 10^{-5}$, $T_{\text{CutMKN}} = 10^{-4}$), such that DLPNO-CCSD(T) can be used in a black-box fashion. LoosePNO and NormalPNO treat MP2 pairs semicanonically but TightPNO pairs canonically. (Since this study, T_{CutMKN} has been increased from 10^{-4} to 10^{-3} in TightPNO settings.¹⁷) In the study of Liakos *et al.*,¹⁶ DLPNO-CCSD(T)/cc-pVTZ with LoosePNO, NormalPNO and TightPNO settings produced 2.6, 1.3, 0.5 kJ mol⁻¹ mean absolute deviations, respectively, for the Friedrich and Hänchen reaction energies compared to CCSD(T)/cc-pVTZ. The S66 dataset performed even better and a mean absolute deviation of 0.4 kJ mol⁻¹ was obtained for TightPNO.

Energy deviations for the systems of melatonin and butane-1,4- diol with TightPNO settings were within 1 kJ mol⁻¹.

A second study by Liakos and Neese has shown that DLPNO-CCSD(T) can reproduce canonical CCSD(T) energies to within 1 kJ mol⁻¹ with TightPNO for organic isomerisation energies and binding energies of weakly bound organic dimers such as a parallel displaced benzene and neutral molecules with neon.¹⁸ The TightPNO settings incur a two- to four-fold increase in cost compared to the default NormalPNO settings, however are still magnitudes cheaper than canonical CCSD(T). The study concluded that CCSD(T) level accuracy can be reproduced at near density functional theory cost.

Chen *et al.* have investigated the use of DLPNO-CCSD(T) in the determination of CCSD(T) values with a complete basis set (CBS) by replacing conventional CCSD(T) with the DLPNO analogue.¹⁹ This was tested in neutral dimers of hydrogen bonded complexes, dispersion-dominated complexes and mixed complexes, in datasets S22, HSG, HBC6, NBC10, and S66 – for which both electrostatics and dispersion play equal roles. Mean average errors were found to be below 1 kJ mol⁻¹ with respect to CCSD(T)/CBS. Larger errors were seen in chemical systems with strong electron correlation, although these errors still fell within chemical accuracy. The authors also reported that the LoosePNO and NormalPNO settings were more likely to exclude important weakly interacting electronic states that contributed to correlation energies of non-covalent systems, thus the use of cutoffs in the TightPNO settings was necessary. Additionally, larger dispersion components had a larger impact on the accuracy of DLPNO non-iterative triples. Iterative triples were also employed, although differences in errors between the two approaches were found to be negligible.

In a study of Paulechka and Kazakov, organic enthalpies of formation were calculated using DLPNO-CCSD(T) with TightPNO settings and compared with experimental data.²⁰ The experimental data was collected from the literature on 45 systems containing only C, H, O, and N and included systems as large as biphenyl and 1-naphthol. The prediction of this challenging thermodynamic property was achieved within 3 kJ mol⁻¹ when coupled with the def2-QZVP basis set and outperformed results determined with G4 which had a maximum error of over 8 kJ mol⁻¹.

A number of benchmarking studies have reported the successful application of DLPNO for use in larger systems inaccessible to CCSD(T). Experimental gas phase Ag⁺, Cu⁺, and Au⁺-ligand dissociation enthalpies have been compared to DLPNO-CCSD(T)/cc-pVTZ calculations giving a mean absolute error of 8.9 kJ mol⁻¹ with the NormalPNO settings, across 72 systems.²¹ DLPNO-CCSD(T)/CBS was also benchmarked for small methyl ester + OH reactions so that the method can be used to investigate larger biodiesel molecules. The method predicted barrier heights within 4.6 kJ mol⁻¹ with respect to CCSD(T)/CBS.²² Electronic energies of species in the reaction of hydroarylation and oxidative coupling catalyzed by Ru(II) chloride carbonyls by DLPNO-CCSD(T) were compared to CCSD(T) using a def2-TZVPP basis set.²³ With NormalPNO, absolute errors of up to 14.7 kJ mol⁻¹ were seen, whereas the tightening of the settings to TightPNO reduced the MAE to as little as 1.5 kJ mol⁻¹ for the reaction energies. Mean absolute errors for the carbonyls, intermediates and transition states were 4.4, 6.5 and 6.6 kJ mol⁻¹. By including the iterative triples¹⁰ in the DLPNO-CCSD(T) routine, the carbonyls, intermediates and transition states mean absolute errors were reduced to 2.5, 3.3 and 4.3 kJ mol⁻¹. Energy storage capacities for photochromic molecules were also interrogated with both NormalPNO and TightPNO. DLPNO-CCSD(T)/cc-pVTZ with NormalPNO and TightPNO produced errors of 4.7 and 2.0 kJ mol⁻¹, respectively, when compared to CCSD(T)-F12a/VDZ-F12.²⁴

The application of DLPNO methods to studying energetics of ionic liquids has not been yet achieved. Ionic liquids represent a challenge for quantum chemical methods due to a complex interplay of intermolecular forces that were found to correlate with experimental melting point and conductivity.⁴ Depending on the nature of the ionic liquid, electrostatic contributions²⁵ of single ion pairs vary between 300 and 479 kJ mol⁻¹ as calculated using symmetry adapted perturbation theory (SAPT).^{26,27} In ionic liquids, dispersion and induction forces flatten the potential energy surface and play a lesser but defining role in their geometry, when compared to electrostatics.²⁸ In single ion pairs these forces were shown to contribute up to 11% and 15%, respectively.^{4,29} On the absolute scale, this contribution could be as much as 59 kJ mol⁻¹ in single ion pairs, with the ratio of dispersion to electrostatics steadily increasing with a number of ion pairs in the system.^{1,5} Additionally, the induction largely contributes to the stabilisation of hydrogen bonding in these systems where hydrogen bonding is known to affect macroscopic properties through the cation and anion arrangements.³⁰ Charge-transfer, defined as the excitation of an electron into the virtual orbital on a secondary molecule within SAPT, is very significant in ILs, allowing for the electron density to flow from the anion to the cation, whereby reducing their formal charges below the unity charge on the absolute scale. Previously it was shown that charge transfer of as much as 0.2 *e* from the anion to the cation could be observed for imidazolium and pyrrolidinium ionic liquids.²⁵ The stabilising effect of charge transfer is shown to be important in molecular dynamics simulations to reproduce experimental data and hence, it is now common to account for charge fluctuations via various approaches.^{31,32}

A substantial contribution from dispersion forces and the importance of charge transfer requires the application of highly correlated levels of theory to accurately extract electron correlation. The sheer size of ionic liquid ions makes them computationally demanding candidates for conventional

CCSD(T), limiting the application of the latter to 2 ion paired clusters of medium-sized ions.³³ Already, a single ion pair of a N,N-butyl-methyl pyrrolidinium cation and a bulky anion such as tosylate could not be computed with conventional CCSD(T). Therefore, this study aims to determine whether DLPNO-CCSD(T) can be reliably used for studying energetics of single ion pairs of ionic liquids. In this study DLPNO-CCSD(T) correlation interaction energies are compared with conventional CCSD(T) for correlation interaction energies of a series of protic (obtained by a proton transfer from an acid to a base) and aprotic (all ionic liquids other than protic) single ion pair systems previously published by our group. A set of parameters used in the DLPNO approach will be thoroughly tested with the view of finding the “Goldilocks zone” that allows for reliable compromise between accuracy and cost.

Theoretical Procedures

Two datasets of single ion paired ionic liquids – IL174^{4,33} and HBIL42^{34,35} – have been used to test the application of DLPNO-CCSD(T) (Figs. 1 & 3). The dataset, termed IL174, comprises of ion pairs (IPs) of aprotic ionic liquids (AILs). All possible combinations of 8 different ionic liquid anions – chloride (Cl^-), bromide (Br^-), bis(trifluoromethane)sulfonimide (NTf_2^-), dicyanamide ($\text{N}(\text{CN})_2^-$), mesylate (CH_3SO_3^-), tetrafluoroborate (BF_4^-), hexafluorophosphate (PF_6^-), tosylate ($\text{CH}_3\text{C}_6\text{H}_4\text{SO}_3^-$) – and 2 families of ionic liquid cations – N,N'-alkyl-methylpyrrolidinium (C_nmpyr^+) and 1-alkyl-3-methylimidazolium (C_nmim^+) – were considered except for NTf_2^- with C_4mim^+ and C_4mpyr^+ , thus making the total number of 179 systems. Anions range from single atom-based anions such as Cl^- to anions with strong delocalisation over the entire structure such as NTf_2^- . The alkyl chain length (n) on the cations varies from methyl ($n = 1$), ethyl ($n = 2$), n -propyl ($n = 3$) to n -butyl ($n = 4$). Single ion pairs of all possible combinations of these ions were

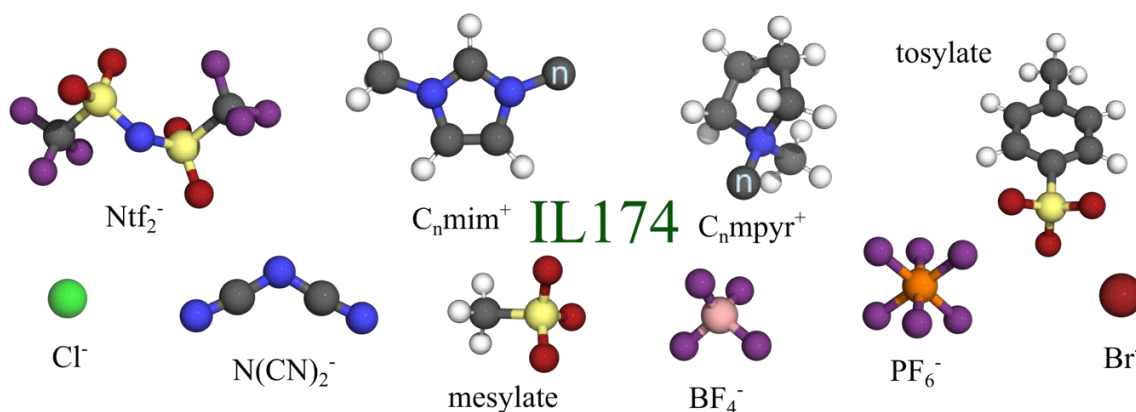


Figure 1. Ions in the aprotic dataset AIL. Cations: 1-alkyl-3-methylimidazolium ($C_n\text{mim}^+$) and N,N'-alkyl-methylpyrrolidinium ($C_n\text{mpyr}^+$). Anions (from left to right): chloride, bis(trifluoromethane)sulfonimide (Ntf_2^-), dicyanamide ($\text{N}(\text{CN})_2^-$), mesylate (CH_3SO_3^-), tetrafluoroborate (BF_4^-), hexafluorophosphate (PF_6^-), tosylate ($\text{CH}_3\text{C}_6\text{H}_4\text{SO}_3^-$) and bromide.

conformationally screened in our previous work⁴ and energetically favourable configurations were selected based on the 10 kJ mol^{-1} difference to the lowest energy configuration for each cation-anion combination.

The second dataset, termed HBIL, contains 42 single ion pairs of protic ionic liquids (PILs) that are synthesised by a proton transfer from a Brønsted acid to a Brønsted base. As a result, ion pairs of these ionic liquids exhibit strong and directional hydrogen bonding between the cation and anion (Fig. 2). The complete list of cations and anions included in the HBIL dataset is shown in Fig. 3. Interaction energies of CCSD(T)/aug-cc-pVDZ (aVDZ) and CCSD(T) with a complete basis set

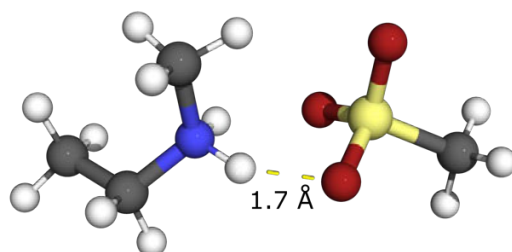


Figure 2. Hydrogen bond in N,N-methyl-ethylammonium and mesylate.

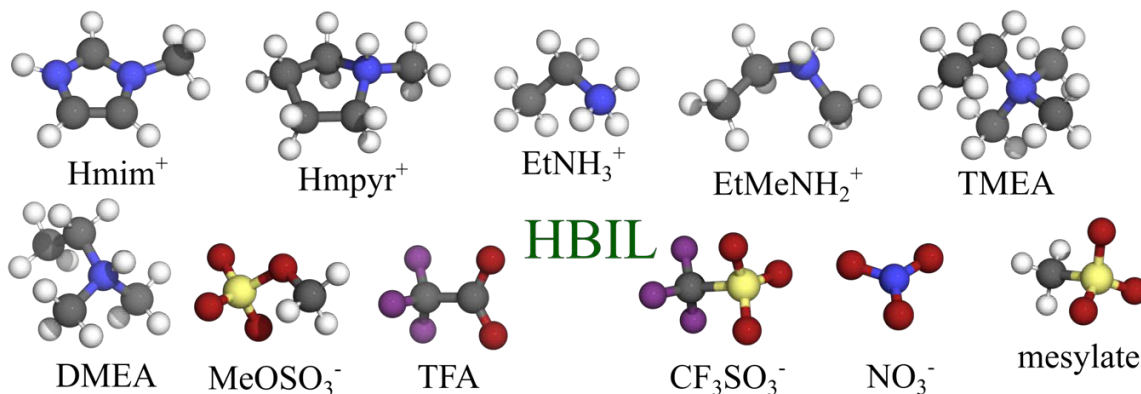


Figure 3. Ions in the HBIL42 dataset. Cations: 3-methylimidazolium (Hmim^+); N-methylpyrrolidinium (Hmpyr^+); N-ethylammonium (EtNH_3^+); N,N-methyl-ethylammonium (EtMeNH_2^+); trimethyl-ethylammonium (TMEA); and N,N-dimethyl-ethylammonium (DMEA). Anions: methyl sulfate (MeOSO_3^-), trifluoroacetate (TFA), triflate (CF_3SO_3^-), nitrate (NO_3^-) and mesylate (CH_3SO_3^-).

(CBS) of the IL174 and HBIL42 datasets were taken from previously published work by our group.^{33–35} Correlation interaction energies calculated with CCSD(T)/CBS were extrapolated as follows:^{36,37}

$$E_{\text{MP2/CBS}}^{\text{corr}} = \frac{X^3 E_{\text{MP2}/X}^{\text{corr}} - Y^3 E_{\text{MP2}/Y}^{\text{corr}}}{X^3 - Y^3} \quad (1)$$

where $X=3$ and $Y=4$ for aug-cc-pVTZ and aug-cc-pVQZ, respectively and

$$E_{\Delta\text{CCSD}(T)}^{\text{corr}} = E_{\text{CCSD}(T)}^{\text{corr}} - E_{\text{MP2}}^{\text{corr}} \quad (2)$$

corrects the perturbative energy via:

$$E_{\text{CCSD}(T)/\text{CBS}}^{\text{corr}} = E_{\Delta\text{CCSD}(T)}^{\text{corr}} + E_{\text{MP2/CBS}}^{\text{corr}} \quad (3)$$

Single point energies of DLPNO-CCSD(T) with cc-pVTZ and aug-cc-pVDZ were calculated using *ab initio*, DFT and semi-empirical SCF-MO package, ORCA version 4.2.^{38,39} Calculations were performed with both non-iterative and iterative triples which will be referred to here as

DLPNO-CCSD(T₀) and DLPNO-CCSD(T₁), respectively. “TightSCF” and “TightPNO” settings were requested unless specified otherwise, where “TightPNO” uses the PNO and TNO expansion cutoffs, $T_{CutPNO} = 1 \times 10^{-7}$ and $T_{CutTNO} = 1 \times 10^{-9}$, the pair energies required for coupled cluster calculation as $T_{CutPairs} = 1 \times 10^{-5}$ and the fit to PNOs $T_{CutMKN} = 1 \times 10^{-3}$. Resolution of identity approximation, RIJCOSX, was employed to speed up both coulomb and exchange two electron integrals with the view of testing its reliability and impact on correlation energies in ionic liquids. Corresponding “/C” auxiliary basis sets were used with the basis sets to satisfy the RI approximation. All correlation energies were counterpoise corrected using the Boys and Bernadi approach except for the CCSD(T)/CBS results of HBIL.⁴⁰

Comparison of methods – DLPNO-CCSD(T) and traditional CCSD(T) – use correlation interaction energies to quantify the recovery of correlation energy and are calculated as:

$$E_{INT} = E_{IP} - \sum_{i=1}^{ions} E_i \quad (4)$$

where E_i represents the energy of individual ions in the geometry adopted in the corresponding ion pair (IP).

Energy differences are reported using the following statistical measures - minimum errors (min), mean absolute errors also known as mean unsigned errors (MAE), maximum errors (max) and sample standard deviations (SD):

$$SD = \sqrt{\frac{\sum_{i=1}^N (x_i - \bar{x})^2}{N - 1}} \quad (5)$$

where N is the number of values, \bar{x} is the mean.

A state-of-the-art method of symmetry adapted perturbation theory (SAPT), SAPT2+3, has previously been used to decompose the interaction energy into five foundational forces - Electrostatics (E_{Elst}), induction (E_{Ind}), dispersion (E_{Disp}), charge transfer (E_{CT}) and exchange

energies (E_{Exch}).^{25,27} These forces populate two categories: long-range and short-range.⁴¹ The long-range forces decay with an inverse power with distance and are electrostatic, induction and dispersion, whereas short-range forces such as charge transfer and exchange decay exponentially with increasing distance due to decreasing orbital overlap. SAPT is inherently free from basis set superposition error. For more detail on the components of the five fundamental forces within SAPT2+3 see Refs 42–44. The raw SAPT values can be found in reference.²⁵

Percentiles for SAPT energies were calculated with the empirical cumulative distribution (\hat{F}_n) function in R. The function returns the fraction of observations less than or equal to the queried value (t) via:

$$\hat{F}_n = \frac{1}{n} \sum_{i=1}^n \mathbf{1}_{X_i \leq t} \quad (11)$$

where n is the number of elements in the sample and $\mathbf{1}_{X_i \leq t}$ is one when element $X_i \leq t$ and zero otherwise. These were converted to percentages.

Results and discussion

Performance of DLPNO-CCSD(T₀)

DLPNO-CCSD(T₀)/aug-cc-pVDZ errors in correlation interaction energies are given in Table 1, where T₀ denotes the use of non-iterative triples.

Table 1. Correlation interaction energy errors (in kJ mol^{-1}) of DLPNO-CCSD(T_0)/aug-cc-pVDZ for the IL174 dataset. CCSD(T)/aug-cc-pVDZ interaction energies were used as the benchmark.

Cation	Anion	#Systems	Min	MAE	Max	SD
C ₁₋₄ mim	BF ₄ ⁻	7	1.5	1.6	1.7	0.1
	Br ⁻	14	1.9	2.4	2.8	0.3
	Cl ⁻	14	1.0	1.2	1.4	0.1
	N(CN) ₂ ⁻	17	1.5	2.1	2.5	0.3
	mesylate	7	2.0	2.1	2.3	0.2
	NTf ₂ ⁻	8	0.2	0.9	1.9	0.6
	PF ₆ ⁻	7	1.4	1.6	1.8	0.1
	tosylate	7	1.3	1.4	1.6	0.1
C ₁₋₄ mpyr	BF ₄ ⁻	11	1.0	1.2	1.3	0.1
	Br ⁻	11	1.9	2.1	2.3	0.1
	Cl ⁻	11	1.0	1.1	1.2	0.1
	N(CN) ₂ ⁻	19	1.0	1.3	1.6	0.2
	mesylate	11	1.3	1.7	2.1	0.2
	NTf ₂ ⁻	16	0.4	0.9	1.4	0.3
	PF ₆ ⁻	11	1.0	1.3	1.4	0.1
	tosylate	8	0.2	1.1	1.4	0.4

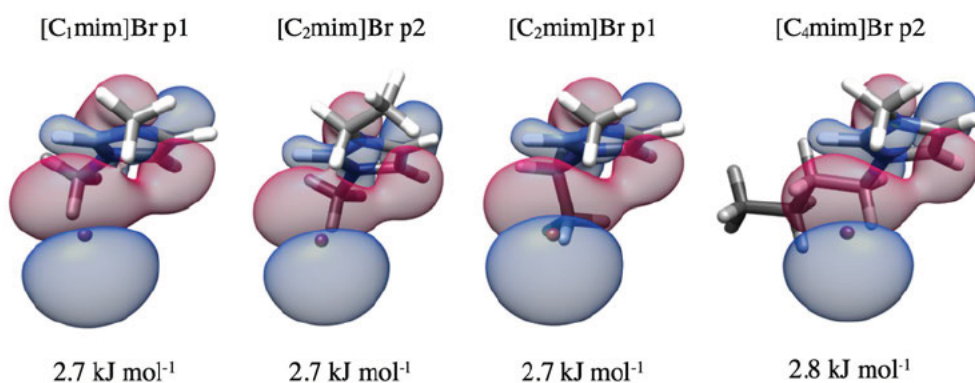
The differences between DLPNO-CCSD(T_0) and CCSD(T) are consistent, providing mean absolute errors in the range of 0.9 and 2.4 kJ mol^{-1} and an overall MAE and standard deviation of 1.5 and 0.5 kJ mol^{-1} , respectively. Surprisingly, out of the anions studied, the NTf₂⁻ anions give the smallest values for MAE with both cations, with the highest SD value of 0.6 kJ mol^{-1} when paired with the imidazolium cations. Errors above 2 kJ mol^{-1} were observed in bromide- and mesylate-containing ion pairs with both cations as well as imidazolium dicyanamides. None of these particularly stand out as supported by the standard deviations of these systems falling in the range of 0.1 to 0.3 kJ mol^{-1} . [C_nmim]Br ion pairs have the largest MAE of 2.4 kJ mol^{-1} and a maximum error of 2.84 kJ mol^{-1} , which may be attributed to the electron rich nature of the anion, which leads to a more slowly decaying electron density. However, this is not observed in the chloride systems that have relatively low MAEs of 1.2 and 1.1 kJ mol^{-1} in imidazolium- and pyrrolidinium-based ion pairs, respectively.

Table 2. Percentiles (P) of SAPT2+3 of IL174 energies including electrostatics (Elst), induction (Ind), dispersion (Disp), charge transfer (CT) and exchange-repulsion (Exch), the HOMO-LUMO gap (Gap, eV) and associated DLPNO-CCSD(T₀) Error (kJ mol⁻¹).

Ion pair config	Percentiles of SAPT energies						Error
	P _{Elst}	P _{Exch}	P _{Ind}	P _{Disp}	P _{CT}	Gap	
[C ₄ mim]Br p3	32	84	22	39	14	8.32	2.3
[C ₃ mim]Br p1	7	97	14	20	3	8.50	2.7
[C ₁ mim]Br p1	3	98	16	23	1	8.53	2.7
[C ₂ mim]Br p2	6	96	15	22	2	8.51	2.7
[C ₄ mim]Br p2	6	99	12	11	2	8.53	2.7
[C ₂ mim]Br p1	7	95	18	23	3	8.48	2.7
[C ₃ mim]Br p2	4	100	13	13	1	8.53	2.8
[C ₄ mim]Br p1	8	97	13	18	4	8.51	2.8

Percentiles for each of the SAPT interaction types have been given in Table 2 for systems with errors larger than 2.5 kJ mol⁻¹ and also the next largest bromide error for comparison. Percentile values indicate the percentage of data that lies below that value. Higher percentiles in the case of exchange, whose values are positive, represents systems of larger exchange whereas for the other negative components, lower percentiles mean that fewer other systems have more negative contributions. The seven imidazolium bromide systems have quantities of exchange all within the

Figure 4. HOMOs and associated DLPNO/aug-cc-pVDZ error of the larger error systems.



95th percentile and dominate the top end of the distribution of exchange. They additionally show large negative contributions of electrostatics and charge transfer in the 1st – 4th percentile. The imidazolium bromide structures of errors $< 2.5 \text{ kJ mol}^{-1}$ have smaller charge transfer components between the 12th and 18th percentile. While electrostatics and exchange are not likely to play a role in correlation errors, incomplete treatment of charge transfer could lead to incorrect dispersion values. The magnitude of the imidazolium bromide interaction correlation from CCSD(T)/aug-cc-pVDZ is roughly average with respect to the IL174 database.

The HOMOs of four imidazolium bromide systems and their errors are shown in Figure 4. Imidazolium bromide configurations, denoted here as p1 and p2, contain the bromide interacting below the imidazolium ring and differ in the orientation of the alkyl chain. All of these p1 and p2 structures in IL174 obtained errors greater than 2.5 kJ mol^{-1} . In contrast, configurations of this ionic liquid where the bromide interacts with the acidic hydrogen of the cation ring in the plane either closer or further from the alkyl chain all had errors below 2.3 kJ mol^{-1} regardless of the alkyl chain length. The error magnitude correlates with larger magnitude of their interaction correlation energy and charge transfer. To this end, there is no obvious link between the chain length, cation-anion distance and errors in DLPNO. The only trend that could be discerned showed that ionic systems of halide anions exhibiting high charge transfer, in this case $-58.3 - -68.0 \text{ kJ mol}^{-1}$ and high exchange and electrostatics can potentially have increased errors.

Table 3. Correlation interaction energy errors (in kJ mol^{-1}) of DLPNO-CCSD(T_0)/aug-cc-pVDZ for the HBIL dataset. CCSD(T)/aug-cc-pVDZ interaction energies were used as the benchmark.

Anion	#Systems	Min	MAE	Max	SD
CF_3SO_3^-	7	0.7	1.4	2.1	0.5
Cl^-	7	0.7	0.8	1.1	0.2
MeOSO_3^-	6	1.2	1.5	1.9	0.3
mesylate	7	1.1	1.4	2.0	0.3
NO_3^-	7	1.4	1.7	2.3	0.3
TFA	8	0.7	1.1	1.5	0.3

Table 3 and Figure 5 show the performance of DLPNO-CCSD(T_0) on the HBIL dataset with respect to CCSD(T), both with the aug-cc-pVDZ basis set. The standard deviations in Table 3 are presented with respect to the anion. When the standard deviations are determined with respect to the cation they span a narrow range of 0.3 to 0.4 kJ mol^{-1} . The errors are equally dependent on both the anion and cation involved. Again, the chloride systems perform extremely well as was seen in the IL174 dataset. These systems have the smallest SD of 0.2 kJ mol^{-1} . The MAE of chloride systems, 0.8 kJ mol^{-1} , is 0.6 kJ mol^{-1} lower than the overall MAE (1.4 kJ mol^{-1}) calculated for the HBIL set with T_0 triples and TightPNO settings. EtNH_3^+ and Hmim^+ ion pairs perform equally well, with an MAE of 1.1 kJ mol^{-1} , with exception for one of the two configurations of $[\text{Hmim}][\text{NO}_3]$ that had an MAE of 2.3 kJ mol^{-1} . This configuration has the anion located above/below the ring, whereas in the other configuration with an MAE of 1.4 kJ mol^{-1} the nitrate sits in the plane of the ring forming two hydrogen bonds. To this end, all of the combinations of anions and cations studied here perform within the chemical accuracy.

Performance of DLPNO-CCSD(T_1)

A summary of the DLPNO-CCSD(T)/aug-cc-pVDZ with iterative triples (T_1) errors is given in Table 4 for the IL174 dataset and Table 5 for the HBIL dataset. On average, the MAE is decreased only slightly, by 0.3 kJ mol^{-1} compared to DLPNO-CCSD(T_0) without iterative triples. The largest

decrease is seen in dicyanamide systems, for the MAE decreased from 2.1 to 1.5 and from 1.3 to 0.9 kJ mol⁻¹ in imidazolium and pyrrolidinium systems, respectively. This is closely followed by bromide ion pairs, whose MAE values are now 2.0 and 1.6 kJ mol⁻¹ when paired with imidazolium and pyrrolidinium, cations, respectively which corresponds to a reduction in errors between 0.4 and 0.5 kJ mol⁻¹. Imidazolium chloride ion pairs have the least reduction in MAE of 0.1 kJ mol⁻¹. Imidazolium bromide systems still have the largest MAE of 2.0 kJ mol⁻¹ and the maximum error of 2.5 kJ mol⁻¹. Maximum errors of over 2 kJ mol⁻¹ are found for both cations coupled with bromide. The low standard deviations of the bromide systems (0.3 kJ mol⁻¹ in both cases) point towards a systematic error when using this diffuse anion. Similarly, mesylate systems produce second largest MAEs (1.5 kJ mol⁻¹) accompanied with low standard deviations (0.2 kJ mol⁻¹).

Table 4. Correlation interaction energy errors (in kJ mol⁻¹) of DLPNO-CCSD(T₁)/aug-cc-pVDZ for the IL174 dataset. CCSD(T)/aug-cc-pVDZ interaction energies were used as the benchmark.

Cation	Anion	#Systems	Min	MAE	Max	SD
C ₁₋₄ mim	BF ₄ ⁻	7	1.3	1.4	1.5	0.1
	Br ⁻	14	1.3	2.0	2.5	0.3
	Cl ⁻	14	0.8	1.1	1.2	0.1
	N(CN) ₂ ⁻	17	1.1	1.5	1.8	0.2
	mesylate	7	1.7	1.8	2.0	0.1
	NTf ₂ ⁻	8	-0.1	0.5	1.5	0.5
	PF ₆ ⁻	7	1.2	1.3	1.5	0.1
	tosylate	7	1.0	1.2	1.4	0.1
C ₁₋₄ mpyr	BF ₄ ⁻	11	0.8	1.0	1.1	0.1
	Br ⁻	11	1.2	1.6	2.1	0.3
	Cl ⁻	11	0.8	0.9	1.0	0.1
	N(CN) ₂ ⁻	19	0.5	0.9	1.4	0.2
	mesylate	11	1.1	1.5	1.8	0.2
	NTf ₂ ⁻	16	0.2	0.6	1.1	0.3
	PF ₆ ⁻	11	0.8	1.1	1.2	0.1
	tosylate	8	0.1	0.9	1.3	0.4

Table 5: Correlation interaction energy errors (in kJ mol^{-1}) of DLPNO-CCSD(T₁)/aug-cc-pVDZ for the HBIL dataset. CCSD(T)/aug-cc-pVDZ interaction energies were used as the benchmark.

Anion	#Systems	Min	MAE	Max	SD
CF ₃ SO ₃ ⁻	7	0.5	1.1	1.7	0.4
Cl ⁻	7	0.4	0.6	0.8	0.1
MeOSO ₃ ⁻	6	1.0	1.2	1.5	0.2
mesylate	7	0.9	1.2	1.6	0.3
NO ₃ ⁻	7	0.9	1.3	2.0	0.4
TFA	8	0.6	0.9	1.3	0.3

Pyrrolidinium ion pairs coupled with tetrafluoroborate, dicyanamide, tosylate, NTf₂⁻ and chloride all have MAEs within spectroscopic accuracy, with mesylate and hexafluorophosphate producing MAEs slightly higher than 1 kJ mol^{-1} . In the case in imidazolium systems, only imidazolium ion pairs coupled with NTf₂⁻ meet this criterion.

Inclusion of iterative triples in the DLPNO calculations for the HBIL set (see Table 5) also reduces all MAEs by as little as 0.3 kJ mol^{-1} on average. Separated into anions (see Fig. 5), the most improvement was found for the NO₃⁻ systems, whose MAE shrinks by 0.4 to 1.3 kJ mol^{-1} .

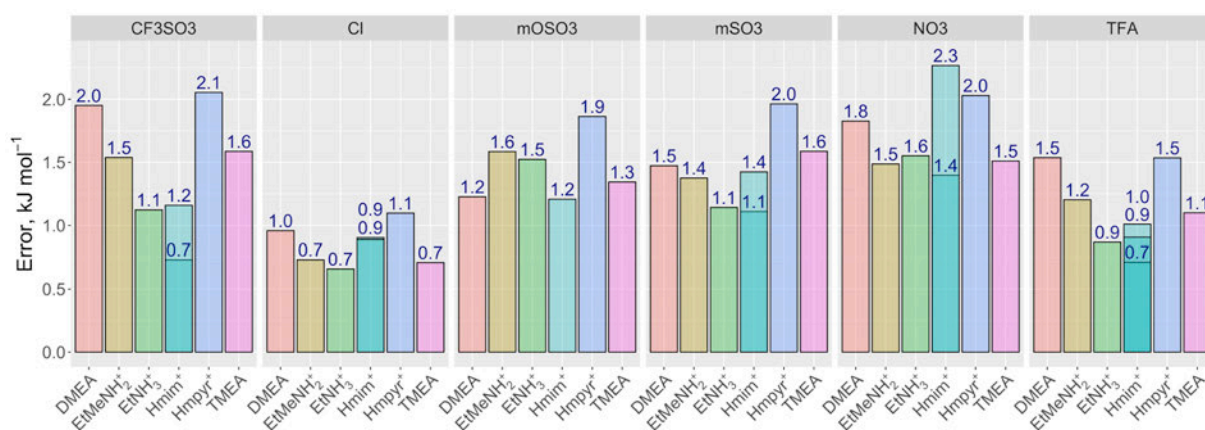


Figure 5. Errors in DLPNO-CCSD(T₀) correlation interaction energy errors in HBIL. Error bars of [Hmim][anion] systems with more than one configuration are overlaid and multiple errors are printed above the bars.

The maximum error, belonging to the out-of-plane configuration of [Hmim][NO₃] (MAE of 2.3 kJ mol⁻¹ for non-iterative triples), is also reduced by 0.5 kJ mol⁻¹.

Varying cutoff parameters in DLPNO-CCSD(T)

The performance of DLPNO-CCSD(T) was tested with respect to individual cutoff parameters as well as their combinations to identify whether relaxed parameters could be used in the prediction of interaction energies of ionic systems, thus allowing us to further reduce the cost of each calculation. In particular, cutoffs such as $T_{CutPairs}$, T_{CutPNO} and T_{MKN} were considered (for more detail see introduction). Currently three standards of the DLPNO approach have been implemented in ORCA defined by keywords: LoosePNO, NormalPNO and TightPNO. As accuracy is the ambition of this study, the larger cutoffs of LoosePNO and NormalPNO have not been tested. TightPNO has cutoffs of $T_{CutPNO} = 1 \times 10^{-7}$, $T_{CutPairs} = 1 \times 10^{-5}$ and $T_{CutMKN} = 1 \times 10^{-3}$. A combination of tighter cutoffs by two orders of magnitude were tested and corresponding DLPNO errors are presented in Figure 6. In addition, the use of the RIJCOSX approximation and the iterative triples treatment, T_1 , were also considered. Imidazolium bromides were chosen as test subjects as they exhibited the highest MAE of 2.4 and 2.0 kJ mol⁻¹ for non-iterative (T_0) and iterative (T_1) DLPNO calculations, respectively, and low standard deviations of 0.3 kJ mol⁻¹ suggesting systematic

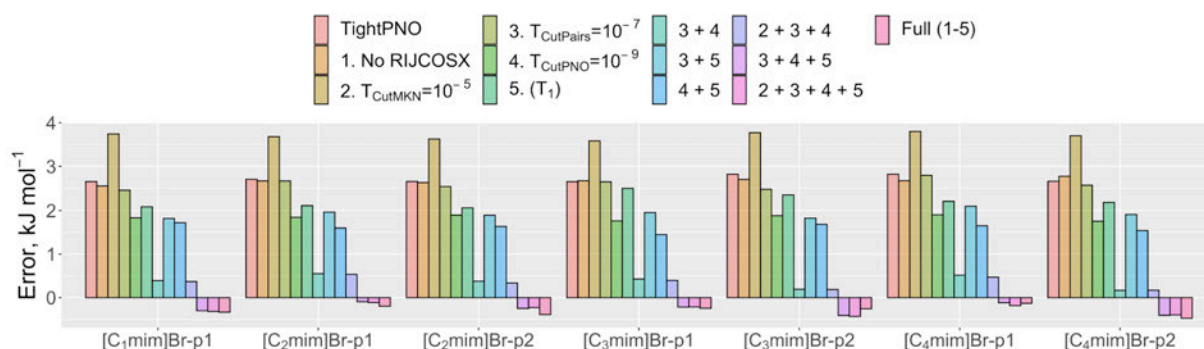


Figure 6. Errors in DLPNO-CCSD(T) correlation interaction energy for different types of calculations on imidazolium bromide ion pairs that had errors of > 2.5 kJ mol⁻¹ with (T_0).

improvement could be achieved. The effect of performance of the calculation parameters on the imidazolium bromide ion energies are shown in Fig. 6. Each calculation uses TightPNO, non-iterative triples (T_0) and the RIJCOSX approximation unless specified otherwise; this is the first calculation type shown. Across the set of systems each calculation type gives consistent results with standard deviations of less than 0.2 kJ mol^{-1} . Calculation type ‘1’ does not employ the density fitting cut-off, RIJCOSX, and does not have a significant impact on the result. The TightPNO calculations in combination with No RIJCOSX produce mean errors of 2.7 kJ mol^{-1} . Calculation type ‘2’, ‘3’, and ‘4’ refer to tightening of T_{CutMKN} , T_{CutPairs} , and T_{CutPNO} by two order of magnitude, respectively, compared to TightPNO where the other two parameters for the three calculation types are held at TightPNO settings. Type ‘5’ has TightPNO settings, however, the triples are calculated iteratively. The remaining settings are a combination of these alterations ending in a full calculation: $T_{\text{CutMKN}} = 10^{-5}$, $T_{\text{CutPairs}} = 10^{-7}$, and $T_{\text{CutPNO}} = 10^{-9}$, iterative treatment of triples and no RIJCOSX approximation. Tightening T_{CutPairs} improves the mean by a mere 0.1 kJ mol^{-1} . However, the same change in T_{CutMKN} has adverse effects where the error is significantly worsened gaining a mean error of 3.7 kJ mol^{-1} . The two single changes that have the most impact on the errors are decreasing T_{CutPNO} by a factor of two and enforcing iterative triples. These obtain mean errors of 1.8 and 2.2 kJ mol^{-1} , respectively. This is in agreement with the previous work conducted by Neese *et al.*⁷ The importance of T_{CutPairs} becomes more obvious when it is combined with a change in T_{CutPNO} , reducing the mean error to 0.4 kJ mol^{-1} . Smaller MAEs are produced by combining the iterative triples treatment with either a tighter T_{CutPairs} (1.9 kJ mol^{-1}) or a tighter T_{CutPNO} (1.6 kJ mol^{-1}). The lowest errors are achieved by the five calculation types that combine tighter criteria of T_{CutPairs} (3) and T_{CutPNO} (4) such as [3 + 4], [2 + 3 + 4], [3 + 4 + 5], [2 + 3 + 4 +

5] and Full (*i.e.* $T_{\text{CutPNO}} = 1 \times 10^{-9}$, $T_{\text{CutPairs}} = 1 \times 10^{-7}$, $T_{\text{CutMKN}} = 1 \times 10^{-5}$ and T_1), with MAEs being 0.4, 0.4, 0.3, 0.3 and 0.3 kJ mol^{-1} , respectively.

From these results, it can be concluded that, regardless of the triples treatment, when T_{CutPNO} and T_{CutPairs} are tightened, T_{CutMKN} still does not have much influence on the overall error. The same conclusion can be made for including the density fitting protocol, which is known to speed up the calculation, and is, therefore, recommended. With the addition of iterative triples, the recovered correlation energy increases and when paired with an increased number of pairs and triples calculated at CCSD(T) level, an increased number of PNO's recovers more correlation energy than that of CCSD(T). This is likely due to the contributions from MP2 and the multipole treatment of doubles and triples, which otherwise cancels with the smaller recovery of correlation when the triples are considered non-iteratively.

The T_{CutPNO} and T_{CutPairs} parameters were further reduced in combination with both triples treatments. The errors of the corresponding calculations are shown in Figure 7 and are plotted against the computation cost calculated relative to the original parameters in TightPNO - $T_{\text{CutPNO}} = 1 \times 10^{-7}$, $T_{\text{CutPairs}} = 1 \times 10^{-5}$. T_1 calculations consistently outperform T_0 ones in terms of

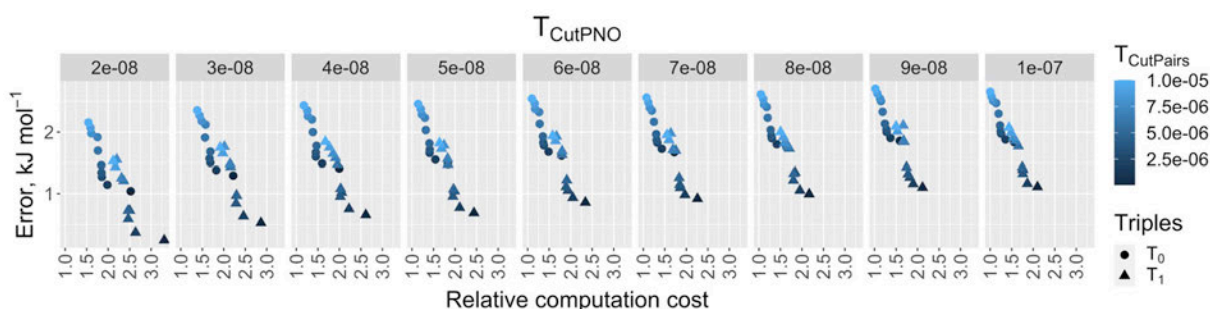


Figure 7. Relative computational cost with respect to TightPNO settings and their associated error when varying T_{CutPairs} (colour), T_{CutPNO} (left to right), and triples type (shape). Calculations were performed on the [C4mim]Br ion pair configuration with the alkyl chain in the plane of the ring and anion above the plane.

accuracy and cost. The most accurate T_0 calculation has an error of 1 kJ mol^{-1} and takes 2.5 times longer than the original calculation. For the same cost, an accuracy of 0.6 kJ mol^{-1} can be achieved for the iterative triples treatment with larger cutoffs for the other two parameters. For results within spectroscopic accuracy the lowest cost was achieved with $T_{\text{CutPNO}} = 5 \times 10^{-8}$ and $T_{\text{CutPairs}} = 4 \times 10^{-6}$ and the iterative triples treatment. The cost became 1.9 times more expensive than that of the original calculations with the TightPNO settings. These cutoffs, referred to further in the text as IL1PNO, have been used on both IL174 and HBIL datasets (see Tables 6 and 7) to analyse whether spectroscopic accuracy can be obtained for the rest of the ionic liquid systems studied.

Performance of DLPNO-CCSD(T_1) with IL1PNO cutoffs

Table 6. Correlation interaction energy errors (in kJ mol^{-1}) of DLPNO-CCSD(T_1)/aug-cc-pVDZ with IL1PNO cutoffs for the IL174 dataset. CCSD(T)/aug-cc-pVDZ interaction energies were used as the benchmark.

Cation	Anion	#Systems	Min	MAE	Max	SD
C ₁₋₄ mim	BF ₄ ⁻	7	1.4	1.5	1.6	0.1
	Br ⁻	14	0.8	1.0	1.3	0.2
	Cl ⁻	14	0.6	0.8	0.9	0.1
	N(CN) ₂ ⁻	17	0.9	1.4	1.7	0.2
	mesylate	7	1.6	1.7	1.9	0.1
	NTf ₂ ⁻	8	-2.0	1.3	2.1	1.3
	PF ₆ ⁻	7	1.2	1.3	1.5	0.1
	tosylate	7	1.1	1.3	1.4	0.1
C ₁₋₄ mpyr	BF ₄ ⁻	11	1.0	1.1	1.2	0.1
	Br ⁻	11	0.5	0.8	1.1	0.2
	Cl ⁻	11	0.5	0.6	0.7	0.1
	N(CN) ₂ ⁻	22	0.9	1.0	1.6	0.2
	mesylate	11	1.1	1.4	1.6	0.2
	NTf ₂ ⁻	16	0.5	1.0	2.0	0.3
	PF ₆ ⁻	11	0.7	1.0	1.1	0.1
	tosylate	8	0.5	0.9	1.1	0.2

With respect to the results with the TightPNO settings, the largest improvement of the proposed IL1PNO settings occurs in the bromide systems, whose MAEs are reduced by 1.0 and 0.8 kJ mol^{-1} in imidazolium and pyrrolidinium ion pairs, respectively. IL1PNO can also achieve spectroscopic accuracy for chloride-based ion pairs. For example, imidazolium chlorides have an MAE of 0.8 kJ mol^{-1} reduced from 1.1 kJ mol^{-1} , whereas pyrrolidinium chlorides fall to just 0.6 kJ mol^{-1} from 0.9 kJ mol^{-1} . This is not surprising since the cutoffs were tested on bromide systems and the similarity of its anionic nature to chloride. The improvement, however, cannot be generalised for the other anions. Tetrafluoroborate errors increase by 0.1 kJ mol^{-1} with MAEs of 1.5 and 1.1 kJ mol^{-1} for imidazolium- and pyrrolidinium-based systems, respectively; although their standard deviations stay constant at 0.1 kJ mol^{-1} . The MAE of imidazolium dicyanamide is reduced by a mere 0.1 kJ mol^{-1} and the minimum error is reduced by as little as 0.2 kJ mol^{-1} . Errors of pyrrolidinium dicyanamides are increased by 0.1 kJ mol^{-1} . Systems of mesylate are treated marginally better as the MAE for both cations is reduced by 0.1 kJ mol^{-1} , however maximum errors of over 1.8 kJ mol^{-1} are still attained. The errors of imidazolium NTf_2^- increases

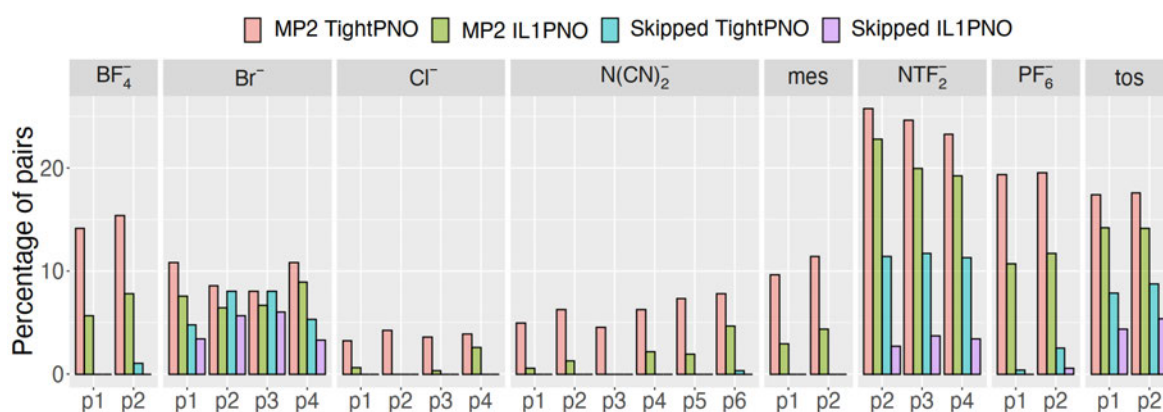


Figure 8. Percentage of pairs treated with MP2 or skipped depending on the TightPNO or IL1PNO restrictions in the system calculation of $[\text{C}_2\text{mim}][\text{anion}]$ for configurations (pn) of the ion pair (x axis).

by 0.7 kJ mol^{-1} and the maximum error is increased to 2.1 from 1.5 kJ mol^{-1} . For pyrrolidinium-base ion pairs, the average MAE increases by 0.4 kJ mol^{-1} and the maximum error increases from 1.1 to 2.0 kJ mol^{-1} . As the MAEs of NTf_2^- with TightPNO settings and the T_1 treatment are below spectroscopic accuracy, tighter cutoffs, in fact, worsen the error. Imidazolium hexafluorophosphates are mostly unaffected, whereas pyrrolidinium hexafluorophosphates are consistently reduced by 0.1 kJ mol^{-1} . The reverse effect is seen in imidazolium tosylates, for which the MAE is increased by 0.1 kJ mol^{-1} and now lies at 1.2 kJ mol^{-1} . For pyrrolidinium systems containing tosylates, the MAE is unchanged, although the maximum error is reduced by 0.2 kJ mol^{-1} . Therefore, TightPNO settings are recommended for ionic liquids of pyrrolidinium tosylates, pyrrolidinium tetrafluoroborates, pyrrolidinium chlorides, pyrrolidinium dicyanamides, as well as those with NTf_2^- anions. IL1PNO settings are recommended for ionic liquids containing bromide and chloride anions, as well as pyrrolidinium hexafluorophosphates and hydrogen bonded ionic liquids.

Figure 8 shows the percentage of ‘weak pairs’ included at the MP2 level of theory (also referred to as MP2 pairs) or those skipped and corrected for with the multipole estimate, for TightPNO and the more inclusive IL1PNO settings. The C_2mim^+ based ion pairs coupled with BF_4^- , $\text{N}(\text{CN})_2^-$ and PF_6^- anions have a negligible number of skipped pairs for either set of cutoffs but a marked decrease in pairs treated with MP2. This leads to a negligible difference in the recovery of correlation interaction error ($\pm 0.1 \text{ kJ mol}^{-1}$). In the case of $[\text{C}_2\text{mim}]\text{Cl}$, similarly, no MP2 pairs were skipped; however, the error reduction of 0.3 kJ mol^{-1} (also observed for $[\text{C}_n\text{mim}]\text{Cl}$ and $[\text{C}_n\text{mpyr}]\text{Cl}$) identified that at least $\sim 5\%$ of weak pairs treated with MP2 were important, which is clearly not the case in BF_4^- , $\text{N}(\text{CN})_2^-$ and PF_6^- . Possibly the error of the latter comes from the cutoff

used for T_{CutPNO} . Bromide systems, for which these cutoffs were tested, have significant contributions from both skipped and weak pairs for both TightPNO and IL1PNO cutoffs.

Table 7. Correlation interaction energy errors (in kJ mol^{-1}) of DLPNO-CCSD(T₁)/aug-cc-pVDZ with IL1PNO cutoffs for the HBIL dataset. CCSD(T)/aug-cc-pVDZ interaction energies were used as the benchmark.

Anion	#Systems	Min	MAE	Max	SD
CF ₃ SO ₃ ⁻	7	0.6	1.0	1.3	0.3
Cl ⁻	7	0.1	0.3	0.4	0.1
MeOSO ₃ ⁻	6	1.0	1.2	1.4	0.2
mesylate	7	0.8	1.0	1.3	0.2
NO ₃ ⁻	7	0.9	1.1	1.5	0.2
TFA	8	0.7	0.9	1.4	0.3

However, the C₂mim-based systems shown in Fig. 8 (which had the largest errors with TightPNO settings) have their errors significantly reduced by 0.8 kJ mol^{-1} . Overall, for the imidazolium systems the error was reduced by 0.2 kJ mol^{-1} when changing from TightPNO to IL1PNO. NTf₂⁻ has contributions of $> 23\%$ MP2 pairs and $\sim 11\%$ skipped pairs. Skipped pairs are reduced to $\sim 3\%$ while MP2 pairs fall by a few percent when the parameters are changed from TightPNO to IL1PNO. This results in an increase of error by 0.6 kJ mol^{-1} suggesting that the accompanying T_{CutPNO} cutoff may need to be increased to correctly ascertain the correlation of these systems. Lastly, the change in error for tosylate systems is unchanged by the more tolerant cutoffs even though both MP2 pairs and skipped pairs is a reduction of 3.3 and 3.4% (~ 70 pairs) reduction, respectively, reduced in favour of the coupled cluster treatment. The remaining error could be corrected by increasing the number of PNOs included suggesting that the cutoffs of in TightPNO settings are already efficient in eliminating calculating pairs and triples of negligible worth.

More consistent improvements are seen in the HBIL dataset, for which all errors are improved. The overall error for the dataset is 0.9 kJ mol^{-1} and the maximum error is now 1.5 kJ mol^{-1} observed for [Hmim][MeOSO₃]. The largest improvement is again observed in the halide ions where chloride systems have decreased errors by 0.3 kJ mol^{-1} . Chloride, CF₃SO₃, mesylate and TFA systems have MAEs within spectroscopic accuracy.

IL1PNO performs exceptionally well for halides and hydrogen bonded complexes. However, for all other anions of the aprotic systems, little difference was seen in the errors except in the case of NTf₂⁻ where the errors increased – by 0.7 kJ mol^{-1} in the case of imidazolium NTf₂⁻. It is likely that the cutoffs are not tightened satisfactorily to recover the correlation energy of the complete set of anions. On average, 40 more MP2 pairs and 52 more skipped pairs are treated with CCSD(T) when IL1PNO settings are used in place of TightPNO with only an increase in accuracy of 0.1 kJ mol^{-1} . Thus, these pairs do not make a significant difference to the errors of the non-halide ion pairs.

Performance of DLPNO-CCSD(T) with IL2PNO cutoffs

The systems presenting larger errors with IL1PNO were run with a further set of cutoffs, termed IL2PNO: $T_{\text{CutPNO}} = 1 \times 10^{-9}$, $T_{\text{CutPairs}} = 1 \times 10^{-7}$, and $T_{\text{CutMKN}} = 1 \times 10^{-3}$. T_{CutPNO} was increased by the same magnitude as T_{CutPairs} , both by two orders of magnitude such that the errors seen in IL1PNO could be possibly reduced by including a larger number of PNOs while also increasing the number of pairs treated with coupled cluster theory. These results are displayed in Table 8. The systems include imidazolium-base ion pairs coupled with tetrafluoroborate, dicyanamide, mesylate and hexafluorophosphate, for which MAE values of less than 1.0 kJ mol^{-1} have not yet been attained. This finding also holds for tosylate systems, although these cutoffs expanded the

external space such that only one calculation was practically feasible. Additionally, the bromide systems from Figure 6 were also included here.

Table 8. Correlation interaction energy errors (in kJ mol⁻¹) of DLPNO-CCSD(T₁)/aug-cc-pVDZ with IL2PNO cutoffs for the IL174 dataset. CCSD(T)/aug-cc-pVDZ interaction energies were used as the benchmark.

Cation	Anion	#Systems	Min	MAE	Max	SD
C ₁₋₄ mim	BF ₄ ⁻	7	0.4	0.5	0.5	0.0
	Br ⁻	7	-0.4	0.3	-0.1	0.1
	N(CN) ₂ ⁻	17	0.3	0.4	0.6	0.1
	mesylate	7	0.3	0.6	0.8	0.2
	PF ₆ ⁻	7	0.5	0.6	0.7	0.1
	tosylate	1	0.0	0.0	0.0	NA
C ₁₋₄ mpyr	BF ₄ ⁻	11	0.4	0.5	0.5	0.0
	N(CN) ₂ ⁻	14	0.1	0.3	1.1	0.3
	mesylate	11	0.3	0.5	0.7	0.1
	PF ₆ ⁻	11	0.3	0.5	0.5	0.0

Table 9. Summary of DLPNO-CCSD(T) settings, their cutoffs, errors (in kJ mol⁻¹) and the anions these settings are recommended for spectroscopic accuracy.

	Triples	T_{CutPNO}	$T_{CutPairs}$	T_{CutMKN}	MAE	Max	SD	Recommendations
TightPNO	T ₀	1×10^{-7}	1×10^{-5}	1×10^{-3}	1.5	2.8	0.5	NTf ₂ ⁻
TightPNO	T ₁	1×10^{-7}	1×10^{-5}	1×10^{-3}	1.2	2.5	0.4	Same as T ₀
IL1PNO	T ₁	5×10^{-8}	4×10^{-6}	1×10^{-3}	1.1	2.1	0.4	Br ⁻ , Cl ⁻ , CF ₃ SO ₃ ⁻ , TFA
IL2PNO	T ₁	1×10^{-9}	1×10^{-7}	1×10^{-3}	0.4	1.1	0.2	BF ₄ ⁻ , N(CN) ₂ ⁻ , mesylate, PF ₆ ⁻ , tosylate

Analysis of Table 8 reveals that all the systems considered now have MAE values within spectroscopic accuracy, below 0.6 kJ mol⁻¹. Table 9 summarizes the overall statistics of each of the tested DLPNO-CCSD(T) settings and their associated cutoffs and provides recommendations for spectroscopic accuracy. IL1PNO has been shown to remarkably increase the accuracy of ion pairs containing halide anions, especially bromides. Disappointingly, smaller or even negative

differences were seen in the other systems, notably those containing NTf₂, for which TightPNO cutoffs gave lower MAEs. IL2PNO, which was tested on a subset of the IL174 dataset that gave larger errors with the TightPNO settings, performs outstandingly and can be recommended when spectroscopic accuracy is required.

Comparison of DLPNO-CCSD(T₀)/VTZ with CCSD(T)/CBS

A thorough analysis of the CCSD(T) performance with respect to the basis set indicated that due to the non-iterative treatment of triples, CCSD(T) produced its performance in combination with a triple-zeta basis set.³⁷ CCSD(T)/cc-pVTZ is considered to be a reliable combination and give energies within chemical accuracy for single molecules.⁴⁵ In this study, the performance of DLPNO-CCSD(T₀)/cc-pVTZ was investigated with respect to the “gold standard” for non-covalent interactions, CCSD(T)/CBS. The goal was to identify whether the use of the cc-pVTZ basis set within the DLPNO approach without the counterpoise correction could potentially replace the more time consuming CCSD(T)/CBS treatment.

Table 10 shows correlation interaction energies for DLPNO-CCSD(T₀)/cc-pVTZ with respect to CCSD(T)/CBS for the IL174 dataset. All errors are larger than chemical accuracy. Tosylate, mesylate and bromide anions give the largest mean errors within each cation series. With the imidazolium cation, average errors are greater than 11 kJ mol⁻¹. All anions have similar or larger variations of error when coupled with imidazolium cations, with the SD of bromide increasing eightfold when paired with the imidazolium cation. Additionally, the maximum errors of the imidazolium ion pairs are larger than those of pyrrolidinium ones, with the errors of the former ranging from 9.8 to 12.5 and the latter from 6.2 to 9.6 kJ mol⁻¹. The small standard deviations present for the pyrrolidinium systems highlights a systematic underestimation of correlation energy with this basis set.

Table 10. Correlation interaction energy errors (in kJ mol^{-1}) of DLPNO-CCSD(T₀)/cc-pVTZ with TightPNO settings for the IL174 dataset. CCSD(T)/CBS interaction energies were used as the benchmark.

Cation	Anion	#Systems	Min	MAE	Max	SD
C ₁₋₄ mim	BF ₄ ⁻	7	8.7	9.3	9.8	0.4
	Br ⁻	14	7.5	11.2	13.7	2.4
	Cl ⁻	14	4.4	7.7	10	2.3
	N(CN) ₂ ⁻	16	7.1	10.7	11.7	1.2
	mesylate	7	11.2	11.7	12.4	0.6
	NTf ₂ ⁻	7	3.6	8.5	12.1	3.1
	PF ₆ ⁻	7	9.0	9.6	10.7	0.7
	tosylate	7	11.1	11.9	12.5	0.5
C ₁₋₄ mpyr	BF ₄ ⁻	11	5.8	6.2	6.8	0.4
	Br ⁻	11	8.6	9.1	9.6	0.3
	Cl ⁻	11	5.6	5.9	6.2	0.2
	N(CN) ₂ ⁻	17	5.4	6.9	7.5	0.6
	mesylate	11	6.8	7.7	8.7	0.7
	NTf ₂ ⁻	16	4.7	5.6	6.4	0.4
	PF ₆ ⁻	11	5.9	6.3	6.9	0.3
	tosylate	6	7.4	8.1	8.8	0.5

Table 11. Correlation interaction energy errors (in kJ mol^{-1}) of DLPNO-CCSD(T₀)/cc-pVTZ with TightPNO settings for the HBIL dataset. CCSD(T)/CBS interaction energies were used as the benchmark.

Anion	#Systems	Min	MAE	Max	SD
CF ₃ SO ₃ ⁻	7	4.9	7.4	9.6	1.4
Cl ⁻	7	4.4	6.0	7.3	0.9
MeOSO ₃ ⁻	6	7.7	10.1	15.6	2.8
mesylate	7	6.4	8.7	10.9	1.4
NO ₃ ⁻	7	3.8	6.0	11.0	2.4
TFA	8	4.4	6.0	8.9	1.6

The results of the HBIL dataset are shown in Table 11. Neither systems of a particular cation nor anion perform well, with MAEs being outside the chemical accuracy range. Overall, DLPNO-CCSD(T₀)/cc-pVTZ without the counterpoise correction cannot be recommended to be used as the benchmark method for the prediction of energetics of ionic liquid systems.

Comment of the performance of DLPNO-CCSD(T₀)/cc-pVTZ for clusters of two ion pairs

Two ion pairs [C₁mim][BF₄] and [C₁mim]Cl have errors 13.3 and 13.8 kJ mol⁻¹ per ion pair. These errors are larger than the maximum errors of 9.8 and 10.0 kJ mol⁻¹, respectively, for the single ion pairs. The chloride system has an error 5.6 kJ mol⁻¹ larger than the MAE of the single ion pairs of imidazolium chloride. The preliminary results indicate that the DLPNO-CCSD(T₀)/cc-pVTZ error may increase with increasing number of ions in the system.

Conclusions

In this study, cutoff parameters used within the DLPNO-CCSD(T) method were scrutinised for the prediction of correlation interaction energies of ionic liquids, both protic and aprotic. TightPNO settings were tested for non-iterative, T₀, and iterative, T₁, treatment of triples. Both approaches produced mean absolute and maximum errors within chemical accuracy, with no significant improvement being achieved when iterative triples were used. The DLPNO error was found to strongly depend on the cation-anion combination. MAEs of anion NTf₂⁻, with both cations, were the only two ILs to reach spectroscopic accuracy with TightPNO and T₀ settings. The impact of cation was seen more dramatically in DLPNO-CCSD(T₁) results with TightPNO where five pyrrolidinium ionic liquids reached spectroscopic accuracy while for imidazolium this is only true for one. Spectroscopic accuracy was only achieved for the following cation-anion combinations: imidazolium and NTf₂⁻; pyrrolidinium and NTf₂⁻; pyrrolodinium and BF₄⁻; pyrrolidinium and chloride; pyrrolidinium and dicyanamide; and pyrrolodinium and tosylate combinations, while bromide and mesylate-based ion pairs systematically produced the largest errors among the aprotic ionic liquids and nitrates, mesylates and trifluorosulfonates among the protic ionic liquids.

Varying the three main cutoff parameters, T_{CutPNO} , $T_{CutPairs}$ and T_{CutMKN} , demonstrated how the DLPNO error could be systematically reduced. The iterative treatment of triples was essential to achieve spectroscopic accuracy while keep looser thresholds, and hence reduce computational cost. Based on the analysis of a series of the cutoffs, the IL1PNO settings were suggested, for which T_{CutPNO} was set to 5×10^{-8} and $T_{CutPairs}$ to 4×10^{-6} . The performance of these IL1PNO settings produced average errors below 1.5 kJ mol^{-1} , with the maximum errors falling below 2.1 kJ mol^{-1} . On average this improved the MAE by only 0.1 kJ mol^{-1} but the maximum error in IL1PNO became 0.4 kJ mol^{-1} smaller than that in TightPNO with iterative triples. The largest improvements were observed for chlorides and bromides, with the bromide systems and the imidazolium chlorides reaching spectroscopic accuracy for MAEs. Negligible improvements were found for the rest of the aprotic ILs. The HBIL dataset seemed to benefit more from these settings, with the majority of MAEs falling within spectroscopic accuracy. Further tightening of the T_{CutPNO} and $T_{CutPairs}$ by two orders of magnitude with respect to the TightPNO settings resulted in all types of errors – mean absolute and maximum – falling within spectroscopic accuracy.

Therefore, this study demonstrated the successful application of DLPNO-CCSD(T) to protic and aprotic ionic liquids. Non-iterative triples and TightPNO settings obtain errors within chemical accuracy for all systems tested. In order to obtain spectroscopic accuracy, the iterative treatment of triples was found to be critical to keep looser thresholds for the main cutoffs and hence, maintain shorter calculation times. It is recommended to use the IL1PNO settings for ionic liquids based on Br^- , Cl^- , CF_3SO_3^- and TFA anions and IL2PNO settings for ionic liquids of anions BF_4^- , $\text{N}(\text{CN})_2^-$, mesylate, PF_6^- and tosylate for spectroscopic accuracy, although they come with higher computational cost. The use of DLPNO-CCSD(T₀)/cc-pVTZ to replace CCSD(T)/CBS interaction energies of ionic liquids is not recommended due to large errors, well above chemical accuracy. It

appears that DLPNO-CCSD(T₁)/aug-cc-pVTZ could be reliably used in the calculation of CCSD(T)/CBS provided recommended settings are used in the process.

Reference

- (1) Halat, P.; Seeger, Z. L.; Barrera Acevedo, S.; Izgorodina, E. I. Trends in Two- and Three-Body Effects in Multiscale Clusters of Ionic Liquids. *J. Phys. Chem. B* **2017**, *121* (3), 577–588. <https://doi.org/10.1021/acs.jpcc.6b10101>.
- (2) Brüssel, M.; Brehm, M.; Voigt, T.; Kirchner, B. *Ab Initio* Molecular Dynamics Simulations of a Binary System of Ionic Liquids. *Phys. Chem. Chem. Phys.* **2011**, *13* (30), 13617–13620. <https://doi.org/10.1039/C1CP21550G>.
- (3) Izgorodina, E. I.; Seeger, Z. L.; Scarborough, D. L. A.; Tan, S. Y. S. Quantum Chemical Methods for the Prediction of Energetic, Physical, and Spectroscopic Properties of Ionic Liquids. *Chem. Rev.* **2017**, *117* (10), 6696–6754. <https://doi.org/10.1021/acs.chemrev.6b00528>.
- (4) Izgorodina, E. I.; Golze, D.; Maganti, R.; Armel, V.; Taige, M.; Schubert, T. J. S.; MacFarlane, D. R. Importance of Dispersion Forces for Prediction of Thermodynamic and Transport Properties of Some Common Ionic Liquids. *Phys. Chem. Chem. Phys.* **2014**, *16* (16), 7209–7221. <https://doi.org/10.1039/C3CP53035C>.
- (5) Seeger, Z. L.; Kobayashi, R.; Izgorodina, E. I. Cluster Approach to the Prediction of Thermodynamic and Transport Properties of Ionic Liquids. *J. Chem. Phys.* **2018**, *148* (19), 193832. <https://doi.org/10.1063/1.5009791>.
- (6) Tsuzuki, S.; Tokuda, H.; Hayamizu, K.; Watanabe, M. Magnitude and Directionality of Interaction in Ion Pairs of Ionic Liquids: Relationship with Ionic Conductivity. *J. Phys. Chem. B* **2005**, *109* (34), 16474–16481. <https://doi.org/10.1021/jp0533628>.
- (7) Neese, F.; Wennmohs, F.; Hansen, A. Efficient and Accurate Local Approximations to Coupled-Electron Pair Approaches: An Attempt to Revive the Pair Natural Orbital Method. *J. Chem. Phys.* **2009**, *130* (11), 114108. <https://doi.org/10.1063/1.3086717>.

- (8) Neese, F.; Hansen, A.; Liakos, D. G. Efficient and Accurate Approximations to the Local Coupled Cluster Singles Doubles Method Using a Truncated Pair Natural Orbital Basis. *J. Chem. Phys.* **2009**, *131* (6), 064103. <https://doi.org/10.1063/1.3173827>.
- (9) Riplinger, C.; Sandhoefer, B.; Hansen, A.; Neese, F. Natural Triple Excitations in Local Coupled Cluster Calculations with Pair Natural Orbitals. *J. Chem. Phys.* **2013**, *139* (13), 134101. <https://doi.org/10.1063/1.4821834>.
- (10) Guo, Y.; Riplinger, C.; Becker, U.; Liakos, D. G.; Minenkov, Y.; Cavallo, L.; Neese, F. Communication: An Improved Linear Scaling Perturbative Triples Correction for the Domain Based Local Pair-Natural Orbital Based Singles and Doubles Coupled Cluster Method [DLPNO-CCSD(T)]. *J. Chem. Phys.* **2018**, *148* (1), 011101. <https://doi.org/10.1063/1.5011798>.
- (11) Boys, S. F. Construction of Some Molecular Orbitals to Be Approximately Invariant for Changes from One Molecule to Another. *Rev. Mod. Phys.* **1960**, *32* (2), 296–299. <https://doi.org/10.1103/RevModPhys.32.296>.
- (12) Saebø, S.; Pulay, P. Local Treatment of Electron Correlation. *Ann. Rev. Phys. Chem.* **1993**, *44*, 213.
- (13) Edmiston, C.; Krauss, M. Configuration-Interaction Calculation of H₃ and H₂. *J. Chem. Phys.* **1965**, *42* (3), 1119–1120. <https://doi.org/10.1063/1.1696050>.
- (14) Riplinger, C.; Neese, F. An Efficient and near Linear Scaling Pair Natural Orbital Based Local Coupled Cluster Method. *Journal Chem. Phys.* **2013**, *138* (3), 034106. <https://doi.org/10.1063/1.4773581>.
- (15) Friedrich, J.; Hänchen, J. Incremental CCSD(T)(F12*)|MP2: A Black Box Method To Obtain Highly Accurate Reaction Energies. *J. Chem. Theory Comput.* **2013**, *9* (12), 5381–5394. <https://doi.org/10.1021/ct4008074>.
- (16) Liakos, D. G.; Sparta, M.; Kesharwani, M. K.; Martin, J. M. L.; Neese, F. Exploring the Accuracy Limits of Local Pair Natural Orbital Coupled-Cluster Theory. *J. Chem. Theory Comput.* **2015**, *11* (4), 1525–1539. <https://doi.org/10.1021/ct501129s>.

- (17) Neese, F.; Wennmohs, F. ORCA Manual: An *Ab Initio*, DFT and Semiempirical SCF-MO Package Version 4.1.2. 2019 2018.
- (18) Liakos, D. G.; Neese, F. Is It Possible To Obtain Coupled Cluster Quality Energies at near Density Functional Theory Cost? Domain-Based Local Pair Natural Orbital Coupled Cluster vs Modern Density Functional Theory. *J. Chem. Theory Comput.* **2015**, *11* (9), 4054–4063. <https://doi.org/10.1021/acs.jctc.5b00359>.
- (19) Chen, J.-L.; Sun, T.; Wang, Y.-B.; Wang, W. Toward a Less Costly but Accurate Calculation of the CCSD(T)/CBS Noncovalent Interaction Energy. *J Comput Chem.* **2020**, 1–9. <https://doi.org/10.1002/jcc.26171>.
- (20) Paulechka, E.; Kazakov, A. Efficient DLPNO–CCSD(T)-Based Estimation of Formation Enthalpies for C-, H-, O-, and N-Containing Closed-Shell Compounds Validated Against Critically Evaluated Experimental Data. *J. Phys. Chem. A* **2017**, *121* (22), 4379–4387. <https://doi.org/10.1021/acs.jpca.7b03195>.
- (21) Minenkov, Y.; Chermak, E.; Cavallo, L. Accuracy of DLPNO–CCSD(T) Method for Noncovalent Bond Dissociation Enthalpies from Coinage Metal Cation Complexes. *J. Chem. Theory Comput.* **2015**, *11* (10), 4664–4676. <https://doi.org/10.1021/acs.jctc.5b00584>.
- (22) Shang, Y.; Ning, H.; Shi, J.; Wang, H.; Luo, S.-N. Benchmarking Dual-Level MS-Tor and DLPNO-CCSD(T) Methods for H-Abstraction from Methyl Pentanoate by an OH Radical. *Phys. Chem. Chem. Phys.* **2019**, *21* (37), 20857–20867. <https://doi.org/10.1039/C9CP03832A>.
- (23) Efremenko, I.; Martin, J. M. L. Coupled Cluster Benchmark of New Density Functionals and of Domain Pair Natural Orbital Methods: Mechanisms of Hydroarylation and Oxidative Coupling Catalyzed by Ru(II) Chloride Carbonyls. *AIP Conf. Proc* **2019**, *2186* (1), 030005. <https://doi.org/10.1063/1.5137916>.
- (24) Koerstz, M.; Elm, J.; Mikkelsen, K. V. Benchmark Study of the Structural and Thermochemical Properties of a Dihydroazulene/Vinylheptafulvene Photoswitch. *J. Phys. Chem. A* **2017**, *121* (16), 3148–3154. <https://doi.org/10.1021/acs.jpca.7b01207>.

- (25) Tan, S. Y. S.; Izgorodina, E. I. Comparison of the Effective Fragment Potential Method with Symmetry-Adapted Perturbation Theory in the Calculation of Intermolecular Energies for Ionic Liquids. *J. Chem. Theory Comput.* **2016**, *12* (6), 2553–2568. <https://doi.org/10.1021/acs.jctc.6b00141>.
- (26) Kitaura, K.; Morokuma, K. A New Energy Decomposition Scheme for Molecular Interactions within the Hartree-Fock Approximation. *Int. J. Quantum Chem.* **1976**, *10* (2), 325–340. <https://doi.org/10.1002/qua.560100211>.
- (27) Jeziorski, B.; Moszynski, R.; Szalewicz, K. Perturbation Theory Approach to Intermolecular Potential Energy Surfaces of van Der Waals Complexes. *Chem. Rev.* **1994**, *94* (7), 1887–1930. <https://doi.org/10.1021/cr00031a008>.
- (28) Zahn, S.; Uhlig, F.; Thar, J.; Spickermann, C.; Kirchner, B. Intermolecular Forces in an Ionic Liquid ([Mmim][Cl]) versus Those in a Typical Salt (NaCl). *Angew. Chem. Int. Ed.* **2008**, *47* (19), 3639–3641. <https://doi.org/10.1002/anie.200705526>.
- (29) Izgorodina, E. I.; MacFarlane, D. R. Nature of Hydrogen Bonding in Charged Hydrogen-Bonded Complexes and Imidazolium-Based Ionic Liquids. *J. Phys. Chem. B* **2011**, *115* (49), 14659–14667. <https://doi.org/10.1021/jp208150b>.
- (30) Hayes, R.; Imberti, S.; Warr, G. G.; Atkin, R. The Nature of Hydrogen Bonding in Protic Ionic Liquids. *Angew. Chem. Int. Ed.* **2013**, *52* (17), 4623–4627. <https://doi.org/10.1002/anie.201209273>.
- (31) Lynden-Bell, R. M.; Youngs, T. G. A. Simulations of Imidazolium Ionic Liquids: When Does the Cation Charge Distribution Matter? *J. Phys.: Condens. Matter* **2009**, *21* (42), 424120. <https://doi.org/10.1088/0953-8984/21/42/424120>.
- (32) Schröder, C. Comparing Reduced Partial Charge Models with Polarizable Simulations of Ionic Liquids. *Phys. Chem. Chem. Phys.* **2012**, *14* (9), 3089–3102. <https://doi.org/10.1039/C2CP23329K>.

- (33) Rigby, J.; Izgorodina, E. I. New SCS- and SOS-MP2 Coefficients Fitted to Semi-Coulombic Systems. *J. Chem. Theory Comput.* **2014**, *10* (8), 3111–3122. <https://doi.org/10.1021/ct500309x>.
- (34) S. Tan, S. Y.; Wylie, L.; Begic, I.; Tran, D.; I. Izgorodina, E. Application of Spin-Ratio Scaled MP2 for the Prediction of Intermolecular Interactions in Chemical Systems. *Phys. Chem. Chem. Phys.* **2017**, *19* (42), 28936–28942. <https://doi.org/10.1039/C7CP04391K>.
- (35) Low, K.; Tan, S. Y. S.; Izgorodina, E. I. An *Ab Initio* Study of the Structure and Energetics of Hydrogen Bonding in Ionic Liquids. *Front. Chem.* **2019**, *7*, 208. <https://doi.org/10.3389/fchem.2019.00208>.
- (36) Halkier, A.; Helgaker, T.; Jørgensen, P.; Klopper, W.; Koch, H.; Olsen, J.; Wilson, A. K. Basis-Set Convergence in Correlated Calculations on Ne, N₂, and H₂O. *Chem. Phys. Lett.* **1998**, *286* (3), 243–252. [https://doi.org/10.1016/S0009-2614\(98\)00111-0](https://doi.org/10.1016/S0009-2614(98)00111-0).
- (37) Helgaker, T.; Jorgensen, P.; Olsen, J. *Molecular Electronic-Structure Theory*; John Wiley & Sons, 2014.
- (38) Neese, F. The ORCA Program System. *WIREs: Comput. Mol. Sci.* **2012**, *2* (1), 73–78. <https://doi.org/10.1002/wcms.81>.
- (39) Neese, F. Software Update: The ORCA Program System, Version 4.0. *WIREs: Comput. Mol. Sci.* **2018**, *8* (1), e1327. <https://doi.org/10.1002/wcms.1327>.
- (40) Boys, S. F.; Bernardi, F. The Calculation of Small Molecular Interactions by the Differences of Separate Total Energies. Some Procedures with Reduced Errors. *Mol. Phys.* **1970**, *19* (4), 553–566. <https://doi.org/10.1080/00268977000101561>.
- (41) Stone, A. *The Theory of Intermolecular Forces*; Oxford University Press, 2013. <https://doi.org/10.1093/acprof:oso/9780199672394.001.0001>.
- (42) Misquitta, A. J.; Stone, A. J. Accurate Induction Energies for Small Organic Molecules: 1. Theory. *J. Chem. Theory Comput.* **2008**, *4* (1), 7–18. <https://doi.org/10.1021/ct700104t>.

- (43) Misquitta, A. J.; Stone, A. J.; Price, S. L. Accurate Induction Energies for Small Organic Molecules. 2. Development and Testing of Distributed Polarizability Models against SAPT(DFT) Energies. *J. Chem. Theory Comput.* **2008**, 4 (1), 19–32. <https://doi.org/10.1021/ct700105f>.
- (44) Parker, T. M.; Burns, L. A.; Parrish, R. M.; Ryno, A. G.; Sherrill, C. D. Levels of Symmetry Adapted Perturbation Theory (SAPT). I. Efficiency and Performance for Interaction Energies. *J. Chem. Phys.* **2014**, 140 (9), 094106. <https://doi.org/10.1063/1.4867135>.
- (45) Spackman, P. R.; Jayatilaka, D.; Karton, A. Basis Set Convergence of CCSD(T) Equilibrium Geometries Using a Large and Diverse Set of Molecular Structures. *J. Chem. Phys.* **2016**, 145 (10), 104101. <https://doi.org/10.1063/1.4962168>.

Supporting Information.

IL174 correlation energies and interaction energies with the aug-cc-pVDZ and cc-pVTZ basis sets; HBIL correlation energies and interaction energies with the aug-cc-pVDZ and cc-pVTZ basis sets; 2IP correlation energies and interaction energies with the cc-pVTZ basis set

Corresponding Author

*katya.pas@monash.edu

Author Contributions

The manuscript was written through contributions of all authors. All authors have given approval to the final version of the manuscript.

Funding Sources

This work was supported through the Australian Government Research Training Program.

Notes

None.

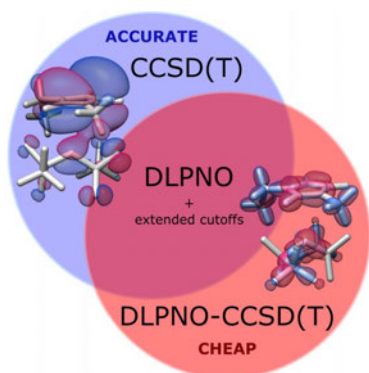
Acknowledgments

The authors gratefully acknowledge a generous allocation of computer resources through the Monash eResearch Centre and the National Computational Infrastructure. This research was supported by an Australian Government Research Training Program (RTP) Scholarship. The authors would like to thank Assoc. Prof. Amir Karton (University of Western Australia) for fruitful discussions.

Abbreviations

Chloride, Cl⁻; bromide, Br⁻; bis(trifluoromethane)sulfonimide, NTf₂⁻; dicyanamide, N(CN)₂⁻; mesylate, CH₃SO₃⁻; tetrafluoroborate, BF₄⁻; hexafluorophosphate, PF₆⁻; tosylate, CH₃C₆H₄SO₃⁻; methyl sulfate, MeOSO₃⁻; trifluoroacetate, TFA; triflate, CF₃SO₃⁻; nitrate, NO₃⁻; N,N'-alkyl-methylpyrrolidinium, C_nmpyr⁺; 3-methylimidazolium, Hmim⁺; N-methylpyrrolidinium, Hmpyr⁺; N-ethylammonium (EtNH₃⁺); N,N-methyl-ethylammonium, EtMeNH₂⁺; trimethyl-ethylammonium, TMEA; N,N-dimethyl-ethylammonium, DMEA; coupled cluster single-double- and perturbative triple-excitations, CCSD(T); complete basis set, (CBS); domain-based local pair natural orbital coupled-cluster method with singles and doubles and non-iterative triples, DLPNO-CCSD(T₀); domain-based local pair natural orbital coupled-cluster method with singles and doubles and iterative triples, DLPNO-CCSD(T₁); Møller-Plesset second order perturbation theory, MP2; symmetry adapted perturbation theory, SAPT.

For Table of Contents Only



In this work, the application of cost-effective DLPNO-CCSD(T) was successfully tested for two classes of ionic liquids, protic and aprotic. Two sets of cut-off parameters were proposed to achieve chemical and spectroscopic accuracy regardless of the cation-anion combination.

4.3 References

- [1] Frank Neese, Andreas Hansen, and Dimitrios G. Liakos. Efficient and Accurate Approximations to the Local Coupled Cluster Singles Doubles Method Using a Truncated Pair Natural Orbital Basis. *The Journal of Chemical Physics* **131**(6) (2009), 064103. DOI: [10.1063/1.3173827](https://doi.org/10.1063/1.3173827).
- [2] Frank Neese, Frank Wennmohs, and Andreas Hansen. Efficient and Accurate Local Approximations to Coupled-Electron Pair Approaches: An Attempt to Revive the Pair Natural Orbital Method. *The Journal of Chemical Physics* **130**(11) (2009), 114108. DOI: [10.1063/1.3086717](https://doi.org/10.1063/1.3086717).
- [3] Christoph Riplinger, Barbara Sandhoefer, Andreas Hansen, and Frank Neese. Natural Triple Excitations in Local Coupled Cluster Calculations with Pair Natural Orbitals. *The Journal of Chemical Physics* **139**(13) (2013), 134101. DOI: [10.1063/1.4821834](https://doi.org/10.1063/1.4821834).
- [4] Christoph Riplinger and Frank Neese. An Efficient and near Linear Scaling Pair Natural Orbital Based Local Coupled Cluster Method. *The Journal of Chemical Physics* **138**(3) (2013), 034106. DOI: [10.1063/1.4773581](https://doi.org/10.1063/1.4773581).
- [5] Yang Guo, Christoph Riplinger, Ute Becker, Dimitrios G. Liakos, Yury Minenkov, Luigi Cavallo, and Frank Neese. Communication: An Improved Linear Scaling Perturbative Triples Correction for the Domain Based Local Pair-Natural Orbital Based Singles and Doubles Coupled Cluster Method [DLPNO-CCSD(T)]. *The Journal of Chemical Physics* **148**(1) (2018), 011101. DOI: [10.1063/1.5011798](https://doi.org/10.1063/1.5011798).
- [6] Svein Saebø and Peter Pulay. Local Treatment of Electron Correlation. **44** (1993), 213.
- [7] Dimitrios G. Liakos and Frank Neese. Is It Possible To Obtain Coupled Cluster Quality Energies at near Density Functional Theory Cost? Domain-Based Local Pair Natural Orbital Coupled Cluster vs Modern Density Functional Theory. *Journal of Chemical Theory and Computation* **11**(9) (2015), 4054–4063. DOI: [10.1021/acs.jctc.5b00359](https://doi.org/10.1021/acs.jctc.5b00359).
- [8] Dimitrios G. Liakos, Manuel Sparta, Manoj K. Kesharwani, Jan M. L. Martin, and Frank Neese. Exploring the Accuracy Limits of Local Pair Natural Orbital Coupled-Cluster Theory. *Journal of Chemical Theory and Computation* **11**(4) (2015), 1525–1539. DOI: [10.1021/ct501129s](https://doi.org/10.1021/ct501129s).

Chapter 5

Sampling vast ionic liquid surfaces for the minima of bulk properties

5.1 Introduction

As the number of molecules in a system increases linearly the number of minima on the potential energy surface increases exponentially.¹ The optimisation of the system becomes dependent on the weak interaction forces where the electrostatic and dispersion components can be balanced to stabilise the system in seemingly infinite ways. Thus, additional minima of similar energy to the global minimum arise in the condensed system and influence macroscopic properties. The ratio of the fundamental energetic components of interaction energy that vary across local minima has been shown to impact properties such as melting point and conductivity in single ion pairs of ionic liquids.^{2,3} Physical properties of liquids are described through ensemble averages and thus account for these thermodynamically accessible states.

Section 5.2 contains a manuscript submitted to *The Journal of Chemical Physics*. An intuitive approach is presented whereby starting structures are strategically designed to span the potential energy surface of ionic liquids 1-methyl-3-butylimidazolium chloride ([C₄mim]Cl) and N-methyl-N-ethylpyrrolidinium tetrafluoroborate ([C₂mpyr][BF₄]). Four ion pair configurations are created by the replication of low energy IIP structures that undergo a series of rotations and inversions such that the configurations span the whole intermolecular potential

energy surface. The local environment around each starting structure is explored via molecular dynamics. Thus, the inability of molecular dynamics to overcome large energy barriers is circumvented by the strategic generation of starting structures. Unique low energy configurations were identified using agglomerative clustering and structural differences were analysed.

More than 80,000 low energy structures for each of the ionic liquids were extracted from the molecular dynamics simulations. Analysis of the structures showed that $[\text{C}_4\text{mim}]\text{Cl}$ has few distinct minima. Contrastingly, $[\text{C}_2\text{mpyr}][\text{BF}_4]$, which is known to undergo tumbling, can vary its geometry without an energetic penalty.^{4,5} Fifteen unique geometries of $[\text{C}_2\text{mpyr}][\text{BF}_4]$ and 2 unique geometries of $[\text{C}_4\text{mim}]\text{Cl}$ have been located. Geometries were located for both ionic liquids of lower energy than obtained from simulated annealing which was verified by wavefunction-based method SRS-MP2. The new methodology can successfully locate important minima of liquids that contribute to bulk properties.

An intuitive approach to finding local minima in ionic materials: a balancing of starting geometry and dynamic evolution

Zoe L. Seeger* and Ekaterina I. Izgorodina*

School of Chemistry, Monash University, 17 Rainforest Walk, Clayton, Victoria 3800, Australia

Abstract

The physicochemical properties of liquids at a given temperature are dependent on an ensemble of lower-energy minima available to the system. The prediction of these properties requires the accurate description of fundamental forces at play in each individual minimum resulting in a macroscopic picture of the system. This study presents a new methodology for finding unique lower-energy configurations that contribute to bulk properties of ionic liquids (ILs) and is applied to four ion-paired clusters of two ILs, N,N'-methyl-ethyl-pyrrolidinium tetrafluoroborate, [C₂mpyr][BF₄], and 1-methyl-3-butyl-imidazolium chloride, [C₄mim]Cl. Computationally cheap molecular dynamics simulations, using the OPLS-AA force field, are applied to a range of starting structures generated to span the potential energy surfaces of these ILs. The lower-energy structures are extracted from the simulations and principal component analysis and agglomerative clustering are used to identify unique structural arrangements. [C₂mpyr][BF₄] was found to undergo large structural changes with little impact on energy, whereas [C₄mim]Cl was very sensitive to the ion arrangement, thus resulting in far fewer minima on its potential energy surface. Simulated annealing global minima were found to be $> 7 \text{ kJ mol}^{-1}$ higher in energy for both ILs compared to those of the proposed methodology. With respect to the benchmark method used, OPLS-AA has average errors above chemical accuracy of 4 kJ mol^{-1} , with its systematic error being estimated at 15 kJ mol^{-1} for ILs. The proposed methodology was also applied to clusters of DMSO, for which the simulated annealing approach successfully located the global minimum identical to that found with the proposed methodology.

Introduction

Navigation through a molecule's potential energy surface (PES) allows for the location of stationary points such as ground and transition states as well as local minima and saddle points.

As the most common practice in computational chemistry, many techniques have been developed to find important minima when their approximate location is unknown and energy barriers must be overcome. Molecular geometries may lie in numerous low-lying minima if kinetically available. In addition, the number of energetically favourable configurations increases with the complexity of the molecule. In most cases of single small- to medium-sized molecules location of the equilibrium geometry of the global minimum on the PES successfully captures the energetics of the system such that properties dominated by this equilibrium geometry can be reliably predicted.¹ For example, gauge-including atomic orbital (GIAO) is used for calculating nuclear magnetic shielding tensors from single molecules and has been applied to large organic molecules like taxol from which it can accurately predict the NMR chemical shifts against experimental data.²⁻⁴ Atomisation energies have also been predicted in small molecules like F₂, N₂ and H₂O₂, to within chemical accuracy which is highly dependent on determining the most stable molecular structure.⁵ Global minimum structures are required to accurately predict interconversion reaction energy, for example, for the conversion between benzvalene and benzene,⁶ or the interconversion between the T-shaped and parallel-shaped benzene dimers.⁷ The intrinsic reaction coordinate (IRC) concept, the minimum-energy pathway connecting reactants and products via the transition state, can only be applied when both the reactant and the product are taken in the geometry dominating the bulk population, *i.e.* the global minimum. This concept has been successfully used to regularly locate the transition state of chemical reactions.^{8,9} In polymer studies the ability of various thioketones to act as radical trapping agents has been predicted by determining the radical stabilisation energies for the mediation of free radical polymerisation.¹⁰ Furthermore, it has been demonstrated that propagation rate coefficients in free-radical polymerization can be predicted provided the global minimum has been located.¹¹

Indeed, early global search algorithms were aimed at single molecule energy minimisation where a combination of important bond distances, angles and dihedrals could be varied simultaneously to find the global minimum while the rest of the configuration is allowed to be optimised to accommodate these variations^{12,13} These techniques work well for small-sized molecules. Since the PES is a function of atom coordinates, the increase in atoms in the molecule leads to a high cost of the PES exploration, making it intractable for large biomolecules. Simply, without the inclusion of temperature, like in molecular dynamics, or geometry deformations, that appear in stochastic approaches, complex surfaces such as the PES cannot be widely explored by scanning several geometric variables.

In condensed systems, the PES becomes infinitely more complex and laden with local minima as the degrees of freedom in the configuration increases and an interplay of forces can be minimised in seemingly unlimited ways.¹⁴ The energetic minimisation is no longer dependent on the molecular geometry alone due to the presence of the weaker intermolecular forces between molecules, which create shallow minima compared to those corresponding to changes in covalent bonds. Although the intermolecular forces are relatively weak, increasing the strength of interaction between molecules is also likely to result in increasing deformation energy that moves molecules away from their lowest energy configuration. Additionally, it becomes less likely that only the global minimum contributes to the energetic properties of the condensed system, as energetically close local minima are very likely to be accessible at a given temperature and pressure and hence, contribute to the bulk properties of the system. It has been demonstrated for ionic liquids that the ratio among the fundamental energetic components of interaction energy of their single ion pairs – electrostatics, induction and dispersion – vary between energetically accessible local minima, thus impacting physical properties such as melting point and conductivity.¹⁵ As well as the strength of interaction, molecular functional groups impact the ease at which molecules may undergo conformational (*e.g.* rotation around single bonds) and configurational (*e.g.* translation of molecules in the bulk). Goldstein *et al.* argued that the availability of multiple energetically accessible configurations separated by low-energy barriers on the PES generally leads to a decrease in viscosity.¹⁶ Since each bulk property of any condensed system such as a liquid or a solid can be best described through an ensemble average of energetically accessible configurations at given conditions, the prediction of these properties strongly depends on the knowledge of these accessible configurations.

There is a growing interest in developing theoretical and computational techniques aiming to reduce the size of the PES while searching for the global minimum of molecular systems consisting of up to thousands of atoms. Molecular dynamics (MD) has solved this problem by allowing the system to evolve through different kinetically available states over an infinite period of time.¹⁷ To-date, only significantly truncated simulations are possible and therefore, MD alone is not well suited to explore the PES in depth due to limitations in sampling. Six MD simulations of maltose in 150 water molecules were analysed according to their glycosidic linkage and hydroxymethyl groups.¹⁸ All simulations adopted the glycosidic linkage torsion angles of the global minimum but no transition from the global minimum to a second stable structure approximately 11 kJ mol⁻¹ higher in energy was observed within a total of 5.4 ns. The authors concluded that a simulation of at least 150 ns is required to reach an

equilibrium of this small molecule in water as the global minimum was estimated to have an average lifetime of 8 ns. Strong dependence of MD simulations on minimising the configuration energy means that once a deep local minimum is reached, it is unlikely that the geometry will increase its energy sufficiently to overcome the barrier and explore surrounding minima. However, it is a powerful tool when an additional strategy is introduced that adds either a geometry perturbation or energy biases, allowing the geometry to explore all possible minima. One such scheme is simulated annealing, by which the geometry begins its evolution at an extremely high temperature and is cooled slowly.^{17,19,20} Theoretically, if cooling is performed infinitely slowly, the geometry will finally become trapped within the global minimum. In practice, the technique has the same shortcomings as equilibrated MD simulations, whereby it is too slow to solve problems where sampling of minima across a vast PES is desired.

Metadynamics, also utilising MD, has great potential in finding equally important minima as it uses degrees of freedom based on the atom coordinates to which bias potentials are added.²¹ The chosen degrees of freedom, generally three or four to limit simulation cost, are termed collective variables (CV) and are identified to be important dimensions of system evolution similar to intrinsic reaction coordinates. Adding bias potentials along these dimensions allows barriers to be overcome in specific directions of the PES during simulation. Choosing the CV, however, turns out to be difficult and system dependent. CVs have been developed that describe dihedral angles in small peptides,²² the reaction pathway connecting metastable states of β -hairpin folding in proteins,²³ the puckering of cyclic compounds,²⁴ and the lattice vectors of calcium phases.²⁵ In order to increase the sampling region to the whole PES, the bias would need to span a dimension that accounts for the highest energy barriers that must be crossed using a handful of CVs. Therefore, metadynamics requires in-depth *a priori* knowledge of the PES of each molecular system to construct robust and reliable CVs.²⁶

The introduction of stochastic based methods is a logical and necessary step in solving optimisations of complex problems where traditional thermodynamic approaches require significant amount of computational resources. However, it is not clear that these methods solve the issue of sampling as they also need to sample all of the configurational space. These methods increase in cost with increasing space, especially in the situation when all minima are required for analysis. Metropolis Monte Carlo samples the PES by adding a random displacement to the geometry and accepting or rejecting the move depending on the change in energy.²⁷ Metropolis Monte Carlo by design creates micro-states in each snapshot of the ensemble which when averaged follow the Boltzmann distribution. In the similar manner as

MD, MC simulations can become stuck in a low energy region of the PES jumping between the same minima for a very long time.

Ionic liquids, discovered in 1914²⁸ but popularised in 1992²⁹ are used in industrial processes including acid scavenging³⁰, catalyst activation^{31,32}, gas absorption³³ and more as detailed in this extensive review.³³ Although, the application of ionic liquids is extremely broad, only particular combinations of cations and anions usually work for an application at hand.³⁴ Due to a countless number of these combinations, ionic liquids vary considerably in their thermodynamic and transport properties and therefore, the main challenge in the field lies in finding a high-throughput method to predict these properties *a priori*. Here computer modelling has stepped-in to bare light on the topic.

A literature search of modelling ionic liquids shows a plethora of molecular dynamics simulations of the condensed phase^{35–45} as well as many *ab initio* studies of single ion pairs^{46–52} and larger numbers of ion pairs.^{53–55} Molecular dynamics has provided insight into structural and dynamic properties of the liquids in multi-scale simulation boxes, while *ab initio* studies on small numbers of ion pairs have offered insightful links between bulk properties and the fundamental forces at play. Our group has determined correlations between electrostatic and dispersion forces with melting point and conductivity in a series of imidazolium- and pyrrolidinium-based ionic liquids using single and two ion paired lower energy configurations.^{56,57} The exact link between the fundamental forces and physicochemical properties is still elusive as research continues into how to unlock the potential of ionic liquids. However, lower energy structures consisting of a single ion pair or two ion pairs have given insight into the role of both cation and anion in governing the strength of interionic interactions and hence, their physicochemical properties. As such, each ionic liquid is unique and broad generalisations tend not to be attainable for this class of materials. It has also been seen that ions with multiple interaction sites lead to an increased number of minima that are of similar energy.⁵⁷ It is not surprising that classical force fields have been found to exhibit serious limitations in the prediction of bulk properties of ionic liquids due to their shortcoming to accurately describe dispersion and account for induction and charge transfer effects.^{58,59} Polarisable force fields, which account for induction via the Drude oscillator model, are currently emerging in the literature^{60–63} with promising results. If large-scale *ab initio* calculations of condensed phases were yet possible, it is likely more answers would have been found, however the cost of high accuracy quantum calculations still limits these studies. With the constant increase in capability of computers, *ab initio* calculations are becoming more frequent and accessible to researchers, and the size of clusters studied are also becoming larger.

With the gap between the cluster size being studied by quantum and molecular dynamics decreasing, it seems possible to combine the two approaches to drive the development of robust and reliable high-throughput algorithms for predicting structural and energetic properties of ionic liquids.

Our previous studies on single and two-ion paired configurations of ionic liquids screened through thousands of configurations to identify those of low-energy as well as the global minima.^{56,57} The geometry screening process consisted of creating starting structures in a comprehensive set of combinations of cation and anion orientations. The ion orientations took into account the $\pi^+ - \pi^+$ stacking, alternating charge arrangements, hydrogen bonding, T-shape interactions of the rings, and alkyl chain position. Fifteen different 2 ion-paired configurations for each imidazolium ionic liquid were optimised to complete a full configurational screening. Introducing complexity to the structure of cations and anions as well as increasing the number of ions in the configuration drastically increases the configurational space that must be screened to identify energetically preferred ion arrangements. This conventional way of finding local and global minima becomes an infeasible task for more realistic numbers of ion pairs.

The approach taken in this study aims to systematically generate chemically intuitive as well as diverse starting structures that span across high energy barriers of the PES and use molecular dynamics to search the potential energy surface (PES) for low energy minima. These geometries are then optimised with the same force field to remove the effects of temperature. Agglomerative clustering is performed on these minima to group similar structures together and create clear boundaries between unique structures and thus identify low energy geometries that contribute to bulk properties of ionic liquids. The developed approach is applied to four ion-paired configurations of two ionic liquids: 1-methyl-3-butylimidazolium chloride ([C4mim]Cl) and N-methyl-N-ethylpyrrolidinium tetrafluoroborate ([C2mpyr][BF₄]) and these results are contrasted with those for 4-molecule configurations of traditional solvent dimethyl sulfoxide (DMSO).

Theoretical Procedures

Starting structures

Lower energy structures of single ion pairs of [C4mim]Cl and [C2mpyr][BF₄] were taken from previously published work by our group.⁶⁴ Configurations exhibiting a varying mode of

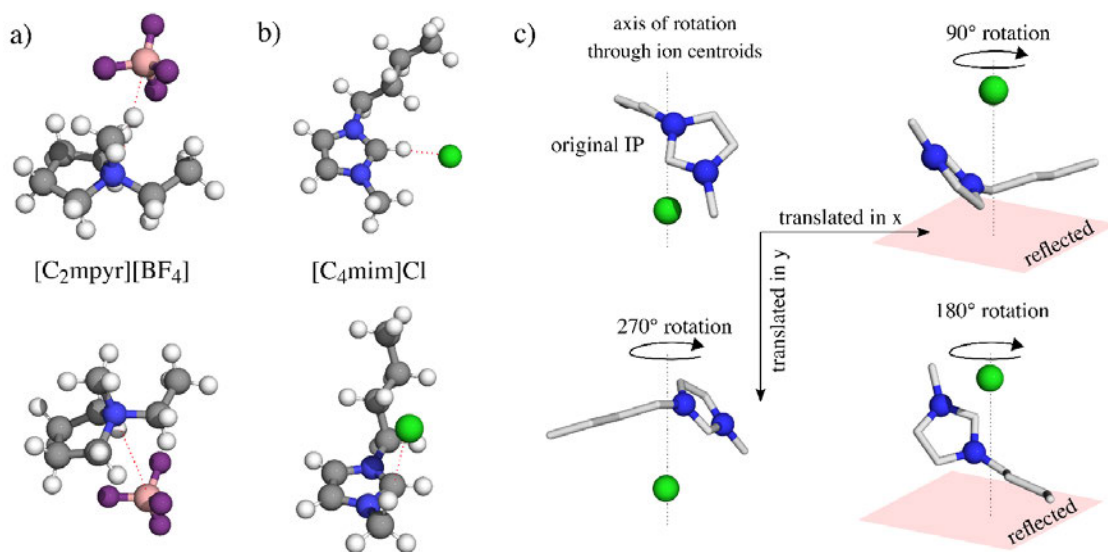


Figure 1. The two lower energy configurations of [C₂mpyr][BF₄] (a) and [C₄mim]Cl (b) ion pairs used to construct four ion-paired configurations. (c) shows a configuration of the imidazolium ion pair through replication of the original low energy structure. The ion pairs undergo rotations of 0°, 90°, 180° and 290° around the axis bisecting the anion and cation centroids, reflection in the plane orthogonal to the axis of rotation; and translation in the x and y planes.

interaction between the cation and anion were chosen in this study. Figure 1a shows the two starting ion-pair configurations of [C₂mpyr][BF₄], in which the tetrafluoroborate anion interacts with the nitrogen on the pyrrolidine ring from two different positions. The two starting ion pairs of [C₄mim]Cl are depicted in Figure 1b. In these configurations, the chloride interacts either in the imidazolium ring plane with the C₂-H bond through hydrogen bonding or above the imidazole ring.

Each ion pair was replicated and manipulated to create multiple configurations of four ion pairs. A systematic approach was applied, by which 90, 180 or 270-degree rotations were performed about an axis going through the cation and anion centroids (see Figure 1c). Additionally, two more operations – mirror reflection in the z plane and translation in the x, y and/or z direction – were applied to ensure that all possible combinations of four single ion pairs were generated, except for those being symmetrically equivalent. An example of this protocol is shown in Figure 1c. Mixing two lower energy configurations of single ion pairs to construct configurations of four ion pairs was deemed unnecessary as the protocol presented in Figure 1c generated all possible configurations exhibiting a series of interionic interactions – alkyl-alkyl van der Waals interactions, $\pi^+ - \pi^+$ stacking, alternating charge arrangements and mixtures of these to varying degrees. Due to the number of geometries constructed, visually similar configurations and configurations that were suspected to have high energy such as structures with large interionic distances between the charge centres were removed from further

analysis, although many unconventional configurations remained in order to be as unbiased as possible. Since all interaction sites of the tetrafluoroborate anion are symmetrically equivalent and chloride is a single atom anion, rotation of the anion itself was not considered.

Molecular Dynamics

The OPLS-AA (All Atom Optimized Potentials for Liquid Simulations) force field developed by Canongia Lopes and Padua^{65,66} was used to perform molecular dynamic simulations of ionic liquids and dimethylsulfoxide (DMSO). These simulations were carried out using LAMMPS.⁶⁷ The production runs of four ion pair geometries were simulated in an NVT ensemble for 0.5 ns at 298 K to explore the local space. The relatively small size of these configurations was equilibrated in a prior step, taking only 0.04 ns. Charges on ionic liquid ions were not intentionally scaled as lowered charges do not adequately correct for the lack of polarisation effects in classical force fields.⁶⁸

Statistical Analysis

Root mean square deviations (RMSD) were used to distinguish the difference between two geometries a and b each consisting of n atoms:

$$RMSD = \sqrt{\frac{1}{n} \sum_i^n \|a_i - b_i\|^2} \quad (1)$$

where a_i and b_i are vectors of the Cartesian coordinates of the atom i . The minimised RMSD is determined after alignment of the two geometries. Alignment minimises the root mean squared distance between the two geometries. RMSDs are found repeatedly after considering reflections of the geometries and accounting for reorganisation of the ions during the molecular dynamics simulation and the best alignment, that with the lowest RMSD, determines the similarity between two geometries. RMSDs of the ion centroids are used to identify the arrangement of the ions in the configurations. As the configurations of both ionic liquids were all found to adopt an alternating charge structure and the anion positions were constant, RMSDs based on a selection of cation ring positions are used to determine the orientations of the cations and used in agglomerative clustering. As such alkyl chain positions are similarly not used to discriminate between configurations. These findings are presented and further rationalised in the results and discussion.

Density-based spatial clustering of applications with noise (DBSCAN) is a computationally fast clustering algorithm, which clusters samples into distinct groups based on a distance threshold. If the number of samples that lie within the selected threshold is greater than a predefined value, referred to as required neighbours, the samples are determined to be of the same cluster, *i.e.* a distinct group. When the value of required numbers is greater than 0, samples that do not meet this criterion are considered noise and are not considered to belong to a cluster. The number of required neighbours was set to zero in this study as all configurations were considered to be important.

Agglomerative clustering was used to distinguish unique patterns in the cation orientations. Agglomerative clustering starts with each observable as its own cluster and iteratively combines the two clusters with the smallest linkage distance.⁶⁹ Where DBSCAN will expand a cluster from each observable within the cluster, agglomerative clustering joins clusters using the minimum difference of the chosen linkage criterion. The linkage criterion used was the maximum RMSD between all geometries of the two clusters. Thus, the distance, $D(A,B)$, between the two clusters - A and B - is defined as:

$$D(A,B) = \max_{a \in A, b \in B} RMSD(a,b) \quad (2)$$

and the two clusters with the smallest $D(A,B)$ are merged. After clustering, the lowest energy geometry of each cluster was considered to be the representative structure of that cluster. Combinations of ion pairs of ionic liquids are commonly called clusters. Further in the text, clusters refer to groups of geometries (*i.e.* several structures of similar geometry), while the four ion pair configurations are referred to as configurations, structures or geometries.

Principal component analysis (PCA) was used to orthogonally transform any correlated properties –a redundant set of Cartesian coordinates – into a set of linearly uncorrelated variables, known as principal components (PCs).⁷⁰ The principal components are constructed such that the first principal component accounts for the largest possible variance and, therefore, describes the most variability in the data. The amount of variability in the data explained by a principal component is referred to as the explained variance. The second PC is then attributed as much remaining variance as possible, with further PCs being identified in an iterative fashion. As the PCs are ordered by their importance, the number of PCs studied can be truncated and those that add little information can be excluded. In PCA, an original data point

x consisting of correlated properties (x_1, x_2, \dots, x_n) can be written in terms of the new principal components via:

$$X_i = x_1 l_{1,i} + x_2 l_{2,i} + \dots + x_n l_{n,i} \quad (3)$$

where $l_{n,i}$ is the loading value for property n and the X_i is the new coordinate of x for principal component number i . The loadings describe how much each property contributes to the given PC. The principal components have been used to provide insight into how sensitive the energies of configurations are to their geometry.

The machine learning toolkit, *scikit-learn*, was used to perform PCA, DBSCAN and agglomerative clustering.⁷¹

***Ab initio* calculations**

Single point energy calculations were performed on the lowest energy geometry for each cluster identified after agglomerative clustering. These calculations were performed with the Fragment Molecular Orbital (FMO) approach^{72–74} accounting for three-body corrections (i.e., FMO3) and spin-ratio scaled second order Møller-Plesset perturbation method (SRS-MP2).^{75,76} The SRS-MP2 method has been designed to work equally well for ionic and neutral systems and reproduces counterpoise corrected energies with maximum errors below 4 kJ mol⁻¹. FMO3-SRS-MP2/cc-pVTZ energies were found with GAMESS-US without any approximations and cut-offs.⁷⁷

Simulated annealing

Simulated annealing, using the same OPLS-AA force field as the classical molecular dynamics, has been performed to benchmark the unique structures obtained from clustering. The simulated annealing simulations started at 400 K and were cooled to 10 K. This was followed by a minimisation with the steepest descent algorithm. Four ion pair configurations of each ionic liquid were run for 5 ns. Simulated annealing of DMSO consisted of four molecules and was run for 25 ns.

For each material studied here (be it an ionic liquid or DMSO) the following protocol was adopted to generate low-energy configurations:

1. Generation of starting structures across the PES via replication and rotations of ion pairs
2. Molecular dynamics simulation of each starting structure
3. Extraction of low energy structures from each simulation

4. DBSCAN clustering to remove the identical structures that came from *the same* simulation to reduce the number of structures
5. Principal component analysis to analyse the dependence of energy on structure
6. Agglomerative clustering is performed to group similar structures such that different clusters represent different structures
7. Extraction of lowest OPLS energy structure from each cluster
8. FMO3-SRS-MP2 single point energy calculations on structures extracted from agglomerative clustering
9. Removal of structures with large FMO3-SRS-MP2 energies
10. Agglomerative clustering on remaining structures after step (9)
11. Extraction of lowest FMO3-SRS-MP2 energy structure from each cluster

Results and discussion

The configurations generated using the protocol outlined in Theoretical procedures (see also Figure 1c) sample across high energy barrier ion rearrangements which are not sampled during a classical MD simulation. As a result, 1761 and 2040 configurations of [C₂mpyr][BF₄] and [C₄mim]Cl were created, respectively, which represents an exhaustive set of ionic arrangements. Molecular dynamics simulations were run for each of the structures to locate low energy structures for both ionic liquids.

The energy of every second step of the simulation was recorded and those with energies within 20 kJ mol⁻¹ of the lowest found in the simulation were saved for further processing. Approximately 47 geometries per simulation of each starting structure of [C₂mpyr][BF₄] and 56 for each starting structure of for [C₄mim]Cl were found to meet this criterion, making over 80,000 geometries for each of the ionic liquids.

Results of DBSCAN clustering for ionic liquids

The DBSCAN clustering approach was used to the configurational space to a set of unique minima on the PES for the two ionic liquids. The geometries from the MD simulations were compared to those within the same simulation to eliminate identical structures (see section 2 of the Supporting Information). The lowest energy geometry from each DBSCAN cluster was

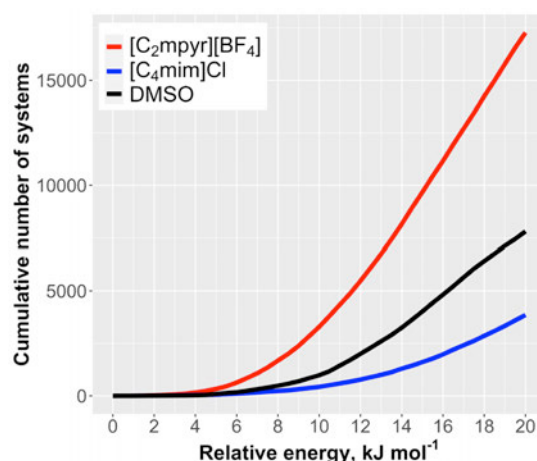


Figure 2. Cumulative number of configurations with increasing relative energy with respect to the global minimum for [C₂mpyr][BF₄], [C₄mim]Cl and DMSO.

retained for further processing. These geometries were subsequently minimised with a steepest descent algorithm with the OPLS-AA force field to remove the effect of temperature. Those within 20 kJ mol⁻¹ of the overall lowest energy identified for each ionic liquid were extracted for further analysis.

The cumulative number of structures obtained after energy minimization is shown in Figure 2 with respect to increasing relative energy (calculated with respect to the identified global minimum). The shape of the curve suggests that the observed PES has several narrow regions of lower energy. 44 structures of [C₄mim]Cl and 148 structures of [C₂mpyr][BF₄] fall within 4 kJ mol⁻¹ (*i.e.* chemical accuracy) and this is approximately 0.3 % of all the structures considered in energy minimization. An exponential increase in the number of structures occurs up to 15 kJ mol⁻¹ for [C₂mpyr][BF₄] and 18 kJ mol⁻¹ for [C₄mim]Cl, after which the growth becomes linear. After the steepest decent algorithm, 17,234 structures of [C₂mpyr][BF₄] and 3,853 structures of [C₄mim]Cl met the 20 kJ mol⁻¹ criterion. It is not surprising that compared to the imidazolium-based clusters, the number of the pyrrolidinium clusters is 4.5 times larger within the same energetic criterion. There are no energetically distinct sites on the pyrrolidinium cation for the anion to interact with, whereas the imidazolium cation has two energetically favourable sites – the in-plane interaction with the C₂-H bond and the above-the-plane interaction with the imidazolium ring.⁵⁶ These findings reflect the experimental trends highlighting varying melting points and viscosities of imidazolium- and pyrrolidinium-based ionic liquids. Additionally, pyrrolidinium cations (especially those with shorter alkyl chains) were found to undergo tumbling, resulting in multiple solid-solid transitions with low entropic penalty. This suggests that the rotation is of lower energy and may lead to numerous similar-

energy configurations.^{78,79} Contrary to this trend, the bulk structure of the imidazolium ionic liquids was found to be governed by strong hydrogen bonding with the C₂-H bond, which is suggested to lead to lower viscosities and lower melting points.^{59,80–84} Other interaction sites in the imidazole ring – especially around the C=C backbone – were found to be of much higher energy and therefore, it is fitting that a smaller number of energetically favourable configurations have been identified in [C₄mim]Cl.^{50,80,85} Electrostatic interactions in ionic liquids govern the long-range order of their bulk structure. In broader terms, there are two main types of arrangement: alternating charge and $\pi^+ - \pi^+$ stacking. Due to the presence of charged organic-type species, dispersion forces in ionic liquids were found to be of importance, even between the cation and anion.^{15,83,86} For some ILs, these forces outcompete electrostatic ones.⁸⁷ Due to the nature of dispersion forces they are more likely to govern the short-range order, thus affecting the number of energetically accessible local minima.

The possibility of decreasing the amount of starting structures was investigated by comparing the global minimum to all other extracted geometries within 20 kJ mol⁻¹ of the global minimum. If the global minimum can be identified in multiple simulations with similar starting structures, it can be reasoned that some of the starting structures can be discarded. Approximately half of the [C₄mim]Cl structures within 20 kJ mol⁻¹ had similar orientations of the cations (produced RMSDs of less than 0.5 Å for the cation positions) when compared to the global minimum. However, the structure of [C₄mim]Cl that had the smallest RMSD with the global minimum for all non-hydrogen atoms, produced an RMSD of 1.2 Å with respect to the global minimum and has large deviations in the alkyl chains positions of up to 2.7 Å and small deviations in the plane of the imidazolium ring of 0.5 Å. The small deviations in imidazolium ring and large deviations in alkyl chain position result in a difference in energy of 11.6 kJ mol⁻¹ and as such it can be concluded that the global minimum of [C₄mim]Cl was found by only one starting structure. The starting structure of the global minimum was a cuboid of alternating charge structure (see Figure 3). The starting structure that produced the most similar structure to the global minimum had the translations in the x and y directions without any reflection. Although many other starting structures were cuboids with an alternating charge arrangement, these did not produce geometries with all non-hydrogen RMSDs of less of than 2.3 Å with respect to the global minimum. Overall, only 44 configurations of [C₄mim]Cl were found to fall within 4 kJ mol⁻¹ of the global minimum despite approximately half having similar orientations of the imidazolium rings and therefore, a reduction in the number of starting structures would require much longer simulation times to ensure a complete coverage of the

lower-energy configurational region of the PES. Due to its shorter alkyl chain, the C₂mpyr⁺ cation in [C₂mpyr][BF₄] has a smaller configurational space. When comparing all structures with the global minimum of [C₂mpyr][BF₄], the most similar geometries have a large deviation of up to 3.7 Å in the positions of the pyrrolidinium ring atoms from which it can be stated that the global minimum was only identified in one simulation. Therefore, it is beneficial to include all generated starting structures to retain short simulations and ensure that the global minimum is located.

In order to determine the preferred arrangement of ions in the ionic liquid clusters optimized with MD, the following procedure was followed. Firstly, the centroid of each ion was calculated for all the MD optimised ionic liquid configurations. One structure was randomly chosen as a reference and the centroid of each ion in all structures were aligned with the centroid of the chemically equivalent ion in the chosen reference structure. As an example, the four ion-pair configurations constitute four identical cations and four identical anions. During the MD simulation, the ions move around and as such we cannot always compare the first cation of the first optimized geometry with the first cation of the second optimized geometry. However, for the atoms in the first geometry a chemically equivalent ion can be found in the second geometry. Therefore, a list of all possible combinations (referred here as mappings) of chemically equivalent atoms was created. To find one RMSD, the root mean squared distance of the atom positions of the second configuration mapped onto the first is minimised to align the two configurations and the RMSD can be calculated.

Comparison of two structures requires determination of numerous RMSD values, *i.e.* if two configurations consisting of four chemically identical molecules, four RMSD values can be determined by changing which molecule of the second configuration is mapped to the firstly selected molecule of the first configuration:

$$Conf_1Mol_1 = Conf_2Mol_1$$

$$Conf_1Mol_1 = Conf_2Mol_2$$

$$Conf_1Mol_1 = Conf_2Mol_3$$

$$Conf_1Mol_1 = Conf_2Mol_4$$

For four ion-paired clusters of ionic liquids, there are 576 possible permutations. In the case when a larger similarity is found between the first configuration and a mirror image of the second configuration, RMSD was re-calculated again after the second configuration was mirror

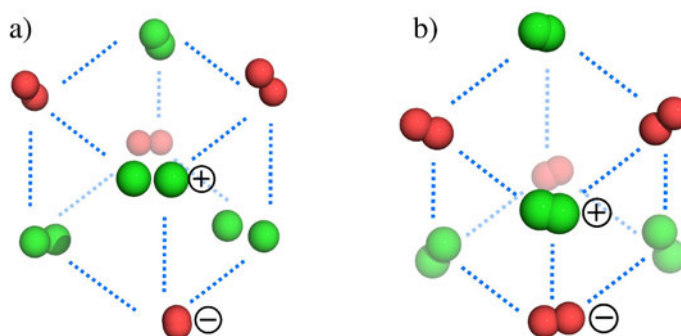


Figure 3. Centroids of cations (green) and anions (red) of the two geometries giving the largest RMSD for (a) [C2mpyr][BF₄], 1.0 Å and (b) [C4mim]Cl, 0.6 Å, showing alternating charge structures.

imaged. As a result, the number of calculated RMSDs doubles to become 1152. As minimisation algorithms depend substantially on the starting point of optimisation which in this case is the reference geometry, $\text{RMSD}(i, j)$ does not always equal $\text{RMSD}(j, i)$. Therefore, the RMSD values for each mapping were calculated a third time to obtain the smallest RMSD values that is the best indicators of the similarity between two configurations. This leads to 2304 alignments and the equal amount of RMSD values for the comparison of two structures consisting of four ion pairs. The smallest RMSD determined represents the similarity between the two structures and this is the value that is referred to as RMSD further in the text.

When comparing RMSDs of the centroids, the largest RMSD value, *i.e.* of the two most different structures, was found to be 0.6 Å for [C4mim]Cl and 1.0 Å for [C2mpyr][BF₄]. For both ionic liquids, the cation centroids aligned well for all selected structures revealing that all lower-energy configurations adopted an alternating charge structure in a cuboid-type arrangement as shown in Figure 3. The chloride anion has only one interacting site, whereas the BF₄⁻ anion has four identical interacting sites due to its tetrahedral symmetry. Therefore, both anions can be considered as “point charges”. As they adopt the same positions in all structures, the anions were excluded from further analysis.

In order to quantify the amount of change in the cation orientation, several positions on each cation were chosen for comparison using RMSD. In the case of the imidazolium cation, there are 3 main interaction sites – in-plane with the C₂-H bond through hydrogen bonding, above/below the imidazolium ring and near the C=C backbone of the ring, with the last site being the least thermodynamically preferred. Therefore, it is critical to take into account the location of the plane and its orientation with respect to other cations when comparing structures. Mathematically, the plane of the imidazolium ring can be defined with three points; however, four points were used in this study such that RMSD penalises any deviation from the

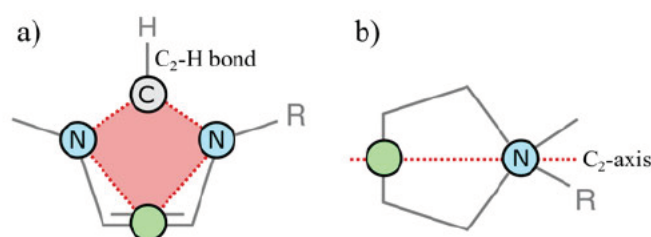


Figure 4. Positions in the imidazolium (a) and pyrrolidinium (b) cations used to differentiate between structures in RMSDs.

plane. The cation positions used to determine RMSDs between structures are shown in Figure 4a. The pyrrolidinium structures, for which 4.5 times as many structures were found within 20 kJ mol⁻¹, were allowed to undergo rotation around the C₂ axis without penalty while position and orientation of the C₂ axis was determined to dictate differences in the structures (see Figure 4b). In the description of the two types of cations, the alkyl chains were not used to discriminate between structure types. Since these short chains stabilise the cluster to a much lesser extent than the strong electrostatic forces between the ion centres, their weaker dispersion interactions do not significantly change the nature or strength of interaction greatly with chain orientation. Ionic liquids with shorter alkyl chains are dominated by cation-anion interactions and this is demonstrated through decreasing melting point with increasing alkyl chain length.⁵⁶ It can, therefore, be argued that after the structures have been grouped by their cationic orientations the alkyl chains become the differentiating factor determining the energy and as such, taking the lowest energy structure of the grouped structures implicitly selects the alkyl chain orientation that best minimises the energy.

Results of PCA for ionic liquids

Principal component analysis (PCA) was performed to understand the energy landscape of the two ionic liquids. Figure 5 shows the first four principal components and their associated energies for 17,234 structures of [C₂mpyr][BF₄] and 3,853 configurations of [C₄mim]Cl. The four principal components are the four axes that explain the most variance, with PC1 explaining the highest variance. The principal components are built on the Cartesian coordinates of the cation positions depicted in Figure 4 after the alignment of all structures to one structure chosen at random. When analysing the input data for PCA, it was found that on average 99.5% of the values for each coordinate spanned 2.5 Å for [C₂mpyr][BF₄] and 0.9 Å for [C₄mim]Cl (determined via interquartile range). Thus, the minima of [C₂mpyr][BF₄] span a much greater configurational space than those of [C₄mim]Cl. The ranges of the Cartesian coordinates on average span 3.0 Å for [C₂mpyr][BF₄] and 1.8 Å for [C₄mim]Cl emphasising that outliers of

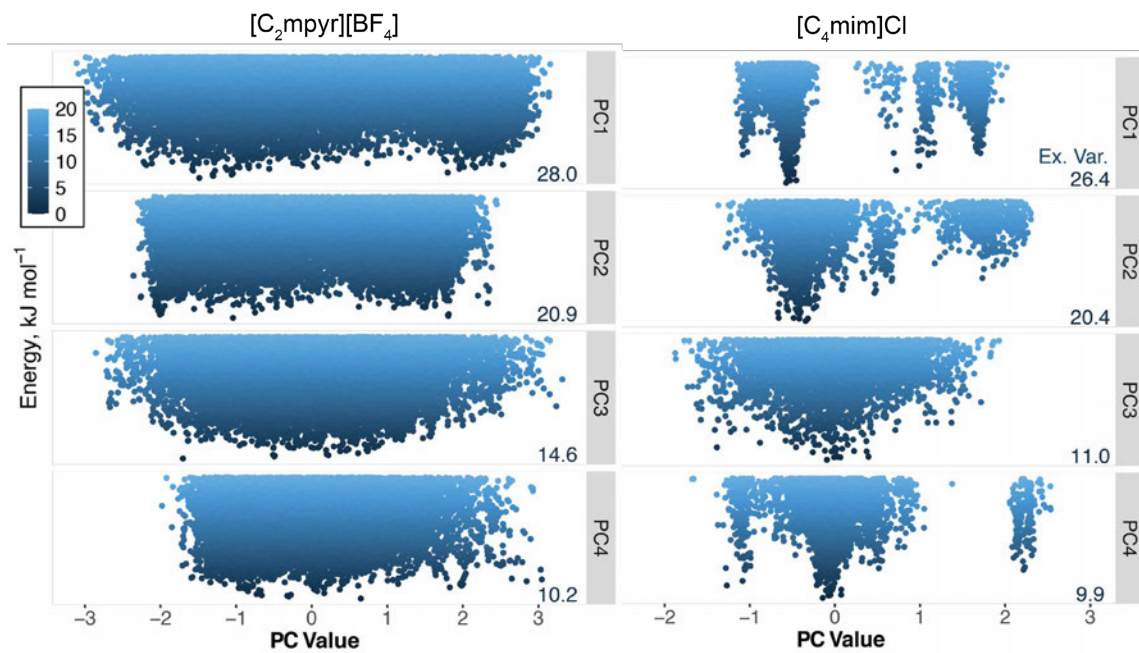


Figure 5. Four main principal component values labelled PC1, PC2, PC3 and PC4 – of the $[\text{C}_2\text{mpyr}][\text{BF}_4]$ (left) and $[\text{C}_4\text{mim}]\text{Cl}$ (right) structures within 20 kJ mol^{-1} of the global minimum and their respective relative energies. Explained variance (Ex. Var.) is shown on the right bottom corner for each PC.

the imidazolium structures span a much longer distance by 0.9 \AA , although the majority of the data can be assigned to a rather narrow range. This information corroborates Figure 5, in which the peaks corresponding to the PCs of the imidazolium-based structures show a strong dependence on cation position and hence, the overall energy. PC values (which represent a certain set of coordinates) between peaks that are not occupied by energy data for the imidazolium-based structures as these must not lead to configurations within 20 kJ mol^{-1} off the global minimum. Furthermore, the graphs represent the potential energy surface, on which low energy geometries are limited to narrow ranges of PC values. This suggests that imidazolium-based ionic liquids are more likely to adopt distinct configurations. Contrastingly, the pyrrolidinium-based structures can have significantly varied cation positions with little impact on energy as demonstrated by the absence of distinct peaks on the PC graphs. This suggests that clustering might have limited success for the pyrrolidinium structures, like clustering of any continuous property.

The configurations of $[\text{C}_2\text{mpyr}][\text{BF}_4]$ require 10 PCs to describes 95% of their variance while the configurations of $[\text{C}_4\text{mim}]\text{Cl}$ require 12 to describe 95% of their variance, suggesting that the arrangement of the cations in the $[\text{C}_2\text{mpyr}][\text{BF}_4]$ configurations are more correlated, however these arrangements are not correlated with energy and span larger interionic distances.

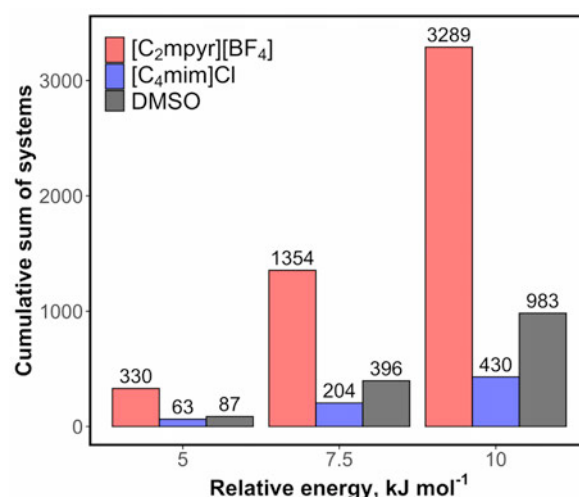


Figure 6. Number of configurations with energies within 5.0, 7.5 and 10.0 kJ mol⁻¹ with respect to the global minimum for [C₂mpyr][BF₄], [C₄mim]Cl and DMSO.

This could be attributed to the longer alkyl chain of [C₄mim]Cl that subtly impacts the cationic positions in the configurations that were not included in the PCA.

Results of agglomerative clustering for ionic liquids

Agglomerative clustering was performed to group similar geometries in nearby minima, thus determining borders between differing geometries. The linkage criterion, which determines the proximity of clusters by which structures are combined, impacts the results of clustering. The agglomerative clustering routine used here determines the distance between clusters to be the largest RMSD between geometries of the two clusters. The two clusters with the smallest maximum RMSD between them are merged. Therefore, merges are recorded as the RMSD between their most different structures to ensure only similar geometries are grouped together. A distance matrix, a symmetric matrix populated with pairwise RMSDs, was used to perform the clustering where n configurations, thus requiring $n!/2(n-2)!$ values of RMSD to be determined. As there are 3,289 configurations of [C₂mpyr][BF₄] within 10 kJ mol⁻¹ of the global minimum the distance matrix is created from 5,407,116 RMSDs. As there is no straightforward approach to pre-align all of the structures with each other simultaneously, the comparison of Cartesian coordinates or z-matrix parameters becomes erroneous and as such a distance matrix is required.

The energy cut-off that determines the structures that are used in the clustering analysis has a direct impact on the number of clusters found due to the increased size of the configurational space being considered. As can be seen more distinctly in the PCA of

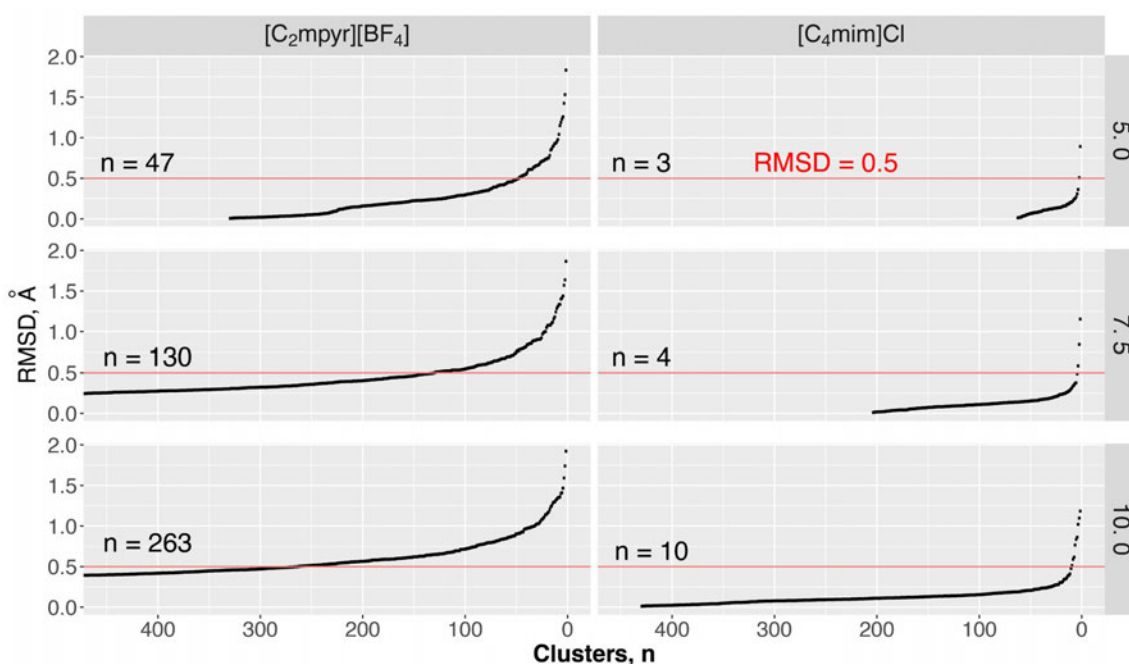


Figure 7. Agglomerative clustering results with energetic constraints of configurations within 5.0, 7.5 and 10.0 kJ mol⁻¹ of the global minimum, showing the number of clusters with an RMSD of 0.5 Å to determine similarity within clusters (red line).

[C₄mim]Cl in Figure 5, as the energy increases a larger variation of coordinates are explored. A larger portion of the PES is also explored for the pyrrolidinium configurations with increasing energy, where different combinations of values for the PCs are obtained with an increasing energy cutoff. It is critical to employ an energy cut-off that reduces the number of clusters determined to reduce the computational cost, especially in the view of optimising these structures with state-of-the-art *ab initio* methods.

Geometries with energies within the range of kinetic energy plus the error of the method (here the OPLS-AA force field) should be included in clustering. The error of the OPLS-AA force field with respect to these ionic liquids is not known. The kinetic energy at 300 K is 3.7 kJ mol⁻¹. Figure 6 shows the number of structures considered in the agglomerative clustering when the energy cutoff is set to 5.0, 7.5 and 10.0 kJ mol⁻¹. It is not surprising that when increasing the energetic cutoff, the number of structures satisfying this criterion increases. The rate, at which this number increases, depends on the ionic liquid. [C₄mim]Cl, with directional hydrogen bonding, has 983 structures within 10 kJ mol⁻¹, compared to 3,290 structures in [C₂mpyr][BF₄]. As previously identified, the pyrrolidinium cation can easily undergo a rotation around its C₂ axis with a little impact on energy.

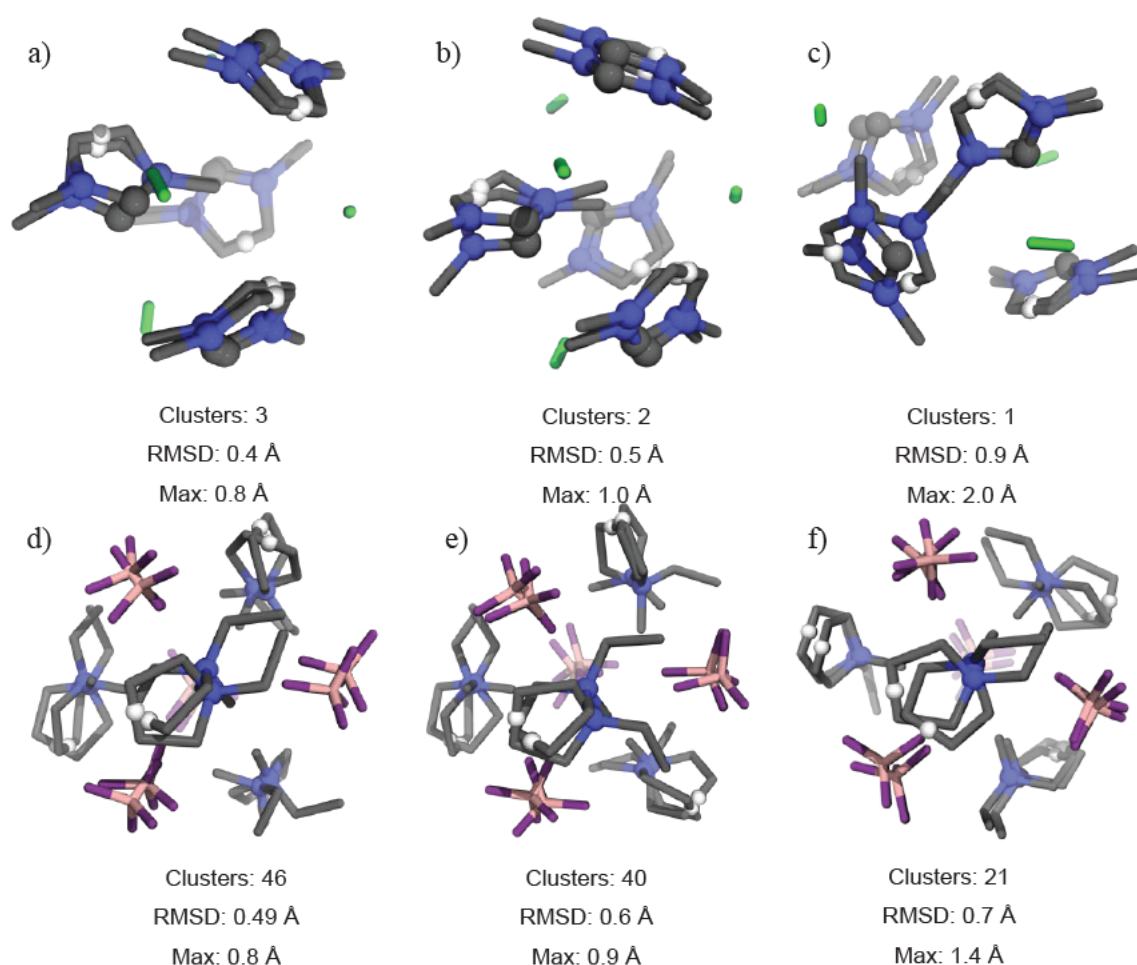


Figure 8. Maximum intra-cluster RMSDs and number of unique clusters within 5 kJ mol^{-1} using in the agglomerative clustering. Maximum distances are also given between the points of reference shown as white spheres. A green line is drawn between the chloride ions as a visual guide to the difference in position between the two clusters.

The effect of including larger portions of the PES into agglomerative clustering is given in Figure 7. At $n-1$ clusters, the two clusters with the smallest maximum RMSD between them are merged and this becomes the maximum intra-cluster RMSD of n clusters and is the RMSD value shown in Figure 7. As the number of cluster merges increases, the respective maximum RMSD increases due to the inclusion of diverse geometries. This is evident from the increasing number of clusters with an increasing predefined energy cutoff. In $[\text{C}_2\text{mpyr}][\text{BF}_4]$ the predefined energy cutoffs of 5.0 to 7.5 to 10.0 kJ mol^{-1} lead to 47, 130 and 263 unique clusters, respectively; whereas in $[\text{C}_4\text{mim}]\text{Cl}$, these lead 3, 4 and 10 clusters, respectively. In both ionic liquids, an RMSD cutoff of 0.5 Å was used. Using the same protocol, configurations of both ionic liquids can be seen to differ considerably with an RMSD of 0.5 Å , for which 48 clusters are found for $[\text{C}_2\text{mpyr}][\text{BF}_4]$ and 2 clusters for $[\text{C}_4\text{mim}]\text{Cl}$ with an energy cutoff of 5 kJ mol^{-1} .

This clearly suggests that in $[\text{C}_2\text{mpyr}][\text{BF}_4]$ a number of different configurations have similar energy.

Figure 8 shows the geometries with the maximum intra-cluster RMSDs overlayed and the associated number of clusters when agglomerative clustering is performed with the energy cutoff of 5 kJ mol^{-1} . Maximum intra-cluster RMSDs of 1.4, 1.5 and 1.8 Å are obtained when $[\text{C}_2\text{mpyr}][\text{BF}_4]$ geometries are grouped into three, two and one clusters, respectively, with 5 kJ mol^{-1} for the energy cutoff. In $[\text{C}_4\text{mim}]\text{Cl}$, three, two and one clusters have RMSD values of 0.4, 0.5 and 0.9 Å, respectively, determining that the low energy configurational space of these imidazolium structures spans a relatively limited region compared to that covered by the low energy pyrrolidinium structures.

An RMSD of 0.4 Å in these imidazolium systems, shown in Figure 8a, represents two well aligned structures, in which the largest difference between cation positions is 0.8 Å. Figure 8b contains the two structures that have the largest intra-cluster RMSD of 0.5 Å and a maximum deviation of 1.0 Å, whereas Figure 8c shows the overlayed two geometries with an RMSD of 0.9 Å and a maximum difference of 2.0 Å. In the latter one imidazolium cation is rotated by approximately 90° around an axis orthogonal to the plane of the imidazolium rings. Similar positions are found for all other cations and anions of these two geometries. The rotation of the cation depicts an obvious change in the structure.

Three RMSDs for $[\text{C}_2\text{mpyr}][\text{BF}_4]$ show the increasing deviation of the “forefront” cation in Figure 8d-f. The maximum deviation in its position increases from 0.8 to 0.9 to 1.4 Å to achieve the RMSDs of 0.5, 0.6 and 0.7 Å, respectively. Each merge of clusters from 46 groups to 21 groups increases the maximum intra-cluster RMSD by a mere 0.02 Å, revealing a flat nature of the PES with respect to the cation position, even when the position changes by up to 1.4 Å on the absolute scale. Contrastingly, discontinuity in structures occurs below an RMSD of 0.5 Å as shown in Figure 7, where similarly low energy structures are separated on the PES.

Intra-cluster RMSDs $< 0.5 \text{ Å}$ were conservatively chosen to represent uniqueness within clusters, which corresponds to maximum distance differences of approximately 1.0 Å and 0.8 Å in $[\text{C}_4\text{mim}]\text{Cl}$ and $[\text{C}_2\text{mpyr}][\text{BF}_4]$, respectively.

In $[\text{C}_2\text{mpyr}][\text{BF}_4]$, 47, 130 and 263 clusters are found for configurations of energies within 5.0, 7.5 and 10.0 kJ mol^{-1} for a maximum intra-cluster RMSD of 0.5 Å. The 47 representative structures obtained from the 5.0 kJ mol^{-1} energy cutoff have been calculated since higher cutoffs include more structures, which was not feasible because of the

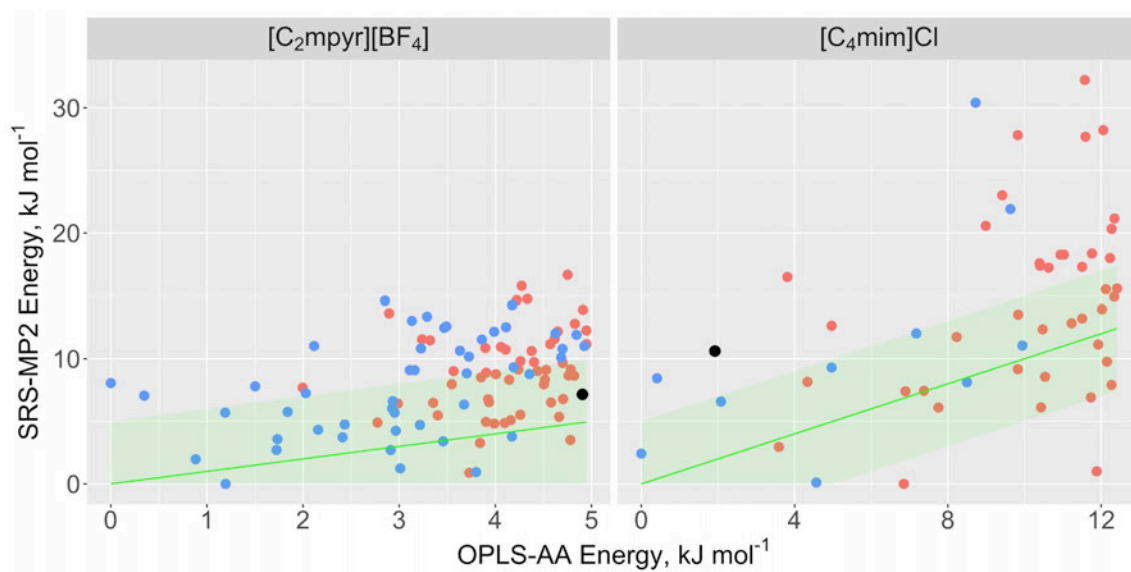


Figure 9. Relative FMO3-SRS-MP2 energies of clustering minima (blue) and other minima (red) against their relative OPLS-AA energies. A green line sits on $y=x$ and is bordered by a region of $\pm 5 \text{ kJ mol}^{-1}$ and the black points show the results of simulated annealing.

computational cost associated with it. For $[\text{C}_4\text{mim}]\text{Cl}$, where maximum intra-cluster RMSDs of 0.5 \AA clearly divides grouped structures on the PES. Clustering of these structures within 10 kJ mol^{-1} leads to 10 distinct geometries and allows for approximately 7 kJ mol^{-1} of error in the OPLS-AA force field. All these 10 representative clusters were taken for further analysis.

Improved electronic energies of representative clusters of ionic liquids

Here we decided to use a state-of-the-art method to improve electronic energies of the lower energy distinct geometries identified in the previous section. This was achieved by performing single-point energy calculations with the FMO3-SRS-MP2/cc-pVTZ level of theory. The comparison of SRS-MP2 and OPLS-AA total electronic energies relative are shown in Figure 9. SRS-MP2 relative energies were calculated with respect to the lowest SRS-MP2 energy cluster, whereas OPLS-AA relative energies were calculated with respect to the OPLS-AA global minimum. The distinct geometries – those with the lowest energy from each cluster – are shown in blue, while additional minima (not the lowest energy within each cluster), are shown in red and have been included to assess the application of the OPLS-AA force field to determining lower energy minima.

Out of the 47 structures determined for $[\text{C}_2\text{mpyr}][\text{BF}_4]$, given in blue in Figure 9, only 29 have SRS-MP2 relative energies below 10 kJ mol^{-1} . The OPLS-AA force field and SRS-MP2 determined different global minima (shown in Figure 10a). The global minimum determined by OPLS-AA has an SRS-MP2 energy of 8.1 kJ mol^{-1} larger than that of the SRS-

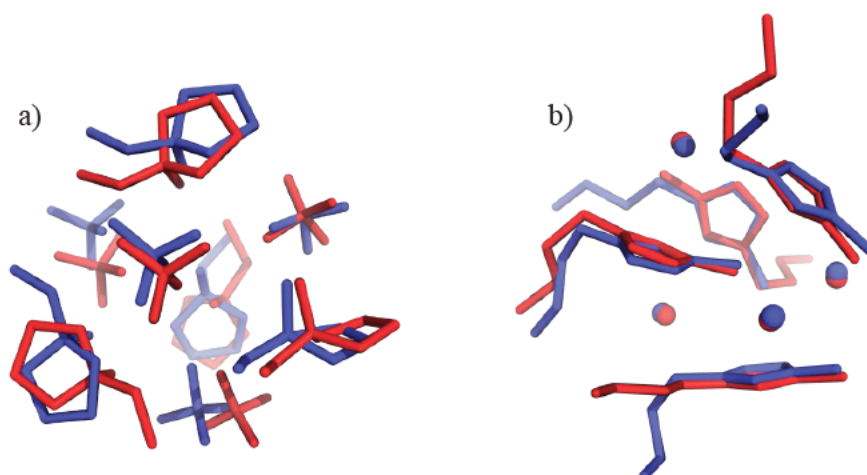


Figure 10. The FMO3-SRS-MP2/cc-pVTZ global minimum (blue) and OPLS-AA global minimum (red) of a) [C₂mpyr][BF₄] and b) [C₄mim]Cl.

MP2 global minimum. The stabilisation of the SRS-MP2 global minimum can be mostly attributed to the electrostatic component of the interaction energy that becomes more negative by 10.5 kJ mol⁻¹.

However, the SRS-MP2 global minimum of [C₂mpyr][BF₄] differs only by 1.2 kJ mol⁻¹ from the OPLS-AA global minimum when calculated with OPLS-AA. For this ionic liquid, the MAE of the OPLS-AA force field is 5.0 kJ mol⁻¹ with a maximum error of 11.9 kJ mol⁻¹. These errors are expected to increase when including structures with relative energies > 5 kJ mol⁻¹.

For [C₄mim]Cl, six of the ten lower energy structures, have SRS-MP2 relative energies of greater than 10 kJ mol⁻¹. As in the case of [C₂mpyr][BF₄], SRS-MP2 and OPLS-AA determine two different global minima. The SRS-MP2 global minimum has an energy of 6.8 kJ mol⁻¹ higher than the OPLS-AA global minimum when calculated with OPLS-AA. Moreover, the cluster, in which the SRS-MP2 global minimum was identified, does not include the geometry with the lowest OPLS-AA energy. The lowest SRS-MP2 energy geometry was not determined to be the lowest energy structure of its cluster by OPLS-AA either. Therefore, the geometry was not used as the representative structure of that cluster and is therefore not located by the methodology presented here. However, the lowest energy structure located with OPLS-AA and recalculated with SRS-MP2 is only 0.1 kJ mol⁻¹ higher in energy than the SRS-MP2 global minimum. These two geometries are shown in Figure 10b. The RMSD of the imidazolium rings of these two systems is only 0.2 Å and as such energetically and geometrically these structures can be considered similar. Overall, for [C₄mim]Cl, the MAE of

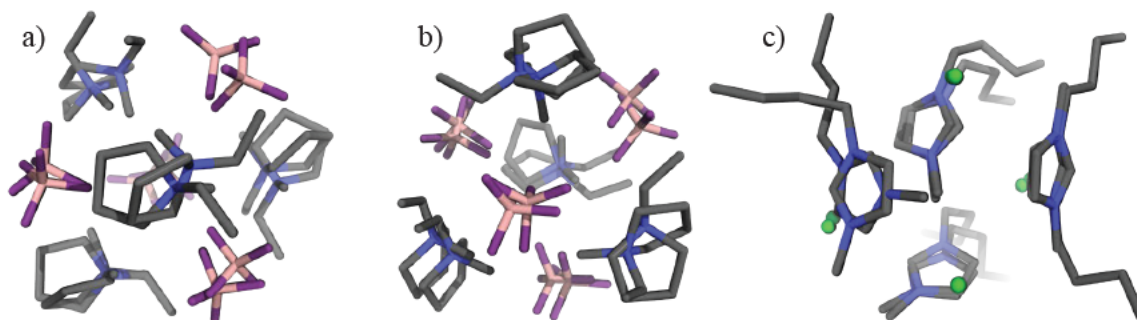


Figure 11. Unique structures of $[\text{C}_2\text{mpyr}][\text{BF}_4]$ and $[\text{C}_4\text{mim}]\text{Cl}$ overlaid for comparison including a) geometries of $[\text{C}_2\text{mpyr}][\text{BF}_4]$ that have an RMSD of 1.0 Å b) geometries of $[\text{C}_2\text{mpyr}][\text{BF}_4]$ that have the largest RMSD of 1.3 Å and c) the two unique geometries of $[\text{C}_4\text{mim}]\text{Cl}$.

the OPLS-AA force field is 6.4 kJ mol^{-1} with a standard deviation and maximum error of 6.9 and 21.7 kJ mol^{-1} , respectively.

Based on the analysis presented, it is recommended to choose structures with OPLS-AA total energy differences of at least 15 kJ mol^{-1} before agglomerative clustering in order to ensure the location of all lower-energy minima. This high energy cutoff presents a problem for materials such as $[\text{C}_2\text{mpyr}][\text{BF}_4]$, whose low energy configuration space expands rapidly with increasing the cutoff. A potential solution includes an increase in the maximum intra-cluster RMSD such that the PES is still accurately sampled with less overlap between the representative configurations.

The results of the simulated annealing simulations are given in black in Figure 9. The four ion-paired configuration of $[\text{C}_2\text{mpyr}][\text{BF}_4]$ that underwent simulated annealing obtained an OPLS-AA energy of 4.9 kJ mol^{-1} higher than that of the lowest energy structure found with the OPLS-AA force field using the protocol described in Theoretical procedures. The FMO3-SRS-MP2/cc-pVTZ energy of this geometry is 7.2 kJ mol^{-1} higher in energy than that of the SRS-MP2 global minimum defined via the proposed methodology. The simulated annealing geometry and global minimum geometry have an RMSD of 0.8 Å. The simulated annealing configuration of $[\text{C}_4\text{mim}]\text{Cl}$ has a small OPLS-AA energy difference of only 1.9 kJ mol^{-1} and a rather large FMO3-SRS-MP2 energy difference of 10.6 kJ mol^{-1} when compared to the corresponding SRS-MP2 global minimum. The RMSD between the cations of these two structures is 0.2 Å, although the alkyl chains differ by up to 5.1 Å. Thus, OPLS-AA did not locate the global minimum for either of the ionic liquids, especially when the global minimum energy was improved with SRS-MP2. OPLS-AA has successfully obtained a range of lower energy geometries; however, it did not distinguish the relative ordering of their thermodynamic

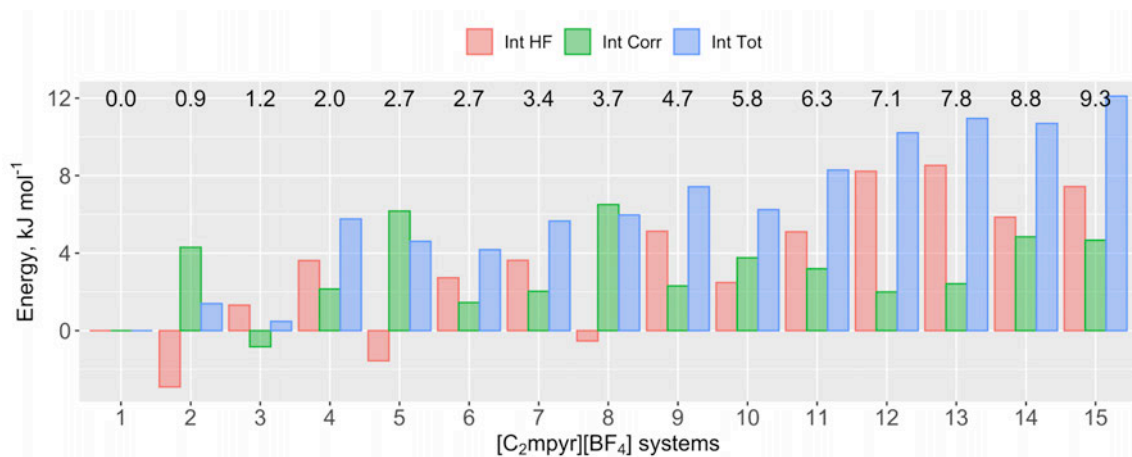


Figure 12. Relative FMO3-SRS-MP2/cc-pVTZ correlation (Int Corr), Hartree-Fock (Int HF) and total interaction energies (Int Tot) of the fifteen unique $[\text{C}_2\text{mpyr}][\text{BF}_4]$ configurations. The relative total energies are given above the bars. All energies are in kJ mol^{-1} .

stability. Therefore, a higher-level method must be applied to confirm the stability of these configurations.

Unique geometries from agglomerative clustering

The lowest energy geometry of each cluster was used as the representative structure for this cluster. The lowest energy structure does not necessarily reside in the centre of the cluster. Therefore, cases exist where two cluster minima have an RMSD of less than 0.5 \AA . Redundant structures of comparatively higher SRS-MP2 energy were removed by repeating agglomerative clustering on the structures with SRS-MP2 energies within 10 kJ mol^{-1} . The linkage criterion was changed to the minimum RMSD between two clusters and clustering was terminated when 0.5 \AA was exceeded. This process resulted in 15 unique structures of $[\text{C}_2\text{mpyr}][\text{BF}_4]$ and 2 unique structures of $[\text{C}_4\text{mim}]\text{Cl}$ down from 29 and 6 structures, respectively. RMSDs between the unique structures of $[\text{C}_2\text{mpyr}][\text{BF}_4]$ span a range of 0.5 to 1.3 \AA . Figure 11a shows the difference between two structures with RMSD of 1.0 \AA , in which the change in the pyrrolidinium cation positions also affected the anion positions. The maximum distance between the cationic reference positions from Figure 4 is 1.4 \AA . The position of the nitrogen atoms from four different cations differ from 0.5 to 1.1 \AA . Figure 11b shows the two unique structures with the largest RMSD of 1.3 \AA . Here the two structures differ in the nitrogen positions from 0.3 to 1.0 \AA , however the largest deviation of 2.8 \AA comes from the mid-point between two carbons on the C_2 axis (see Figure 4b), thus resulting in a different direction of the alkyl chain. For comparison, two unique configurations of $[\text{C}_4\text{mim}]\text{Cl}$, with an RMSD of 1.1 \AA are shown in Figure 11c. These predominantly differ by the alkyl chain position. In

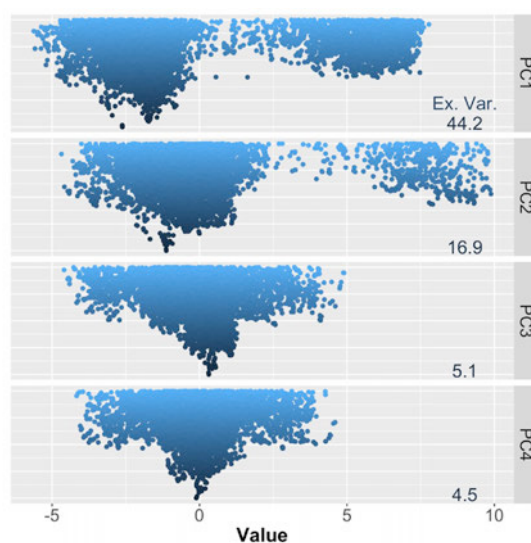


Figure 13. Principal component values of PCs 1-4 and explained variance (Ex. Var.) for dimethyl sulfoxide configurations within 20 kJ mol⁻¹ of the global minimum and their respective relative energies.

addition, one imidazolium cation is rotated by approximately 90 degrees in the plane of the ring. The configuration of higher energy has a relative energy of 6.5 kJ mol⁻¹ such that the global minimum is greatly preferred at room temperature. The relative interaction energy of the higher energy configuration is 13.4 kJ mol⁻¹ and has a favourable interaction correlation energy than the global minimum by 4.3 kJ mol⁻¹.

Relative interaction energies together with the HF and correlation components of the unique structures of [C₂mpyr][BF₄] are given Figure 12. Their SRS-MP2 interaction energies differ within 9.3 kJ mol⁻¹ and come with slight variations in the HF and correlation components not exceeding 8 kJ mol⁻¹. The two structures presented in Figure 3a differ by only 3.4 kJ mol⁻¹. These results clearly highlight the energetic similarity of the structures despite configurational differences. All these structures are expected to contribute to the bulk properties of [C₂mpyr][BF₄].

Application of the proposed methodology to clusters of DMSO

The same protocol described in Theoretical Procedures has been applied to clusters of four molecules of dimethyl sulfoxide (DMSO), for which 1008 starting configurations were simulated for 0.1 ns bounded by walls generating a Lennard-Jones potential to inhibit evaporation. After energy minimisation, 7,808 structures of DMSO were found to be within 20 kJ mol⁻¹ of the lowest energy cluster. This lies below the number of structures for [C₂mpyr][BF₄] and above that for [C₄mim]Cl (see Figure 2). On average, 99.5% of the values for each coordinate span 3.4 Å, which is 0.8 Å larger than the range of pyrrolidinium structures

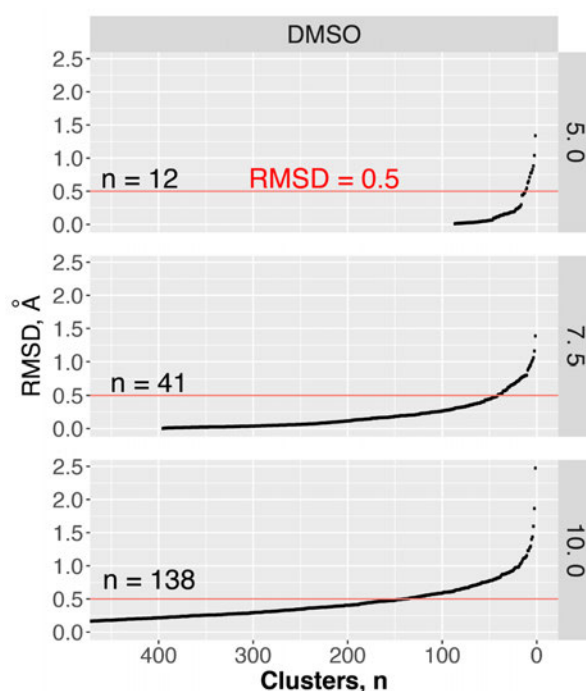


Figure 14. Agglomerative clustering results with energetic constraints of configurations within 5.0, 7.5 and 10.0 kJ mol⁻¹ of the global minimum, showing the number of clusters when an RMSD threshold of 0.5 Å is used to determine sameness within clusters (red line).

suggesting a broader region of the PES is covered for each atom to generate these minima. PCA was performed on the non-hydrogen atoms and is shown in Figure 13. The analysis, as in the case of [C4mim]Cl, shows preference for the adoption of particular configurations and low energy structures are achieved by a very narrow selection of PC values suggesting that clustering will yield a small number of representative geometries. The first principal component of DMSO explains 44% of the variance – approximately one and a half times that of either of the ionic liquids – which identifies a strong order of in the structure.

Results of the agglomerative clustering are shown in Figure 14. All non-hydrogen atoms were used in finding the RMSDs and an energy cutoff of 7.5 kJ mol⁻¹ was used to keep the number of structures below 100. An energy cutoff of 10.0 kJ mol⁻¹ leads to the location of 138 clusters. 41 clusters were identified to have the intra-cluster RMSD < 0.5 Å. The SRS-MP2 and OPLS-AA relative energies for these unique configurations are shown in Figure 15. The SRS-MP2 global minimum has an OPLS-AA relative energy of > 6 kJ mol⁻¹ and as such is not the geometry that was used to represent the cluster and is therefore not located by the proposed methodology.

The SRS-MP2 global minimum was grouped with structures with RMSDs of less than 0.3 Å. This structure has an RMSD of 0.2 Å with respect to the geometry of the same cluster

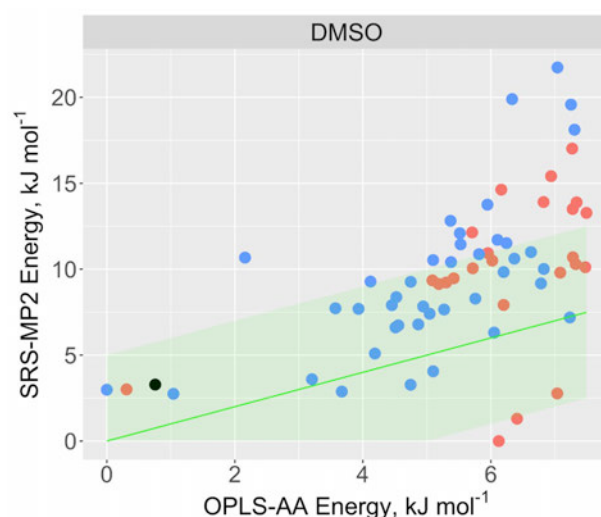


Figure 15. Relative FMO3-SRS-MP2/cc-pVTZ energies of unique structures from clustering (blue), the result of simulated annealing (black) and other minima (red) against their relative OPLS-AA energies. A green line sits on $y=x$ and is bordered by a region of ± 5 kJ mol^{-1} and the black point shows the result of simulated annealing.

with the lowest OPLS-AA energy that is selected to be the representative geometry of the cluster. The SRS-MP2 energy of the lowest OPLS-AA energy geometry in the same cluster as the SRS-MP2 global minimum is 4.1 kJ mol^{-1} higher in energy than the SRS-MP2 global minimum. 21 of the 41 geometries have SRS-MP2 energies above 10 kJ mol^{-1} and were removed from further analysis. The MAE of the OPLS-AA force field when applied to DMSO configurations is 4.6 kJ mol^{-1} with a standard deviation and a maximum error of 3.8 and 14.7 kJ mol^{-1} , respectively. This is similar to the performance of the OPLS-AA force field when applied to $[\text{C}_2\text{mpyr}][\text{BF}_4]$.

Figure 15 also shows the result of the simulated annealing simulation run for 25 ns from 400 K to 10 K followed by a minimisation with the steepest descent algorithm. The structure produced has a relative OPLS-AA energy of 0.8 kJ mol^{-1} , an SRS-MP2 relative energy of 3.3 kJ mol^{-1} and an RMSD of 0.1 \AA with respect to the OPLS-AA lowest energy geometry.

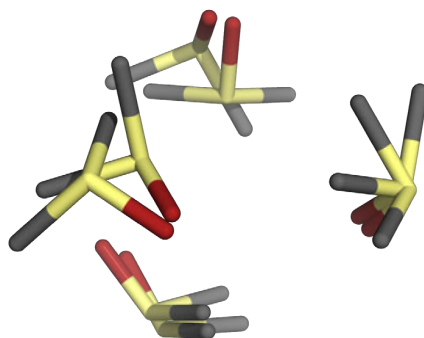


Figure 16. The two unique structures of DMSO with the largest RMSD of 0.9 \AA .

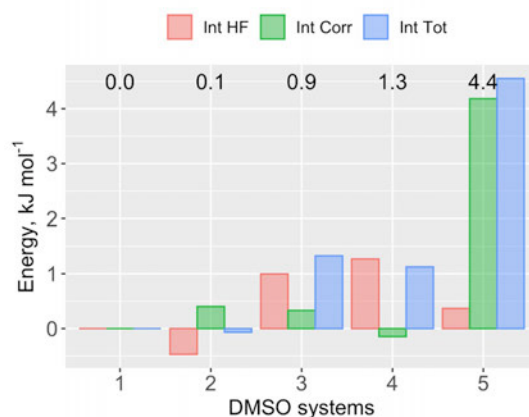


Figure 17. Relative FMO3-SRS-MP2/cc-pVTZ correlation (Int Corr), Hartree-Fock (Int HF) and total (Int Tot) interaction energies of the five unique DMSO configurations. The relative total energies are given above the bars. All energies are in kJ mol⁻¹.

Agglomerative clustering was repeated on the low energy SRS-MP2 structures, as in the case of the ionic liquids, and the unique geometries were taken to be the lowest SRS-MP2 energy configuration of each cluster. This approach identified 5 unique geometries including one very close in geometry to the geometry from simulated annealing (RMSD of < 0.1 Å). The RMSDs vary from 0.6 to 0.9 Å between the structures of DMSO. Figure 17 shows the two most different structures. Two of the molecules are a mirror image of one another with respect to their bent shape but the position of the oxygen atoms is relatively constant. In fact, in all the structures the oxygen positions stay constant determining that only one arrangement of DMSO exists with respect to the oxygen atoms. This is also true of the sulphur atoms, although larger deviations are seen in their positions.

SRS-MP2 interaction energies of the five configurations relative to the SRS-MP2 global minimum are given in Figure 18 along with their HF and correlation components. The total relative energies are all below 5 kJ mol⁻¹. The RMSD between global minimum and second lowest energy structure is 0.6 Å and the difference lies in one DMSO molecule being rotated around its S-O bond. Energetically these structures differ by as little as 0.1 kJ mol⁻¹ in energy. When the global minimum is compared with the structure of a relative error of 4.4 kJ mol⁻¹, the difference was attributed to the direction of one of methyl groups, resulting in a much larger interaction energy.

The four molecule configurations of DMSO have been clustered and the unique low energy geometries have been extracted according to their FMO3-SRS-MP2/cc-pVTZ energy. The geometry obtained from simulated annealing was located via this methodology as well as four other distinct geometries. A randomly calculated minimum was found to be at least 2.5 kJ

mol⁻¹ lower than both the structures obtained from clustering (it was not the lowest energy structure in its cluster as per its OPLS-AA energy) as well as the geometry from simulated annealing.

Conclusions

A new methodology for finding lower energy configurations of condensed systems such as ionic liquids is presented, which uses molecular dynamic simulations on a number of systematically generated starting configurations followed by PCA, agglomerative clustering and further refinement based improved energy calculations performed with FMO3-SRS-MP2. In this work the proposed protocol was applied to finding lower-energy configurations consisting of four ion pairs of the ionic liquids - [C₂mpyr][BF₄] and [C₄mim]Cl - and 4 molecules of an organic solvent, DMSO.

Initial MD simulations on systematically generated 4 ion-paired configurations produced a large number of structures within 20 kJ mol⁻¹, with [C₂mpyr][BF₄] having 4.5 times the amount of structures. All of these structures had an alternating charge arrangement, with the pyrrolidinium cation exhibit an increased variation in its position with no effect on energy. The ionic liquid configurations were grouped using agglomerative clustering according to the RMSDs calculated with respect to the selected positions on the imidazolium/pyrrolidinium ring. An intra-cluster RMSD of 0.5 Å was conservatively defined to have variability within clusters such that the cluster no longer contained only identical structures. The RMSD cutoff of 0.5 Å was applied to clustering results when configurations within 5.0, 7.5 and 10.0 kJ mol⁻¹ of the global minimum were included. 10 and 263 clusters were determined for [C₄mim]Cl and [C₂mpyr][BF₄], respectively, when configurations within 10.0 kJ mol⁻¹ of the global minimum were included. Clustering of [C₂mpyr][BF₄] leads to a much larger number of clusters as the geometries of [C₂mpyr][BF₄] span a large configuration space. In order to concentrate on a smaller more important subset of geometries, the clustering results of the configurations within 5.0 kJ mol⁻¹ of the global minimum were used which resulted in 47 clusters.

FMO3-SRS-MP2/cc-pVTZ single point energy calculations were performed on the lowest energy structure from each cluster of the 47 clusters of [C₂mpyr][BF₄] and the 10 clusters of [C₄mim]Cl. Out of the 47 structures of [C₂mpyr][BF₄], 29 of these had FMO3-SRS-MP2 energies below 10 kJ mol⁻¹ and 6 of the 10 [C₄mim]Cl structures from clustering had FMO3-SRS-MP2 energies below 10 kJ mol⁻¹. Redundant configurations of comparatively higher SRS-MP2 energy were removed by repeating clustering on configurations with FMO3-

SRS-MP2 relative energies less than 10 kJ mol^{-1} . 15 unique geometries of $[\text{C}_2\text{mpyr}][\text{BF}_4]$ and 2 unique geometries of $[\text{C}_4\text{mim}]\text{Cl}$ have been identified that differ by at least 0.5 \AA in their cation orientations. The pyrrolidinium cation showed a high degree of rotation around the C_2 axis with small changes in energy. On the other hand, the imidazolium cation clearly preferred to interact through two specific sites that were previously shown to be energetically favourable. The two unique structures of 4 ion-paired configurations of $[\text{C}_4\text{mim}]\text{Cl}$ differed only slightly in their total energy (0.1 kJ mol^{-1}), with varying position of the alkyl chains and only one imidazolium cation being rotated in the plane of the ring by 90 degrees.

The classical MD simulations with the OPLS-AA force field were excellent at generating a vast number of structures within 20 kJ mol^{-1} . When compared to the SRS-MP2 method, which is considered the benchmark method for ionic liquids, it showed rather large deviations in the total energy of the selected clusters that contained representative geometries. Based on the energy analysis, OPLS-AA and SRS-MP2 produced different global minima. The mean absolute error of the OPLS-AA force field with $[\text{C}_4\text{mim}]\text{Cl}$ was 6.4 kJ mol^{-1} with a maximum error of 21.7 kJ mol^{-1} . The mean absolute error of OPLS-AA with $[\text{C}_2\text{mpyr}][\text{BF}_4]$ was 5.0 kJ mol^{-1} with a maximum error of 11.9 kJ mol^{-1} . The global minimum of $[\text{C}_2\text{mpyr}][\text{BF}_4]$ as determined by the OPLS-AA force field had an energy 8.1 kJ mol^{-1} larger than the global minimum determined by the FMO3-SRS-MP2 method. The global minimum defined by OPLS-AA has an FMO3-SRS-MP2 relative energy of 1.2 kJ mol^{-1} . These findings suggest that configurations with relative energies of up to 15 kJ mol^{-1} should be included in higher level calculations to account for the systematic error of the force field.

It appears that simulated annealing does not converge to the same global minimum as the proposed protocol for 4 ion-paired configurations of both ionic liquids. The SRS-MP2 global minimum identified for $[\text{C}_2\text{mpyr}][\text{BF}_4]$ is 7.2 kJ mol^{-1} lower than the geometry from simulated annealing, whereas the SRS-MP2 global minimum identified for $[\text{C}_4\text{mim}]\text{Cl}$ is 10.5 kJ mol^{-1} lower in energy than that of the simulated annealing geometry. The SRS-MP2 global minimum and the simulated annealing of $[\text{C}_2\text{mpyr}][\text{BF}_4]$ have a large RMSD of 0.8 \AA for their cation positions. Contrastingly, the SRS-MP2 global minimum and the simulated annealing of $[\text{C}_4\text{mim}]\text{Cl}$ have a small RMSD of 0.2 \AA however the terminal carbon of their alkyl chains deviated by up to 5.1 \AA .

The same methodology was applied to DMSO, for which five unique structures were identified, highlighting a small variability in geometry. All structures differed in the position of the methyl groups, with the oxygen and sulphur atoms maintaining similar positions. One of these structures was very close in its geometry to the one produced with simulated annealing.

The OPLS-AA global minimum was within chemical accuracy off the FMO3-SRS-MP2 global minimum. These structures were at least 2.5 kJ mol^{-1} larger than the global minimum which is within chemical accuracy. For a traditional organic solvent, a good agreement was found between the simulated annealing and the proposed protocol, thus highlighting the reliability of the OPLS-AA force field for the prediction of energetics of condensed systems consisting of neutral molecules.

The proposed methodology allows for a robust identification of lower-energy configurations of condensed systems such as ionic liquids consisting of several ion pairs. The analysis of the unique geometries leads to the understanding of which configurations contribute to their thermodynamic and transport properties. For example, for $[\text{C}_2\text{mpyr}][\text{BF}_4]$ the pyrrolidinium cation demonstrated its unique ability of rotating around the C_2 axis without any significant effect on energy, which was confirmed experimentally by the presence of solid-solid transitions at low temperatures. Contrary to this, for $[\text{C}_4\text{mim}]\text{Cl}$ the imidazolium cation clearly preferred to maintain two energetically favourable interactions within its ring in the 4 ion-paired clusters. The proposed methodology can now be applied to studying how variations in the chemical identity of the ionic liquid cation and anion modify their energetic landscape and result in varying thermodynamic and transport properties. The thus determined lower-energy structures of medium- to large-sized clusters of condensed systems such as ionic materials will aid in the development of insightful collective variables to be used in metadynamics studies to observe transitions between local minima on the potential energy surface of these materials. Equally important, the knowledge of the relationship between the local structure of lower energy configurations of condensed systems with their physicochemical properties will also help improve on machine learning models used for the design of novel materials with desired properties.

Author's contributions

The manuscript was written through contributions of all authors. All authors have given approval to the final version of the manuscript.

Acknowledgments

The authors gratefully acknowledge a generous allocation of computer resources through the Monash eResearch Centre and the National Computational Infrastructure. This research was

supported by an Australian Government Research Training Program (RTP) Scholarship. ZLS would like to thank Peter Halat for his advice on principal component analysis.

Data Availability

The data that supports the findings of this study are available within the article [and its supplementary material].

References

- (1) Maranas, C. D.; Floudas, C. A. Global Minimum Potential Energy Conformations of Small Molecules. *J. Glob. Optim.* **1994**, *4* (2), 135–170. <https://doi.org/10.1007/BF01096720>.
- (2) Ditchfield, R. Self-Consistent Perturbation Theory of Diamagnetism. *Mol. Phys.* **1974**, *27* (4), 789–807. <https://doi.org/10.1080/00268977400100711>.
- (3) Cheeseman, J. R.; Trucks, G. W.; Keith, T. A.; Frisch, M. J. A Comparison of Models for Calculating Nuclear Magnetic Resonance Shielding Tensors. *J. Chem. Phys.* **1996**, *104* (14), 5497–5509. <https://doi.org/10.1063/1.471789>.
- (1) Maranas, C. D.; Floudas, C. A. Global Minimum Potential Energy Conformations of Small Molecules. *Struct. Chem.* **1994**, *4* (2), 135–170. <https://doi.org/10.1007/BF01096720>.
- (5) Bak, K. L.; Jørgensen, P.; Olsen, J.; Helgaker, T.; Klopper, W. Accuracy of Atomization Energies and Reaction Enthalpies in Standard and Extrapolated Electronic Wave Function/Basis Set Calculations. *J. Chem. Phys.* **2000**, *112* (21), 9229–9242. <https://doi.org/10.1063/1.481544>.
- (6) Dewar, M. J. S.; Kirschner, S. Conversion of Benzvalene to Benzene. *J. Am. Chem. Soc.* **1975**, *97* (10), 2932–2933. <https://doi.org/10.1021/ja00843a070>.
- (7) Tsuzuki, S.; Uchimaru, T.; Sugawara, K.; Mikami, M. Energy Profile of the Interconversion Path between T-Shape and Slipped-Parallel Benzene Dimers. *J. Chem. Phys.* **2002**, *117* (24), 11216–11221. <https://doi.org/10.1063/1.1523057>.
- (8) Schmidt, M. W.; Gordon, M. S.; Dupuis, M. The Intrinsic Reaction Coordinate and the Rotational Barrier in Silaethylene. *J. Am. Chem. Soc.* **1985**, *107* (9), 2585–2589. <https://doi.org/10.1021/ja00295a002>.
- (9) Wiest, O.; Black, K. A.; Houk, K. N. Density Functional Theory Isotope Effects and Activation Energies for the Cope and Claisen Rearrangements. *J. Am. Chem. Soc.* **1994**, *116* (22), 10336–10337. <https://doi.org/10.1021/ja00101a078>.

- (10) Chaffey-Millar, H.; Izgorodina, E. I.; Barner-Kowollik, C.; Coote, M. L. Radical Addition to Thioketones: Computer-Aided Design of Spin Traps for Controlling Free-Radical Polymerization. *J. Chem. Theory Comput.* **2006**, 2 (6), 1632–1645. <https://doi.org/10.1021/ct600128t>.
- (11) Izgorodina, E. I.; Coote, M. L. Accurate Ab Initio Prediction of Propagation Rate Coefficients in Free-Radical Polymerization: Acrylonitrile and Vinyl Chloride. *Chem. Phys.* **2006**, 324 (1), 96–110. <https://doi.org/10.1016/j.chemphys.2005.09.042>.
- (12) Wiberg, K. B.; Boyd, R. H. Application of Strain Energy Minimization to the Dynamics of Conformational Changes. *J. Am. Chem. Soc.* **1972**, 94 (24), 8426–8430. <https://doi.org/10.1021/ja00779a023>.
- (13) Lipton, M.; Still, W. C. The Multiple Minimum Problem in Molecular Modeling. Tree Searching Internal Coordinate Conformational Space. *J. Comput. Chem.* **1988**, 9 (4), 343–355. <https://doi.org/10.1002/jcc.540090409>.
- (14) Goedecker, S. Minima Hopping: An Efficient Search Method for the Global Minimum of the Potential Energy Surface of Complex Molecular Systems. *J. Chem. Phys.* **2004**, 120 (21), 9911–9917. <https://doi.org/10.1063/1.1724816>.
- (15) Bernard, U. L.; Izgorodina, E. I.; MacFarlane, D. R. New Insights into the Relationship between Ion-Pair Binding Energy and Thermodynamic and Transport Properties of Ionic Liquids. *J. Phys. Chem. C* **2010**, 114 (48), 20472–20478. <https://doi.org/10.1021/jp1048875>.
- (16) Goldstein, M. Viscous Liquids and the Glass Transition: A Potential Energy Barrier Picture. *J. Chem. Phys.* **2003**, 119 (9), 3728. <https://doi.org/10.1063/1.1672587>.
- (17) van Laarhoven, P. J. M.; Aarts, E. H. L. Simulated Annealing. In *Simulated Annealing: Theory and Applications*; van Laarhoven, P. J. M., Aarts, E. H. L., Eds.; Mathematics and Its Applications; Springer Netherlands: Dordrecht, 1987; Vol. 37, pp 7–15. https://doi.org/10.1007/978-94-015-7744-1_2.
- (18) Molecular Dynamics Simulations of Maltose in Water. *Carbohydr. Res.* **1996**, 281 (1), 11–34. [https://doi.org/10.1016/0008-6215\(95\)00320-7](https://doi.org/10.1016/0008-6215(95)00320-7).
- (19) Kirkpatrick, S.; Gelatt, C. D.; Vecchi, M. P. Optimization by Simulated Annealing. *Science* **1983**, 220 (4598), 671–680. <https://doi.org/10.1126/science.220.4598.671>.
- (20) Mestres, J.; Scuseria, G. E. Genetic Algorithms: A Robust Scheme for Geometry Optimizations and Global Minimum Structure Problems. *J. Comput. Chem.* **1995**, 16 (6), 729–742. <https://doi.org/10.1002/jcc.540160609>.

- (21) Barducci, A.; Bonomi, M.; Parrinello, M. Metadynamics. *Wiley Interdiscip. Rev. Comput. Mol. Sci.* **2011**, *1* (5), 826–843. <https://doi.org/10.1002/wcms.31>.
- (22) Vymětal, J.; Vondrášek, J. Metadynamics As a Tool for Mapping the Conformational and Free-Energy Space of Peptides — The Alanine Dipeptide Case Study. *J. Phys. Chem. B* **2010**, *114* (16), 5632–5642. <https://doi.org/10.1021/jp100950w>.
- (23) Bonomi, M.; Branduardi, D.; Gervasio, F. L.; Parrinello, M. The Unfolded Ensemble and Folding Mechanism of the C-Terminal GB1 β -Hairpin. *J. Am. Chem. Soc.* **2008**, *130* (42), 13938–13944. <https://doi.org/10.1021/ja803652f>.
- (24) Sega, M.; Autieri, E.; Pederiva, F. On the Calculation of Puckering Free Energy Surfaces. *J. Chem. Phys.* **2009**, *130* (22), 225102. <https://doi.org/10.1063/1.3147642>.
- (25) Ishikawa, T.; Ichikawa, A.; Nagara, H.; Geshi, M.; Kusakabe, K.; Suzuki, N. Theoretical Study of the Structure of Calcium in Phases IV and V via *Ab Initio* Metadynamics Simulation. *Phys. Rev. B* **2008**, *77* (2), 020101. <https://doi.org/10.1103/PhysRevB.77.020101>.
- (26) Sutto, L.; Marsili, S.; Gervasio, F. L. New Advances in Metadynamics. *Wiley Interdiscip. Rev. Comput. Mol. Sci.* **2012**, *2* (5), 771–779. <https://doi.org/10.1002/wcms.1103>.
- (27) Hammond, B. L.; Lester, W. A.; Reynolds, P. J. *Monte Carlo Methods in Ab Initio Quantum Chemistry*; World Scientific, 1994.
- (28) Walden, P. Molecular Weights and Electrical Conductivity of Several Fused Salts. *Bull. Acad. Imper. Sci. (St. Petersburg)* **1914**, *8*, 405–422.
- (29) S. Wilkes, J.; J. Zaworotko, M. Air and Water Stable 1-Ethyl-3-Methylimidazolium Based Ionic Liquids. *J. Chem. Soc. Chem. Comm.* **1992**, *0* (13), 965–967. <https://doi.org/10.1039/C39920000965>.
- (30) Maase, M.; Massonne, K. Biphasic Acid Scavenging Utilizing Ionic Liquids: The First Commercial Process with Ionic Liquids. In *Ionic Liquids IIIB: Fundamentals, Progress, Challenges, and Opportunities*; ACS Symposium Series; American Chemical Society, 2005; Vol. 902, pp 126–132. <https://doi.org/10.1021/bk-2005-0902.ch010>.
- (31) Chauvin, Y.; Hirschauer, A.; Olivier, H. Alkylation of Isobutane with 2-Butene Using 1-Butyl-3-Methylimidazolium Chloride—Aluminium Chloride Molten Salts as Catalysts. *J. Mol. Catal.* **1994**, *92* (2), 155–165. [https://doi.org/10.1016/0304-5102\(94\)00065-4](https://doi.org/10.1016/0304-5102(94)00065-4).
- (32) Rogers, R. D.; Seddon, K. R.; Volkov, S. *Green Industrial Applications of Ionic Liquids*; Nato Science Series II; Springer Netherlands, 2012.

- (33) V. Plechkova, N.; R. Seddon, K. Applications of Ionic Liquids in the Chemical Industry. *Chem. Soc. Rev.* **2008**, *37* (1), 123–150. <https://doi.org/10.1039/B006677J>.
- (34) Wylie, L.; Oyaizu, K.; Karton, A.; Yoshizawa-Fujita, M.; Izgorodina, E. I. Toward Improved Performance of All-Organic Nitroxide Radical Batteries with Ionic Liquids: A Theoretical Perspective. *ACS Sustainable Chem. Eng.* **2019**, *7* (5), 5367–5375. <https://doi.org/10.1021/acssuschemeng.8b06393>.
- (35) D. Smith, G.; Borodin, O.; Li, L.; Kim, H.; Liu, Q.; E. Bara, J.; L. Gin, D.; Nobel, R. A Comparison of Ether - and Alkyl-Derivatized Imidazolium-Based Room-Temperature Ionic Liquids : A Molecular Dynamics Simulation Study. *Phys. Chem. Chem. Phys.* **2008**, *10* (41), 6301–6312. <https://doi.org/10.1039/B808303G>.
- (36) Kobrak, M. N. Characterization of the Solvation Dynamics of an Ionic Liquid via Molecular Dynamics Simulation. *J. Chem. Phys.* **2006**, *125* (6), 064502. <https://doi.org/10.1063/1.2227026>.
- (37) Kowsari, M. H.; Alavi, S.; Ashrafizaadeh, M.; Najafi, B. Molecular Dynamics Simulation of Imidazolium-Based Ionic Liquids. I. Dynamics and Diffusion Coefficient. *J. Chem. Phys.* **2008**, *129* (22), 224508. <https://doi.org/10.1063/1.3035978>.
- (38) Jiang, W.; Wang, Y.; Voth, G. A. Molecular Dynamics Simulation of Nanostructural Organization in Ionic Liquid/Water Mixtures. *J. Phys. Chem. B* **2007**, *111* (18), 4812–4818. <https://doi.org/10.1021/jp067142l>.
- (39) Znamenskiy, V.; Kobrak, M. N. Molecular Dynamics Study of Polarity in Room-Temperature Ionic Liquids. *J. Phys. Chem. B* **2004**, *108* (3), 1072–1079. <https://doi.org/10.1021/jp035891m>.
- (40) Liu, H.; Maginn, E.; Visser, A. E.; Bridges, N. J.; Fox, E. B. Thermal and Transport Properties of Six Ionic Liquids: An Experimental and Molecular Dynamics Study. *Ind. Eng. Chem. Res.* **2012**, *51* (21), 7242–7254. <https://doi.org/10.1021/ie300222a>.
- (41) Rey-Castro, C.; Vega, L. F. Transport Properties of the Ionic Liquid 1-Ethyl-3-Methylimidazolium Chloride from Equilibrium Molecular Dynamics Simulation. The Effect of Temperature. *J. Phys. Chem. B* **2006**, *110* (29), 14426–14435. <https://doi.org/10.1021/jp062885s>.
- (42) Wang, Y.; Jiang, W.; Yan, T.; Voth, G. A. Understanding Ionic Liquids through Atomistic and Coarse-Grained Molecular Dynamics Simulations. *Acc. Chem. Res.* **2007**, *40* (11), 1193–1199. <https://doi.org/10.1021/ar700160p>.

- (43) Maginn, E. J. Molecular Simulation of Ionic Liquids: Current Status and Future Opportunities. *J. Phys.: Condens. Matter* **2009**, *21* (37), 373101. <https://doi.org/10.1088/0953-8984/21/37/373101>.
- (44) Varela, L. M.; Méndez-Morales, T.; Carrete, J.; Gómez-González, V.; Docampo-Álvarez, B.; Gallego, L. J.; Cabeza, O.; Russina, O. Solvation of Molecular Cosolvents and Inorganic Salts in Ionic Liquids: A Review of Molecular Dynamics Simulations. *J. Mol. Liq.* **2015**, *210*, 178–188. <https://doi.org/10.1016/j.molliq.2015.06.036>.
- (45) Zhao, W.; Leroy, F.; Heggen, B.; Zahn, S.; Kirchner, B.; Balasubramanian, S.; Müller-Plathe, F. Are There Stable Ion-Pairs in Room-Temperature Ionic Liquids? Molecular Dynamics Simulations of 1-n-Butyl-3-Methylimidazolium Hexafluorophosphate. *J. Am. Chem. Soc.* **2009**, *131* (43), 15825–15833. <https://doi.org/10.1021/ja906337p>.
- (46) Dong, K.; Zhang, S.; Wang, Q. A New Class of Ion-Ion Interaction: Z-Bond. *Sci. China Chem.* **2015**, *58* (3), 495–500. <https://doi.org/10.1007/s11426-014-5147-2>.
- (47) Fedorova, I. V.; Safonova, L. P. Ab Initio Investigation of the Interionic Interactions in Triethylammonium-Based Protic Ionic Liquids: The Role of Anions in the Formation of Ion Pair and Hydrogen Bonded Structure. *J. Phys. Chem. A* **2019**, *123* (1), 293–300. <https://doi.org/10.1021/acs.jpca.8b10906>.
- (48) Dong, K.; Zhang, S. Hydrogen Bonds: A Structural Insight into Ionic Liquids. *Chem. Eur. J.* **2012**, *18* (10), 2748–2761. <https://doi.org/10.1002/chem.201101645>.
- (49) Hunt, P. A.; Gould, I. R. Structural Characterization of the 1-Butyl-3-Methylimidazolium Chloride Ion Pair Using Ab Initio Methods. *J. Phys. Chem. A* **2006**, *110* (6), 2269–2282. <https://doi.org/10.1021/jp0547865>.
- (50) Hunt, P. A.; Gould, I. R.; Kirchner, B. The Structure of Imidazolium-Based Ionic Liquids: Insights From Ion-Pair Interactions. *Aust. J. Chem.* **2007**, *60* (1), 9. <https://doi.org/10.1071/CH06301>.
- (51) Dong, K.; Song, Y.; Liu, X.; Cheng, W.; Yao, X.; Zhang, S. Understanding Structures and Hydrogen Bonds of Ionic Liquids at the Electronic Level. *J. Phys. Chem. B* **2012**, *116* (3), 1007–1017. <https://doi.org/10.1021/jp205435u>.
- (52) Turner, E. A.; Pye, C. C.; Singer, R. D. Use of *Ab Initio* Calculations toward the Rational Design of Room Temperature Ionic Liquids. *J. Phys. Chem. A* **2003**, *107* (13), 2277–2288. <https://doi.org/10.1021/jp021694w>.
- (53) I. Izgorodina, E.; Rigby, J.; R. MacFarlane, D. Large-Scale *Ab Initio* Calculations of Archetypical Ionic Liquids. *Chem. Commun.* **2012**, *48* (10), 1493–1495. <https://doi.org/10.1039/C1CC15056A>.

- (54) Rigby, J.; Barrera Acevedo, S.; Izgorodina, E. I. Novel SCS-IL-MP2 and SOS-IL-MP2 Methods for Accurate Energetics of Large-Scale Ionic Liquid Clusters. *J. Chem. Theory Comput.* **2015**, *11* (8), 3610–3616. <https://doi.org/10.1021/acs.jctc.5b00551>.
- (55) Halat, P.; Seeger, Z. L.; Barrera Acevedo, S.; Izgorodina, E. I. Trends in Two- and Three-Body Effects in Multiscale Clusters of Ionic Liquids. *J. Phys. Chem. B* **2017**, *121* (3), 577–588. <https://doi.org/10.1021/acs.jpcc.6b10101>.
- (56) Izgorodina, E. I.; Golze, D.; Maganti, R.; Armel, V.; Taige, M.; Schubert, T. J. S.; MacFarlane, D. R. Importance of Dispersion Forces for Prediction of Thermodynamic and Transport Properties of Some Common Ionic Liquids. *Phys. Chem. Chem. Phys.* **2014**, *16* (16), 7209–7221. <https://doi.org/10.1039/C3CP53035C>.
- (57) Seeger, Z. L.; Kobayashi, R.; Izgorodina, E. I. Cluster Approach to the Prediction of Thermodynamic and Transport Properties of Ionic Liquids. *J. Chem. Phys.* **2018**, *148* (19), 193832. <https://doi.org/10.1063/1.5009791>.
- (58) Kirchner, B.; Hollóczki, O.; Canongia Lopes, J. N.; Pádua, A. A. H. Multiresolution Calculation of Ionic Liquids. *Wiley Interdiscip. Rev. Comput. Mol. Sci.* **2015**, *5* (2), 202–214. <https://doi.org/10.1002/wcms.1212>.
- (59) Izgorodina, E. I.; Seeger, Z. L.; Scarborough, D. L. A.; Tan, S. Y. S. Quantum Chemical Methods for the Prediction of Energetic, Physical, and Spectroscopic Properties of Ionic Liquids. *Chem. Rev.* **2017**, *117* (10), 6696–6754. <https://doi.org/10.1021/acs.chemrev.6b00528>.
- (60) Yan, T.; Burnham, C. J.; Del Pópolo, M. G.; Voth, G. A. Molecular Dynamics Simulation of Ionic Liquids: The Effect of Electronic Polarizability. *J. Phys. Chem. B* **2004**, *108* (32), 11877–11881. <https://doi.org/10.1021/jp047619y>.
- (61) Borodin, O. Polarizable Force Field Development and Molecular Dynamics Simulations of Ionic Liquids. *J. Phys. Chem. B* **2009**, *113* (33), 11463–11478. <https://doi.org/10.1021/jp905220k>.
- (62) Pádua, A. A. H. Resolving Dispersion and Induction Components for Polarizable Molecular Simulations of Ionic Liquids. *J. Chem. Phys.* **2017**, *146* (20), 204501. <https://doi.org/10.1063/1.4983687>.
- (63) Goloviznina, K.; Canongia Lopes, J. N.; Costa Gomes, M.; Pádua, A. A. H. Transferable, Polarizable Force Field for Ionic Liquids. *J. Chem. Theory Comput.* **2019**, *15* (11), 5858–5871. <https://doi.org/10.1021/acs.jctc.9b00689>.

- (64) Rigby, J.; Izgorodina, E. I. New SCS- and SOS-MP2 Coefficients Fitted to Semi-Coulombic Systems. *J. Chem. Theory Comput.* **2014**, *10* (8), 3111–3122. <https://doi.org/10.1021/ct500309x>.
- (65) Canongia Lopes, J. N.; Deschamps, J.; Pádua, A. A. H. Modeling Ionic Liquids Using a Systematic All-Atom Force Field. *J. Phys. Chem. B* **2004**, *108* (6), 2038–2047. <https://doi.org/10.1021/jp0362133>.
- (66) Canongia Lopes, J. N.; Pádua, A. A. H. Molecular Force Field for Ionic Liquids Composed of Triflate or Bistriflylimide Anions. *J. Phys. Chem. B* **2004**, *108* (43), 16893–16898. <https://doi.org/10.1021/jp0476545>.
- (67) Plimpton, S. Fast Parallel Algorithms for Short-Range Molecular Dynamics. *J. Chem. Phys.* **1995**, *117*, 1–19.
- (68) Schröder, C. Comparing Reduced Partial Charge Models with Polarizable Simulations of Ionic Liquids. *Phys. Chem. Chem. Phys.* **2012**, *14* (9), 3089–3102. <https://doi.org/10.1039/C2CP23329K>.
- (69) Kaufman, L.; Rousseeuw, P. J. *Finding Groups in Data: An Introduction to Cluster Analysis*; John Wiley & Sons, 2009.
- (70) Jolliffe, I. T. Principal Components in Regression Analysis. In *Principal Component Analysis*; Jolliffe, I. T., Ed.; Springer Series in Statistics; Springer: New York, NY, 1986; pp 129–155. https://doi.org/10.1007/978-1-4757-1904-8_8.
- (71) Pedregosa, F.; Varoquaux, G.; Gramfort, A.; Michel, V.; Thirion, B.; Grisel, O.; Blondel, M.; Prettenhofer, P.; Weiss, R.; Dubourg, V.; Vanderplas, J.; Passos, A.; Cournapeau, D.; Brucher, M.; Perrot, M.; Duchesnay, E. Scikit-Learn: Machine Learning in Python. *J. Mach. Learn. Res.* **2011**, *12*, 2825–2830.
- (72) Fedorov, D. G.; Olson, R. M.; Kitaura, K.; Gordon, M. S.; Koseki, S. A New Hierarchical Parallelization Scheme: Generalized Distributed Data Interface (GDDI), and an Application to the Fragment Molecular Orbital Method (FMO). *J. Comput. Chem.* **2004**, *25* (6), 872–880. <https://doi.org/10.1002/jcc.20018>.
- (73) Fedorov, D. G.; Kitaura, K. Second Order Møller-Plesset Perturbation Theory Based upon the Fragment Molecular Orbital Method. *J. Chem. Phys.* **2004**, *121* (6), 2483–2490. <https://doi.org/10.1063/1.1769362>.
- (74) Fedorov, D. G.; Kitaura, K. The Importance of Three-Body Terms in the Fragment Molecular Orbital Method. *J. Chem. Phys.* **2004**, *120* (15), 6832–6840. <https://doi.org/10.1063/1.1687334>.

- (75) Tan, S.; Barrera Acevedo, S.; Izgorodina, E. I. Generalized Spin-Ratio Scaled MP2 Method for Accurate Prediction of Intermolecular Interactions for Neutral and Ionic Species. *J. Chem. Phys.* **2017**, *146* (6), 064108. <https://doi.org/10.1063/1.4975326>.
- (76) S. Tan, S. Y.; Wylie, L.; Begic, I.; Tran, D.; I. Izgorodina, E. Application of Spin-Ratio Scaled MP2 for the Prediction of Intermolecular Interactions in Chemical Systems. *Phys. Chem. Chem. Phys.* **2017**, *19* (42), 28936–28942. <https://doi.org/10.1039/C7CP04391K>.
- (77) Gordon, M. S.; Schmidt, M. W. Chapter 41 - Advances in Electronic Structure Theory: GAMESS a Decade Later. In *Theory and Applications of Computational Chemistry*; Dykstra, C. E., Frenking, G., Kim, K. S., Scuseria, G. E., Eds.; Elsevier: Amsterdam, 2005; pp 1167–1189. <https://doi.org/10.1016/B978-044451719-7/50084-6>.
- (78) Adebahr, J.; Seeber, A. J.; MacFarlane, D. R.; Forsyth, M. Thermal Analysis, Nuclear Magnetic Resonance Spectroscopy, and Impedance Spectroscopy of N,N-Dimethyl-Pyrrolidinium Iodide: An Ionic Solid Exhibiting Rotator Phases. *J. Appl. Phys.* **2005**, *97* (9), 093904. <https://doi.org/10.1063/1.1889245>.
- (79) Adebahr, J.; Grimsley, M.; Rocher, N. M.; MacFarlane, D. R.; Forsyth, M. Rotational and Translational Mobility of a Highly Plastic Salt: Dimethylpyrrolidinium Thiocyanate. *Solid State Ion.* **2008**, *178* (35), 1798–1803. <https://doi.org/10.1016/j.ssi.2007.12.017>.
- (80) Izgorodina, E. I.; MacFarlane, D. R. Nature of Hydrogen Bonding in Charged Hydrogen-Bonded Complexes and Imidazolium-Based Ionic Liquids. *J. Phys. Chem. B* **2011**, *115* (49), 14659–14667. <https://doi.org/10.1021/jp208150b>.
- (81) Fumino, K.; Wulf, A.; Ludwig, R. Strong, Localized, and Directional Hydrogen Bonds Fluidize Ionic Liquids. *Angew. Chem. Int. Ed.* **2008**, *47* (45), 8731–8734. <https://doi.org/10.1002/anie.200803446>.
- (82) Fumino, K.; Peppel, T.; Geppert-Rybczyńska, M.; H. Zaitsau, D.; K. Lehmann, J.; P. Verevkin, S.; Köckerling, M.; Ludwig, R. The Influence of Hydrogen Bonding on the Physical Properties of Ionic Liquids. *Phys. Chem. Chem. Phys.* **2011**, *13* (31), 14064–14075. <https://doi.org/10.1039/C1CP20732F>.
- (83) Zahn, S.; Bruns, G.; Thar, J.; Kirchner, B. What Keeps Ionic Liquids in Flow? *Phys. Chem. Chem. Phys.* **2008**, *10* (46), 6921–6924. <https://doi.org/10.1039/B814962N>.
- (84) Hunt, P. A. Why Does a Reduction in Hydrogen Bonding Lead to an Increase in Viscosity for the 1-Butyl-2,3-Dimethyl-Imidazolium-Based Ionic Liquids? *J. Phys. Chem. B* **2007**, *111* (18), 4844–4853. <https://doi.org/10.1021/jp067182p>.

- (85) P. Matthews, R.; Welton, T.; A. Hunt, P. Competitive Pi Interactions and Hydrogen Bonding within Imidazolium Ionic Liquids. *Phys. Chem. Chem. Phys.* **2014**, *16* (7), 3238–3253. <https://doi.org/10.1039/C3CP54672A>.
- (86) Zahn, S.; Uhlig, F.; Thar, J.; Spickermann, C.; Kirchner, B. Intermolecular Forces in an Ionic Liquid ([Mmim][Cl]) versus Those in a Typical Salt (NaCl). *Angew. Chem. Int. Ed.* **2008**, *47* (19), 3639–3641. <https://doi.org/10.1002/anie.200705526>.
- (87) Shimizu, K.; Tariq, M.; Gomes, M. F. C.; Rebelo, L. P. N.; Lopes, J. N. C. Assessing the Dispersive and Electrostatic Components of the Cohesive Energy of Ionic Liquids Using Molecular Dynamics Simulations and Molar Refraction Data. *J. Phys. Chem. B* **2010**, *114* (17), 5831–5834. <https://doi.org/10.1021/jp101910c>.

5.3 References

- [1] Stefan Goedecker. Minima Hopping: An Efficient Search Method for the Global Minimum of the Potential Energy Surface of Complex Molecular Systems. *The Journal of Chemical Physics* **120**(21) (2004), 9911–9917. DOI: [10.1063/1.1724816](https://doi.org/10.1063/1.1724816).
- [2] Uditha L. Bernard, Ekaterina I. Izgorodina, and Douglas R. MacFarlane. New Insights into the Relationship between Ion-Pair Binding Energy and Thermodynamic and Transport Properties of Ionic Liquids. *The Journal of Physical Chemistry C* **114**(48) (2010), 20472–20478. DOI: [10.1021/jp1048875](https://doi.org/10.1021/jp1048875).
- [3] Ekaterina I. Izgorodina, Dorothea Golze, Radha Maganti, Vanessa Armel, Maria Taige, Thomas J. S. Schubert, and Douglas R. MacFarlane. Importance of Dispersion Forces for Prediction of Thermodynamic and Transport Properties of Some Common Ionic Liquids. *Physical Chemistry Chemical Physics* **16**(16) (2014), 7209–7221. DOI: [10.1039/C3CP53035C](https://doi.org/10.1039/C3CP53035C).
- [4] Josefina Adebahr, Aaron J. Seeber, Douglas R. MacFarlane, and Maria Forsyth. Thermal Analysis, Nuclear Magnetic Resonance Spectroscopy, and Impedance Spectroscopy of N,N-Dimethyl-Pyrrolidinium Iodide: An Ionic Solid Exhibiting Rotator Phases. *Journal of Applied Physics* **97**(9) (2005), 093904. DOI: [10.1063/1.1889245](https://doi.org/10.1063/1.1889245).
- [5] J. Adebahr, M. Grimsley, N. M. Rocher, D. R. MacFarlane, and M. Forsyth. Rotational and Translational Mobility of a Highly Plastic Salt: Dimethylpyrrolidinium Thiocyanate. *Solid State Ionics* **178**(35) (2008), 1798–1803. DOI: [10.1016/j.ssi.2007.12.017](https://doi.org/10.1016/j.ssi.2007.12.017).

Chapter 6

Use of a cluster approach for the prediction of thermodynamic and transport properties

6.1 Introduction

The targeted design of ionic liquids would soon earn the promising materials widespread use, as their potential applications seem endless.¹ To this end, the prediction of physicochemical properties through the descriptions of electronic structure, rather than by synthetic trial and error, seems to be the most effective means. Although there is no doubt that macroscopic properties are a result of the subtle interplay of forces present at the atomic level, the exact nature of their relationship is unknown and it is currently impossible to extrapolate meaningful thermodynamic and transport properties from small calculations.² Larger calculations with density functional theory and classical methods also struggle with prediction as the lack of detail in the molecular description leads to compounding errors within larger clusters. This is especially true for systems with strong intermolecular dispersion forces like those present in ionic liquids.^{3–5}

Previous work has shown that the ratio of total interaction energy to dispersion interaction energy correlates with melting point for each of the $C_n\text{mim}^+$ and $C_n\text{mpyr}^+$ cationic series

with a particular anion in ion pairs.^{6,7} A trend between dispersion interaction energy and viscosity was also shown. The research within this chapter extends this study into two ion pairs which accounts for same-ion interactions and therefore changes the magnitudes of forces present. The publication presented in section 6.2, published in *The Journal of Chemical Physics*, details a full geometry screen of twenty-four two ion pair ionic liquids resulting in sixty-four unique, energetically favourable geometries. Each geometry is of sufficiently low energy with respect to the global minimum to be present in the liquid form and thus contribute to the macroscopic properties of the material. From these systems, correlations between interaction energy components and melting point and conductivity were made.

It was seen that while interaction energy doubled from one ion pair to two, dispersion increased three fold and the amount of dispersion present is predominantly dependent on the anion. While melting point trends in one ion pair showed separate trends for the anions tested with each cationic series, the trends in two ion pairs converged such that a general trend was made by the majority of ionic liquids. These trends are expected to improve with larger clusters.



Cluster approach to the prediction of thermodynamic and transport properties of ionic liquids

Zoe L. Seeger,¹ Rika Kobayashi,² and Ekaterina I. Izgorodina^{1,a)}

¹*School of Chemistry, Monash University, 17 Rainforest Walk, Clayton, VIC 3800, Australia*

²*Australian National University, Leonard Huxley Building 56, Mills Road, Canberra, ACT 2601, Australia*

(Received 20 October 2017; accepted 5 February 2018; published online 28 February 2018)

The prediction of physicochemical properties of ionic liquids such as conductivity and melting point would substantially aid the targeted design of ionic liquids for specific applications ranging from solvents for extraction of valuable chemicals to biowaste to electrolytes in alternative energy devices. The previously published study connecting the interaction energies of single ion pairs (1 IP) of ionic liquids to their thermodynamic and transport properties has been extended to larger systems consisting of two ion pairs (2 IPs), in which many-body and same-ion interactions are included. Routinely used cations, of the imidazolium and pyrrolidinium families, were selected in the study coupled with chloride, tetrafluoroborate, and dicyanamide. Their two ion pair clusters were subjected to extensive configuration screening to establish most stable structures. Interaction energies of these clusters were calculated at the spin-ratio scaled MP2 (SRS-MP2) level for the correlation interaction energy, and a newly developed scaled Hartree-Fock method for the rest of energetic contributions to interaction energy. A full geometry screening for each cation-anion combination resulted in 192 unique structures, whose stability was assessed using two criteria—widely used interaction energy and total electronic energy. Furthermore, the ratio of interaction energy to its dispersion component was correlated with experimentally observed melting points in 64 energetically favourable structures. These systems were also used to test the correlation of the dispersion contribution to interaction energy with measured conductivity. *Published by AIP Publishing.* <https://doi.org/10.1063/1.5009791>

INTRODUCTION

The prediction of physicochemical properties of condensed systems such as ionic liquids from first principles represents a holy grail of theoretical chemistry. Ionic liquids have emerged as promising and superior alternatives to currently used electrolytes in electrochemical devices and solvents for a myriad of applications from CO₂ capture to extraction of natural products from biowaste.^{1–11} Ideally, *ab initio* molecular dynamics simulations must be used for the accurate prediction of thermodynamic and transport properties of condensed materials as these allow for the inclusion of not only enthalpic but also entropic effects. To date, these types of simulations are limited to approximately 100 ps for medium-sized simulation boxes of ionic liquids, not long enough to achieve statistically sound accuracy for individual ion trajectories and hence the calculation of bulk transport properties such as conductivity and viscosity.^{12,13} Classical and polarisable force fields have offered a tremendous capability for studying condensed systems as these allow for significantly longer simulations at the cost of reduced accuracy for bulk properties.^{12,14–27} In addition, these force fields do not allow us to study reactivity of ionic liquids as they cannot be used to break bonds. Due to a complex interplay of intermolecular forces in the bulk of ionic liquids, the predictive power of these force fields for

ionic liquids has not reached its full potential as force fields are continuing to be further improved.

Static quantum chemical calculations of single ion pairs have been used as a simple model to predict physicochemical properties of ionic liquids with varying success.¹³ Recently, our group has shown how the combination of the second law of thermodynamics and interaction energies of single ion pairs (1 IP) may be used to understand the behaviour of melting points of ionic liquids.²⁸ It was established that the ratio of interaction energy to its dispersion component could be correlated with melting point (T_m) for a range of *N*-methyl-*N*-alkylpyrrolidinium- and *N*-methyl-*N*-alkylimidazolium-based ionic liquids as shown in Eq. (1). Additionally, the dispersion component of the interaction energy in these systems was shown to correlate well with conductivity,^{28,29}

$$T_m = f \left(\frac{E_{INT}}{E_{INT}^{disp}} \right). \quad (1)$$

However, the single ion pair model does not account for many-body effects found to be far from negligible in ionic liquids.^{13,30} These effects are shown to increase not only with increasing alkyl chain on the cation^{31–33} but also due to the bulky nature of ionic liquid ions.³⁰ This finding suggests that larger-scale clusters are necessary in order to accurately account for intermolecular forces observed in the bulk of ionic liquids.

In addition to molecular dynamics and single ion models, the quantitative structure–property relationship (QSPR) approach, Volume-Based Thermodynamics (VBT), and

^{a)}Author to whom correspondence should be addressed: katya.pas@monash.edu

conductor like screening model for real solvents (COSMO-RS) have been employed in relating the ionic liquids' electronic structure to their thermodynamic and transport properties. QSPR,^{34–36} VBT,^{37,38} and COSMO-RS^{39,40} have accurately predicted physicochemical properties based on *ab initio* calculations of single ion pairs and parametrization of the underlying formulation for different ionic liquid types. The required parametrization results from the omission of many-body effects, thus affecting the transferability of these techniques to novel systems.¹³ An example of this was explained in a review by Valderrama,³⁶ which stated that QSPR models in the literature give melting points to within 25 K in the best case and 102 K in the worst case. Improved predictions are possible with the sacrifice of narrowing down the type of species present in the training set and thus limiting the ionic liquids for which the model can be applied. A satisfactory balance between accuracy and transferability has not been found. Relatively few publications have attempted to use VBT to predict melting point as it has similar shortcomings as QSPR. Gutowski⁴¹ used this method instead for the prediction of lattice enthalpies and it was found that average errors of less than 15 kJ mol⁻¹ were achieved only when extra parametrisation was applied for each ionic liquid family. The result reflects the disregard of dispersion interactions which are not correlated with an ion pair's volume. COSMO-RS has also been applied to the prediction of thermodynamic and transport properties. The Krossing group⁴² has applied a least-squares regression to a large database of molecules reporting an average error of 36 K, later including added parametrisation for the ring interaction enthalpy and van der Waals interaction enthalpy, which only slightly decreased the average error and reduced the maximum error from 116 K to 89 K. The outliers suggest that the relationship does not viably connect the descriptors to the melting point. This is observed again when conductivity is considered.⁴³

A cluster approach originally proposed by Ludwig has been used to predict thermodynamic properties (i.e., entropy, enthalpy of vaporization) of water and ionic liquids using minimum energy structures of up to 14 ion pairs.^{44–47} For [C₁mim][SCN], binding energies per ion pair converged in the clusters of 10 IPs highlighting the importance of many-body effects over a long range.⁴⁶ The approach was also used to correlate RHF/3-21G binding energies and experimental melting points of imidazolium-based NTf₂⁻ ionic liquids and would need to be tested with correlated levels of theory.^{48,49} Weinhold developed the quantum cluster equilibrium (QCE) methodology that requires a series of increasing cluster sizes to extract partition functions and hence the Gibbs free energy and other thermodynamic properties.^{50,51} Ludwig and Weinhold used the QCE methodology to treat clusters of small neutral species such as methanol, ammonia, and water.^{52–59} The Kirchner group has recently showed that the level of theory is extremely important in the treatment of hydrogen bonding.^{60–62} Overall, the cluster approach has been rather successful in extracting thermodynamic and spectroscopic properties of ionic liquids.^{63–67}

However, the direct correlation of physicochemical properties with cluster energies has not yielded interpretable relationships. This is partly due to the difficulty in predicting the

crystal structure which governs the physicochemical properties of the materials and is best modeled by periodic structures. However, the size of these periodic structures needs to vary depending on the property being calculated to ensure meaningful prediction. To find energies of these large systems with theories able to accurately represent dispersion is challenging. Correlations of single ion pair structures were attempted with transport and thermodynamic (such as melting point) properties in the past and it was shown that their energies do not represent the bulk properties of the ionic liquid.^{28,68,69} Recently, many-body effects have been shown to be significant in large clusters of ionic clusters.^{28,70,71} Therefore, it has become clear that in order to reliably predict physicochemical properties of ionic liquids, large scale systems, those of many ion pairs, must be used. To date, the only spectroscopic properties have been successfully determined.^{63–67}

Muller-Dethlefs and Hobza⁷² published a review that highlighted the importance of interaction energy in describing condensed systems. While interaction energy is magnitudes smaller than the covalent interactions, these noncovalent interactions control dynamics of clustered systems and are made up of electrostatics, induction, dispersion, and exchange-repulsion. While many quantum methods deal with electrostatics quite well, to accurately reproduce physicochemical properties dispersion must be properly accounted for. Furthermore, the non-additive components, induction and exchange-repulsion, need to be considered in larger clusters to mimic the forces in the bulk. Since large clusters are dominated by cumulative causal motion, an equilibrium structure is not truly representative of the system and thereby minima of the potential energy surface are better found by minimising the Gibbs free energy. In practice, interaction energy is commonly used as the criterion to determine the most stable structure. The interaction energy is an artefact and is widely used in large-scale calculations due to the simplicity of the calculation. Interaction energy is not observable by experiment and lacks important contributions such as deformation energy associated with the energy penalty due to the changes in geometry of interacting molecules/ions, zero-point vibrational energy, entropic contribution, and temperature correction. Interaction energy is an excellent quantity to benchmark quantum chemical methods. It might not be as reliable as in determining the most stable structure. To determine realistic minima on the potential energy surfaces, free energy that includes the aforementioned contributions is preferred. This can also be achieved by analysing a series of non-equilibrium geometries on the potential energy surface.⁷³

It is well known that single ion pairs do not accurately represent the interactions in an ionic liquid.^{68,70,74–77} The importance of many-body effects, induction and dispersion, is magnified by the additional ion pairs and therefore clusters must be considered to extract correct ionic liquid properties. Therefore, an extensive study of 2 ion-paired clusters of 24 ionic liquids of imidazolium and pyrrolidinium families has been conducted to investigate: whether total energy and interaction energy can be reliably used as criteria for finding thermodynamically stable geometries, the correlation of melting point with the fundamental energetic components of interaction energy, and the correlation of the dispersion component

to interaction energy with conductivity. The last two points are then compared to the study of ion pair systems²⁸ to tease out the effect of including the same ion interactions to the energy components. There is also a description of a scaled Hartree-Fock method to produce accurate HF interaction energies of many ion-paired clusters of ionic liquids at a small basis set.

THEORETICAL PROCEDURES

All geometry optimisations were performed with the Fragment Molecular Orbital (FMO) approach^{78,79} accounting for the two-body correction (i.e., FMO2) coupled with the recently developed spin-ratio scaled second-order Møller-Plesset perturbation method (SRS-MP2) which was designed to achieve high accuracy for interaction energies in multi-scale clusters of ionic liquids.⁸⁰ The SRS-MP2 method called a spin ratio-based scaled MP2 method is an improved version of the original spin-component scaled second-order Møller-Plesset perturbation method scaled for ionic liquids (SCS-IL-MP2) and was designed to work equally well for ionic and neutral complexes.³⁰ The advantage of the method lies in its high accuracy (maximum errors below 4 kJ mol⁻¹) and the inclusion of basis set superposition error into the scaling coefficients of the MP2 correlation energy, thus allowing for more accurate geometry optimisations of multi-scale clusters without the need for a counterpoise correction. In this work, the SRS-MP2 method was combined with Dunning's cc-pVDZ basis set for geometry optimisations and only the opposite-spin (OS) component was scaled to 1.752 to improve correlation energy (for more details, see Ref. 30). All optimized structures were subjected to single-point energy calculations using two- and three-body corrections (i.e., FMO3) coupled with the SRS-MP2 method by scaling the OS component with 1.640 and Dunning's cc-pVTZ basis set. Our group recently showed that the three-body correction was already sufficient to accurately approximate MP2 interaction energies in multi-scale clusters of ILs.⁷⁰ Non-counterpoise corrected HF interaction energies calculated at the cc-pVTZ basis set were scaled to reproduce those of HF/aug-cc-pVQZ using the recently developed scheme, which is discussed in full detail below. No cutoffs for both two-electron integrals and many-body effects were employed in the FMO calculations presented. Calculations were performed using the GAMESS-US,⁸¹ PSI4,⁸² and Gaussian09⁸³ packages of quantum chemical methods.

Deformation energies were calculated using the energy of the ion in the configuration it adopts in the cluster and subtracting the energy of the ion optimised in a vacuum, resulting in the energy that the ion uses to contort in its environment.

The mean of signed errors, called mean for simplicity (\bar{x}), the mean absolute error (MAE), the standard deviation, $SD = \sqrt{\sum_i^n (x_i - \bar{x})^2 / (N - 1)}$, of N instances where x_i is an instance, and the maximum absolute error (max) are presented for data predictions.

RESULTS AND DISCUSSION

Construction of two ion-paired clusters

Commonly used imidazolium ($C_n\text{mim}^+$) and pyrrolidinium ($C_n\text{mpyr}^+$) cations were considered with the alkyl

chain increasing from methyl to n -butyl ($n = 1-4$). Two ion-paired clusters were constructed using low energy configurations of single ion pairs coupled with chloride, tetrafluoroborate, and dicyanamide ($N(\text{CN})_2^-$) from our previous study.²⁸ 15 and 16 different types of cluster configurations were geometry optimised for the imidazolium- and pyrrolidinium-based cations, respectively (for more details, see Fig. 1). In the case of the $C_n\text{mim}^+$ cation, the imidazolium rings are considered either in a $\pi^+-\pi^+$ stacked arrangement⁸⁴ (see configurations p1, p2a, p2b, p3a, p3b, p8a, and p8b in Fig. 1) or an alternating charge arrangement (configurations p4–p7 in Fig. 1). In the case of the pyrrolidinium cation, only alternating charge structures were considered due to the absence of a delocalised π -conjugated ring. Increasing alkyl chains were also allowed to interact through van der Waals dispersion, thus leading to additional configurations for both the imidazolium cations [see configurations pna ($n = 2-8$) in Fig. 1] and the pyrrolidinium cations (see configurations p1, p2a, p2b, p3, and p9 in Fig. 1). In addition, the alkyl chains, R, were also allowed to alternate their position in configurations p1 and p4–p7 in the pyrrolidinium clusters, thus generating additional configurations analogous to pnb configurations ($n = 2-8$) in the imidazolium clusters (not shown in Fig. 1 for the sake of simplicity). Some of the initial ionic clusters optimized to the same structure. Overall, between 5 and 12 unique structures were located for the selected combinations of the cation and anion, with the total number of 194 clusters being optimized (for more details, see the [supplementary material](#)).

Lowest energy configurations of 2 ion-paired clusters

Figure 2 shows the lowest energy structures for the imidazolium and pyrrolidinium ionic liquids studied, with SRS-MP2/cc-pVTZ total electronic energies being used to determine the lower energy structures.

Analysis of Fig. 2 reveals that both the anion and the alkyl chain appear to determine the energetically preferred arrangement in ionic liquids. Further in the text, abbreviations of two ion-paired configurations are taken from Fig. 1.

For imidazolium-based clusters with the BF_4^- anion, there is an energetic preference for the alternate charge arrangement such as the p4a structure in Fig. 1, with the stacking configuration having a much higher energy by at least 21 kJ mol⁻¹ regardless of the alkyl chain length. The alternating charge arrangement, in which alkyl chains interact such as the structure p4a or the planes of the imidazolium ring are perpendicular to each other such as the p7a/b structures, becomes the second energetically preferred configuration. As seen in Fig. 2, for the $[C_n\text{mim}]\text{Cl}$ clusters, the $\pi^+-\pi^+$ stacking configuration (p2a/b and p8b) competes with the alternative arrangement (p4b) and becomes preferred by only a couple of kJ mol⁻¹. For longer alkyl chains starting with ethyl, the p7b configuration falls within 10 kJ mol⁻¹. Other optimized configurations are much higher in energy, between 20 and 40 kJ mol⁻¹. For the imidazolium-based clusters with the $N(\text{CN})_2^-$ anion, the alternating arrangement (p4a) is preferred for shorter alkyl chains such as methyl and ethyl, with the $\pi^+-\pi^+$ stacking (p2a and p2b) becoming most energetically stable for longer alkyl chains such as propyl and butyl. The alternate arrangement

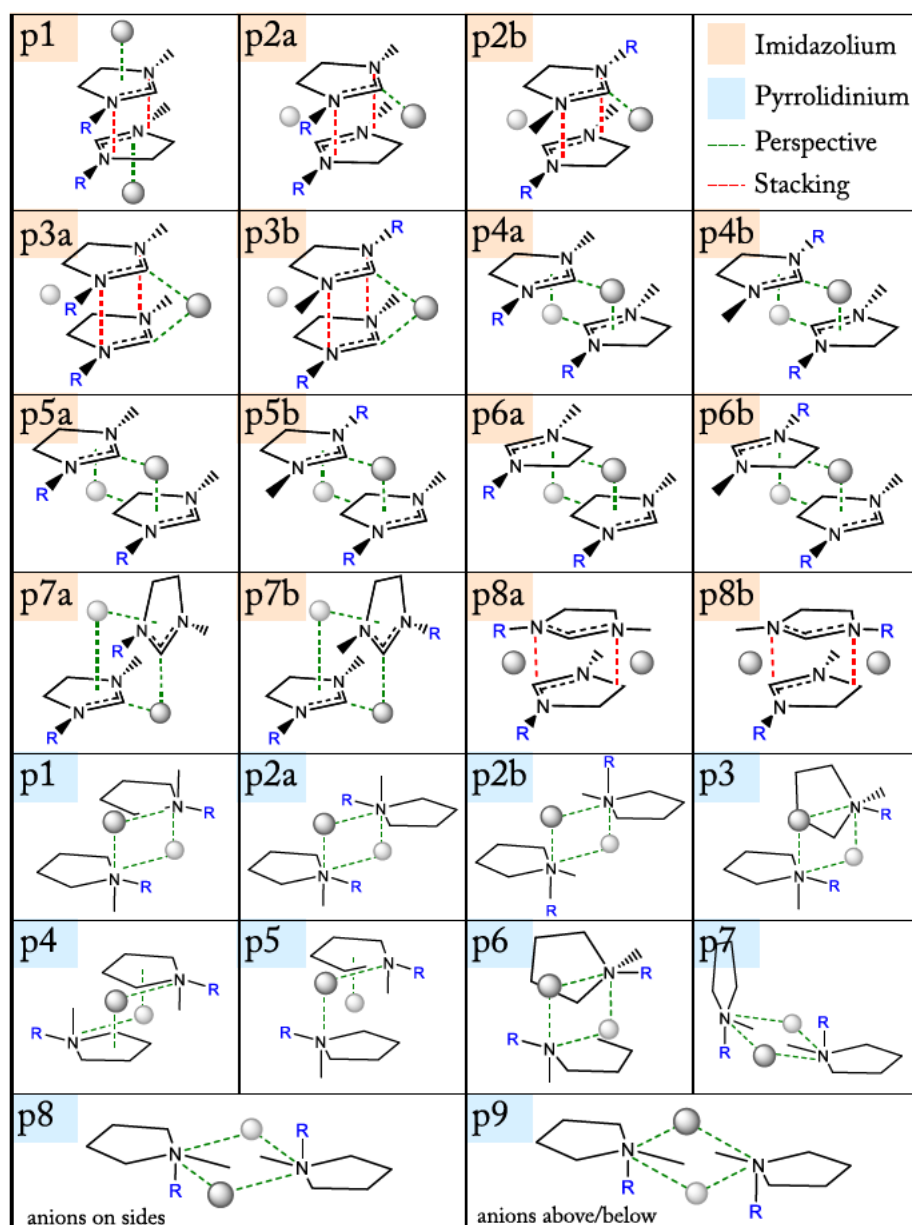


FIG. 1. Schematic of starting geometries of 2 ion-paired clusters [$X = \text{Cl}^-$, BF_4^- , and $\text{N}(\text{CN})_2^-$]. Green dashed lines show the shortest distance between the cation and anion, whereas red dashed lines indicate $\pi^+ - \pi^+$ in imidazolium-based ionic liquids.

configurations (p4a/b and p5a) are still within 10 kJ mol^{-1} . Apart from a few exceptions such as $[\text{C}_1\text{mim}]\text{X}$ ($X = \text{BF}_4^-$, Cl^- , and $\text{N}(\text{CN})_2^-$) and $[\text{C}_2\text{mim}][\text{BF}_4]$, the rest have between 3 and 6 configurations falling within 10 kJ mol^{-1} , thus giving rise to a large number of 2 ion paired configurations.

In the case of the $[\text{C}_n\text{mpyr}][\text{BF}_4]$ ionic liquids, the p2 configuration is the most stable for the methyl and ethyl substitutions on the pyrrolidinium ring and this changes to p1 for longer chains, with the alkyl chain preferring to interact with the pyrrolidinium ring. There are between 2 and 5 optimized configurations for each alkyl chain within 10 kJ mol^{-1} . For the chloride-based clusters, the situation becomes reversed, with the p1 configuration being preferred for shorter alkyl chains and p2 for longer alkyl chains. The chloride-based clusters are also unusual as there are only 2 ionic configurations falling within 10 kJ mol^{-1} of each other, with the rest of the

optimised structures having much higher energies of up to 45 kJ mol^{-1} . For the dicyanamide anion, between 4 and 7 configurations fall within 10 kJ mol^{-1} , with the only exception being $[\text{C}_3\text{mpyr}][\text{N}(\text{CN})_2]$, for which only one configuration (p3) was located in the 10 kJ mol^{-1} range. For the methyl and ethyl groups of C_3mpyr^+ , at least three configurations are within 2 kJ mol^{-1} , with the butyl chain having 3 configurations within 3 kJ mol^{-1} . The rest of the configurations have higher energies of up to 66 kJ mol^{-1} . These findings indicate that anions with multiple interaction sites, such as tetrafluoroborate and dicyanamide, tend to have a number of energetically preferred configurations on the potential energy surface, whereas chloride usually produces a small number of these configurations.

The Hunt group studied 2 ion-paired clusters of the 1,3-dimethyl-imidazolium cation coupled with the

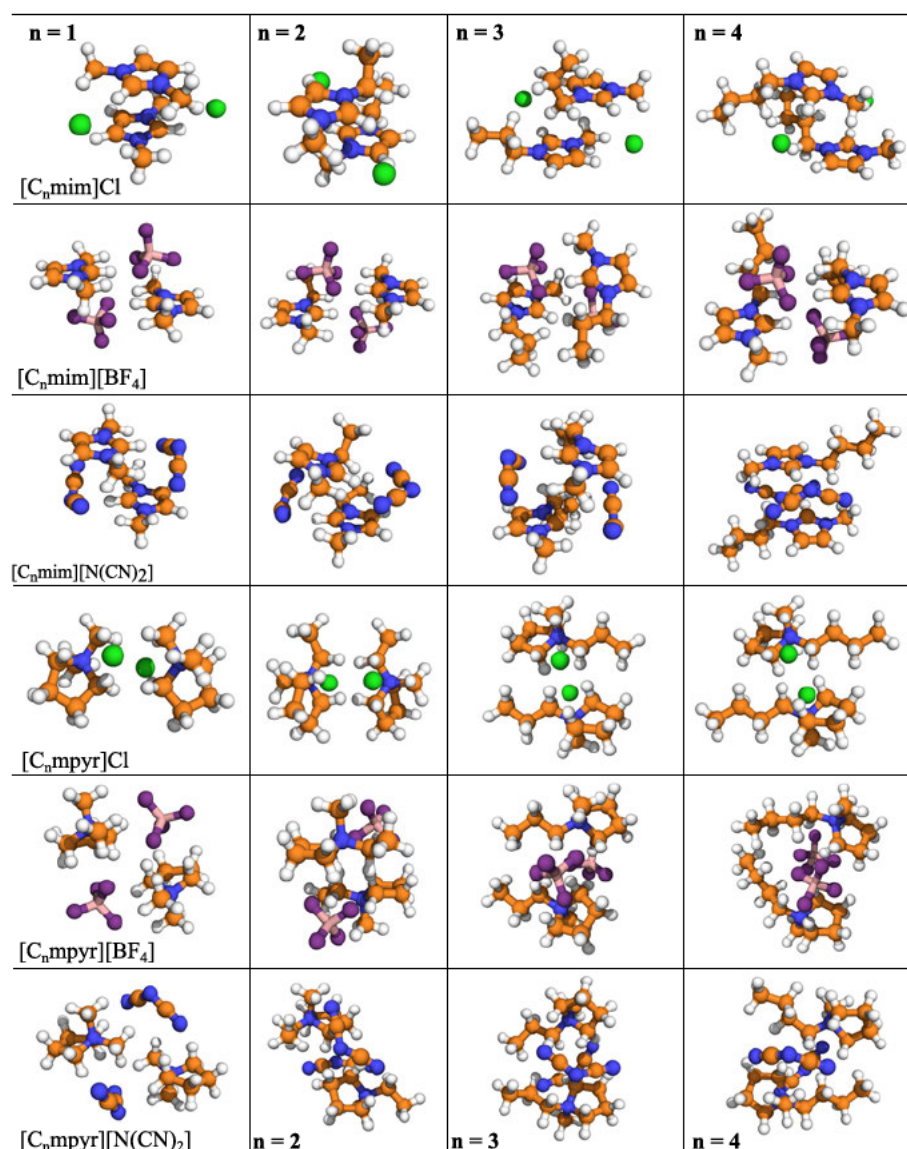


FIG. 2. Lowest energy configurations of [C_nmim]X and [C_nmpyr]X ionic liquids, where n = 1–4 and X = Cl[−], BF₄[−], and N(CN)₂[−].

tetrafluoroborates and chloride anions at the B3LYP-D3/aug-cc-pVTZ level of theory.^{85,86} D3 represents Grimme's third generation empirical correction for dispersion.^{87–89} It has been shown before that many density functional theory (DFT) functionals such as B3LYP suffer from poor description of dispersion forces.^{29,91} The inclusion of the empirical dispersion correction⁹⁰ usually results in the decrease of errors in interaction energies to 10 kJ mol^{−1}. There are obvious discrepancies between our and previously published data. In the case of [C₁mim]Cl, only two configurations were located within 10 kJ mol^{−1}, whereas as many as 6 were identified with B3LYP-D3. There is good agreement between the two most stable structures located, whereas the four additional structures located with B3LYP-D3 had electronic energies well above 18 kJ mol^{−1} in energy as calculated with SRS-MP2/cc-pVTZ. A similar situation is observed for [C₁mim][BF₄], for which only two configurations within 10 kJ mol^{−1} were located in our study, whereas 3 configurations were found with B3LYP-D3. The SRS-MP2/cc-pVTZ configurations are in good agreement

geometry-wise and relative energy-wise with the previously published data, whereas the third favourable configuration with B3LYP-D3 was found to have an energy of 26 kJ mol^{−1} higher when optimized with SRS-MP2 and was therefore discarded in our study. It has to be noted that configurations that were within 2–3 kJ mol^{−1} of the lowest energy geometry were in good agreement between the SRS-MP2 and B3LYP-D3 levels of theory. Obviously, B3LYP-D3 could locate the lowest energy configurations for [C₁mim][BF₄] and [C₁mim]Cl. It appears that B3LYP-D3 has difficulty in the prediction of energy of other configurations due to a complex interplay of fundamental forces, with the combination of the B3LYP functional and D3 correction needing to be tested further to confirm its reliability for ionic liquids. These findings highlight the importance of using a reliable and accurate level of theory even for geometry optimisations of large-scale clusters of ionic liquids.

In summary, the increasing alkyl chain length leads to a large number of energetically preferred configurations. The

availability of multiple interaction sites on the anion such as tetrafluoroborate and dicyanamide tends to also increase the number of viable configurations. There are a few exceptions to this rule. $[C_1\text{mim}]X$ ($X = \text{BF}_4$, Cl , and $\text{N}(\text{CN})_2$) and $[C_n\text{mpyr}]\text{Cl}$ ($n = 1\text{--}4$) clusters have either one or two configurations within 10 kJ mol^{-1} . The ionic arrangement in the most energetically stable configuration is strongly dependent on the cation and anion combination. It appears that a full conformational screening is required for each cation-anion combination to determine the most stable structures. This might also explain complexity in thermodynamic and transport properties that are not transferrable between each family of cations.

Interionic distances and dispersion forces in 2 ion-paired clusters

Table I presents ranges of interionic distances in the optimized 2 ion-paired clusters whose electronic energies were within 10 kJ mol^{-1} off the lowest energy configuration. The three types of interionic distances were considered—namely, cation...cation, cation...anion, and anion...anion. For each unique cation and anion, a centre atom of the ion was identified and interionic distances were measured between centres of ions. The B and N central atoms were taken as the centre of the tetrafluoroborate anion and pyrrolidinium cations, respectively. For the imidazolium cations, the middle point between the two nitrogen atoms of the imidazolium ring was assigned the centre, whereas for the dicyanamide anion the central nitrogen atom was taken as the centre. For pyrrolidinium clusters, the cation...anion distance is longer compared to that in imidazolium.

Analysis of Table I reveals that in general the lower bound of the cation...anion distance in the pyrrolidinium-based clusters is longer by at least 0.8 Å than those in imidazolium clusters. The smaller interionic distances in the imidazolium-based ILs, mainly due to the absence of steric hindrance, allows for a higher degree of dispersion forces. This trend was also observed in single ion pairs of imidazolium ionic liquids.²⁸ The presence of the $\pi^+\text{--}\pi^+$ stacking of imidazolium rings also results in shorter cation...cation distances in imidazolium ionic liquids. This is reflected in a similar trend in the anion...anion distances that are $0.7\text{--}1.1\text{ Å}$ shorter in the imidazolium salts compared to those in analogous pyrrolidinium-based ILs. Compared to the previously published optimised structures of single ion pairs of both imidazolium and pyrrolidinium cations,^{91,92} interionic distances in 2 ion-paired clusters tend

to be longer—in the range of $0.5\text{--}1\text{ Å}$ —thus affecting the interplay of fundamental forces. This observation further highlights the importance of considering large-scale clusters and non-equilibrium geometries (in which ions are further removed from the equilibrium) for drawing reliable conclusions for ionic liquids.

Scaling of HF interaction energies

The MP2 energy is comprised of the HF energy and the contribution from electron correlation. Our new method, SRS-MP2, predicts the latter very well with cc-pVTZ, a relatively small basis set.³⁰ However, the HF energy is not yet converged and requires much more expensive basis sets to give comparable errors. This section outlines a new scaling method to allow anyone to correct the HF energy to the complete basis set and was used for the cluster calculations in this work.

It is well known that HF electronic energies converge fast with an increasing basis set for single molecules. In this study, we tested the convergence for interaction energies of two ion-paired clusters. HF interaction energies of the two ion-paired configurations within 10 kJ mol^{-1} for each cation-anion combination were calculated for a series of Dunning's basis sets, non-augmented cc-pVXZ, and augmented aug-cc-pVXZ ($X = \text{D, T, and Q}$) with the view of establishing the reliability of smaller basis sets for the prediction of HF interaction energies in larger clusters. These interaction energies were calculated with and without counterpoise corrections developed by Boys and Bernardi.⁹³ Overall, 64 two ion-paired configurations were used for further analysis.

Table II shows statistical measures such as mean absolute errors (MAEs), standard deviations (SDs), and maximum absolute errors (Max) for the standard HF interaction energies given per ion pair. HF/aug-cc-pVQZ interaction energies without counterpoise correction were used as the benchmark data. Without counterpoise correction, the errors are large for the double- ζ basis sets as well as for cc-pVTZ. The maximum errors fall between 20 and 55 kJ mol^{-1} . The aug-cc-pVTZ basis set is needed to produce errors below chemical accuracy, with

TABLE II. Error statistics (in kJ mol^{-1}) for standard and scaled HF interaction energies per one ion pair with and without counterpoise corrections. Errors are per one ion pair.

CP	Basis	Standard HF			Scaled HF				
		Max	MAE	SD	α	β	Max	MAE	SD
No	VDZ	52.1	40.1	6.4	0.874	-10.913	12.6	3.9	4.7
	VTZ	20.1	14.9	3.3	0.928	-12.505	3.5	1.5	1.8
	VQZ	8.4	5.1	2.2	0.963	-8.791	2.7	1.4	1.6
	AVDZ	24.9	10.5	6.9	0.977	1.906	14.4	6.2	6.9
	AVTZ	4.0	1.9	1.3	1.004	3.468	2.0	1.2	1.2
Yes	VDZ	11.9	5.5	4.0	0.941	-16.459	5.8	2.5	3.0
	VTZ	6.2	2.6	2.6	0.967	-9.789	3.7	1.8	2.1
	VQZ	2.6	1.4	1.5	0.985	-5.087	2.0	1.3	1.4
	AVDZ	1.7	0.9	0.4	1.002	-0.088	0.8	0.3	0.4
	AVTZ	1.5	0.7	0.4	0.999	1.010	0.8	0.4	0.4

TABLE I. Interionic distances (in Å) in two ion-paired clusters of $[C_n\text{mim}]X$ and $[C_n\text{mpyr}]X$ ionic liquids [$n = 1\text{--}4$ and $X = \text{Cl}^-$, BF_4^- , and $\text{N}(\text{CN})_2^-$].

Ionic liquid	Cation...Cation	Cation...Anion	Anion...Anion
$[C_1\text{mim}][\text{BF}_4]$	4.6–5.8	3.1–4.8	4.8–5.9
$[C_1\text{mim}]\text{Cl}$	3.2–5.3	3.0–4.6	4.7–7.4
$[C_1\text{mim}][\text{N}(\text{CN})_2]$	3.4–5.1	3.2–6.1	6.1–8.2
$[C_2\text{mpyr}][\text{BF}_4]$	5.2–6.5	3.9–4.9	5.5–6.8
$[C_2\text{mpyr}]\text{Cl}$	5.1–5.4	3.8–4.4	5.7–6.0
$[C_2\text{mpyr}][\text{N}(\text{CN})_2]$	5.3–6.5	3.9–5.9	7.2–8.0

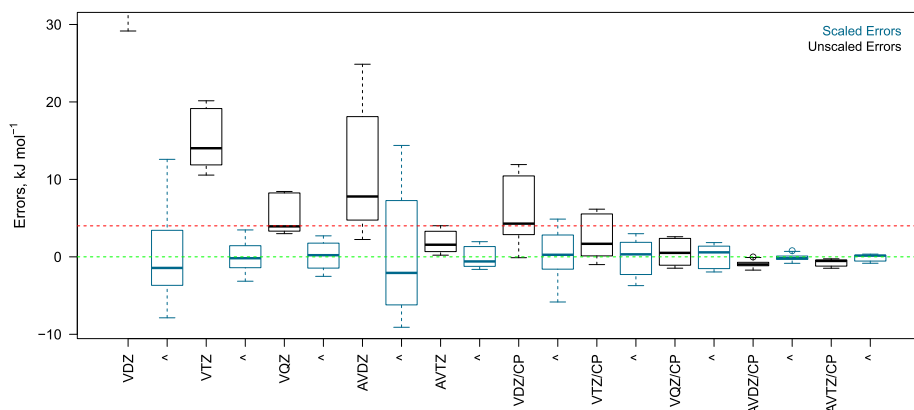


FIG. 3. Errors for 2 IP systems for unscaled (black) and scaled (blue) against cc-pVQZ energies where VDZ represents cc-pVDZ, A is augmentation, and CP is the counterpoise correction. The green and red dashed lines indicated 0.0 and 4.0 kJ mol⁻¹ errors, respectively.

the maximum error of as little as 4 kJ mol⁻¹. Counterpoise correction (CP) was necessary to reduce the error to below chemical accuracy for the cc-pVTZ basis set. The correction produces excellent results for the augmented basis sets as well as for cc-VTZ and cc-pVQZ.

Counterpoise corrected calculations are very time consuming when larger clusters are considered. The use of augmented basis sets such as aug-cc-pVTZ, even without the counterpoise correction, is not a solution either as these require a significant increase in computational resources and usually show very slow convergence of the HF energy for multi-scale clusters of ionic liquids due to the presence of degenerate molecular orbitals on anions.

The exponential convergence of the HF electronic energy has been well established for systematically improved basis sets such as Dunning's basis sets.^{94–96} In this study, this type of convergence [see Eq. (2)] was adopted to scale HF interaction energies to reproduce the benchmark energies,

$$E_{pred}^{INT} = \alpha \cdot E_{HF}^{INT} + \beta, \quad (2)$$

where E_{pred}^{INT} is the predicted interaction energy, E_{HF}^{INT} is the HF interaction energy with smaller basis sets, and α and β are the scaling coefficients. The latter were fitted using chi-squared minimisation (weighted sum of squared deviations) as implemented in the lmfit package for Python.⁹⁷ The fitted coefficients together with statistical measures are given in Table II. As one can see, a significant improvement has been achieved for non-counterpoise corrected HF interaction energies. For the cc-pVTZ basis set, the maximum error is reduced to below chemical accuracy (see Fig. 3), with the MAE falling below 2 kJ mol⁻¹. The fitted scaling coefficients were also applied to the previously studied single ion pairs. Similar errors were observed for non-counterpoise corrected HF/cc-pVTZ interaction energies, with a MAE of 1.8 kJ mol⁻¹ and SD of 1.7 kJ mol⁻¹ (for more details, see the [supplementary material](#)). Further in the text, scaled HF/cc-pVTZ interaction energies were used for the selected 2 ion-paired configurations.

TOTAL ELECTRONIC ENERGY VS. INTERACTION ENERGY

In this study, total electronic energy was used as the criterion to select the most stable 2 ion-paired configurations.

There are two other criteria commonly used in the field of theoretical chemistry—namely, binding energy and interaction energy. Binding energy, E_{BIND} , is defined as the energy difference between that of a cluster, $E_{cluster}$, and the sum of energies of individual ions, E_{ion}^i , taken in their minimum energy geometry [see Eq. (3)]. In order to obtain the latter, individual ions need to be geometry optimized separately,

$$E_{BIND} = E_{cluster} - \sum_i E_{ion}^i(min) + \Delta ZPVE, \quad (3)$$

where *min* indicates that the ion is taken in its lowest energy geometry and $\Delta ZPVE$ is the difference in zero-point vibration energies of the cluster and constituting ions. In two ion paired clusters, it was expected to contribute within 5 kJ mol⁻¹ on average per mole of ionic liquid (i.e., calculated per ion pair). For example, [C₁mim][BF₄], [C₃mim]Cl, and [C₁mpyr][N(CN)₂] have the values of $\Delta ZPVE$ of 4.7, 1.9, and 5.3 kJ mol⁻¹, respectively. Vibrational frequency calculations are very time consuming as these require computation of the Hessian matrix. Although the effect of vibrational frequency contribution is not negligible for some ionic liquids, it is not computationally feasible to perform this type of calculations for large-scale clusters on the routine basis.

It is usually customary to include counterpoise correction to account for molecular orbital overlap due to an incomplete basis set. The use of energies of ions in their lowest energy geometry introduces a reference point and allows for the calculation of the energy gain in the formation of the cluster. This energy gain is usually attributed to intermolecular fundamental forces that ensure the stability of the cluster. If the counterpoise correction is not included, especially for wavefunction-based methods, binding energies become significantly over-estimated up to 20 kJ mol⁻¹ in some cases.⁹² This effect has been shown to drastically increase with inclusion of more ions in the system.⁸⁰ Due to the constant reference point for individual ions, the use of binding energy as a criterion to determine thermodynamically stable structures becomes similar to total electronic energy, provided both are corrected for basis set superposition error. For ionic liquids, individual ions represent an unrealistic reference point as it is well known that these ions cannot exist on their own without either the counter-ions present or a stabilising medium. Nonetheless, binding energy directly relates to total interaction energy

with the difference being the reference point for the cation and anion.

Interaction energy, E_{INT} , is different from both total electronic energy and binding energy as the energy of individual ions is calculated using the geometry these adopt in the cluster as shown in the following figure:

$$E_{INT} = E_{cluster} - \sum_i E_{ion}^i(cluster), \quad (4)$$

where the ions are in the geometry they adopt in the cluster. It is important to account for counterpoise corrections to make interaction energy more reliable and realistic.

The main difference between binding and interaction energies lies in the deformation energy that is associated with an increase in the energy of individual ions due to the geometry deformation that each ion undergoes in an ionic cluster. This deformation occurs as a result of the presence of intermolecular interactions. For example, hydrogen bonding can result in a stretch of the C–H and N–H bonds,⁹⁸ whereas phosphonium cations are known to have greater flexibility about the phosphorus centre due to the larger range of allowed bond angles.⁹⁹ To this end, interaction energy quantifies the pure energy gain as a result of intermolecular interactions, whereas binding energy also includes the geometry and zero-point vibrational energy effect for constituting ions. It must be pointed out that total electronic energy already includes deformation energy of ions, which is more likely to be the larger contributor of the two.

Out of all the criteria, binding energies are much more computationally demanding as these require the calculation of the Hessian to confirm the minimum on the potential energy surface and cannot be applied to non-equilibrium geometries. It is computationally infeasible to perform Hessian calculations for multi-scale clusters of ionic liquids beyond 4 ion pairs and therefore this criterion is hardly used for studying intermolecular complexes.⁷² In the field of molecular dynamics simulations, it is common to minimise Gibbs free energy to locate the most stable structure of a condensed system at a given temperature.^{100–103} For quantum chemical calculations of multi-scale clusters of ionic liquids, interaction energy has been widely used to analyze their thermodynamic stability, thus excluding the deformation energy. Deformation energy becomes exceedingly important when increasing the number of ions in the cluster as well as when investigating complex ions, such as those with long alkyl chains or polar groups with strong hydrogen bonding ability.

In this study, both criteria, interaction energy and total electronic energy (further in the text referred to as total energy), are contrasted for the selection of energetically stable configurations of two ion-paired clusters, with total energy serving as the benchmark. The same lowest energy configurations could only be located in 14 out of 24 studied systems (in approximately 58% of systems) with interaction energy as a criterion. This has been achieved for the clusters of $[C_n\text{mim}]X$ ($X = \text{BF}_4^-$ and $\text{N}(\text{CN})_2^-$), $[C_n\text{mpyr}]\text{Cl}$, $[C_2\text{mpyr}][\text{BF}_4]$, and $[C_3\text{mpyr}][\text{N}(\text{CN})_2]$ ($n = 1\text{--}4$). Interaction energy fails to locate the lowest energy structures for imidazolium chlorides and the majority of pyrrolidinium ILs coupled with the

tetrafluoroborate and dicyanamide anions (see Fig. 2). In all the 24 systems, the criterion still identified the lowest energy configuration by total energy within 10 kJ mol^{-1} . In 13 of these systems (in approximately 54% of systems), the order of lower energy configurations within 10 kJ mol^{-1} by interaction energy does not correspond to that by total energy. Some typical examples are shown in Fig. 4. In $[C_4\text{mpyr}][\text{BF}_4]$, the third lowest energy configuration was not identified by interaction energy, placing it almost 15 kJ mol^{-1} above in energy, whereas an opposite trend was observed for $[C_3\text{mpyr}]\text{Cl}$ and $[C_2\text{mim}][\text{N}(\text{CN})_2]$. The use of interaction energy locates a couple of configurations within 10 kJ mol^{-1} , whereas their total energies are at least 15 kJ mol^{-1} higher in energy than the lowest energy configuration (see Fig. 4). These findings indicate that a configuration with the strongest interaction energy does not necessarily possess the lowest total energy. The latter represents a more realistic result from the conceptual point of view and when compared with experiment.

Examples of the difference between relative interaction energies and relative total energies are shown in Figs. 4(a) and 4(b). Configurations within 10 kJ mol^{-1} are labeled and can be found in Fig. 2. The differences between relative total energy and relative interaction energy fall consistently on the absolute scale between 3.3 (for $[C_n\text{mpyr}][\text{BF}_4]$) and 5.4 kJ mol^{-1} (for $[C_n\text{mim}]\text{Cl}$) on average (see Table III) with no particular trend with respect to the ionic liquid type. The differences can be equally positive and negative as demonstrated by low values of mean yet can be significant with a maximum difference of 31.2 kJ mol^{-1} .

To this end, interaction energy does not appear to be a reliable criterion for determining not only the lowest energy configuration but also the order of configurations within 10 kJ mol^{-1} . In 58% of the 2 ion paired systems studied, interaction energy could not locate the lowest energy configuration, and in 54% of the systems the order of lower energy configuration was not correctly identified, with some higher energy structures having interaction energy within 10 kJ mol^{-1} .

The two ion pair deformation energies in Table IV show that the cations and the BF_4^- anion contribute significantly through the deformation of their covalent bonds. Although chloride cannot deform, its ability to form strong electrostatic interactions has a significant effect on the cation which becomes more destabilised in its presence when compared to either BF_4^- or $\text{N}(\text{CN})_2^-$. The imidazolium cations tend to undergo a larger deformation than the pyrrolidinium ones except when dicyanamide is involved. The dicyanamide anion preferentially interacts through both of the terminal nitrogens, which can be easier accommodated by the imidazolium ring. Since the pyrrolidinium ring lacks this feature, in order to allow for unobstructed access to the nitrogen centres and hence an increase interaction energy, it requires to move the alkyl chains out of the way, thus resulting in puckering of the nitrogen centre. Imidazolium coupled with tetrafluoroborate and dicyanamide gives similar values for the deformation energy, further highlighting the ability of this cation to be easily polarised in response to changes in environment without a geometric change. As deformation energies are the result of the re-arrangement of internal molecular structure to

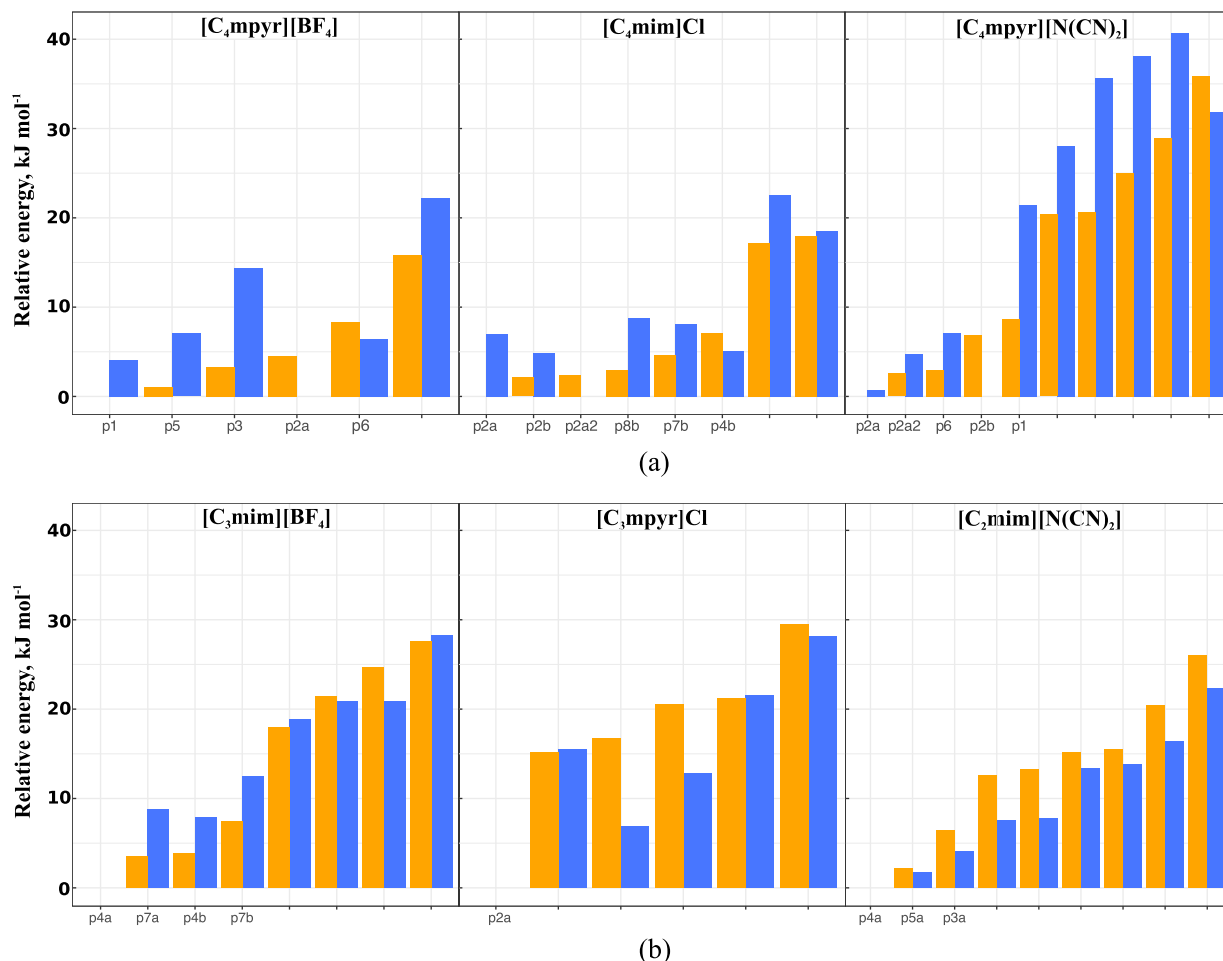


FIG. 4. Comparison of relative interaction energy (blue) and relative total energy (orange) of configurations optimized for 2 ion-paired clusters of (a) [C₄mpyr][BF₄], [C₄mim]Cl, and [C₄mpyr][N(CN)₂] and (b) [C₃mim][BF₄], [C₃mpyr]Cl, and [C₂mim][N(CN)₂].

enhance interaction and are quantitatively larger than chemical accuracy, it is unquestioningly important to consider them to accurately represent the bulk material.

Dispersion forces and ratio

The probability of encountering energy state i out of all possible states I is given by

$$p_i = \frac{e^{-E_i^{\text{tot}}/k_B T}}{\sum_j^I e^{-E_j^{\text{tot}}/k_B T}}, \quad (5)$$

TABLE III. Error statistics (in kJ mol⁻¹) for the difference between relative interaction energy and relative total energy.

Ionic liquids	No. of systems	MAE	Mean	Max
[C _n mim][BF ₄]	34	3.4	-0.6	8.3
[C _n mim]Cl	34	5.4	1.7	31.2
[C _n mim][N(CN) ₂]	29	3.7	3.6	10.8
[C _n mpyr][BF ₄]	27	3.3	-0.5	-11.1
[C _n mpyr]Cl	29	3.9	3.8	11.3
[C _n mpyr][N(CN) ₂]	41	5.1	0.4	18.4

where k_B is the Boltzmann constant, T is the temperature, and the Boltzmann distribution is dependent on the total energy of the state, E^{tot} . A Boltzmann averaged property is therefore the sum of each state multiplied by its probability. For example, the interaction dispersion energy weighted by the Boltzmann distribution is

$$E_{\text{INT}}^{\text{disp}} = \sum_i^I (p_i \times E_{\text{INT},i}^{\text{disp}}). \quad (6)$$

The ranges of ratios and interaction dispersion energy determined via Eqs. (5) and (6) for the two ion pairs are given

TABLE IV. Deformation energies (kJ mol⁻¹) averaged for the cations and anions of each configuration.

Ionic liquids	Cation			Anion		
	Max	Mean	SD	Max	Mean	SD
[C _n mim][BF ₄]	9.1	6.6	1.4	6.8	4.7	1.1
[C _n mim]Cl	26.7	12.6	3.9	0.0	0.0	0.0
[C _n mim][N(CN) ₂]	9.6	6.0	1.7	4.8	2.7	1.2
[C _n mpyr][BF ₄]	12.1	5.6	2.6	6.3	4.5	1.0
[C _n mpyr]Cl	13.3	8.7	2.1	0.0	0.0	0.0
[C _n mpyr][N(CN) ₂]	16.1	7.6	3.7	4.9	3.3	0.8

TABLE V. Ratio and dispersion energy per ion pair (kJ mol^{-1}) ranges for 2 ions paired systems and 1 ion pair model.

	Ratio 2 IP	Ratio 1 IP ²⁸	E_{Disp} 2 IP	E_{Disp} 1 IP ²⁸
$[\text{C}_n\text{mim}][\text{BF}_4]$	5.8–7.3	10.1–11.0	–63.3 to –52.2	–37.4 to –34.5
$[\text{C}_n\text{mim}]\text{Cl}$	5.4–6.4	9.0–9.8	–72.9 to –63.1	–45.6 to –42.5
$[\text{C}_n\text{mim}][\text{N}(\text{CN})_2]$	3.4–4.2	6.5–7.0	–95.3 to –82.2	–32.0 to –30.8
$[\text{C}_n\text{mpyr}][\text{BF}_4]$	5.1–6.5	11.4–12.0	–69.2 to –57.2	–56.4 to –50.7
$[\text{C}_n\text{mpyr}]\text{Cl}$	5.5–6.8	10.7–11.3	–71.8 to –60.2	–36.5 to –35.0
$[\text{C}_n\text{mpyr}][\text{N}(\text{CN})_2]$	3.6–5.5	8.7–9.2	–89.8 to –63.0	–39.7 to –38.0

in Table V as well as the previously published 1 ion pair data for comparison.²⁸ The previously published approach has been improved in three ways. First, previously the ion pair model energies were calculated with a different method, symmetry-adapted perturbation theory, which has a different definition for dispersion energy than post-HF methods such as SRS-MP2 as the former accounts for exchange component of dispersion. Second, the Boltzmann distribution used to weight the one ion pair data was based on the interaction energy of the system, in contrast to the two ion pairs which were weighted based on their total electronic energy. Third, the previously published correlations only included ionic liquids whose melting point continued to decrease with increasing alkyl chain length. This was done to ensure that interactions among like-charged ions were not the main contributor to thermodynamic and transport properties. In the current work, this limitation has been lifted, with all ionic liquids for which experimental data have been published being included in the analysis.

Analysis of Table V reveals that, on average, the ratio range for 2 IP clusters is almost half that of 1 IP systems. While two ion pair clusters experience an increase from both electrostatics and dispersion forces, the electrostatic interactions do not increase as drastically therefore causing the ratio to reduce. The slow increase in electrostatic forces can be explained by the presence of both attractive and repulsive interactions, whereas the dispersion forces between ions are by definition always attractive regardless of their charge. For example, the average HF interaction energy of the 2 IP $[\text{C}_1\text{mim}][\text{BF}_4]$ structures ($-590.0 \text{ kJ mol}^{-1}$) is ~ 1.7 times that of the 1 IP systems ($-342.2 \text{ kJ mol}^{-1}$). The average dispersion interaction energy in $[\text{C}_1\text{mim}][\text{BF}_4]$ structures increases by a factor of 3.5 from 1 IP ($-35.1 \text{ kJ mol}^{-1}$) to 2 IPs ($-124.6 \text{ kJ mol}^{-1}$).

With an increasing number of ions, the potential energy surface is expected to flatten out due to the increased contribution from dispersion forces. The latter is demonstrated in a wider spread of the dispersion component from 3.0 kJ mol^{-1} for single ion pairs to 11.5 kJ mol^{-1} for 2 ion-paired systems. In addition, the inclusion of same-ion interactions impacts the distribution of the dispersion component to interaction energy for all the ILs studied increasing from 25.6 kJ mol^{-1} on average for 1 IPs to 37.6 kJ mol^{-1} on average for 2 IPs. In some cases, such as $[\text{C}_n\text{mpyr}][\text{N}(\text{CN})_2]$ and $[\text{C}_n\text{mim}][\text{N}(\text{CN})_2]$, the dispersion component increases nearly three-fold. This also explains wider ranges for the ratio in the 2 IP systems. It is important to note that for two ion-paired systems the ratio becomes less dependent on the cation-anion

combination, falling within a small range of 3.4–5.5 (compared to the range of 6.5–12.0 for 1 IP models). As has been showcased for ionic liquid clusters of varying size from 4 to 32 ion pairs,³⁰ dispersion energy continues to grow with increasing cluster size and therefore the ratio might not have converged for two ion-paired systems. More studies on larger clusters are required to confirm whether the distribution of the ratio becomes even narrower regardless of the ionic liquid type.

Behaviour of the dispersion component in 2 IPs suggests that the anion has a larger effect than the type of cation. The dispersion component increases in the series of BF_4^- to Cl^- to $\text{N}(\text{CN})_2^-$ for both imidazolium- and pyrrolidinium-based cations. Contrary to this trend, the ratio is affected inversely in the same series, with the outlier being $[\text{C}_n\text{mpyr}]\text{Cl}$, whose ratio range is larger than that of $[\text{C}_n\text{mpyr}][\text{BF}_4]$. In the former, the electrostatic and induction energies appear to have the largest contribution to interaction energy out of the ionic liquids studied. This trend is attributed to the tight alternative packing arrangement (see Table I).

In general, the ratio decreases with increasing cluster size, with the exception of $[\text{C}_n\text{mim}][\text{BF}_4]$ and $[\text{C}_n\text{mpyr}][\text{N}(\text{CN})_2]$ where n increases from 3 to 4. The decrease in the ratio going from n -propyl to n -butyl when combined with the same anion and cation is small (maximum of 0.5) compared to the distribution range of the ratio. The original hypothesis that the ratio correlates with melting point suggests that the trend in the ratio should follow that of melting point in order to produce good correlations. For some ionic liquids, the ratio continues to decrease, whereas the corresponding melting point increases. An example of this is $[\text{C}_3\text{mim}][\text{BF}_4]$ and $[\text{C}_4\text{mim}][\text{BF}_4]$, where the increase in melting point from 333 to 342 K is accompanied by a slight decrease in the ratio from 5.7 to 5.4. This suggests that larger clusters might be needed to produce correlations that can be used to predict melting points of novel ionic liquids.

The relative contribution of dispersion to interaction energy is defined as follows:

$$E_{\text{INT}}^{\text{disp}} = E_{\text{cluster}}^{\text{disp}} - \sum_i E_{\text{ion}}^{i,\text{ion}}. \quad (7)$$

The relative dispersion for 2 ion-paired systems is plotted against the interaction energy in Fig. 5. The figure also illustrates the number of low energy structures (within 20 kJ mol^{-1}) for each system and how it follows no particular trend. For the BF_4^- and Cl^- anions, the relative dispersion is comparable regardless of the alkyl chain length ranging from 12.0% to 16.2% for imidazolium-based ILs and 12.3% to 15.7% for pyrrolidinium-based ionic liquids. The importance of the dispersion component of interaction energy is most clearly demonstrated in the $\text{N}(\text{CN})_2^-$ clusters. The $\text{N}(\text{CN})_2^-$ systems exhibit a greater contribution from dispersion due to its delocalised structure falling in the range of -110.9 (C_1mpyr^+) and -193.2 (C_4mim^+) kJ mol^{-1} which is up to $\sim 20\%$ of the interaction energy. This non-negligible component is expected to continue to increase disproportionately with the interaction energy in larger-scale clusters, i.e., the percentage of dispersion in the interaction energy will increase. Larger clusters will need to be investigated until it is seen that the dispersion

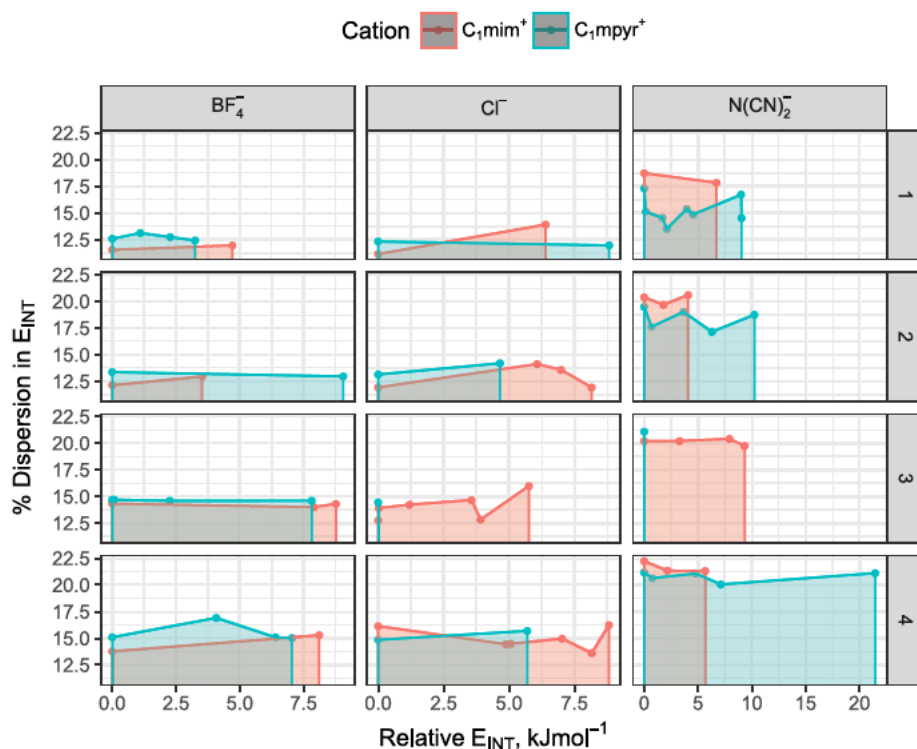


FIG. 5. The relative dispersion (in %) against relative interaction energy compared in imidazolium- and pyrrolidinium-based ionic liquids for the different anions (columns) and alkyl chain lengths (rows) of low energy configurations.

component has converged with cluster size as a proportion of interaction energy.

Correlation of the ratio with melting point

Here, an attempt to correlate the ratio of interaction energy to its dispersion component observed in clusters of 2 IPs is presented. In our previous work, the same ratio could not be used to predict melting points of ionic liquids when applied to single ion pairs. This conclusion is not surprising since single ion pairs do not account for many-body effects present in the bulk of ionic liquids. It is informative to investigate whether the inclusion of 2 ion pairs in a cluster would result in better trends. It has to be pointed out that the prediction of melting point represents one of the most challenging tasks that is yet to be solved. The results below by no means achieve this goal. On the other hand, they clearly indicate that the ratio is a valid concept and shows promise towards the development of a methodology for the prediction of melting points using the cluster approach.

Figure 6 and Table VI present the established correlations between the ratio and melting point. It was found that the imidazolium tetrafluoroborate ionic liquids formed their own correlation to the remaining ionic liquids and were thus treated separately. It has to be noted that the melting point correlations do not include the data for $[C_3mim][N(CN)_2]$ and $[C_2mpyr]Cl$ as melting points for these ionic liquids have not been published. Apart from $[C_nmim][BF_4]$, the remaining ionic liquids were found to fall in a similar range to allow for a general correlation to be established (see Fig. 6). This is a significant improvement in its own right on the previously established correlations for single ion pair models.

In general, the established correlation (see Table VI) allows for the prediction of the melting point of the studied ionic liquids within 54 K on average, which is comparable to the accuracy of currently used force fields.^{104–106} The melting points span from 202 to 613 K, a range of 411 K. The lowest MAEs as well as standard deviations of 21.3 K on average were found for dicyanamide-based ionic liquids. The delocalized dicyanamide anion with multiple interaction sites appears to favour alternating charge stacking, which might already be accounted well in smaller-sized clusters.

The worst performing systems are the $[C_nmpyr][BF_4]$ ionic liquids, whose collective standard deviation is 88.4 K which is over 35 K greater than the standard deviations of the other ionic liquids. The most plausible explanation lies in the fact that the $[C_1mpyr][BF_4]$ and $[C_2mpyr][BF_4]$ systems form plastic crystals that undergo a few solid-solid transitions prior

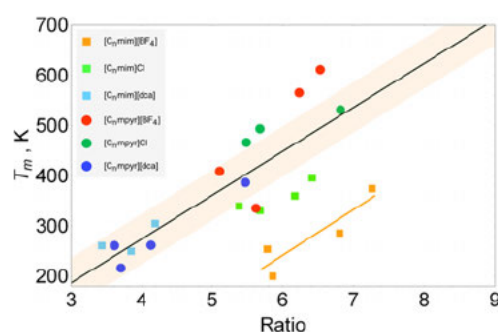


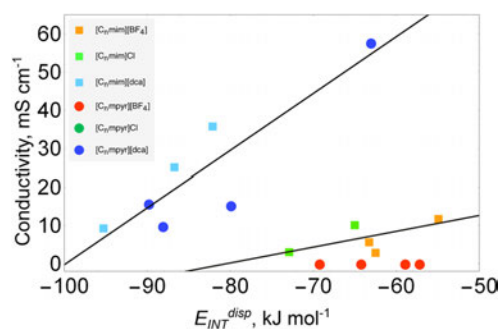
FIG. 6. Correlation of the ratio with experimental melting points with one general correlation (black) which includes all ionic liquids except for $[C_nmim][BF_4]$ whose correlation is depicted by an orange line. The region highlighted about the general trend shows ± 50 K.

TABLE VI. Melting point correlations with correlation statistics including the mean absolute error (MAE), standard deviation (SD), and maximum error (Max). All data are given in K.

Property	Ionic liquids	Correlation equation	MAE	SD	Max
Melting point	[C _n mim][BF ₄]	$-301.65 + 90.64 \times \text{ratio}$	27.0	31.7	34.0
	[C _n mim]Cl				
	[C _n mim][N(CN) ₂]				
	[C _n mpyr][BF ₄]	$-73.95 + 87.14 \times \text{ratio}$	53.7	65.7	118.0
	[C _n mpyr]Cl				
	[C _n mpyr][N(CN) ₂]				

to melting.^{107–112} These transitions are caused by rotation of ions around their internal axis of symmetry, which results in the entropic penalty. As a result, the latter is excluded from the entropy of fusion, thus resulting in higher melting points for this type of compounds. The [C_nmim]Cl ionic liquids have the second highest MAE of 82.2 K and an SD of 20.6 K. Out of all imidazolium-based ionic liquids this series was the only to exhibit the $\pi^+-\pi^+$ stacking of imidazolium rings in the lowest energy geometries. This suggests that the bulk structure might not be modeled properly with the 2 ion pair model and larger-scale clusters are needed to establish a reliable trend in the ratio of interaction energy to its dispersion component. It is not well understood why the [C_nmim][BF₄] ionic liquids form their own trend that is separate from the rest of ionic liquids. This observation might be attributed to slow convergence of the dispersion component with increasing cluster size.

The current findings illustrate a greater role of the anion compared to the cation in determining the melting point of ionic liquids. The ratio correctly captures the relationship between the dispersion component and melting point for more diffuse anions such as dicyanamide. This might be also attributed to slower convergence of the ratio for more spherical anions such as tetrafluoroborates and chloride. This hypothesis needs to be tested on larger clusters for these anions. To this end, a significant improvement over the single ion pair model has been achieved, with the average error of 54 K suggesting that more accurate correlation is most likely possible for larger-sized ionic liquid clusters.

FIG. 7. Correlation of the dispersion interaction energy with experimental conductivity with two correlations (black lines). One encapsulates the N(CN)²⁻ systems and the other is for imidazolium with BF₄⁻ and chloride.TABLE VII. Conductivity correlations with correlation statistics in mS cm⁻¹.

Property	Ionic liquids	Correlation	MAE	SD	Max
Conductivity	[C _n mim][BF ₄]	$33.37 + 0.41 \times E_{\text{INT}}^{\text{disp}}$	2.2	3.1	4.6
	[C _n mim]Cl				
	[C _n mim][N(CN) ₂]	$147.58 + 1.48 \times E_{\text{INT}}^{\text{disp}}$	6.6	8.4	14.0
	[C _n mpyr][N(CN) ₂]				

Correlation of dispersion component with conductivity

The conductivity correlations shown in Fig. 7 and Table VII do not include points for [C₁mim][BF₄], [C₁mim]Cl, [C₃mim]Cl, [C₃mim][N(CN)₂], and [C_nmpyr]Cl (n = 1–4) for which conductivity data have not been published.

A similar trend observed for melting points is that the dicyanamide ionic liquids form a good correlation between the dispersion component and conductivity with the MAE of 6.6 mS cm⁻¹ and the maximum error of 14 mS cm⁻¹. Conductivities have been predicted using molecular dynamics with a mean absolute error of 23%.^{22,113} This represents an excellent result, considering that the ionic liquid conductivity data span a range of 57.7 mS cm⁻¹. The imidazolium-based ionic liquids coupled with tetrafluoroborates and chloride anions produce excellent correlations with the MAE as low as 2.2 mS cm⁻¹ and the maximum error of 4.6 mS cm⁻¹, with both tetrafluoroborate and chloride systems performing equally well and producing MAE ± SD of 2.4 ± 2.9 and 1.9 ± 2.9, respectively. It has to be noticed that the series of the [C_nmpyr][BF₄] ionic liquids (n = 1–4) do not seem to correlate with the dispersion component due to very low values of conductivity ranging from 4.2 × 10⁻¹¹ to 8.8 × 10⁻⁷ mS cm⁻¹. To this end, it appears that good correlations between conductivity and the dispersion component can already be achieved for 2 ion-paired models.

CONCLUSIONS

In this work, two ion-paired clusters of [C_nmim]X and [C_nmpyr]X (n = 1–4), where X = BF₄⁻, Cl⁻, and N(CN)₂⁻, have been studied with the newly developed SRS-MP2 method with the view of predicting their thermodynamic (such as melting point) and transport (such as conductivity) properties. Each cation-anion combination was thoroughly screened to locate all possible minima and hence global minima on the potential energy surfaces, with 192 unique structures being identified. Increasing alkyl chain on the cation leads to an increased number of lower energy configurations as do anions with multiple interaction sites. Based on the analysis of the lowest energy configurations, it can be concluded that both cation and anion play a role in governing the most stable structure, opposed to the general belief that the anion was the main driving force. The preference for the $\pi^+-\pi^+$ stacking interaction was only observed for imidazolium-based ionic liquids when coupled with the chloride anion, whereas both tetrafluoroborate and dicyanamide preferred alternating charge arrangement. In the case of pyrrolidinium-based ionic liquids, the position of the alkyl groups appeared to be dictated by the anion. In the case of anions with multiple interaction sites such as tetrafluoroborate

and dicyanamide, longer alkyl chains preferred to align with each other in order to further increase the cluster stability.

Out of the two criteria, interaction energy and total electronic energy, the latter was found to be less biased due to the inclusion of deformation energy of constituting ions. Although interaction energy is often used to identify the stability of intermolecular complexes in the field of theoretical chemistry, the deformation energy was found to be far from negligible in two ion-paired ionic liquid clusters, reaching up to 27 kJ mol⁻¹ for imidazolium ionic liquids. This study clearly highlights the importance of using total electronic energy to determining the most stable structures from quantum chemical calculations.

The dispersion component of interaction energy was found to increase up to three-fold going from 1 to 2 ion-paired systems. The relative contribution of dispersion fell between 12.0% and 16.2% for BF₄⁻ and Cl⁻-based ionic liquids, whereas dicyanamide salts exhibited the highest dispersion component reaching 22%. The most striking difference to the single ion pair model results lies in the fact that no appreciable differences in the relative dispersion component were found between imidazolium and pyrrolidinium ionic liquids when coupled with the same anion.

The previously suggested correlation between the ratio of interaction energy to its dispersion component and experimentally measured melting points was tested for 2 ion paired systems. Contrary to the single ion pair model, the ionic liquids studied now formed a good correlation with the MAE of 54 K which is comparable to the accuracy of current MD simulations. The [C_nmim][BF₄] ionic liquids that appeared to produce their own correlation with the largest deviations were observed for [C_nmpyr][BF₄] and [C_nmim]Cl. The former belongs to the class of plastic crystals that undergo solid-solid transitions that result in higher melting points. The entropic effects appear to play a particularly important role for these ionic liquids, thus highlighting the limitation of our approach. Dicyanamide-based ionic liquids generated the best correlation, with the MAE as low as 21 K. Two distinct trends were observed for the prediction of conductivity. One includes [C_nmim][BF₄] and [C_nmim]Cl ionic liquids, whose conductivity can be predicted with the MAE of 2.2 mS cm⁻¹. The second trend was formed by the N(CN)₂⁻ ionic liquids with the MAE of 6.6 mS cm⁻¹. Good correlations for both melting point and conductivity represent a significant improvement over the single ion pair model, thus highlighting the importance of many-body effects in ionic liquids induced by interionic interactions of the same charge. It is also suggested that such good correlations could only be achieved due to the use of the recently developed SRS-MP2 method that shows high accuracy (2 kJ mol⁻¹ on average) for the prediction of dispersion forces in large-scale clusters of ionic liquids. In addition, a reliable scaled HF method was proposed to predict interaction energies of large-scale clusters of ionic liquids with a relatively small basis set and without the need to account for counterpoise correction.

In summary, the proposed approach of correlating the interaction energy and its dispersion component with thermodynamic and transport properties has been successful when applied to two ion-paired systems, especially when applied

to dicyanamide-based ionic liquids. Further improvement is expected for spherical anions such as tetrafluoroborates and chloride when larger-scale clusters are considered. Currently a study is underway to identify whether the inclusion of 4 ion pairs in the cluster would further result in the improvement of the established correlations.

SUPPLEMENTARY MATERIAL

See [supplementary material](#) for the literature melting points, conductivity, and interaction energies for the correlations of ionic liquids.

ACKNOWLEDGMENTS

The authors acknowledge generous support from the Australian Research Council through a Discovery Project Grant and a Future Fellowship for E.I.I. Z.L.S. is grateful to the Department of Education and Training for an Australian Postgraduate Award.

- 1 S. J. Andersen, J. K. E. T. Berton, P. Naert, S. Gildemyn, K. Rabaey, and C. V. Stevens, *ChemSusChem* **9**, 2059–2063 (2016).
- 2 S. Bhattacharyya, A. Filippov, and F. Shah, *Phys. Chem. Chem. Phys.* **18**, 28617–28625 (2016).
- 3 N. Daud, E. Bakis, J. P. Hallett, C. C. Weber, and T. Welton, *Chem. Commun.* **53**, 11154–11156 (2017).
- 4 G. F. Gregorio, C. C. Weber, J. Gräsvik, T. Welton, A. Brandt, and J. P. Hallett, *Green Chem.* **18**, 5456–5465 (2016).
- 5 J. P. Hallett and T. Welton, *Chem. Rev.* **111**, 3508–3576 (2011).
- 6 A. Izgorodin, E. Izgorodina, and D. R. MacFarlane, *Energy Environ. Sci.* **5**, 9496–9501 (2012).
- 7 S. Kwon, J. Choi, S. Cho, H. Lee, W. Oh, and S.-J. Choi, *J. Radioanal. Nucl. Chem.* **311**, 1605–1611 (2016).
- 8 J. V. Langham, R. A. O'Brien, J. H. Davis, and K. N. West, *J. Phys. Chem. B* **120**, 10524–10530 (2016).
- 9 T. Lee, S. Oh, T. R. Gohndrone, O. Morales-Collazo, S. Seo, J. F. Brennecke, and W. F. Schneider, *J. Phys. Chem. B* **120**, 1509–1517 (2016).
- 10 S. Menne, T. Vogl, and A. Balducci, *Chem. Commun.* **51**, 3656–3659 (2015).
- 11 A. Rout, K. A. Venkatesan, T. G. Srinivasan, and V. P. R. Rao, *Solvent Extr. Ion Exch.* **29**, 602–618 (2011).
- 12 B. Kirchner, O. Hollóczki, J. N. Canongia Lopes, and A. A. H. Pádua, *Wiley Interdiscip. Rev.: Comput. Mol. Sci.* **5**, 202–214 (2014).
- 13 E. I. Izgorodina, Z. L. Seeger, D. L. A. Scarborough, and S. Y. S. Tan, *Chem. Rev.* **117**, 6696–6754 (2017).
- 14 K. Shimizu, A. Pensado, P. Malfreyt, A. A. H. Pádua, and J. N. Lopes, *Faraday Discuss.* **154**, 155–169 (2011).
- 15 S. Lectez, J. Roques, M. Salanne, and E. Simoni, *J. Chem. Phys.* **137**, 154705 (2012).
- 16 F. Dommert, J. Schmidt, B. Qiao, Y. Zhao, C. Krekeler, L. Site, R. Berger, and C. Holm, *J. Chem. Phys.* **129**, 224501 (2008).
- 17 W. Jiang, D. J. Hardy, J. C. Phillips, A. D. MacKerell, K. Schulten, and B. Roux, *J. Phys. Chem. Lett.* **2**, 87–92 (2011).
- 18 C. Merlet, M. Salanne, B. Rotenberg, and P. A. Madden, *J. Phys. Chem. C* **115**, 16613–16618 (2011).
- 19 T. Méndez-Morales, J. Carrete, O. Cabeza, L. J. Gallego, and L. M. Varela, *J. Phys. Chem. B* **115**, 6995–7008 (2011).
- 20 A. Kandratsenka, J. Schroeder, D. Schwarzer, and V. S. Vikhrenko, *J. Chem. Phys.* **130**, 174507 (2009).
- 21 A. C. F. Mendonça, A. A. H. Pádua, and P. Malfreyt, *J. Chem. Theory Comput.* **9**, 1600–1610 (2013).
- 22 O. Borodin, *J. Phys. Chem. B* **113**, 11463–11478 (2009).
- 23 J. C. Wu, J.-P. Piquemal, R. Chaudret, P. Reinhardt, and P. Ren, *J. Chem. Theory Comput.* **6**, 2059–2070 (2010).
- 24 K. Shimizu and J. N. Lopes, *J. Mol. Liq.* **210**, 257–263 (2015).
- 25 F. Lipparini, L. Lagardère, B. Stamm, E. Cancès, M. Schnieders, P. Ren, Y. Maday, and J.-P. Piquemal, *J. Chem. Theory Comput.* **10**, 1638–1651 (2014).

- ²⁶A. Dequidt, J. Dev  my, and A. A. H. P  dua, *J. Chem. Inf. Model.* **56**, 260–268 (2016).
- ²⁷J.-M. Andanson, E. Bordes, J. Dev  my, F. Leroux, A. A. H. P  dua, and M. F. Gomes, *Green Chem.* **16**, 2528–2538 (2014).
- ²⁸E. I. Izgorodina, D. Golze, R. Maganti, and V. Armel, *Phys. Chem. Chem. Phys.* **16**, 7209–7221 (2013); E. I. Izgorodina *et al.*, *ibid.* **16**, 7129 (2014).
- ²⁹E. I. Izgorodina, and U. L. Bernard, *J. Phys. Chem. A* **113**, 7064–7072 (2009).
- ³⁰S. Tan, S. Barrera Acevedo, and E. I. Izgorodina, *J. Chem. Phys.* **146**, 064108 (2017).
- ³¹N. V. Plechkova and K. R. Seddon, *Chem. Soc. Rev.* **37**, 123–150 (2008).
- ³²C. M. Gordon, J. D. Holbrey, A. R. Kennedy, and K. R. Seddon, *J. Mater. Chem.* **8**, 2627–2636 (1998).
- ³³J. D. Holbrey and S. Seddon, *J. Chem. Soc., Dalton Trans.* 2133–2140 (1999).
- ³⁴R. N. D. Das and K. Roy, *Mol. Diversity* **17**, 151–196 (2013).
- ³⁵D. C. Weis and D. R. MacFarlane, *Aust. J. Chem.* **65**, 1478–1486 (2012).
- ³⁶J. O. Valderrama, *Ind. Eng. Chem. Res.* **53**, 1004–1014 (2014).
- ³⁷H. D. B. Jenkins, D. Tudela, and L. Glasser, *Inorg. Chem.* **41**, 2364–2367 (2002).
- ³⁸H. D. B. Jenkins, H. K. Roobottom, J. Passmore, and L. Glasser, *Inorg. Chem.* **38**, 3609–3620 (1999).
- ³⁹A. Klamt, *Wiley Interdiscip. Rev.: Comput. Mol. Sci.* **1**, 699–709 (2011).
- ⁴⁰A. Klamt, F. Eckert, and W. Arlt, *Annu. Rev. Chem. Biomol. Eng.* **1**, 101–122 (2010).
- ⁴¹K. E. Gutowski, J. D. Holbrey, R. D. Rogers, and D. D. Dixon, *J. Phys. Chem. B* **109**, 23196–23208 (2005).
- ⁴²U. Preiss, S. Bulut, and I. Krossing, *J. Phys. Chem. B* **114**, 11133–11140 (2010).
- ⁴³P. Eiden, S. Bulut, T. K  chner, C. Friedrich, T. Schubert, and I. Krossing, *J. Phys. Chem. B* **115**, 300–309 (2010).
- ⁴⁴K. Dong, L. Zhao, Q. Wang, Y. Song, and S. Zhang, *Phys. Chem. Chem. Phys.* **15**, 6034–6040 (2013).
- ⁴⁵C. Spickermann, S. C. Lehmann, and B. Kirchner, *J. Chem. Phys.* **128**, 244506 (2008).
- ⁴⁶R. Ludwig, *Phys. Chem. Chem. Phys.* **10**, 4333–4339 (2008).
- ⁴⁷V. N. Emel'yanenko, G. Boeck, S. P. Verevkin, and R. Ludwig, *Chem. - Eur. J.* **20**, 11640–11645 (2014).
- ⁴⁸K. Fumino, T. Peppel, M. Geppert-Rybczynska, D. H. Zaitsau, J. K. Lehmann, S. P. Verevkin, M. K  ckerling, and R. Ludwig, *Phys. Chem. Chem. Phys.* **13**, 14064–14075 (2011).
- ⁴⁹T. Peppel, C. Roth, K. Fumino, P. Paschek, M. K  ckerling, and R. Ludwig, *Angew. Chem., Int. Ed.* **50**, 6661–6665 (2011).
- ⁵⁰F. Weinhold, *J. Chem. Phys.* **109**, 367–372 (1998).
- ⁵¹F. Weinhold, *J. Chem. Phys.* **109**, 373–384 (1998).
- ⁵²R. Ludwig, F. Weinhold, and T. C. Farrar, *J. Chem. Phys.* **102**, 5118–5125 (1995).
- ⁵³R. Ludwig, *ChemPhysChem* **6**, 1376–1380 (2005).
- ⁵⁴R. Ludwig, F. Weinhold, and T. C. Farrar, *Ber. Bunsenges. Phys. Chem.* **102**, 205–212 (1998).
- ⁵⁵R. Ludwig and F. Weinhold, *J. Chem. Phys.* **110**, 508–515 (1999).
- ⁵⁶R. Ludwig, F. Weinhold, and T. C. Farrar, *Mol. Phys.* **97**, 479–486 (1999).
- ⁵⁷R. Ludwig, F. Weinhold, and T. C. Farrar, *Mol. Phys.* **97**, 465–477 (1999).
- ⁵⁸R. Ludwig, *ChemPhysChem* **6**, 1369–1375 (2005).
- ⁵⁹R. Ludwig, F. Weinhold, and T. C. Farrar, *J. Chem. Phys.* **107**, 499–507 (1997).
- ⁶⁰B. Kirchner, *J. Chem. Phys.* **123**, 204116 (2005).
- ⁶¹J. Friedrich, E. Perlt, M. Roatsch, C. Spickermann, and B. Kirchner, *J. Chem. Theory Comput.* **7**, 843–851 (2011).
- ⁶²C. Spickermann, E. Perlt, M. von Domaros, M. Roatsch, J. Friedrich, and B. Kirchner, *J. Chem. Theory Comput.* **7**, 868–887 (2011).
- ⁶³K. Fumino, A. Wulf, and R. Ludwig, *Phys. Chem. Chem. Phys.* **11**, 8790–8794 (2009).
- ⁶⁴K. Fumino, A. Wulf, and R. Ludwig, *Angew. Chem., Int. Ed.* **48**, 3184–3186 (2009).
- ⁶⁵K. Fumino, A. Wulf, and R. Ludwig, *Angew. Chem., Int. Ed.* **47**, 3830–3834 (2008).
- ⁶⁶A. Wulf, K. Fumino, R. Ludwig, and P. F. Taday, *ChemPhysChem* **11**, 349–353 (2010).
- ⁶⁷K. Fumino, V. Fossog, P. Stange, K. Wittler, W. Polet, R. Hempelmann, and R. Ludwig, *ChemPhysChem* **15**, 2604–2609 (2014).
- ⁶⁸E. A. Turner, C. C. Pye, and R. D. Singer, *J. Phys. Chem. A* **107**, 2277–2288 (2003).
- ⁶⁹S. Zahn, G. Bruns, J. Thar, and B. Kirchner, *Phys. Chem. Chem. Phys.* **10**, 6921–6924 (2008).
- ⁷⁰E. I. Izgorodina, J. Rigby, and D. R. MacFarlane, *Chem. Commun.* **48**, 1493–1495 (2011).
- ⁷¹P. Halet, Z. L. Seeger, S. Barrera Acevedo, and E. I. Izgorodina, *J. Phys. Chem. B* **121**, 577–588 (2017).
- ⁷²K. Muller-Dethlefs and P. Hobza, *Chem. Rev.* **100**, 143–168 (2000).
- ⁷³J. Rezac and P. Hobza, *Chem. Rev.* **116**, 5038–5071 (2016).
- ⁷⁴J. Rigby and E. I. Izgorodina, *Phys. Chem. Chem. Phys.* **15**, 1632–1646 (2012).
- ⁷⁵O. Holl  czki, F. Malberg, T. Welton, and B. Kirchner, *Phys. Chem. Chem. Phys.* **16**, 16880–16890 (2014).
- ⁷⁶P. A. Hunt, *J. Phys. Chem. B* **111**, 4844–4853 (2007).
- ⁷⁷P. A. Hunt, I. R. Gould, and B. Kirchner, *Aust. J. Chem.* **60**, 9–14 (2007).
- ⁷⁸D. G. Fedorov and K. Kitaura, *Chem. Phys. Lett.* **389**, 129–134 (2004).
- ⁷⁹D. G. Fedorov, R. M. Olson, and K. Kitaura, *J. Comput. Chem.* **25**, 872–880 (2004).
- ⁸⁰J. Rigby, S. Barrera Acevedo, and E. I. Izgorodina, *J. Chem. Theory Comput.* **11**, 3610–3616 (2015).
- ⁸¹M. W. Schmidt, K. K. Baldrige, J. A. Boatz, S. T. Elbert, M. S. Gordon, J. H. Jensen, S. Koseki, N. Matsunaga, K. A. Nguyen, and S. Su, *J. Comput. Chem.* **14**, 1347–1363 (1993).
- ⁸²R. M. Parrish, L. A. Burns, and D. G. A. Smith, A. C. Simmonett, A. DePrince, E. G. Hohenstein, U. Bozkaya, A. Y. Sokolov, R. D. Remigio, R. M. Richard, J. F. Gonthier, A. M. James, H. R. McAlexander, A. Kumar, M. Saitow, X. Wang, B. P. Pritchard, P. Verma, H. F. Schaefer, K. Patkowski, R. A. King, E. F. Valeev, F. A. Evangelista, J. M. Turney, T. D. Crawford, and C. D. Sherrill, *J. Chem. Theory Comput.* **13**, 3185–3197 (2017).
- ⁸³M. J. Frisch, G. W. Trucks, H. B. Schlegel, G. E. Scuseria, M. A. Robb, J. R. Cheeseman, G. Scalmani, V. Barone, B. Mennucci, G. A. Petersson, H. Nakatsuji, M. Caricato, X. Li, H. P. Hratchian, A. F. Izmaylov, J. Bloino, G. Zheng, J. L. Sonnenberg, M. Hada, M. Ehara, K. Toyota, R. Fukuda, J. Hasegawa, M. Ishida, T. Nakajima, Y. Honda, O. Kitao, H. Nakai, T. Vreven, J. A. Montgomery, J. E. Peralta, F. Ogliaro, M. Bearpark, J. J. Heyd, E. Brothers, K. N. Kudin, V. N. Staroverov, R. Kobayashi, J. Normand, K. Raghavachari, A. Rendell, J. C. Burant, S. S. Iyengar, J. Tomasi, M. Cossi, N. Rega, J. M. Millam, M. Klene, J. E. Knox, J. B. Cross, V. Bakken, C. Adamo, J. Jaramillo, R. Gomperts, R. E. Stratmann, O. Yazyev, A. J. Austin, R. Cammi, C. Pomelli, J. W. Ochterski, R. L. Martin, K. Morokuma, V. G. Zakrzewski, G. A. Voth, P. Salvador, J. J. Dannenberg, S. Dapprich, A. D. Daniels, Farkas, J. B. Foresman, J. V. Ortiz, J. Cioslowski, and D. J. Fox, GAUSSIAN 09, Revision E.01, Gaussian, Inc., Wallingford, CT, 2016.
- ⁸⁴R. P. Matthews, T. Welton, and P. A. Hunt, *Phys. Chem. Chem. Phys.* **16**, 3238–3253 (2014).
- ⁸⁵R. P. Matthews, T. Welton, and P. A. Hunt, *Phys. Chem. Chem. Phys.* **17**, 14437–14453 (2015).
- ⁸⁶R. P. Matthews, C. Ashworth, T. Welton, and P. A. Hunt, *J. Phys.: Condens. Matter* **26**, 284112 (2014).
- ⁸⁷S. Grimme, J. Antony, S. Ehrlich, and H. Krieg, *J. Chem. Phys.* **132**, 154104 (2010).
- ⁸⁸S. Grimme, *Wiley Interdiscip. Rev.: Comput. Mol. Sci.* **1**, 211–228 (2011).
- ⁸⁹S. Grimme, A. Hansen, J. Brandenburg, and C. Bannwarth, *Chem. Rev.* **116**, 5105–5154 (2016).
- ⁹⁰S. Zahn, D. R. MacFarlane, and E. I. Izgorodina, *Phys. Chem. Chem. Phys.* **15**, 13664–13675 (2013).
- ⁹¹E. I. Izgorodina, D. Golze, R. Maganti, and V. Armel, *Phys. Chem. Chem. Phys.* **16**, 7209–7221 (2013).
- ⁹²J. Rigby and E. I. Izgorodina, *J. Chem. Theory Comput.* **10**, 3111–3122 (2014).
- ⁹³S. F. Boys and F. Bernardi, *Mol. Phys.* **19**, 553–566 (2006).
- ⁹⁴F. Jensen, *J. Chem. Phys.* **110**, 6601–6605 (1999).
- ⁹⁵A. Halkier, T. Helgaker, P. Jorgensen, W. Klopper, and J. Olsen, *Chem. Phys. Lett.* **302**, 437–446 (1999).
- ⁹⁶A. Karton and J. M. L. Martin, *Theor. Chem. Acc.* **115**, 330–333 (2006).
- ⁹⁷M. Newville, T. Stensitzki, D. B. Allen, and A. Ingargiola, LMFIT: Non-Linear Least-Square Minimization and Curve-Fitting for Python (2014).
- ⁹⁸K. Fumino, V. Fossog, P. Stange, D. Paschek, R. Hempelmann, and R. Ludwig, *Angew. Chem., Int. Ed.* **54**, 2792–2795 (2015).
- ⁹⁹L. Scarbath-Evers, P. A. Hunt, B. Kirchner, D. R. MacFarlane, and S. Zahn, *Phys. Chem. Chem. Phys.* **17**, 20205–20216 (2015).
- ¹⁰⁰M. Levitt, *J. Mol. Biol.* **170**, 723–764 (1983).
- ¹⁰¹S. Erkoc and E. Guneyler, *Phys. E* **8**, 40–49 (2000).
- ¹⁰²A. Ince and S. Erkoc, *Comput. Mater. Sci.* **50**, 865–870 (2011).

- ¹⁰³B. Leimkuhler, C. Matthews, B. Leimkuhler, and C. Matthews, *Molecular Dynamics With Deterministic and Stochastic Numerical Methods* (Springer, 2015), Vol. 39, pp. 211–260.
- ¹⁰⁴E. J. Maginn, *Acc. Chem. Res.* **40**, 1200–1207 (2007).
- ¹⁰⁵D. M. Eike, J. F. Brennecke, and E. J. Maginn, *Green Chem.* **5**, 323–328 (2003).
- ¹⁰⁶S. Jayaraman and E. J. Maginn, *J. Chem. Phys.* **127**, 214504 (2007).
- ¹⁰⁷L. Glasser, *Thermochim. Acta* **421**, 87–93 (2004).
- ¹⁰⁸S. Forsyth, J. Golding, D. R. MacFarlane, and M. Forsyth, *Electrochim. Acta* **46**, 1753–1757 (2001).
- ¹⁰⁹J. Golding, N. Hamid, D. R. MacFarlane, M. Forsyth, C. Forsyth, C. Collins, and J. Huang, *Chem. Mater.* **13**, 558–564 (2001).
- ¹¹⁰W. A. Henderson, V. G. Young, S. Passerini, P. C. Trulove, and H. C. DeLong, *Chem. Mater.* **18**, 934–938 (2006).
- ¹¹¹D. R. MacFarlane, P. Meakin, J. Sun, N. Amini, and M. Forsyth, *J. Phys. Chem. B* **103**, 4164–4170 (1999).
- ¹¹²T. Kanatani, R. Ueno, K. Matsumoto, T. Nohira, and R. Hagiwara, *J. Fluorine Chem.* **130**, 979–984 (2009).
- ¹¹³B. L. Bhargava and S. Balasubramanian, *J. Chem. Phys.* **123**, 144505 (2005).

6.3 References

- [1] Robin D. Rogers and Kenneth R. Seddon. Ionic Liquids–Solvents of the Future? *Science* **302**(5646) (2003), 792–793. DOI: [10.1126/science.1090313](https://doi.org/10.1126/science.1090313).
- [2] Ekaterina I. Izgorodina, Zoe L. Seeger, David L. A. Scarborough, and Samuel Y. S. Tan. Quantum Chemical Methods for the Prediction of Energetic, Physical, and Spectroscopic Properties of Ionic Liquids. *Chemical Reviews* **117**(10) (2017), 6696–6754. DOI: [10.1021/acs.chemrev.6b00528](https://doi.org/10.1021/acs.chemrev.6b00528).
- [3] Alston J. Misquitta, Bogumil Jeziorski, and Krzysztof Szalewicz. Dispersion Energy from Density-Functional Theory Description of Monomers. *Physical Review Letters* **91**(3) (2003), 033201. DOI: [10.1103/PhysRevLett.91.033201](https://doi.org/10.1103/PhysRevLett.91.033201).
- [4] O. Anatole von Lilienfeld, Ivano Tavernelli, Ursula Rothlisberger, and Daniel Sebastiani. Optimization of Effective Atom Centered Potentials for London Dispersion Forces in Density Functional Theory. *Physical Review Letters* **93**(15) (2004), 153004. DOI: [10.1103/PhysRevLett.93.153004](https://doi.org/10.1103/PhysRevLett.93.153004).
- [5] Richard P. Matthews, Tom Welton, and Patricia A. Hunt. Competitive Pi Interactions and Hydrogen Bonding within Imidazolium Ionic Liquids. *Physical Chemistry Chemical Physics* **16**(7) (7 2014), 3238–3253. DOI: [10.1039/C3CP54672A](https://doi.org/10.1039/C3CP54672A).
- [6] Ekaterina I. Izgorodina, Uditha L. Bernard, and Douglas R. MacFarlane. Ion-Pair Binding Energies of Ionic Liquids: Can DFT Compete with *Ab Initio*-Based Methods? *The Journal of Physical Chemistry A* **113**(25) (25 2009), 7064–7072. DOI: [10.1021/jp8107649](https://doi.org/10.1021/jp8107649).
- [7] Ekaterina I. Izgorodina, Dorothea Golze, Radha Maganti, Vanessa Armel, Maria Taige, Thomas J. S. Schubert, and Douglas R. MacFarlane. Importance of Dispersion Forces for Prediction of Thermodynamic and Transport Properties of Some Common Ionic Liquids. *Physical Chemistry Chemical Physics* **16**(16) (2014), 7209–7221. DOI: [10.1039/C3CP53035C](https://doi.org/10.1039/C3CP53035C).

Chapter 7

Conclusions

The aim within this thesis was to facilitate the prediction of properties of ionic liquids from large scale wavefunction-based methods. This has been achieved by:

- I. Examining the energetics of larger clusters of ionic liquids that can be linked to structural motifs
- II. Exploring quantum chemical methods that have the potential to be used as cheaper alternatives with high accuracy
- III. Identifying key low energy geometries in larger clusters that contribute to physicochemical properties of ionic liquids
- IV. Investigating the link between fundamental forces and desired properties in larger clusters of ionic liquids

Chapter 2 introduced the fragment molecular orbital approach (FMO) and investigated the two- and three- body effects to further decrease the resources required for large scale calculations beyond that of using the fragmentation scheme. FMO was applied to systems of imidazolium, pyrrolidinium, quaternary ammonium, and pyridinium cations that were combined with chloride and tetrafluoroborate anions. The calculations were performed with second-order Møller-Plesset perturbation theory (MP2). All two-body HF contributions were seen to be important for all cluster sizes. Two-body correlation contributions were found to converge

to within 1 kJ mol^{-1} at $\log(N) - 0.5$ where N is the number of ion pairs and this on average accounted for 71% of the two-body correlation calculations. Two-body correlation contributions surprisingly extended into the third solvation shell. Three-body effects did not extend past the first solvation shell and larger cutoffs were thus recommended. Between 70 and 89% of three-body calculations can be omitted resulting in a drastically reduced consumption of resources.

Chapter 3 determined the quality of density functional theory (DFT) functional and MP2 variant optimisations in two and four ion pair structures. The benchmark geometries were optimised with FMO3-SRS-MP2/cc-pVTZ. Seven DFT functionals with added dispersion corrections and FMO2/3-SRS-MP2 were combined with four Dunning basis sets to make 43 levels of optimisation. Single point energy calculations were performed on all geometries with FMO3-SRS-MP2/cc-pVTZ. Good agreement with the benchmark geometry in the two ion pair geometries did not always translate to accurate geometries of four ion pairs despite the interionic distances of the four ion pair benchmark geometries being identical to that of the two ion pairs. The functionals that performed the best for both two and four ion pairs are PBE-D3/cc-pVTZ, ω B97X-D/aug-cc-pVDZ and BLYP-D3/cc-pVTZ where PBE-D3/cc-pVTZ obtained an average relative total energy and standard deviation of 2.3 and 3.4 kJ mol^{-1} , respectively, for the 4 ion pair clusters.

Chapter 4 studied the accuracy of domain-based local pair natural orbital theory applied to coupled cluster with single-, double-, and perturbative triple-excitations (DLPNO-CCSD(T)) with respect to canonical CCSD(T). The use of DLPNO theory would dramatically reduce the cost of high accuracy calculations of ionic liquids. The theory was applied to protic and aprotic single ion pairs of the datasets IL174 and HBIL. Both TightPNO settings with non-iterative triples (T_0) and with iterative triples (T_1) produced errors all within chemical accuracy. The three parameters controlling the size of the external space, T_{CutPNO} , T_{CutPairs} and T_{CutMKN} , were varied to obtain spectroscopic accuracy for the ionic liquids. Two sets of cutoffs are recommended for spectroscopic accuracy. IL1PNO, where T_{CutPNO} is 5×10^{-8} and T_{CutPairs} is 4×10^{-6} , obtained mean absolute errors within spectroscopic accuracy for the ionic liquids containing halides and the majority of protic ionic liquids. IL2PNO, where T_{CutPNO} is 1×10^{-9} and T_{CutPairs} is 1×10^{-7} , achieved spectroscopic accuracy for all errors.

Chapter 5 presented a methodology for sampling vast areas of a potential energy surface and converting sampled configurations into a set of unique low energy geometries. As the geometries are energetically favourable, they are therefore present in a bulk solution and influence the physical properties of the material. Ion pairs were replicated and subjected to 90 degree rotations of the cations and inversions in all combinations to create a geometrically diverse set of four ion pairs. Molecular dynamics was performed for each starting structure such that the local region of the potential energy surface was adequately sampled and all low energy geometries were extracted from the trajectories. All configurations of $[\text{C}_2\text{mpyr}][\text{BF}_4]$ and $[\text{C}_4\text{mim}]\text{Cl}$ adopted alternating charge structures. Principal component analysis of the structures revealed that while relative low energies were only possible for a small set of very specific cation orientations in the case of $[\text{C}_4\text{mim}]\text{Cl}$, the $[\text{C}_2\text{mpyr}][\text{BF}_4]$ cations could reorient with little affect on the energy. Agglomerative clustering was used to group clusters by their geometry. 15 unique geometries of $[\text{C}_2\text{mpyr}][\text{BF}_4]$ and 2 unique geometries of $[\text{C}_4\text{mim}]\text{Cl}$ were located. For both ionic liquids geometries of lower energy than that of simulated annealing were obtained.

Chapter 6 correlated thermodynamic and transport properties with interaction energies in two ion pair clusters. Imidazolium and pyrrolidinium cations with alkyl chain lengths of methyl to butyl were coupled with anions chloride, tetrafluoroborate and dicyanamide. Each ionic liquid was subjected to extensive geometry screening such that the low configuration energies found in the bulk liquid could be located. It was found that both the anion and cation were responsible for determining the most stable structure. The dispersion component of these two ion pairs increased by a factor of three from previously studied one ion pair systems. The melting point temperatures were correlated with the ratio of the total interaction energy to the dispersion interaction energy where all energies were determined from a Boltzmann distribution of the low energy geometries. For one ion pair clusters, separate trends were formed for each cation family and anion. Conversely, a general trend was formed for the two ion pair systems where the mean absolute error was 54 K which rivals the accuracy of molecular dynamics simulations. Two trends were observed in the correlation of viscosity with dispersion interaction energy.

7.1 Future Work

Employing the developed cutoffs for the fragment molecular orbital approach and employing a DFT functional such as PBE-D3/cc-pVTZ, which provides accurate geometries of larger clusters, enables further investigations of the physicochemical properties of ILs. One interesting application would be to expand on the work of chapter 6 and observe the correlation of interaction energies of four ion pair clusters with melting point and viscosity. As the dispersion energy increased 3-fold from one ion pair systems to two, and the trends of independent cation families were seen to converge, the question is will the predictive power of the trends strengthen in four ion pairs? Furthermore, it can be established whether the dispersion per ion pair continues to increase as a function of the interaction energy.

Principal component analysis on the unique four ion pair geometries of $[\text{C}_2\text{mpyr}][\text{BF}_4]$ and $[\text{C}_4\text{mim}]\text{Cl}$ obtained from the developed methodology of chapter 5 can be used to construct collective variables for use in metadynamics. Bias potentials would be added to the atomic coordinates of a structure such that it would be guided through the low energy regions collecting the unique geometries in its trajectory. The development of transferable collective variables for ionic liquid systems would significantly circumvent the issue of geometry screening in larger clusters. Furthermore, geometries produced in the methodology of chapter 5 are only as good as the force field used to determine them and errors of up to 21.7 kJ mol^{-1} were seen. Polarised force fields are beginning to appear in the literature that account for induction effects. If polarised force fields can determine relative energies with higher accuracy, more realistic geometries would be obtained.

Appendices

Appendix A

A systematic study of DFT performance for geometry optimisations of ionic liquid clusters – Supporting Information

Supplementary Information

A systematic study of DFT performance for geometry optimisations of ionic liquid clusters

Zoe Luisa Seeger and Ekaterina I. Izgorodina*

School of Chemistry, Monash University, 17 Rainforest Walk, Clayton, Victoria 3800,
Australia

Contents

1	Information	1
2	Energies of 2IPs with b3lyp	2
3	Energies of 2IPs with b3lyp-d3	2
4	Energies of 2IPs with blyp	3
5	Energies of 2IPs with blyp-d3	3
6	Energies of 2IPs with bp86-d3	3
7	Energies of 2IPs with df-mp2	4
8	Energies of 2IPs with m062x	4
9	Energies of 2IPs with pbe	4
10	Energies of 2IPs with pbe-d3	5
11	Energies of 2IPs with srs-fmo2	5
12	Energies of 2IPs with srs-fmo3	5
13	Energies of 2IPs with tpss-d3	6
14	Energies of 2IPs with wb97xd	6
15	Energies of 4IPs with b3lyp	6
16	Energies of 4IPs with b3lyp-d3	7

17 Energies of 4IPs with blyp	7
18 Energies of 4IPs with blyp-d3	7
19 Energies of 4IPs with hf	8
20 Energies of 4IPs with m062x	8
21 Energies of 4IPs with pbe	8
22 Energies of 4IPs with pbe-d3	9
23 Energies of 4IPs with srs-fmo2	9
24 Energies of 4IPs with srs-fmo3	9
25 Energies of 4IPs with tpss-d3	10
26 Energies of 4IPs with wb97xd	10

1 Information

All energies are given in kJ/mol. Basis sets **ccd**, **cct**, **accd** and **acct** represent cc-pVDZ, cc-pVTZ, aug-cc-pVDZ and aug-cc-pVTZ, respectively. **Diff** columns refer to difference in energies of the geometry optimised with the **Theory** and the geometry optimised with FMO3-SRS-MP2/cc-pVTZ.

The column names are as follows:

System	Ionic liquid system
Theory	Ab initio method + basis set
HF	Total FMO3-HF/cc-pVTZ energy
Cor	Total FMO3-SRS-MP2/cc-pVTZ correlation energy
Int HF	FMO3-HF/cc-pVTZ interaction energy
Int Cor	FMO3-SRS-MP2/cc-pVTZ interaction correlation energy
HF Diff	Difference in total FMO3-HF/cc-pVTZ energies
Cor Diff	Difference in total FMO3-SRS-MP2/cc-pVTZ correlation energies
Int HF Diff	Difference in FMO3-HF/cc-pVTZ interaction energies
Int Cor Diff	Difference in FMO3-SRS-MP2/cc-pVTZ interaction correlation energy

This is an abbreviated version of the supplementary information where the Cartesian coordinates of 320 DFT and MP2 optimised geometries have been removed. These are available on request and are included in the supplementary information of the publication.

2 Energies of 2IPs with b3lyp

System	Theory	HF	Cor	Int HF	Int Cor	HF Diff	Cor Diff	Int HF Diff	Int Cor Diff
c1mim-bf4-conf1	b3lyp-accd	-3814469.8	-15105.3	-809.9	-78.9	-4.9	10.0	-10.2	13.9
c1mim-bf4-conf1	b3lyp-acct	-3814493.7	-15078.9	-812.2	-75.6	-28.8	36.4	-12.5	17.2
c1mim-bf4-conf1	b3lyp-ccd	-3814456.0	-15120.7	-806.1	-92.9	8.9	-5.4	-6.4	-0.1
c1mim-bf4-conf1	b3lyp-cct	-3814493.2	-15080.9	-813.2	-78.4	-28.2	34.4	-13.5	14.5
c1mim-bf4-conf2	b3lyp-accd	-3814469.3	-15105.4	-805.4	-79.1	-6.8	11.8	-9.6	15.1
c1mim-bf4-conf2	b3lyp-acct	-3814491.3	-15080.3	-809.6	-77.0	-28.9	37.0	-13.7	17.2
c1mim-bf4-conf2	b3lyp-ccd	-3814455.1	-15120.4	-800.5	-92.8	7.4	-3.2	-4.6	1.3
c1mim-bf4-conf2	b3lyp-cct	-3814494.6	-15079.6	-808.8	-77.9	-32.2	37.6	-12.9	16.2
c1mim-cl-conf1	b3lyp-accd	-4007054.8	-9309.6	-875.0	-83.3	-29.0	42.4	-26.3	37.2
c1mim-cl-conf1	b3lyp-acct	-4007070.0	-9291.0	-873.5	-80.8	-44.1	61.0	-24.8	39.8
c1mim-cl-conf1	b3lyp-ccd	-4007041.6	-9325.2	-874.6	-93.2	-15.7	26.8	-25.9	27.3
c1mim-cl-conf1	b3lyp-cct	-4007068.3	-9295.2	-875.1	-83.7	-42.4	56.7	-26.4	36.8
c1mim-cl-conf2	b3lyp-accd	-4007061.0	-9303.3	-880.5	-79.1	-14.6	23.2	-15.3	23.1
c1mim-cl-conf2	b3lyp-acct	-4007075.4	-9287.3	-880.0	-78.2	-28.9	39.2	-14.8	24.0
c1mim-cl-conf2	b3lyp-ccd	-4007049.8	-9312.5	-879.3	-83.6	-3.3	14.0	-14.1	18.6
c1mim-cl-conf2	b3lyp-cct	-4007074.1	-9289.6	-879.9	-80.1	-27.6	37.0	-14.7	22.1

3 Energies of 2IPs with b3lyp-d3

System	Theory	HF	Cor	Int HF	Int Cor	HF Diff	Cor Diff	Int HF Diff	Int Cor Diff
c1mim-bf4-conf1	b3lyp-d3-accd	-3814462.7	-15116.2	-803.0	-90.7	2.2	-0.9	-3.3	2.1
c1mim-bf4-conf1	b3lyp-d3-acct	-3814487.1	-15090.9	-806.9	-88.1	-22.2	24.4	-7.1	4.7
c1mim-bf4-conf1	b3lyp-d3-ccd	-3814444.7	-15130.1	-795.0	-103.0	20.2	-14.9	4.7	-10.1
c1mim-bf4-conf1	b3lyp-d3-cct	-3814485.9	-15092.0	-807.0	-90.0	-21.0	23.3	-7.2	2.8
c1mim-bf4-conf2	b3lyp-d3-accd	-3814458.7	-15120.7	-800.4	-94.8	3.8	-3.5	-4.5	-0.7
c1mim-bf4-conf2	b3lyp-d3-acct	-3814484.2	-15093.8	-804.8	-90.8	-21.8	23.4	-8.9	3.3
c1mim-bf4-conf2	b3lyp-d3-ccd	-3814438.8	-15133.1	-786.8	-105.4	23.7	-15.9	9.1	-11.2
c1mim-bf4-conf2	b3lyp-d3-cct	-3814482.1	-15093.7	-801.1	-91.3	-19.6	23.5	-5.2	2.8
c1mim-cl-conf1	b3lyp-d3-accd	-4007028.2	-9347.4	-851.4	-119.4	-2.3	4.5	-2.7	1.2
c1mim-cl-conf1	b3lyp-d3-acct	-4007046.3	-9327.5	-854.1	-114.3	-20.4	24.4	-5.4	6.3
c1mim-cl-conf1	b3lyp-d3-ccd	-4007017.0	-9356.3	-851.3	-123.4	8.9	-4.4	-2.5	-2.9
c1mim-cl-conf1	b3lyp-d3-cct	-4007044.8	-9329.1	-853.9	-115.4	-18.9	22.8	-5.2	5.2
c1mim-cl-conf2	b3lyp-d3-accd	-4007053.3	-9317.6	-877.7	-93.6	-6.9	9.0	-12.5	8.5
c1mim-cl-conf2	b3lyp-d3-acct	-4007068.5	-9300.8	-878.2	-91.6	-22.1	25.8	-13.0	10.6
c1mim-cl-conf2	b3lyp-d3-ccd	-4007042.2	-9325.0	-879.2	-96.1	4.2	1.5	-14.0	6.1
c1mim-cl-conf2	b3lyp-d3-cct	-4007066.5	-9302.7	-878.0	-93.2	-20.1	23.8	-12.8	9.0

4 Energies of 2IPs with blyp

System	Theory	HF	Cor	Int HF	Int Cor	HF Diff	Cor Diff	Int HF Diff	Int Cor Diff
c1mim-bf4-conf1	blyp-accd	-3814420.8	-15136.9	-808.4	-73.1	44.1	-21.6	-8.7	19.7
c1mim-bf4-conf1	blyp-acct	-3814455.8	-15109.9	-809.6	-70.0	9.1	5.4	-9.9	22.8
c1mim-bf4-conf1	blyp-ccd	-3814408.1	-15154.6	-807.2	-90.2	56.8	-39.4	-7.5	2.7
c1mim-bf4-conf1	blyp-cct	-3814456.7	-15112.6	-811.7	-73.7	8.2	2.7	-12.0	19.1
c1mim-bf4-conf2	blyp-accd	-3814419.0	-15137.4	-803.2	-73.5	43.5	-20.2	-7.4	20.7
c1mim-bf4-conf2	blyp-acct	-3814454.3	-15109.9	-804.0	-69.9	8.2	7.4	-8.2	24.2
c1mim-bf4-conf2	blyp-ccd	-3814404.1	-15151.8	-801.2	-85.8	58.4	-34.6	-5.3	8.4
c1mim-bf4-conf2	blyp-cct	-3814457.7	-15111.5	-806.3	-73.5	4.7	5.7	-10.4	20.6
c1mim-cl-conf1	blyp-accd	-4007023.8	-9331.6	-878.6	-79.5	2.1	20.3	-29.9	41.0
c1mim-cl-conf1	blyp-acct	-4007047.2	-9311.4	-875.7	-76.7	-21.3	40.5	-27.0	43.9
c1mim-cl-conf1	blyp-ccd	-4007006.8	-9348.9	-880.2	-89.8	19.1	3.0	-31.5	30.7
c1mim-cl-conf1	blyp-cct	-4007045.5	-9316.6	-878.3	-80.3	-19.6	35.3	-29.6	40.2
c1mim-cl-conf2	blyp-accd	-4007029.3	-9324.4	-881.0	-74.4	17.2	2.2	-15.8	27.8
c1mim-cl-conf2	blyp-acct	-4007052.2	-9307.0	-880.2	-73.2	-5.8	19.6	-15.0	28.9
c1mim-cl-conf2	blyp-ccd	-4007014.4	-9335.5	-880.5	-79.8	32.1	-9.0	-15.3	22.3
c1mim-cl-conf2	blyp-cct	-4007050.8	-9309.8	-880.9	-75.4	-4.4	16.8	-15.7	26.8

5 Energies of 2IPs with blyp-d3

System	Theory	HF	Cor	Int HF	Int Cor	HF Diff	Cor Diff	Int HF Diff	Int Cor Diff
c1mim-bf4-conf1	blyp-d3-ccd	-3814397.0	-15165.4	-794.7	-102.3	67.9	-50.1	5.1	-9.5
c1mim-bf4-conf1	blyp-d3-cct	-3814451.4	-15125.5	-806.5	-87.8	13.5	-10.2	-6.8	5.1
c1mim-bf4-conf1	blyp-d3-ccd	-3814391.5	-15168.3	-786.2	-104.6	71.0	-51.0	9.7	-10.4
c1mim-bf4-conf2	blyp-d3-cct	-3814453.1	-15124.4	-803.4	-87.4	9.3	-7.2	-7.5	6.8
c1mim-cl-conf1	blyp-d3-ccd	-4006980.6	-9383.6	-855.0	-124.2	45.3	-31.7	-6.3	-3.6
c1mim-cl-conf1	blyp-d3-cct	-4007021.3	-9353.1	-857.4	-114.9	4.6	-1.2	-8.7	5.6
c1mim-cl-conf2	blyp-d3-ccd	-4007006.6	-9349.2	-881.9	-93.1	39.9	-22.6	-16.7	9.1
c1mim-cl-conf2	blyp-d3-cct	-4007043.8	-9323.9	-880.1	-89.5	2.7	2.7	-14.9	12.7

6 Energies of 2IPs with bp86-d3

System	Theory	HF	Cor	Int HF	Int Cor	HF Diff	Cor Diff	Int HF Diff	Int Cor Diff
c1mim-bf4-conf1	bp86-d3-accd	-3814421.3	-15147.3	-800.0	-92.1	43.6	-32.1	-0.3	0.7
c1mim-bf4-conf1	bp86-d3-acct	-3814455.4	-15122.5	-803.9	-89.7	9.5	-7.2	-4.1	3.1
c1mim-bf4-conf1	bp86-d3-ccd	-3814400.1	-15162.3	-790.8	-105.4	64.8	-47.1	8.9	-12.6
c1mim-bf4-conf1	bp86-d3-cct	-3814454.1	-15123.9	-803.9	-91.9	10.8	-8.6	-4.1	1.0
c1mim-bf4-conf2	bp86-d3-accd	-3814420.5	-15147.7	-796.2	-92.2	42.0	-30.5	-0.3	2.0
c1mim-bf4-conf2	bp86-d3-acct	-3814455.4	-15121.5	-799.6	-88.8	7.1	-4.3	-3.7	5.3
c1mim-bf4-conf2	bp86-d3-ccd	-3814393.4	-15165.0	-781.8	-107.2	69.1	-47.8	14.1	-13.1
c1mim-bf4-conf2	bp86-d3-cct	-3814449.7	-15125.8	-797.6	-93.1	12.8	-8.6	-1.7	1.0
c1mim-cl-conf1	bp86-d3-accd	-4006987.6	-9381.3	-846.6	-130.7	38.3	-29.4	2.1	-10.1
c1mim-cl-conf1	bp86-d3-acct	-4007012.9	-9361.4	-850.0	-125.1	13.0	-9.5	-1.3	-4.6
c1mim-cl-conf1	bp86-d3-ccd	-4006972.6	-9389.8	-847.8	-133.4	53.2	-37.9	0.9	-12.9
c1mim-cl-conf1	bp86-d3-cct	-4007011.2	-9362.6	-849.9	-125.8	14.7	-10.7	-1.2	-5.3
c1mim-cl-conf2	bp86-d3-accd	-4007017.3	-9345.7	-875.7	-98.9	29.1	-19.2	-10.5	3.2
c1mim-cl-conf2	bp86-d3-acct	-4007039.1	-9328.8	-876.3	-96.4	7.4	-2.3	-11.1	5.8
c1mim-cl-conf2	bp86-d3-ccd	-4007002.0	-9353.2	-877.1	-100.4	44.5	-26.7	-11.9	1.8
c1mim-cl-conf2	bp86-d3-cct	-4007036.7	-9330.5	-876.3	-97.4	9.8	-4.0	-11.1	4.7

7 Energies of 2IPs with df-mp2

System	Theory	HF	Cor	Int HF	Int Cor	HF Diff	Cor Diff	Int HF Diff	Int Cor Diff
c1mim-bf4-conf1	df-mp2-ccd	-3814430.5	-15144.4	-793.5	-101.8	34.5	-29.1	6.2	-9.0
c1mim-bf4-conf1	df-mp2-cct	-3814477.7	-15100.8	-800.9	-95.5	-12.8	14.5	-1.2	-2.6
c1mim-bf4-conf2	df-mp2-ccd	-3814423.9	-15148.6	-785.8	-105.2	38.5	-31.4	10.1	-11.1
c1mim-bf4-conf2	df-mp2-cct	-3814472.6	-15104.2	-794.6	-98.1	-10.1	13.0	1.3	-4.0
c1mim-cl-conf1	df-mp2-ccd	-4007000.6	-9373.0	-845.9	-128.0	25.3	-21.0	2.8	-7.5
c1mim-cl-conf1	df-mp2-cct	-4007022.6	-9352.2	-837.5	-132.0	3.3	-0.3	11.2	-11.4
c1mim-cl-conf2	df-mp2-ccd	-4007031.5	-9338.1	-874.1	-100.7	15.0	-11.5	-8.9	1.5
c1mim-cl-conf2	df-mp2-cct	-4007050.0	-9321.0	-864.7	-107.7	-3.6	5.6	0.5	-5.5

8 Energies of 2IPs with m062x

System	Theory	HF	Cor	Int HF	Int Cor	HF Diff	Cor Diff	Int HF Diff	Int Cor Diff
c1mim-bf4-conf1	m062x-accd	-3814457.0	-15116.5	-786.7	-105.0	7.9	-1.2	13.1	-12.1
c1mim-bf4-conf1	m062x-acct	-3814480.6	-15090.7	-793.4	-100.5	-15.7	24.5	6.3	-7.7
c1mim-bf4-conf1	m062x-ccd	-3814438.0	-15127.9	-775.9	-114.2	26.9	-12.6	23.8	-21.3
c1mim-bf4-conf1	m062x-cct	-3814478.7	-15091.7	-792.7	-102.0	-13.7	23.6	7.0	-9.2
c1mim-bf4-conf2	m062x-accd	-3814448.9	-15123.7	-780.0	-111.7	13.5	-6.5	15.9	-17.6
c1mim-bf4-conf2	m062x-acct	-3814474.1	-15097.0	-788.4	-106.2	-11.6	20.2	7.5	-12.1
c1mim-bf4-conf2	m062x-ccd	-3814428.5	-15134.3	-765.5	-119.6	34.0	-17.1	30.4	-25.5
c1mim-bf4-conf2	m062x-cct	-3814472.1	-15097.9	-787.4	-107.8	-9.6	19.3	8.5	-13.6
c1mim-cl-conf1	m062x-accd	-4007024.7	-9348.4	-837.7	-129.4	1.2	3.5	11.0	-8.9
c1mim-cl-conf1	m062x-acct	-4007038.0	-9333.2	-839.3	-126.6	-12.2	18.7	9.5	-6.0
c1mim-cl-conf1	m062x-ccd	-4007020.2	-9352.9	-840.8	-130.2	5.7	-1.0	8.0	-9.6
c1mim-cl-conf1	m062x-cct	-4007038.9	-9332.8	-840.7	-125.8	-13.0	19.1	8.0	-5.3
c1mim-cl-conf2	m062x-accd	-4007055.4	-9314.9	-874.0	-100.6	-8.9	11.6	-8.8	1.5
c1mim-cl-conf2	m062x-acct	-4007066.9	-9300.8	-875.2	-98.8	-20.4	25.7	-10.0	3.4
c1mim-cl-conf2	m062x-ccd	-4007048.0	-9319.9	-876.8	-102.0	-1.5	6.6	-11.6	0.1
c1mim-cl-conf2	m062x-cct	-4007065.2	-9302.2	-875.3	-99.9	-18.7	24.3	-10.1	2.3

9 Energies of 2IPs with pbe

System	Theory	HF	Cor	Int HF	Int Cor	HF Diff	Cor Diff	Int HF Diff	Int Cor Diff
c1mim-bf4-conf1	pbe-accd	-3814433.5	-15133.0	-808.0	-80.7	31.4	-17.7	-8.2	12.1
c1mim-bf4-conf1	pbe-acct	-3814465.5	-15108.1	-810.7	-77.9	-0.6	7.2	-11.0	14.9
c1mim-bf4-conf1	pbe-ccd	-3814416.3	-15149.6	-802.3	-96.6	48.6	-34.3	-2.6	-3.7
c1mim-bf4-conf1	pbe-cct	-3814464.7	-15110.5	-811.4	-81.3	0.2	4.8	-11.7	11.5
c1mim-bf4-conf2	pbe-accd	-3814431.7	-15134.1	-802.2	-81.8	30.8	-16.9	-6.3	12.3
c1mim-bf4-conf2	pbe-acct	-3814461.1	-15109.0	-805.5	-78.2	1.4	8.2	-9.6	15.9
c1mim-bf4-conf2	pbe-ccd	-3814410.7	-15149.4	-794.5	-95.5	51.8	-32.2	1.4	-1.4
c1mim-bf4-conf2	pbe-cct	-3814465.6	-15110.0	-806.0	-81.6	-3.1	7.2	-10.1	12.6
c1mim-cl-conf1	pbe-accd	-4007022.4	-9341.1	-874.7	-94.8	3.4	10.8	-26.0	25.7
c1mim-cl-conf1	pbe-acct	-4007043.4	-9322.4	-874.8	-90.7	-17.5	29.5	-26.0	29.8
c1mim-cl-conf1	pbe-ccd	-4007004.5	-9356.2	-872.4	-104.5	21.4	-4.3	-23.7	16.0
c1mim-cl-conf1	pbe-cct	-4007040.1	-9326.9	-874.3	-94.2	-14.3	25.0	-25.6	26.3
c1mim-cl-conf2	pbe-accd	-4007032.0	-9328.3	-880.2	-85.4	14.5	-1.7	-15.0	16.8
c1mim-cl-conf2	pbe-acct	-4007050.2	-9313.9	-879.7	-84.4	-3.8	12.7	-14.5	17.7
c1mim-cl-conf2	pbe-ccd	-4007016.5	-9337.9	-878.3	-90.0	29.9	-11.3	-13.1	12.1
c1mim-cl-conf2	pbe-cct	-4007048.2	-9316.1	-879.5	-86.3	-1.7	10.4	-14.3	15.9

10 Energies of 2IPs with pbe-d3

System	Theory	HF	Cor	Int HF	Int Cor	HF Diff	Cor Diff	Int HF Diff	Int Cor Diff
clmim-bf4-conf1	pbe-d3-accd	-3814429.5	-15140.0	-803.8	-88.4	35.4	-24.7	-4.1	4.4
clmim-bf4-conf1	pbe-d3-acct	-3814461.6	-15115.6	-807.5	-85.8	3.3	-0.3	-7.7	7.0
clmim-bf4-conf1	pbe-d3-ccd	-3814409.2	-15155.5	-795.3	-102.9	55.7	-40.2	4.4	-10.0
clmim-bf4-conf1	pbe-d3-cct	-3814460.2	-15117.5	-807.5	-88.6	4.7	-2.2	-7.7	4.3
clmim-bf4-conf2	pbe-d3-accd	-3814428.9	-15140.6	-799.7	-89.0	33.6	-23.4	-3.8	5.1
clmim-bf4-conf2	pbe-d3-acct	-3814461.6	-15115.1	-802.9	-85.6	0.9	2.1	-7.0	8.5
clmim-bf4-conf2	pbe-d3-ccd	-3814402.7	-15158.5	-786.0	-105.2	59.8	-41.3	9.9	-11.0
clmim-bf4-conf2	pbe-d3-cct	-3814455.9	-15119.5	-801.0	-90.1	6.6	-2.2	-5.1	4.0
clmim-cl-conf1	pbe-d3-accd	-4007004.0	-9366.1	-857.5	-119.3	21.9	-14.2	-8.8	1.3
clmim-cl-conf1	pbe-d3-acct	-4007026.0	-9347.5	-860.3	-114.1	-0.1	4.4	-11.6	6.4
clmim-cl-conf1	pbe-d3-ccd	-4006987.9	-9376.3	-857.1	-124.1	38.0	-24.4	-8.4	-3.6
clmim-cl-conf1	pbe-d3-cct	-4007023.7	-9349.3	-860.0	-115.2	2.1	2.6	-11.3	5.3
clmim-cl-conf2	pbe-d3-accd	-4007027.1	-9337.2	-878.6	-94.5	19.3	-10.6	-13.4	7.7
clmim-cl-conf2	pbe-d3-acct	-4007045.9	-9322.0	-878.6	-92.5	0.6	4.6	-13.4	9.7
clmim-cl-conf2	pbe-d3-ccd	-4007011.2	-9345.9	-879.2	-97.4	35.3	-19.3	-14.0	4.7
clmim-cl-conf2	pbe-d3-cct	-4007043.2	-9324.0	-878.5	-93.9	3.3	2.6	-13.3	8.3

11 Energies of 2IPs with srs-fmo2

System	Theory	HF	Cor	Int HF	Int Cor	HF Diff	Cor Diff	Int HF Diff	Int Cor Diff
clmim-bf4-conf1	srs-fmo2-ccd	-3814387.7	-15173.6	-788.7	-103.5	77.2	-58.3	11.0	-10.7
clmim-bf4-conf1	srs-fmo2-cct	-3814467.0	-15114.6	-802.1	-92.3	-2.1	0.7	-2.4	0.6
clmim-bf4-conf2	srs-fmo2-ccd	-3814380.7	-15178.6	-780.6	-107.5	81.8	-61.3	15.3	-13.3
clmim-bf4-conf2	srs-fmo2-cct	-3814461.4	-15117.5	-795.8	-93.9	1.1	-0.2	0.1	0.2
clmim-cl-conf1	srs-fmo2-ccd	-4006958.7	-9400.4	-837.2	-133.5	67.2	-48.5	11.5	-13.0
clmim-cl-conf1	srs-fmo2-cct	-4007001.6	-9368.0	-828.4	-135.1	24.3	-16.1	20.3	-14.6
clmim-cl-conf2	srs-fmo2-ccd	-4006996.6	-9362.0	-869.8	-104.3	49.9	-35.5	-4.6	-2.2
clmim-cl-conf2	srs-fmo2-cct	-4007044.0	-9328.6	-863.2	-104.7	2.5	-2.1	2.0	-2.5

12 Energies of 2IPs with srs-fmo3

System	Theory	HF	Cor	Int HF	Int Cor	HF Diff	Cor Diff	Int HF Diff	Int Cor Diff
clmim-bf4-conf1	srs-fmo3-ccd	-3814390.1	-15172.2	-790.6	-101.7	74.8	-56.9	9.1	-8.8
clmim-bf4-conf1	srs-fmo3-cct	-3814464.9	-15115.3	-799.7	-92.9	0.0	0.0	0.0	0.0
clmim-bf4-conf2	srs-fmo3-ccd	-3814383.7	-15176.5	-783.4	-105.1	78.8	-59.3	12.5	-10.9
clmim-bf4-conf2	srs-fmo3-cct	-3814462.5	-15117.2	-795.9	-94.1	0.0	0.0	0.0	0.0
clmim-cl-conf1	srs-fmo3-ccd	-4006975.5	-9389.1	-851.5	-123.5	50.4	-37.2	-2.8	-3.0
clmim-cl-conf1	srs-fmo3-cct	-4007025.9	-9351.9	-848.7	-120.5	0.0	0.0	0.0	0.0
clmim-cl-conf2	srs-fmo3-ccd	-4007004.8	-9355.9	-873.9	-98.5	41.6	-29.4	-8.7	3.6
clmim-cl-conf2	srs-fmo3-cct	-4007046.5	-9326.6	-865.2	-102.2	0.0	0.0	0.0	0.0

13 Energies of 2IPs with tpss-d3

System	Theory	HF	Cor	Int HF	Int Cor	HF Diff	Cor Diff	Int HF Diff	Int Cor Diff
clmim-bf4-conf1	tpss-d3-accd	-3814442.2	-15132.1	-803.4	-87.7	22.7	-16.8	-3.7	5.2
clmim-bf4-conf1	tpss-d3-acct	-3814471.7	-15107.5	-807.1	-85.0	-6.8	7.8	-7.4	7.9
clmim-bf4-conf1	tpss-d3-ced	-3814424.1	-15147.4	-795.3	-101.5	40.9	-32.1	4.4	-8.7
clmim-bf4-conf1	tpss-d3-cct	-3814470.5	-15109.3	-807.1	-87.6	-5.6	6.0	-7.4	5.3
clmim-bf4-conf2	tpss-d3-accd	-3814441.7	-15133.1	-799.7	-88.7	20.8	-15.9	-3.8	5.4
clmim-bf4-conf2	tpss-d3-acct	-3814471.5	-15107.4	-803.0	-85.2	-9.0	9.8	-7.1	9.0
clmim-bf4-conf2	tpss-d3-ced	-3814417.9	-15150.4	-786.8	-103.9	44.6	-33.2	9.1	-9.8
clmim-bf4-conf2	tpss-d3-cct	-3814466.3	-15111.5	-801.4	-89.2	-3.8	5.7	-5.5	4.9
clmim-cl-conf1	tpss-d3-accd	-4007014.0	-9360.7	-854.4	-119.5	11.9	-8.8	-5.6	1.1
clmim-cl-conf1	tpss-d3-acct	-4007034.4	-9341.1	-858.8	-113.0	-8.5	10.8	-10.1	7.5
clmim-cl-conf1	tpss-d3-ced	-4007001.8	-9369.2	-854.1	-123.2	24.0	-17.3	-5.4	-2.7
clmim-cl-conf1	tpss-d3-cct	-4007032.8	-9342.5	-858.4	-114.0	-6.9	9.4	-9.6	6.6
clmim-cl-conf2	tpss-d3-accd	-4007035.9	-9332.3	-877.0	-94.6	10.5	-5.7	-11.8	7.5
clmim-cl-conf2	tpss-d3-acct	-4007051.9	-9317.1	-877.0	-92.3	-5.5	9.4	-11.8	9.9
clmim-cl-conf2	tpss-d3-ced	-4007023.5	-9339.4	-877.8	-96.5	23.0	-12.9	-12.6	5.6
clmim-cl-conf2	tpss-d3-cct	-4007050.2	-9318.7	-876.9	-93.5	-3.8	7.9	-11.7	8.7

14 Energies of 2IPs with wb97xd

System	Theory	HF	Cor	Int HF	Int Cor	HF Diff	Cor Diff	Int HF Diff	Int Cor Diff
clmim-bf4-conf1	wb97xd-accd	-3814469.8	-15107.2	-803.0	-92.4	-4.9	8.0	-3.3	0.5
clmim-bf4-conf1	wb97xd-acct	-3814493.2	-15080.6	-807.2	-89.1	-28.3	34.7	-7.5	3.7
clmim-bf4-conf1	wb97xd-ced	-3814454.5	-15119.2	-796.4	-102.4	10.4	-3.9	3.3	-9.5
clmim-bf4-conf1	wb97xd-cct	-3814492.3	-15081.3	-807.5	-90.4	-27.4	34.0	-7.8	2.5
clmim-bf4-conf2	wb97xd-accd	-3814466.1	-15111.0	-799.9	-95.8	-3.6	6.2	-4.1	-1.6
clmim-bf4-conf2	wb97xd-acct	-3814490.3	-15083.5	-804.8	-91.9	-27.8	33.7	-8.9	2.3
clmim-bf4-conf2	wb97xd-ced	-3814449.6	-15123.4	-792.8	-106.4	12.9	-6.2	3.1	-12.3
clmim-bf4-conf2	wb97xd-cct	-3814488.8	-15084.7	-804.4	-93.6	-26.3	32.5	-8.5	0.5
clmim-cl-conf1	wb97xd-accd	-4007034.2	-9338.1	-848.3	-120.1	-8.3	13.8	0.4	0.5
clmim-cl-conf1	wb97xd-acct	-4007049.4	-9319.7	-850.6	-116.0	-23.5	32.3	-1.9	4.6
clmim-cl-conf1	wb97xd-ced	-4007026.5	-9345.3	-849.7	-123.1	-0.7	6.6	-0.9	-2.5
clmim-cl-conf1	wb97xd-cct	-4007048.4	-9321.0	-850.7	-116.9	-22.5	30.9	-2.0	3.6
clmim-cl-conf2	wb97xd-accd	-4007061.3	-9307.8	-877.6	-94.0	-14.8	18.7	-12.4	8.2
clmim-cl-conf2	wb97xd-acct	-4007074.7	-9291.0	-878.8	-91.3	-28.2	35.6	-13.6	10.9
clmim-cl-conf2	wb97xd-ced	-4007054.0	-9313.8	-879.4	-96.2	-7.6	12.7	-14.2	6.0
clmim-cl-conf2	wb97xd-cct	-4007073.2	-9292.8	-878.8	-92.9	-26.7	33.8	-13.6	9.2

15 Energies of 4IPs with b3lyp

System	Theory	HF	Cor	Int HF	Int Cor	HF Diff	Cor Diff	Int HF Diff	Int Cor Diff
clmim-bf4	b3lyp-cct	-7629042.1	-30174.2	-1673.3	-168.1	-75.0	76.9	-39.4	38.3
clmim-cl	b3lyp-cct	-8014218.8	-18598.9	-1829.2	-177.3	-103.7	120.7	-70.0	88.9
clmpyr-bf4	b3lyp-cct	-7485357.1	-30959.6	-1665.1	-197.9	-83.0	91.0	-62.9	75.1
clmpyr-cl	b3lyp-cct	-7870525.5	-19392.8	-1802.3	-220.0	-66.7	71.0	-48.5	58.3
nme4-bf4	b3lyp-cct	-6677444.4	-26785.2	-1709.2	-192.0	-27.8	37.2	-13.0	24.5
nme4-cl	b3lyp-cct	-7062615.1	-15210.6	-1841.3	-208.4	-59.9	35.9	-46.5	29.2
pyr-bf4	b3lyp-cct	-7858787.4	-31600.0	-1652.3	-210.8	-96.6	119.7	-50.3	80.9
pyr-cl	b3lyp-cct	-8243891.8	-20017.3	-1739.3	-214.2	-129.0	127.8	-94.3	96.5

16 Energies of 4IPs with b3lyp-d3

System	Theory	HF	Cor	Int HF	Int Cor	HF Diff	Cor Diff	Int HF Diff	Int Cor Diff
c1mim-bf4	b3lyp-d3-accd	-7628963.9	-30251.9	-1640.2	-202.3	3.2	-0.7	-6.3	4.1
c1mim-bf4	b3lyp-d3-cct	-7629019.6	-30215.8	-1651.5	-210.0	-52.4	35.4	-17.6	-3.6
c1mim-cl	b3lyp-d3-accd	-8014130.4	-18702.7	-1778.0	-253.3	-15.3	17.0	-18.7	12.8
c1mim-cl	b3lyp-d3-cct	-8014218.8	-18598.9	-1829.2	-177.3	-103.7	120.7	-70.0	88.8
c1mpyr-bf4	b3lyp-d3-accd	-7485272.6	-31053.0	-1615.7	-261.8	1.5	-2.4	-13.5	11.2
c1mpyr-bf4	b3lyp-d3-cct	-7485324.1	-31002.9	-1633.0	-247.4	-50.0	47.7	-30.8	25.6
c1mpyr-cl	b3lyp-d3-accd	-7870450.7	-19476.5	-1747.7	-288.5	8.0	-12.7	6.1	-10.2
c1mpyr-cl	b3lyp-d3-cct	-7870525.5	-19392.8	-1802.3	-220.0	-66.8	71.1	-48.5	58.4
nme4-bf4	b3lyp-d3-accd	-6677376.6	-26857.1	-1671.9	-236.0	39.9	-34.8	24.3	-19.5
nme4-bf4	b3lyp-d3-cct	-6677420.6	-26815.8	-1684.9	-227.1	-4.1	6.6	11.3	-10.6
nme4-cl	b3lyp-d3-accd	-7062524.4	-15274.5	-1769.5	-260.4	30.8	-28.0	25.3	-22.9
nme4-cl	b3lyp-d3-cct	-7062584.6	-15269.8	-1810.6	-271.2	-29.4	-23.3	-15.8	-33.7
pyr-bf4	b3lyp-d3-accd	-7858694.8	-31714.3	-1600.2	-283.4	-4.0	5.4	1.8	8.3
pyr-bf4	b3lyp-d3-cct	-7858749.5	-31654.8	-1614.6	-271.6	-58.7	64.9	-12.6	20.1
pyr-cl	b3lyp-d3-accd	-8243778.6	-20156.9	-1655.9	-326.4	-15.8	-11.7	-10.9	-15.7
pyr-cl	b3lyp-d3-cct	-8243778.6	-20156.9	-1655.9	-326.4	-15.8	-11.7	-10.9	-15.7

17 Energies of 4IPs with blyp

System	Theory	HF	Cor	Int HF	Int Cor	HF Diff	Cor Diff	Int HF Diff	Int Cor Diff
c1mim-bf4	blyp-cct	-7628970.4	-30228.6	-1669.9	-150.4	-3.3	22.6	-36.0	56.1
c1mim-cl	blyp-cct	-8014174.2	-18638.5	-1831.6	-168.8	-59.1	81.1	-72.4	97.4
c1mpyr-bf4	blyp-cct	-7485289.6	-31003.8	-1662.8	-187.4	-15.5	46.8	-60.6	85.6
c1mpyr-cl	blyp-cct	-7870494.3	-19404.3	-1809.4	-202.7	-35.6	59.5	-55.6	75.7
nme4-bf4	blyp-cct	-6677385.9	-26824.6	-1708.5	-182.4	30.6	-2.3	-12.3	34.0
nme4-cl	blyp-cct	-7062577.2	-15238.7	-1834.3	-213.2	-22.0	7.8	-39.5	24.4
pyr-bf4	blyp-cct	-7858725.1	-31650.7	-1655.8	-193.7	-34.4	68.9	-53.8	98.0
pyr-cl	blyp-cct	-8243868.7	-20042.0	-1754.5	-197.6	-106.0	103.1	-109.5	113.1

18 Energies of 4IPs with blyp-d3

System	Theory	HF	Cor	Int HF	Int Cor	HF Diff	Cor Diff	Int HF Diff	Int Cor Diff
c1mim-bf4	blyp-d3-cct	-7628942.4	-30269.0	-1648.7	-194.2	24.8	-17.8	-14.8	12.2
c1mim-cl	blyp-d3-cct	-8014118.8	-18710.9	-1786.5	-242.4	-3.7	8.7	-27.2	23.8
c1mpyr-bf4	blyp-d3-cct	-7485263.0	-31056.4	-1634.3	-248.1	11.1	-5.8	-32.2	24.8
c1mpyr-cl	blyp-d3-cct	-7870453.9	-19469.0	-1761.8	-271.8	4.8	-5.2	-8.0	6.5
nme4-bf4	blyp-d3-cct	-6677369.4	-26860.6	-1685.5	-224.4	47.2	-38.3	10.7	-7.9
nme4-cl	blyp-d3-cct	-7062524.7	-15271.3	-1778.9	-249.6	30.5	-24.8	15.9	-12.1
pyr-bf4	blyp-d3-cct	-7858692.2	-31713.6	-1614.3	-266.7	-1.4	6.1	-12.3	25.0
pyr-cl	blyp-d3-cct	-8243768.8	-20136.5	-1654.1	-296.3	-6.0	8.7	-9.0	14.3

19 Energies of 4IPs with hf

System	Theory	HF	Cor	Int HF	Int Cor	HF Diff	Cor Diff	Int HF Diff	Int Cor Diff
c1mim-bf4	hf-cct	-7629093.9	-30051.2	-1682.8	-145.7	-126.7	199.9	-48.9	60.7
c1mim-cl	hf-cct	-8014256.4	-18503.3	-1833.4	-148.4	-141.3	216.3	-74.1	117.7
c1mpyr-bf4	hf-cct	-7485396.4	-30866.6	-1676.1	-171.9	-122.3	184.0	-74.0	101.1
c1mpyr-cl	hf-cct	-7870551.9	-19322.9	-1811.8	-182.6	-93.2	140.9	-58.0	95.7
nme4-bf4	hf-cct	-6677481.5	-26694.8	-1717.1	-164.1	-65.0	127.6	-20.9	52.4
nme4-cl	hf-cct	-7062639.5	-15147.0	-1850.1	-171.8	-84.3	99.5	-55.3	65.8
pyr-bf4	hf-cct	-7858839.7	-31486.4	-1674.8	-177.8	-148.9	233.3	-72.8	113.9
pyr-cl	hf-cct	-8243940.3	-19928.0	-1765.5	-171.8	-177.6	217.2	-120.5	138.8

20 Energies of 4IPs with m062x

System	Theory	HF	Cor	Int HF	Int Cor	HF Diff	Cor Diff	Int HF Diff	Int Cor Diff
c1mim-bf4	m062x-accd	-7628943.7	-30259.5	-1598.7	-237.5	23.4	-8.4	35.3	-31.1
c1mim-bf4	m062x-cct	-7628989.9	-30208.0	-1614.2	-229.0	-22.7	43.2	19.7	-22.5
c1mim-cl	m062x-accd	-8014123.0	-18706.8	-1759.4	-275.8	-7.9	12.8	-0.2	-9.7
c1mim-cl	m062x-cct	-8014155.8	-18669.7	-1771.6	-262.6	-40.6	49.9	-12.3	3.6
c1mpyr-bf4	m062x-accd	-7485235.5	-31074.2	-1573.1	-295.0	38.6	-23.6	29.0	-22.0
c1mpyr-bf4	m062x-cct	-7485290.9	-31022.9	-1600.0	-277.6	-16.8	27.7	2.2	-4.7
c1mpyr-cl	m062x-accd	-7870446.4	-19473.0	-1744.2	-288.3	12.3	-9.2	9.6	-9.9
c1mpyr-cl	m062x-cct	-7870475.6	-19449.3	-1755.7	-280.2	-16.8	14.5	-1.9	-1.8
nme4-bf4	m062x-accd	-6677337.7	-26876.1	-1626.1	-267.8	78.8	-53.7	70.1	-51.4
nme4-bf4	m062x-cct	-6677397.0	-26839.3	-1657.4	-262.4	19.5	-17.0	38.8	-45.9
nme4-cl	m062x-accd	-7062507.1	-15282.3	-1753.2	-271.6	48.1	-35.7	41.6	-34.0
nme4-cl	m062x-cct	-7062522.2	-15267.0	-1753.1	-268.7	33.0	-20.4	41.7	-31.2
pyr-bf4	m062x-accd	-7858638.4	-31751.0	-1533.5	-337.7	52.4	-31.3	68.5	-46.0
pyr-bf4	m062x-cct	-7858700.0	-31688.5	-1562.4	-319.1	-9.2	31.2	39.6	-27.4
pyr-cl	m062x-accd	-8243790.1	-20157.7	-1661.1	-334.9	-27.3	-12.6	-16.1	-24.3
pyr-cl	m062x-cct	-8243818.7	-20127.3	-1670.3	-330.0	-56.0	17.8	-25.3	-19.3

21 Energies of 4IPs with pbe

System	Theory	HF	Cor	Int HF	Int Cor	HF Diff	Cor Diff	Int HF Diff	Int Cor Diff
c1mim-bf4	pbe-cct	-7629036.1	-30162.0	-1663.9	-179.6	-69.0	89.2	-30.0	26.8
c1mim-cl	pbe-cct	-8014210.6	-18607.1	-1823.4	-196.7	-95.5	112.5	-64.1	69.4
c1mpyr-bf4	pbe-cct	-7485359.6	-30957.3	-1663.1	-210.0	-85.5	93.3	-60.9	63.0
c1mpyr-cl	pbe-cct	-7870510.0	-19410.8	-1793.4	-241.0	-51.3	53.0	-39.6	37.3
nme4-bf4	pbe-cct	-6677446.6	-26782.5	-1707.1	-203.2	-30.1	39.8	-10.9	13.3
nme4-cl	pbe-cct	-7062575.2	-15252.5	-1832.7	-229.0	-20.0	-6.0	-37.9	8.6
pyr-bf4	pbe-cct	-7858789.9	-31600.3	-1647.2	-229.0	-99.1	119.4	-45.2	62.7
pyr-cl	pbe-cct	-8243894.9	-20030.1	-1745.4	-232.4	-132.2	115.0	-100.4	78.3

22 Energies of 4IPs with pbe-d3

System	Theory	HF	Cor	Int HF	Int Cor	HF Diff	Cor Diff	Int HF Diff	Int Cor Diff
c1mim-bf4	pbe-d3-cct	-7628961.0	-30251.6	-1651.6	-194.3	6.2	-0.4	-17.7	12.1
c1mim-cl	pbe-d3-cct	-8014121.2	-18707.7	-1786.8	-247.5	-6.1	12.0	-27.5	18.7
c1mpyr-bf4	pbe-d3-cct	-7485286.3	-31039.6	-1638.5	-240.2	-12.2	11.0	-36.3	32.7
c1mpyr-cl	pbe-d3-cct	-7870448.2	-19476.1	-1760.2	-278.3	10.5	-12.2	-6.4	0.1
nme4-bf4	pbe-d3-cct	-6677382.9	-26851.6	-1689.0	-224.2	33.7	-29.3	7.2	-7.8
nme4-cl	pbe-d3-cct	-7062521.7	-15276.6	-1779.9	-255.1	33.5	-30.1	14.9	-17.6
pyr-bf4	pbe-d3-cct	-7858712.3	-31700.3	-1623.1	-263.7	-21.5	19.4	-21.1	28.1
pyr-cl	pbe-d3-cct	-8243767.9	-20135.9	-1657.3	-298.1	-5.1	9.2	-12.3	12.6

23 Energies of 4IPs with srs-fmo2

System	Theory	HF	Cor	Int HF	Int Cor	HF Diff	Cor Diff	Int HF Diff	Int Cor Diff
c1mim-bf4	srs-fmo2-cct	-7628800.8	-30377.5	-1599.8	-236.9	166.4	-126.3	34.1	-30.5
c1mim-bf4	srs-fmo2-cct	-7628964.4	-30255.0	-1632.7	-209.9	2.8	-3.8	1.2	-3.5
c1mim-cl	srs-fmo2-cct	-8014011.5	-18793.7	-1761.4	-274.0	103.6	-74.1	-2.2	-7.8
c1mim-cl	srs-fmo2-cct	-8014091.9	-18726.3	-1740.6	-272.7	23.2	-6.7	18.7	-6.6
c1mpyr-bf4	srs-fmo2-cct	-7485157.5	-31130.5	-1610.3	-272.2	116.6	-79.8	-8.2	0.8
c1mpyr-bf4	srs-fmo2-cct	-7485302.3	-31027.6	-1632.6	-249.5	-28.2	23.0	-30.4	23.4
c1mpyr-cl	srs-fmo2-cct	-7870363.0	-19522.4	-1738.5	-289.5	95.8	-58.6	15.2	-11.1
c1mpyr-cl	srs-fmo2-cct	-7870440.1	-19476.3	-1736.2	-291.3	18.7	-12.4	17.6	-12.9
nme4-bf4	srs-fmo2-cct	-6677284.6	-26916.0	-1675.7	-239.3	132.0	-93.7	20.5	-22.8
nme4-bf4	srs-fmo2-cct	-6677407.4	-26828.7	-1687.3	-223.7	9.1	-6.3	8.9	-7.2
nme4-cl	srs-fmo2-cct	-7062473.3	-15296.8	-1780.6	-249.6	81.9	-50.3	14.2	-12.1
nme4-cl	srs-fmo2-cct	-7062534.6	-15264.2	-1775.0	-254.9	20.6	-17.7	19.8	-17.3
pyr-bf4	srs-fmo2-cct	-7858506.0	-31854.2	-1542.8	-331.7	184.8	-134.5	59.2	-39.9
pyr-bf4	srs-fmo2-cct	-7858686.8	-31718.8	-1586.7	-293.5	4.0	0.9	15.3	-1.8
pyr-cl	srs-fmo2-cct	-8243601.2	-20262.1	-1591.7	-357.2	161.6	-117.0	53.3	-46.6
pyr-cl	srs-fmo2-cct	-8243709.9	-20186.8	-1598.2	-350.9	52.9	-41.7	46.8	-40.3

24 Energies of 4IPs with srs-fmo3

System	Theory	HF	Cor	Int HF	Int Cor	HF Diff	Cor Diff	Int HF Diff	Int Cor Diff
c1mim-bf4	srs-fmo3-cct	-7628812.4	-30369.4	-1611.2	-227.7	154.7	-118.2	22.7	-21.3
c1mim-bf4	srs-fmo3-cct	-7628967.2	-30251.2	-1633.9	-206.4	0.0	0.0	0.0	0.0
c1mim-cl	srs-fmo3-cct	-8014029.3	-18782.3	-1773.1	-262.4	85.8	-62.7	-13.9	3.7
c1mim-cl	srs-fmo3-cct	-8014115.1	-18719.6	-1759.3	-266.1	0.0	0.0	0.0	0.0
c1mpyr-bf4	srs-fmo3-cct	-7485183.3	-31109.5	-1631.3	-250.8	90.8	-58.9	-29.1	22.2
c1mpyr-bf4	srs-fmo3-cct	-7485274.1	-31050.6	-1602.2	-273.0	0.0	0.0	0.0	0.0
c1mpyr-cl	srs-fmo3-cct	-7870405.5	-19496.0	-1777.1	-264.2	53.2	-32.1	-23.3	14.2
c1mpyr-cl	srs-fmo3-cct	-7870458.8	-19463.8	-1753.8	-278.4	0.0	0.0	0.0	0.0
nme4-bf4	srs-fmo3-cct	-6677299.5	-26906.1	-1685.3	-228.8	117.0	-83.7	10.9	-12.4
nme4-bf4	srs-fmo3-cct	-6677416.5	-26822.3	-1696.2	-216.5	0.0	0.0	0.0	0.0
nme4-cl	srs-fmo3-cct	-7062499.2	-15280.4	-1802.7	-234.1	56.0	-33.8	-7.8	3.5
nme4-cl	srs-fmo3-cct	-7062555.2	-15246.5	-1794.8	-237.6	0.0	0.0	0.0	0.0
pyr-bf4	srs-fmo3-cct	-7858540.0	-31830.1	-1574.0	-307.4	150.8	-110.4	28.0	-15.6
pyr-bf4	srs-fmo3-cct	-7858690.8	-31719.7	-1602.0	-291.7	0.0	0.0	0.0	0.0
pyr-cl	srs-fmo3-cct	-8243670.1	-20232.4	-1652.6	-331.1	92.7	-87.3	-7.6	-20.5
pyr-cl	srs-fmo3-cct	-8243762.8	-20145.1	-1645.0	-310.7	0.0	0.0	0.0	0.0

25 Energies of 4IPs with tpss-d3

System	Theory	HF	Cor	Int HF	Int Cor	HF Diff	Cor Diff	Int HF Diff	Int Cor Diff
c1mim-bf4	tpss-d3-cct	-7628982.3	-30234.2	-1651.8	-191.2	-15.1	17.0	-17.9	15.2
c1mim-cl	tpss-d3-cct	-8014136.3	-18696.0	-1784.3	-246.0	-21.2	23.6	-25.1	20.1
c1mpyr-bf4	tpss-d3-cct	-7485305.0	-31025.8	-1642.7	-236.7	-30.9	24.8	-40.6	36.3
c1mpyr-cl	tpss-d3-cct	-7870453.7	-19474.1	-1756.7	-281.6	5.1	-10.3	-2.9	-3.2
nme4-bf4	tpss-d3-cct	-6677398.3	-26839.7	-1691.4	-222.1	18.2	-17.4	4.8	-5.7
nme4-cl	tpss-d3-cct	-7062524.1	-15276.6	-1775.1	-259.8	31.1	-30.1	19.7	-22.2
pyr-bf4	tpss-d3-cct	-7858738.6	-31690.5	-1636.7	-265.8	-47.8	29.2	-34.7	25.9
pyr-cl	tpss-d3-cct	-8243810.6	-20144.6	-1682.7	-317.6	-47.8	0.5	-37.7	-6.9

26 Energies of 4IPs with wb97xd

System	Theory	HF	Cor	Int HF	Int Cor	HF Diff	Cor Diff	Int HF Diff	Int Cor Diff
c1mim-bf4	wb97xd-accd	-7628976.4	-30235.3	-1637.9	-207.2	-9.2	15.8	-4.0	-0.8
c1mim-bf4	wb97xd-ccd	-7628942.4	-30261.7	-1621.2	-229.1	24.8	-10.6	12.7	-22.6
c1mim-bf4	wb97xd-cct	-7629021.2	-30183.0	-1648.0	-202.1	-54.1	68.2	-14.1	4.3
c1mim-cl	wb97xd-accd	-8014144.0	-18684.4	-1776.1	-255.0	-28.9	35.3	-16.8	11.2
c1mim-cl	wb97xd-ccd	-8014130.3	-18696.0	-1779.8	-258.8	-15.2	23.6	-20.5	7.3
c1mim-cl	wb97xd-cct	-8014175.5	-18646.8	-1785.3	-245.2	-60.4	72.8	-26.1	20.9
c1mpyr-bf4	wb97xd-accd	-7485258.3	-31060.6	-1598.3	-276.5	15.8	-10.0	3.8	-3.5
c1mpyr-bf4	wb97xd-ccd	-7485232.4	-31077.2	-1589.6	-284.9	41.7	-26.5	12.5	-11.9
c1mpyr-bf4	wb97xd-cct	-7485312.7	-31008.1	-1619.3	-261.6	-38.6	42.5	-17.2	11.3
c1mpyr-cl	wb97xd-accd	-7870441.9	-19472.1	-1737.8	-287.9	16.9	-8.2	16.0	-9.5
c1mpyr-cl	wb97xd-ccd	-7870439.4	-19483.2	-1748.4	-292.0	19.4	-19.4	5.4	-13.6
c1mpyr-cl	wb97xd-cct	-7870475.9	-19447.3	-1752.0	-282.6	-17.1	16.5	1.8	-4.2
nme4-bf4	wb97xd-accd	-6677371.5	-26872.3	-1663.9	-257.0	45.1	-50.0	32.3	-40.6
nme4-bf4	wb97xd-ccd	-6677342.0	-26879.8	-1653.4	-257.2	74.6	-57.5	42.8	-40.8
nme4-bf4	wb97xd-cct	-6677418.2	-26827.6	-1679.8	-246.5	-1.7	-5.2	16.4	-30.0
nme4-cl	wb97xd-accd	-7062528.4	-15266.8	-1772.5	-256.0	26.8	-20.3	22.3	-18.4
nme4-cl	wb97xd-ccd	-7062517.7	-15276.9	-1775.0	-259.4	37.5	-30.4	19.8	-21.8
nme4-cl	wb97xd-cct	-7062550.7	-15246.1	-1777.8	-250.2	4.5	0.4	17.0	-12.6
pyr-bf4	wb97xd-accd	-7858694.1	-31711.2	-1592.1	-293.1	-3.3	8.4	9.8	-1.4
pyr-bf4	wb97xd-ccd	-7858661.5	-31734.1	-1570.3	-311.8	29.3	-14.4	31.7	-20.1
pyr-bf4	wb97xd-cct	-7858748.0	-31649.6	-1608.9	-280.0	-57.2	70.1	-6.9	11.7
pyr-cl	wb97xd-accd	-8243788.9	-20116.1	-1658.9	-296.2	-26.1	29.0	-13.9	14.4
pyr-cl	wb97xd-ccd	-8243769.8	-20132.7	-1656.7	-304.9	-7.0	12.4	-11.7	5.8
pyr-cl	wb97xd-cct	-8243846.5	-20081.3	-1695.3	-289.7	-83.8	63.8	-50.3	20.9

Appendix B

A DLPNO-CCSD(T) benchmarking study of intermolecular interactions of ionic liquids – Supporting Informa- tion

Supplementary Information

A DLPNO-CCSD(T) benchmarking study for intermolecular interactions of ionic liquids

Zoe Luisa Seeger and Ekaterina I. Izgorodina*

School of Chemistry, Monash University, 17 Rainforest Walk, Clayton, Victoria 3800, Australia

Contents

1	Information	1
2	IL174 + c1mim cation + aug-cc-pVDZ	2
3	IL174 + c1mim cation + cc-pVTZ	2
4	IL174 + c1mpyr cation + aug-cc-pVDZ	3
5	IL174 + c1mpyr cation + cc-pVTZ	4
6	IL174 + c2mim cation + aug-cc-pVDZ	5
7	IL174 + c2mim cation + cc-pVTZ	6
8	IL174 + c2mpyr cation + aug-cc-pVDZ	7
9	IL174 + c2mpyr cation + cc-pVTZ	8
10	IL174 + c3mim cation + aug-cc-pVDZ	9
11	IL174 + c3mim cation + cc-pVTZ	10
12	IL174 + c3mpyr cation + aug-cc-pVDZ	11

13 IL174 + c3mpyr cation + cc-pVTZ	12
14 IL174 + c4mim cation + aug-cc-pVDZ	13
15 IL174 + c4mim cation + cc-pVTZ	14
16 IL174 + c4mpyr cation + aug-cc-pVDZ	15
17 IL174 + c4mpyr cation + cc-pVTZ	16
18 HBIL + DMEA cation + aug-cc-pVDZ	17
19 HBIL + DMEA cation + cc-pVTZ	17
20 HBIL + EtMeNH2 cation + aug-cc-pVDZ	17
21 HBIL + EtMeNH2 cation + cc-pVTZ	18
22 HBIL + EtNH3 cation + aug-cc-pVDZ	18
23 HBIL + EtNH3 cation + cc-pVTZ	18
24 HBIL + mim cation + aug-cc-pVDZ	19
25 HBIL + mim cation + cc-pVTZ	19

26 HBIL + mpyr cation + aug-cc-pVDZ	20
27 HBIL + mpyr cation + cc-pVTZ	20
28 HBIL + TMEA cation + aug-cc-pVDZ	20
29 HBIL + TMEA cation + cc-pVTZ	21
30 2ip + c1mim cation + cc-pVTZ	21

1 Information

All energies are given in kJ/mol.

Configurations in the publication of [C_nmim][BF₄] p2 were renamed for convenience, and here in the SI and in previously published data of IL174 correspond to configuration p4.

The column names are as follows:

HF	Hartree-Fock energy from full system calculation
DSysCorT0	DLPNO-CCSD(T) correlation energy from full system calculation with non-iterative triples and TightPNO settings
DSysCorT1	DLPNO-CCSD(T) correlation energy from full system calculation with iterative triples and TightPNO settings
DSysCorT1_IL1	DLPNO-CCSD(T) correlation energy from full system calculation with iterative triples and IL1PNO settings
DSysCorT1_IL2	DLPNO-CCSD(T) correlation energy from full system calculation with iterative triples and IL2PNO settings
DIntCorT0	DLPNO-CCSD(T) interaction correlation energy with non-iterative triples and TightPNO settings
DIntCorT1	DLPNO-CCSD(T) interaction correlation energy with iterative triples and TightPNO settings
DIntCorT1_IL1	DLPNO-CCSD(T) interaction correlation energy with iterative triples and IL1PNO settings
DIntCorT1_IL2	DLPNO-CCSD(T) interaction correlation energy with iterative triples and IL2PNO settings
BMIntCorr	CCSD(T)/aug-cc-pVDZ (when basis set is aug-cc-pVDZ) and CCSD(T)/CBS (cc-pVTZ) interaction correlation energy

2 IL174 + c1mim cation + aug-cc-pVDZ

System	HF	DSysCorT0	DSysCorT1	DSysCorT1_IL1	DSysCorT1_IL2	DIntCorT0	DIntCorT1	DIntCorT1_IL1	DIntCorT1_IL2	BMIntCorr
c1mim-bf4-p1	-1906688.3	-5489.3	-5500.3	-5501.0	-5504.9	-72091.4	-27.6	-27.6	-28.5	-29.0
c1mim-br-p1	-7550661.5	-3451.1	-3459.7	-3461.4	-3463.7	-83050.8	-32.2	-33.2	-34.6	-34.3
c1mim-br-p2	-7550672.1	-3434.3	-3442.9	-3443.9	NA	-44736.0	-17.7	-18.1	NA	-19.0
c1mim-cl-p1	-2003262.1	-3481.9	-3489.7	-3490.3	-28.2	-74020.1	-28.2	-28.5	NA	-29.4
c1mim-cl-p2	-2003275.1	-3468.9	-3476.8	-3477.5	NA	-41312.3	-15.9	-16.2	NA	-16.7
c1mim-dca-p1	-1424478.3	-5120.6	-5136.1	-5137.1	-5140.4	-117434.1	-45.4	-45.6	-46.6	-47.0
c1mim-dca-p2	-1424479.0	-5108.3	-5123.5	-5124.5	-5127.4	-84454.8	-32.6	-32.8	-33.4	-33.7
c1mim-nes-p1	-2534114.9	-5553.5	-5567.2	-5568.5	-5573.4	-85756.7	-33.0	-33.1	-34.3	-34.7
c1mim-ntf2-p1	-5578539.0	-10600.3	-10626.9	-10632.9	NA	-147341.7	-56.7	-59.2	NA	-57.2
c1mim-ntf2-p2	-5578549.5	-10566.8	-10593.1	-10595.8	NA	-77220.7	-29.7	-29.8	NA	-30.1
c1mim-ntf2-p3	-5578548.3	-10573.4	-10599.6	-10601.5	NA	-90268.4	-34.6	-33.6	NA	-34.9
c1mim-pf6-p1	-3258572.4	-6767.4	-6781.0	-6782.5	-6788.0	-76393.7	-29.3	-29.3	-30.0	-30.6
c1mim-tos-p1	-3136826.9	-7834.1	-7855.6	-7857.3	-7864.9	-85377.7	-32.8	-32.8	-34.0	-34.0

3 IL174 + c1mim cation + cc-pVTZ

System	HF	DSysCorT0	DSysCorT1	DSysCorT1_IL1	DSysCorT1_IL2	DIntCorT0	DIntCorT1	DIntCorT1_IL1	DIntCorT1_IL2	BMIntCorr
c1mim-bf4-p1	-1907182.4	-6501.0	NA	NA	NA	-67129.2	NA	NA	NA	-34.6
c1mim-br-p1	-7551022.0	-4145.8	NA	NA	NA	-85328.7	NA	NA	NA	-45.4
c1mim-br-p2	-7551030.8	-4134.2	NA	NA	NA	-59601.2	NA	NA	NA	-30.2
c1mim-cl-p1	-2003462.4	-4071.4	NA	NA	NA	-76708.1	NA	NA	NA	-38.5
c1mim-cl-p2	-2003469.3	-4065.0	NA	NA	NA	-60834.0	NA	NA	NA	-27.5
c1mim-dca-p1	-1424777.3	-5923.0	NA	NA	NA	-116636.5	NA	NA	NA	-55.6
c1mim-dca-p2	-1424778.7	-5914.5	NA	NA	NA	-93806.4	NA	NA	NA	-42.8
c1mim-nes-p1	-2534601.1	-6480.9	NA	NA	NA	-81753.9	NA	NA	NA	-42.6
c1mim-ntf2-p1	-5579664.5	-12575.3	NA	NA	NA	-139278.6	NA	NA	NA	-63.9
c1mim-ntf2-p2	-5579678.3	-12550.1	NA	NA	NA	-84262.6	NA	NA	NA	-35.7
c1mim-ntf2-p3	-5579678.7	-12552.2	NA	NA	NA	-87159.4	NA	NA	NA	-41.4
c1mim-pf6-p1	-3259255.4	-8048.3	NA	NA	NA	-71231.2	NA	NA	NA	-36.3
c1mim-tos-p1	-3137439.8	-9109.5	NA	NA	NA	-77562.3	NA	NA	NA	-41.0

4 IL174 + c1mpyr cation + aug-cc-pVDZ

System	HF	DSysCorT0	DSysCorT1	DSysCorT1_IL1	DSysCorT1_IL2	DIntCorT0	DIntCorT1	DIntCorT1_IL1	DIntCorT1_IL2	BMIntCorr
c1mpyr-bf4-p1	-1870777.1	-5629.0	-5636.9	-5637.9	-5641.5	-67154.7	-25.8	-25.7	-26.3	-26.9
c1mpyr-bf4-p2	-1870770.1	-5625.6	-5633.5	-5634.6	-5638.1	-60871.2	-23.4	-23.4	-24.0	-24.4
c1mpyr-br-p1	-7514761.5	-3581.9	-3587.5	-3588.9	NA	-80333.0	-31.3	-31.9	NA	-32.7
c1mpyr-br-p2	-7514757.4	-3579.4	-3584.9	-3586.4	NA	-75949.9	-29.6	-30.3	NA	-30.9
c1mpyr-cl-p1	-1967365.1	-3612.7	-3617.5	-3618.4	NA	-72203.7	-27.7	-28.0	NA	-28.6
c1mpyr-cl-p2	-1967358.6	-3611.2	-3616.0	-3616.9	NA	-69338.6	-26.6	-26.9	NA	-27.5
c1mpyr-dea-p1	-1388592.3	-5226.0	-5237.8	-5238.9	-5242.0	-83134.7	-32.1	-32.0	-32.9	-33.1
c1mpyr-dea-p2	-1388592.8	-5230.9	-5242.7	-5243.7	-5246.8	-91398.1	-35.3	-35.2	-36.1	-36.1
c1mpyr-dea-p3	-1388575.1	-5229.5	-5241.2	-5242.3	-5245.2	-86425.0	-33.2	-33.1	-33.8	-34.0
c1mpyr-dea-p4	-1388592.7	-5229.0	-5240.8	-5241.7	-5244.8	-88098.8	-34.0	-33.8	-34.6	-34.7
c1mpyr-mes-p1	-2498203.9	-5695.1	-5705.8	-5707.4	-5711.9	-75360.9	-29.0	-29.2	-30.0	-30.3
c1mpyr-mes-p2	-2498196.2	-5689.8	-5700.4	-5702.1	-5706.5	-62590.3	-24.1	-24.3	-25.2	-25.9
c1mpyr-ntf2-p1	-5542629.9	-10720.7	-10744.0	-10747.0	NA	-100826.1	-38.7	-38.6	NA	-39.7
c1mpyr-ntf2-p2	-5542633.6	-10707.9	-10731.0	-10733.8	NA	-78562.5	-30.1	-29.8	NA	-30.7
c1mpyr-ntf2-p3	-5542633.4	-10718.1	-10741.4	-10744.3	NA	-97493.3	-37.4	-37.2	NA	-38.1
c1mpyr-ntf2-p5	-5542634.0	-10708.7	-10731.7	-10734.4	NA	-82010.4	-31.4	-31.0	NA	-31.7
c1mpyr-pf6-p1	-3222659.1	-6907.8	-6918.3	-6920.2	-6925.7	-67535.9	-26.0	-26.0	-26.6	-27.1
c1mpyr-pf6-p2	-3222656.1	-6904.5	-6915.0	-6917.1	-6922.5	-61523.8	-23.6	-23.8	-24.4	-24.8
c1mpyr-tos-p1	-3100921.1	-7974.7	-7993.2	-7995.3	NA	-72543.2	-27.8	-28.0	NA	-29.1
c1mpyr-tos-p2	-3100912.2	-7969.2	-7987.6	-7989.8	NA	-62466.8	-23.9	-24.1	NA	-25.0

5 IL174 + c1mpyr cation + cc-pVTZ

System	HF	DSysCorT0	DSysCorT1	DSysCorT1_IL1	DSysCorT1_IL2	DIntCorT1_IL2	DIntCorT0	DIntCorT1	DIntCorT1_IL1	DIntCorT1_IL2	BMIntCorr
c1mpyr-bf4-p1	-1871262.6	-6646.9	NA	NA	NA	NA	-68877.7	NA	NA	NA	-32.7
c1mpyr-bf4-p2	-1871256.2	-6644.5	NA	NA	NA	NA	-64424.3	NA	NA	NA	-30.3
c1mpyr-br-p1	-7515115.2	-4284.9	NA	NA	NA	NA	-90230.5	NA	NA	NA	-43.5
c1mpyr-br-p2	-7515109.9	-4283.6	NA	NA	NA	NA	-87379.4	NA	NA	NA	-41.8
c1mpyr-cl-p1	-1967555.2	-4211.6	NA	NA	NA	NA	-83670.3	NA	NA	NA	-37.8
c1mpyr-cl-p2	-1967551.3	-4210.9	NA	NA	NA	NA	-82340.5	NA	NA	NA	-37.0
c1mpyr-dea-p1	-1388879.7	-6038.0	NA	NA	NA	NA	-86425.8	NA	NA	NA	-39.7
c1mpyr-dea-p2	-1388881.7	-6041.0	NA	NA	NA	NA	-94093.3	NA	NA	NA	-43.2
c1mpyr-dea-p3	-1388864.9	-6039.6	NA	NA	NA	NA	-89034.4	NA	NA	NA	-39.7
c1mpyr-dea-p4	-1388883.2	-6039.6	NA	NA	NA	NA	-91683.1	NA	NA	NA	-41.8
c1mpyr-mes-p1	-2498678.2	-6626.9	NA	NA	NA	NA	-78837.6	NA	NA	NA	-38.3
c1mpyr-mes-p2	-2498668.9	-6623.3	NA	NA	NA	NA	-71727.2	NA	NA	NA	-34.1
c1mpyr-ntf2-p1	-5543750.3	-12703.0	NA	NA	NA	NA	-100814.4	NA	NA	NA	-43.5
c1mpyr-ntf2-p2	-5543751.8	-12690.7	NA	NA	NA	NA	-77217.6	NA	NA	NA	-34.7
c1mpyr-ntf2-p3	-5543744.5	-12702.0	NA	NA	NA	NA	-98971.9	NA	NA	NA	-42.4
c1mpyr-ntf2-p5	-5543752.2	-12691.8	NA	NA	NA	NA	-79962.7	NA	NA	NA	-36.0
c1mpyr-pf6-p1	-3223333.7	-8193.0	NA	NA	NA	NA	-67859.0	NA	NA	NA	-32.3
c1mpyr-pf6-p2	-3223325.8	-8190.9	NA	NA	NA	NA	-63521.6	NA	NA	NA	-30.1
c1mpyr-tos-p1	-3101517.3	-9254.6	NA	NA	NA	NA	-73739.5	NA	NA	NA	-36.4
c1mpyr-tos-p2	-3101508.9	-9250.3	NA	NA	NA	NA	-64858.5	NA	NA	NA	-32.1

6 IL174 + c2mim cation + aug-cc-pVDZ

System	HF	DSysCorT0	DSysCorT1	DSysCorT1_IL1	DSysCorT1_IL2	DIntCorT0	DIntCorT1	DIntCorT1_IL1	DIntCorT1_IL2	BMIntCorr
c2mim-bf4-p1	-2009196.3	-5931.9	-5943.4	-5944.3	-5948.5	-76185.8	-29.2	-29.2	-30.2	-30.7
c2mim-bf4-p2	-2009193.7	-5928.2	-5939.7	-5940.5	-5944.6	-71491.9	-27.4	-27.3	-28.2	-28.7
c2mim-br-p1	-7653166.8	-3893.0	-3902.2	-3903.7	-3906.2	-85758.6	-33.3	-34.1	-35.5	-35.4
c2mim-br-p2	-7653175.2	-3882.5	-3891.7	-3892.9	NA	-52417.4	-20.6	-21.2	NA	-22.1
c2mim-br-p3	-7653174.6	-3879.6	-3888.9	-3890.0	NA	-53464.1	-21.0	-21.6	NA	-22.5
c2mim-br-p4	-7653160.8	-3894.2	-3903.4	-3905.1	-3907.6	-86112.4	-33.4	-34.4	-35.7	-35.5
c2mim-cl-p1	-2105768.2	-3923.6	-3932.1	-3932.8	NA	-77214.2	-29.5	-29.8	NA	-30.7
c2mim-cl-p2	-2105776.6	-3915.1	-3923.7	-3924.3	NA	-46625.7	-17.9	-18.2	NA	-18.9
c2mim-cl-p3	-2105774.9	-3913.2	-3921.7	-3922.5	NA	-48741.6	-18.7	-19.1	NA	-19.8
c2mim-cl-p4	-2105761.3	-3924.3	-3932.7	-3933.4	NA	-76495.3	-29.2	-29.5	NA	-30.3
c2mim-dca-p1	-1526985.7	-5562.5	-5578.5	-5579.6	-5583.2	-120418.2	-46.5	-46.6	-47.6	-48.0
c2mim-dca-p2	-1526987.1	-5558.3	-5574.3	-5575.3	-5579.0	-113660.1	-43.9	-43.9	-45.1	-45.3
c2mim-dca-p3	-1526985.6	-5562.8	-5578.8	-5579.9	-5583.6	-120332.9	-46.5	-46.7	-47.7	-48.2
c2mim-dca-p4	-1526986.7	-5558.7	-5574.7	-5575.8	-5579.5	-114833.2	-44.4	-44.4	-45.4	-45.7
c2mim-dca-p5	-1526984.7	-5560.3	-5576.4	-5577.4	-5581.0	-118461.6	-45.8	-45.9	-46.9	-47.3
c2mim-dca-p6	-1526981.7	-5559.9	-5575.9	-5577.0	-5580.7	-118557.4	-45.8	-46.0	-47.0	-47.5
c2mim-mes-p1	-2636618.7	-5999.8	-6014.2	-6015.5	-6020.4	-96479.3	-37.1	-37.2	-38.2	-39.0
c2mim-mes-p2	-2636618.4	-5993.8	-6008.2	-6009.4	-6014.5	-87617.0	-33.7	-33.7	-34.9	-35.4
c2mim-ntf2-p1	-5681044.2	-11049.0	-11076.2	-11078.2	NA	-173136.2	-66.5	-65.6	NA	NA
c2mim-ntf2-p2	-5681050.2	-11020.4	-11047.3	-11049.6	NA	-101597.5	-39.0	-38.5	NA	-39.0
c2mim-ntf2-p3	-5681059.6	-11016.9	-11043.6	-11045.6	NA	-97180.4	-37.3	-36.4	NA	-37.6
c2mim-ntf2-p4	-5681039.5	-11038.5	-11065.7	-11067.7	NA	-140580.1	-54.1	-53.3	NA	-55.1
c2mim-pf6-p1	-3361080.5	-7212.0	-7226.1	-7227.7	-7233.6	-84074.0	-32.3	-32.3	-33.2	-33.8
c2mim-pf6-p2	-3361079.1	-7207.2	-7221.3	-7222.9	-7228.7	-77507.3	-29.7	-29.7	-30.5	-31.0
c2mim-tos-p1	-3239335.5	-8281.6	-8303.7	-8305.4	NA	-98468.9	-37.8	-37.8	NA	-39.1
c2mim-tos-p2	-3239331.0	-8274.6	-8296.6	-8298.4	NA	-87285.5	-33.5	-33.4	NA	-34.6

7 IL174 + c2mim cation + cc-pVTZ

System	HF	DSysCorT0	DSysCorT1	DSysCorT1_IL1	DSysCorT1_IL2	DIntCorT0	DIntCorT1	DIntCorT1_IL1	DIntCorT1_IL2	BMIntCorr
c2mim-bf4-p1	-2009712.5	-7009.0	NA	NA	NA	-71335.7	NA	NA	NA	-36.7
c2mim-bf4-p2	-2009710.6	-7005.4	NA	NA	NA	-66962.6	NA	NA	NA	-34.2
c2mim-br-p1	-7653549.8	-4652.5	NA	NA	NA	-88511.8	NA	NA	NA	-47.0
c2mim-br-p2	-7653554.6	-4645.6	NA	NA	NA	-65336.4	NA	NA	NA	-33.4
c2mim-br-p3	-7653556.9	-4643.5	NA	NA	NA	-66356.5	NA	NA	NA	-34.0
c2mim-br-p4	-7653542.4	-4653.9	NA	NA	NA	-87780.0	NA	NA	NA	-46.5
c2mim-cl-p1	-2105991.9	-4578.2	NA	NA	NA	-79862.4	NA	NA	NA	-40.3
c2mim-cl-p2	-2105996.7	-4575.2	NA	NA	NA	-64613.6	NA	NA	NA	-29.6
c2mim-cl-p3	-2105997.0	-4573.3	NA	NA	NA	-65218.4	NA	NA	NA	-30.5
c2mim-cl-p4	-2105985.0	-4578.7	NA	NA	NA	-78164.0	NA	NA	NA	-39.3
c2mim-dca-p1	-1527305.7	-6429.3	NA	NA	NA	-120546.5	NA	NA	NA	-56.8
c2mim-dca-p2	-1527306.4	-6426.6	NA	NA	NA	-113746.8	NA	NA	NA	-53.8
c2mim-dca-p3	-1527304.2	-6431.0	NA	NA	NA	-120555.2	NA	NA	NA	-56.9
c2mim-dca-p4	-1527308.3	-6426.1	NA	NA	NA	-114136.0	NA	NA	NA	-54.2
c2mim-dca-p5	-1527305.7	-6427.8	NA	NA	NA	-117308.8	NA	NA	NA	-55.7
c2mim-dca-p6	-1527301.9	-6427.7	NA	NA	NA	-117366.9	NA	NA	NA	-55.8
c2mim-mes-p1	-2637128.4	-6991.9	NA	NA	NA	-93085.7	NA	NA	NA	-47.4
c2mim-mes-p2	-2637128.6	-6986.1	NA	NA	NA	-83842.3	NA	NA	NA	-43.1
c2mim-ntf2-p1	-5682192.3	-13087.3	NA	NA	NA	-152176.0	NA	NA	NA	-70.0
c2mim-ntf2-p2	-5682202.5	-13066.6	NA	NA	NA	-105314.9	NA	NA	NA	-45.3
c2mim-ntf2-p3	-5682208.8	-13060.9	NA	NA	NA	-94364.5	NA	NA	NA	-44.5
c2mim-ntf2-p4	-5682189.5	-13079.7	NA	NA	NA	-133825.6	NA	NA	NA	-61.7
c2mim-pf6-p1	-3361787.4	-8557.9	NA	NA	NA	-78239.5	NA	NA	NA	-40.1
c2mim-pf6-p2	-3361784.1	-8553.2	NA	NA	NA	-71946.5	NA	NA	NA	-36.5
c2mim-tos-p1	-3239966.6	-9622.3	NA	NA	NA	-91578.7	NA	NA	NA	-46.9
c2mim-tos-p2	-3239967.8	-9615.7	NA	NA	NA	-80673.1	NA	NA	NA	-41.8

8 IL174 + c2mpyr cation + aug-cc-pVDZ

System	HF	DSysCorT0	DSysCorT1	DSysCorT1_IL1	DSysCorT1_IL2	DIntCorT0	DIntCorT1	DIntCorT1_IL1	DIntCorT1_IL2	BMIntCorr
c2mpyr-bf4-p1	-1973274.4	-6076.2	-6084.7	-6085.8	-6089.8	-69000.1	-26.5	-26.4	-27.1	-27.6
c2mpyr-bf4-p2	-1973262.8	-6074.1	-6082.5	-6083.6	-6087.5	-64687.7	-24.9	-24.8	-25.3	-25.7
c2mpyr-bf4-p3	-1973268.7	-6073.0	-6081.4	-6082.5	-6086.5	-62712.8	-24.1	-24.1	-24.7	-25.1
c2mpyr-br-p1	-7617258.3	-4029.7	-4035.8	-4037.4	NA	-82313.6	-32.1	-32.6	NA	-33.6
c2mpyr-br-p2	-7617239.7	-4028.8	-4035.0	-4036.4	NA	-79243.1	-30.9	-31.5	NA	-32.3
c2mpyr-br-p3	-7617253.9	-4026.6	-4032.8	-4034.0	NA	-77885.6	-30.4	-30.7	NA	-31.7
c2mpyr-cl-p1	-2069857.8	-4059.9	-4065.3	-4066.3	NA	-73504.3	-28.2	-28.5	NA	-29.2
c2mpyr-cl-p2	-2069841.7	-4059.0	-4064.4	-4065.3	NA	-71693.1	-27.5	-27.8	NA	-28.3
c2mpyr-cl-p3	-2069855.8	-4057.9	-4063.3	-4064.2	NA	-70583.9	-27.1	-27.3	NA	-27.9
c2mpyr-dea-p1	-1491085.4	-5672.6	-5685.0	-5686.1	-5689.6	-83671.7	-32.3	-32.2	-33.1	-33.2
c2mpyr-dea-p2	-1491084.0	-5676.7	-5689.2	-5690.3	-5693.8	-90327.7	-34.9	-34.8	-35.8	-36.0
c2mpyr-dea-p3	-1491087.0	-5677.7	-5690.1	-5691.2	-5694.5	-92292.1	-35.6	-35.5	-36.3	-36.5
c2mpyr-dea-p4	-1491085.0	-5676.7	-5689.1	-5690.2	NA	-90547.8	-35.0	-34.8	NA	-36.0
c2mpyr-dea-p5	-1491087.0	-5677.7	-5690.1	-5691.2	NA	-92292.1	-35.6	-35.5	NA	-36.5
c2mpyr-dea-p6	-1491087.8	-5677.6	-5690.0	-5691.1	NA	-92157.1	-35.6	-35.5	NA	-36.5
c2mpyr-mes-p1	-2600700.5	-6143.4	-6154.7	-6156.4	-6161.4	-77605.3	-29.8	-30.1	-31.0	-31.6
c2mpyr-mes-p2	-2600687.9	-6140.6	-6151.9	-6153.3	-6158.2	-71815.8	-27.6	-27.5	-28.4	-29.0
c2mpyr-mes-p3	-2600692.6	-6138.4	-6149.6	-6151.3	-6156.1	-67494.8	-25.9	-26.2	-26.9	-27.3
c2mpyr-ntf2-p1	-5645131.7	-11169.7	-11193.6	-11196.6	NA	-105403.2	-40.5	-40.3	NA	-41.1
c2mpyr-ntf2-p2	-5645131.3	-11157.4	-11181.1	-11183.9	NA	-83322.5	-31.9	-31.6	NA	-32.7
c2mpyr-ntf2-p3	-5645122.2	-11167.7	-11191.6	-11194.4	NA	-103504.2	-39.7	-38.7	NA	-40.0
c2mpyr-ntf2-p4	-5645128.5	-11166.1	-11190.0	-11193.1	NA	-98467.8	-37.8	-37.7	NA	-38.9
c2mpyr-ntf2-p5	-5645122.1	-11158.4	-11182.1	-11185.0	NA	-88190.7	-32.2	-32.2	NA	-34.2
c2mpyr-ntf2-p6	-5645129.4	-11155.4	-11179.1	-11182.0	NA	-81969.8	-31.4	-31.2	NA	-32.2
c2mpyr-pf6-p1	-3325154.6	-7355.0	-7366.1	-7368.0	-7373.9	-68662.7	-26.4	-26.4	-27.0	-27.5
c2mpyr-pf6-p2	-3325145.1	-7352.8	-7363.9	-7365.6	-7371.5	-65001.5	-25.0	-25.0	-25.6	-26.0
c2mpyr-pf6-p3	-3325153.6	-7351.9	-7363.0	-7365.0	-7370.7	-63204.1	-24.3	-24.4	-24.9	-25.4
c2mpyr-tos-p1	-3203415.6	-8423.5	-8442.6	-8444.8	NA	-76234.9	-29.2	-29.4	NA	-30.5
c2mpyr-tos-p2	-3203403.9	-8420.5	-8439.5	-8441.4	NA	-71305.3	-27.3	-27.1	NA	-28.1

9 IL174 + c2mpyr cation + cc-pVTZ

System	HF	DSysCorT0	DSysCorT1	DSysCorT1_IL1	DSysCorT1_IL2	DIntCorT1_IL1	DIntCorT1_IL2	DIntCorT1_IL1	DIntCorT1_IL2	BMIntCorr
c2mpyr-bf4-p1	-1973781.0	-7158.0	NA	NA	NA	NA	NA	NA	NA	-33.2
c2mpyr-bf4-p2	-1973767.8	-7156.7	NA	NA	NA	NA	NA	NA	NA	-31.2
c2mpyr-bf4-p3	-1973774.8	-7156.0	NA	NA	NA	NA	NA	NA	NA	-30.9
c2mpyr-br-p1	-7617631.1	-4796.0	NA	NA	NA	NA	NA	NA	NA	-44.1
c2mpyr-br-p2	-7617615.3	-4795.5	NA	NA	NA	NA	NA	NA	NA	-42.8
c2mpyr-br-p3	-7617627.3	-4794.4	NA	NA	NA	NA	NA	NA	NA	-42.4
c2mpyr-cl-p1	-2070073.7	-4722.3	NA	NA	NA	NA	NA	NA	NA	-38.1
c2mpyr-cl-p2	-2070058.6	-4721.8	NA	NA	NA	NA	NA	NA	NA	-37.3
c2mpyr-cl-p3	-2070068.6	-4721.4	NA	NA	NA	NA	NA	NA	NA	-37.1
c2mpyr-dea-p1	-1491399.6	-6548.3	NA	NA	NA	NA	NA	NA	NA	-39.6
c2mpyr-dea-p2	-1491396.7	-6551.0	NA	NA	NA	NA	NA	NA	NA	-42.7
c2mpyr-dea-p3	-1491402.5	-6551.5	NA	NA	NA	NA	NA	NA	NA	-43.4
c2mpyr-dea-p4	-1491397.6	-6551.0	NA	NA	NA	NA	NA	NA	NA	NA
c2mpyr-dea-p5	-1491402.5	-6551.5	NA	NA	NA	NA	NA	NA	NA	NA
c2mpyr-dea-p6	-1491401.4	-6551.5	NA	NA	NA	NA	NA	NA	NA	NA
c2mpyr-mes-p1	-2601198.1	-7138.6	NA	NA	NA	NA	NA	NA	NA	-39.3
c2mpyr-mes-p2	-2601184.7	-7136.9	NA	NA	NA	NA	NA	NA	NA	-36.5
c2mpyr-mes-p3	-2601190.5	-7135.2	NA	NA	NA	NA	NA	NA	NA	-35.3
c2mpyr-ntf2-p1	-5646267.7	-13214.8	NA	NA	NA	NA	NA	NA	NA	-44.7
c2mpyr-ntf2-p2	-5646270.9	-13203.2	NA	NA	NA	NA	NA	NA	NA	-36.8
c2mpyr-ntf2-p3	-5646259.8	-13213.9	NA	NA	NA	NA	NA	NA	NA	-43.9
c2mpyr-ntf2-p4	-5646265.6	-13212.9	NA	NA	NA	NA	NA	NA	NA	-42.9
c2mpyr-ntf2-p5	-5646265.3	-13204.3	NA	NA	NA	NA	NA	NA	NA	-38.4
c2mpyr-ntf2-p6	-5646268.1	-13202.8	NA	NA	NA	NA	NA	NA	NA	-36.3
c2mpyr-pf6-p1	-3325850.2	-8704.2	NA	NA	NA	NA	NA	NA	NA	-32.5
c2mpyr-pf6-p2	-3325841.5	-8702.6	NA	NA	NA	NA	NA	NA	NA	-30.9
c2mpyr-pf6-p3	-3325847.8	-8702.0	NA	NA	NA	NA	NA	NA	NA	-30.6
c2mpyr-tos-p1	-3204036.4	-9766.6	NA	NA	NA	NA	NA	NA	NA	-37.6
c2mpyr-tos-p2	-3204022.9	-9764.8	NA	NA	NA	NA	NA	NA	NA	-34.9

10 IL174 + c3mim cation + aug-cc-pVDZ

System	HF	DSysCorT0	DSysCorT1	DSysCorT1_IL1	DSysCorT1_IL2	DIntCorT0	DIntCorT1	DIntCorT1_IL1	DIntCorT1_IL2	BMIntCorr
c3mim-bf4-p1	-2111694.7	-6371.7	-6383.7	-6384.7	-6389.2	-78138.7	-30.0	-29.9	-31.0	-31.5
c3mim-bf4-p2	-2111689.4	-6370.7	-6382.7	-6383.5	-6388.0	-76853.4	-29.5	-29.3	-30.3	-30.7
c3mim-br-p1	-7755663.1	-4334.3	-4344.1	-4345.5	-4348.2	-87525.9	-33.5	-34.8	-36.2	-36.0
c3mim-br-p2	-7755673.3	-4322.8	-4332.6	-4333.9	NA	-53407.4	-20.5	-21.7	NA	-22.5
c3mim-br-p3	-7755672.2	-4324.4	-4334.2	-4335.5	NA	-62198.6	-23.8	-25.0	NA	-25.9
c3mim-br-p4	-7755659.6	-4336.4	-4346.1	-4347.9	-4350.4	-89183.2	-34.4	-35.7	-37.2	-36.8
c3mim-cl-p1	-2208264.9	-4364.0	-4373.0	-4373.8	NA	-78183.5	-29.9	-30.2	NA	-31.1
c3mim-cl-p2	-2208272.7	-4355.3	-4364.4	-4365.1	NA	-47545.9	-18.3	-18.5	NA	-19.2
c3mim-cl-p3	-2208271.1	-4356.3	-4365.4	-4366.3	NA	-55681.9	-21.4	-21.8	NA	-22.5
c3mim-cl-p4	-2208261.3	-4365.7	-4374.6	-4375.3	NA	-79162.6	-30.2	-30.5	NA	-31.3
c3mim-dca-p1	-1629483.4	-6002.2	-6018.7	-6019.8	-6023.6	-122358.4	-47.2	-47.3	-48.3	-48.9
c3mim-dca-p2	-1629480.6	-6003.9	-6020.5	-6021.4	-6025.5	-125351.4	-48.4	-48.4	-49.6	-50.0
c3mim-dca-p3	-1629480.4	-5997.0	-6013.4	-6014.0	-6017.9	-106134.2	-40.9	-40.6	-41.6	-42.0
c3mim-dca-p4	-1629486.2	-6003.8	-6020.3	-6021.4	-6025.5	-127408.2	-49.2	-49.3	-50.5	-51.0
c3mim-dca-p5	-1629483.2	-5999.6	-6016.2	-6017.3	-6021.1	-121720.9	-47.0	-47.2	-48.0	-48.5
c3mim-dca-p6	-1629479.1	-5998.0	-6014.6	-6015.7	-6019.6	-119451.5	-46.2	-46.3	-47.4	-47.7
c3mim-mes-p1	-2739117.4	-6442.0	-6456.9	-6458.2	-6463.5	-101505.0	-39.0	-39.1	-40.2	-41.0
c3mim-mes-p2	-2739115.7	-6432.4	-6447.2	-6448.5	-6453.9	-89183.1	-34.3	-34.3	-35.4	-35.9
c3mim-ntf2-p1	-5783542.7	-11492.5	-11520.3	-11522.2	NA	-168741.5	-64.9	-63.8	NA	NA
c3mim-ntf2-p2	-5783549.8	-11463.7	-11491.2	-11493.5	NA	-110570.0	-42.5	-41.9	NA	-44.0
c3mim-ntf2-p3	-5783555.5	-11458.1	-11485.4	-11487.5	NA	-101268.2	-38.8	-37.9	NA	-38.8
c3mim-ntf2-p4	-5783537.1	-11477.6	-11510.8	-11507.3	NA	-144329.7	-58.9	-54.6	NA	NA
c3mim-pf6-p1	-3463570.0	-7650.6	-7665.3	-7667.0	-7673.2	-86915.1	-33.4	-33.4	-34.2	-34.8
c3mim-pf6-p2	-3463577.6	-7645.4	-7660.0	-7661.6	-7667.7	-78235.7	-30.0	-29.9	-30.7	-31.2
c3mim-tos-p1	-3341832.2	-8724.2	-8746.9	-8748.6	NA	-104808.9	-40.2	-40.2	NA	-41.5
c3mim-tos-p2	-3341828.5	-8721.1	-8743.8	-8745.3	NA	-100471.5	-38.5	-38.4	NA	-39.6

11 IL174 + c3mim cation + cc-pVTZ

System	HF	DSysCorT0	DSysCorT1	DSysCorT1_IL1	DSysCorT1_IL2	DIntCorT0	DIntCorT1	DIntCorT1_IL1	DIntCorT1_IL2	BMIntCorr
c3mim-bf4-p1	-2112234.2	-7514.0	NA	NA	NA	-72726.6	NA	NA	NA	-37.5
c3mim-bf4-p2	-2112230.6	-7513.3	NA	NA	NA	-71291.2	NA	NA	NA	-36.3
c3mim-br-p1	-7756067.5	-5158.0	NA	NA	NA	-89240.6	NA	NA	NA	-47.5
c3mim-br-p2	-7756073.0	-5150.6	NA	NA	NA	-65970.7	NA	NA	NA	-33.7
c3mim-br-p3	-7756072.9	-5152.3	NA	NA	NA	-73338.6	NA	NA	NA	-37.8
c3mim-br-p4	-7756067.2	-5160.0	NA	NA	NA	-89551.8	NA	NA	NA	-47.7
c3mim-cl-p1	-2208511.0	-5083.4	NA	NA	NA	-80676.2	NA	NA	NA	-40.7
c3mim-cl-p2	-2208515.7	-5079.9	NA	NA	NA	-65022.9	NA	NA	NA	-29.7
c3mim-cl-p3	-2208515.8	-5080.9	NA	NA	NA	-69923.4	NA	NA	NA	-33.3
c3mim-cl-p4	-2208508.1	-5084.7	NA	NA	NA	-79702.1	NA	NA	NA	-40.1
c3mim-dca-p1	-1629825.9	-6934.2	NA	NA	NA	-122680.7	NA	NA	NA	NA
c3mim-dca-p2	-1629822.5	-6935.7	NA	NA	NA	-124844.1	NA	NA	NA	-58.9
c3mim-dca-p3	-1629824.6	-6932.0	NA	NA	NA	-111837.4	NA	NA	NA	-51.0
c3mim-dca-p4	-1629831.5	-6936.0	NA	NA	NA	-126584.7	NA	NA	NA	-59.9
c3mim-dca-p5	-1629825.4	-6931.7	NA	NA	NA	-119693.5	NA	NA	NA	-57.0
c3mim-dca-p6	-1629822.8	-6931.2	NA	NA	NA	-117786.0	NA	NA	NA	-55.9
c3mim-mes-p1	-2739650.0	-7498.8	NA	NA	NA	-97771.5	NA	NA	NA	-49.6
c3mim-mes-p2	-2739648.6	-7490.3	NA	NA	NA	-84964.7	NA	NA	NA	-43.5
c3mim-ntf2-p1	-5784711.5	-13594.9	NA	NA	NA	-159206.2	NA	NA	NA	NA
c3mim-ntf2-p2	-5784724.0	-13574.4	NA	NA	NA	-113848.7	NA	NA	NA	NA
c3mim-ntf2-p3	-5784727.9	-13566.8	NA	NA	NA	-98042.7	NA	NA	NA	NA
c3mim-ntf2-p4	-5784708.4	-13583.4	NA	NA	NA	-136443.2	NA	NA	NA	NA
c3mim-pf6-p1	-3464298.6	-9060.9	NA	NA	NA	-79851.6	NA	NA	NA	-40.4
c3mim-pf6-p2	-3464305.2	-9056.9	NA	NA	NA	-72298.2	NA	NA	NA	-36.5
c3mim-tos-p1	-3342486.7	-10129.5	NA	NA	NA	-97325.0	NA	NA	NA	-49.5
c3mim-tos-p2	-3342483.0	-10126.7	NA	NA	NA	-91486.3	NA	NA	NA	-46.8

12 IL174 + c3mpyr cation + aug-cc-pVDZ

System	HF	DSysCorT0	DSysCorT1	DSysCorT1_IL1	DSysCorT1_IL2	DIntCorT0	DIntCorT1	DIntCorT1_IL1	DIntCorT1_IL2	BMIntCorr
c3mpyr-bf4-p1	-2075770.8	-6517.2	-6526.2	-6527.2	-6531.6	-70439.1	-27.1	-26.8	-27.6	-28.1
c3mpyr-bf4-p2	-2075756.6	-6514.7	-6523.7	-6524.8	-6529.0	-65445.9	-25.1	-25.0	-25.6	-26.0
c3mpyr-bf4-p3	-2075764.9	-6513.7	-6522.7	-6523.8	-6528.1	-63903.0	-24.6	-24.5	-25.1	-25.6
c3mpyr-br-p1	-7719755.6	-4471.4	-4478.2	-4479.5	NA	-84531.1	-32.5	-33.3	NA	-34.4
c3mpyr-br-p2	-7719741.6	-4468.6	-4475.3	-4476.9	NA	-79899.7	-30.7	-31.9	NA	-32.4
c3mpyr-br-p3	-7719749.1	-4468.4	-4475.0	-4476.7	NA	-79503.9	-30.5	-31.8	NA	-32.5
c3mpyr-cl-p1	-2172355.3	-4501.3	-4507.3	-4508.4	NA	-75113.6	-28.8	-29.2	NA	-29.8
c3mpyr-cl-p2	-2172338.6	-4499.8	-4505.7	-4506.7	NA	-72556.5	-27.9	-28.2	NA	-28.7
c3mpyr-cl-p3	-2172350.1	-4499.0	-4504.9	-4505.9	NA	-71712.4	-27.5	-27.8	NA	-28.4
c3mpyr-dea-p1	-1593584.7	-6115.0	-6127.9	-6129.1	-6132.7	-86955.6	-33.6	-33.5	-34.3	-34.5
c3mpyr-dea-p2	-1593579.6	-6117.2	-6130.1	-6131.3	-6135.0	-90989.6	-35.1	-35.0	-35.9	-36.0
c3mpyr-dea-p3	-1593560.1	-6115.8	-6128.6	-6129.6	-6133.0	-85497.2	-32.7	-32.5	-33.0	-34.1
c3mpyr-dea-p4	-1593578.3	-6116.4	-6129.3	-6130.4	-6134.0	-89458.6	-34.5	-34.3	-35.1	NA
c3mpyr-dea-p5	-1593584.6	-6117.9	-6130.8	-6131.9	-6135.5	-92576.4	-35.7	-35.6	-36.4	NA
c3mpyr-dea-p6	-1593584.6	-6117.9	-6130.8	-6131.9	NA	-92576.4	-35.7	-35.7	NA	-36.6
c3mpyr-mes-p1	-2703199.2	-6585.2	-6597.1	-6598.8	-6604.0	-80321.6	-30.9	-31.0	-32.0	-32.5
c3mpyr-mes-p2	-2703183.4	-6581.7	-6593.5	-6595.0	-6600.0	-73396.4	-28.2	-28.0	-28.8	-29.4
c3mpyr-mes-p3	-2703191.6	-6580.2	-6592.0	-6593.7	-6598.8	-69557.3	-26.7	-26.9	-27.7	-28.2
c3mpyr-ntf2-p1	-5747628.3	-11612.7	-11637.2	-11640.2	NA	-111013.4	-42.6	-42.4	NA	-42.9
c3mpyr-ntf2-p2	-5747625.8	-11597.5	-11621.7	-11624.6	NA	-83941.0	-32.2	-31.8	NA	-32.6
c3mpyr-ntf2-p3	-5747620.4	-11608.3	-11632.7	-11635.6	NA	-103163.8	-39.6	-39.2	NA	-40.2
c3mpyr-ntf2-p4	-5747623.5	-11608.8	-11633.2	-11636.3	NA	-103534.3	-39.7	-39.6	NA	-40.8
c3mpyr-ntf2-p5	-5747621.5	-11598.6	-11622.8	-11625.9	NA	-87734.4	-33.6	-33.6	NA	-34.3
c3mpyr-ntf2-p6	-5747622.6	-11598.2	-11622.4	-11625.4	NA	-85938.4	-32.9	-32.7	NA	-33.7
c3mpyr-pf6-p1	-3427651.8	-7796.8	-7808.5	-7810.9	-7816.5	-71538.5	-27.5	-27.9	-28.2	-28.6
c3mpyr-pf6-p2	-3427641.8	-7793.1	-7804.7	-7806.5	-7812.5	-65535.3	-25.2	-25.0	-25.6	-26.1
c3mpyr-pf6-p3	-3427647.9	-7793.2	-7804.8	-7806.8	-7812.8	-64687.1	-24.9	-24.9	-25.4	-26.0
c3mpyr-tos-p1	-3305915.6	-8865.4	-8884.9	-8887.1	NA	-79480.9	-30.5	-30.5	NA	-31.5
c3mpyr-tos-p2	-3305898.8	-8861.6	-8881.1	-8883.1	NA	-72409.8	-27.7	-27.6	NA	-28.6

13 IL174 + c3mpyr cation + cc-pVTZ

System	HF	DSysCorT0	DSysCorT1	DSysCorT1_IL1	DSysCorT1_IL2	DIntCorT1_IL1	DIntCorT1_IL2	DIntCorT1_IL1	DIntCorT1_IL2	BMIntCorr
c3mpyr-bf4-p1	-2076302.4	-7663.1	NA	NA	NA	NA	NA	NA	NA	-33.5
c3mpyr-bf4-p2	-2076288.7	-7661.4	NA	NA	NA	NA	NA	NA	NA	-31.4
c3mpyr-bf4-p3	-2076293.2	-7661.0	NA	NA	NA	NA	NA	NA	NA	-31.2
c3mpyr-br-p1	-7720152.3	-5301.4	NA	NA	NA	NA	NA	NA	NA	-44.8
c3mpyr-br-p2	-7720134.5	-5299.8	NA	NA	NA	NA	NA	NA	NA	-42.6
c3mpyr-br-p3	-7720145.6	-5299.8	NA	NA	NA	NA	NA	NA	NA	-43.0
c3mpyr-cl-p1	-2172594.3	-5227.3	NA	NA	NA	NA	NA	NA	NA	-38.4
c3mpyr-cl-p2	-2172577.8	-5226.7	NA	NA	NA	NA	NA	NA	NA	-37.4
c3mpyr-cl-p3	-2172587.8	-5226.5	NA	NA	NA	NA	NA	NA	NA	-37.4
c3mpyr-dea-p1	-1593919.9	-7054.0	NA	NA	NA	NA	NA	NA	NA	-40.6
c3mpyr-dea-p2	-1593918.4	-7055.7	NA	NA	NA	NA	NA	NA	NA	-42.7
c3mpyr-dea-p3	-1593896.6	-7054.7	NA	NA	NA	NA	NA	NA	NA	-38.6
c3mpyr-dea-p4	-1593916.8	-7054.9	NA	NA	NA	NA	NA	NA	NA	-41.5
c3mpyr-dea-p5	-1593921.0	-7056.1	NA	NA	NA	NA	NA	NA	NA	-43.3
c3mpyr-dea-p6	-1593921.0	-7056.1	NA	NA	NA	NA	NA	NA	NA	NA
c3mpyr-mes-p1	-2703719.1	-7643.9	NA	NA	NA	NA	NA	NA	NA	-40.0
c3mpyr-mes-p2	-2703703.0	-7642.1	NA	NA	NA	NA	NA	NA	NA	-36.7
c3mpyr-mes-p3	-2703708.3	-7640.9	NA	NA	NA	NA	NA	NA	NA	-36.0
c3mpyr-ntf2-p1	-5748789.0	-13721.5	NA	NA	NA	NA	NA	NA	NA	-46.7
c3mpyr-ntf2-p2	-5748788.5	-13707.5	NA	NA	NA	NA	NA	NA	NA	-36.4
c3mpyr-ntf2-p3	-5748778.9	-13718.7	NA	NA	NA	NA	NA	NA	NA	-44.1
c3mpyr-ntf2-p4	-5748786.8	-13719.5	NA	NA	NA	NA	NA	NA	NA	-44.8
c3mpyr-ntf2-p5	-5748785.2	-13709.0	NA	NA	NA	NA	NA	NA	NA	-38.3
c3mpyr-ntf2-p6	-5748790.9	-13708.9	NA	NA	NA	NA	NA	NA	NA	-37.8
c3mpyr-pf6-p1	-3428374.5	-9209.5	NA	NA	NA	NA	NA	NA	NA	-33.6
c3mpyr-pf6-p2	-3428358.5	-9207.3	NA	NA	NA	NA	NA	NA	NA	-30.9
c3mpyr-pf6-p3	-3428365.4	-9207.1	NA	NA	NA	NA	NA	NA	NA	-31.0
c3mpyr-tos-p1	-3306556.0	-10272.2	NA	NA	NA	NA	NA	NA	NA	-38.4
c3mpyr-tos-p2	-3306543.7	-10269.8	NA	NA	NA	NA	NA	NA	NA	-35.0

14 IL174 + c4mim cation + aug-cc-pVDZ

System	HF	DSysCorT0	DSysCorT1	DSysCorT1_IL1	DSysCorT1_IL2	DIntCorT0	DIntCorT1	DIntCorT1_IL1	DIntCorT1_IL2	BMIntCorr
c4mim-bf4-p1	-2214191.6	-6810.8	-6823.4	-6824.5	-6829.1	-79580.7	-30.5	-30.5	-31.5	-32.0
c4mim-bf4-p2	-2214189.2	-6809.1	-6821.6	-6822.6	-6827.2	-77460.6	-29.7	-29.6	-30.6	-31.0
c4mim-br-p1	-7858158.3	-4775.2	-4785.5	-4787.1	-4789.6	-89070.0	-34.5	-35.4	-36.9	-36.7
c4mim-br-p2	-7858167.6	-4763.9	-4774.2	-4775.7	NA	-55336.0	-21.2	-22.4	NA	-23.4
c4mim-br-p3	-7858166.2	-4766.2	-4776.6	-4778.0	NA	-65843.1	-25.2	-26.4	NA	-27.4
c4mim-br-p4	-7858156.4	-4776.9	-4787.1	-4788.9	-4791.3	-90792.4	-35.1	-36.3	-37.6	-37.2
c4mim-cl-p1	-2310759.2	-4804.5	-4814.0	-4814.9	NA	-79585.1	-30.4	-30.7	NA	-31.7
c4mim-cl-p2	-2310770.6	-4796.0	-4805.5	-4806.3	NA	-48596.1	-18.7	-18.9	NA	-19.8
c4mim-cl-p3	-2310769.2	-4797.5	-4807.1	-4808.1	NA	-58457.5	-22.4	-22.9	NA	-23.6
c4mim-cl-p4	-2310756.1	-4805.9	-4815.3	-4816.1	NA	-80393.0	-30.7	-30.9	NA	-31.7
c4mim-dca-p1	-1731980.7	-6441.5	-6458.5	-6459.6	-6463.6	-124681.8	-48.1	-48.1	-49.0	-49.5
c4mim-dca-p2	-1731982.9	-6444.1	-6461.2	-6462.2	-6466.4	-131312.0	-50.7	-50.6	-51.8	-52.3
c4mim-dca-p3	-1731979.6	-6438.1	-6455.2	-6456.5	-6460.4	-122630.1	-47.4	-47.5	-48.4	-48.8
c4mim-mes-p1	-2841613.5	-6881.9	-6897.4	-6898.6	-6904.2	-105088.0	-40.4	-40.4	-41.5	-42.1
c4mim-mes-p2	-2841615.1	-6870.3	-6885.6	-6887.1	-6892.6	-89511.5	-34.4	-34.4	-35.6	-36.1
c4mim-pfe-p1	-3566075.7	-8092.7	-8108.0	-8109.7	-8116.0	-90712.0	-34.8	-34.8	-35.5	-36.2
c4mim-pfe-p2	-3566070.8	-8083.6	-8098.7	-8100.6	-8106.7	-78187.9	-30.0	-30.0	-30.7	-31.2
c4mim-tos-p1	-3444327.6	-9165.4	-9188.6	-9190.2	NA	-110154.8	-42.2	-42.0	NA	-43.3
c4mim-tos-p2	-3444328.9	-9159.9	-9183.0	-9184.8	NA	-102176.4	-39.2	-39.1	NA	-40.2

15 IL174 + c4mim cation + cc-pVTZ

System	HF	DSysCorT0	DSysCorT1	DSysCorT1_IL1	DSysCorT1_IL2	DIntCorT0	DIntCorT1	DIntCorT1_IL1	DIntCorT1_IL2	BMIntCorr
c4mim-bf4-p1	-2214755.1	-8018.4	NA	NA	NA	-73930.1	NA	NA	NA	-38.0
c4mim-bf4-p2	-2214750.4	-8017.2	NA	NA	NA	-71777.4	NA	NA	NA	-36.5
c4mim-br-p1	-7858588.6	-5663.5	NA	NA	NA	-91085.2	NA	NA	NA	-48.3
c4mim-br-p2	-7858592.4	-5656.1	NA	NA	NA	-67302.6	NA	NA	NA	-34.5
c4mim-br-p3	-7858593.0	-5658.3	NA	NA	NA	-75895.2	NA	NA	NA	-39.3
c4mim-br-p4	-7858583.4	-5665.1	NA	NA	NA	-90473.6	NA	NA	NA	-48.1
c4mim-cl-p1	-2311030.5	-5588.5	NA	NA	NA	-81689.6	NA	NA	NA	-41.2
c4mim-cl-p2	-2311034.2	-5585.0	NA	NA	NA	-65352.4	NA	NA	NA	-30.2
c4mim-cl-p3	-2311034.4	-5586.5	NA	NA	NA	-72071.0	NA	NA	NA	-34.4
c4mim-cl-p4	-2311027.0	-5589.6	NA	NA	NA	-80500.3	NA	NA	NA	-40.4
c4mim-dca-p1	-1732346.0	-7438.8	NA	NA	NA	-124386.6	NA	NA	NA	-58.1
c4mim-dca-p2	-1732350.3	-7441.4	NA	NA	NA	-130043.4	NA	NA	NA	-61.2
c4mim-dca-p3	-1732345.0	-7435.7	NA	NA	NA	-120218.2	NA	NA	NA	-57.2
c4mim-mes-p1	-2842168.5	-8003.9	NA	NA	NA	-100332.4	NA	NA	NA	-50.7
c4mim-mes-p2	-2842163.3	-7994.1	NA	NA	NA	-84989.9	NA	NA	NA	-43.6
c4mim-pfe-p1	-3566826.1	-9568.8	NA	NA	NA	-83679.1	NA	NA	NA	-42.6
c4mim-pfe-p2	-3566823.9	-9560.6	NA	NA	NA	-72440.9	NA	NA	NA	-36.6
c4mim-tos-p1	-3445004.5	-10635.7	NA	NA	NA	-102025.8	NA	NA	NA	-51.3
c4mim-tos-p2	-3445003.5	-10631.5	NA	NA	NA	-94118.0	NA	NA	NA	-47.6

16 IL174 + c4mpyr cation + aug-cc-pVDZ

System	HF	DSysCorT0	DSysCorT1	DSysCorT1_IL1	DSysCorT1_IL2	DIntCorT0	DIntCorT1	DIntCorT1_IL1	DIntCorT1_IL2	BMIntCorr
c4mpyr-bf4-p1	-2178269.5	-6956.8	-6966.4	-6967.5	-6972.0	-70844.0	-27.2	-27.0	-27.7	-28.2
c4mpyr-bf4-p2	-2178253.6	-6954.3	-6963.7	-6964.9	-6969.2	-66049.5	-25.4	-25.2	-25.8	-26.2
c4mpyr-bf4-p3	-2178262.1	-6953.4	-6962.9	-6964.1	-6968.5	-64441.4	-24.8	-24.7	-25.3	-25.8
c4mpyr-br-p1	-7822250.9	-4911.2	-4918.4	-4920.2	NA	-84998.2	-32.6	-33.8	NA	-34.7
c4mpyr-br-p2	-7822235.4	-4908.5	-4915.7	-4917.3	NA	-80754.8	-31.0	-32.1	NA	-32.8
c4mpyr-br-p3	-7822245.3	-4908.2	-4915.4	-4917.0	NA	-80782.2	-31.0	-32.1	NA	-32.7
c4mpyr-cl-p1	-2274852.5	-4940.8	-4947.3	-4948.4	NA	-75404.1	-29.0	-29.2	NA	-29.9
c4mpyr-cl-p2	-2274835.7	-4940.1	-4946.6	-4947.6	NA	-73830.1	-28.4	-28.6	NA	-29.2
c4mpyr-cl-p3	-2274847.1	-4938.4	-4944.8	-4945.9	NA	-71929.6	-27.6	-27.9	NA	-28.4
c4mpyr-dea-p1	-1696074.5	-6556.1	-6569.5	-6570.4	-6574.2	-88522.4	-34.2	-33.8	-34.5	-34.7
c4mpyr-dea-p2	-1696078.1	-6556.7	-6570.2	-6571.2	-6575.2	-91208.7	-35.2	-35.0	-35.9	-36.1
c4mpyr-dea-p3	-1696080.2	-6555.2	-6568.6	-6569.8	-6573.6	-89256.0	-34.5	-34.2	-35.1	-35.3
c4mpyr-dea-p4	-1696080.8	-6557.3	-6570.7	-6571.5	-6575.4	-90852.8	-35.1	-34.5	-35.4	-36.1
c4mpyr-dea-p5	-1696080.9	-6557.5	-6571.0	-6572.2	-6575.9	-93015.2	-35.9	-35.8	-36.5	NA
c4mpyr-dea-p6	-1696080.9	-6557.5	-6571.0	-6572.2	NA	-93015.2	-35.9	-35.8	NA	-36.7
c4mpyr-mes-p1	-2805695.0	-7024.7	-7037.1	-7038.9	-7044.2	-80987.4	-31.1	-31.3	-32.2	-32.6
c4mpyr-mes-p2	-2805684.5	-7021.9	-7034.2	-7035.6	-7040.9	-74888.6	-28.8	-28.5	-29.3	-29.9
c4mpyr-mes-p3	-2805687.6	-7019.7	-7032.0	-7033.7	-7039.0	-70008.3	-26.9	-27.0	-27.9	-28.5
c4mpyr-ntf2-p1	-5850127.1	-12051.8	-12076.8	-12080.0	NA	-109996.0	-40.1	-42.1	NA	NA
c4mpyr-ntf2-p2	-5850130.1	-12041.9	-12066.7	-12069.5	NA	-93984.9	-36.0	-35.6	NA	NA
c4mpyr-ntf2-p3	-5850113.4	-12049.6	-12074.6	-12077.6	NA	-106178.4	-41.8	-40.6	NA	NA
c4mpyr-ntf2-p4	-5850120.6	-12049.8	-12074.7	-12077.9	NA	-106634.4	-40.9	-40.8	NA	NA
c4mpyr-ntf2-p5	-5850116.6	-12039.1	-12063.9	-12066.8	NA	-89588.7	-34.3	-34.1	NA	NA
c4mpyr-ntf2-p6	-5850121.0	-12039.2	-12063.9	-12066.8	NA	-89610.9	-34.3	-34.1	NA	NA
c4mpyr-pf6-p1	-3530153.4	-8236.3	-8248.5	-8250.6	-8256.9	-71785.6	-27.6	-27.6	-28.3	-28.8
c4mpyr-pf6-p2	-3530138.9	-8233.2	-8245.3	-8247.2	-8253.3	-66918.2	-25.7	-25.5	-26.0	-26.5
c4mpyr-pf6-p3	-3530145.5	-8232.9	-8245.0	-8247.1	-8253.3	-65450.6	-25.1	-25.2	-25.8	-26.2
c4mpyr-tos-p1	-3408409.6	-9305.0	-9325.1	-9327.4	NA	-80024.8	-30.7	-30.8	NA	-31.8
c4mpyr-tos-p2	-3408396.7	-9301.6	-9321.7	-9323.6	NA	-74723.8	-28.6	-28.2	NA	-28.7

17 IL174 + c4mpyr cation + cc-pVTZ

System	HF	DSysCorT0	DSysCorT1	DSysCorT1_IL1	DSysCorT1_IL2	DIntCorT1_IL2	DIntCorT0	DIntCorT1	DIntCorT1_IL1	DIntCorT1_IL2	BMIntCorr
c4mpyr-bf4-p1	-2178821.0	-8167.5	NA	NA	NA	NA	-70515.6	NA	NA	NA	-33.6
c4mpyr-bf4-p2	-2178807.4	-8165.8	NA	NA	NA	NA	-66478.9	NA	NA	NA	-31.5
c4mpyr-bf4-p3	-2178812.7	-8165.6	NA	NA	NA	NA	-67004.4	NA	NA	NA	-31.4
c4mpyr-br-p1	-7822671.2	-5805.9	NA	NA	NA	NA	-93190.6	NA	NA	NA	-45.0
c4mpyr-br-p2	-7822654.4	-5803.9	NA	NA	NA	NA	-88012.3	NA	NA	NA	-42.8
c4mpyr-br-p3	-7822666.2	-5804.3	NA	NA	NA	NA	-90100.6	NA	NA	NA	-43.3
c4mpyr-cl-p1	-2275113.2	-5731.7	NA	NA	NA	NA	-84667.8	NA	NA	NA	-38.5
c4mpyr-cl-p2	-2275096.3	-5731.6	NA	NA	NA	NA	-83671.6	NA	NA	NA	-37.8
c4mpyr-cl-p3	-2275109.2	-5730.7	NA	NA	NA	NA	-82877.9	NA	NA	NA	-37.3
c4mpyr-dea-p1	-1696436.6	-7558.2	NA	NA	NA	NA	-89874.3	NA	NA	NA	-40.4
c4mpyr-dea-p2	-1696435.5	-7560.1	NA	NA	NA	NA	-92591.3	NA	NA	NA	-42.6
c4mpyr-dea-p3	-1696441.2	-7558.6	NA	NA	NA	NA	-89469.0	NA	NA	NA	-41.3
c4mpyr-dea-p4	-1696438.8	-7560.0	NA	NA	NA	NA	-93499.0	NA	NA	NA	-42.1
c4mpyr-dea-p5	-1696441.9	-7560.5	NA	NA	NA	NA	-94715.7	NA	NA	NA	-43.4
c4mpyr-dea-p6	-1696441.9	-7560.5	NA	NA	NA	NA	-94715.7	NA	NA	NA	NA
c4mpyr-mes-p1	-2806237.1	-8148.3	NA	NA	NA	NA	-82295.5	NA	NA	NA	-40.0
c4mpyr-mes-p2	-2806221.3	-8146.8	NA	NA	NA	NA	-77535.5	NA	NA	NA	-37.0
c4mpyr-mes-p3	-2806228.0	-8145.3	NA	NA	NA	NA	-76018.0	NA	NA	NA	-36.2
c4mpyr-ntf2-p1	-5851306.7	-14225.8	NA	NA	NA	NA	-107366.5	NA	NA	NA	NA
c4mpyr-ntf2-p2	-5851314.0	-14215.8	NA	NA	NA	NA	-89779.1	NA	NA	NA	NA
c4mpyr-ntf2-p3	-5851298.3	-14224.3	NA	NA	NA	NA	-103963.0	NA	NA	NA	NA
c4mpyr-ntf2-p4	-5851305.7	-14224.8	NA	NA	NA	NA	-105408.6	NA	NA	NA	NA
c4mpyr-ntf2-p5	-5851305.8	-14213.8	NA	NA	NA	NA	-85607.3	NA	NA	NA	NA
c4mpyr-ntf2-p6	-5851309.7	-14214.4	NA	NA	NA	NA	-86194.4	NA	NA	NA	NA
c4mpyr-pf6-p1	-3530890.8	-9714.1	NA	NA	NA	NA	-70332.2	NA	NA	NA	-33.7
c4mpyr-pf6-p2	-3530877.4	-9712.0	NA	NA	NA	NA	-65809.3	NA	NA	NA	-31.2
c4mpyr-pf6-p3	-3530884.7	-9711.6	NA	NA	NA	NA	-65658.8	NA	NA	NA	-31.2
c4mpyr-tos-p1	-3409077.1	-10776.6	NA	NA	NA	NA	-78243.5	NA	NA	NA	NA
c4mpyr-tos-p2	-3409061.6	-10774.7	NA	NA	NA	NA	-73386.7	NA	NA	NA	NA

18 HBIL + DMEA cation + aug-cc-pVDZ

System	HF	DSysCorT0	DSysCorT1	DSysCorT1_IL1	DSysCorT1_IL2	DIntCorT0	DIntCorT1	DIntCorT1_IL1	DIntCorT1_IL2	BMIntCorr
DMEA-CF3SO3-p1	-3075038.2	-6424.3	-6436.8	-6438.9	NA	-70589.2	-27.2	-27.6	NA	-28.8
DMEA-Cl-p1	-1765500.4	-2808.3	-2811.7	-2812.3	NA	-70157.3	-27.1	-27.4	NA	-27.7
DMEA-mOSO3-p1	-2492873.9	-5412.7	-5423.1	-5424.5	-5428.7	-65848.8	-25.3	-25.3	-26.1	-26.3
DMEA-mSO3-p1	-2296322.6	-4890.8	-4900.1	-4901.1	NA	-66591.9	-25.6	-25.7	NA	-26.8
DMEA-NO3-p1	-1291354.0	-4469.4	-4479.1	-4480.1	-4483.0	-80053.5	-31.1	-31.2	-32.1	-32.3
DMEA-TFA-p1	-1934444.6	-5801.0	-5811.9	-5813.6	NA	-71523.7	-27.5	-27.8	NA	-28.8

19 HBIL + DMEA cation + cc-pVTZ

System	HF	DSysCorT0	DSysCorT1	DSysCorT1_IL1	DSysCorT1_IL2	DIntCorT0	DIntCorT1	DIntCorT1_IL1	DIntCorT1_IL2	BMIntCorr
DMEA-CF3SO3-p1	-3075686.5	-7602.7	NA	NA	NA	-79947.6	NA	NA	NA	-37.6
DMEA-Cl-p1	-1765655.6	-3291.1	NA	NA	NA	-87683.0	NA	NA	NA	-39.7
DMEA-mOSO3-p1	-2493377.8	-6327.2	NA	NA	NA	-76870.3	NA	NA	NA	-37.0
DMEA-mSO3-p1	-2296758.1	-5707.6	NA	NA	NA	-80804.8	NA	NA	NA	-38.6
DMEA-NO3-p1	-1291633.6	-5201.9	NA	NA	NA	-98645.9	NA	NA	NA	-43.1
DMEA-TFA-p1	-1934915.2	-6848.8	NA	NA	NA	-86323.7	NA	NA	NA	-39.6

20 HBIL + EtMeNH2 cation + aug-cc-pVDZ

System	HF	DSysCorT0	DSysCorT1	DSysCorT1_IL1	DSysCorT1_IL2	DIntCorT0	DIntCorT1	DIntCorT1_IL1	DIntCorT1_IL2	BMIntCorr
EtMeNH2-CF3SO3-p1	-2972568.9	-5980.3	-5992.2	-5993.8	NA	-75724.7	-29.1	-29.3	NA	-30.4
EtMeNH2-Cl-p1	-1663016.7	-2358.8	-2361.5	-2361.9	NA	-64008.8	-24.6	-24.9	NA	-25.1
EtMeNH2-mOSO3-p1	-2390390.3	-4976.8	-4986.7	-4988.0	NA	-75745.8	-29.1	-29.2	NA	-30.4
EtMeNH2-mSO3-p1	-2193856.9	-4437.2	-4445.7	-4446.7	NA	-58406.4	-22.5	-22.6	NA	-23.6
EtMeNH2-NO3-p1	-1188873.2	-4018.1	-4027.0	-4027.8	-4030.2	-70483.5	-27.3	-27.4	-28.2	-28.3
EtMeNH2-TFA-p1	-1831964.2	-5349.2	-5359.4	-5360.9	NA	-60934.9	-23.3	-23.6	NA	-24.4

21 HBIL + EtMeNH2 cation + cc-pVTZ

System	HF	DSysCorT0	DSysCorT1	DSysCorT1_IL1	DSysCorT1_IL2	DIntCorT0	DIntCorT1	DIntCorT1_IL1	DIntCorT1_IL2	BMIntCorr
EtMeNH2-CF3SO3-p1	-2973195.4	-7096.0	NA	NA	NA	-86805.2	NA	NA	NA	-40.4
EtMeNH2-Cl-p1	-1663149.3	-2778.6	NA	NA	NA	-82241.1	NA	NA	NA	-37.0
EtMeNH2-mOSO3-p1	-2390871.7	-5822.0	NA	NA	NA	-86829.7	NA	NA	NA	-48.6
EtMeNH2-mSO3-p1	-2194267.4	-5191.3	NA	NA	NA	-71320.6	NA	NA	NA	-35.7
EtMeNH2-NO3-p1	-1189133.9	-4687.5	NA	NA	NA	-89986.5	NA	NA	NA	-38.8
EtMeNH2-TFA-p1	-1832412.0	-6334.6	NA	NA	NA	-77185.9	NA	NA	NA	-35.0

22 HBIL + EtNH3 cation + aug-cc-pVDZ

System	HF	DSysCorT0	DSysCorT1	DSysCorT1_IL1	DSysCorT1_IL2	DIntCorT0	DIntCorT1	DIntCorT1_IL1	DIntCorT1_IL2	BMIntCorr
EtNH3-CF3SO3-p1	-2870089.9	-5537.7	-5549.0	-5550.7	NA	-68302.6	-26.4	-26.5	NA	-27.1
EtNH3-Cl-p1	-1560534.7	-1919.5	-1921.6	-1921.9	NA	-61025.2	-23.5	-23.8	NA	-23.9
EtNH3-mOSO3-p1	-2287911.0	-4532.7	-4541.9	-4543.2	-4546.8	-74843.7	-28.8	-28.9	-29.7	-30.0
EtNH3-mSO3-p1	-2091366.4	-4001.9	-4009.9	-4010.8	NA	-63016.2	-24.2	-24.4	NA	-25.1
EtNH3-NO3-p1	-1086389.3	-3582.1	-3590.6	-3591.3	-3593.5	-72443.6	-28.1	-28.3	-29.0	-29.1
EtNH3-TFA-p1	-1729486.6	-4907.2	-4916.8	-4918.1	NA	-50749.0	-19.4	-19.6	NA	-20.2

23 HBIL + EtNH3 cation + cc-pVTZ

System	HF	DSysCorT0	DSysCorT1	DSysCorT1_IL1	DSysCorT1_IL2	DIntCorT0	DIntCorT1	DIntCorT1_IL1	DIntCorT1_IL2	BMIntCorr
EtNH3-CF3SO3-p1	-2870692.4	-6590.1	NA	NA	NA	-78680.6	NA	NA	NA	-36.9
EtNH3-Cl-p1	-1560644.3	-2275.1	NA	NA	NA	-80009.2	NA	NA	NA	-36.1
EtNH3-mOSO3-p1	-2288363.5	-5319.7	NA	NA	NA	-87259.7	NA	NA	NA	-42.2
EtNH3-mSO3-p1	-2091754.7	-4692.2	NA	NA	NA	-76129.1	NA	NA	NA	-37.3
EtNH3-NO3-p1	-1086625.8	-4186.8	NA	NA	NA	-91739.2	NA	NA	NA	-40.2
EtNH3-TFA-p1	-1729908.6	-5829.4	NA	NA	NA	-69583.8	NA	NA	NA	-30.9

24 HBIL + mim cation + aug-cc-pVDZ

System	HF	DSysCorT0	DSysCorT1	DSysCorT1_IL1	DSysCorT1_IL2	DIntCorT0	DIntCorT1	DIntCorT1_IL1	DIntCorT1_IL2	BMIntCorr
mim-CF3SO3-p1	-3210348.9	-6637.6	-6653.8	-6655.3	NA	-58505.1	-22.5	-22.4	NA	-23.0
mim-CF3SO3-p2	-3210388.9	-6634.3	-6650.6	-6652.2	NA	-46016.1	-17.8	-17.8	NA	-18.7
mim-Cl-p1	-1900814.5	-3020.5	-3027.7	-3028.0	NA	-50433.5	-19.5	-19.7	NA	-20.1
mim-Cl-p2	-1900793.9	-3006.8	-3013.7	-3014.2	NA	-26640.5	-10.2	-10.6	NA	-11.0
mim-mOSO3-p1	-2628157.4	-5627.8	-5641.9	-5643.1	-5647.4	-56484.4	-21.7	-21.5	-22.1	-22.7
mim-mSO3-p1	-2431663.2	-5097.5	-5110.4	-5111.5	NA	-34669.6	-13.4	-13.5	NA	-14.3
mim-mSO3-p2	-2431630.7	-5094.6	-5107.4	-5108.6	NA	-44903.2	-17.2	-17.4	NA	-18.5
mim-NO3-p1	-1426686.4	-4681.4	-4694.9	-4695.5	-4698.5	-55735.1	-21.7	-21.6	-22.3	-22.6
mim-NO3-p2	-1426627.4	-4690.5	-4703.7	-4704.8	-4708.2	-89552.5	-34.7	-34.9	-36.0	-36.4
mim-TFA-p1	-2069742.2	-5993.2	-6007.6	-6009.1	NA	-22226.0	-8.5	-8.7	NA	-9.5
mim-TFA-p2	-2069635.1	-5993.4	-6007.8	-6009.0	NA	-33569.7	-12.9	-12.9	NA	-13.5
mim-TFA-p3	-2069661.3	-6005.9	-6020.6	-6021.9	NA	-54021.7	-20.8	-20.8	NA	-21.5

25 HBIL + mim cation + cc-pVTZ

System	HF	DSysCorT0	DSysCorT1	DSysCorT1_IL1	DSysCorT1_IL2	DIntCorT0	DIntCorT1	DIntCorT1_IL1	DIntCorT1_IL2	BMIntCorr
mim-CF3SO3-p1	-3211020.5	-7866.1	NA	NA	NA	-61024.0	NA	NA	NA	-31.1
mim-CF3SO3-p2	-3211059.9	-7865.5	NA	NA	NA	-58614.5	NA	NA	NA	-27.2
mim-Cl-p1	-1900990.6	-3556.5	NA	NA	NA	-71650.5	NA	NA	NA	-31.7
mim-Cl-p2	-1900964.7	-3539.5	NA	NA	NA	-37974.8	NA	NA	NA	-20.2
mim-mOSO3-p1	-2628680.1	-6591.9	NA	NA	NA	-61377.0	NA	NA	NA	-31.8
mim-mSO3-p1	-2432121.5	-5967.1	NA	NA	NA	-51338.0	NA	NA	NA	-25.9
mim-mSO3-p2	-2432087.9	-5961.1	NA	NA	NA	-47437.0	NA	NA	NA	-27.8
mim-NO3-p1	-1426987.7	-5466.3	NA	NA	NA	-77708.5	NA	NA	NA	-33.4
mim-NO3-p2	-1426929.2	-5465.4	NA	NA	NA	-88553.3	NA	NA	NA	-44.7
mim-TFA-p1	-2070225.2	-7092.0	NA	NA	NA	-31262.0	NA	NA	NA	-16.3
mim-TFA-p2	-2070116.0	-7088.3	NA	NA	NA	-34197.2	NA	NA	NA	-17.9
mim-TFA-p3	-2070139.7	-7101.3	NA	NA	NA	-59091.1	NA	NA	NA	-28.5

26 HBIL + mpyr cation + aug-cc-pVDZ

System	HF	DSysCorT0	DSysCorT1	DSysCorT1_IL1	DSysCorT1_IL2	DIntCorT0	DIntCorT1	DIntCorT1_IL1	DIntCorT1_IL2	BMIntCorr
mpyr-CF3SO3-p1	-3174495.0	-6781.7	-6795.1	-6797.2	NA	-89876.6	-34.6	-35.0	NA	-36.3
mpyr-Cl-p1	-1864953.8	-3157.9	-3162.1	-3162.7	NA	-75718.1	-29.2	-29.5	NA	-29.9
mpyr-mOSO3-p1	-2592319.9	-5769.1	-5780.4	-5781.9	-5786.7	-82427.8	-31.8	-31.8	-32.8	-33.3
mpyr-mSO3-p1	-2395777.0	-5245.4	-5255.4	-5256.9	NA	-81659.5	-31.4	-31.8	NA	-33.1
mpyr-NO3-p1	-1390801.6	-4821.1	-4831.6	-4832.6	-4836.0	-90659.0	-35.1	-35.2	-36.3	-36.6
mpyr-TFA-p1	-2033866.6	-6159.8	-6171.6	-6172.8	NA	-95977.7	-36.9	-36.7	NA	-38.1

27 HBIL + mpyr cation + cc-pVTZ

System	HF	DSysCorT0	DSysCorT1	DSysCorT1_IL1	DSysCorT1_IL2	DIntCorT0	DIntCorT1	DIntCorT1_IL1	DIntCorT1_IL2	BMIntCorr
mpyr-CF3SO3-p1	-3175155.0	-8016.4	NA	NA	NA	-97069.4	NA	NA	NA	-46.6
mpyr-Cl-p1	-1865123.3	-3697.7	NA	NA	NA	-91602.8	NA	NA	NA	-42.2
mpyr-mOSO3-p1	-2592831.3	-6739.4	NA	NA	NA	-91219.5	NA	NA	NA	-45.2
mpyr-mSO3-p1	-2396226.2	-6118.2	NA	NA	NA	-91799.4	NA	NA	NA	-45.9
mpyr-NO3-p1	-1391097.2	-5609.5	NA	NA	NA	-105991.6	NA	NA	NA	-47.1
mpyr-TFA-p1	-2034343.8	-7261.2	NA	NA	NA	-106553.4	NA	NA	NA	-49.5

28 HBIL + TMEA cation + aug-cc-pVDZ

System	HF	DSysCorT0	DSysCorT1	DSysCorT1_IL1	DSysCorT1_IL2	DIntCorT0	DIntCorT1	DIntCorT1_IL1	DIntCorT1_IL2	BMIntCorr
TMEA-CF3SO3-p1	-3177471.1	-6875.7	-6888.9	-6891.0	NA	-67833.4	-26.1	-26.4	NA	-27.4
TMEA-Cl-p1	-1867911.6	-3253.3	-3257.2	-3257.9	NA	-55125.4	-21.2	-21.4	NA	-21.7
TMEA-mOSO3-p1	-2595295.0	-5863.6	-5874.6	-5876.3	-5880.9	-65104.0	-25.0	-25.1	-25.8	-26.1
TMEA-mSO3-p1	-2398747.8	-5336.7	-5346.4	-5348.1	NA	-59652.4	-22.9	-23.2	NA	-24.3
TMEA-NO3-p1	-1393762.2	-4910.3	-4920.3	-4921.6	-4924.5	-58332.0	-22.5	-22.7	-23.3	-23.7
TMEA-TFA-p1	-2036830.8	-6249.5	-6261.0	-6262.5	NA	-68526.4	-26.3	-26.2	NA	-27.2

29 HBIL + TMEA cation + cc-pVTZ

System	HF	DSysCorT0	DSysCorT1	DSysCorT1_IL1	DSysCorT1_IL2	DIntCorT0	DIntCorT1	DIntCorT1_IL1	DIntCorT1_IL2	BMIntCorr
TMEA-CF3SO3-p1	-3178143.5	-8115.3	NA	NA	NA	-71092.5	NA	NA	NA	-35.1
TMEA-Cl-p1	-1868086.3	-3795.9	NA	NA	NA	-62983.7	NA	NA	NA	-30.8
TMEA-mOSO3-p1	-2595814.7	-6838.7	NA	NA	NA	-67692.4	NA	NA	NA	-35.1
TMEA-mSO3-p1	-2399205.0	-6213.4	NA	NA	NA	-63421.1	NA	NA	NA	-33.4
TMEA-NO3-p1	-1394064.3	-5702.5	NA	NA	NA	-67415.2	NA	NA	NA	-31.1
TMEA-TFA-p1	-2037317.4	-7355.2	NA	NA	NA	-72397.3	NA	NA	NA	-35.1

30 2ip + c1mim cation + cc-pVTZ

System	HF	DSysCorT0	DSysCorT1	DSysCorT1_IL1	DSysCorT1_IL2	DIntCorT0	DIntCorT1	DIntCorT1_IL1	DIntCorT1_IL2	BMIntCorr
c1mim-bf4	-3814427.0	-13057.7	NA	NA	NA	-216321.2	NA	NA	NA	-108.9
c1mim-cl	-4007022.0	-8176.2	NA	NA	NA	-230016.8	NA	NA	NA	-115.2

Appendix C

An intuitive approach to finding local minima in ionic materials: a balancing of starting geometry and dynamic evolution – Supporting Information

Supplementary Information

An intuitive approach to finding local minima in ionic materials: a balancing of starting geometry and dynamic evolution

Zoe Luisa Seeger and Ekaterina I. Izgorodina*

School of Chemistry, Monash University, 17 Rainforest Walk, Clayton, Victoria 3800,
Australia

Contents

1	Information	1
2	DBSCAN clustering	1
3	Energies of [C4mim]Cl	2
4	Energies of [C2mpyr][BF ₄]	3
5	Energies of DMSO	6

1 Information

All energies are given in kJ/mol.

The column names are as follows:

Conf	Configuration/Geometry
Low	Lowest energy geometry from first agglomerative clustering: Yes (y) or No (n)
Unique	Lowest energy geometry from second agglomerative clustering: Yes (y) or No (n)
HF	Total FMO3-HF/cc-pVTZ energy
Cor	Total FMO3-SRS-MP2/cc-pVTZ correlation energy
OPLS	Total OPLS-AA energy
Int HF	FMO3-HF/cc-pVTZ interaction energy
Int Cor	FMO3-SRS-MP2/cc-pVTZ interaction correlation energy

This is an abbreviated version of the supplementary information where the Cartesian coordinates of 216 low energy geometries have been removed. These are available on request and are included in the supplementary information of the publication.

2 DBSCAN clustering

Geometries from molecular dynamics simulations were compared to others within the same simulation to eliminate identical structures and principal component analysis was used on their standardised z-matrices to reduce dimensionality before being piped into DBSCAN clustering. The number of principal components was chosen such that 95% explained variance was included. As a clear cutoff value for clustering was not known, a recursive approach was used where the cutoff distance was incrementally increased (Figure 1).

It was seen that, after a sharp decline in the number of groups with increasing cutoff values, a plateau occurred where the number of clusters found was approximately half of the geometries given (i.e. on average each cluster contained two geometries). This plateau indicates that the clusters are separated by a comparatively large difference in principal component space. As the first plateau,

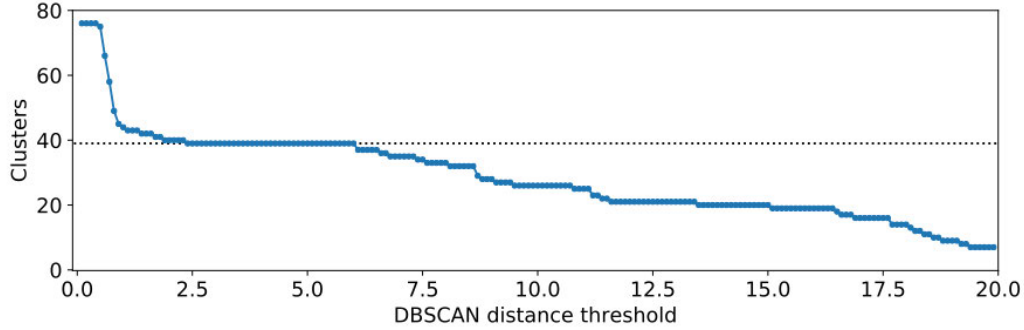


Figure 1: DBSCAN clustering with increasing distance threshold distance in DBSCAN on 76 low energy geometries from an MD simulation. The black line shows the longest plateau which is approximately half of the number of structures.

and thus the most conservative, this was determined to be the best cut-off to use. This plateau was found for each simulation and the geometry with the lowest energy of each cluster was retained. Analysis of the clustering showed that geometries in the same cluster were largely those of similar times in the simulation and had an RMSD of less than 0.05 Å.

3 Energies of [C4mim]Cl

Conf	Low	Unique	HF	Cor	OPLS	Int HF	Int Cor
c4mim-cl-p2-opt-212-90d0d270d90-fofo-step-950314	n	n	-9244427.0	-25660.2	-1336.0	-1755.6	-291.4
c4mim-cl-p2-opt-212-0d0d180d180-oooo-step-245706	n	n	-9244430.2	-25656.0	-1331.0	-1755.7	-288.0
c4mim-cl-p2-opt-122-270d270d180d270-oooo-step-1035504	n	n	-9244421.2	-25663.1	-1339.3	-1749.3	-297.9
c4mim-cl-p2-opt-212-90d0d270d90-fofo-step-955406	n	n	-9244402.8	-25678.3	-1335.1	-1732.2	-313.7
c4mim-cl-p2-opt-212-270d90d180d270-oooo-l-step-583500	n	n	-9244409.8	-25671.3	-1332.4	-1744.3	-299.7
c4mim-cl-p1-opt-212-0d0d0d0-ffoo-step-721478	n	n	-9244401.1	-25678.7	-1335.5	-1740.1	-314.1
c4mim-cl-p2-opt-212-0d180d90d90-fofo-step-379362	n	n	-9244408.6	-25670.7	-1330.6	-1744.4	-301.7
c4mim-cl-p2-opt-212-0d0d270d270-fooo-l-step-1054720	n	n	-9244417.7	-25662.6	-1331.1	-1749.5	-292.5
c4mim-cl-p2-opt-212-90d0d270d90-fofo-step-433950	n	n	-9244419.2	-25660.6	-1336.0	-1738.8	-299.0
c4mim-cl-p2-opt-221-180d0d270d0-foof-step-1064210	n	n	-9244394.5	-25681.6	-1330.9	-1734.9	-313.3
c4mim-cl-p1-opt-221-0d180d270d180-foof-step-586552	n	n	-9244407.0	-25671.6	-1332.3	-1748.0	-295.7
c4mim-cl-p1-opt-212-0d270d0d0-fooo-step-485120	n	n	-9244414.0	-25665.1	-1338.5	-1746.8	-293.8
c4mim-cl-p2-opt-122-0d180d90d90-oooo-step-730020	n	n	-9244415.5	-25662.6	-1333.0	-1734.2	-302.5
c4mim-cl-p1-opt-212-0d90d90d90-fofo-step-725716	n	n	-9244413.2	-25664.3	-1330.7	-1736.8	-298.5
c4mim-cl-p1-opt-212-90d270d180d270-fofo-step-1016164	n	n	-9244401.5	-25674.0	-1334.6	-1740.4	-306.1
c4mim-cl-p1-opt-212-0d0d90d90-ffoo-step-185796	n	n	-9244398.6	-25675.4	-1331.4	-1724.5	-310.9

c4mim-cl-p2-opt-212-270d0d90d270-oooo-step-745168	n	n	-9244405.0	-25669.6	-1337.9	-1737.0	-307.7
c4mim-cl-p1-opt-212-90d90d180d270-fofo-step-377150	n	n	-9244399.0	-25675.4	-1331.6	-1735.6	-306.4
c4mim-cl-p1-opt-212-90d270d180d270-fofo-step-198876	n	n	-9244409.1	-25665.8	-1332.4	-1736.2	-300.0
c4mim-cl-p2-opt-212-0d0d90d270-oooo-l-step-539702	n	n	-9244394.1	-25678.2	-1330.5	-1726.0	-314.8
c4mim-cl-p2-opt-212-90d180d0d90-oooo-step-1006560	n	n	-9244420.0	-25653.7	-1333.0	-1749.2	-283.3
c4mim-cl-p2-opt-212-90d90d180d90-fooo-step-1051158	n	n	-9244406.0	-25667.3	-1330.9	-1742.1	-298.9
c4mim-cl-p2-opt-122-0d180d90d0-fofo-l-step-759326	n	n	-9244408.5	-25663.1	-1330.5	-1732.7	-300.0
c4mim-cl-p1-opt-212-90d180d270d90-fofo-step-845482	n	n	-9244403.0	-25668.7	-1330.7	-1744.5	-300.0
c4mim-cl-p2-opt-212-0d270d90d270-oooo-step-648418	n	n	-9244393.8	-25676.2	-1332.2	-1734.4	-308.1
c4mim-cl-p2-opt-212-0d270d0d0-fofo-step-734210	n	n	-9244391.9	-25678.8	-1339.1	-1731.0	-309.1
c4mim-cl-p1-opt-212-180d180d90d180-fofo-step-815178	n	n	-9244393.1	-25675.7	-1331.1	-1739.0	-307.4
c4mim-cl-p2-opt-212-0d180d90d180-oooo-step-784020	n	n	-9244397.6	-25671.3	-1331.9	-1741.9	-301.0
c4mim-cl-p2-opt-122-0d0d90d90-oooo-l-step-920370	n	n	-9244410.0	-25660.0	-1331.4	-1746.6	-291.5
c4mim-cl-p2-opt-221-90d180d0d90-foof-l-step-570350	n	n	-9244407.6	-25662.0	-1332.5	-1741.4	-294.7
c4mim-cl-p2-opt-212-0d0d0d0-fooo-step-537874	n	n	-9244410.8	-25658.2	-1331.8	-1736.9	-290.0
c4mim-cl-p2-opt-221-180d270d180d270-foof-step-771074	n	n	-9244412.8	-25657.1	-1332.5	-1742.4	-292.7
c4mim-cl-p2-opt-212-0d0d180d0-oooo-step-245482	n	n	-9244420.2	-25649.0	-1330.6	-1743.8	-284.4
c4mim-cl-p2-opt-212-0d180d270d270-fooo-l-step-656542	n	n	-9244392.4	-25673.6	-1330.5	-1723.1	-308.5
c4mim-cl-p2-opt-212-0d270d90d180-fofo-step-1010588	n	n	-9244402.3	-25664.6	-1330.6	-1743.5	-293.6
c4mim-cl-p1-opt-212-0d270d90d90-oooo-step-542922	n	n	-9244395.8	-25670.8	-1333.9	-1741.1	-296.9
c4mim-cl-p2-opt-122-90d90d180d90-oooo-step-996358	n	n	-9244398.9	-25665.3	-1333.5	-1745.8	-294.1
c4mim-cl-p2-opt-122-0d270d0d0-fofo-step-718958	n	n	-9244392.2	-25667.2	-1333.0	-1732.5	-298.8
c4mim-cl-p1-opt-212-0d180d90d0-fooo-step-617152	n	n	-9244396.6	-25663.0	-1331.3	-1736.7	-296.8
c4mim-cl-p1-opt-212-0d180d90d0-fooo-step-613860	n	n	-9244398.2	-25660.8	-1330.8	-1734.6	-292.4
c4mim-cl-p2-opt-122-0d270d0d270-fofo-step-986778	n	n	-9244383.4	-25671.6	-1331.3	-1725.5	-302.0
c4mim-cl-p1-opt-212-90d90d270d90-fooo-step-114926	y	y	-9244418.7	-25668.4	-1338.3	-1750.7	-301.4
c4mim-cl-p2-opt-221-90d0d180d90-foof-step-88658	y	n	-9244418.9	-25665.9	-1342.9	-1741.2	-301.7
c4mim-cl-p2-opt-122-0d180d90d90-oooo-step-211600	y	y	-9244410.8	-25669.9	-1340.8	-1733.0	-305.7
c4mim-cl-p1-opt-212-180d180d90d180-fooo-step-592506	y	n	-9244394.8	-25683.9	-1342.5	NA	NA
c4mim-cl-p2-opt-212-270d90d180d270-fooo-l-step-531766	y	n	-9244405.8	-25672.2	-1337.9	-1732.4	-309.0
c4mim-cl-p2-opt-212-0d90d180d90-fofo-step-367488	y	n	-9244414.1	-25665.0	-1334.4	NA	NA
c4mim-cl-p2-opt-212-0d0d90d270-oooo-l-step-539894	y	n	-9244398.9	-25677.3	-1332.9	NA	NA
c4mim-cl-p2-opt-221-0d0d0d0-foof-step-193318	y	n	-9244403.9	-25671.3	-1335.7	NA	NA
c4mim-cl-p1-opt-212-0d0d90d180-fooo-step-307022	y	n	-9244395.5	-25669.8	-1333.2	NA	NA
c4mim-cl-p1-opt-212-180d180d270d180-fooo-step-899872	y	n	-9244365.0	-25691.8	-1334.1	NA	NA
sa	sa	sa	-9244386.8	-25689.8	-1341.0	NA	NA

4 Energies of [C2mpyr][BF4]

Conf	Low	Unique	HF	Cor	OPLS	Int HF	Int Cor
c2mpyr-bf4-p1-opt-122-180d180d90d180-fofo-step-743114	n	n	-7895317.8	-33277.6	-612.9	-1610.1	-220.1
c2mpyr-bf4-p2-opt-212-90d0d180d90-ffoo-step-1067538	n	n	-7895312.6	-33280.4	-612.8	-1603.4	-222.7
c2mpyr-bf4-p2-opt-221-0d90d180d180-fooo-step-387566	n	n	-7895317.8	-33274.9	-611.9	-1609.9	-217.1
c2mpyr-bf4-p2-opt-221-270d270d180d270-oooo-step-323198	n	n	-7895313.3	-33278.1	-613.9	-1601.7	-221.6
c2mpyr-bf4-p2-opt-221-0d270d90d180-fofo-step-230738	n	n	-7895312.4	-33279.0	-612.7	-1602.2	-222.0
c2mpyr-bf4-p2-opt-212-180d270d90d180-fofo-step-792678	n	n	-7895313.6	-33277.8	-612.6	-1605.0	-220.1
c2mpyr-bf4-p2-opt-212-0d270d90d180-foof-step-479620	n	n	-7895314.7	-33276.1	-613.2	-1601.1	-219.9
c2mpyr-bf4-p1-opt-212-0d180d90d180-oooo-step-581848	n	n	-7895315.5	-33275.9	-612.5	-1607.7	-218.8
c2mpyr-bf4-p2-opt-212-0d90d180d270-foof-step-298780	n	n	-7895316.3	-33274.8	-612.5	-1608.4	-217.7
c2mpyr-bf4-p2-opt-221-0d0d270d0-fooo-step-760972	n	n	-7895317.6	-33273.3	-612.0	-1610.0	-215.2
c2mpyr-bf4-p2-opt-212-90d270d90d270-fofo-step-295600	n	n	-7895316.4	-33274.3	-612.4	-1608.5	-216.7
c2mpyr-bf4-p1-opt-212-180d180d270d0-oooo-step-193816	n	n	-7895312.3	-33277.4	-612.7	-1604.1	-220.4
c2mpyr-bf4-p2-opt-122-0d90d180d180-fooo-step-863636	n	n	-7895312.3	-33277.5	-613.3	-1604.1	-219.8
c2mpyr-bf4-p2-opt-212-0d180d270d0-ffoo-step-386516	n	n	-7895314.7	-33275.1	-612.1	-1606.1	-217.8
c2mpyr-bf4-p2-opt-221-90d180d270d180-ffoo-step-268948	n	n	-7895315.1	-33274.4	-611.9	-1602.2	-218.1
c2mpyr-bf4-p2-opt-221-90d90d180d0-fooo-step-1027236	n	n	-7895310.1	-33279.4	-612.7	-1602.4	-221.8
c2mpyr-bf4-p1-opt-122-0d270d180d270-fofo-step-497048	n	n	-7895313.4	-33276.5	-613.6	-1606.5	-218.8
c2mpyr-bf4-p1-opt-122-0d180d90d0-fofo-step-514900	n	n	-7895309.6	-33279.0	-614.6	-1598.3	-222.3
c2mpyr-bf4-p1-opt-212-270d90d0d270-fofo-step-896380	n	n	-7895313.2	-33275.1	-613.1	-1602.8	-218.2
c2mpyr-bf4-p2-opt-221-180d180d270d180-foof-step-108632	n	n	-7895309.9	-33278.0	-612.1	-1603.8	-219.8
c2mpyr-bf4-p2-opt-212-0d270d90d90-ffoo-step-695360	n	n	-7895313.4	-33274.9	-612.1	-1604.8	-217.9
c2mpyr-bf4-p2-opt-221-0d0d270d270-fooo-step-624566	n	n	-7895307.4	-33280.3	-612.8	-1597.5	-223.0
c2mpyr-bf4-p1-opt-122-180d270d180d270-fofo-step-746254	n	n	-7895312.1	-33275.9	-612.5	-1600.1	-219.5
c2mpyr-bf4-p2-opt-212-0d90d270d270-ffoo-step-357150	n	n	-7895311.5	-33276.1	-611.9	-1599.5	-219.0
c2mpyr-bf4-p1-opt-212-0d270d90d270-fofo-step-757132	n	n	-7895307.4	-33279.8	-613.1	-1597.0	-222.8
c2mpyr-bf4-p2-opt-221-0d180d90d270-oooo-step-583910	n	n	-7895312.1	-33275.5	-611.8	-1604.2	-217.2
c2mpyr-bf4-p2-opt-212-0d270d180d0-oooo-step-278472	n	n	-7895312.2	-33274.9	-611.8	-1599.9	-218.0
c2mpyr-bf4-p1-opt-221-270d180d90d270-foof-step-275856	n	n	-7895310.3	-33276.8	-612.4	-1603.8	-218.9
c2mpyr-bf4-p1-opt-122-0d90d180d270-fofo-step-878884	n	n	-7895311.7	-33275.5	-612.2	-1600.6	-218.9
c2mpyr-bf4-p2-opt-122-270d180d0d270-ffoo-step-321836	n	n	-7895310.5	-33276.9	-612.7	-1600.3	-219.7
c2mpyr-bf4-p1-opt-221-90d180d270d180-foof-step-908420	n	n	-7895312.0	-33275.5	-612.6	-1604.7	-217.7
c2mpyr-bf4-p1-opt-221-270d180d0d90-foof-step-451848	n	n	-7895310.3	-33276.3	-612.2	-1604.1	-217.8
c2mpyr-bf4-p2-opt-122-90d270d180d270-fofo-step-609930	n	n	-7895308.1	-33278.5	-611.9	-1597.6	-221.5
c2mpyr-bf4-p2-opt-122-0d180d270d0-oooo-step-632590	n	n	-7895312.1	-33275.1	-612.1	-1603.7	-217.0
c2mpyr-bf4-p1-opt-212-0d180d270d270-fofo-step-172898	n	n	-7895309.7	-33276.7	-612.4	-1599.2	-219.8
c2mpyr-bf4-p1-opt-122-0d270d0d0-fofo-step-586380	n	n	-7895304.2	-33281.2	-612.7	-1593.0	-223.9
c2mpyr-bf4-p2-opt-122-0d90d180d90-ffoo-step-967384	n	n	-7895309.4	-33276.2	-612.3	-1601.5	-218.2
c2mpyr-bf4-p2-opt-221-90d180d270d90-ffoo-step-996394	n	n	-7895308.8	-33276.5	-612.6	-1601.1	-218.7
c2mpyr-bf4-p2-opt-122-0d90d180d90-foof-step-123838	n	n	-7895310.2	-33275.3	-612.5	-1602.5	-217.3

c2mpyr-bf4-p2-opt-122-90d270d0d90-fofo-step-543220	n	n	-7895309.4	-33275.7	-611.7	-1598.9	-218.3
c2mpyr-bf4-p2-opt-212-0d180d90d270-fooo-step-224920	n	n	-7895305.8	-33278.9	-613.4	-1595.6	-221.7
c2mpyr-bf4-p2-opt-212-180d270d90d180-fofo-step-1079698	n	n	-7895305.4	-33279.3	-612.0	-1598.6	-221.0
c2mpyr-bf4-p2-opt-122-0d0d270d270-fooo-step-1074784	n	n	-7895312.6	-33272.5	-612.1	-1600.7	-215.1
c2mpyr-bf4-p2-opt-122-180d180d270d0-fofo-step-155006	n	n	-7895308.4	-33276.4	-613.3	-1598.7	-219.3
c2mpyr-bf4-p2-opt-212-0d270d90d180-ffoo-step-716340	n	n	-7895305.8	-33278.3	-612.0	-1601.4	-219.2
c2mpyr-bf4-p2-opt-122-0d90d180d180-oooo-step-679874	n	n	-7895306.5	-33277.5	-611.7	-1594.5	-220.6
c2mpyr-bf4-p1-opt-122-90d90d270d90-fofo-step-595874	n	n	-7895305.0	-33278.4	-611.8	-1597.5	-219.9
c2mpyr-bf4-p2-opt-221-0d180d270d180-ffoo-step-794014	n	n	-7895304.2	-33278.4	-613.7	NA	NA
c2mpyr-bf4-p2-opt-212-0d180d90d180-fofo-step-810142	n	n	-7895306.4	-33276.0	-611.7	NA	NA
c2mpyr-bf4-p2-opt-122-90d90d270d90-oooo-step-926242	n	n	-7895301.7	-33279.9	-612.3	-1594.8	-222.4
c2mpyr-bf4-p2-opt-212-0d90d90d90-ffoo-step-356430	n	n	-7895306.2	-33275.4	-612.4	-1595.6	-218.6
c2mpyr-bf4-p1-opt-122-90d0d180d270-fofo-step-380338	n	n	-7895305.7	-33274.8	-612.4	-1593.2	-218.6
c2mpyr-bf4-p1-opt-221-180d270d90d180-foof-step-465390	n	n	-7895300.8	-33278.8	-611.9	-1589.2	-221.8
c2mpyr-bf4-p2-opt-221-0d180d90d180-fofo-step-691410	y	y	-7895315.5	-33280.8	-615.4	-1608.4	-223.3
c2mpyr-bf4-p2-opt-212-0d180d90d90-foof-step-777850	y	y	-7895313.7	-33281.3	-613.6	-1607.1	-224.2
c2mpyr-bf4-p1-opt-212-180d180d270d0-oooo-step-269456	y	y	-7895318.7	-33276.6	-612.8	-1611.3	-219.0
c2mpyr-bf4-p2-opt-221-270d270d180d270-oooo-step-322986	y	y	-7895316.7	-33277.6	-615.7	-1604.8	-221.2
c2mpyr-bf4-p2-opt-212-0d180d180d180-oooo-step-1035592	y	y	-7895319.0	-33274.6	-613.7	-1610.0	-217.2
c2mpyr-bf4-p2-opt-212-180d270d90d180-fofo-step-792834	y	y	-7895314.1	-33279.4	-614.9	-1605.7	-221.9
c2mpyr-bf4-p2-opt-212-90d0d180d90-ffoo-step-1067662	y	y	-7895313.5	-33279.3	-613.2	-1604.8	-221.3
c2mpyr-bf4-p2-opt-221-0d270d90d0-oooo-step-1018302	y	n	-7895314.5	-33278.2	-614.9	NA	NA
c2mpyr-bf4-p2-opt-221-0d270d0d270-fooo-step-496428	y	y	-7895317.9	-33274.7	-614.2	-1608.9	-216.8
c2mpyr-bf4-p1-opt-122-0d180d90d180-fofo-step-561030	y	n	-7895314.7	-33277.8	-612.5	-1606.8	-220.3
c2mpyr-bf4-p2-opt-122-180d0d270d0-oooo-step-533090	y	n	-7895312.0	-33280.0	-613.7	-1599.3	-222.9
c2mpyr-bf4-p2-opt-122-180d90d270d90-oooo-step-862422	y	n	-7895312.4	-33279.5	-614.5	-1604.8	-221.7
c2mpyr-bf4-p2-opt-212-0d270d270d270-fofo-step-687596	y	y	-7895313.7	-33277.8	-614.2	-1603.3	-221.0
c2mpyr-bf4-p2-opt-221-0d0d270d0-fooo-step-760996	y	n	-7895316.7	-33274.8	-613.4	-1609.0	-216.8
c2mpyr-bf4-p2-opt-221-90d0d180d270-ffoo-step-1016814	y	n	-7895312.5	-33278.0	-615.4	-1602.0	-221.1
c2mpyr-bf4-p2-opt-221-0d0d90d90-oooo-step-844336	y	y	-7895313.4	-33277.1	-614.8	-1605.9	-219.6
c2mpyr-bf4-p1-opt-122-0d270d180d270-fofo-step-496980	y	n	-7895312.3	-33278.3	-613.7	-1605.8	-220.9
c2mpyr-bf4-p2-opt-221-180d0d270d180-fooo-step-961398	y	n	-7895312.7	-33277.6	-613.7	-1604.5	-219.6
c2mpyr-bf4-p1-opt-212-180d180d270d0-oooo-step-198300	y	y	-7895312.5	-33277.5	-613.0	-1603.3	-220.1
c2mpyr-bf4-p1-opt-212-180d90d270d90-fooo-step-755206	y	n	-7895312.4	-33277.2	-613.7	-1600.8	-219.7
c2mpyr-bf4-p1-opt-122-180d90d270d90-fofo-step-192456	y	y	-7895311.2	-33278.0	-616.3	-1600.2	-221.3
c2mpyr-bf4-p1-opt-212-0d270d180d270-fofo-step-745882	y	n	-7895309.3	-33279.7	-614.6	-1597.5	-222.4
c2mpyr-bf4-p2-opt-221-180d180d270d180-fooo-step-230336	y	y	-7895311.3	-33277.2	-615.1	-1599.9	-220.9
c2mpyr-bf4-p1-opt-221-90d90d180d90-foof-step-264634	y	n	-7895309.1	-33279.1	-616.6	-1597.9	-222.3
c2mpyr-bf4-p2-opt-212-0d0d90d180-fofo-step-832418	y	n	-7895309.0	-33278.4	-612.3	-1601.2	-220.5
c2mpyr-bf4-p1-opt-212-0d180d0d180-fofo-step-1075326	y	y	-7895310.9	-33276.5	-612.9	-1602.5	-218.5
c2mpyr-bf4-p2-opt-221-0d90d270d270-foof-step-266770	y	n	-7895312.0	-33275.1	-613.5	-1600.4	-218.4

c2mpyr-bf4-p2-opt-122-270d90d180d270-fooo-step-585470	y	y	-7895312.2	-33274.8	-612.4	-1601.0	-218.7
c2mpyr-bf4-p2-opt-221-0d180d90d180-fooo-step-416866	y	n	-7895311.0	-33276.2	-613.5	-1606.8	-217.7
c2mpyr-bf4-p2-opt-122-90d90d270d0-foof-step-1014810	y	n	-7895308.2	-33277.9	-611.9	-1601.6	-219.3
c2mpyr-bf4-p1-opt-212-0d270d270d270-fofo-step-263926	y	n	-7895307.9	-33278.2	-612.9	-1597.0	-221.5
c2mpyr-bf4-p2-opt-221-0d180d180d180-foof-step-677062	y	n	-7895306.1	-33279.4	-611.9	-1595.2	-222.9
c2mpyr-bf4-p1-opt-221-0d180d270d180-foof-step-124776	y	n	-7895307.7	-33278.0	-613.0	-1596.6	-220.3
c2mpyr-bf4-p2-opt-221-0d90d0d0-foof-step-721294	y	n	-7895307.7	-33277.5	-614.5	-1600.5	-219.3
c2mpyr-bf4-p2-opt-221-0d0d180d0-oooo-step-791592	y	n	-7895306.0	-33279.2	-611.7	-1595.9	-221.8
c2mpyr-bf4-p1-opt-221-90d90d180d270-ffoo-step-322032	y	n	-7895307.7	-33277.7	-613.4	NA	NA
c2mpyr-bf4-p2-opt-212-180d180d270d0-fofo-step-256150	y	n	-7895304.9	-33279.9	-612.8	-1593.8	-223.3
c2mpyr-bf4-p2-opt-212-0d0d270d270-oooo-step-683328	y	n	-7895304.3	-33280.0	-611.8	-1597.9	-221.9
c2mpyr-bf4-p2-opt-221-180d90d0d180-oooo-step-917918	y	n	-7895305.3	-33278.8	-612.6	-1596.3	-221.2
c2mpyr-bf4-p1-opt-212-0d0d90d90-fofo-step-829496	y	n	-7895305.9	-33277.8	-613.2	NA	NA
c2mpyr-bf4-p2-opt-221-90d180d0d90-ffoo-step-681056	y	n	-7895308.4	-33275.8	-612.0	-1600.6	-218.2
c2mpyr-bf4-p2-opt-212-180d90d270d90-fofo-step-598844	y	n	-7895305.8	-33277.8	-613.1	NA	NA
c2mpyr-bf4-p2-opt-212-90d0d180d90-fofo-step-327324	y	n	-7895305.0	-33278.7	-612.5	-1597.7	-220.1
c2mpyr-bf4-p1-opt-122-0d0d90d0-fofo-step-167138	y	n	-7895305.3	-33277.9	-613.5	NA	NA
c2mpyr-bf4-p2-opt-212-270d270d90d270-fooo-step-596750	y	n	-7895302.0	-33280.9	-613.3	-1590.1	-223.7
c2mpyr-bf4-p2-opt-221-90d180d90d180-ffoo-step-478814	y	n	-7895303.1	-33278.6	-613.8	-1591.2	-221.7
c2mpyr-bf4-p1-opt-221-90d180d270d0-foof-step-852046	y	n	-7895306.4	-33275.6	-612.5	-1597.5	-217.4
sa	sa	sa	-7895310.7	-33278.4	-611.7	NA	NA

5 Energies of DMSO

Conf	Low	Unique	HF	Cor	OPLS	Int HF	Int Cor
dms0-122-90d90d180d270-oooo-step-19944-last	n	n	-5793531.2	-10334.8	-199.6	-63.6	-56.0
dms0-122-90d90d180d90-ffoo-step-28087-last	n	n	-5793529.0	-10335.7	-199.3	-61.1	-57.0
dms0-212-90d180d270d0-fofo-step-8113-last	n	n	-5793530.9	-10332.1	-205.4	-63.3	-53.6
dms0-212-90d90d270d90-oooo-step-48973-last	n	n	-5793529.5	-10333.7	-198.7	-61.6	-55.0
dms0-221-0d270d0d270-ffoo-step-32608-last	n	n	-5793520.6	-10337.5	-199.5	-52.1	-59.6
dms0-221-90d270d180d90-oooo-step-38107-last	n	n	-5793517.4	-10339.4	-200.4	-49.4	-61.1
dms0-221-0d270d180d180-fooo-step-25500-last	n	n	-5793514.3	-10342.6	-200.5	-46.1	-64.1
dms0-212-90d90d180d270-ffoo-step-18912-last	n	n	-5793521.8	-10334.7	-200.3	-52.9	-56.6
dms0-122-0d90d270d270-oooo-step-35796-last	n	n	-5793516.0	-10340.7	-200.6	-47.9	-62.4
dms0-212-0d0d270d0-fofo-step-9813-last	n	n	-5793518.2	-10338.0	-198.6	-50.0	-59.8
dms0-212-0d270d90d270-oooo-step-44093-last	n	n	-5793515.1	-10340.9	-200.0	-47.4	-62.4
dms0-221-0d180d270d0-oooo-step-29314-last	n	n	-5793516.2	-10339.7	-198.3	-48.0	-61.3
dms0-122-0d270d90d270-fooo-step-30771-last	n	n	-5793519.0	-10336.7	-198.4	-50.6	-58.1
dms0-122-90d270d0d90-fooo-step-33161-last	n	n	-5793528.8	-10326.7	-199.7	-61.2	-48.6
dms0-122-0d0d180d270-ffoo-step-23415-last	n	n	-5793516.0	-10339.3	-198.4	-48.3	-60.6

dms0-212-180d270d0d180-oooo-step-12195-last	n	n	-5793514.7	-10340.4	-199.8	-46.4	-61.7
dms0-212-90d0d270d0-fooo-step-16441-last	n	n	-5793516.6	-10337.3	-200.0	-49.0	-58.8
dms0-212-0d90d90d90-oooo-step-28899-last	n	n	-5793512.7	-10340.0	-198.2	-45.4	-61.5
dms0-122-0d0d180d270-ffoo-step-4467-last	n	n	-5793520.1	-10332.5	-198.5	-51.5	-54.5
dms0-122-270d180d90d270-ffoo-step-42113-last	n	n	-5793507.0	-10345.1	-198.4	-38.6	-67.5
dms0-221-0d180d180d180-oooo-step-21152-last	n	n	-5793513.7	-10338.4	-198.9	-46.2	-59.9
dms0-122-0d90d180d0-oooo-step-46803-last	n	n	-5793509.0	-10342.4	-199.6	-40.5	-64.0
dms0-221-0d180d90d270-ffoo-step-44991-last	n	n	-5793509.4	-10341.3	-198.8	-40.3	-63.3
dms0-212-90d0d180d270-fofo-step-20624-last	n	n	-5793506.7	-10342.3	-198.5	-38.0	-64.2
sa	sa	sa	-5793524.1	-10338.6	-205.0	NA	NA
dms0-221-270d90d0d270-oooo-step-34249-last	y	y	-5793525.9	-10337.4	-204.7	-57.7	-58.8
dms0-221-0d90d0d0-oooo-step-11444-last	y	y	-5793525.7	-10337.4	-202.1	-58.2	-58.4
dms0-212-90d180d270d0-fofo-step-8105-last	y	n	-5793530.3	-10332.7	-205.7	NA	NA
dms0-221-0d270d90d270-fofo-step-33288-last	y	n	-5793520.2	-10342.6	-201.0	NA	NA
dms0-122-0d270d90d0-fofo-step-26068-last	y	y	-5793525.2	-10337.2	-202.5	-56.7	-58.5
dms0-221-0d270d0d0-fooo-step-26064-last	y	y	-5793524.0	-10338.0	-200.6	-56.4	-59.0
dms0-221-0d180d270d180-oooo-step-33621-last	y	n	-5793518.9	-10342.0	-201.5	NA	NA
dms0-221-270d270d90d180-ffoo-step-10766-last	y	n	-5793523.0	-10336.4	-201.2	-55.3	-57.8
dms0-212-90d90d180d270-ffoo-step-22844-last	y	n	-5793524.4	-10335.4	-199.7	NA	NA
dms0-221-270d0d180d270-ffoo-step-39916-last	y	n	-5793524.2	-10335.0	-200.9	NA	NA
dms0-122-90d90d180d270-oooo-step-7032-last	y	n	-5793516.6	-10342.7	-201.2	NA	NA
dms0-221-90d0d180d90-ffoo-step-10202-last	y	n	-5793521.5	-10337.1	-200.7	NA	NA
dms0-221-0d180d270d180-oooo-step-42832-last	y	y	-5793525.8	-10333.1	-198.5	-57.3	-54.7
dms0-212-0d270d180d270-fooo-step-34075-last	y	n	-5793520.3	-10338.0	-201.8	NA	NA
dms0-221-0d0d90d180-fofo-step-31957-last	y	n	-5793525.4	-10332.7	-201.3	NA	NA
dms0-221-0d90d270d90-fofo-step-20883-last	y	n	-5793519.2	-10339.1	-200.5	NA	NA
dms0-122-0d90d180d270-fofo-step-9105-last	y	n	-5793514.6	-10343.7	-202.2	NA	NA
dms0-122-0d90d0d90-oooo-step-48310-last	y	n	-5793517.8	-10340.0	-200.0	NA	NA
dms0-212-180d90d0d180-fofo-step-46788-last	y	n	-5793516.1	-10342.1	-200.8	NA	NA
dms0-122-180d270d90d180-ffoo-step-31229-last	y	n	-5793516.4	-10341.2	-201.2	NA	NA
dms0-221-180d270d0d180-fooo-step-22814-last	y	n	-5793522.0	-10334.8	-198.9	NA	NA
dms0-212-0d0d0d0-fooo-step-42729-last	y	n	-5793526.0	-10330.8	-201.0	NA	NA
dms0-122-0d90d270d270-oooo-step-37088-last	y	n	-5793516.9	-10339.9	-201.6	NA	NA
dms0-212-0d0d270d0-fofo-step-9917-last	y	n	-5793517.1	-10339.1	-199.5	NA	NA
dms0-212-0d180d270d270-fooo-step-35766-last	y	n	-5793525.4	-10330.6	-198.9	-57.4	-52.0
dms0-122-270d0d180d270-oooo-step-7922-last	y	n	-5793518.8	-10336.6	-199.4	NA	NA
dms0-212-90d90d180d270-ffoo-step-18866-last	y	n	-5793519.7	-10335.9	-200.4	NA	NA
dms0-122-90d180d0d90-oooo-step-20972-last	y	n	-5793513.0	-10342.5	-200.6	NA	NA
dms0-221-0d270d180d0-fofo-step-33508-last	y	n	-5793523.2	-10332.2	-203.6	NA	NA
dms0-212-0d0d0d0-fooo-step-48310-last	y	n	-5793524.2	-10330.8	-199.1	NA	NA
dms0-221-0d180d180d180-oooo-step-21475-last	y	n	-5793516.4	-10338.8	-199.9	NA	NA

dms0-212-0d270d90d270-fooo-step-20684-last	y	n	-5793508.0	-10346.4	-199.6	NA	NA
dms0-221-270d270d90d180-fooo-step-28207-last	y	n	-5793521.6	-10333.0	-199.5	-53.2	-54.7
dms0-221-180d180d270d180-fofo-step-31133-last	y	n	-5793527.5	-10327.1	-200.2	-59.6	-48.7
dms0-122-90d90d180d270-oooo-step-12940-last	y	n	-5793510.8	-10343.2	-200.2	NA	NA
dms0-221-0d270d180d270-oooo-step-16605-last	y	n	-5793513.0	-10340.2	-200.4	NA	NA
dms0-122-0d90d0d90-fofo-step-8738-last	y	n	-5793505.7	-10346.6	-199.8	NA	NA
dms0-212-270d0d180d270-oooo-step-32116-last	y	n	-5793516.4	-10331.5	-198.4	NA	NA
dms0-122-180d0d270d0-oooo-step-24683-last	y	n	-5793499.3	-10346.8	-199.4	NA	NA
dms0-212-0d0d0d0-oooo-step-8657-last	y	n	-5793514.4	-10332.1	-198.5	NA	NA
dms0-212-270d0d90d270-oooo-step-44079-last	y	n	-5793497.7	-10346.6	-198.7	NA	NA

Appendix D

Cluster approach to the prediction of thermodynamic and transport properties of ionic liquids – Supporting Information

Cluster approach to the prediction of thermodynamic and transport properties of ionic liquids

Zoe L. Seeger, Rika Kobayashi and Ekaterina I. Izgorodina*

Ionic liquid statistics for melting point, K (MP), and conductivity, S cm⁻¹ (Cond), correlations with interaction energy and dispersion interaction energy Boltzmann weighted over all configurations and given in kJ mol⁻¹.

Cation	Anion	n	MP	Ref.	Cond	Ref.	Total Interaction 2IP	Ratio 2IP	Dispersion Interaction 2IP	Predicted MP	Pred Cond
C _n mim ⁺	BF ₄ ⁻	1	376.6	1	N/A	-	-379.4	7.3	-52.2	356.5	11.9
C _n mim ⁺	BF ₄ ⁻	2	288.0	2	12.0	2	-373.6	6.8	-54.9	314.9	10.9
C _n mim ⁺	BF ₄ ⁻	3	256.0	3	5.9	3	-365.6	5.8	-63.3	222.0	7.4
C _n mim ⁺	BF ₄ ⁻	4	202.0	4	3.1	2	-366.1	5.9	-62.5	229.2	7.7
C _n mim ⁺	Cl ⁻	1	398.0	5	N/A	-	-404.6	6.4	-63.1	485.1	7.5
C _n mim ⁺	Cl ⁻	2	362.0	6	10.4	6	-400.9	6.2	-65.0	463.4	6.7
C _n mim ⁺	Cl ⁻	3	333.0	7	N/A	-	-395.6	5.7	-69.7	420.5	4.8
C _n mim ⁺	Cl ⁻	4	341.8	6	3.3	6	-392.2	5.4	-72.9	394.8	3.5
C _n mim ⁺	N(CN) ₂ ⁻	1	307.0	8	36.0	8	-344.2	4.2	-82.2	290.8	25.9
C _n mim ⁺	N(CN) ₂ ⁻	2	252.0	2	25.3	2	-333.1	3.8	-87.4	258.0	18.2
C _n mim ⁺	N(CN) ₂ ⁻	3	N/A	-	N/A	-	-332.8	3.8	-87.3	258.2	18.4
C _n mim ⁺	N(CN) ₂ ⁻	4	263.0	8	9.5	2	-327.2	3.4	-95.3	225.3	6.6
C _n mpyr ⁺	BF ₄ ⁻	1	613.0	9	0.0	9	-373.3	6.5	-57.2	495.0	N/A
C _n mpyr ⁺	BF ₄ ⁻	2	567.0	10	0.0	10	-367.0	6.2	-58.9	468.8	N/A
C _n mpyr ⁺	BF ₄ ⁻	3	337.0	9	0.0	9	-360.9	5.6	-64.2	415.6	N/A
C _n mpyr ⁺	BF ₄ ⁻	4	411.0	9	0.0	9	-353.4	5.1	-69.2	370.9	N/A
C _n mpyr ⁺	Cl ⁻	1	533.0	11	N/A	-	-410.3	6.8	-60.2	519.8	N/A
C _n mpyr ⁺	Cl ⁻	2	N/A	-	N/A	-	-401.6	6.3	-63.7	475.0	N/A
C _n mpyr ⁺	Cl ⁻	3	495.0	2	N/A	-	-396.6	5.7	-69.9	420.5	N/A
C _n mpyr ⁺	Cl ⁻	4	468.0	2	N/A	-	-393.7	5.5	-71.8	403.9	N/A
C _n mpyr ⁺	N(CN) ₂ ⁻	1	388.0	12	57.7	6	-344.9	5.5	-63.0	402.8	54.3
C _n mpyr ⁺	N(CN) ₂ ⁻	2	263.2	13	15.3	6	-330.3	4.1	-79.9	286.3	29.3
C _n mpyr ⁺	N(CN) ₂ ⁻	3	262.4	13	15.7	13	-324.7	3.6	-89.8	241.1	14.7
C _n mpyr ⁺	N(CN) ₂ ⁻	4	218.0	12	9.8	2	-326.6	3.7	-88.1	249.2	17.2

1. D. Holbrey, J.; R. Seddon, K. J. Chem. Soc., Dalton Trans. 1999, 2133-2140.
2. IoLiTec Ionic Liquids Technologies GmbH, S., D-74076 Heilbronn, Deutschland.
3. Nishida, T.; Tashiro, Y.; Yamamoto, M. J. Fluorine Chem. 2003, 120, 135-141.
4. <http://www.merck-chemicals.com/July 2010>.
5. Fannin, A. A.; Floreani, D. A.; King, L. A.; Landers, J. S.; Piersma, B. J.; Stech, D. J.; Vaugh, R. L.; Wilkes, J. S.; Williams, J. L. J. Phys. Chem. 1984, 88, 22614-22621.
6. Izgorodina, E. I.; Golze, D.; Maganti, R.; Armel, V.; Taige, M.; Schubert, T. J. S.; MacFarlane, D. R., PCCP, 2013, Supplementary Information.
7. Ngo, H. L.; LeCompte, K.; Hargens, L.; McEwen, A. B. Thermochim. Acta, 2000, 357-358, 97-102
8. Yoshida, Y.; Baba, O.; Saito, G. J. Phys. Chem. B, 2007, 111, 4742-4749.
9. Forsyth, S.; Golding, J.; MacFarlane, D. R.; Forsyth, M., Electrochim. Acta, 2001, 46, 1753-1757.

10. Kanatani, T.; Ueno, R.; Matsumoto, K.; Nohira, T.; Hagiwara, R. J. Fluorine Chem. 2009, 130, 979-984.
11. Smiglak, M.; Hines, C. C.; Rogers, R. D. Green Chem. 2010, 12, 491-501.
12. MacFarlane, D. R.; Golding, J.; Forsyth, S.; Forsyth, M.; Deacon, G. B. Chem. Commun. 2001, 1430-1431.
13. Annat, G., 2012, PhD thesis, School of Chemistry, Monash University.

Energies of lowest energy configurations (see Table I of MS) of $[C_n\text{mim}]X$ and $[C_n\text{mpyr}]X$ ionic liquids where $n = 1 - 4$ and $X = \text{Cl}^-$, BF_4^- and $\text{N}(\text{CN})_2^-$ and energies are given in kJ mol^{-1} unless stated otherwise.

Cation	Anion	n	Total energy (Hartrees)	Interaction energy*	Dispersion interaction energy
$C_n\text{mim}^+$	BF_4^-	1	-1458.608295	-760.9	-103.6
$C_n\text{mim}^+$	BF_4^-	2	-1537.154698	-749.9	-108.0
$C_n\text{mim}^+$	BF_4^-	3	-1615.694539	-732.8	-127.6
$C_n\text{mim}^+$	BF_4^-	4	-1694.232259	-738.1	-122.8
$C_n\text{mim}^+$	Cl^-	1	-1529.754438	-799.2	-134.7
$C_n\text{mim}^+$	Cl^-	2	-1608.300870	-794.8	-136.4
$C_n\text{mim}^+$	Cl^-	3	-1686.841356	-788.3	-141.3
$C_n\text{mim}^+$	Cl^-	4	-1765.380296	-784.8	-144.1
$C_n\text{mim}^+$	$\text{N}(\text{CN})_2^-$	1	-1090.591112	-688.3	-164.7
$C_n\text{mim}^+$	$\text{N}(\text{CN})_2^-$	2	-1169.132822	-665.3	-176.6
$C_n\text{mim}^+$	$\text{N}(\text{CN})_2^-$	3	-1247.674959	-665.9	-174.7
$C_n\text{mim}^+$	$\text{N}(\text{CN})_2^-$	4	-1326.215356	-652.7	-193.2
$C_n\text{mpyr}^+$	BF_4^-	1	-1431.388589	-744.0	-117.0
$C_n\text{mpyr}^+$	BF_4^-	2	-1509.929539	-734.3	-118.0
$C_n\text{mpyr}^+$	BF_4^-	3	-1588.467651	-722.1	-128.4
$C_n\text{mpyr}^+$	BF_4^-	4	-1667.004711	-699.9	-148.0
$C_n\text{mpyr}^+$	Cl^-	1	-1502.539588	-820.8	-120.5
$C_n\text{mpyr}^+$	Cl^-	2	-1581.080203	-803.8	-127.1
$C_n\text{mpyr}^+$	Cl^-	3	-1659.620290	-793.2	-139.8
$C_n\text{mpyr}^+$	Cl^-	4	-1738.158988	-787.8	-143.4
$C_n\text{mpyr}^+$	$\text{N}(\text{CN})_2^-$	1	-1063.355851	-689.6	-127.6
$C_n\text{mpyr}^+$	$\text{N}(\text{CN})_2^-$	2	-1141.900866	-658.7	-160.3
$C_n\text{mpyr}^+$	$\text{N}(\text{CN})_2^-$	3	-1220.443749	-649.3	-179.7
$C_n\text{mpyr}^+$	$\text{N}(\text{CN})_2^-$	4	-1298.979214	-655.0	-176.5

*Includes scaled HF interaction energy